

# **Sedimentology and Stratigraphy of the Middle to Upper Jurassic Succession of Northern Iraq**



Royal Holloway University of London

Thesis submitted for the degree of Doctor of Philosophy

Azad Saeed

## DECLARATION OF AUTHORSHIP

I Azad Tahir Saeed declare that this thesis and the work presented in it is entirely my own. Where I have consulted the work of others, this is always clearly stated.

Signed: 

Date: 20 /Feb /2017

## **Acknowledgments**

Thanks are due to the Ministry of Higher Education and Scientific Research / Bagdad and Salahaddin University/ Erbil for providing financial support to this project. Acknowledgment is also expressed to Dr Ahmad Aqrawi from the Head Department of Geology for support of this research.

My greatest gratitude goes to my supervisor Professor Peter Burgess, who with his comments and valuable suggestions has helped me throughout different stages of my Ph.D. Furthermore, thanks to Dr Le Heron and Dr Bosence for their efforts as co-supervisor and adviser. Special thanks are also due to Margaret Collinson, who was kind enough to read early chapter drafts of the thesis and provided valuable feedback for improvements.

I am also grateful to Drs Hennig, Browning, Andres–Martinez, and Rudyawan for invaluable help with proofreading. I would like to express my special thanks to my wife Gona, who was my greatest supporter during my study. My thanks are, of course, due to all members of staff, postgraduates and at the Royal Holloway Earth Sciences department; their assistance and support are gratefully acknowledged. Dr Fouad Mohammad, Dr Kamal Haji Kareem, Mr. Shaker Ismail, Hemn Sabah, Abdulsamad Abdullah, and Dilshad Ali deserve special thanks for their kind cooperation and help with the field works.

## Abstract

This study investigates the Middle–Upper Jurassic strata of Northern Iraq. These Jurassic strata crop out as isolated patches in eroded cores of a highly folded and imbricate thrust zone of the Kurdistan region of Northern Iraq. Three field campaigns covered seven different areas, in a transect approximately 450 km long from Chnaran to Bank village. In total almost 500 samples were collected, and approximately 350 thin-sections were prepared. The goal of this study was to describe lithofacies in detail and establish a better understanding of the depositional environments and basin evolution through field description, petrography, SEM, and microfacies analyses. The study also aimed to understand the sequence stratigraphic development of the Upper Jurassic in the Gotnia Basin generally, and their influence on the study area specifically. Specific work focused on investigating the possible causes of *Posidonia* and radiolaria concentrations, and reconstruct their depositional environment. Determine the causative factors in facies transitions that may represent rapid shifts from open-marine pelagic to sabkha environment.

The upper part of the Sargelu Formation comprises a mixture of three different lithofacies alternating with each other at intervals of several decimetres thick, and these lithofacies comprise *Posidonia*-bearing limestone, radiolarian bedded chert, and black shale. Seasonal monsoonal upwelling can explain radiolarite deposition in the central Neotethyan basins during the Jurassic. The upwelling is the most likely source of chert formation at the upper part of Sargelu Formation. Detailed examination of different lithofacies in Sargelu Formation also reveals sedimentary features interpreted here as resedimented carbonate turbidite strata.

Five members are recognised in the Naokelekan Formation composed of a mix of black shale, limestones, including thick-bedded mottled limestones, and evaporites. The topmost strata in the formation include evidence for relatively shallow environments such as oolites and oncolites. Deep-sea microbial stromatolite overgrowths on ammonite shells, oncolites, bioturbation, encrusting foraminifera, coccoliths, and calcispheres are the most distinctive features of the Naokelekan Formation, which can be prominently observed at all localities. Condensed pelagic microbial stromatolite facies are comparable in many respects to the ammonitico rosso facies.

Three lithofacies are distinguished in the Barsarin Formation; including microbial laminite limestone, blister and flat laminated limestones and thick interbeds of dolomite and limestone. These strata are interpreted as several higher-frequency cycles, comparable in many ways with the Trucial Coast sabkha model. The ideal shallowing-upward cycles

comprise microbial stromatolite of subtidal environment, (ii) blister and flat, of an intertidal environment, and (iii) thick-bedded dolomite and limestone, of a supratidal environment.

## Contents

Sedimentology and Stratigraphy of the Middle to Upper Jurassic Succession of Northern Iraq.....		1
Declaration of Authorship.....		2
Acknowledgments .....		3
Abstract.....		4
List of Figures.....		15
List of tables.....		25
1	INTRODUCTION .....	25
1.1	Introduction.....	26
1.2	Aims of the study: .....	29
1.3	Methodology .....	29
1.4	Brief History of the area .....	30
1.5	Layout of the thesis .....	31
1.6	Localities .....	32
1.6.1	Chnaran Location (567924, E3934178) .....	32
1.6.2	Sargelu Location (514783, E3969364) .....	32
1.6.3	Hanjera Location (486759, E 4015920) .....	32
1.6.4	Nora Location (478324, E4022850).....	33
1.6.5	Barsarin Location (469705, E4053123) .....	33
1.6.6	Gara Location (368619, E4095981).....	33
1.6.7	Banik Location (319657, E4121871).....	33
2	A REVIEW OF TECTONIC AND BASIN DEVELOPMENT ON THE ARABIAN PLATE AND IN THE STUDY AREA.....	34
2.1	Aims .....	35
2.2	Tectono–physiographic subdivisions of Iraq .....	35

2.3	Unstable Zone .....	41
2.3.1	Zagros Suture Zone.....	41
2.3.2	The imbricated zone .....	41
2.3.3	The folded zone.....	43
2.4	Tectonostratigraphic Megasequences of the AP.....	43
2.4.1	Pre–Jurassic.....	45
2.4.2	Extension and passive subsidence associated with the opening of the Neotethys Ocean, the Early Permian–Early Triassic rifting .....	45
2.4.3	Middle Triassic–Early Jurassic.....	52
2.4.4	Early Jurassic: Sinemurian to Aalenian.....	57
2.4.5	Early Jurassic Sequence of Iraq .....	58
2.4.6	Middle Jurassic–Early Tithonian Differential Subsidence and Rifting, AP7 61	
2.4.7	Late Middle Jurassic: Callovian to Oxfordian .....	67
2.4.8	Late Jurassic: Kimmeridgian to Tithonian .....	75
2.5	Summary .....	80
3	<i>DESCRIPTION AND INTERPRETATION OF THE UPPER PART OF THE SARGELU FORMATION BAJOCIAN–EARLY CALLOVIAN</i> .....	83
3.1	Aims .....	84
3.2	A General view .....	84
3.3	Basal Saccharoidal Dolomite Member (BSDM) (10–50 m thick) .....	86
3.4	Middle <i>Posidonia</i> Limestone Member (MPLM) (7–30 m thick) .....	88
3.5	Black Shale, Radiolarian Bedded Chert and <i>Posidonia</i> –Bearing Limestone Member (BRPLM) (10–31 m thick) .....	94
3.5.1	<i>Posidonia</i> -bearing Limestone lithofacies (PBLL).....	97

3.5.2	Microscopic description .....	101
3.5.3	The preservation style of <i>Posidonia</i> .....	105
3.6	Interpretation .....	110
3.6.1	Preservation type and environment .....	111
3.6.2	Associated fossils.....	113
3.6.3	Mode of life of <i>Posidonia</i> .....	114
3.6.4	Age.....	116
3.7	Radiolarian Bedded Chert Lithofacies (RBCL).....	116
3.7.1	Field description .....	116
3.7.2	Microscopic description .....	118
3.7.3	Interpretation .....	123
3.7.4	Radiolarian formation and upwelling current.....	128
3.8	Potential mechanism for the high-productivity.....	132
3.8.1	The Caribbean river plume model.....	132
3.8.2	Equatorial upwelling current.....	133
3.9	<i>Posidonia</i> and radiolaria relation.....	135
3.10	Palaeobasin geometry .....	136
3.11	Resedimentation.....	141
3.12	Turbidity currents.....	141
3.12.1	Coarse-grained turbidites .....	143
3.12.2	Medium-grained sandy turbidites (siliciclastics and carbonates) .....	143
3.12.3	Carbonate turbidites .....	146

3.13	Turbidites of the Sargelu Formation.....	148
3.14	Mutual relationship between different lithofacies.....	152
3.15	Initiation of turbidity current.....	154
3.16	Distance from source.....	154
3.17	Folded Unit.....	155
3.17.1	Slumping .....	155
3.18	The morphology of slopes .....	157
3.19	Transformations between different kinds of gravity deposits .....	158
3.20	Summary .....	159
4	DESCRIPTION AND INTERPRETATION OF THE NAOKELEKAN FORMATION OXFORDIAN–EARLY KIMMERIDGIAN .....	162
4.1	Aims .....	163
4.2	Facies analysis.....	163
4.3	Black shale member (BSM) .....	164
4.3.1	Bajocian–Bathonian and Oxfordian–Early Kimmeridgian boundary .....	165
4.3.2	Interpretation .....	172
4.3.3	Oceanic Anoxic Events (OAE).....	173
4.4	Carbonaceous limestone member (CLM) .....	173
4.4.1	Interpretation .....	178
4.5	Medium-bedded microbial-bearing limestone member (MBMLM) .....	180
4.5.1	Interpretation .....	181
4.6	Thick-bedded mottled limestone member (TBMLM) .....	185
4.6.1	Dark patches .....	190
4.6.2	Light patches .....	200

4.6.3	Scanning electron microscope (SEM).....	205
4.6.4	Interpretation .....	205
4.6.5	Discussion .....	212
4.6.6	Summary of TBMLM formation .....	217
4.7	Argillaceous limestone member (ALM) .....	218
4.7.1	Microscopic evidence for the transition from ALM to MLL (Oxfordian–Early Kimmeridgian and Middle–Late Kimmeridgian boundary) .....	218
4.7.2	Facies interpretation of the ALM .....	224
4.8	Summary .....	227
5	<i>DESCRIPTION AND INTERPRETATION OF THE BARSARIN FORMATION MID–LATE KIMMERIDGIAN</i> .....	229
5.1	Introduction.....	230
5.2	Microbial laminite lithofacies (MLL). .....	234
5.2.1	Interpretation .....	242
5.3	Blister–flat laminated lithofacies (BFLL) .....	245
5.3.1	Interpretation .....	255
5.3.2	Conclusion.....	259
5.4	Thick-bedded dolomite–limestone lithofacies (TBDLL) .....	260
5.4.1	Interpretation .....	273
5.4.2	Conclusions.....	278
5.5	Summary .....	279
6	<i>SEQUENCE STRATIGRAPHY OF THE SARGELU, NAOKELEKAN AND BARSARIN FORMATIONS MID–LATE JURASSIC</i> .....	280
6.1	Aims .....	281

6.2	Introduction.....	281
6.3	Potential difficulties in sequence stratigraphy application in the study area.	282
6.3.1	Post collision deformation.....	282
6.3.2	Geometry of the basin .....	282
6.4	Sequence boundaries on submarine plateaus .....	283
6.5	Sequence boundaries.....	284
6.5.1	Type 1 sequence boundaries.....	284
6.5.2	Type 2 sequence boundaries.....	284
6.5.3	Type 3 sequence boundaries or drowning unconformity .....	284
6.6	Depositional sequences.....	285
6.7	Depositional sequence 1 (Latest Triassic–Early Jurassic Period) .....	287
6.8	Depositional sequence 2 (Middle Jurassic Period).....	288
6.8.1	Sequence boundary (Sb2).....	288
6.8.2	Drowning .....	289
6.8.3	TST2 <i>Posidonia</i> and radiolarians-rich facies.....	290
6.8.4	MFS2.....	292
6.8.5	HST2.....	295
6.9	Depositional sequence 3 (Late Callovian–Oxfordian).....	295
6.9.1	Sb3.....	295
6.9.2	TST3 microbial rich Medium-bedded facies .....	295
6.9.3	HST3 Mottled facies .....	296
6.10	Depositional sequence 4 (Late Oxfordian–Late Kimmeridgian).....	297
6.10.1	Sb4.....	297

6.10.2	HST4 calcispheres-rich facies .....	297
6.11	Problematic boundary between Early–Middle Kimmeridgian.....	298
6.11.1	HST5 Sabkha facies.....	299
6.11.2	The Barsarin sequence.....	301
6.11.3	Sb6.....	303
6.12	Summary .....	303
7	<i>ANALYSIS OF A CONDENSED INTERVAL ON A NEOTETHYAN MARGIN: IMPLICATIONS FOR BASIN EVOLUTION</i> .....	306
7.1	Aims .....	307
7.2	Introduction.....	307
7.3	Condensation facies .....	313
7.4	Condensed facies and tectonic setting .....	317
7.4.1	Starved basin floor.....	317
7.4.2	Bathymetric high.....	317
7.5	Tectonics .....	318
7.6	Evidence for fault controlled bathymetry .....	321
7.7	Eustatic and relative sea-level control.....	326
7.8	Gotnia Basin accommodation .....	328
7.9	Microbial stromatolite overgrowth on ammonites “ammonitico rosso” .....	331
7.9.1	Condense ammonitico rosso facies and bathymetry high .....	334
7.9.2	Disappearance of ammonitico rosso.....	334
7.10	Factors controlling condensed intervals related to Jurassic ammonitico rosso 335	
7.10.1	Current sweeping and reworking .....	335
7.10.2	Rate of sedimentation.....	337

7.10.3	Paucity of planktonic organisms .....	338
7.10.4	Hardground and low rate of sedimentation .....	338
7.10.5	Depth.....	339
7.10.6	Climate controlled.....	340
7.11	Naokelekan Barsarin boundary.....	343
7.12	Discussion .....	344
8	<i>DISCUSSION</i> .....	346
8.1	Tectonic development of the study area .....	347
8.2	Correlation between subsurface sections and Kurdistan outcrops .....	347
8.3	Sargelu Formation .....	348
8.3.1	Radiolarian bedded chert.....	349
8.3.2	Potential mechanism for the high-productivity.....	350
8.3.3	Posidonia-bearing limestone.....	351
8.3.4	Age.....	352
8.3.5	Resedimentation.....	353
8.3.6	Allodapic limestones or carbonate turbidites .....	354
8.3.7	<i>Posidonia</i> and radiolaria relation.....	355
8.3.8	Fold structures.....	356
8.3.9	Oceanic Anoxic Events (OAE) .....	356
8.4	Naokelekan Formation.....	357
8.4.1	Black shale in the Naokelekan Formation .....	358
8.4.2	Carbonate units in the Naokelekan Formation .....	358

8.4.3	Mottled limestone .....	359
8.4.4	Argillaceous limestone member and calcispheres .....	360
8.5	Barsarin formation .....	361
8.5.1	Microbial laminite lithofacies (MLL).....	361
8.5.2	Blister-flat laminated lithofacies (BFLL).....	362
8.5.3	Thick-bedded dolomite-limestone lithofacies (TBDLL) .....	363
8.5.4	Dolomite related to sabkha environments.....	364
8.6	Sequence stratigraphy.....	365
8.6.1	Sb2.....	365
8.6.2	Sb3.....	366
8.6.3	HST3.....	367
8.6.4	Sb4.....	367
8.6.5	Problematic boundary between Early-Middle Kimmeridgian.....	367
8.6.6	Sequence stratigraphy of Middle-Late Kimmeridgian .....	368
8.7	Condensed facies.....	369
9	<i>CONCLUSIONS AND RECOMMENDATIONS</i> .....	372
9.1	Conclusions.....	373
9.1.1	Sargelu Formation .....	373
9.1.2	Naokelekan Formation.....	374
9.1.3	Barsarin Formation .....	375
9.2	Recommendations.....	376
	References.....	387

## List of Figures

Figure 1.1: Geographic map of Iraq with the location of the study sections.....	29
Figure 2.1: Geographic map of Iraq with the location of the study sections.....	37
Figure 2.2: Tectonic map of Iraq, modified from Aqrawi et al. (2010).....	38
Figure 2.3: diagram showing simplified layout of tectonic zones of Iraq, modified from Aqrawi et al. (2010) and Fouad (2015).....	39
Figure 2.4: Geographic map showing different structure belts of the Zagros Mountains in Iraq and Iran.....	40
Figure 2.5: Geological Map of the study area, after Sissakian (2000). ....	42
Figure 2.6: diagram showing stratigraphic summary form Permian to Jurassic sediments of the Arabian Plate, tectonostratigraphic megasequences (TMS) development of the Arabian Plate.....	46
Figure 2.7: Schematic plate reconstruction megasequence AP5. The Hercynian Orogeny resulted in non-depositional uplift in Late Carboniferous to Late Permian times .....	47
Figure 2.8: Schematic plate reconstruction with its cross-section A–B for the megasequence AP5 during Late Carboniferous–Middle Permian showing blocks.....	49
Figure 2.9: Diagram showing cross section through Triassic successions in northern Iraq and western of Zagros of Iran. Note lateral variation in thickness and facies. Modified from Aqrawi et al. (2010).....	50
Figure 2.10: Middle–Late Triassic palaeo–tectonic setting of Iraq and west of Iran, modified after Aqrawi et al. (2010).....	51
Figure 2.11 Schematic diagram shows the distribution of the main structures of the Arabian Plate, modified after Ziegler (2001).....	52
Figure 2.12: Regional lithostratigraphic correlation chart of the Late Triassic and Jurassic for study area, after Alsharhan (2003).....	55
Figure 2.13: Lithostratigraphic correlation chart of the Late Triassic and Jurassic for Iraq, after Jassim and Goff (2006).....	56
Figure 2.14: A; Diagram showing stratigraphic correlation of the Late Triassic–Jurassic formations across northeast-southwest Iraq.....	57
Figure 2.15: A; Palaeofacies of the latest Triassic–Early Jurassic in the Arabian Plate, modified from Ziegler (2001). B; The palaeogeographic of Early Jurassic of Iraq, after Jassim and Goff (2006).....	60
Figure 2.16: Diagram showing reconstruction for megasequence AP8. During Early–Late Jurassic, a new passive margin developed at the northeastern AP.....	63

- Figure 2.17: A; Palaeofacies of the Early Jurassic in the Arabian Plate. In this period, a new passive margin developed due to the eastern Mediterranean opening modified from Ziegler (2001).....64
- Figure 2.18: Diagram showing depositional evolution of Jurassic successions with Idealised model for Gotnia Basin fill.....71
- Figure 2.19: A; Generalized depositional model of Middle–Late Jurassic condensed basin at central basin to the margin of the Gotnia Basin at western desert. B; locations of sections, modified after Aqrabi et al. (2010).....72
- Figure 2.20 A; Palaeofacies of the Middle Jurassic in the Arabian Plate During this time period, the passive margins along the northeast and north of the Arabian Plate are well-developed, and sediments were generally characterized for an open-marine environment.....77
- Figure 2.21: A; Palaeofacies of the Late Jurassic in the Arabian Plate, which is characterized by including differential intra-plate subsidence that .....80
- Figure 2.22: Thickness map of the late Jurassic period in Iraq, note the depocentres at south and north of Iraq, from Jassim and Goff, 2006.....81
- Figure 2.23: Stratigraphic column of the Jurassic succession showing tectonic history and different stratigraphic units from northwest, across Kermanshah to southwest Iran, modified from (Lasemi and Jalilian, 2010).....84
- Figure 2.24: A; Palaeofacies of the Late Jurassic in the Arabian Plate. This time period spanned the deposition of the Barsarin and Gotnia Formations in Iraq with Arab, and Hith, Formations in Arabia Basin.....87
- Figure 3.1: different locations of studied areas in northern Iraq, Kurdistan region.....95
- Figure 3.2: diagram showing correlation between BRPLM, MPLM, and BSDM .....97
- Figure 3.3: Generalized stratigraphic column of the upper part “black shale radiolarian bedded chert and *Posidonia*-bearing limestone member “of the Sargelu Formation.....98
- Figure 3.4: Basal Saccharoidal Dolomite Unit: A; medium-bedded saccharoidal dolomite. B; the lower boundary between Sargelu and Sehkaniyan Formations.....100
- Figure 3.5: A; medium-bedded of thin-shelled bivalve bearing limestone of the MPLM with black shale interbedding .....101
- Figure 3.6: A; partially Alizarin Red S photomicrograph showing *Protoglobigerina* foraminifers (red arrows), PPL, partially stained with red alizarin. ....102
- Figure 3.7: A; upper part of the BRPLM showing alternation between different lithofacies; PBLL (p lst), RBCL (ch), and BSALL (b sh).....104
- Figure 3.8: A; intense folded structures (bounded by red dashed lines) characterizing upper part of Sargelu Formation, note, overlaying and underlying beds are not folded, Gara location.....105

- Figure 3.9: A; BRPLM showing interbedding between limestone, bedded chert, and black shale, note, the beds are tabular-shape.....107
- Figure 3.10: A; photograph showing high abundance of thin-shelled bivalves "*Posidonia*." B; ammonite C; ammonite–aptychus (white arrows) which have been observed at the top of the Sargelu Formation.....108
- Figure 3.11: photographs showing vertical variation of textures in the *Posidonia*-bearing limestone at different localities of the PBL.....109
- Figure 3.12: A; different range size of horizontal disarticulated intact thin-shelled *Posidonia*. B; *Posidonia ornati* Quenstedt .....112
- Figure 3.13: photomicrograph showing textural comparison between MPLM and MPLM. A; the MPLM showing Protoglobigerina (red arrows) and broken *Posidonia* mudstone. The Protoglobigerina are always not more than three chambers.....113
- Figure 3.14: thin-shelled filamentous packstone showing.....116
- Figure 3.15: photomicrographs of thin-shelled filamentous wackestone–packstone showing different stages (from A–D) of transformation from parallel layers of *Posidonia* filament (fil pos) to the coalescent debris (coa de).....117
- Figure 3.16: photographs (A–F) showing gradual upward increase in elongated lensoid bodies: A; scattered dolomite (dol) crystals between *Posidonia* filaments (pos).....118
- Figure 3.17: A; thin to medium-bedded cherts alternating with, *Posidonia*-bearing limestone. B; interbedding between bedded chert, *Posidonia*-bearing limestone.....127
- Figure 3.18: A; bedded chert showing numerous dissolved radiolarian tests (black arrows). B; photomicrograph showing both radiolarian chert at the bottom.....129
- Figure 3.19: A; bedded chert showing radiolarian pore–space and sheltered pores filled with kerogeneous matter (Ke m), note scattered *Posidonia* shells.....130
- Figure 3.20; photomicrographs bedded chert with various kind of radiolaria, their origin cannot be ascertained, due to the poor preservation of their outer wall. Note the groundmass contains a great number of perhaps radiolarian test ghosts (white arrows).....131
- Figure 3.21: (A–C) photomicrographs showing *Cinguloturris carpatica* Dumitrica. Note the groundmass contains a great number of perhaps radiolarian test .....132
- Figure 3.22: diagram showing the relative role of different organisms for extraction of silica from seawater since the beginning of the Cambrian Period (modified from Kidder and Erwin, 2001).....134
- Figures 3.23: Distribution and age of Jurassic ribbon radiolarites in the continental–margin sequences of the Neotethys. Note the radiolarians are usually followed by pelagic facies such as Ammonitico Rosso or pelagic oolites, and are highly diachronous. (Modified from Jenkyns and winterer, 1982).....139

- Figure 3.24: Comparison between the Hawasina basin (A) which could be considered an extension to the studied Sargelu basin of Middle–Jurassic time with modern Somalia and Owen basins (B).....140
- Fig 3.25: diagram showing a simplified upwelling area with high surface fertility and principal sedimentary palaeoenvironments. ....140
- Figure 3.26: palaeogeographic map showing major oceanic high productivities of radiolarian bio-provenance and potential high productivity upwelling zones during Bathonian age (modified from Baumgartner, 2013).....141
- Figure 3. 27: diagram showing relationship between radiolarites(R) and monsoonal activities at different periods (Modified from DE Wever et al., 2014).....144
- Figure 3.28: depositional model showing relation between *Posidonia*-bearing limestone and radiolaria (modified from Jach, 2007).....145
- Figure 3.29: Hypothetical model representing depositional environments of Sargelu Formation.....149
- Figure 3.30: Restored relations of the passive margin sediments and the tectonic fault control of the Oman rifted margin (Modified from Robertson & Searle, 1990).....149
- Figure 3.31: Simplified tectonic diagram showing the main palaeogeographic domains in central Tunisia and the main Jurassic faults .....150
- Figure 3.32: the range of different processes that occur in deep sea and their products (adapted from Stow, 1992; Reading, 2009).....152
- Figure 3.33: Diagram showing different intervals of the Bouma Sequence model with depositional interpretation (adapted from Bouma, 1962).....155
- Figure 3.34: Meischner Sequence showing ideal allodapic limestone turbidity model and its subdivisions (adapted from Meischner, 1964).....157
- Figure 3.35: Cross-sectional view of posidonia bearing limestone and thin-bedded chert showing gradual fining upward.....160
- Figure 3.36: photograph showing normal graded bedding and laminated structures in posidonia bearing limestone, which may suggest turbidity processes. Note the bedded cherts cap the turbidite limestone.....161
- Figure 3.37: Generalized turbidity model of the upper part of the Sargelu Formation showing turbidity units and their interpretation.....163
- Figure 3.38: Slumped structure showing folded beds, note the bedding kept their parameters (red arrows) which indicate early lithification.....168
- Figure 3.39: Schematic diagram showing different types of gravity–driven processes which transport sediments into deep water environments.....169

- Figure 3.40: Hypothetical diagram showing upwelling current, high productivity and slumping structures of the upper part of the Sargelu Formation during Bathonian age.....170
- Figure 4.1: different locations of studied areas in northern Iraq, Kurdistan region.....175
- Figure 4.2: Generalized stratigraphic column of the Naokelekan Formation showing different members and the nature of underlying and overlaying contacts with Sargelu and Barsarin Formations respectively.....176
- Figure 4.3: Panoramic photography showing the M–U Jurassic succession at Barsarin village locality. The Naokelekan Formation is represented by four different units CLM, MBMLM, TBMLM, and ALM .....178
- Figure 4.4: A; Black shale member intercalated with a few dolomite beds. Note the sharp contact with the overlying medium-bedded microbial-bearing .....179
- Figure 4.5: A; contact between the Naokelekan and Sargelu formations (dashed line). Note the changes from convoluted structures at the top of the Sargelu Formation to normal bedding at the base of black shale member .....180
- Figure 4.6: Black shale unit: A; crudely laminated carbonaceous wackestone, including poorly preserved fossils (F), few dolomitized crystals (D).....181
- Figure 4.7: carbonaceous lithofacies subdivisions: (a); medium to thin-bedded carbonaceous limestone, and (b); thin-bedded highly fissile and recrystallized carbonaceous limestone.....185
- Figure 4.8: A; stained recrystallized limestone with Alizarin Red S showing selective dolomitization. ....186
- Figure 4.9: A; photomicrograph showing *Protoglobigerina* foraminifers (white arrows) that make up the majority of fossil contents of the upper unit of carbonaceous limestone member.....187
- Figure 4.10: A; highly fractured, and well bedded MBMLM. B; photomicrograph of the upper part of MBMLM showing small lath shapes of limestone pseudomorphs of evaporite.....193
- Figure 4.11: A; upper and lower sharp boundaries of medium-bedded microbial-bearing limestone member.....194
- Figure 4.12: A; thick-bedded mottled limestone member appears persistent and forms a prominent cliff. B; bedding thickness variation and detail of dark and light patches.....197
- Figure 4.13: A; vertical section view; sharp boundary between light (L) and dark (D) patches, (white arrows). Red arrows show scattered dark non-laminated patches surrounded by light patches.....198
- Figure 4.14: Sharp contact between thick-bedded mottled limestone and the overlying limestone member (dashed line).....199

- Figure 4.15: A cross section showing distribution and arrangements of the dark and light patches. The laminated dark patches normally develop on the nodular limestones (NL) and ammonite shells (A).....201
- Figure 4.16: A; and B; laminated dark patches growing on ammonite shell and nodular limestones (NL). Note, (B) is the artistic effected photo. C and D; photograph and sketch showing laminated dark patches stacking on ammonite shells.....202
- Figure 4.17: vertical section view showing differential resistance to weathering (top of the photo), the light patches appear as recessive producing pits, whereas the dark patches appear more resistance and standing out fossils.....203
- Figure 4.18: Thick-bedded mottled limestone member showing three different kinds of laminated dark patches textures. A; high relief laterally linked hemisphere. Note the laterally linked laminated structures stacking on nodular limestones (NL).....204
- Figure 4.19: A; dark laminated patches over growth on ammonite shells, the lamina couplets consisting of fine dark and coarse-grained calcite spars. ....206
- Figure 4.20: Micro-fabric of laminated dark patches, rich in different size of peloids, calcispheres (black arrows), and large clasts. B; detail of the black rectangle in (A), showing microbial filaments (white arrows).....207
- Figure 4.21: cross-section views show dark grey structureless patches (D) and light patches (L) at different locations A; Nora location.....208
- Figure 4.22: A; dark structureless patch contains a lot of microbial filament traces (black arrows), and few bioclasts and gastropods are also included (G). B; photomicrograph shows detailed microbial filament.....209
- Figure 4.23: photomicrograph showing microbial filaments over growth on an ammonite shell. Note, the sketch of the microbial filaments has similar direction with the microbial of photomicrograph.....210
- Figure 4.24: Photograph showing increasing in the light patches proportion upward by comparison with dark patches.....211
- Figure 4.25: A; bedding plane surface view shows differential weathering effects and rounded net-shaped pits on the mottled lithofacies. The light patches (L) always appear recessive and less resistance than the darker patches (D).....212
- Figure 4.26: A; Fossil debris and calcispheres in the light patches (white arrows). B; shows a sharp boundary between dark and light patches (white arrows).....213
- Figure 4.27: Scanning electron microscope photographs showing both dark (I) and light (II) patches The SEM analysis reveals dominance of nanofossils in both dark and light patches (arrows).....214
- Figure 4.28: diagram showing comparison between Naokelekan Formation microbial structures and modified Logan et al. (1964) model.....221

- Figure 4.29 A; homogenized texture of TBMLM contains scattered remnants of dark patches. B; photograph showing different stages of bioturbation and scoured surface of laminated stromatolites.....224
- Figure 4.30: A; boundary between argillaceous limestone member of the Naokelekan Formation (B) and microbial laminated lithofacies of the Barsarin Formation (C) (white dashed line) showing sharp changes in lithofacies characteristics from black shale dominance to the stromatolitic strata.....230
- Figure 4.31: Sharp lithofacies change between argillaceous limestone member ALM (A) and microbial laminate lithofacies MLL .....231
- Figure 4.32: details of lithological change from the Naokelekan (I) to the Barsarin Formation (II). The wide grey arrow pointing to the dramatic lithofacies change. A; calcispheric packstone in argillaceous limestone member (white arrows), PPL.....32
- Figure 4.33: A; Lamination bent around fenestral calcite (EC), the white arrows pointing to the lamination displacement. ....233
- Figure 4.34 Distribution of member types of the Naokelekan Formation in Kurdistan exposures and lithostratigraphy correlation between different members. ....237
- Figure 5.1: Different locations of the studied area in northern Iraq, Kurdistan region.....240
- Figure 5.2: Generalized stratigraphic column of the Barsarin Formation showing different lithofacies and the nature of the underlying and overlying contacts with the Naokelekan and Chia Gara Formations respectively.....241
- Figure 5.3: A; diagram showing panoramic photograph and lithostratigraphic log of the lower part of the Barsarin Formation, note a repetition of lithofacies (curved red arrows).....243
- Figure 5.4: Microbial laminite lithofacies MLL. A; polished slab showing couplets of light coarse and dark fine calcitic laminae. The laminae show undulating macrofabric, note small fenestrae fabrics.....245
- Figure 5.5: Domal stromatolites from different locations. A; top view showing domal stromatolite at Barsarin village. B; partially exposed domal stromatolites, showing alternation between domal and planar beddings.....246
- Figure 5.6: Microbial laminite lithofacies. A; laminated couplet, showing thin dark laminae (D), and thick light laminae (L).....249
- Figure 5.7: A; intact ostracod carapaces are infilled by calcite cement (black arrows), and clotted structures (white arrows).....250
- Figure 5.8 A; couplets of dark fine (D) and light microsparite (L) laminae. The light laminae are rich in fenestral fabrics (F). Note the dark laminar are so susceptible to pressure solution.....251
- Figure 5.9: A; the Barsarin Formation exposure showing blistered–flat lamination lithofacies (2) is underlain by microbial laminite lithofacies (1), and overlain by thick-bedded dolomite lithofacies (3) respectively.....257

- Figure 5.10: A; blistered–flat lamination lithofacies, the sequence normally commences with blistered then followed by flat laminae. The boundary between blistered and flat laminae is determined by white dashed line.....258
- Figure 5.11: A; blister–flat laminated lithofacies, as illustrated in reflected–light, showing large fenestrae at the base that infilled by calcite cement.....261
- Figure 5.12: A; distinct lamination of dolomite (dol) and neomorphosed calcite (neo cal) couplets, note large fenestrae at left of photo. ....262
- Figure 5.13: A; Clusters and arrays of cyanobacterial filaments (white arrows) in the darker laminae (D) surrounded by lighter laminae (L) with many signs of evaporite pseudomorphs (red arrows) B; Photomicrograph showing filaments in the dark micritic laminae (black arrows).....263
- Figure 5.14: A; dolomite rhombs within (Au qz) crystals forming poikilotopic texture. B; calcite cement pseudomorphs of gypsum (black arrows) and authigenic quartz (Au qz) C; Lensoidal and rhomb-shaped micrite pseudomorphs of evaporite associated with length–slow chalcedony (ch).....264
- Figure 5.15: Photograph showing stratigraphic section of the lower part of the Barsarin Formation which consists of three different lithofacies (1, 2, and 3). ....272
- Figure 5.16: A; Black laminated elongate chert nodules, note the preservation of original lamination B; large lensoidal chert nodules C; scattered chert nodules in the massive dolomite lithofacies.....273
- Figure 5.17: A; showing two intervals of polygonal mudcrack at the top of thick-bedded dolomite–limestone lithofacies. B; detail of the white square in the (A) photo showing polygonal fracture network which are filled with limestone sediments.....274
- Figure 5.18: A; red coloured highly porous and brecciated carbonate-rich soil-like horizon (white arrows) separating thick-bedded dolomite–limestone lithofacies and microbial laminite lithofacies.....275
- Figure 5.19: A; thick bedding dolomite in the top of the Barsarin Formation display noticeable undulation and tilted structures. B; the boundary between Barsarin and Chia Gara Formations (white dashed line).....276
- Figure 5.20: A; fine crystalline dolomite (F Cr Dol) showing intraclasts (red arrows), fenestrae structures, truncated, and fractured laminae (blue arrow).....279
- Figure 5.21: A; anhydrite lath shapes in fine crystalline dolomite show fenestral structures. B; fenestral structures are formed by calcite pseudomorphs of evaporite in microcrystalline dolomite.....280
- Figure 5.22: couplets of fine crystalline dolomitized mudstone and fenestral dolomite, note that the fenestral dolomite laminae are much richer with elongated pelloids than darker one.....281

- Figure 5.23: Couplets of fine crystalline dolomite (F Cr Dol) and coarse poikilotopic blocky calcite laminae, note dolomitic including calcite pseudomorphs of evaporite, whereas poikilotopic blocky calcite laminae containing rhombs of dolomite and kerogen.....282
- Figure 5.24: Depositional model showing different lithofacies locations of the Barsarin Formation on tidal flat.....287
- Figure 6.1: Generalized stratigraphic correlation between Iraq and Arabian Plate (AP) showing comparison between tectonic, eustatic, relative sea-level development.....295
- Figure 6.2: diagram showing sequence stratigraphy and facies change between Sehkaniyan and Sargelu formations of Early–Middle Jurassic.....298
- Figure 6.3: summary of description and 3rd order sequence stratigraphy development of the upper part of the Sargelu and Naokelekan Formations.....303
- Figure 6.4: diagram showing panorama of field section in Barsarin locality with stratigraphic column and sequence stratigraphy of the upper part of the Sargelu–Naokelekan–Barsarin and–Chia Gara Formations.....304
- Figure 6.5: Generalized of description and 3rd with 4th order sequence stratigraphy development of the Barsarin Formation.....310
- Figure 6.6: Diagram showing typical shallowing-upward succession of two selected cycles of the Barsarin Formation with their relationship to fluctuating of sea-level.....314
- Figure 7.1: Diagram showing poorly understood lateral facies changes from Naokelekan to the subsurface section of Najmah Formation.....318
- Figure 7.2: A; The palaeogeographic of Late Jurassic of Iraq, after Jassim and Goff (2006). (B) Correlation between condensed Naokelekan and Najmah Formations.....319
- Figure 7.3: Simplified stratigraphic column of the Naokelekan Formation showing different members and the nature of underlying and overlying contacts with Sargelu and Barsarin.....320
- Figure 7.4: Distribution of the ammonitico rosso and condensed facies across Northern Neotethys Ocean. Note growing of condensed facies over the bathymetric highs in passive margins.....324
- Figure 7.5: (A) Oncoids in the thick-bedded mottled limestone member TBMLM, Naokelekan Formation. (B) Oncoids of the Betic Cordillera, Southern Spain, modified from Vera and Martín–Algarra (1994).....325
- Figure 7.6: distributions and abundance of microbial ammonitico rosso on the intra Prebetic Zone, southern Spain during Middle Oxfordian–Lower Kimmeridgian.....329
- Figure 7.7: Diagram showing prevailing Phanerozoic reef types and reef builders. The left column represents cumulative curves of reefs and reef mounds .....331
- Figure 7.8: hypothetical model for fault–block platform of condensed facies in the Naokelekan Formation during Oxfordian.....334

Figure 7.9: Correlation between global mean sea-level of Miller (2005) and relative sea-level Fluctuation in the study area.....	336
Figure: 7.10: Palaeofacies of the Late Jurassic in the Arabian Plate, which is characterized by including differential intra-plate subsidence .....	338
Figure: 7.11: (A); the passive margin development with differential subsidence in Oman showing condensed ammonitico rosso facies development on a bathymetric high.....	339
Figure 7.12: I–Comparison between; (A) a slab showing taphonomy of cephalopod assemblages with hardground of macro-oncoids with microbial Fe–Mn crusts encrustations on ammonoids .....	342
Figure 7.13: diagram showing current impact on the condensed intervals. A bimodal histogram explaining that only trapped coccoliths and ammonite could preserve on the tilted fault block, whereas the rest sizes were swept away by current.....	345
Figure 7.14: (A) Palaeogeographic diagram showing migrations and distributions of boreal ammonite. Note migration towards subtropical latitudes of boreal ammonite fauna during the Late Callovian–Early Oxfordian age.....	351

## List of tables

Table 2.1: List of different members and lithofacies of the Sargelu, Naokelekan and Barsarin Formations with their abbreviation.....	84
Table 4.1: Comparison between thick-bedded mottled limestone member and medium-bedded microbial-bearing limestone member .....	192
Table 4.2: Comparison between dark and light patches.....	218
Table 4.3: Comparison between deep and peritidal stromatolites.....	226

# *CHAPTER ONE*

## *1 INTRODUCTION*

## 1.1 Introduction

The Jurassic formations of Kurdistan exposures are generally characterized by the dominance of carbonate rocks, but the Sargelu and Naokelekan Formations contain well-known organic-rich intervals also seen elsewhere in the Middle–Upper Jurassic successions of Iraq, and they are the most important hydrocarbon source rocks in the region (Buday, 1980; Jassim and Goff, 2006; Aqrabi et al., 2010; Al-Ameri et al., 2013; Hussein et al., 2013; Abdula, 2014; Al-Ameri and Al-Nagshbandi, 2014).

Traditional interpretations divide the Bajocian–Bathonian Sargelu Formation into a basal saccharoidal dolomite member, a middle *Posidonia* limestone member and the upper black shale, radiolarian bedded chert and *Posidonia*-bearing limestone member. This formation was initially interpreted as a basinal deposit, and its age is still a subject of controversy. Although Jurassic strata of Kurdistan outcrops are rich in ammonites, the last time these fossils were studied was by Spath (1950). This study focuses on the upper member, which commonly comprises mixtures of three lithofacies that are interbedded at intervals of several decimetres. The facies typically start with *Posidonia*-bearing limestone, which is followed by radiolarian bedded chert, and capped by black shale and argillaceous limestone. The causes of this facies mixture and their repetitions within many separate packages are not systematically examined in a comprehensive study. Current investigations in this study are an initial attempt to explore the high abundance of *Posidonia* and radiolarians and their connection to Jurassic monsoonal upwelling current. Also, a model is presented that helps interpreting the periodical repetitions of different lithofacies which show some evidence for the presence of re-sedimentation.

The Naokelekan Formation was interpreted to be a deep-marine condensed facies (Bellen et al., 1959; Jassim and Goff, 2006; Aqrabi et al., 2010; Salae, 2001). Spath (1950) studied ammonites from the formation, and determined the age to be Late Oxfordian to Early Kimmeridgian. The two main aspects to be considered in the Naokelekan Formation are the probable existence of condensed intervals, and the origin of the mottled textures, which have been questioned initially by Bellen et al. (1959). The average thickness of the formation in the study area is about 14 metres. Based on Salae (2001) the formation can be subdivided into three units, an uppermost argillaceous limestone, an underlying mottled limestone with ammonite traces, and a lowermost unit of thinly bedded, bituminous limestones and intercalated black bituminous calcareous shales. The boundary between the Early and Middle Kimmeridgian shows dramatic sea-level fall with an abrupt basinward shift of facies from ammonitico rosso to sabkha. According to Miller et al. (2005) the eustatic sea-level fall from Early to Middle

Kimmeridgian was about 20 metres, suggesting that this shift of facies may not be eustatic. This problematic boundary needs to be carefully considered.

The Naokelekan and Barsarin Formations are interpreted as a deposit formed in a sediment starved environment in unfilled accommodation space (Jassim and Goff, 2006; Aqrawi et al., 2010). However, the entire Barsarin Formation is related to a peritidal sabkha setting similar to the Trucial Coast area of the Arabian Gulf (Salae, 2001). It seems unlikely that the Barsarin Formation deposited in a deep starved basin, because there are significant observations consistent with supratidal environments. More evidence is necessary to support this assumption. The Barsarin Formation is not fossiliferous, and its Middle–Late Kimmeridgian age is estimated from stratigraphic position alone. A prominent characteristic of this formation is the possibly cyclical repetition of lithofacies assemblages. According to Salae (2001) each assemblage usually begins with a subtidal microbial laminite lithofacies, followed by blister–flat laminated lithofacies, and ends with thickly bedded dolomite lithofacies. Common desiccation features, such as, chicken-wire gypsum, mud cracks and tepee structures, provide evidence of subaerial exposure.

Numerous studies about hydrocarbon evaluation of the Middle–Upper Jurassic strata have been published in the last three decades (Othman, 1990; Al-Ahmed, 2006; Al-Ameri et al., 2009; Al-Ameri and Zumberge, 2012; Al-Badry, 2012; Al Ahmed, 2012; Al-Ameri et al., 2013; Baban and Ahmed, 2013; Hussein et al., 2013; Abdula, 2014; Al-Ameri and Al-Nagshbandi, 2014; Al-Jaafary and Hadi, 2015; English et al., 2015). However, the sedimentology and palaeo–environments remained poorly understood. Despite some recent studies on the sedimentology of the Jurassic strata (Surdashy 2000; Salae, 2001; Balaky 2004; Sherwani and Balaky, 2006) many important questions about the exact depositional environment of the different facies remain unanswered. The present study will introduce a new perspective on these formations, and could be used for correlation with their subsurface equivalents in future studies.

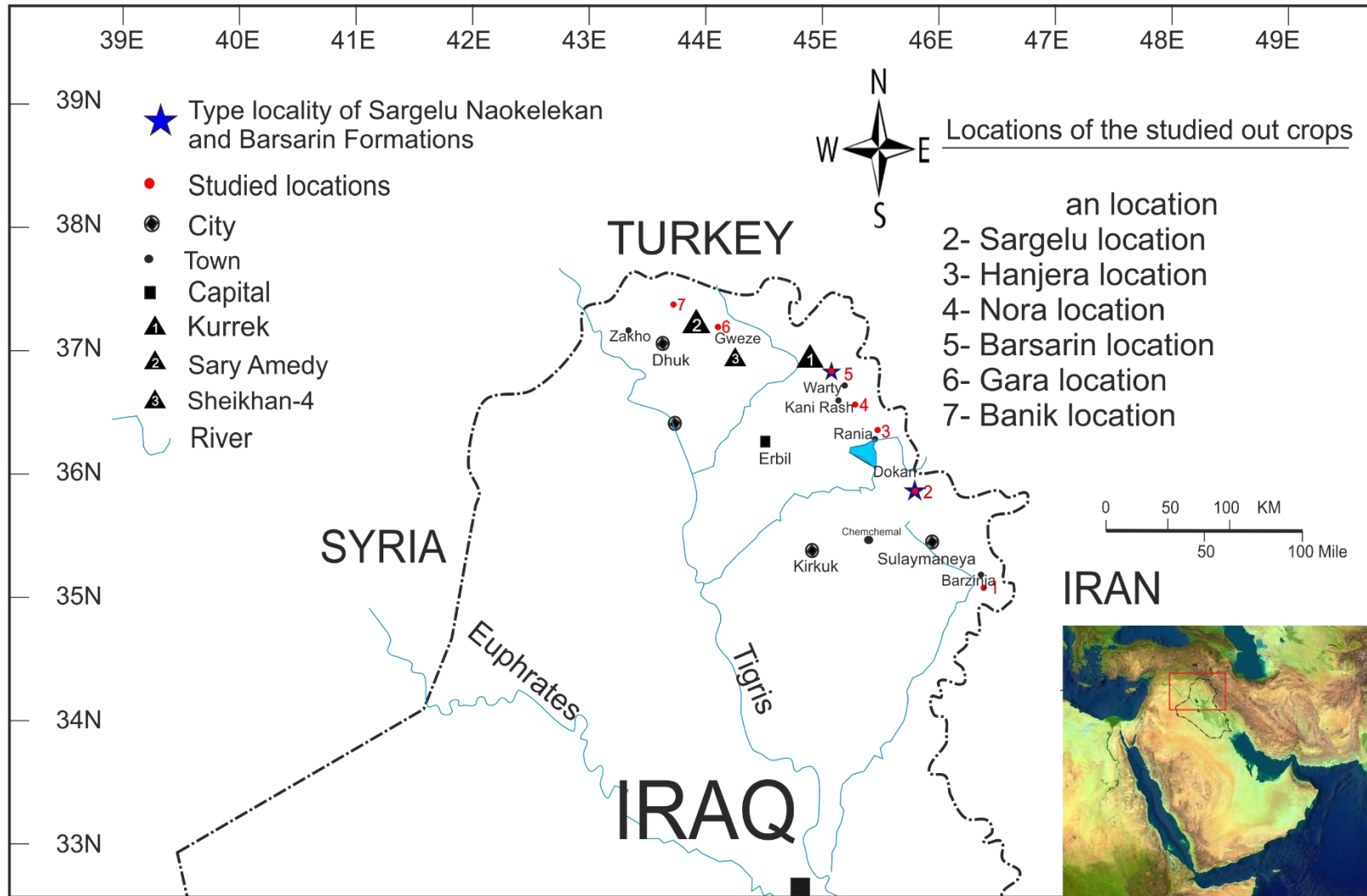


Figure 1.1: Geographic map of Iraq with the location of the studied sections.

## 1.2 Aims of the study:

- Describe lithofacies in detail and provide a better understanding of depositional environments through field description, petrography, and microfacies analyses for selected sections of the Middle to Upper Jurassic strata in the Kurdistan region outcrops.
- Interpret the occurrence of bedded chert, black shales, and carbonate beds of the upper part of the Sargelu Formation, and identify the causative factors that are responsible for the flourishing of *Posidonia* fossils, and reconstruct their depositional environment locally. One of the main quests in these studies is to determine the origin of the bedded chert, and suggest potential models of the relationship between radiolarians and the monsoonal-driven upwelling currents in study area.
- Discuss some evidence regarding resedimentation by turbidity currents and slumps in the Sargelu Formation. Interpret the mechanism that causes the occurrence of folding at the top of the Sargelu Formation.
- Reveal the causes of the ammonitico rosso facies development in the condensed strata in the Naokelekan Formation, and find a closer analogue in this respect. Within the scope of this thesis to discuss in detail, the processes that controlled condensed facies formation in the Naokelekan Formation, including the possibility of tectonic development, eustatic sea-level change, and bottom current activities. Suggest an appropriate model to explain the condensed facies in the study area.
- Determine if repeated peritidal facies packages could represent shallowing-upward cycles in the Barsarin Formation, and suggest mechanisms that could cause the observed cyclicity. Also, determine the relevant processes that caused apparently rapid environmental changes from an open-marine pelagic setting to sabkha environments.

## 1.3 Methodology

Fieldwork for this study was undertaken in three separate field campaigns and covered seven different areas: April 2012, April 2013 and August 2014. Most outcrops in the study area occur in either highly folded or imbricate zones (the details described in Chapter 2). Field areas are easily accessible by road from towns. There are relatively wide areas of the Jurassic carbonate exposures, and there are good opportunities for the selection of suitable sections. Outcrop sections were studied and described in detail, including closely spaced sampling. The total number of samples is about 500, collected at 0.3–0.7 metre intervals or at each change in lithology. All sections are accurately represented,

and relevant photographs were well documented. 350 thin-sections were studied and detailed petrographical study and microfacies analysis were performed for this thesis. Full-field stratigraphic descriptions presented in the attached appendix. Scanning electron microscope analysis was carried out on freshly broken etched, polished and coated surfaces with gold samples. About 193 SEM images have been investigated for information on calcareous nanofossils and evidence of microbialites.

#### **1.4 Brief History of the area**

The discovery and use of oil “asphalt” in Iraq dates back more than four thousand years. There are many natural asphaltic seeps in springs in Hit City in southern Iraq. Natural asphalt was employed for construction since a long time ago, and it is used for the walls and bricks of Babylon. Northern Iraq also has many bitumen and crude oil and gas seeps. Perhaps the most famous gas show is the eternal fire at Baba Gurgur in Kirkuk City. The fire is estimated to have been burning for several thousand years; Herodotus (c. 484–425 BC) described the eternal fire of Baba Gurgur. The Baba Gurgur is a giant oil-field of Kirkuk Governorate discovered in 1927. It was the largest oil-field globally prior to discovery of the Ghawar field in Saudi Arabia in 1948.

The history of oil production dates back more than a century, when the first exploration well in the Middle East was drilled in 1901 on the Chia Surkh anticline in Kurdistan (Figure 1.1) (Mackertich and Samarrai, 2015). In spite of promising geological indicators from 1922 to 2005, few wells were drilled. Long-term military conflicts between Kurdish Revolutionaries and successive governments in Baghdad were the main cause that prevented exploration and production in Kurdistan until 2003. Following the Iraq War in 2003, the Kurdistan region drew up a first draft ‘block map’ of the region. This comprises 48 blocks with one surface structure per block. From 2005 onwards, many international companies started to invest and explore acreage in Kurdistan. It is clear that hydrocarbon exploration in Kurdistan only started relatively recently. Consequently, the area suffers from a lack of an adequate geological database. Geological understanding of the area remains basic especially in the areas of tectonic development, basin analysis and bio- and sequence stratigraphy. Despite some seismic and well-log data acquired by recently involved oil companies, confusions in the interpretation of stratigraphy between different companies are clearly evident. In the current thesis, there is an attempt to answer a small part of the large number of questions about geology of the area. Results presented here should motivate future studies.

## 1.5 Layout of the thesis

This thesis is composed of nine chapters. The introduction is part of this chapter that covers an overview to the problem proposed along with an outline of the thesis aims, methodology and locations. A brief outline of the subsequent chapters is provided in the following:

Chapter 2 reviews the tectonic and basin development of the Arabian Plate (AP) and the study area. The chapter focuses on the different phases of the Neotethyan Ocean opening from Late Permian to the Late Jurassic which was accompanied by the passive margin development along the NE margin of the AP. Also, different Jurassic formations of study area will be described and correlated with their equivalents in the AP.

Chapter 3, 4 and 5 present descriptions and environmental interpretations of the Bathonian–Early Callovian Sargelu Formation, Oxfordian Early Kimmeridgian Naokelekan Formation and Middle–Late Kimmeridgian Barsarin Formation respectively. Chapter 3 explains the high abundance of *Posidonia* and radiolarian fossils with their connection to Jurassic monsoonal upwelling current. Furthermore, mutual relationship between different structures within carbonate and bedded chert rocks indicates the presence of re-sedimentation. Chapter 4 presents an in–depth discussion on how deep-sea microbial stromatolite overgrowths on ammonite shells occurred as well as how bioturbated mottled limestone occurred. Also, the argument is extended to estimate the origin of the organic-rich argillaceous limestone deposition. Chapter 5 will provide a broad overview of the sabkha peritidal facies. Many shallowing-upward cycles suggest facies changes upward from subtidal to intertidal and supratidal facies with periodic subaerial exposure at the top.

Chapter 6 presents sequence stratigraphy of the Middle–Late Jurassic Sargelu, Naokelekan and Barsarin formations. The developments of the depositional sequences are discussed in terms of the eustatic sea-level changes, tectonic subsidence and uplift, and type of sedimentation. An attempt is made to reveal the problematic boundary between Early–Middle Kimmeridgian that shows an abrupt basinward shift of facies from deep marine to sabkha.

Chapter 7 focuses on analysis of a condensed interval on the Neotethyan margin. Relationships between the microbial overgrowth with ammonitico rosso facies and development of the condensed interval on the bathymetric high are presented and discussed.

Chapter 8 involves an overall discussion of the sedimentology and stratigraphy of the Middle to Upper Jurassic succession of Northern Iraq. Previous chapters will be discussed in a larger correlation to create a comprehensive and clear view of the research results and problems.

Chapter 9: In this chapter, the conclusions of the studied chapters are summarized and recommendations for future studies are given.

## **1.6 Localities**

Seven different outcrops were chosen in the northern Iraq, Kurdistan Region as representative sections for the study of sedimentology and stratigraphy of the Middle–Late Jurassic System (Figure 1.1). The Middle–Upper Jurassic strata are represented by Sargelu, Naokelekan, and Barsarin Formations, exposed as isolated patches in the deeply eroded cores of the highly folded anticlines, thrust, and imbricated zones along transects totalling approximately 450 km in length, from Chnaran to Banik villages (Figure 1.1, attached appendix). The locations were chosen in the Kurdistan Region of northern Iraq for the present study

### **1.6.1 Chnaran Location (567924, E3934178)**

At the Chnaran section, the Middle–Upper Jurassic strata crop out in the Waraska Dom anticline structure, which tectonically belongs to the thrust zone. The anticline shows strong structural deformation, and much caution is needed for logging due to the probability of repetition by faulting or folding. The Jurassic formations crop out about 2 kilometres northeast of the Chnaran village, and Barzinja Town, Sulaymaniya Governorate.

### **1.6.2 Sargelu Location (514783, E3969364)**

The Jurassic section crops out in the core of the Surdash anticline structure at the Sargelu Formation type location. Tectonically it belongs to the high folded zone (Buday, 1980). The Jurassic succession crops out approximately 30 metres to the west of Sargelu village, Dokan District Sulaymaniya Governorate.

### **1.6.3 Hanjera Location (486759. E 4015920)**

Jurassic strata in the Hanjera location crop out in the core of the Rania anticlinal structure. Tectonically Hanjera location belongs to the High Folded zone. In this section,

Naokelekan and Sargelu strata include the lowest amount of organic matter in comparison with other locations. The location is 70 metres west of the Hanjera village at Dopî Qabran.

#### **1.6.4 Nora Location (478324, E4022850)**

Jurassic rocks in the Nora location crop out in the core of the Rania anticlinal structure, in Shelana valley, Rania District Sulaymaniya Governorate. Tectonically this area belongs to the High Folded zone. It is about 18 km north west of the Hanjera section. Despite the relatively short distance between them, they show some interesting differences, where this section is rich in organic matter intervals by comparison with Hanjera section. The upper part of the Naokelekan Formation at Kani Rash (Nora) section was covered by recent soil; for this reason, a supplementary section was taken in Warty village.

#### **1.6.5 Barsarin Location (469705, E4053123)**

Jurassic strata in Barsarin village crop out in a thrust part of the Zozik anticlinal structure that tectonically belongs to the thrust zone. The Naokelekan and Barsarin Formations crop out about 40 metres upstream from the footbridge, whereas the upper part of the Sargelu Formation crops out about 10 metres downstream from the footbridge.

#### **1.6.6 Gara Location (368619, E4095981)**

Jurassic formations in the Gara location crop out in the northern limb of Gara anticline structure that tectonically belongs to the High Folded Zone, Sulaymaniya–Zakho Subzone. The study section is located about 200 metres west of the new Gweze village.

#### **1.6.7 Banik Location (319657, E4121871)**

The studied section in Banik village crops out in the southern limb of the Banik anticlinal structure, and it tectonically belongs to the northern Ora thrust zone. The Jurassic strata are located at about 40 metres west of Banik village. The Banik location represents the most northwesterly section studied, 23 km north east of Zakho District.

## *CHAPTER TWO*

### *2 A REVIEW OF TECTONIC AND BASIN DEVELOPMENT ON THE ARABIAN PLATE AND IN THE STUDY AREA*

## 2.1 Aims

- Present the detailed palaeogeographic development and regional geology of the Triassic–Jurassic in the Arabian Plate (AP), with emphasis on the Kurdistan Region of Iraq.
- Demonstrate the tectonic history of the Triassic–Jurassic strata in the area, and discuss the tectonic development in the Zagros Mountains and Iraq.
- Describe the different phases of the Neotethyan Ocean opening that occurred from Late Permian to the Late Jurassic and to show evidence for the Middle Triassic–Jurassic rifting which followed by formation of the passive margins along the NE margin of the AP with subsequent intrashelf basin development.

## 2.2 Tectono–physiographic subdivisions of Iraq

About 95 percent of the Iraqi territory belongs to the northern part of the Arabian platform, whereas the remaining terrain consists of the thrust Sanandaj–Serjan Zone of the Eurasian plate (Fouad, 2015). Iraq is divided into two main tectonic zones: Stable Shelf (Inner Platform) and Unstable Shelf (Outer Platform) used by the Geological Survey of Iraq (GSI) in referring to tectonic subdivisions (Figures 2.2 and 2.3) (Bellen et al., 1959; Buday, 1980; Jassim and Goff, 2006; Aqrawi et al., 2010).

A. Stable Shelf (Inner Platform): it occupies the Western Desert and the Zagros Mountains foredeep of Iraq (Figure 2.1). This platform is usually non-or slightly folded by the effect of the Late Cretaceous–Tertiary Arabian Plate subduction. The Stable Shelf was subdivided into two zones: Mesopotamian Foredeep and Western Zones (Figures 2.2 and 2.3).

B. Unstable Shelf (Outer Platform): this zone is usually located in the north/northeast of Iraq, where the Kurdistan Region and the study area (Figure 2.1). As a part of the northern AP, the Unstable Zone of Iraq is located mainly on the northeastern plate margin. The Unstable Shelf, which is also called the Zagros Fold-Thrust Belt (ZFTB), developed due to collision and convergence between the northeastern part of the AP and the Central Iran/Eurasia Plate (Figure 2.4). There has been southwest directed obduction of ophiolitic blocks that were derived from the Neo-Tethyan oceanic crust as a result of the collision and continued convergence of AP and Iran/Eurasian (Koyi, 1988; Fouad, 2010; Karim et al., 2011; Navabpour et al., 2011; Fouad, 2015).

Based on the intensity of the structural deformation, the Unstable Shelf has been subdivided into four zones, which are oriented from northeast to southwest: Suture Zone, Imbricated Zone, High Folded Zone, and Low Folded Zone. The study area, which forms a part of the North Western Zagros convergence, was subjected to intense tectonic events.

ZFTB can be defined as the deformed part of the Unstable Zone which formed from the former AP passive margin. The belt includes thick folded and faulted successions of Palaeozoic–Cenozoic sediments. These tectonic zones in Iraq are commonly aligned on a northwest-southeast trend, which appears subparallel to the palaeo-AP margin. These trends may be influenced by the deep-seated tectonic lineaments that were inherited from previous extensional phases that reactivated the Caledonian and Hercynian faults (Jassim and Goff, 2006; Beydoun, 1991). A knowledge of the structural type of the Zagros Fold-Thrust Belt is crucial for understanding the trap style which can help in predicting the presence of hydrocarbons in exploitation programs. The study area is located in the Unstable Zones, and the following section will describe the structure, stratigraphy and history of this zone in more detail.

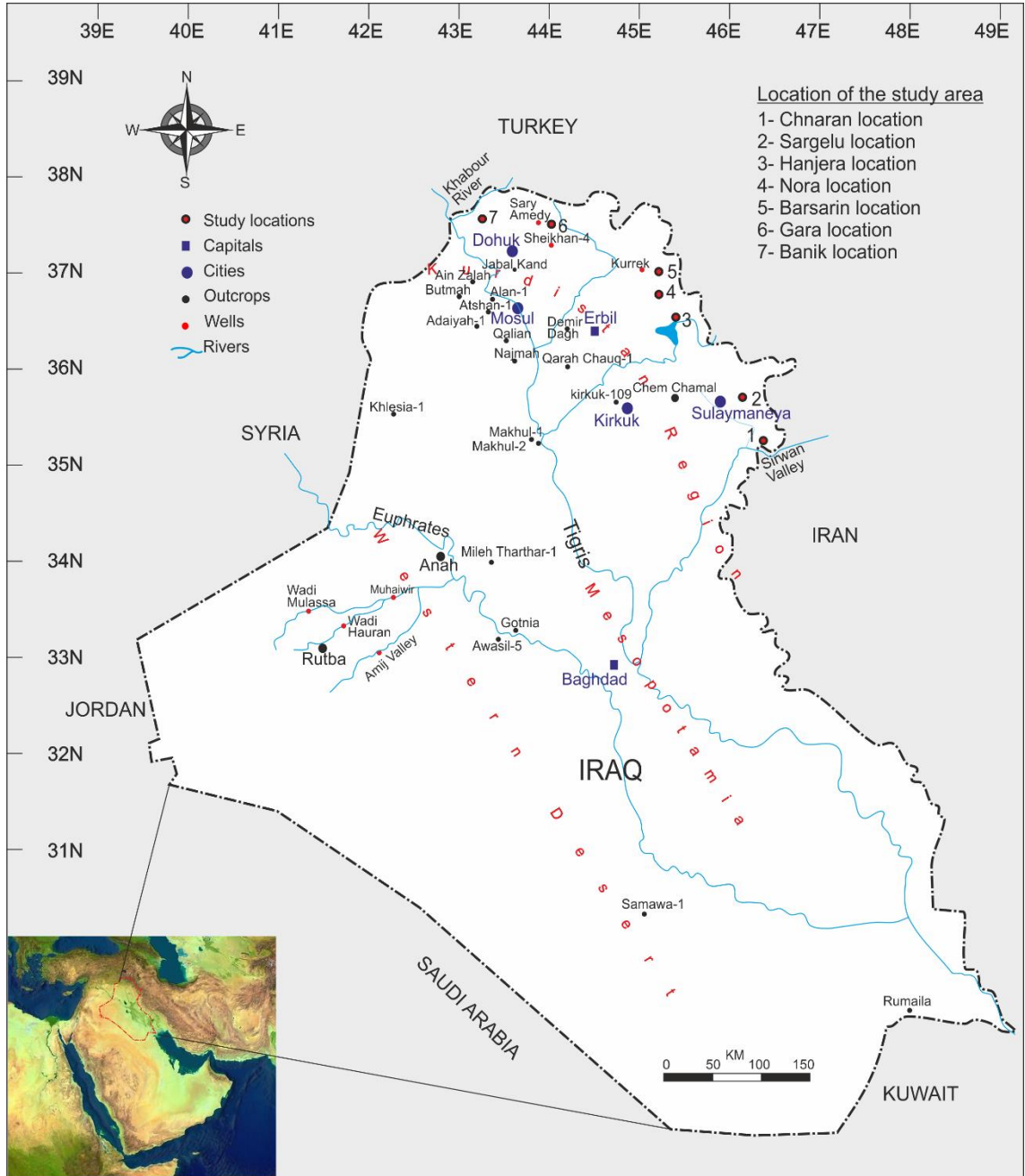


Figure 2.1: Geographic map of Iraq with the location of the study sections.

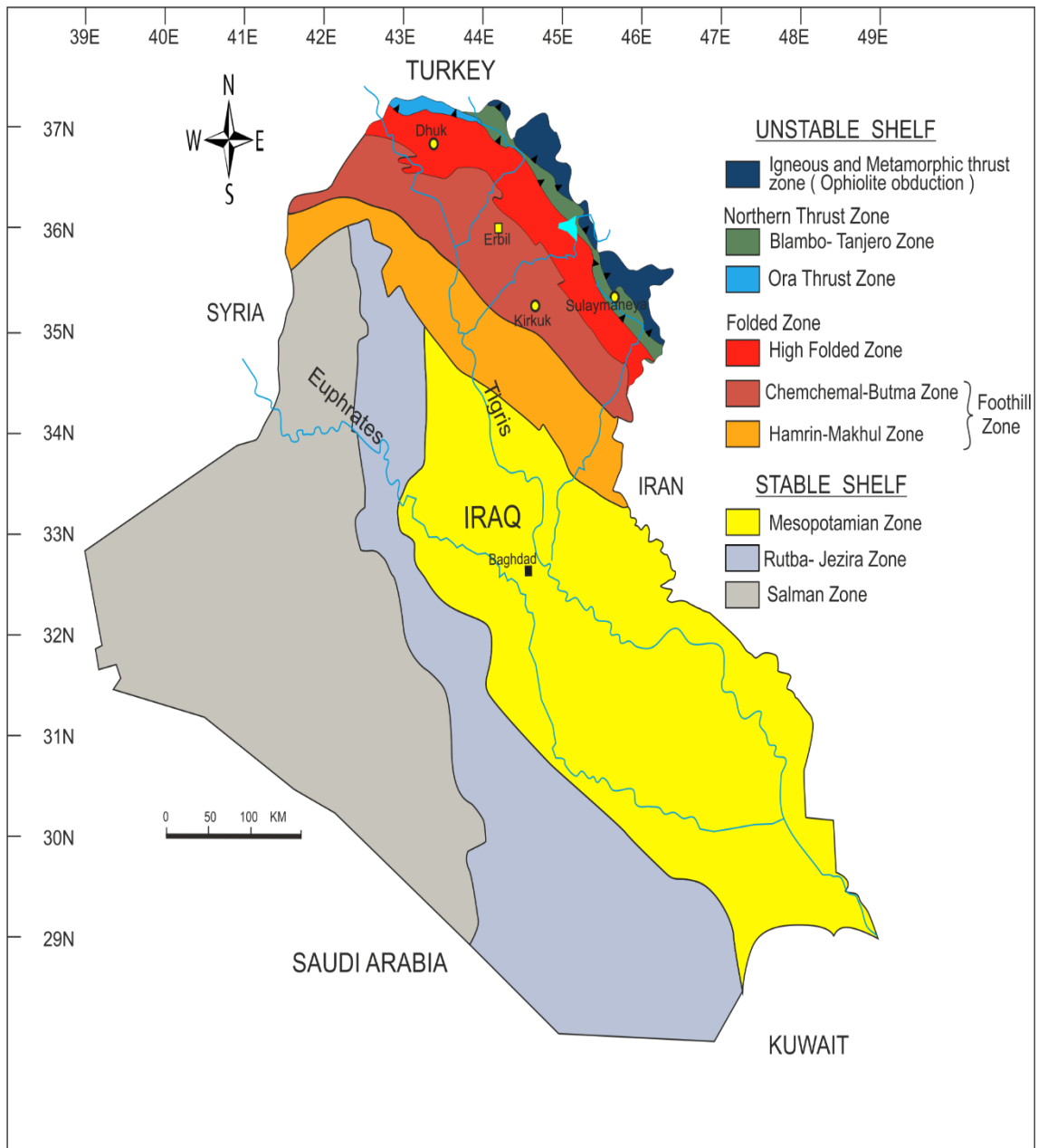


Figure 2.2: Tectonic map of Iraq, modified from Aqrawi et al. (2010).

West		ARABIAN PLATE										East
STABLE SHELF					UNSTABLE SHELF							
Non-Folded		Mesopotamian Zone			Folded Zone				Northern Imbricated and Thrust Zone			
Western Zones					Foothill Zone	High Folded Zone		Imbricated Zone	Zagros Suture Zone			
Salman Zone	Rutba- Jezira Zone	Zubair Subzone	Euphrates Subzone	Tigirs Subzone	Hamrin-Makhul Subzone	Chemchemal-Butma Subzone	Amedia Shaqlawa Subzone	Qamchuqa -Ranya Subzone	Blambo- Tanjero Subzone	Ora Thrust Subzone	Igneous and Metamorphic Thrust Zone ( Ophiolite obduction )	

Figure 2.3: diagram showing simplified layout of tectonic zones of Iraq, modified from Aqrawi et al. (2010) and Fouad (2015).

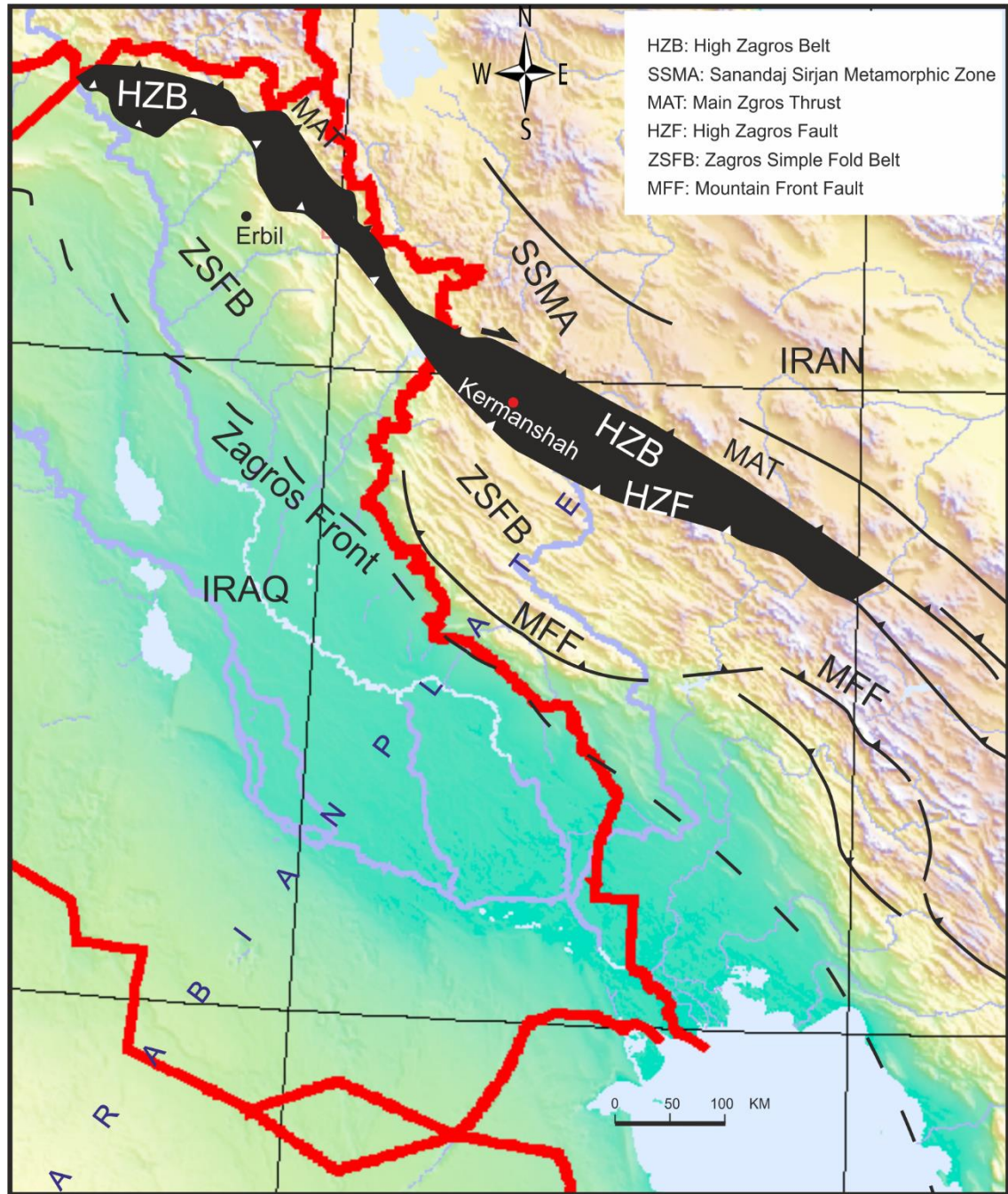


Figure 2.4: Geographic map showing different structural belts of the Zagros Mountains in Iraq and Iran. The black coloured belt (HZB) represents a potential extension of the studied strata, modified from Navabpour et al. (2011).

## **2.3 Unstable Zone**

### **2.3.1 Zagros Suture Zone**

The Zagros suture units comprise a stack of the thrust ophiolite complexes, which mainly consist of a mixture of peridotite, serpentinite, gabbro, basalt, local dykes and sedimentary rocks with radiolarian interbeds. These ophiolite complexes formed within the Neotethyan Ocean, and they were thrust over the AP during two different stages of obduction and collision. The stages occurred in the Late Cretaceous and Mio–Pliocene stages (Jassim and Goff, 2006). The greater area of the thrust sheets are located in Iran, whereas the thrust ophiolite complex of Kurdistan, which is about 5–50 kilometres wide and a few hundred kilometres long, appears as a narrow stripe along the north/north-eastern Iraqi border (Figure 2.2, 2.4, and 2.5). Three major tectonic zones have been identified within Kurdistan, and these are: 1) Qulqula–Khwakurk Zone with deformed radiolarite 2) Penjween–Walash Thrust Zone of metamorphosed volcanics with carbonates and 3) Shalair Zone consisting of thrust sheets of metacarbonates of the Mesozoic and metamorphosed Palaeozoic rocks of the Sanandaj–Sirjan strata. As a consequence of this overthrusting in the study area, the eastern margin of the Jurassic successions has been completely covered by ophiolite complex (Figure 2.5).

### **2.3.2 The imbricated zone**

This zone is located in south/southeast of the Zagros Suture Zone, which is characterised by thrust anticlinal structures and imbricated structures with overriding anticlinal structures. The imbricated zone consists of a narrow belt of highly folded and faulted structures of the Early Palaeozoic and Mesozoic sedimentary rocks. Three sections of this research: Banik, Barsarin and Chnaran, are located within this zone, and they belong to Ora and Balambo–Tanjero Subzones (Figure 2.2 and 2.3).

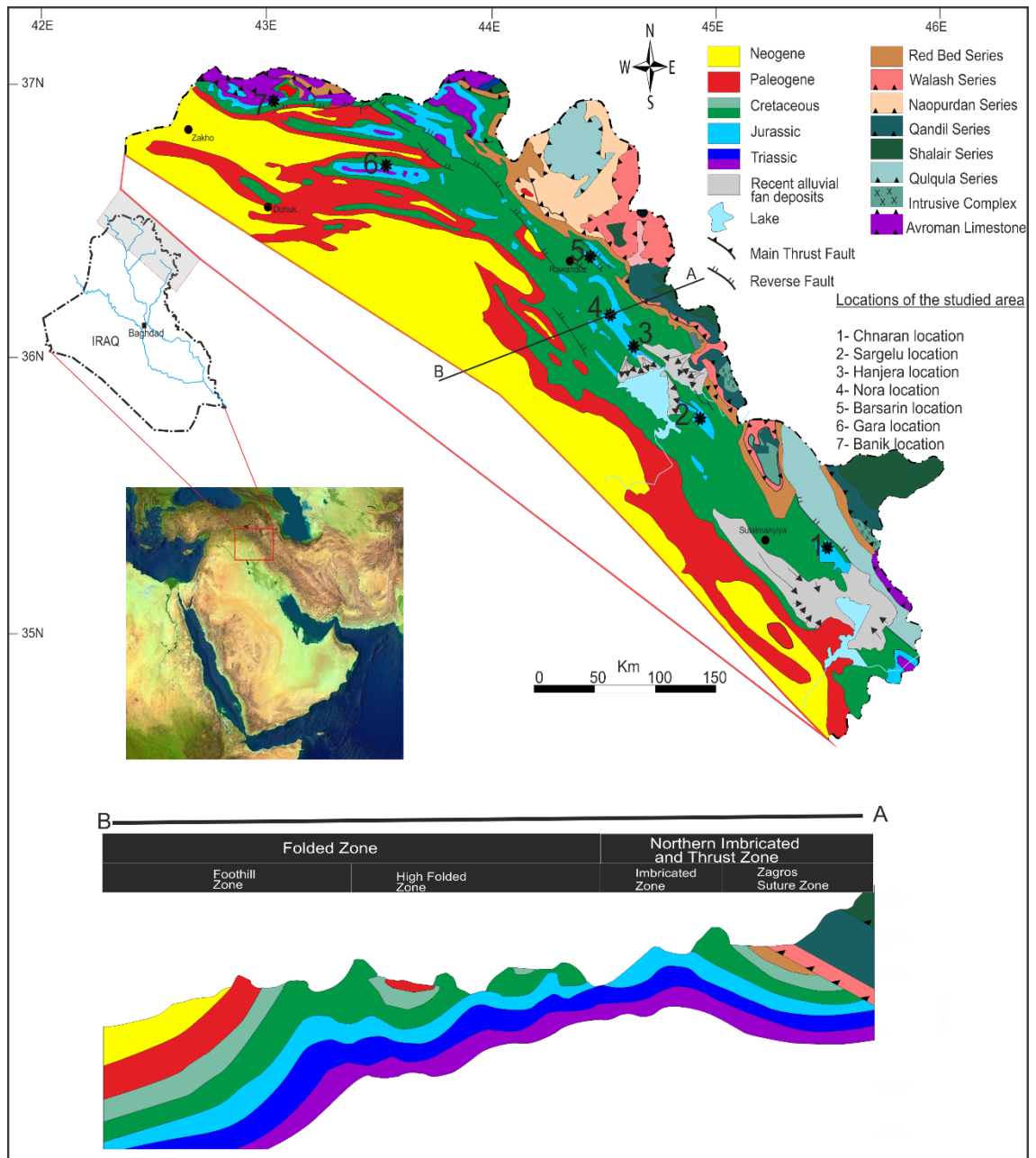


Figure 2.5: Geological map of the study area, after Sissakian (2000).

### 2.3.3 The folded zone

#### A–High Folded Zone

This zone extends for about 450 kilometres in an approximately northwest-southeast direction, from the Sirwan Valley to the Khabour River (Figure 2.1), whereas its width ranges from 25 to 50 kilometres. The High Folded Zone consists of several series of the parallel anticlines, which are separated by narrow synclines. The anticline axes range between 60 and 30 kilometres in length with strike orientation in a general northwest-southeast direction, and are usually asymmetrical in geometry. The dips on the southern and southwestern limb are much steeper than those on the northern or northeastern limb.

The northern boundary of the High Folded Zone is determined by the thrust zone structures, whereas the southern boundary is marked by Foothill or Low Folded Zones (Figures 2.2 and 2.3). The borderline between the High and Low Folded Zones is sharp. According to Aqrabi et al. (2010), the rapid transforms from High to Low Folded Zones of the southern boundary could be related to the reactivated major faults, which occurred in the Late Miocene. Usually massive carbonate strata of the Middle–Late Cretaceous crop out in the cores in the cores of anticlines, but in some cases the anticline cores are deeply eroded down into the Upper Triassic strata. The Sargelu, Hanjera, Nora, and Gara sections are located within this zone.

#### B–The Low Folded (Foothill) Zone

This zone occupies a large area in northern Iraq. It represents the area between the High Folded Zone in the north and the Makhul Hamrin and Sinjar in the South (Figure 2.2). The Foothill Zone is distinguished by high wavelengths with low amplitude structures. Presumably the Neogene strata only crop out in the centres of anticlines. The width of the low Folded Zone varies from 100 to 150 km. The Foothill Zone includes the most important giant oilfields of Iraq such as Kirkuk, Chemchemal and Hamrin oilfields. This zone is subdivided into many subzones (Figures 2.2 and 2.3).

## 2.4 Tectonostratigraphic Megasequences of the AP

Sharland et al. (2001) have studied different stages of the palaeobasin development of the AP from an intra-cratonic setting, through back-arc, to passive margin, and finally to the active margin setting of today. Based on the major unconformities, which occurred during the eustatic fall and tectonic uplift, the AP has been subdivided into eleven

tectonostratigraphic megasequences (TMS) (Figure 2.6). Although, the study sections are found within AP7 which lasted for about 33 My, the current chapter will also focus on the tectonic megasequence of AP6 to understand the palaeobasin development of the region.

The following five points show the major tectonic phases that have brought about the AP (Sharland et al., 2001) (Figure 2.6):

1. The Late Proterozoic terrane accretion 715–610 Ma which resulted in the assembly of the AP.
2. The Late Proterozoic to Late Devonian extensional phase AP1 to AP3: This took place from 610 to 364 Ma, and the depositional setting was characterised by the dominance of siliciclastic rocks in an intra-cratonic basin with a passive margin in low to moderate southern latitudes.
3. The Late Devonian to Middle–Permian phases AP4–AP5: This took place from 364 to 255 Ma. The Late Palaeozoic phase occurred concurrently with the European Hercynian Orogeny. During this time span, the AP was located in a general back–arc setting in southern latitudes 20°–40°. In the Middle–Permian, the Sanandaj–Sirjan, central Iran terrains, Alborz and Lut continental blocks were rifted. Subsequently, the Neotethys Ocean and a new passive continental margin were created along the northeast AP margin.
4. The Middle Permian–Middle Cretaceous phase AP6, AP7, and AP8: it lasted from 255 to 92 Ma. In this phase, the AP was located in an equatorial position. The continuous continental rifting in and around the north and north-eastern plate margins resulted in the development of a further passive margin. Triassic and Jurassic sedimentation was generally characterised by the dominance of carbonate-evaporite deposition, whereas during the Early Cretaceous open-marine clastic-carbonate deposits were more common.
5. The Late Mesozoic–Recent AP9–AP11: the last phase is from 92 Ma to the present day. During this phase, the AP was characterised by a compressive and broadly active margin, starting with the onset of the first ophiolite obduction along the northern and eastern margin. Consequently, a narrow foredeep basin developed on the eastern margins of the AP. During this phase, in addition to the closure of Neotethys, the uplift of the Zagros and Oman Mountains took place, with rifting and opening of the Red Sea and the Gulf of Aden.

### 2.4.1 Pre-Jurassic

Palaeozoic strata are exposed in some deeply eroded and thrust folds in the far north of the study area, close to the Turkish frontier. The oldest recorded exposure is from the Ordovician succession, which is represented by the Khabour Quartzite Formation. The Ordovician succession is overlain by the shale-rich Late Devonian Kaista and Ora Formations (Bellen et al., 1959; Omer, 2012). The infra-Cambrian to Cambrian Hormuz salt intrusions with dome structures are common in southern Zagros. At least nine diapiric provinces have been distinguished in Iran (Arian and Noroozpour, 2015; Abdolizadeh et al. 2016). Though the direction, dimensions, positions and trends of pre-Ordovician basins in the study area are unknown, no evidence was recorded for the presence of the Hormuz Salt beneath the Zagros in the Kurdistan Region (Fouad, 2014).

### 2.4.2 Extension and passive subsidence associated with the opening of the Neotethys Ocean, the Early Permian–Early Triassic rifting

Early–Middle Permian rifting is interpreted to have taken place along the northeastern margin of the AP. The rifting started with continental separation of the Sanandaj–Sirjan terrain and Central Iran (Figure 2.7). During this interval, the AP commonly occupied a 40°S–20°S position (Sharland et al., 2001). In the same period, Iraq was gently uplifted as a landmass in the central part of the AP, and was relatively unaffected by the Early–Middle Permian rifting. Due to the absence of the Early–Middle Permian sedimentary successions over large areas in the AP, there is little recorded direct evidence for Middle–Permian rifting in the poorly dated continental clastics. This hiatus is the evidence for the boundary between AP5 and AP6.

Farther northwards, drifting of fragmented blocks occurred in the Late Permian–Early Triassic period. The Iran–Laurasia continent fragmented from the Arabian–Gondwana supercontinent, and a passive continental margin developed in the north and northeast of the AP (Figures 2.8 and 2.10) (Sharland et al., 2001; Haq and Al-Qahtani, 2005). The Neotethys Ocean started opening and broadening up in the Late Permian time, and the ocean continued to expand progressively into the Early Triassic period (Beydoun, 1991). In Iraq, the Mesopotamian Basin developed, where the eastern flank of the Rutba Uplift determined its western margin (Figure 2.8). The Triassic successions are well-known from many exposures in Kurdistan, Ga'ara Depression in the southwest Iraqi desert, and deep-well sections on the Qalian, Atshan, and Butmah areas (Figure 2.1) (Bellen et al., 1959; Buday, 1980; Jassim and Goff, 2006).

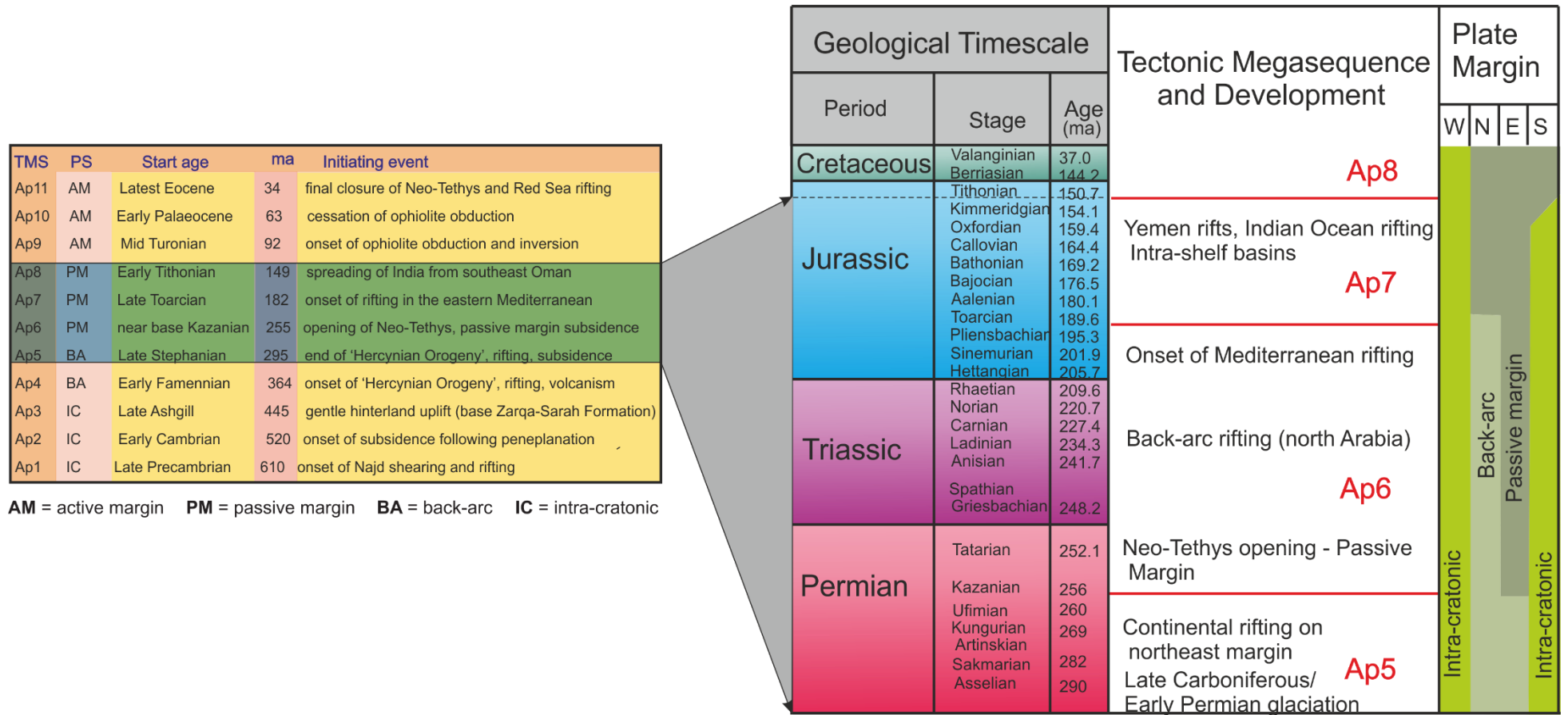


Figure 2.6: diagram showing stratigraphic summary form Permian to Jurassic sediments of the Arabian Plate, tectonostratigraphic megasequences (TMS) development of the Arabian Plate, and the nature of plate margin. Note that each tectonostratigraphic megasequence separated by a major unconformity, modified from Sharland et al. (2001).

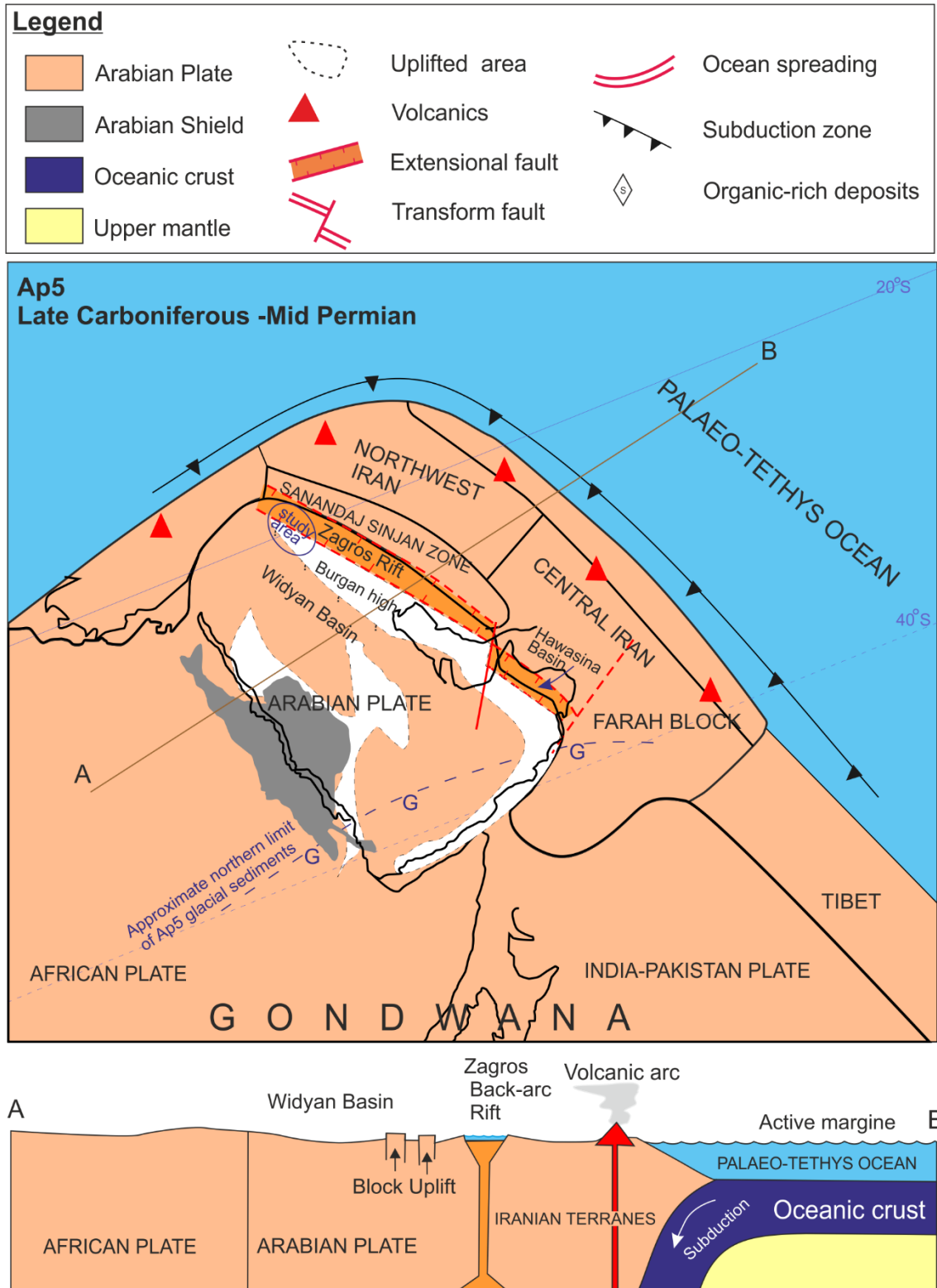


Figure 2.7: Schematic plate reconstruction megasequence AP5. The Hercynian Orogeny resulted in uplift in Late Carboniferous to Late Permian times at the Central Arabian with south and east margins of the Arabian Plate (white areas). Note development the Widyan Basin between the Arabian Shield and the Burgan high and Zagros rift between Sanandaj–Sirjan Zones and Arabian Plate. The A–B line shows the cross-section for megasequence AP5, modified from Sharland et al. (2001).

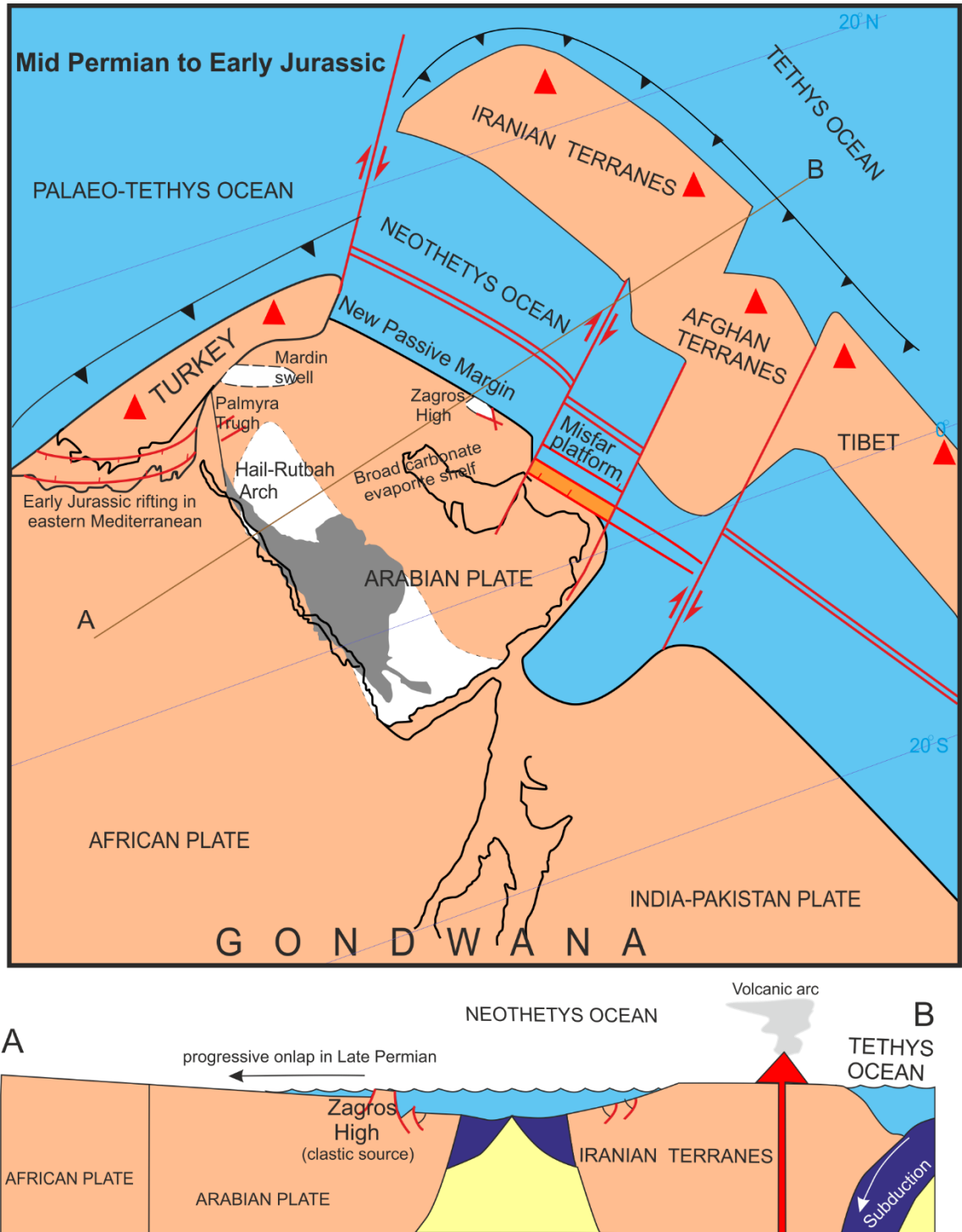


Figure 2.8: Schematic plate reconstruction with its cross-section A–B for the megasequence AP5 during Late Carboniferous–Middle Permian showing the separation between the Iranian and the Arabian blocks. Note creation of the Neotethys Ocean with a new northeast Arabian Plate passive margin modified from Sharland et al. (2001).



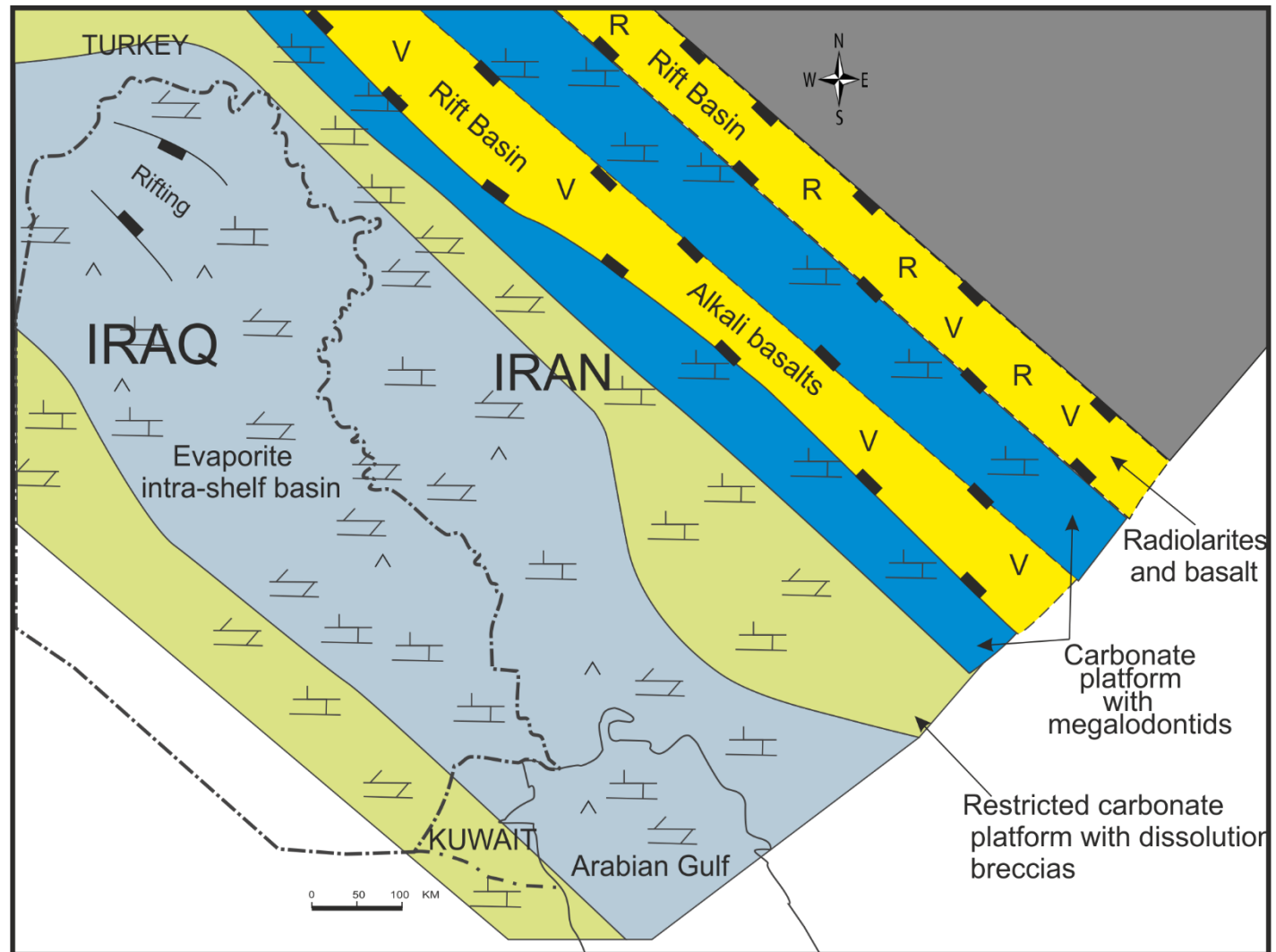


Figure 2.10: Middle-Late Triassic palaeo-tectonic setting of Iraq and west of Iran, modified after Aqrabi et al. (2010).

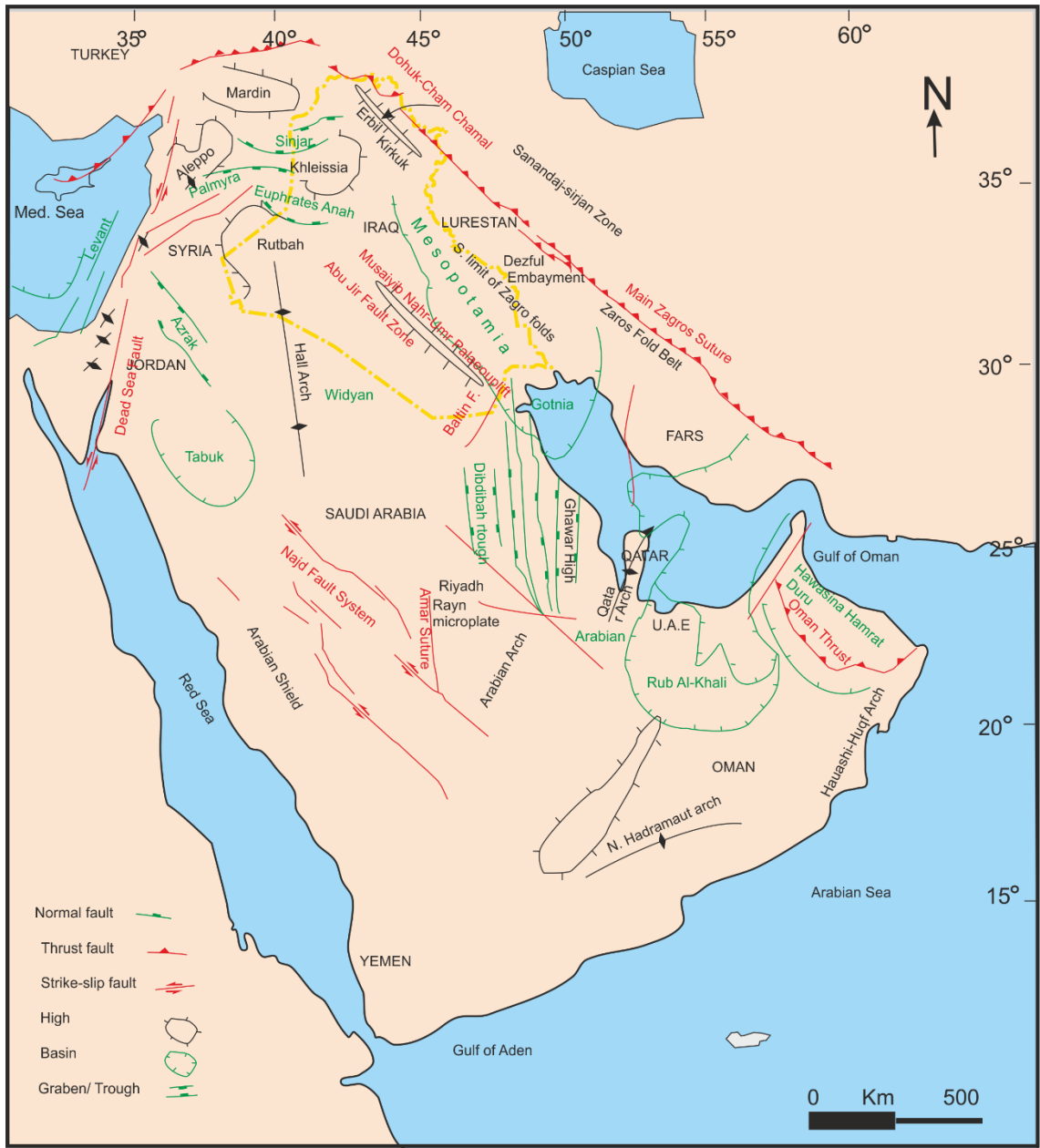


Figure 2.11: Schematic diagram shows the distribution of the main structures of the Arabian Plate, modified after Ziegler (2001).

### 2.4.3 Middle Triassic–Early Jurassic

A second major rifting phase in the Neotethyan Ocean, which led to drowning of the northern and eastern margins of the Arabian Platform, occurred during the Middle–Late Triassic (Beydoun, 1991) (Figure 2.9). A large-scale intra-shelf basin developed as a result of differential subsidence of tilted fault blocks with the fault–bounded troughs in the front eastern edge of the AP and in northern and eastern Iraq as well (Aqrabi et al., 2010; Beydoun, 1991). The troughs are characterised by thick radiolarian succession overlying alkali basalts (Figure 2.10) (De Wever, 1989; Fontaine, 1989; Searle, 2007; Aqrabi et al., 2010). Furthermore, Fontaine (1989) studied the renewed extension evolution of the Oman. Similarly to the northern margin of the AP, it has been found that the rifting of the southern Neotethyan passive continental margin led to the development of many faulted troughs, and basins accompanied by a significant radiolarian deposition with magmatic activity.

During the Late Triassic–Jurassic period, the AP was an interior platform located in an equatorial position. A drop in eustatic sea-level during the Late Triassic–Early Jurassic is well-recognized (Aqrabi, 2010), and an unconformity at this time appears to be a regional event which is recorded in all sections around the AP (Haq and Al-Qahtani, 2005). The Upper Triassic facies show that most of Arabia was an exposed continent. The Rhaetian–Hettangian strata are commonly absent over much of the AP, and this may suggest regional erosion and non-deposition over the area (Figures 2.12 and 2.13). Non-deposition or erosion during this period may correspond with a sea-level lowstand, structural uplift, and the onset of the Mediterranean rifting (Hirsch and Picard, 1988; Al-Husseini, 1997; Beydoun, 1991). In spite of a regional unconformity, in the Kurdistan outcrops, the depositional sequence from the Triassic to Early–Jurassic was not interrupted, where the Early Jurassic Sarki Formation conformably overlies the Late Triassic Baluti Formation (Bellen et al., 1959; Surdashy, 1999; Jassim and Goff, 2006; Beydoun, 1991). Gardosh et al. (2011) studied the sequence stratigraphy of the Mesozoic in the Levant basin, northwest of the AP, in detail. The study suggested a clear unconformity between the Late Triassic and Early Jurassic. The exposure of large areas of the eastern Mediterranean and the AP and their weathering inferred either by the existence of lateritic units, or by existence of ferruginous soil crusts, indicate post-Rhaetian emergence. This unconformity is most likely related to a eustatic fall in sea-level (Beydoun, 1991).

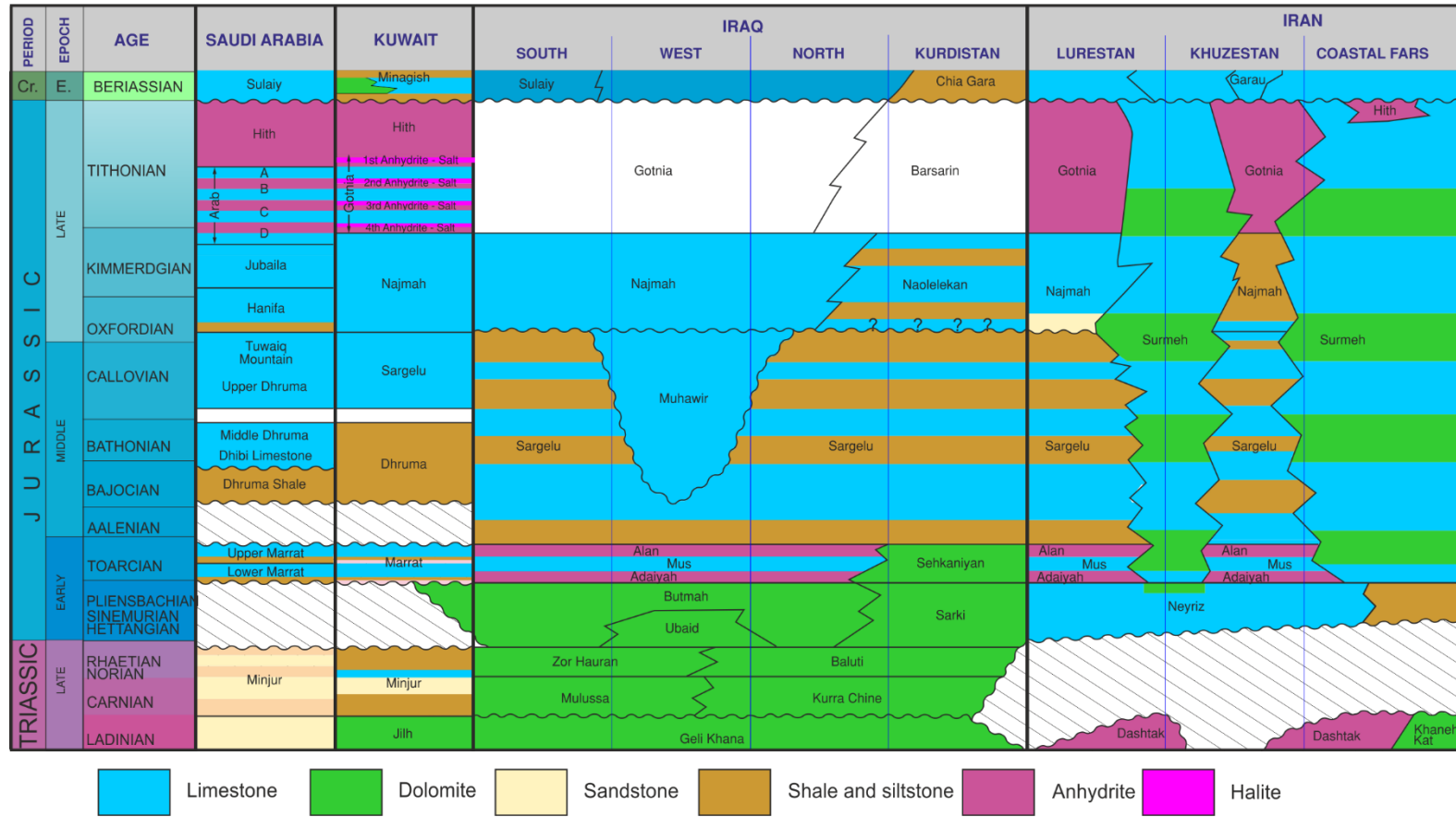


Figure 2.12: Regional lithostratigraphic correlation chart of the Late Triassic and Jurassic for the study area, after Alsharhan (2003).

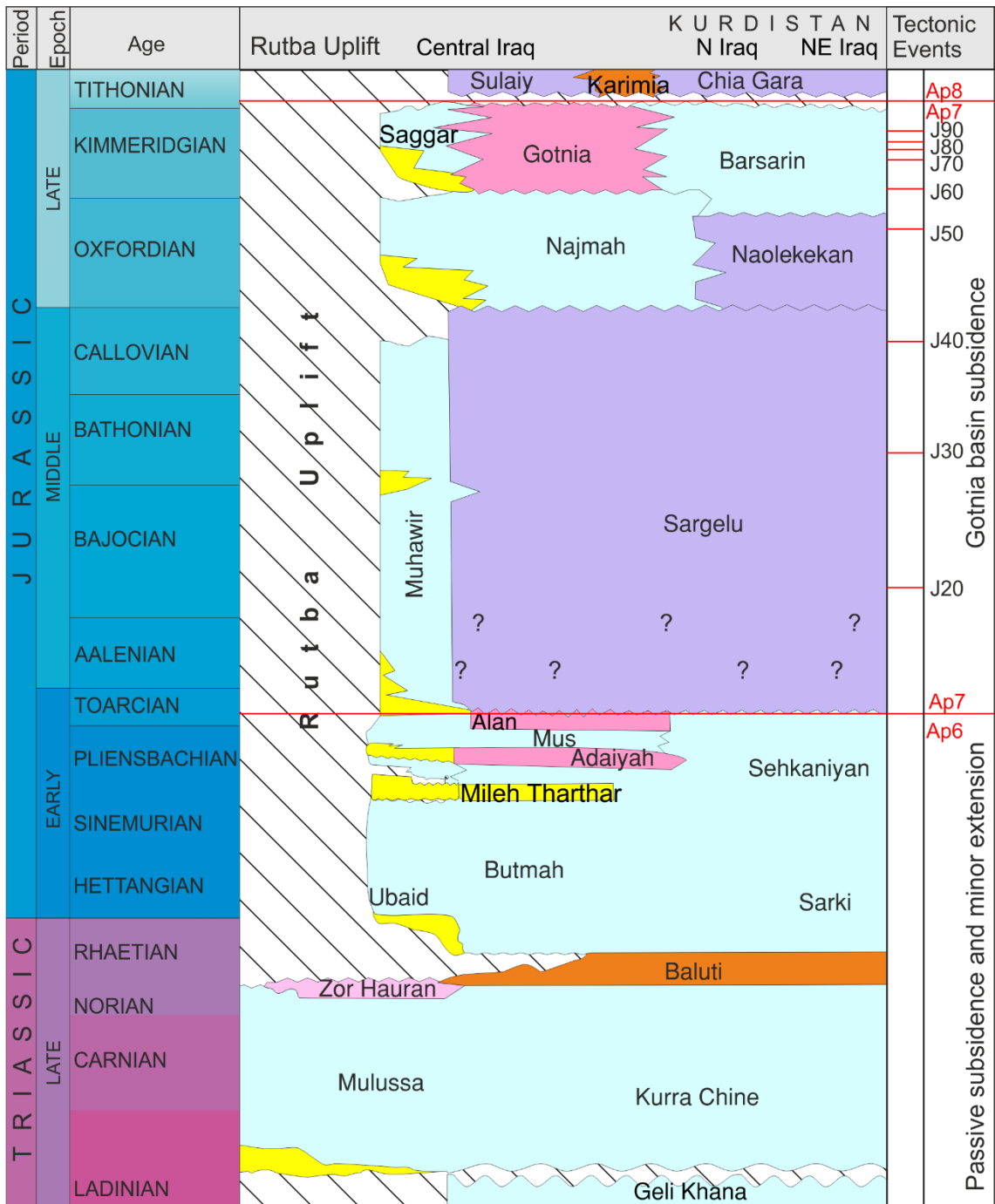


Figure 2.13: Lithostratigraphic correlation chart of the Late Triassic and Jurassic for Iraq, after Jassim and Goff (2006).

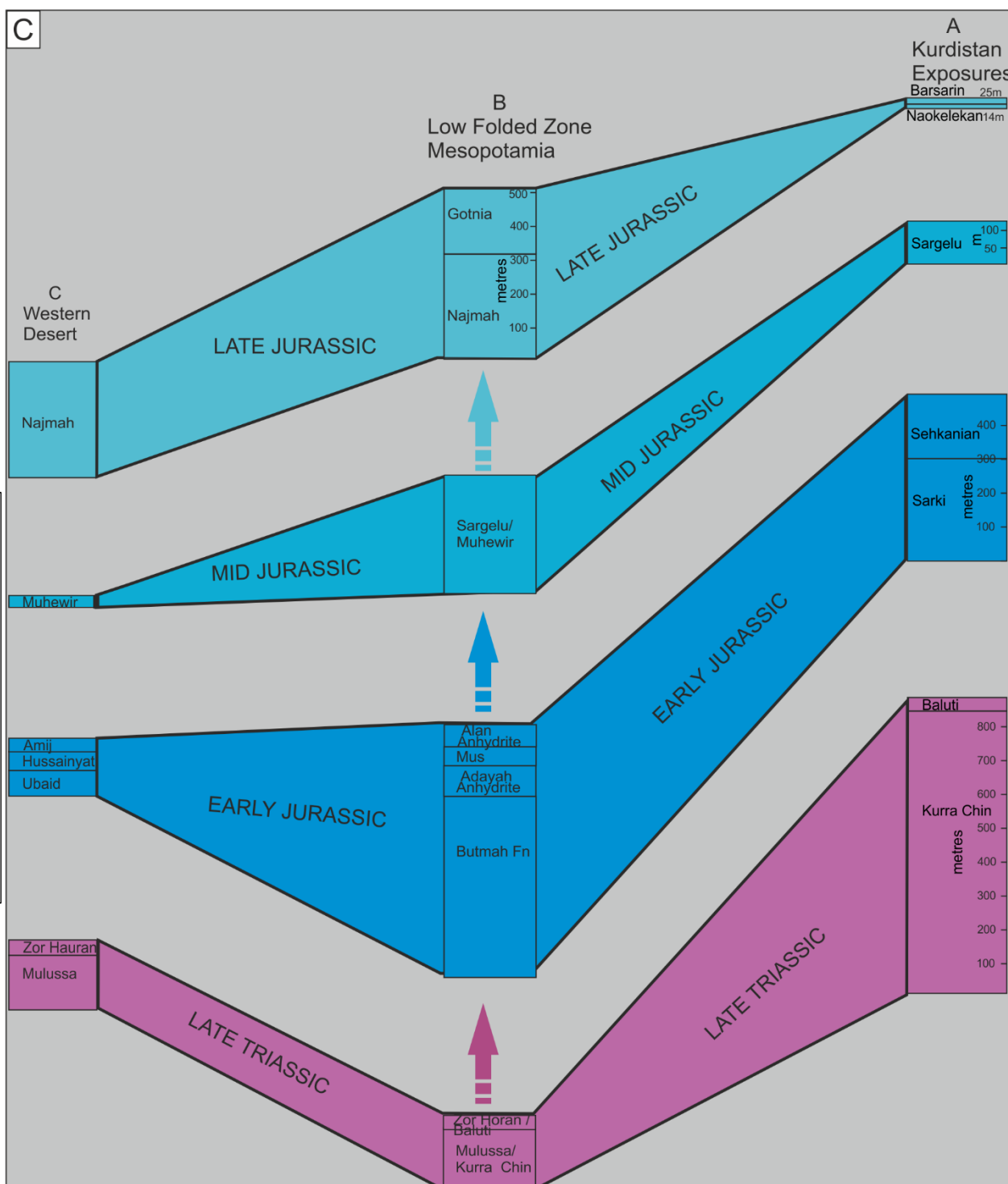
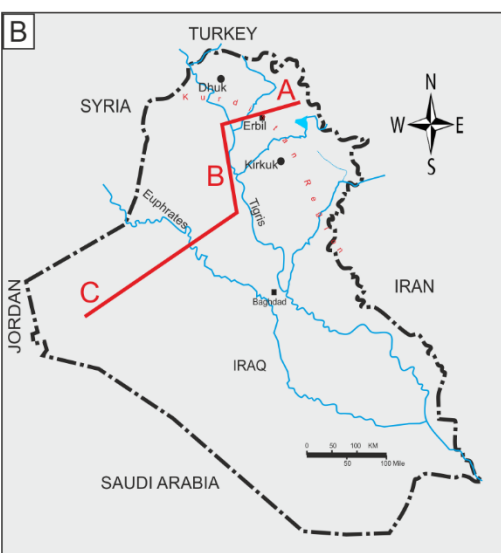
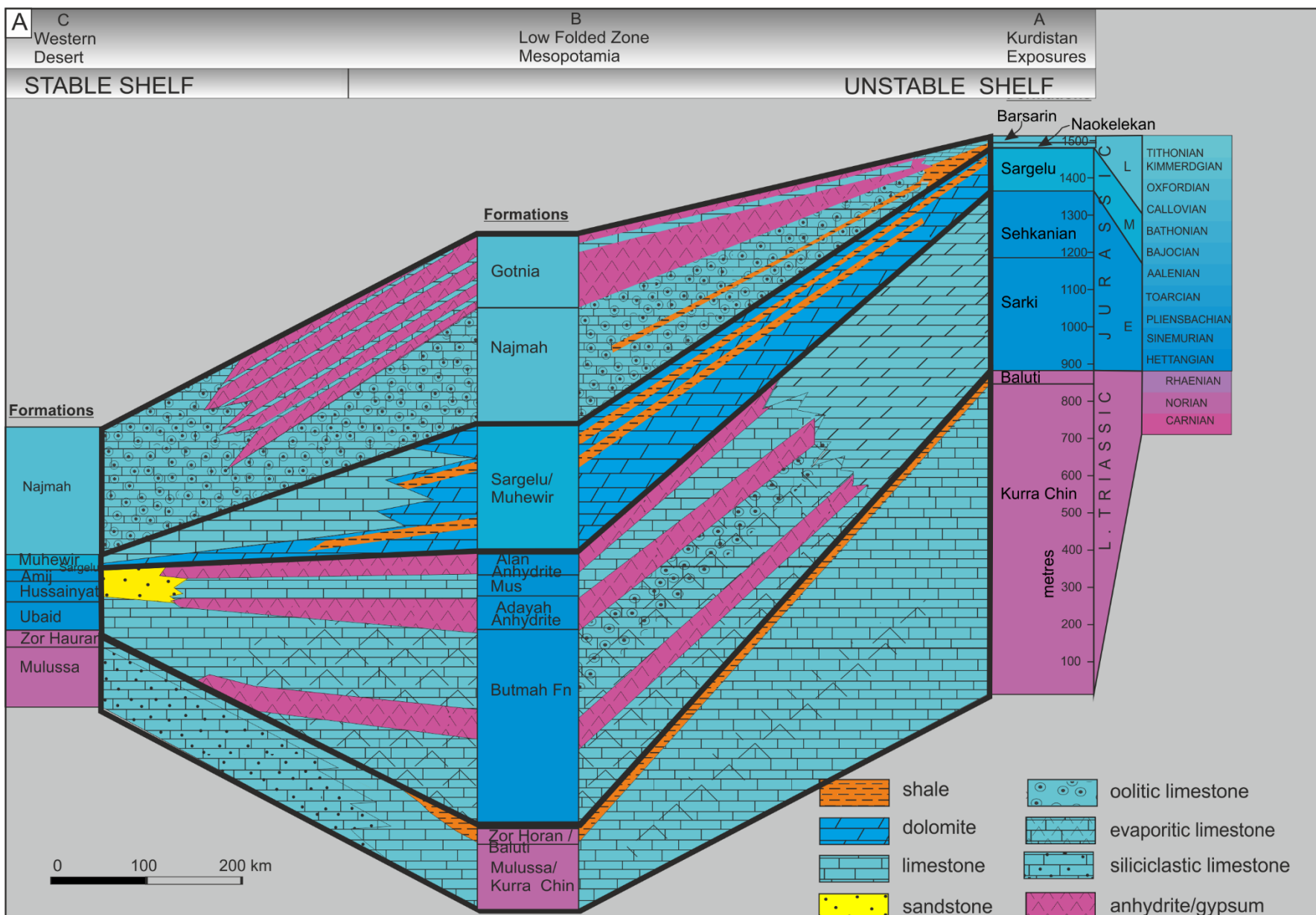


Figure 2.14: A: Diagram showing stratigraphic correlation of the Late Triassic–Jurassic formations across northeast-southwest Iraq. Note East–West dramatic inversion in terms of depositional accommodation through the Jurassic period. Modified from Buday (1980); Jassim et al. (1984); Numan (1997). B: map showing the section location of the diagram A. C: fragmented Jurassic period into different stages to show accommodation development across Iraq.

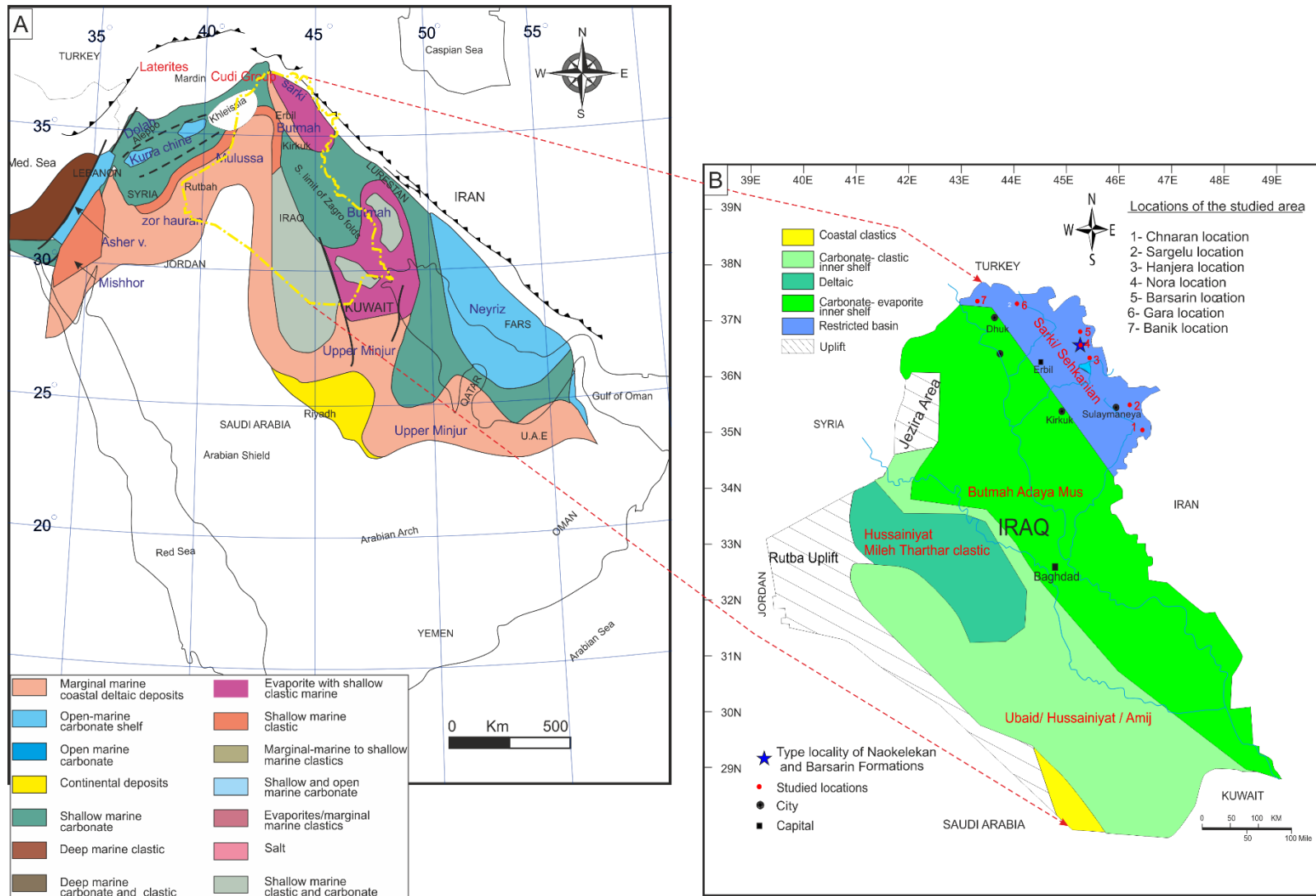


Figure 2.15: A: Facies of the latest Triassic - Early Jurassic in the Arabian Plate, modified from Ziegler (2001). B: The palaeogeography of the Early Jurassic in Iraq, after Jassim and Goff (2006).

#### 2.4.4 Early Jurassic: Sinemurian to Aalenian

Generally, during the Jurassic period, the Neotethys Ocean progressively expanded (Figure 2.16), and rifting accelerated, producing graben-type basins trending north/northwest to southeast in the AP (Sharland et al., 2001; Jassim and Goff, 2006). This time interval is equivalent to mfs J10 to intra-J20 which is located at the top AP6 and the base of the AP7 (Sharland et al., 2001). The base of AP7 is marked by the Early Toarcian unconformity at 182 Ma. This stage is also characterized by the opening of the eastern margin of the Mediterranean to create a new passive margin (Beydoun, 1991). Based on an unconformity, the Early Jurassic Epoch can be subdivided into two intervals; Hettangian–Pliensbachian, and Toarcian–Aalenian ages:

I–Hettangian–Pliensbachian ages; as a result of a long term relative sea-level lowstand during the Hettangian–Pliensbachian ages, a distinct hiatus is recorded in most parts of the AP. This hiatus is not reported in Iraq and the study area, where the Late Triassic Baluti Formation was followed conformably by the Hettangian–Pliensbachian Sarki, Ubaid, and Butmah Formations (Figures 2.12 and 2.13).

II–Toarcian–Aalenian age; the lowermost Jurassic hiatus of the AP was briefly interrupted during the Early–Middle Toarcian age, where a new passive margin developed on the north-northeastern margin of the AP, and a widespread marine transgression covered the Arabian shelf in the Toarcian. The depositional environment varied from a siliciclastic platform in the west to non-deposition and erosion in Southern Arabia, whereas a shallow-marine carbonate platform developed in the north and east of the plate (Al-Husseini, 1997). The Toarcian–Aalenian ages spanned the deposition of the Adaya, Mus and Alan Formations of the Stable zone, and the Sehkaniyan Formation in the unstable zone of Iraq (Figure 2.17). Moreover, in this period, the Qamchuqa Formation in Syria, and the Marrat Formation in Kuwait, United Arab Emirates, and Saudi Arabia, were deposited. However, the Late Triassic–Early Jurassic rocks are absent in Oman. During the latest Toarcian and Aalenian ages, relative sea-level dropped again resulting in another period of non-deposition in most of the Arabian Gulf countries (Al-Husseini, 1997). However, the shallow carbonate and evaporitic Alan and Sehkaniyan Formations pass up in the deep-water Sargelu Formation in Iraq, (Figures 2.12 and 2.13).

The Mardin palaeohigh in south-eastern Turkey continued as a positive feature and created a barrier isolating the shallow open-marine of the northern margin of the AP from the region to the east, which led to the formation of evaporites in parts of the northern

and eastern margins of the Arabian Platform (Figure 2.17). Deep-water sediments accumulated in an intrashelf basin in western Iran and north-eastern Iraq. Post-Jurassic movements led to differential vertical uplift over western Jordan, southeast Turkey, and southern Arabia, followed by the erosion of the older part of the section from many of the palaeohighs. With this erosion and uplift, the Upper Jurassic sediments were removed from much of central Syria and parts of Lebanon.

#### **2.4.5 Early Jurassic Sequence of Iraq**

After exposure in the latest Triassic, a series of transgressive–regressive pulses occurred and in the Early Jurassic period, which is well recorded along the edge of the Rutba Uplift in the Western Desert (Figures 2.15 and 2.17). The Lower Jurassic sequence in Iraq can be divided into three facies, i) fluviomarine siliciclastic shelf to coastal carbonates of the Ubaid, Hussainiyat and Amij Formations in the Western Desert, ii) lagoonal evaporitic–carbonates of the Butmah, Adaiyah, Alan and Mus Formations in Mesopotamia and low folded zones, and iii) the restricted lagoonal with minor evaporites of the Sarki and Sehkaniyan Formations in the High Folded and Balambo–Tanjero zones in Kurdistan. According to Jassim and Goff (2006), the Lower Jurassic sequence is about 200 metres thick in the Western Desert, whereas in Mesopotamia and the High Folded Zones, its thickness is up to 800 metres. The Lower Jurassic strata of Iraq include the following formations (Figure 2.13):

##### **A–Ubaid Formation**

The Ubaid Formation was first described from exposures in Wadi Hauran in the north-eastern Rutba in western Iraq (Bellen et al., 1959) (Figure 2.1). The formation attains a thickness of about 70 metres in the type locality. According to Al-Naqib and Al-Juboury (2014) the formation can be divided into two parts: (i) a lower clastic part, 5–10 metres thick, it comprises yellowish brown to red, pebbly sandstone, and (ii) an upper carbonate part, 50–70 metres thick characterised by an alternation of marl and dolomite with dolomitic limestone. Abundant chert nodules occur in the uppermost part of this member as well.

The formation is assumed to be Late Triassic–Early Jurassic in age (Buday, 1980). The lower siliciclastic unit was deposited in a fluvial environment, whereas the upper carbonates formed in shallow hypersaline peritidal and lagoonal environments (Buday, 1980; Jassim and Goff, 2006; Sissakian and Mohammad, 2007). The lower contact with the underlying Zor Hauran Formation is unconformable. The upper contact with the

Hussainiyat Formation is disconformable. The topmost level of the Ubaid Formation is intensely karstified with dolines that range from 1 to 50 metres (Jassim and Goff, 2006).

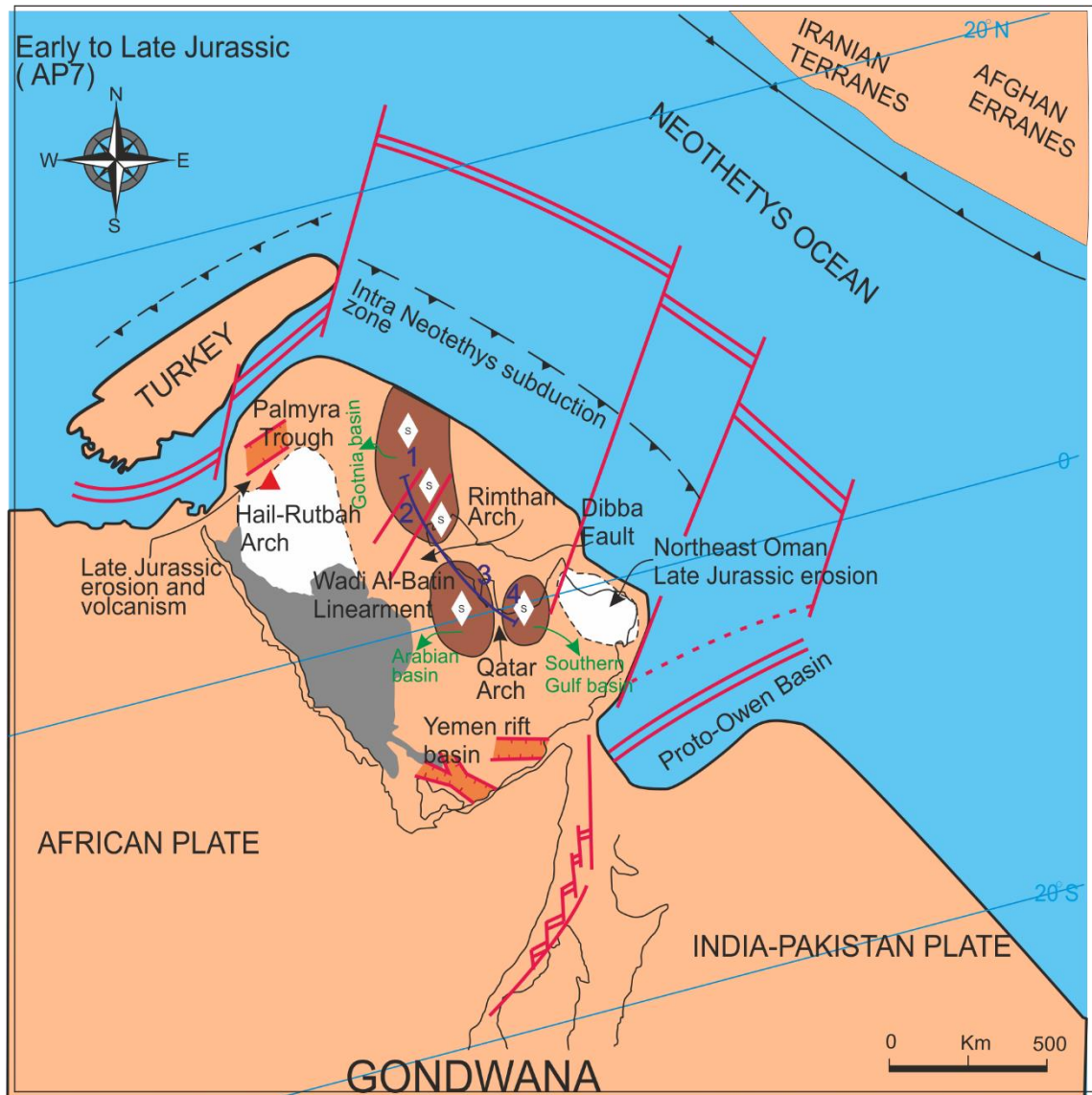


Figure 2.16: Diagram showing reconstruction for megasequence AP8. During the Early-Late Jurassic, a new passive margin developed at the northeastern AP, and the Jurassic rift basins were activated in Palmyra in Syria and southeast Yemen as well. The sequential numbers (1-4) next to the green line show the stages of source rock deposition from Bathonian to Callovian. The structural lineaments such as Dibba fault and Wadi Al-Batin Fault could have controlled the trends of the intrashelf basins, from Sharland et al. (2001).

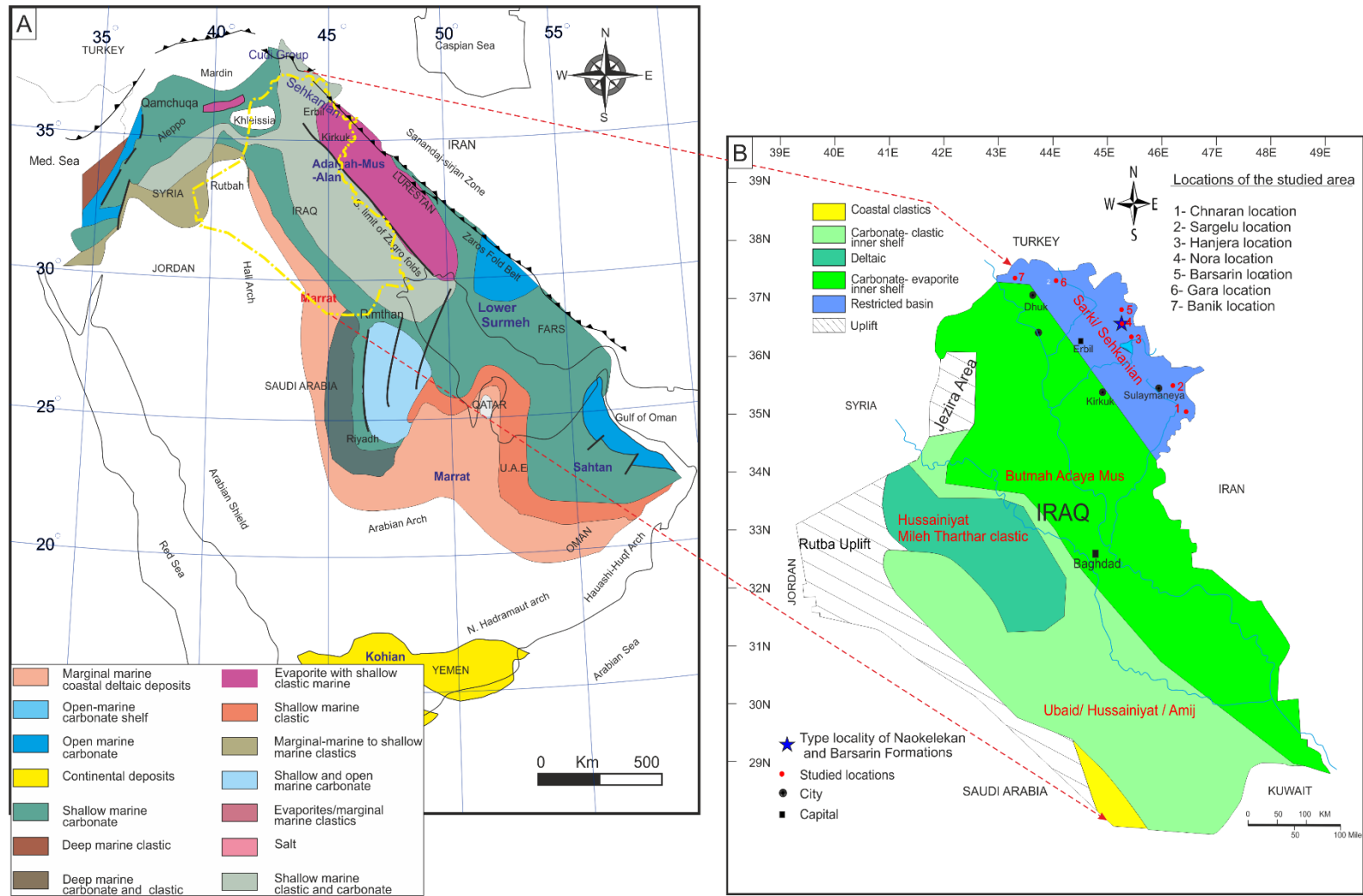


Figure 2.17: A: Facies of the Early Jurassic in the Arabian Plate. In this period, a new passive margin developed due to the eastern Mediterranean opening. Modified from Ziegler (2001). B: Palaeogeography of the Early Jurassic of Iraq, after Jassim and Goff (2006).

#### 2.4.6 Middle Jurassic–Early Tithonian Differential Subsidence and Rifting, AP7

The Middle–Late Jurassic or AP7 is equivalent to mfs intra-J20 to J110 (Figure 2.6 and Figure 2.13) (Sharland et al., 2001). The opening of the Neotethys Ocean continued throughout the Middle–Late Jurassic period (Figure 2.16). Many normal faults developed along the eastern passive margin of the AP. Fault activity results in differential subsidence in different sectors of the basin, which is well-documented in Oman exposures (Pratt and Smewing, 1990; Rabu et al., 1990; Robertson and Searle, 1990; Robertson, 2007). Jassim and Goff (2006) considered that this phase of Oman rifting may have extended farther north along the margin of the AP, separating an outer carbonate ridge from the restricted Gotnia Basin. The Gotnia Basin can be defined as a basin that occupied most parts of the north-east, central and southern Iraq (Figures 2.18 and 2.19). The margin of this basin was perhaps controlled by a system of conjugate northwest-southeast and southwest-northeast trending lineaments (Aqrabi et al., 2010). Similarly, Schettino and Scotese (2002) pointed to the great rifting event, which occurred during the Bajocian–Middle Tithonian in the Mediterranean. It has been suggested that this rifting resulted in the formation of continental fragmentation, which rifted away from the northern margin of Gondwana, and many horsts and grabens formed with about 1000 m of relief. Schettino and Scotese (2002) suggested that the rifting was caused by the tensional forces of the north-eastern subduction of the Tethyan Ocean crust beneath the active margin of Eurasia.

Generally, in the vast area of the AP, the lower boundary of tectonostratigraphic megasequence AP7 is marked by the Latest Toarcian unconformity on the top of the Mus, Marrat and Mulussa Formations (Figures 2.12 and 2.13). However, in Kurdistan exposures, this unconformity is not confirmed, where the Sargelu Formation of Middle Jurassic age lies conformably on the Sehkanian Formation of Lower Jurassic age (Surdashy, 1999). The upper boundary of the AP7 is also marked by the widespread unconformity layer of the Early Tithonian which is underlain by thick evaporite beds of the Gotnia and Hith Formations; however, no evidence for stratigraphic interruption in the Late Jurassic has been confirmed in the study area. Sharland et al. (2001) interpreted that the Early Tithonian unconformity surface and relative sea-level fall occurred as a result of the spreading of India from Oman and the opening of the proto–Owen basin, with structural inversion in the north part of the AP. These events caused great unconformity, where the Aptian to Albian strata unconformably rest on the Middle Jurassic Sargelu Formation in northwestern Iraq. Similarly, a west–east direction across

Oman shows Cretaceous successions unconformably overlying Jurassic strata. In Kirkuk wells and Kurdistan exposures, this stratigraphic break is not observed, which suggests that the stratigraphic break decreases eastwards (Sharland et al., 2001).

#### 2.4.6.1 Bajocian to Bathonian Middle Jurassic

After the Aalenian depositional hiatus, Bajocian–Bathonian carbonates were deposited over most of the AP. This time period is equivalent to mfs J20 to intra-J40 (Sharland et al., 2001) (Figure 2.13). At this point in time, a passive margin was well developed in the north and to the northeast of the AP (Beydoun, 1991). A shallow-water shelf environment usually characterised the west and southern side of the AP, whereas the deeper mixed siliciclastic and carbonate shelf of the Gotnia Basin and Saudi–Arabian Basin developed in the north-northeastern part of the plate (Figure 2.20). Commonly, the Gotnia and Saudi–Arabian Basins were characterised by a widespread open-marine environment. The Gotnia Basin of Iraq and Kuwait was separated from the Saudi Arabian Basin by the Rimthan Arch (Figure 2.20), which was intersected by sets of north-trending Hercynian faults. The Gotnia province basin appears to have been controlled by a north-westerly fault–trend. In this period, the Araej, Izhara and Dhurma Formations were deposited in Qatar, the United Arab Emirates and Saudi Arabia respectively, and the Muhaiwir and Sargelu Formations in Iraq (Figure 2.20). Far to the south of the AP, in the eastern part of the Rub Al-Khali Basin, particularly in Oman, shallow-water limestone of the Middle to Late Jurassic Sahtan Group were deposited, which correspond roughly to the Middle Jurassic palaeoslope and passed off the continental margin into the Al Ayn sub-basin of the Hawasina Basin (Beydoun, 1991) (Figure 2.20).

According to Ziegler (2001) the Middle Jurassic represents a phase of the general sea-level rise. The Neotethys Ocean transgressed westward far on to the Arabian Craton in this period. Coastal and near–shore facies Dhurma (Saudi Arabia, Oman) at the west part of AP pass eastward into shallow-marine shales of Izhara and Araej Qatar and the United Arab Emirates, and then into shallow-marine bioclastic carbonates of the lower Surmeh formation in Iran (Beydoun, 1991).

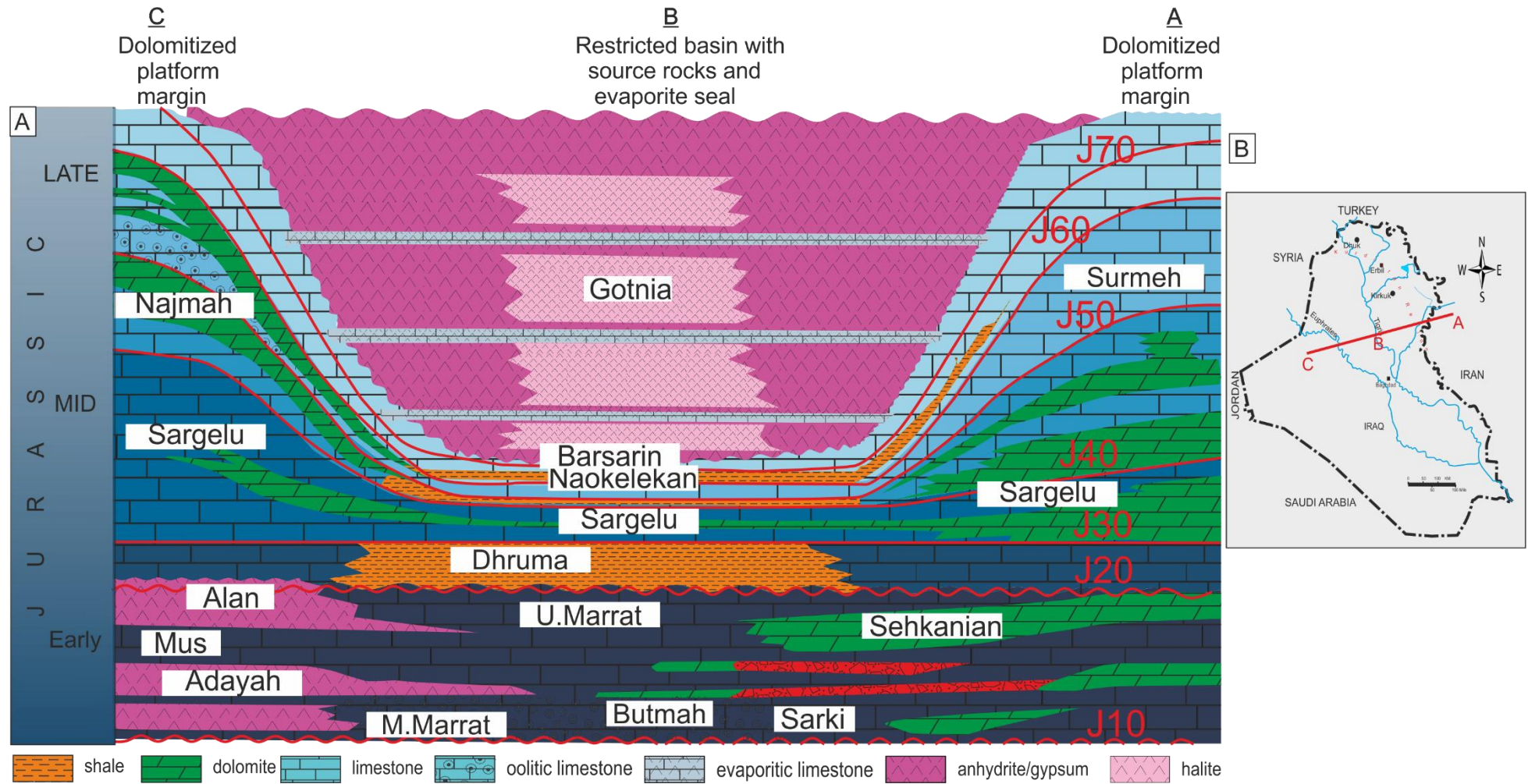
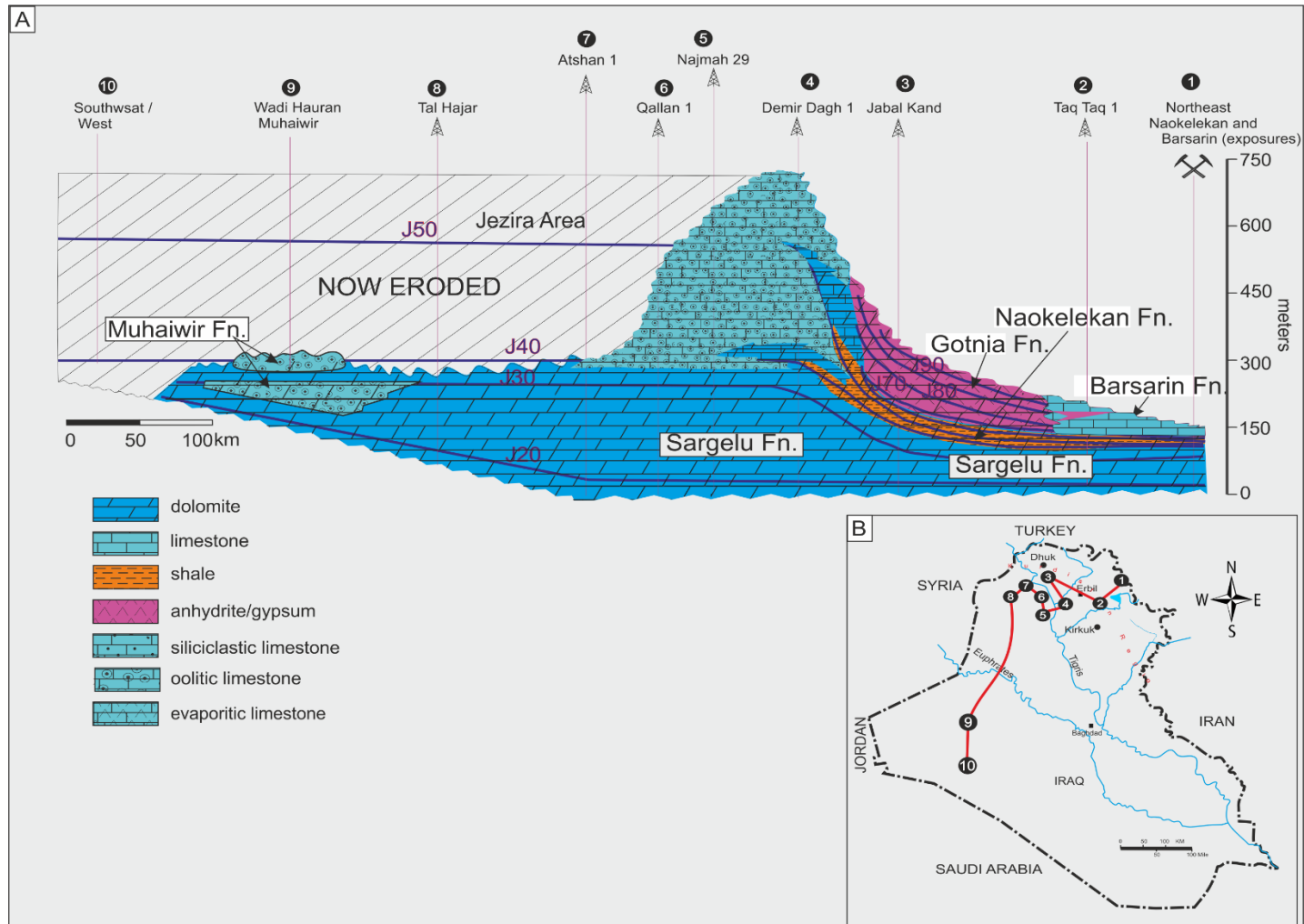


Figure 2.18: Diagram showing depositional evolution of the Jurassic successions with an idealised model for Gotnia Basin fill. Note only the margins of the Gotnia Basin were filled, leaving significant unfilled accommodation space in the sediment-starved centre, modified from Goff (2005).



In the Saudi–Arabian Basin, differential subsidence resulted in the formation of horst and graben in the areas located over the Precambrian basement high at the south-western end of the Central Arabian Arch (Al-Husseini, 1997). In the subsiding areas, shales and deeper-marine carbonates were deposited such as the Middle–Dhurma shales of mfs J20. The Dhurma Formation, which is interrupted by significant unconformities, corresponds to Middle Jurassic sequences. The lower unit or Lower Dhurma Shale of Bajocian age is underlain and overlain by clear unconformities, whereas the Upper Dhurma Formation together with the Tuwaiq Mountain Limestone Formation is interpreted as a single Callovian–Oxfordian sequence (Al-Husseini, 1997).

These intrashelf basins, which are distinguished for their richness in source-rocks, were developed in central Saudi Arabia, Iraq and Kuwait during this period. The source rocks in the different intrashelf basins of AP were not deposited concurrently. The onset of source-rock deposition in Iraq was during the Early Bajocian, which was followed by Middle Callovian in south Iraq and Kuwait, whereas in Saudi Arabia and the United Arab Emirates, it started in the Middle Oxfordian (Figure 2.1).

#### 2.4.6.2 Middle Jurassic of Iraq

##### A–Sargelu Formation

This formation was first described in the core of the Surdash Anticline of the high folded zone, near Sargelu village (Figure 2.1) (Bellen et al., 1959). The total thickness of the Sargelu Formation in the type section is about 115 metres, but the thickness is reduced to 30 metres westward near Banik village (Figure 2.1). The subsurface sections are usually thicker than exposures, for example; the well Samawa-1 (Figure 2.1) is about 450 metres in thickness. The age of the formation is still a subject of controversy, but some biostratigraphic studies indicate a Bajocian–Bathonian age. According to Balaky (2004), and Aqrabi et al. (2010) the basal beds of the formation could be of the Latest Toarcian age. However, as yet, no evidence has proved the existence of Toarcian strata in the study areas. The Sargelu Formation has been considered as the most important organic-rich succession of the Gotnia Basin (Figure 2.16) (Buday, 1980; Hussein et al., 2013; Abdula, 2014; Al-Ameri et al., 2014; Al-Ameri and Al-Nagshbandi, 2014).

Based on lithological and palaeontological evidence, Balaky (2004) divided the Sargelu Formation into three main units in ascending order: (a) Dolomite unit; distinguished by destructive dolomitization, where no fossils or sedimentary structures can be recognized (b) *Posidonia*-bearing limestone unit; characterised by the first appearance of *Posidonia*, generally comprises medium-bedded limestone with few thin interbeds of argillaceous

limestone, and (c) cherty limestone unit; this part is characterised by disrupted and folded strata and consists of medium-bedded, kerogeneous, black-coloured limestone interbedded with thin-bedded cherts and black shale. The formation generally interpreted to be deposited in a basinal euxinic marine environment (Buday, 1980; Aqrabi et al., 2010; Abdula, 2014). However, in the Salman Zone of the Stable Shelf (Figure 2.2), the formation includes a higher proportion of shale and fine-grained sandstone with evidence of shallower and well-aerated water, which have been inferred as tongues of the Muhaiwir Formation.

The lower contact with the Sehkaniyan formation in north and northeastern Iraq is usually gradational and conformable, but in subsurface sections, the boundary, which is characterised by sharp transitional facies, is determined by the last occurrence of evaporite at the top of the Alan Formation. In the Jezira area (Figure 2.20), the formation has been truncated at the Base Cretaceous unconformity. The Sargelu Formation passes laterally into the Amij Bajocian and Muhaiwir Bathonian Formations in the Western Desert. The Sargelu Formation is equivalent to parts of the Cudi Group of southeast Turkey (Figure 2.20) (Altinli, 1966). The formation is also equivalent to the black shale of the uppermost part of the Dolaa Group of northeast and central Syria (Jassim and Goff, 2006). The Dhurma Formation of Saudi Arabia and the lower part of the Surmeh Formation in southeast Iran is age equivalent of the Sargelu Formation (Figure 2.12).

#### B–Muhaiwir Formation

The Muhaiwir Formation was first described in Wadi Hauran in the Western Desert (Figure 2.1). The thickness of the outcrops varies from 12 to 35 metres, whereas in the subsurface sections, the thickness ranges between 110 and 200 metres. The formation is a typical example of the widely transgressive period of the Middle Jurassic on the Stable Shelf zone of Iraq (Jassim and Goff, 2006; Aqrabi et al., 2010). This formation is relatively heterogeneous, and has been divided into three units: (a) the lower 13 metres are characterised by argillaceous sandstone with oolitic limestone, and also some sponge debris, brachiopods and chert nodules, (b) the middle unit consists of 12 metres of interbedded sandstone, marly limestone, coralline limestone, and oolitic limestone, and (c) the upper unit, which is rich with brachiopods, gastropods, bivalves and echinoids, comprises 14 metres of limestone and marly limestone.

The Muhaiwir Formation is Bathonian in age (Jassim and Goff, 2006), and it could be correlated with: the upper part of the Sargelu Formation of Iraq, the lowermost Surmeh Formation of Iran, the upper parts of the Dolaa Group of Syria, and the middle to upper

part of the Dhurma Formation of Saudi Arabia (Figure 2.12, Figure 2.13, and Figure 2.14). This formation has been observed in both outcrop and subsurface sections at the southern side of the Euphrates River in the Stable Shelf Zone of Iraq (Figure 2.1), whereas it is absent on the northern side of the river, most probably because of post Jurassic erosion. Northeast ward from the river, the upper part of the Sargelu Formation usually replaces the Muhaiwir Formation. The Muhaiwir Formation is characterised by wide variation in facies, the result of peritidal, normal salinity, shallow reef and deltaic environments (Buday, 1980; Sissakian and Mohammad, 2007). Al-Naqib and Al-Juboury (2014) pointed to the existence of five incomplete coarsening-upward cycles in both lower and upper units, which may suggest deltaic deposition. However, there is no clear evidence of the deltaic sequence. The lower and upper boundaries of the Muhaiwir Formation with the overlying and underlying Amij and Najmah Formations are unconformable.

#### **2.4.7 Late Middle Jurassic: Callovian to Oxfordian**

This time period is equivalent to mfs J40 to J60 (Beydoun, 1991). During this period, four intra-shelf basins were developed in the AP, and they are the Gotnia, Rub' Al Khali, Ras al Khaima and Central Arabia Basins (Figure 2.21). The Gotnia Basin occupied the northern area of the AP, whereas the others occur in the central and lower parts of Arabian Plate. The distribution of these intra-shelf basin structure appears to have been controlled by rejuvenated N-trending Hercynian tectonic faults; the dimension of the southern Gulf Basin was possibly based on the Dibba fault zone (Beydoun, 1991). Shallow-marine carbonates are interpreted to have been deposited in the AP basins during a period of relative lowstand in sea-level. This period is well-known for organic-rich deposition under anoxic conditions, in which the Hanifa, Naokelekan and Diyab Formations represent significant source rocks in the AP (Buday, 1980; Jassim and Goff, 2006; Aqrabi et al., 2010).

In this time period, differential subsidence occurred across the AP resulting in formation of intra-shelf basins. In Iraq and Kuwait, differential subsidence during Late Callovian–Kimmeridgian time segmented the Gotnia Basin into three sub-basins: (i) Naokelekan basin in the north, (ii) central platform area, and (iii) a smaller Gotnia Basin of south Iraq and Kuwait (Figure 2.22) (Yousif and Nouman, 1997; Sharland, 2001). This period includes the Naokelekan and Najmah Formations in Iraq with the Hanifa, Dhurma, Tuwaiq Mountain Limestone, Upper Araej Formations in the Gulf countries, and the Surmeh dolomite in Iran (Figure 2.12).

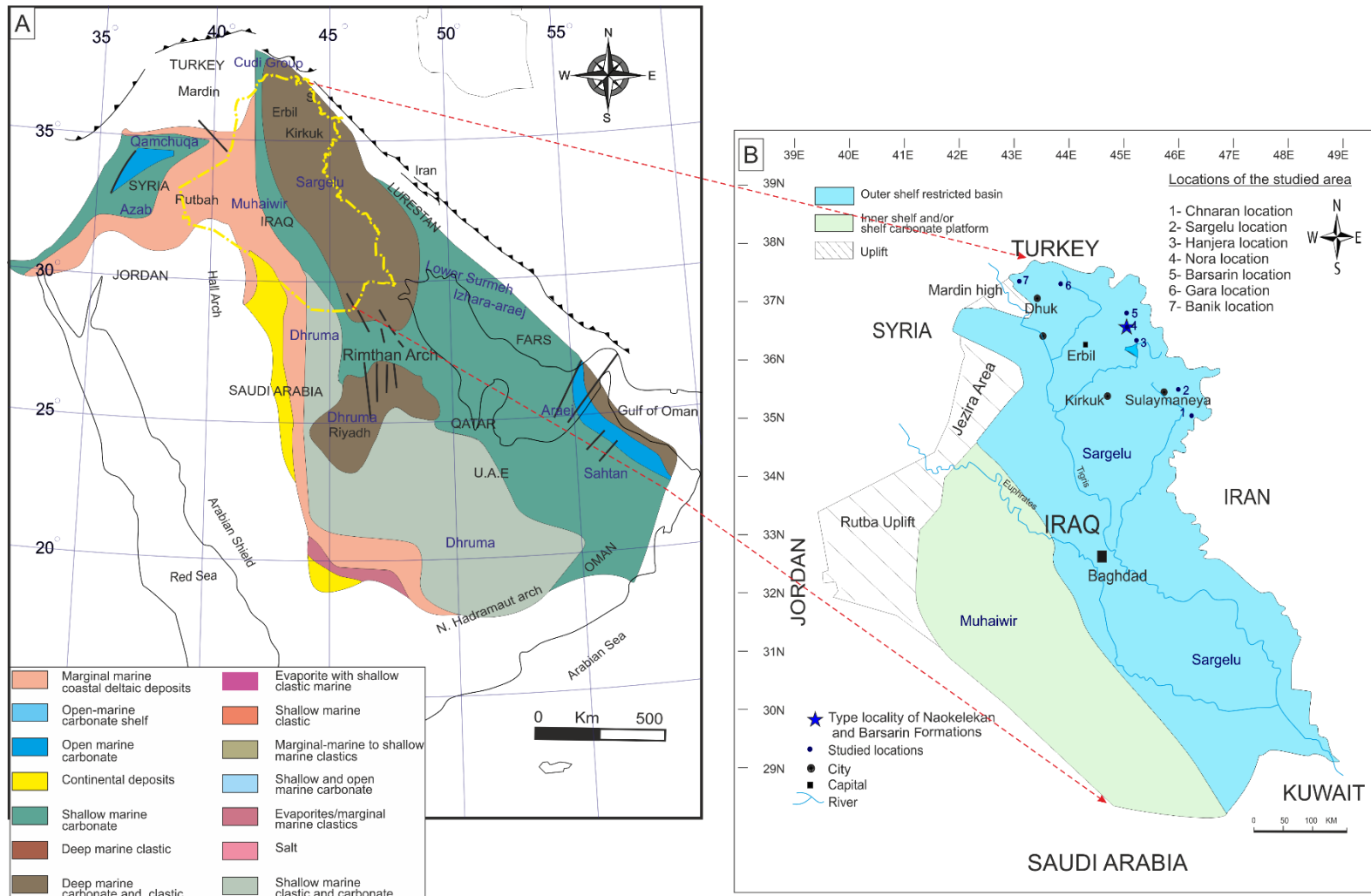


Figure 2.20 A: Facies of the Middle Jurassic on the Arabian Plate. During this period, the passive margins along the northeast and north of the Arabian Plate are well-developed, and sediments were generally characterized by open-marine facies, modified from Ziegler (2001). B: The palaeogeography of Middle Jurassic of Iraq, after Jassim and Goff (2006).

#### 2.4.7.1 Condensed section

Although the depositional succession in the Gotnia Basin was thicker on the eastern side than the western side during the Early–Middle Jurassic, this pattern of the thickness distribution is distinctively reversed during Callovian to Kimmeridgian time (Figure 2.14, Figure 2.22). For instance, the Naokelekan and Barsarin Formations on the eastern side of the basin, which palaeontological evidence indicates are of Late Callovian–Late Kimmeridgian age, are near 14 m and 20 m in thickness respectively. However, in the same span of time, about 530 metres of the Najmah and the Gotnia Formations were deposited on the quasiplatform. Numan (1997) stipulated that this difference in thickness could represent the time of incipient subduction, and commencement of gentle bending of the passive Arabian continental margin resulting from strain accumulating in the oceanic crust. This differential thickness occurred due to gentle bending significantly slowing down thermal subsidence in the foreland basin, in contrast with enhanced subsidence on the quasiplatform and marginal cratonic platforms (Numan, 1997). However, Sharland et al. (2001) inferred that the development of the large accommodation condensed rocks, and source rock deposition of the Sargelu, Naokelekan Hanifa, Tuwaiq Mountain and Najmah Formations in Iraq, Saudi Arabia, United Arab Emirates and Kuwait may have been controlled by faults. The faults plugged with either carbonate or evaporite sedimentation (Lapointe, 1991).

#### 2.4.7.2 Callovian hiatus

The Late Bathonian–Callovian hiatus has been recorded across wide areas: Saudi Arabia, Abu Dhabi, Qatar, Bahrain, and Iraq (Alsharhan and Nairn, 2003). Likewise, in the north-western parts of the AP, Hirsch and Picard (1988), and Hirsch et al. (1995) introduced evidence of post-depositional subaerial emergence during the end of the Middle–Late Callovian age. This missing time is also supported by widespread marine erosion in eastern Lebanon and Sinai. The hiatus is well represented in Tuwaiq Mountain Limestone, which shows a hardground and an unconformity with weathering phenomena during the Late Callovian section (Figure 2.12). The unconformable surface is overlain by the Late Oxfordian shales at the base of the Hanifa Formation (Beydoun, 1991).

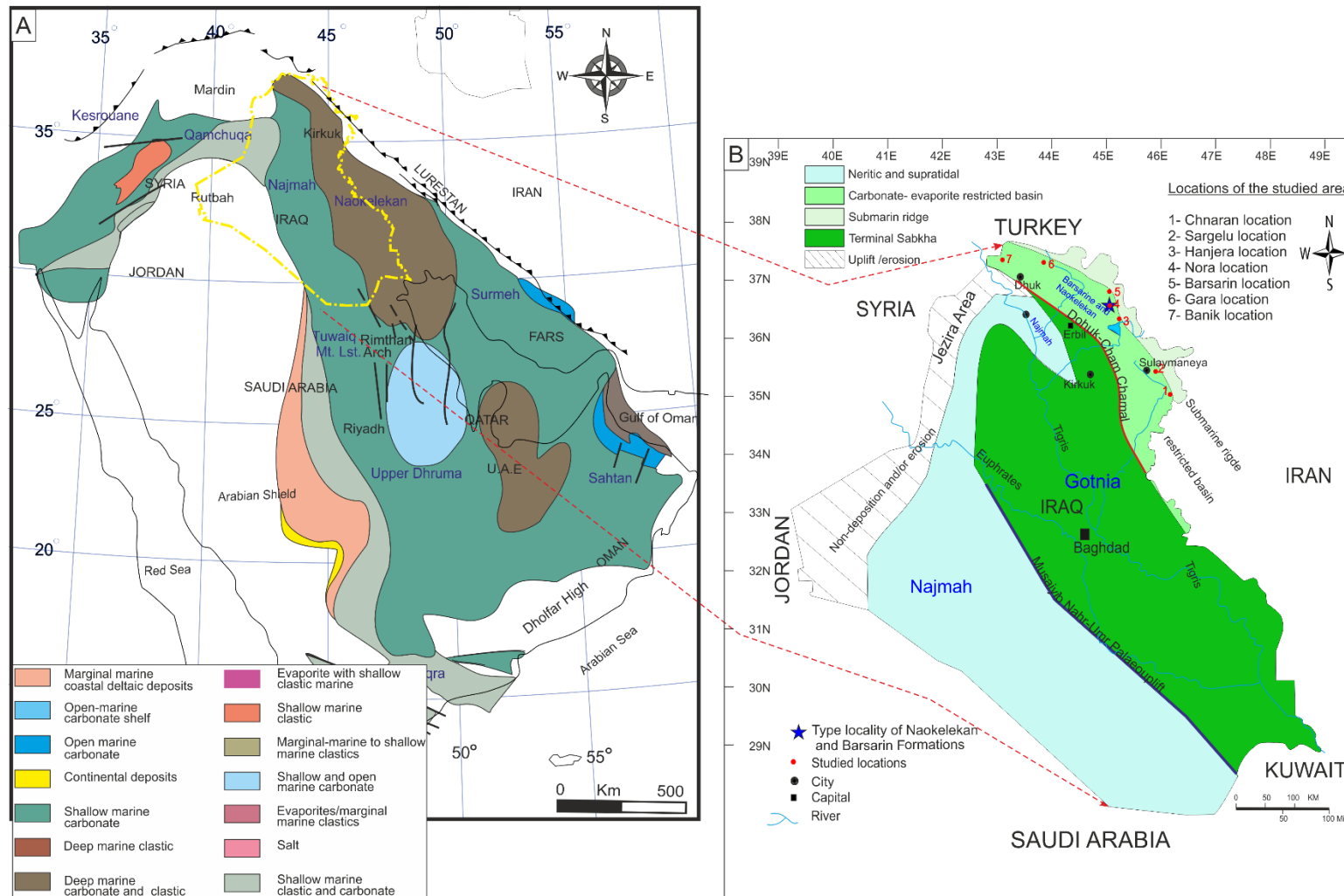


Figure 2.21: A: Palaeofacies of the Late Jurassic in the Arabian Plate, which is characterized by including differential intra-plate subsidence that resulted in the development of intrashelf basins on the plate, modified from Ziegler (2001). B: The palaeogeography of the Late Jurassic of Iraq, after Jassim and Goff (2006).

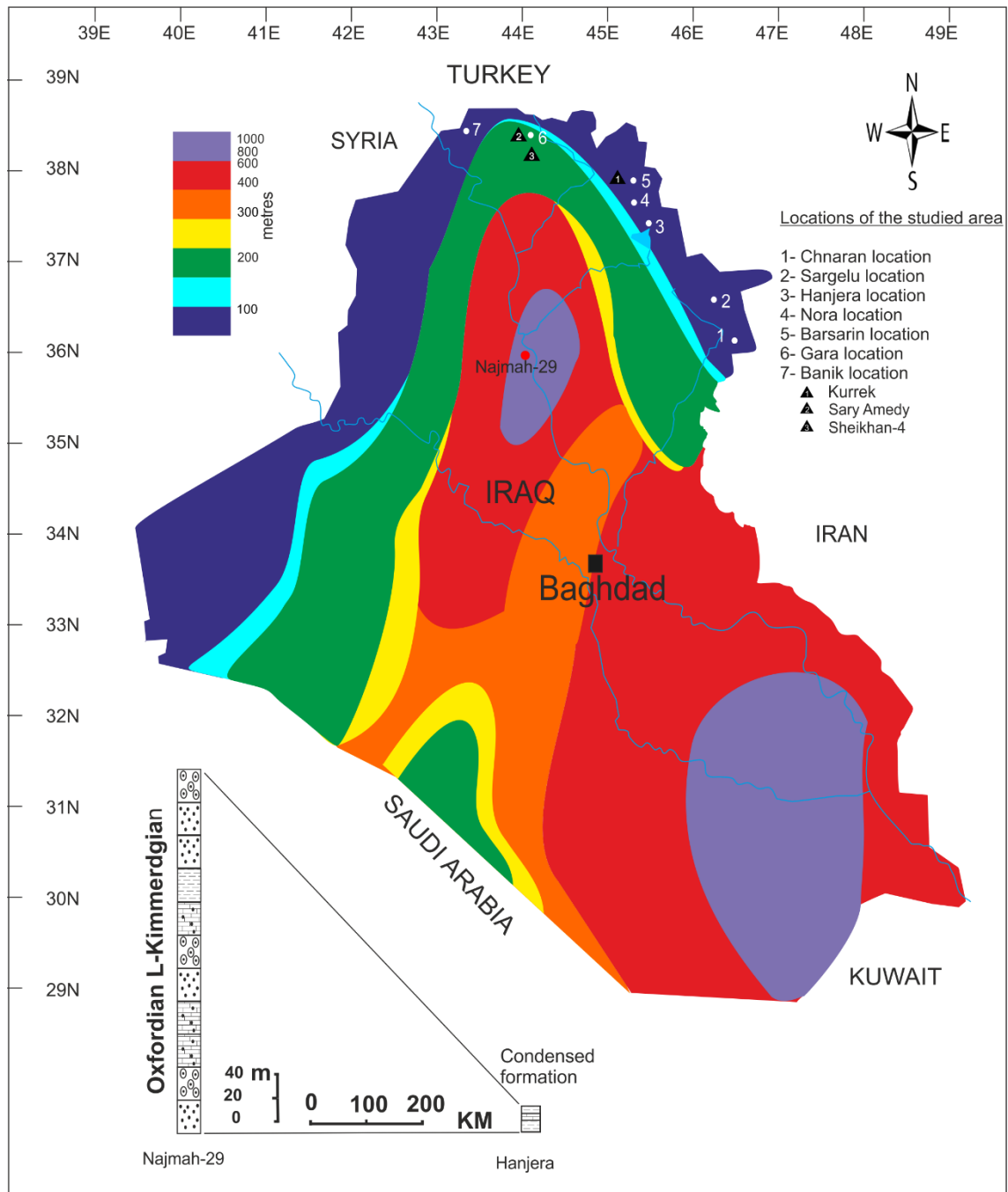


Figure 2.22: Thickness map of the late Jurassic period in Iraq, note the depocentres in the south and north of Iraq, from Jassim and Goff, 2006. B; Diagram showing significance difference in thickness between study sections and Najmah well.

### A–Naokelekan Formation

This was first described near Naokelekan village, in the imbricated zone of the Kurdistan Region in Iraq (Figure 2.1) (Bellen et al., 1959). The formation exists in the High, and perhaps Low Folded Zone as well (Jassim and Goff, 2006; Sissakian and Al-Jiburi, 2014). The Naokelekan Formation is regarded as one of the most well-known organic-rich Jurassic successions in Iraq and surrounding countries (Buday, 1980; Jassim and Goff, 2006; Aqrabi et al., 2010). The depositional basin margins of the formation are poorly understood. Ditmar and the Iraqi–Soviet Team (1971) suggested that the southern edge of the basin could coincide with the Dhuk–Chemchemal palaeouplift (Figure 2.11), whereas the northern margin is completely unknown because of overthrusting of an ophiolite complex on the Jurassic succession during the Cretaceous–Palaeogene period (Figure 2.5). The total thickness of the Naokelekan Formation in the type section is about 14 metres, generally divided into three units (Bellen et al., 1959; Buday, 1980; Salae, 2001); they are in ascending order: (a) 7 metres of thin-bedded, bituminous limestone and dolomite, with intercalated, black, highly bituminous, calcareous shale. Although no coal exists in this unit, it is informally called the ‘coal horizon’. This is due to the highly bituminous rock which is used by local people for cooking. (b) 4 metres of ammonitic mottled limestone (c) the upper unit consists of 3 metres of laminated shaly limestone. The formation was deposited in a euxinic environment in a very slightly subsiding or starved basin (Figure 2.18) (Aqrabi et al., 2010).

The Upper Jurassic successions of Kurdistan are characterized by condensed formations (Figure 2.14 and Figure 2.22), and there has been very little controversy over the cause and interpretation of the condensed formations as mentioned in previous sections. Spath (1950) assumed that a break may have occurred within the formation on the top of the mottled unit, but (Bellen et al., 1959) presumed a conformable boundary with the overlying Barsarin Formation. The fossils that were found in the mottled bed and in the coal horizon suggest an Oxfordian to Early Kimmeridgian age (Buday, 1980). In contrast, the top of the Najmah Formation, which is equivalent to the Naokelekan Formation, is considered as the Oxfordian or younger in northern Iraq (Aqrabi et al., 2010). Furthermore, regional correlations support that the Najmah Formation does not extend into the Kimmeridgian (Aqrabi et al., 2010).

The existence of the Naokelekan Formation has not been fully confirmed on the south/southwestern side of the Dhuk–Chemchemal ridge, but the formation is replaced by its equivalent Najmah Formation to the west of Kirkuk. However, in the Jezira area, and northwestern of Mosul, all Late Jurassic sediments are absent due to the post-

Jurassic uplift (Figure 2.19 and Figure 2.21), where Aptian–Albian facies unconformably rest on the Early–Middle Jurassic successions. The upper contacts of the formation with the Barsarin Formation are assumed to be conformable. The Naokelekan Formation extends into Kuwait and Saudi Arabia, and its age is equivalent to that of the Arab and Jubaila Formations (Jassim and Goff, 2006). The existence of the Naokelekan Formation in southwest Iran is not clearly demonstrated, but it could be correlated with the middle carbonate, upper shaley unit, and lower part of the upper carbonate unit of the Surmeh Formation (Figure 2.21, and Figure 2.23) (Lasemi and Jalilian, 2010). However, the Naokelekan Formation has not been reported towards Syria and in Turkey yet.

#### B–Najmah Formation

The Najmah Formation was first described from the Najmah well in the Foothill Zone (Bellen et al., 1959) (Figure 2.1), and the formation exists in the Mesopotamian and Stable Shelf Zones as well (Figure 2.14 and Figure 2.19). The depositional basin includes two depocentres (Figure 2.22), where the 340 metres thick type section is located in the northern depocentre. The thickness of the formation could reach up to 485 metres thickness in the southern depocentres. The only known outcrop is located in Wadi Hauran, in the western desert of Iraq which is about 38 metres.

Most authors have agreed that the Najmah Formation roughly divides into two parts; the lower part is dominated by siliciclastic deposition, which is carbonate cemented, whereas the upper part mainly consists of white coloured carbonate rocks (Al-Mubarak and Amin, 1983; Al-Naqib et al., 1986; Al-Azzawi and Dawood, 1996; Sissakian and Mohammad, 2007). According to Jassim and Goff (2006) the Najmah Formation can be divided into four parts; these are in ascending order: i) fine-grained, featureless, recrystallized limestone with relict fauna or oolitic grains, ii) oolitic and pseudo–oolitic limestone with an abundance of macrofossil debris; iii) coarsely granular dolomite; and iv) fluffy–textured limestone with thin anhydrite layers intercalated, and in some subsurface sections thin units of black shale are included as well. The Najmah Formation represents the calcareous shallow-marine facies with some intercalations of restricted lagoonal facies (Buday, 1980).

The formation is usually underlain and overlain unconformably by Sargelu and Gotnia Formations respectively (Figure 2.13). However, the Najmah Formation is conformably overlain by the Gotnia Formation in the south of Iraq. Also, near well Makhul–2, the Najmah Formation interfingers with the Gotnia Formation. In the western desert outcrops, the Najmah Formation is overlain unconformably either by the Rutbah Formation of Cenomanian age or by the Ghar Formation of the Early Miocene (Al-Jiburi

and Karim, 2009), and the lower boundary of Najmah Formation with the Muhaiwir Formation is unconformable.

The location of the northeastern shelf margin of the Najmah Formation is not well-known, but based on Ditmar and the Iraqi–Soviet Team (1971), it may be determined by the Dhuk–Chemchemical palaeouplift. Northeast of this palaeouplift, the Najmah Formation passes into the organic-rich argillaceous and condensed basinal Naokelekan Formation. Since the Dhuk–Chemchemical palaeouplift is located about 45 km east of the Kirkuk wells, Ditmar and the Iraqi–Soviet Team (1971) have assumed that the Late Jurassic in well Kirkuk–109 (Figure 2.1) represents the Najmah and Gotnia Formations rather than the Naokelekan and Barsarin Formations (Buday, 1980; Jassim and Goff, 2006).

Age		Kermanshah stratigraphic units		Tectonic history
		SW	NE	
Cenozoic		Shallow marine to continental deposits		Zagros shortening Onset of collision Neotethyan closure Ophiolite obduction
Cretaceous	Maastrichtian	Gurpi	Amiran	Kermanshah Radiolarite Trough
	Campanian			
	Santonian	Ilam		
	Coniacian			
	Turonian	Sarvak		
	Cenomanian			
	Albian			
	Aptian neocomian	Garau		
Jurassic	Upper	Gotnia		Marginal basin opening NE-Arabian passive margin Neotethyan opening
	Middle			
	Lower			
Triassic	Upper	Terrigenous to shelf carbonate		
	Middle			
	Lower			
Palaeozoic		Epicontinental detrital deposits		
Precambrian		Arabian Basement		

Figure 2.23: Stratigraphic column of the Jurassic succession showing tectonic history and different stratigraphic units from northwest, across Kermanshah to southwest Iran. Modified from Lasemi and Jalilian, (2010).

#### 2.4.8 Late Jurassic: Kimmeridgian to Tithonian

This time period is equivalent to mfs J60–K10 of the Sharland et al. (2001) scheme. It is characterised by the dominance of evaporites and shallow marine carbonates. As a result of the continental rifting and sea–floor spreading between the Afro–Arabian and Indian, a new passive margin was developed along the south-eastern coast of the AP in this period (Beydoun, 1991). Generally, the Late Jurassic succession of the AP was deposited in two main basins; the Arabian Basin in the south and the Gotnia Basin in the north (Figure 2.24).

i. The Arabian Basin, which includes the Arab and Hith Formations, is located in Saudi Arabia, Qatar and the United Arab Emirates. The Arab Formation is subdivided into four cycles of shallowing-upward of carbonate–anhydrite strata. These are labelled from top–down A, B, C and D Members (Al-Husseini, 1997; Cantrell and Hagerty, 1999). The Arab Formation members have uniform thickness and are laterally extensive both in terms of thickness and facies throughout the 250 km width of the Arabian Basin (Beydoun, 1991). The thickest part of the Hith Anhydrite Formation exists in the Arabian Basin, which overlies the Arab Formation. The thickness of the Hith Formation decreases northward into the Gotnia Basin. Based on Beydoun (1991) the Arab and Hith Formations deposited in a protected, shallow-marine basin with slow continuous subsidence.

ii. The Gotnia Basin, which is occupied by the Gotnia and Barsarin Formations, was distributed throughout wide areas of Iraq and Kuwait (Figure 2.24). Iraq is distinguished by including both Gotnia and Barsarin Formations, whereas only the Gotnia Formation was deposited in Kuwait. The Gotnia Formation generally shows several thick anhydrite units up to tens of metres with subordinate thin interbeds of calcareous shales (Figure 2.18). The southern part of the Gotnia Basin is comparable to the Arabian Basin, where the four–fold division of the Arab Formation can be easily recognised (Figure 2.18). The southern margin of the basin demonstrates more isolated conditions where shale–sulphate–halite rhythmites have been recorded. At the north-eastern margin of the Gotnia Basin, a condensed Barsarin Formation was deposited, which usually comprises shallowing-upward cycles of dolomitic limestone of a peritidal environment (Salae, 2001). The thickness of the Barsarin Formation has been estimated at about 20 metres, and includes some thin terminal anhydrite as well. According to Aqrabi et al. (2010), significant differences in thickness between the Barsarin and Gotnia Formations may be related to Late Jurassic fault reactivation. Subsequently, segmentation occurred in the Gotnia Basin, and thick halite and anhydrite units were deposited in SE Iraq whereas deposition of thin evaporites was taking place in northern Iraq. Likewise, Carman (1996)

also suggested basin extension and reactivation of Devonian faults in the Late Kimmeridgian period in Kuwait, and this could be comparable with what occurred in northern Iraq.

Based on Aqrabi et al. (2010), by the end of Megasequence AP7, only the margins of the Gotnia Basin were filled, leaving significant unfilled accommodation in the sediment-starved centre (Figure 2.18). By the end of the Tithonian time, a new tectonic stage began, when subduction started to the north and north-east of the oceanic crust below the Anatolian and Iranian plates (Numan, 1997). The Arabian Basin locally shows evidence of subaerial exposure such as brecciation and karstification with geopetal cement fills during the Late Tithonian. A sea-level lowstand has been also reported by (Hirsch and Picard, 1988), where canyons incised the Levant coast (Beydoun, 1991). Furthermore, in the Rimthan field on the northern extension of the Summan Platform and the Marjan field of the Saudi offshore area, numerous stacked erosional surfaces and microbial mats and crusts were recorded.

#### A–Barsarin Formation

The Barsarin Formation was first described at Barsarin village in the Rowanduz area of Kurdistan. The formation consists of laminated limestone and dolomitic limestone with some chert nodules and breccia intercalations (Bellen et al., 1959). Salae (2001) studied the type locality of the Barsarin Formation in detail. It has been revealed that the Barsarin Formation comprises a peritidal facies with the dominance of the microbial structures, and more than nine cycles of shallowing-upward were interpreted. Based on (Salae, 2001) an ideal Barsarin cycle may be composed in the following lithofacies ascending order: A–Stratiform stromatolite lithofacies; It consists of microbial laminated limestone that includes few algal spores, ostracods, and unidentified fossil fragments. B–Blister–flat stromatolite lithofacies; comprised microbial dolomitic limestone, with signs of evaporites and grains of chert. C–Thick-bedded dolomite lithofacies; composed of fine crystalline dolomite with large chert nodules, intraclasts, and tepee structures. D–Thick-bedded limestone lithofacies; composed of dense, fine grained–limestone containing grains of chert, evaporite pseudomorphs, and some signs of desiccation.

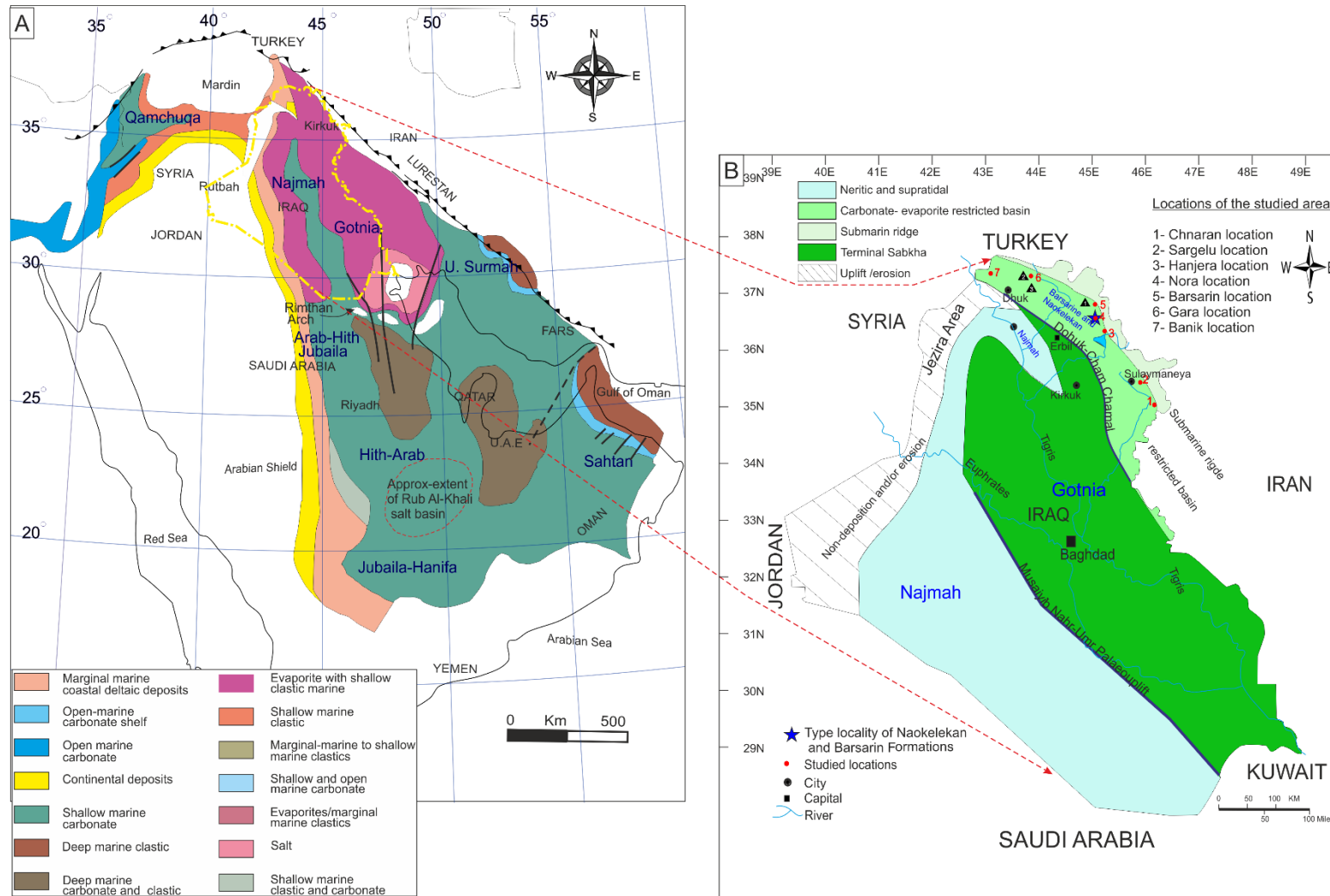


Figure 2.24: A: Facies of the Late Jurassic on the Arabian Plate. This period spanned the deposition of the Barsarin and Gotnia Formations in Iraq with Arab and Hith, Formations in the Arabia Basin. The Late Jurassic was distinguished for deposition of evaporites. Modified from Ziegler (2001). B; The palaeogeographic of the Late Jurassic of Iraq, after Jassim and Goff (2006).

Even though fossils are absent in both surface and subsurface sections of the Barsarin Formation, a Middle–Late Kimmeridgian age has been estimated from its stratigraphic position. The total thickness of the Barsarin Formation in the type section is about 20 metres. The thickness increases westward to about 30 metres near Banik village, whereas subsurface sections are thicker than exposures. The Barsarin Formation is distributed all over the High Folded, Imbricated and northern Thrust Zones, but its continuation towards the Foothill Zone in the south west is uncertain. Based on the stratigraphic position, the Barsarin Formation could be correlated partially with the Gotnia Formation of Iraq and Kuwait. Furthermore, it can be fully correlated with the Arab Formation of Saudi Arabia and the Hith Anhydrite (Buday, 1980). The Middle Surmeh of the eastern Zagros in Iran and the Sharifeh Shale Formation of Syria are equivalent in age to the Barsarin Formation as well. The upper contact with the Chia Gara Formation is apparently sharp, and no evidence for a break or uniformity was determined. However, at the base of the Chia Gara Formation, a thick unit of conglomerate was recorded in the Kirkuk wells.

#### B–Gotnia Formation

The Gotnia Formation was first described from the Awasil–5 well in central Iraq (Figure 2.1) (Bellen et al., 1959). The formation is about 200 metres thick at the type locality, and comprises mainly bedded anhydrite with subordinate thin interbeds of brown calcareous shale, thin black bituminous shale, and oolitic limestones (Figure 2.18). In the Rumaila well in south Iraq, the anhydrite beds are intercalated with four units of halite, which is quite similar to that seen in the Arab Formation of the Arabian Basin (Kadhim and Nasr, 1971). The south western margin of the depositional basin may be determined by the Musaiyib–Nahr Umr palaeouplift, whereas the northern margin could extend up to the Dhuk Chemchemical palaeouplift (Figure 2.24) (Buday, 1980). Subsurface data discovered three depocentres in the depositional basin; two of them located within the Mesopotamian Zone (Figure 2.22), whereas the third one, which is about 620 metres in thickness, is situated in the southern part of the Gotnia Basin and extends into Kuwait. The maximum thickness of Gotnia Formation has been recorded in Kuwait, and is about 700 metres (Jassim and Goff, 2006).

In addition to the Mesopotamia Zone, the Gotnia Formation is widely distributed in the Low Folded Zone in northern Iraq as well, such as Qarah Chauq–1, and Makhul–1, and Jabal Qand well (Figure 2.1) (Sadooni, 1997). The Late Jurassic succession in the Jabal Qand well, which is about 70 kilometres northwest to Kirkuk, comprises 216 metres of a combination Gotnia and Barsarin Formations. No surface outcrops of this formation were

recognized in the Western Desert (Jassim and Goff, 2006), but Buday (1980) pointed to the existence of the Gotnia Formation along the Euphrates River and southern desert of the stable shelf zone, and it mostly appears as a tongue within the Najmah Formation. Bellen et al. (1959), and Ditmar and the Iraqi–Soviet Team (1971) stated that the Gotnia Formation may be also deposited to the north east of Makhul, but it have been subsequently eroded by the post-Jurassic uplift.

The age of the Gotnia Formation is not precisely determined, but based on regional correlations, Callovian–Early Tithonian Stages were assigned. The Gotnia Formation is equivalent in age to the Hith and partly the A–C of Arab Formation. The upper and lower boundaries of the formation are mostly conformable with the Makhul and Najmah Formations respectively. However, the upper contact with the Makhul Formation could be locally erosional.

#### C–Chia Gara Formation

This formation was first described in the Chia Gara anticline and the High Folded Zone in Kurdistan (Figure 2.1) (Bellen et al., 1959). According to Aqrabi et al. (2010) the Chia Gara Formation represents mfs of J110 to K30. It is the most typical widely distributed formation across Iraq. The formation is rich in fossils, mainly ammonites, and radiolarians. The lithology of the formation is uniform throughout the study area, and can be divided into two units; they are: (i) lower unit: composed of thin-bedded limestones and calcareous shale, with a consistent zone of discoidal or "phacoidal" structures, up to 1 metre in diameter at the base. (ii) upper unit: comprised of marls and marly limestones with some shale interbeds.

The thickness of the formation ranges from 30 to 300 metres, but in the type locality it is about 230 metres. Based on (Buday, 1980; Salae, 2001; Jassim and Goff, 2006) the contact with the underlying Barsarin Formation is conformable in the high folded, imbricated and northern thrust zones. However, its lower boundary in Kirkuk–109 well is marked by a conglomeratic unit with the Gotnia and Najmah Formations, which are assumed to be equivalents of the Barsarin in the Foothill Zone (Buday, 1980). Ditmar and the Iraqi–Soviet Team (1971) inferred the possible existence of an uplifted structure, where the Chia Gara Formation unconformably rests on conglomerate in some areas south of the foot–hill zone.

Combining palaeontological data and sedimentary structure analysis confirm a deep basin for the Chia Gara Formation (Mohyaldin, 2008; Sissakian and Al-Jiburi, 2014). The local occurrence of silty layers in the upper part suggests interfingering with the Makhul Formation that consists of argillaceous limestone and pseudoolitic limestone with some

siltstone and anhydrite nodules interbedded. This may imply shallowing of the sea and uplift of the surrounding continental areas (Buday, 1980). The northern margin of the formation is marked by the high folded, imbricated and northern thrust zones, whereas in the south west of the Low Folded Zone the formation gradually passes into the Makhul Formation that is equivalent in age to it.

## 2.5 Summary

Iraq is basically divided into two main tectonic zones: Stable Zone and Unstable Zone. The former zone occupies the Western Desert, whereas the latter is usually located in the north/northeast of Iraq, where the study area is located. The Unstable Zone has developed due to the convergence and collision between the northeastern part of the AP and the Central Iran/Eurasia Plate, forming the Zagros Fold-Thrust Belt. The Unstable Zone is divided into: i–Zagros Suture Zone that comprises a stack of the thrustured ophiolite complexes, ii–the Imbricated Zone characterised by thrustured anticlinal structures and imbricated structures with overriding anticlinal structures, and iii–the Folded Zone consisting of series of parallel anticlines and synclines.

Based on the major unconformities the AP is subdivided into eleven tectonostratigraphic megasequences, and the study sections are found within Middle–Upper Jurassic AP7 which lasted for about 33 My. In this phase, the AP was located in an equatorial position. The continental rifting in and around the north and north-eastern AP margins resulted in the development of passive margin and depositional accommodation.

During Jurassic period, Gotnia Basin was developed in the northern AP. Due to continued rifting and differential subsidence across the AP, many intra-shelf basins were developed. Commonly, the impact of the tectonic and basin development is well-established. In the Western Desert, the Lower Jurassic strata are dominated by thin units of terrestrial–derived sediments, whereas in the same span of time, thick units of shallow-water carbonate rocks accumulated in the study area. Furthermore, the Middle–Upper Jurassic successions in the study area are characterised by deep-water condensed carbonate facies, whereas thick siliciclastic–carbonate rocks accumulated on the west side of the basin. Late stage of the AP7 is capped by the dominance of evaporites and shallow marine carbonates.

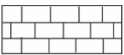
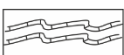
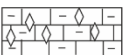
Subsequently to the AP7, the last stage of the extensional opening of the Neotethys Ocean started during Late Tithonian and lasted until the Cenomanian. During this period of rifting, thick deep-water carbonate successions accumulated throughout the study area.

Foreland basin formation of the Neotethys commenced in the Turonian–Eocene. Lastly, the closure of the Neotethys and the continental collision of the Arabian Plate with the Persian and Anatolian Plates took place. Consequently, ophiolite complexes were thrust over the AP during two different stages of obduction and collision. The stages occurred in the Late Cretaceous and Mio–Pliocene.

Barsarin Fm.	1. Thick Bedded Dolomite–Limestone Lithofacies ( <b>TBDLL</b> )	
	2. Blister–Flat Laminated Lithofacies ( <b>BFLL</b> )	
	3. Microbial laminite lithofacies ( <b>MLL</b> )	
Naokelekan Formation	1. Argillaceous Limestone Member ( <b>ALM</b> )	
	2. Thick Bedded Mottled Limestone Member ( <b>TBMLM</b> )	
	3. Medium Bedded Microbial–Bearing Limestone Member ( <b>MBMLM</b> )	
	4. Carbonaceous Limestone Member ( <b>CLM</b> )	
	5. Black shale member ( <b>BSM</b> )	
Sargelu Formation	1. Black Shale, Radiolarian Bedded Chert and <i>Posidonia</i> –Bearing Limestone Member ( <b>BRPLM</b> )	i. <i>Posidonia</i> –Bearing Limestone Lithofacies ( <b>PBLL</b> )
		ii. Radiolarian Bedded Chert Lithofacies ( <b>RBCL</b> )
		iii. Black Shale and Argillaceous Limestone Lithofacies ( <b>BSALL</b> )
	2. Middle <i>Posidonia</i> Limestone Member ( <b>MPLM</b> )	
3. Basal Saccharoidal Dolomite Member ( <b>BSDM</b> )		

Table 1: List of different members and lithofacies of the Sargelu, Naokelekan and Barsarin Formations with their abbreviation.

**LEGEND**

	bedded chert		limestone		flat stromatolite
	black shale		dolomitic limestone		blister stromatolite
	thick bedded eroded limestone		dolomite		microbialites
	convolute bedding		recrystallized		domal stromatolite
	argillaceous limestone		thick bedded eroded dolomite		microbial laminites
	interlayered fenestrae		ammonite		
	solution collapse		<i>Protoglobigerines</i>		
	tepee structure		ostracods		
	mud crack		radiolarians		
	evaporite		<i>Posidonia</i>		
	filled vug		broken <i>Posidonia</i>		
	scoured surface		algal spores		
	intraclast		grumeleuse		
	flat pebble		<i>Aggregatella pseudohieroglyphicus</i>		
	chert grains		peloid		
	chert nodule		fecal pellet		
	flocculated intraclast		undifferentiated microfossil		
	burrow		calcisphere		
	hardground		mottled		
	micritized grains		coalescent debris		
	coccoliths		bioclasts		
	filamentous bivalves		butterfly <i>Posidonia</i>		
	intact <i>Posidonia</i>		lamination		

## **CHAPTER THREE**

### **3 DESCRIPTION AND INTERPRETATION OF THE UPPER PART OF THE SARGELU FORMATION BAJOCIAN–EARLY CALLOVIAN**

### 3.1 Aims

- Fully describe the occurrence of chert beds, black shales, and carbonate beds of the upper part of the Sargelu Formation.
- Describe the different members in detail and establish a better understanding of depositional environments.
- Interpret the processes that may account for black shale formation and explore their link to Oceanic Anoxic Events (OAE).
- Determine the causative factors that led to the flourishing of *Posidonia* fossils, and reconstruct their depositional environment locally.
- Determine the origin of bedded chert sequences, discuss problems of chert origin and suggest possible models.
- Understand the nature of the boundaries between different lithostratigraphic members, and identify lateral and vertical relationships between bedded chert, black shale, and carbonates throughout the stratigraphic sections. Explore the likely mechanisms that could generate ordered or disorder strata in this case.
- Interpret the mechanism that causes the occurrence of folding at the top of the Sargelu Formation.

Although, there is a general agreement among the majority of researchers about the basinal deposition of the Sargelu Formation, the palaeo-water depth remains uncertain and its depositional and tectonic settings are also poorly understood. One cause of this uncertainty is the poor correlation between the Sargelu Formation exposures and the presumed age equivalent subsurface Bathonian–Bajocian equivalent strata in the rest of Iraq.

### 3.2 A General view

The Sargelu Formation is one of the most well-known organic-rich succession of the Middle Jurassic successions of Iraq in which the TOC content ranges up to 28% with an average of 4.7% (Buday, 1980; Jassim and Goff, 2006; Aqrabi et al., 2010; Al-Ameri et al., 2013; Hussein et al., 2013; Abdula, 2014; Al-Ameri and Al-Nagshbandi, 2014). It was first described in a highly folded zone in the core of the Surdash Anticline, near Sargelu village in the Kurdistan Region (Bellen et al., 1959) (Figure 3.1) (Bellen et al., 1959). As is the case with all other Jurassic formations in Kurdistan, the Sargelu Formation is generally characterized by the dominance of carbonate rocks. The total thickness of the Sargelu Formation in the type section is about 115 metres, but over a distance of more than 450 kilometres, the Sargelu Formation exposures of Kurdistan display a significant

variety in thickness. The maximum thickness which is about 130 m, has been recorded in the Rania location, whereas in the Banik area, a condensed section was identified, the whole section is less than 30 m thick (Figure 3.2). Roughly, based on lithological and palaeontological evidence, the Sargelu Formation has been subdivided into three main members (Figure 3.1):

1. Basal Saccharoidal Dolomite Member (BSDM)
2. Middle Posidonia Limestone Member (MPLM)
3. Black Shale, Radiolarian Bedded Chert and *Posidonia*-bearing Limestone Member (BRPLM)

The lower part of the formation or basal saccharoidal dolomite member is distinguished by destructive dolomitization, where no fossils or sedimentary structures can be recognized, whereas the middle part, which is characterized by the first appearance of *Posidonia*, generally comprises medium-bedded limestone with few thin interbeds of argillaceous limestone. The upper part, which is characterized by disrupted and folded strata, consists of medium-bedded, kerogeneous, black-coloured limestone interbedded with thin-bedded cherts and black shale. What caused the transitions between such different lithologies over relatively small vertical thicknesses remains unclear. Furthermore, the upper part of the Sargelu Formation is also of great interest because it contains a considerable amount of black shale that is thought to be the main source rock for oil in Iraq, Iran and most other Gulf countries as well.

The thickness variation becomes greater when Kurdistan outcrop sections are correlated with those of the westward subsurface in the foothill and Mesopotamian zones, where the Sargelu Formation could reach up to 400 metres thick in subsurface sections (Jassim and Goff, 2010). The link between Kurdistan outcrop and subsurface sections is poorly understood due to lack of research in this area. Most studies have considered the Sargelu Formation as a basinal facies that was widespread during a Middle Jurassic transgressive phase in Iraq (Bellen et al., 1959; Buday, 1980; Jassim and Goff, 2006; Aqrawi et al., 2010). Despite the noticeable lateral variation in thickness of different members, generally, the lateral extensions of these members are maintained continuously with a similar vertical arrangement throughout the study area, and they can be easily correlated lithologically because of the distinct character of each member (Figure 3.2).

The Sargelu Formation has been determined as Bajocian–Bathonian age, and its basal beds may be of Latest Toarcian age (Aqrawi et al., 2010). However, the age is still a

subject of controversy; the upper boundary of the Sargelu Formation is not determined precisely because of an absence of zone fossils and because the degree of erosion on the base of the Oxfordian unconformity in the Kurdistan region is uncertain. A more exact age for the lower boundary cannot be determined due to the obscured lower boundary as a result of the destructive dolomitization which makes it impossible to determine fossils.

The next sections will mainly focus on the upper part of the formation, i.e. “BRPLM,” which is characterized by black bedded chert intercalated with highly fissile black shale and posidonia-bearing carbonates (Figure 3.3). However, at the beginning of this chapter, and, in order to establish a general conception about the Sargelu Formation succession, a brief description of BSDM and MPLM will be included as well:

### **3.3 Basal Saccharoidal Dolomite Member (BSDM) (10–50 m thick)**

BSDM is thick-to medium-bedded saccharoidal dolomite 40–60 cm, grey to dark brown in colour with a grey to bluish colour on weathering surfaces (Figure 3.4, A). The dark colour is related to the saturation of intercrystalline pores of saccharoidal dolomite with bitumen, which gives a strong odour of oil on a fresh surface. The original texture is completely destroyed by dolomitization, so no fossils or sedimentary structures were recognized. At the uppermost of this member, there are a few thin intercalations of black shale.

The lower boundary between the Sargelu and Sehkaniyan Formations, which represents the boundary between Early and Middle Jurassic as well, can be determined in the field by the transformation from the massive to bedded limestone. The medium-thick beds of the MPLM usually overlie the brownish, massive-bedded, brecciated dolomite of the Sehkaniyan Formation, which represents the lower boundary between Sargelu and Sehkaniyan Formations well (Figure 3.4, B).

Microscopically, the BSDM is composed of equigranular dolomite crystals, ranging from 0.6–0.75 mm in diameter with a clear rim but a cloudy centre, and intercrystalline pores are usually filled with bitumen (Figure 3.4, C). The initial texture cannot be recognized due to the strong destructive dolomitization.

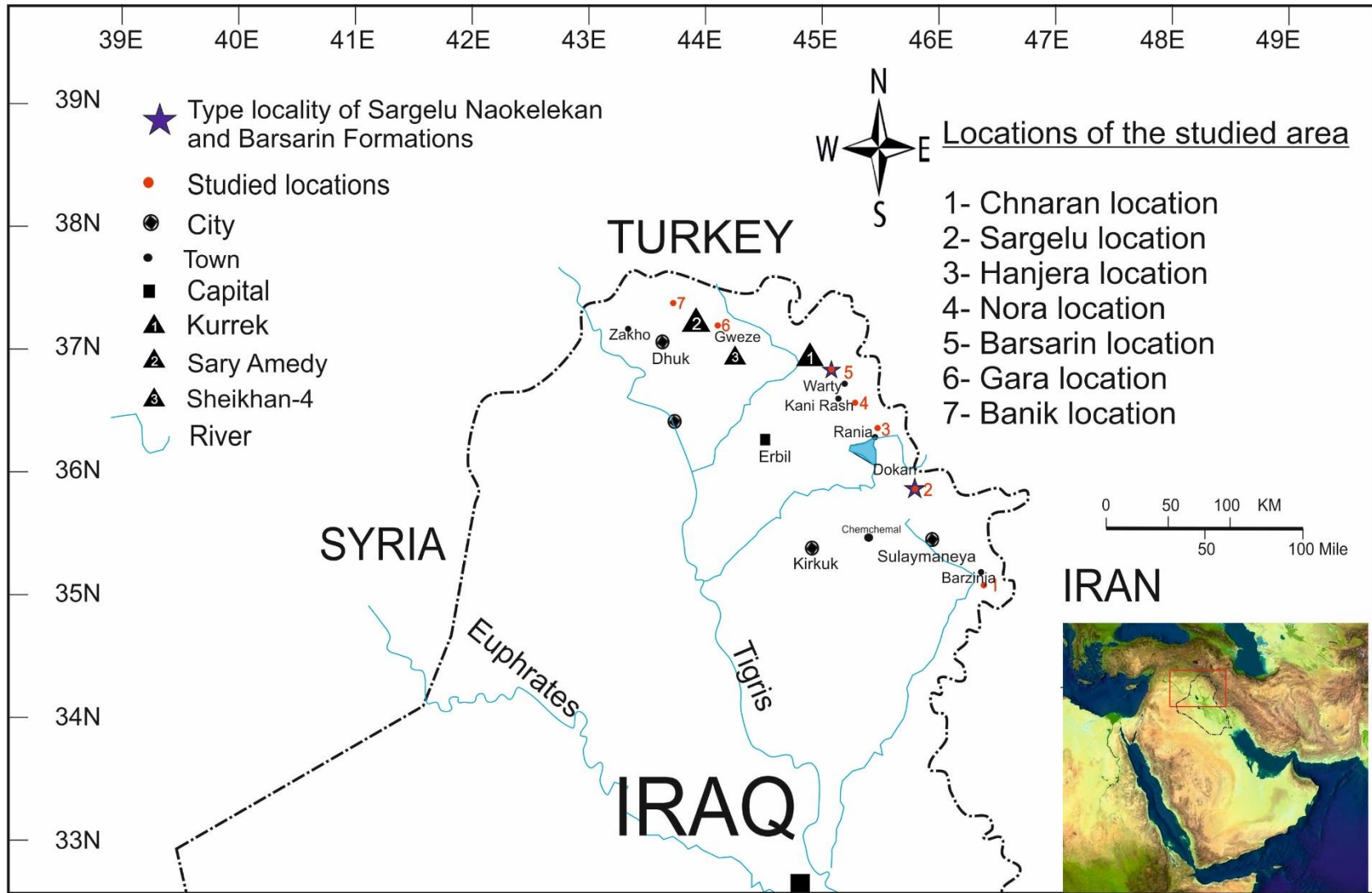


Figure 3.1: Different locations of the studied areas in northern Iraq, Kurdistan

### 3.4 Middle *Posidonia* Limestone Member (MPLM) (7–30 m thick)

MPLM, usually comprise medium to thick-bedded (10–60 cm beds thick), dark grey kerogeneous limestone, with few a thin units of argillaceous limestone interbeds (Figure 3.5, A). This u member nit is characterized by the first abundant appearance of *Posidonia* fossils; some ammonites are also observed, though occasionally.

The bedding surfaces are predominantly flat, though, a few thick beds (50–80 cm) in the at upper part of this member seem to be quite different from the others, with their surfaces displaying lobate structures (Figure 3.5, C). The cross-section of these lobate structures is distinguished by narrow, folded structures, with some rupture-like features (Figure 3.5, B & E). The recessive areas between lobate structures on the bedding surface usually display a different colour and lithology (Figure 3.5, C). In the current study, these folded structures of MPLM will be termed “first folded structures,” and this is because of the existence of another type of folded structure in the next member BRPLM that will be termed “the main folded structure.”

The boundary between MPLM and the underling BSDM can be easily determined in the field or from thin-section studies. It is from the point at which the facies changes upwards from the saccharoidal dolomite of the BSDM into the MPLM is marked by the first appearance of mudstone–wackestone containing broken thin-shelled bivalves (Figure 3.5, D).

Microscopically, the rock textures generally consist of intensely broken *Posidonia* wackestone to packstone (Figure 3.6, A & B), and the amount of broken shells gradually decreases upward. On the lower part of this member, some bioturbated structures have been observed as well (Figure 3.6, B). In addition to *Posidonia*, ammonites and *Protoglobigerina* have also been recorded (Figure 3.6, A). Noteworthy, this is the first appearance of the planktonic foraminifera *Protoglobigerina* in the Jurassic succession of the studied area. This is considered a significant event, which will be discussed further in a later section of this chapter.

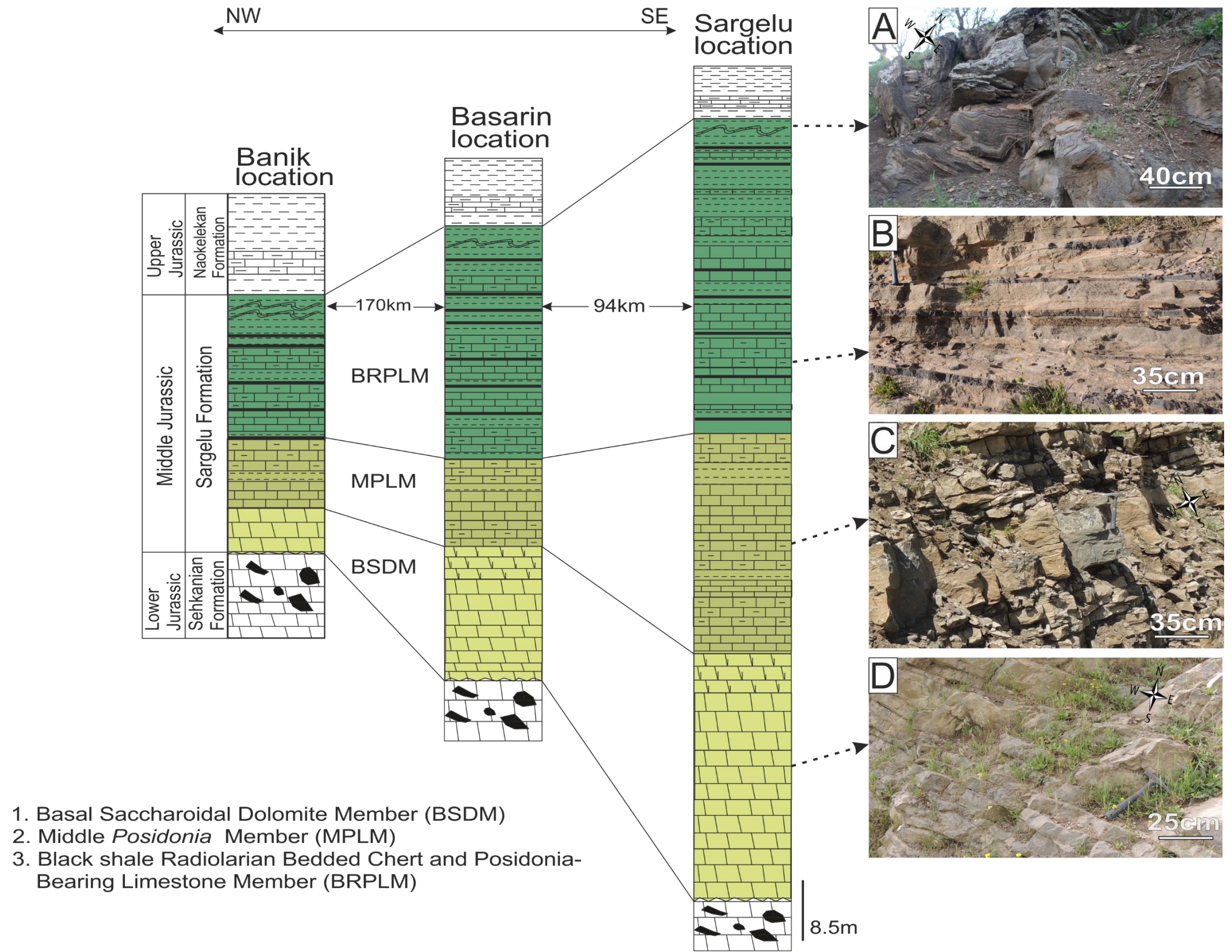


Figure 3.2: diagram showing lithostratigraphic correlation between BRPLM, MPLM, and BSDM for three selected locations of the Sargelu Formation, A: Gara location, B: Hanjera location, camera pointing north east, C: Nora location and D: Barsarin location.





Figure 3.4: Basal saccharoidal dolomite member: A: medium-bedded saccharoidal dolomite, camera pointing north, Barsarin location B: the lower boundary between Sargelu and Sehkaniyan Formations showing bedding surface of the brecciated dolomite at the top of Sehkaniyan Formation, Chnaran location. C: equigranular crystals of the saccharoidal dolomite showing a cloudy centre and clear rim, note the initial texture cannot be recognized because of the strong dolomitization, and their intercrystalline pores are filled by organic materials, PPL, Gara location.

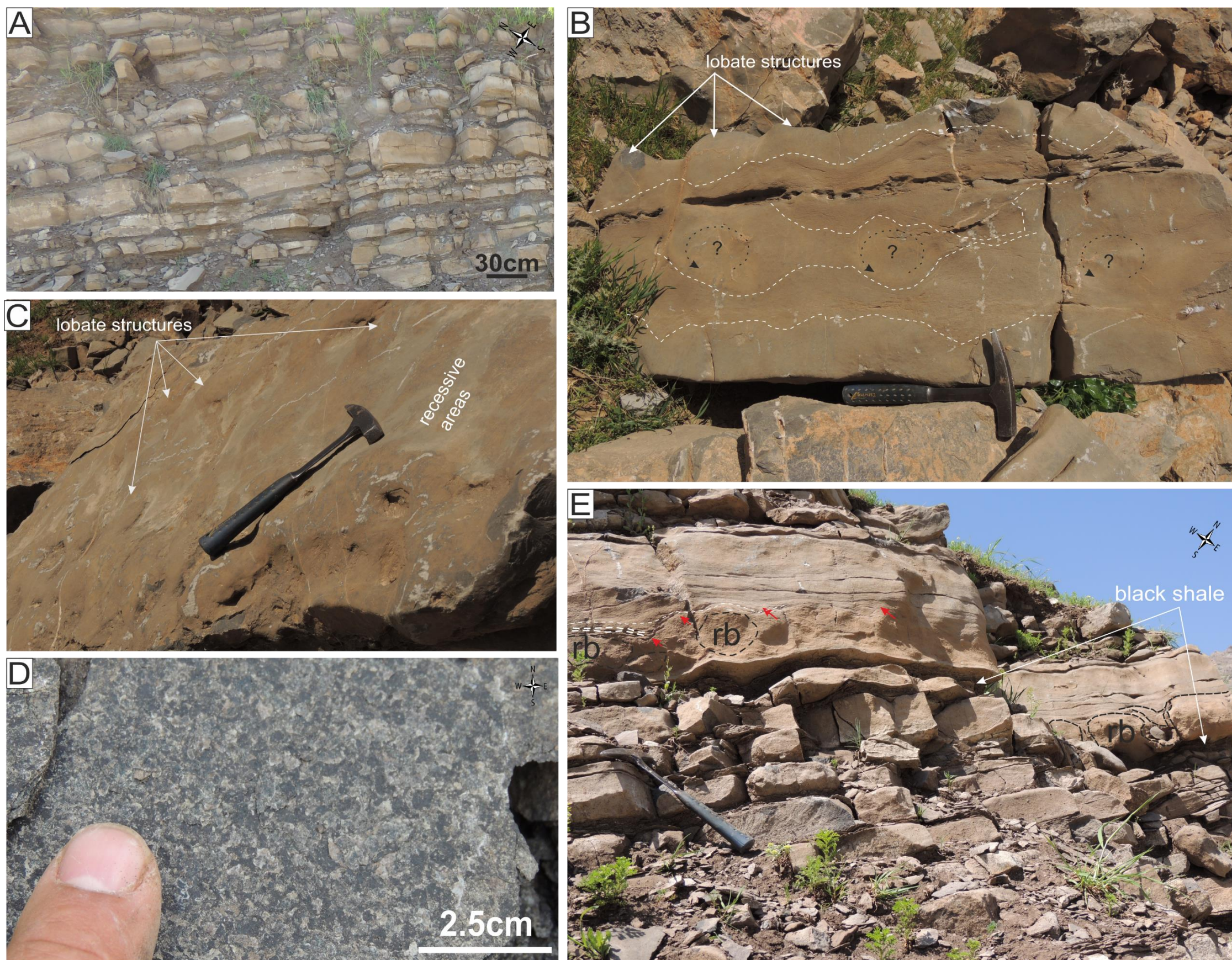


Figure 3.5: A: medium-bedded of thin-shelled bivalve bearing limestone of the MPLM with black shale interbedding, Nora location. B: cross-sectional view of the upper part of the MPLM, showing folded structures and local narrowing of the bedding thickness (white dashed lines), the black dashed and rounded arrows with the question marks represent areas that probably display the rolling structures. Note lobated structures at the top of the bedding plane, Chnaran location, camera pointing north east. C: plane surface view of "figure B" showing the lobate and recessive structures, note the colour and lithological difference between both. D: freshly fractured surface showing the dominance of intensely broken thin-shelled bivalves, which appear as white coloured flakes, while the black coloured spots are kerogen saturated porosities, Banik location. E: cross-sectional view showing the truncated surface (red arrows) with ruptured bed (rb), Nora location.

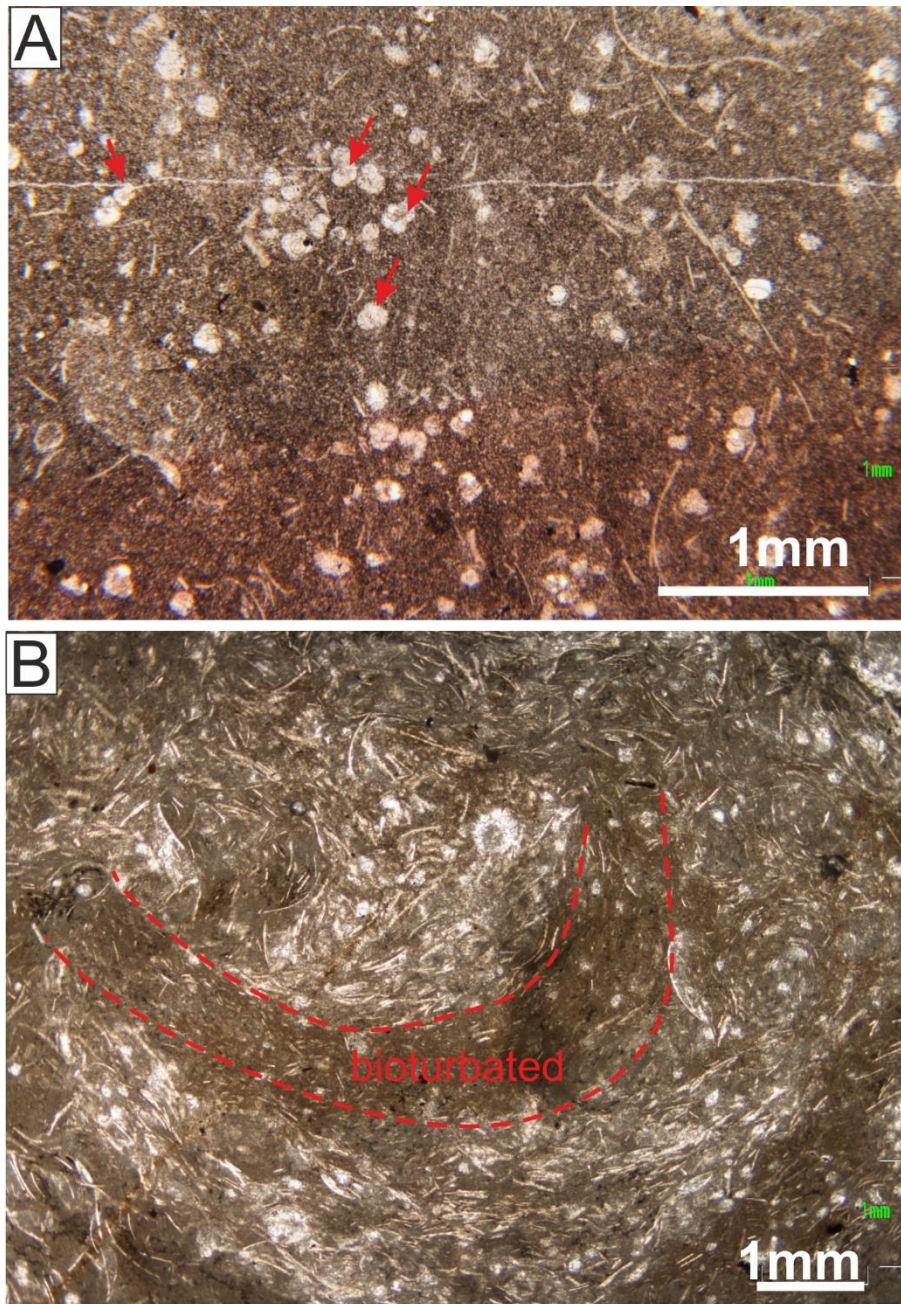


Figure 3.6: A: photomicrograph showing *Protoglobigerina* foraminifera (red arrows), PPL, partially stained with Alizarin Red S. B: broken thin-shelled bivalves showing bioturbated structures (bounded with red dashed lines), PPL, both photomicrographs are from Sargelu location.

### 3.5 Black Shale, Radiolarian Bedded Chert and *Posidonia*-Bearing Limestone Member (BRPLM) (10–31 m thick)

The BRPLM basically comprises a mixture of three different lithofacies alternating with each other at intervals of several decimetres thick with no clear regular cyclic arrangement (Figure 3.7 A, B, & C), and the lithofacies are as the follows:

- 1) *Posidonia*-bearing limestone lithofacies (P BLL)
- 2) Radiolarian bedded chert lithofacies (RBCL)
- 3) Black shale and argillaceous limestone lithofacies (BSALL)

The beds of each lithofacies are interbedded with each other. Radiolarian bedded chert lithofacies is interbedded with *Posidonia*-bearing limestone lithofacies and black shale and argillaceous limestone lithofacies about 30 times at most localities.

The BRPLM section as a whole may suggest a possible differentiation in terms of fossil content and lithological variation, where the lowermost part is normally dominated by *posidonia*-bearing limestone lithofacies (Figure 3.7, C) which changed gradually upward to the radiolarian bedded chert lithofacies (Figure 3.7, B), whereas the uppermost part of this member, in addition to the few contributions of RBCL and BSALL, shows the dominance of black shale and argillaceous limestone lithofacies (Figure 3.7, A). The existence of bedded chert often represents a prominent feature of the upper part of the Sargelu Formation, so it can be used as a marker bed in Jurassic sequences due to its peculiar lithology within carbonate successions, and its exposures can be traced over hundreds of kilometres from the Sirwan Valley in the north east to Zakho in northern Iraq (Figure 3.1).

The folded structure, which also can be termed as the main folded structure, is located at the top of Sargelu Formation, may represent the most prominent feature and distinguishes this member from the whole section (Figure 3.8, A–C). In addition to the main folded structure, some slightly folded structures also exist within some beds (Figure 3.8, C), and their intensity gradually increases upward through the section. The top of folded structures represents the upper boundary between the Sargelu and Naokelekan Formations.

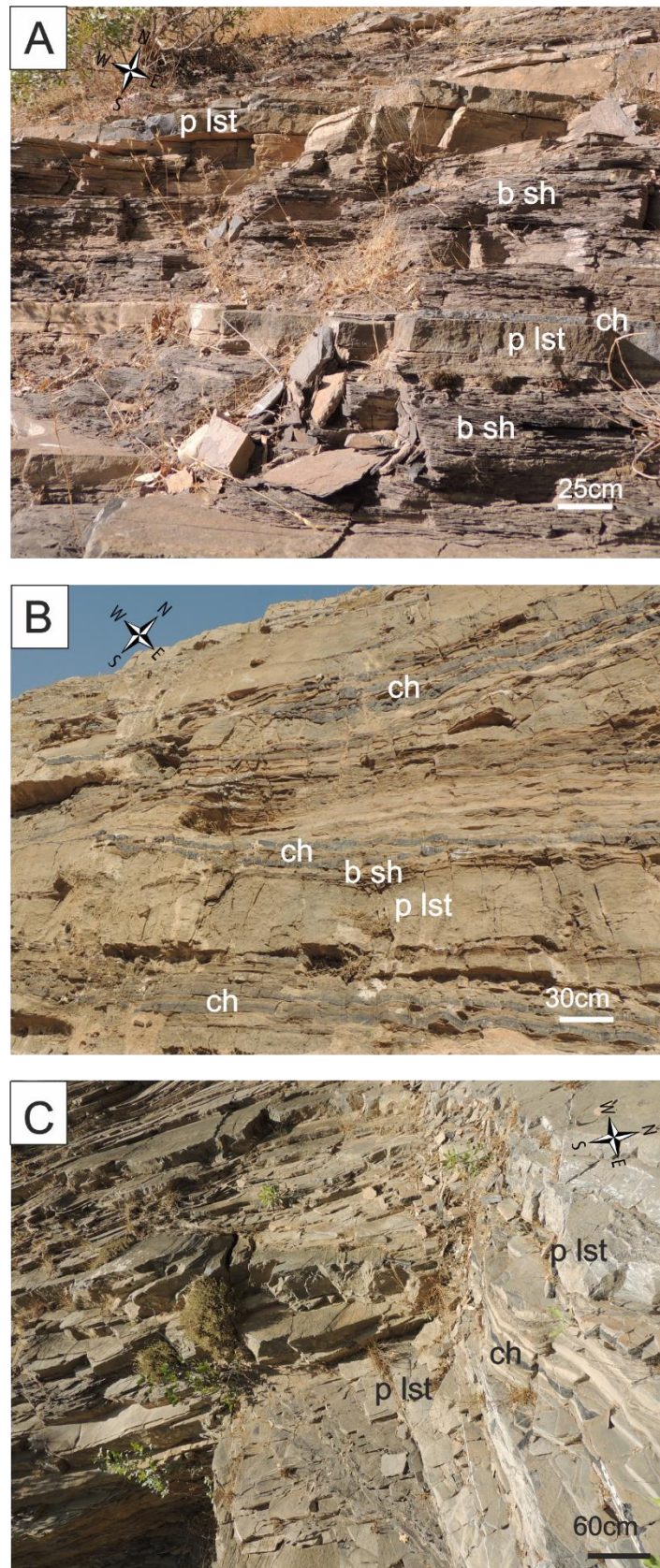


Figure 3.7: A: upper part of the BRPLM showing the alternation between different lithofacies; PBL (p lst), RBCL (ch) and BSALL (b sh), note the dominance of black shale (b sh), Gara location. B: middle part of the BRPLM showing alternation between different lithofacies; PBL, RBCL, and BSALL, note the dominance of bedded chert (ch), Hanjera location. C: lower part of the BRPLM showing alternation between different lithofacies; PBL, RBCL, and BSALL. Note that the sequence BRPLM shows a- an upward increase of black shale and b- the lack of a regular arrangement between different lithofacies, Barsarin location.

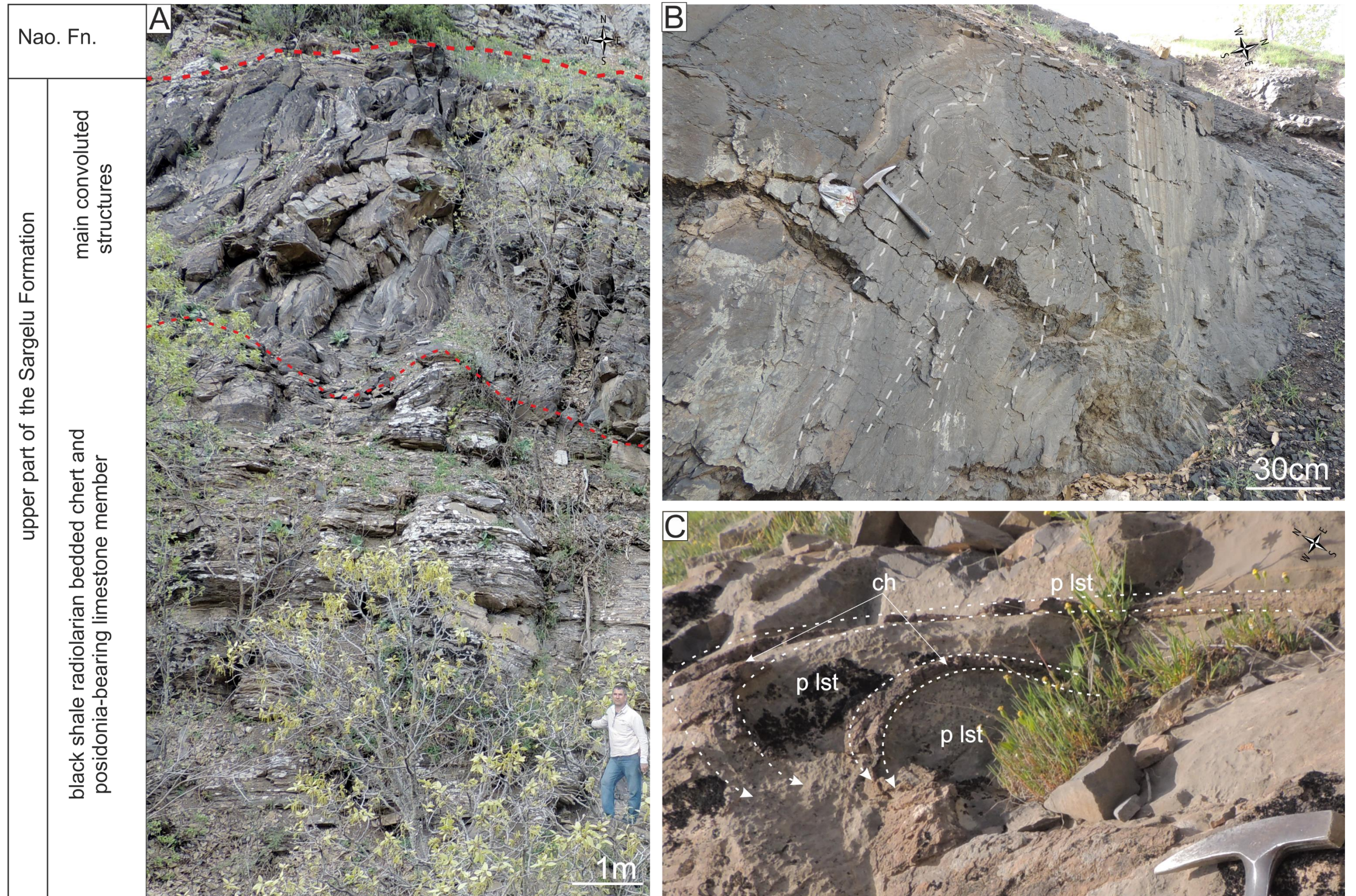


Figure 3.8: A; intense folded structures (bounded by red dashed lines) characterizing the upper part of the Sargelu Formation, note, overlying and underlying beds are not folded, Gara location. B; folded structures (white dashed lines) at the top of the Sargelu Formation, note the dominance of organic-rich shale, Banik location. C; photograph showing rolling structures in chert (ch) and Posidonia-bearing limestone (p lst), Barsarin location.

### 3.5.1 *Posidonia*-bearing Limestone lithofacies (P BLL)

#### 3.5.1.1 Field description

*Posidonia*-bearing limestone lithofacies (P BLL) is dominantly dark grey in colour and thickness of beds ranges from 10 to 50 cm. In addition to limestone, some intervals of the P BLL may appear as saccharoidal dolomite and/or silicified *posidonia*-bearing limestone. This lithofacies is interbedded with both RBCL and BSALL, but its proportion gradually decreases upward through the section. Although the dominant bedding type is tabular in shape, the bedding geometries are variable from location to location. The Hanjera location, for example, includes many elongated lenticular bedding structures (Figure 3.9, A–B). The intercrystalline pores are filled by bitumen, and fresh–fracture surfaces have a strong bitumen odour.

This lithofacies is dominated by thin-shelled bivalves *Posidonia*, with some poorly preserved ammonites and aptychi, especially in the upper part. The thin-shelled bivalves are up to 1.5 cm across, and they may make up more than 90% of the rock mass in some beds (Figure 3.10, A–C). In addition, many intervals of almost equigranular juvenile *Posidonia* bivalves of 1–2 mm in size have been recorded, especially when the P BLL approaches the black shale beds in the uppermost part of the section.

Field observations demonstrate that the beds of the P BLL, which are mostly overlain or underlain by bedded cherts or black shales, usually contain three types of internal sedimentary structure (Figure 3.11, A–D). These structures locally follow definite trends, in ascending order from base to top: i) this type is usually underlain by the bedded chert, and its lower part often shows normal graded bedding (fining upward) with very few truncation surfaces, whereas the upper part has some diffuse laminae (Figure 3.11, A–C). The vertical change in grain size in the graded structures is best seen in the beds of different sizes of ammonite shells, in which the larger size may rest at the bottom of the bed, and the size decreases gradually upward with *Posidonia* dominance at the top. In places, the underlying bedded cherts seem to be interjected by the *posidonia*-bearing limestone beds or P BLL resulting in the formation of rip-up clasts of bedded chert (Figure 3.11, E). ii) parallel laminated *posidonia*-rich laminae limestone, and iii) folded and undulating *Posidonia*-rich laminated limestone (Figure 3.11, A–D). The folded beds usually include small internal clasts up to 1 cm across.



Figure 3.9: A: BRPLM showing interbedding between limestone, bedded chert, and black shale, note, the beds are tabular, Nora location. B: Hanjera location situated about 20 km east of the photo A, showing lateral variation in the bedding thickness and some elongated lenticular structures in the Posidonia-bearing limestone beds (red dashed lenticular shapes).

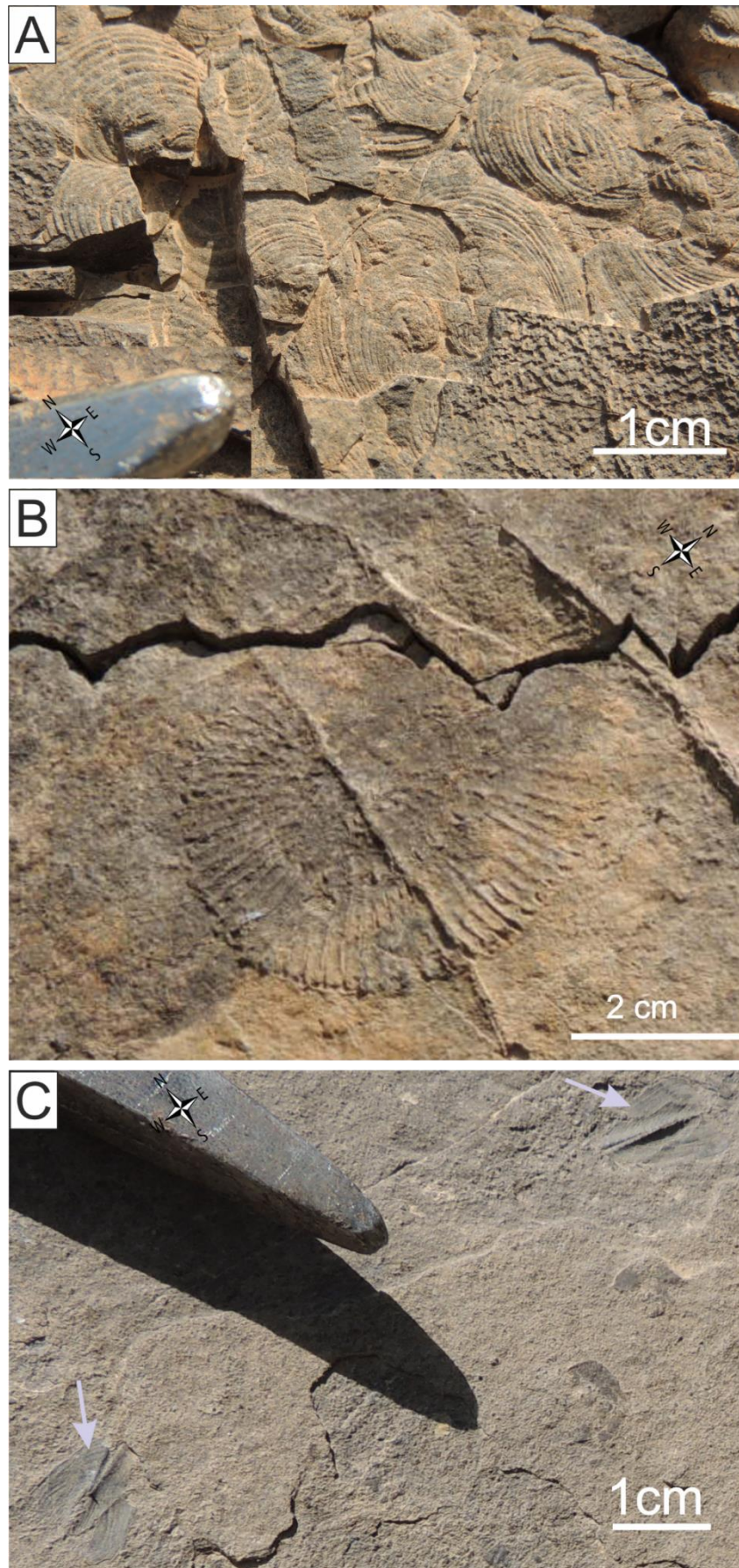


Figure 3.10: A; photograph showing high abundance of thin-shelled bivalves *Posidonia*, Chnaran location B; ammonite in Barsarin location C; ammonite-aptychi (white arrows) which have been observed at the top of the Sargelu Formation, Gara location.

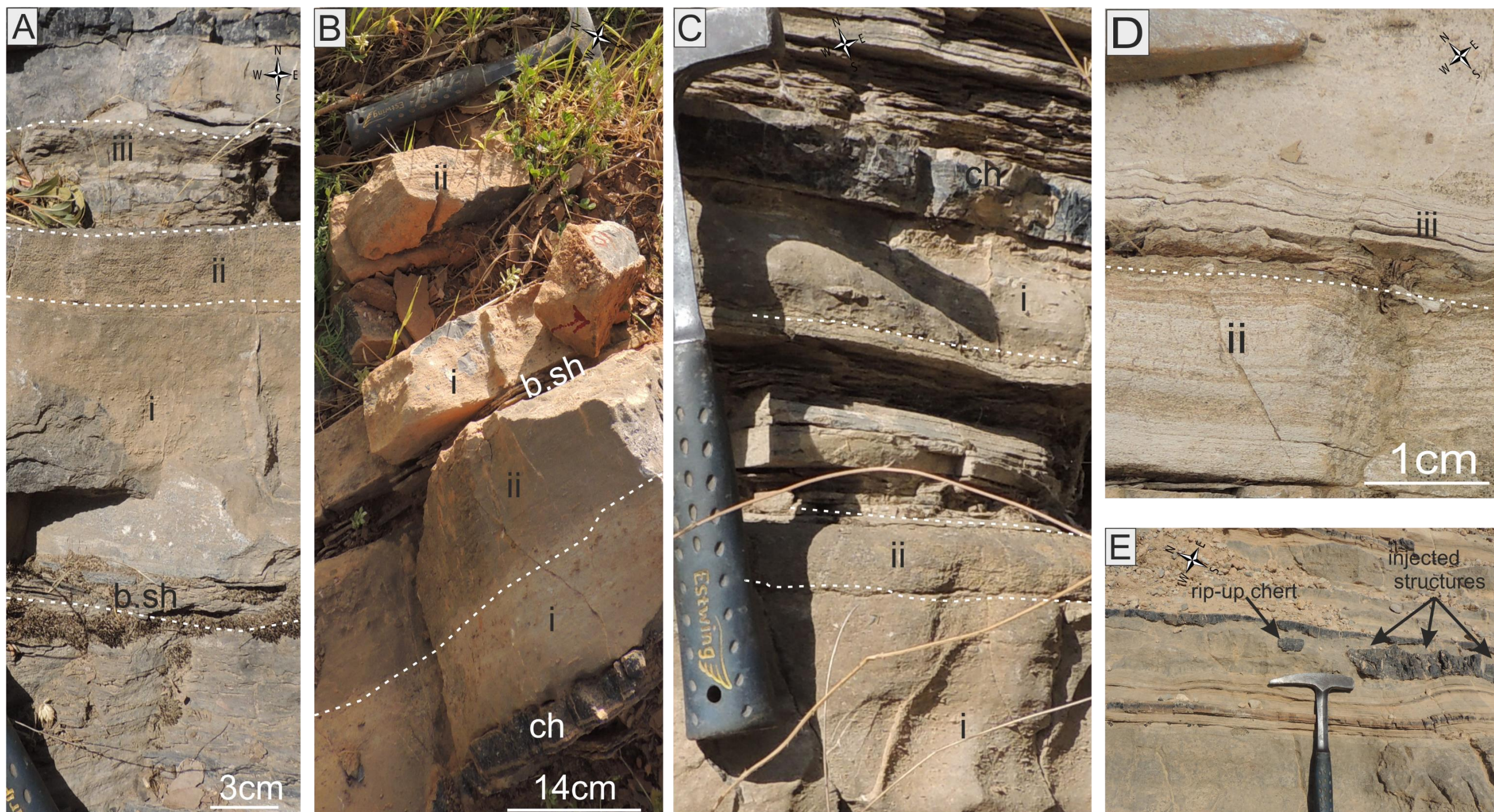


Figure 3.11: photographs showing vertical variation of textures in the *Posidonia*-bearing limestone at different localities of the PBLL: A: Hanjera location, B: Chnaran location, C: Barsarin location D: Sargelu location. The sequences are usually initiated with chert (ch) or black shale (b sh), which were then followed by massive bed shows diffused lamination, and normal graded bedding (i) , *Posidonia*-rich limestone with parallel laminae (ii), and folded *Posidonia*-rich laminated limestone (iii) respectively or repeatedly. Note the beds underlying and overlying folded *Posidonia* (iii) are not folded. E; photograph showing rip-up clasts of chert in *Posidonia*-bearing limestone.

### 3.5.1.2 *Posidonia* classification

The thin-shelled bivalves, which are collectively and informally called “paper pectens” or “flat clams” due to their abnormally thin shells (Etter, 1996), are fairly small in size 0.5–1.5 cm (Figure 3.12, A). Their surfaces are ornamented with many regular concentric ribs, which are strongly developed on the medial and ventral parts of the shell but become indistinct towards the anterior and posterior margin interspaces (Figure 3.12, B). The shells normally appear obliquely ovate and become more oblique during growth by extension of the oblique postero-ventral part with equivalves but in equilateral. Their straight hinge-lines are situated anterior to the middle of the dorsal at about two-thirds; whereas beaks, which are very small and barely project beyond the hinge line. Based on the morphological description, these thin shells are quite comparable to *Posidonia ornati* Quenstedt.

Based on the classification of the Schatz (2005), the *Posidonia ornati* Quenstedt shells of the Sargelu Formation appear to be preserved in different styles such as butterfly (Figure 3.12, E), horizontal disarticulated valves (Figure 3.12, A), articulated with closed valves, and cone-in-cone (Figure 3.12, C). Sizes of *Posidonia* valves reduce to 2–4 mm near the top of the BRPLM which is characterized by a dominance of black shale (Figure 3.12, F).

### 3.5.1.3 Ammonite classification

The upper part of the Sargelu Formation is characterized by different kinds of poorly preserved ammonites. No systematic classification or ammonite zonation have been presented since the first description by Wetzel in 1948 (Bellen et al., 1959). Though the Sargelu Formation contains many different kinds of ammonite, only one species has been determined in the current study, and this is due to the poor preservation of fossils. This can be tentatively identified as a *Kosmoceras* sp. of Middle Callovian (Figure 3.10, B). *Kosmoceras* sp. has occasionally been recorded from the Callovian of the Middle East, though it is much more common to the north in the Caucasus (John Wright. personal communication).

## 3.5.2 Microscopic description

The thin-shelled bivalves are ubiquitous in the Sargelu Formation. The first appearance of *Posidonia* fossils in the Sargelu Formation occurs in the middle *posidonia* limestone Member (MPLM), which is underlain by the Basal Saccharoidal Dolomite member (BSDM) and is overlain by the PBLM. The *Posidonia* shells preserved in many different

textures will be described in detail in the next sections. In order to illustrate the most important differences and main distinguishing criteria between PBLM and MPLM with regards to *Posidonia* preservation, the following points are relevant:

- I. ***Posidonia* of MPLM**; It is made up of dark grey to black limestone of *Posidonia* mudstone to wackestone texture alternating with thin-bedded argillaceous limestone. The thin-shelled bivalves of *Posidonia* were intensely broken into small fragments with no preferred orientation of broken shells. Bedded cherts never occur in this member (Figure 3.6, A&B) and (Figure 3.12, D).
- II. ***Posidonia* of PBLM**; It is made up of dark grey to black limestone of *Posidonia* wackestone to packstone texture (Figure 3.12, B–C). Microscopic study shows that the thin-shelled bivalve preservation varies; they appear to be distributed in a specific arrangement upwards through the member (i) intact disarticulated, (ii) articulated with closed valves, (iii) folded with fragmented shells, and (iv) stripe-like or filamented *Posidonia*. The intact thin-shelled bivalves are about 1.5 mm in average length and 0.5 mm in average thickness, (Figure 3.12, C). Generally, the shells do not exhibit any encrustations or borings, and are commonly preferentially oriented parallel to stratification. (Figure 3.13, B–C). PBLM is always interbedded with black shale and bedded chert.

Microscopic study shows the existence of the *Protoglobigerina* in the lower part of the PBLM as well. The *Protoglobigerina* are usually associated with highly fragmented *Posidonia* and display mudstone–wackestone textures. The *Protoglobigerina* are characterized by a relatively small size, 0.1–0.5 mm, with 1 to 3 chambers, and all chambers are filled with sparry calcite cement. Rare calcified radiolaria have also been observed.

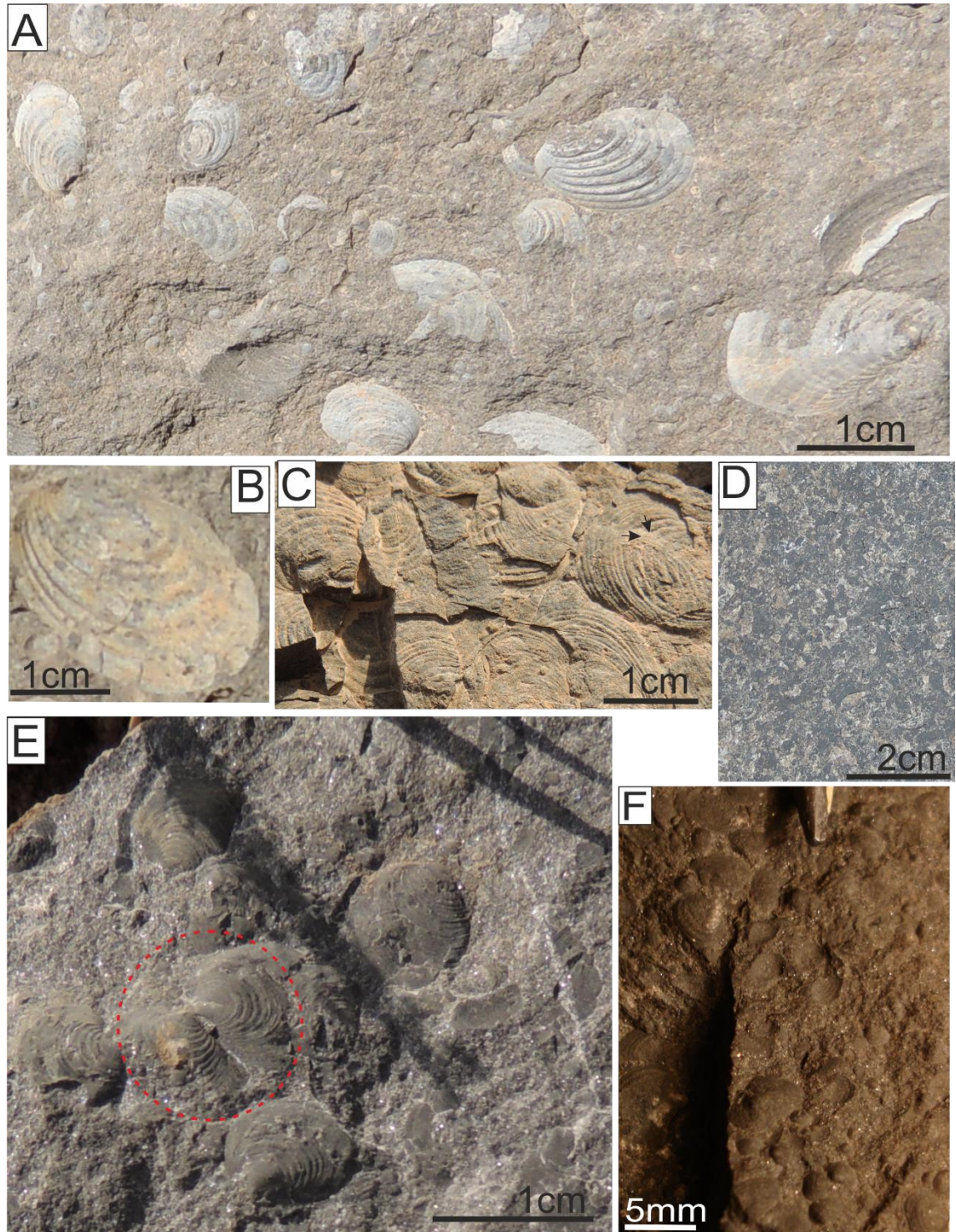


Figure 3.12: A: different size range of horizontal disarticulated intact thin-shelled *Posidonia*, Nora location. B: *Posidonia ornat*i Quenstedt, showing regular concentric ribs, which are relatively strong on the medial and ventral parts of the shell and their hinge-lines are situated anterior to the middle of the hinge line, Nora location. C: cone-in-cone preservation, Chnaran location. D: intensely fractured *Posidonia*, Gara location. E: butterfly preservation (red circle), Chnaran location F: decrease in size of the *Posidonia* valves in the upper part of the BRPLM, Banik location.

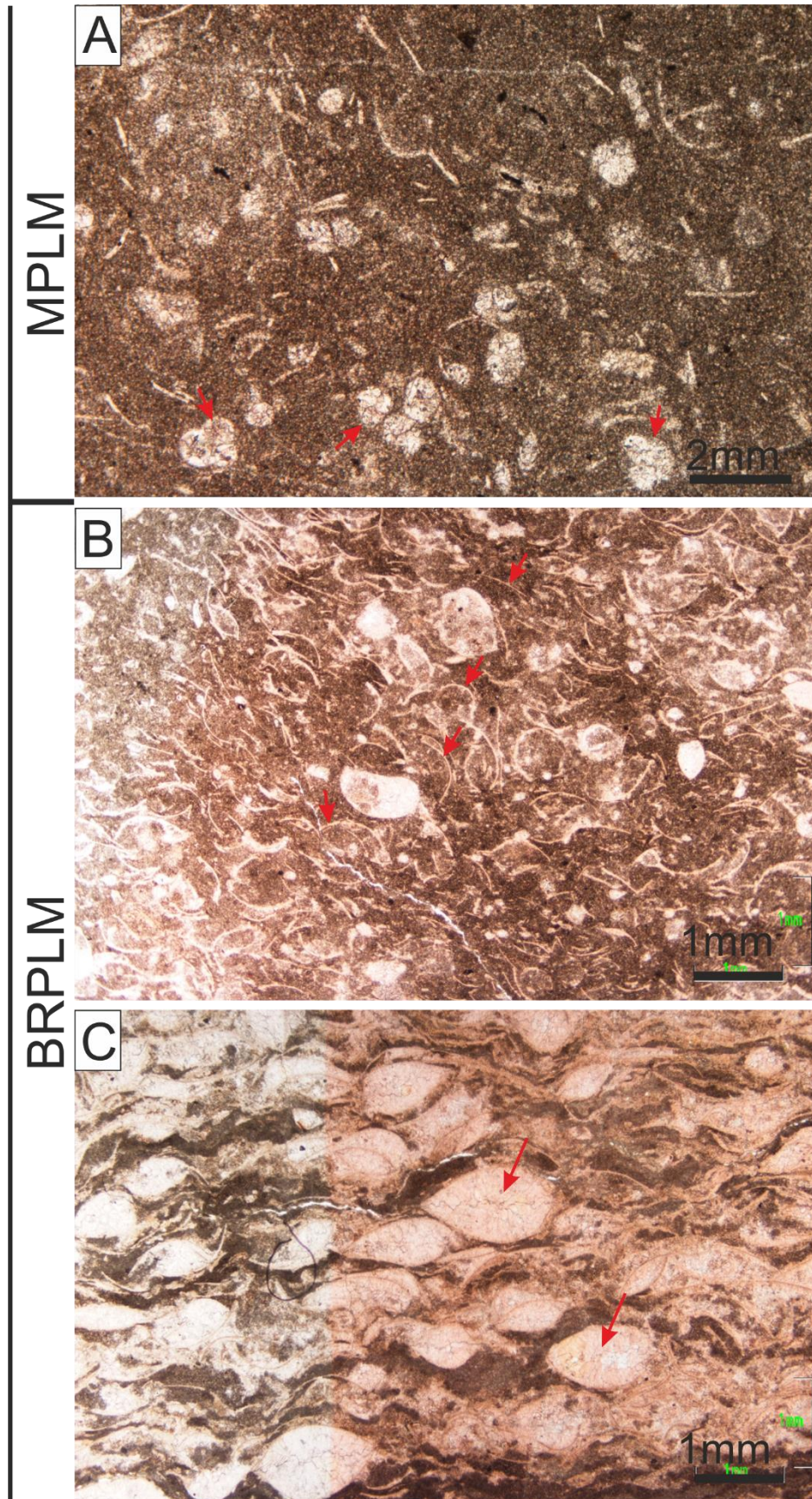


Figure 3.13: photomicrograph showing textural comparison between MPLM and BRPLM. A; the MPLM showing *Protoglobigerina* (red arrows) and broken *Posidonia* mudstone. The *Protoglobigerina* are always not more than three chambers, Sargelu location. B; disarticulated *Posidonia* (red arrows) wackestone, alizarin Red S, PPL, Barsarin location. C; packstone, including the intact *Posidonia* (red arrows), note, the *Posidonia* lay parallel to stratification, partially stained with Alizarin Red S, PPL, Hanjera location.

### 3.5.3 The preservation style of *Posidonia*

Petrographically, the PBL is usually dominated by densely packed *Posidonia* with few calcified radiolaria and foraminifera in a micritic matrix. The *Posidonia* contribution in the PBL may range from 10 to 90%, either forming wackestone or packstone textures (Figures 3.12, A–F; 3.13, A–C; 3.14, A–F). In the case of high abundance of continuous stripe-like *Posidonia*, the texture could be termed “filament,” and the filament texture can be defined as an event which is characterized by an interval with dominant thin-bivalve shells that constitute up to 90% of all grains (Figures 3.16 and 3.15).

The PBL exhibits a wide variety of internal textures and compositions depending on its position within the succession. Besides, *Posidonia ornati* Quenstedt shells were preserved in different styles, such as butterfly-like, horizontally disarticulated valves, rolled and folded shells, articulated with closed valves, and cone-in-cone. Although the variety of preservation styles of *Posidonia* seemingly lacks specific arrangement in the strata, they can be roughly categorized into the different horizons in which there is an abundance of specific texture. After study and comparison of different sections at all localities, it appears, there is a kind of organization and general pattern, and quantitative analysis might be useful in future research in order to interpret preservation styles. The following arrangement is in ascending order with respect to the predominant preservation textures:

- i. **Intact disarticulated shells:** this usually overlies the intensely fragmented shells of the IFPL, and the shells tend to lie parallel to bedding (, A). Some small broken thin-shelled bivalves are also included, especially at lower part of this member.
- ii. **Articulated with closed valves:** this texture is observed in several intervals in the lower part of PBL, which consists of either *Posidonia* packstone or juvenile *Posidonia* packstone. The *Posidonia* fossils generally lie parallel to the bedding plane, and all fossil moulds are filled with relatively coarse calcite cement (Figure 3.14, B). Ascendingly, the articulated with closed valves are normally followed by horizontal disarticulated textures, which usually characterized by folded and broken shells.
- iii. **Undulated and fractured shells texture:** it consists of *Posidonia* wackestone to packstone. The shells appear either as layers of broken, undulated thin-shelled bivalves (Figure 3.14, C–E) or as thin broken shells that show warping around more rigid bioclasts such as ammonite shells (Figure 3.14, F). This kind of preservation is quite rich with coalescent debris (Figure 3.14, C–D). The coalescent debris

comprises flocculated *Posidonia* valves with internal folding and rolling textures (Figure 3.14, D). The debris lithology varies from limestone, dolomite, to silica. In some places, they have an abundance of up to 20%, with the grain size ranging from 0.5 to 5 mm.

- iv. **Layers of thin-shelled bivalve filaments;** the thin-shelled filamentous packstone can normally occur when the *Posidonia* bivalves stack horizontally and accumulate as continuous thread-like layers (Figure 3.15, A–D). The filaments usually exhibit irregular to zigzag and undulated or rolled textures (Figure 3.15, A–D), and they often associate with significant amounts of thin-bivalve coalescent debris as well.

Some rock beds, particularly near the top of this lithofacies, are characterized by the dominance of rosette-shape and elongated lensoid bodies up to 1 mm in length and 0.4 mm across, which are composed of clusters of equigranular dolomitic crystals (Figure 3.16, B–F). A single lensoidal structure usually consists of two parallel rows of dolomite crystals (Figure 3.16, D). However, it appears that the relationship between *Posidonia* filament and lensoidal structures is inverse, because *Posidonia* filament content decreases upward whereas elongated lensoid bodies become the predominant lithology in the upper part of this member.

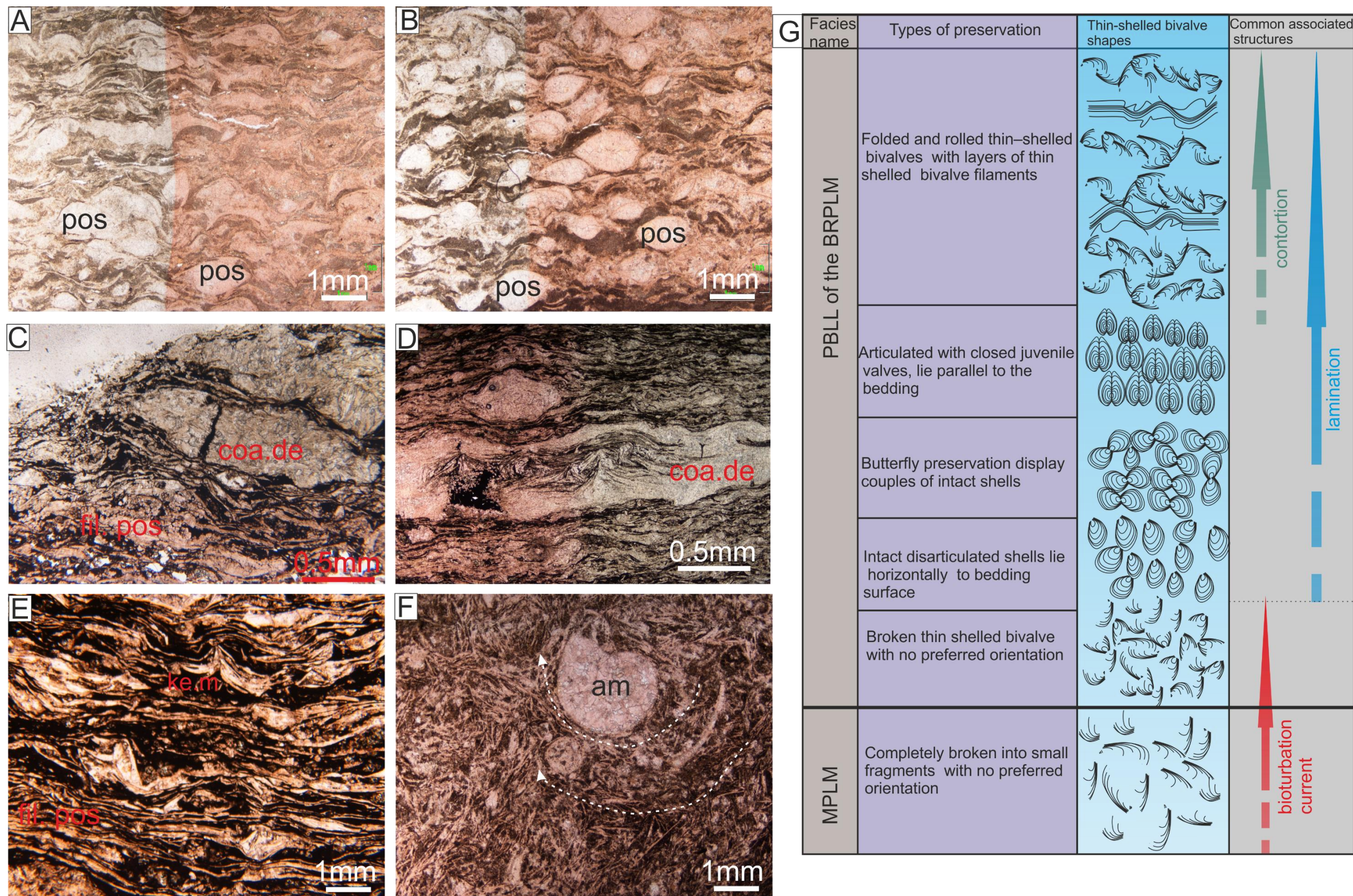


Figure 3.14: thin-shelled filamentous packstone showing: A: horizontal disarticulated textures, which usually include unbroken *Posidonia* valves (pos), PPL, alizarin red S, Hanjera location. B: articulated *Posidonia* valves (pos) lying parallel to the bedding plane, note all fossils are filled with calcite cement, PPL, Alizarin Red S, Hanjera location. C: local dominance of thin-bivalve coalescent debris (coa.de), note saturation of the fracture pores with kerogen PPL, Alizarin Red S, Hanjera location. D: internal structures of coalescent debris showing intense folded and rolled *Posidonia* valves PPL, Alizarin Red S. E: irregular and fractured filamented *Posidonia*, Hanjera location. F: intensely fragmented shells, note broken thin-shells of *Posidonia* wrapping (white dashed curves) around rigid ammonite (am), PPL, Alizarin Red S, Hanjera location. G: A sketch representing the distribution of different kinds of thin-shelled bivalve preservation and associated structures in the PBLL.

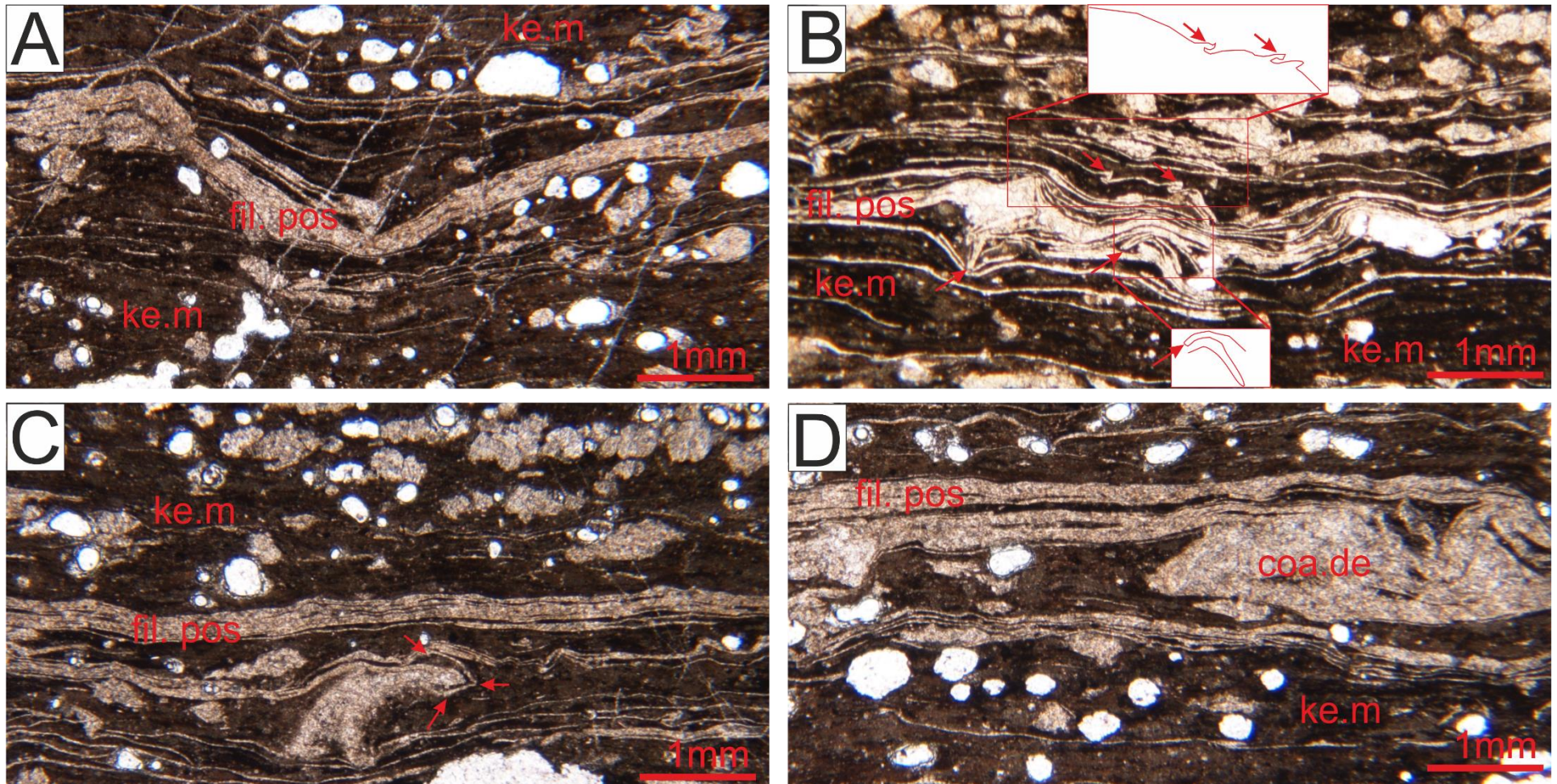


Figure 3.15: photomicrographs of thin-shelled filamentous wackestone and packstone showing different stages (from A–D) of transformation from parallel layers of *Posidonia* filament (fil pos) to the coalescent debris (coa de). A; filamentous wackestone (fil pos) aligned parallel to bedding and rich in kerogeneous material (ke. M). B; Layers of thin-shelled bivalve filaments showing the folded form (red arrows). C; rolling (red arrows) and D, coalescent debris formation, all photomicrographs are from Barsarin location. .

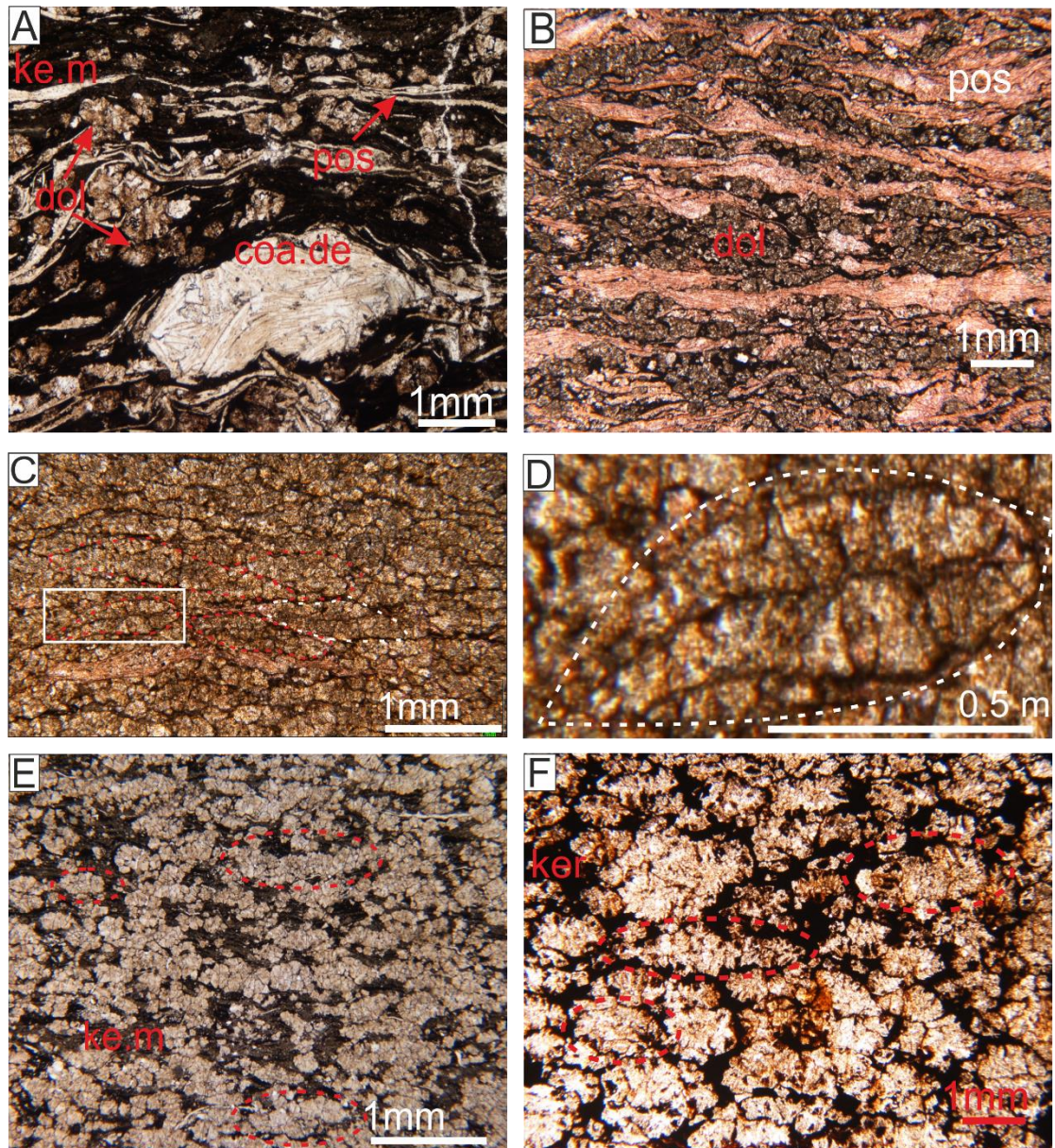


Figure 3.16: photographs (A–F) showing gradual upward increase in elongated lensoid bodies: A: scattered dolomite (dol) crystals between *Posidonia* filaments (pos). Note, the coalescent debris made of accumulation of thin-shelled bivalves, Banik location. B: alternation between *Posidonia* filament (pos) and elongated lensoid bodies clusters of dolomite, Gara location. C: photomicrograph showing elongated bodies, which are formed by clusters of equigranular dolomitic crystals (red dashed lenticular shapes) with few *Posidonia* filaments, Barsarin location. D: Detail of white rectangular of figure (C) showing single elongated lensoid bodies (white dashed lenticular shape). Each singular lensoidal structure usually comprises two parallel rows of dolomite crystals. E: dominance of elongated lensoid bodies with kerogene material (ke. M), Hanjera location. F: clusters of equiangular dolomitic crystals (red dashed lenticular shape), with few rosette-shaped crystals floating in the kerogeneous matter, Banik location.

### 3.6 Interpretation

#### Introduction

In this study, the limestone beds of the upper part of Sargelu Formation, which are characterized by the dominance of *Posidonia* fossil, have been named posidonia-bearing limestone lithofacies (PBL). The Tethys Ocean is well-known for many events of mass accumulations of thin-shelled bivalves, yet the three intervals described here represent the most prominent events that have been recorded throughout the Mesozoic Era:

a–Triassic period; mass accumulations of thin-shelled bivalves with thin filaments-like structures are assumed to represent occurrences of halobiid and pectinid bivalves of the *Entolium* group (Parrish et al., 2001; Schatz, 2005; Waller and Stanley Jr, 2005; McRoberts, 2011).

b–Jurassic period; although mass accumulation of thin-shelled bivalves have been found in many parts of the world during Bajocian Early Callovian, the Toarcian *Posidonia* Shale is one of the most well-known events when the mass accumulation of thin-shelled bivalve occurred in the same stratigraphic interval, described in different areas around the world (Imlay, 1963; Oschmann, 1993; Caswell et al., 2009; Trabucho–Alexandre et al., 2012). The thin-shelled bivalve *Posidonia* of the Jurassic period are attributed to protoconchs or/and posidoniid bivalves (Flügel, 2004).

c–Middle Cretaceous period; which is represented by *Posidonia* filament lumachelles, and no attribution to a genus has been proposed (Navarro et al., 2008; Negra et al., 2011).

Although *Posidonia* events occurred at different periods in the Mesozoic Era, they were all consistent with deposition in a pelagic setting with high faunal productivity, and their facies are usually characterized by the dominance of monospecific assemblages (Imlay, 1963; Conti, 1986; Oschmann, 1993; Parrish et al., 2001; Röhl et al., 2001; Schmid–Röhl et al., 2002; Schatz, 2005; Waller and Stanley Jr, 2005; Caswell et al., 2009; Trabucho–Alexandre et al., 2012; Baumgartner and Föllmi, 2013). The frequent occurrences of thin-shelled bivalves in organic-rich shale are very common, which may imply that they could survive in low oxygen conditions (Kauffman, 1978; Kauffman, 1981; Jenkyns, 1988; Wignall and Simms, 1990; Oschmann, 1993; Wignall, 1993; Etter, 1996; Röhl et al., 2001; Schmid–Röhl et al., 2002; Caswell et al., 2009; Meesook et al., 2009).

There are no modern analogues for the massive accumulation of *Posidonia* in the Recent Oceans, so depth of depositional environment is difficult to determine, but based on studying the associated ammonite fossils, Meesook et al. (2009) have estimated the depth of a *posidonia*-rich basin as several hundred metres. Furthermore, sedimentological features such as black shale and chert bands, and associated fossils such as planktonic foraminifera, ammonite, and radiolarians, may suggest that this member could represent deposition in the deep-marine environment.

### 3.6.1 Preservation type and environment

Both field and petrographic observations demonstrate that the *Posidonia* fossils have been preserved in several different styles, such as, butterfly, horizontal disarticulated valves, articulated with closed valves, cone-in-cone preservations, and the shells display considerable variation with respect to the degree of shell integrity, and orientation (Figure 3.12, A–F) and (Figure 3.14, A–G). Although these various types of preservation occur in intervals (decimetres to metre) that usually alternate with each other, the sections normally demonstrate dominance of fragmented bivalve shells at the base which passes into butterfly and articulated *Posidonia* gradually, whereas the folded and rolled thin-shelled bivalves mainly occur in the upper part of the Sargelu Formation. The variations of the *Posidonia* preservation could be related to the depositional environments, as explained in the following points:

#### **Intact or fragmented bivalve shells**

The presence of intact and well-preserved pelagic thin-shelled bivalves suggests a low-energy depositional environment probably below fair-weather wave base, whereas randomly oriented and fragmented thin-shelled bivalves probably imply shallower depth where the storm event conditions are able to disturb the sea bottom (Negra et al., 2011) (Figure 3.12, D) and (Figure 3.13, B). However, care has to be taken with this interpretation because compaction can also cause breakage of the thin bivalve shells (Rivas et al., 1997).

#### **Butterfly**

Butterfly preservation consists of intact shells (Figure 3.12, E) lacking bioturbation, and characterizes the middle part of the PBLL. It is underlaid by intact disarticulated thin shells. Schatz (2005) has found similar thin-shelled bivalve preservation in the Triassic period, and examined proposed modes of life, in order to apply these criteria

investigations in the field of taphonomy, shell morphology, and spatial and facies distribution. Based on interpretation, the butterfly preservation of Sargelu Formation, may suggest low velocity currents and slow decay of articulating ligament in oxygen deficient waters. It can be suggested that butterfly preservation indicates autochthonous accumulation of *Posidonia*.

### **Articulated and cone-in-cone *Posidonia***

The articulated *Posidonia* with closed valves are characterized by horizontal orientation of shells, and have been reported from deposits intra-or interplatform basin strata (Figure 3.13, C) and ( B), whereas cone-in-cone and randomly oriented shells may point to platform-slopes (Figure 3.12, C) (Schatz, 2005). The sagittal planes of articulated *Posidonia* are always horizontally orientated, and shells are resting on their more inflated valves, which may represent normal life position (Schatz, 2005). Therefore, the articulated shells are assumed to be preserved in life position.

### **Folded and rolled thin-shelled bivalves**

The folded and rolled thin-shelled bivalve textures are rich with dispersed coalescent debris, and are common in all Sargelu Formation sections (Figure 3.14, D–F) and (Figure 3.15, A–D), and their contribution increase gradually upward across the sections. They also represent the dominant kind of preservation in comparison with those other kinds. Similar structures of folded *Posidonia* filament shells have been observed by Navarro et al. (2008) and (Negra et al., 2011) in the Middle Cretaceous of Tunisia, and the Middle Jurassic of Spain. These textures have been interpreted as having formed through compaction, with a solid fragment serving as a rigid obstacle above which the filaments have been broken or upturned. However, in addition to the assumed compaction that led to the broken bivalves, micro- and macrostructures are evidence that may suggest other reasons such as mass transportation and redeposition for occurring folding and rolling structures in Sargelu Formation, as the following.

- a) Breakage of the thin shells by compaction effects can probably be excluded because some layers of *posidonia*-bearing limestone are not folded or broken even though they are directly above or below beds that contain broken, folded and rolled *Posidonia* (Figure 3.11, D).

- b) Thin bivalve shells are clearly rolled tangentially around ammonite shells or rigid materials (Figure 3.14, F) and (Figure 3.15, C).
- c) Large slumping structures association that indicates redeposition (Figure 3.8, A–C) and for more detail see next chapter.
- d) Existence of a significant amount of *Posidonia* coalescent debris within folded and rolled shells, which is more consistent with lithified grain transportation through rolling (Figure 3.14, C–D).

However, it seems that not all broken thin shelled bivalves represent transportation and redeposition, where at the initial stages of the *Posidonia* appearance in the MPLM, the broken shells show: (i) random spread of could suggest the current impact on broken shells (more detail in Chapter 6), (ii) bioturbation association, which could be one of the reasons that led to the broken shells as well (Figure 3.6, 2B).

### 3.6.2 Associated fossils

*Posidonia*-bearing sediments of the Sargelu Formation are characterized by a low diversity and high abundance of *Posidonia* fossils. The *Posidonia* are abundant in monospecific assemblages with the association of rare ammonites, *protoglobigerina*, and radiolarians. Low diversity and high abundance of monospecific assemblages of thin-shelled bivalves, which are more tolerant to oxygen deficiency, is a common scenario in organic-rich deposits, and are reported by many authors (Parrish et al., 2001; Röhl et al., 2001; Schmid–Röhl et al., 2002; Schatz, 2005; Waller and Stanley Jr, 2005; Caswell et al., 2009). Close relationships between *Posidonia* with either black shale or global Oceanic Anoxic Events (OAE) are well documented (Jenkyns, 1988). Paucity of associated fossils in the PBLM probably represents an ecological response to low oxygen marine conditions, which are generally considered to be above the tolerance of the majority of the fauna.

In addition, the lack of associated benthonic organisms can be easily assumed due to well-preserved lamination in the black shale facies has studied thin-shelled bivalves of Western Interior basin, in North America. He found that the predominantly non-burrowed and well-laminated strata indicate low oxygen or dysaerobic benthic oxygen levels. Additional evidence on low oxygen condition may be indicated by lack boring, micritization and encrustation of shells (Navarro et al., 2008; Negra et al., 2011).

### 3.6.3 Mode of life of *Posidonia*

Thin-shelled bivalves do not have a counterpart in recent oceans, so their mode of life has been a subject of intense controversy for the last five decades. Pseudoplanktonic and benthic mods of life are the two most plausible interpretations:

- (a) Pseudoplanktonic;** previous speculation on the mode of life of *Posidonia* was a pseudoplanktonic life habit (Seilacher, 1982). This was largely based on the functional morphology, and the assumption that the constant anoxic sea bed could not support epifauna. There have also been cases observed where *Posidonia* attached to driftwood. Subsequently, Wignall and Simms (1990) have stated that the presence of pseudoplanktonic mode of life for different kinds of posidoniform such as *Posidonia*, *Bositra* can be considered very rare in the fossil record, and pseudoplanktonic mode occurs only a minor proportion of the fauna in organic-rich mudstones or black shales.
- (b) Benthic mode of life;** this mode of life depends on the oxygen level fluctuates on the seafloor. Based on results obtained from palaeoecological analyses of benthic fauna of the Early Toarcian, Kauffman (1978), and Kauffman (1981) pointed to strong oxygen fluctuations. Thin-shelled *Posidonia* is considered a taxon resistant to low oxygen condition. Fluctuations of the redox boundary curve are in good accordance with thrive and distinction of fauna, where very short of the oxygenate period may be led to flourish benthic fauna. This Interpreted mode of life is supported by many researchers such as Wignall and Simms (1990), Oschmann (1993), Schatz (2005), Etter (1996), Röhl et al. (2001) Schmid-Röhl et al. (2002), Röhl (2005), Caswell et al. (2009), and McRoberts (2011). They all have suggested that the *Posidonia* "*Bositra*" organic-rich shales, which have been inferred as epibenthonic organisms, could form in low oxygen environments but not anoxic bottom waters. Benthic organism that adapted to low O<sub>2</sub>-values as a mode of life for much longer than the life cycles is one of a probability.

Because Toarcian *Posidonia* shale has regarded as the main source rock in the onshore part of the Central European Basin System (Littke et al., 1991), its environments have been studied in detail. Toarcian *Posidonia* Shale, was deposited during an OAE that was widespread across Europe has been chosen as exemplary embodiment to describe and help the understanding mass accumulation of *Posidonia* fossils of Sargelu Formation.

Many sections of the *Posidonia* shale in SW-Germany studied by Rohl et al. 2001, using high-resolution geochemical, sedimentological and palaeoecological investigations. The

results suggest that oxygen availability was variable, which ranged from long-term anoxia to short oxygenated periods. The short periods of oxygenated bottom water conditions were indicated by some benthic macrofauna intervals such as, thin-shelled bivalves.

Based on size–frequency distributions, density of growth lines related to shell size of *Bositra buchi* (formerly *Posidonia*), and total organic carbon (TOC) Röhl et al. (2001), and Schmid–Röhl et al. (2002) have re–evaluated the mode of life of the thin-shelled bivalves. As following:

- They have revealed that a fast growth is indicated by low density of growth lines and relatively large average sizes about 13 mm, characterizing appropriate life conditions at the sea floor. In contrast, a very small average size 5 mm and dense growth lines point to reduced oxygen availability within the benthic environment. This evidence suggests that variations in seafloor oxygen variations can be linked to changes in growth rate in the *Posidonia* they were probably benthic fauna.
- The monospecific and mass occurrence of tiny post-larval and juvenile bivalves of 1–2 mm in size are common in studied sections. Their textures are characterized by a distinct wavy lamination and usually occur in relatively rich organic carbon content intervals. Based on Schmid–Röhl et al. (2002) this kind of juvenile accumulation may indicate very short oxygenated periods possibly only a few weeks in duration, and they died because of new anoxic condition that occurred soon after colonizing the sediment surface (Figure 3.13, C) and (Figure 3.14, B).

The studied *Posidonia* of the Sargelu Formation, in many respects, are comparable to the Early Toarcian *Posidonia* shale. Evidence for an inverse relationship between the TOC and density of growth lines related to shell size *Posidonia* prominently noticeable at upper part of the Sargelu Formation as well (Figure 3.12, F). So, occasional mass occurrences of larger-sized *Posidonia* which have been recorded at lower part of the BRPLM may indicate oxygenated benthic conditions. In contrast, the occurrence of smaller examples of thin-shelled bivalves at the upper part of the BRPLM, which is characterised high TOC, are clearly observed. The gradual upward decrease in *Posidonia* size could be attributed to the decline of seafloor oxygen.

Furthermore, recently, Caswell et al. (2009) have re–investigated horizons of the marine mass extinction interval that occurred during Pliensbachian–Toarcian boundary. They found that *Pseudomytiloides dubius*, which is thin-shelled bivalve, is the only abundant benthic macro-invertebrate survived in the most hostile environmental conditions, i.e. low oxygenate, whereas all other benthic species are almost completely absent for many

thousands of years directly after each abrupt negative carbon isotope excursion. Also, Etter (1996) analysed taphonomic patterns of the thin-shelled bivalve, and found that postulated gradient of decreasing oxygen is correlated with a gradually increasing articulation ratio. It has been also observed that the bioturbations decrease with gradual oxygen depletion.

#### 3.6.4 Age

The thin-shelled bivalves are represented by *Posidonia ornati* Quenstedt, which have been observed for first time by Wetzel in 1948 (internal report of Geological Survey of Iraq) in the Sargelu Formation type section (Bellen et al., 1959). Based on Imlay (1945; 1963; and 1964); Waller and Stanley Jr (2005), and Cant (2001), the *Posidonia ornati* can be considered as an indicator for Bajocian to Callovian age, and they similarly have been found in the pelagic environment. The *Posidonia*-bearing limestone lithofacies is principally constituted by thin-shelled bivalves and are accompanied by *Kosmoceras* species of ammonite. The Middle Callovian age is also ascertained through recording *Kosmoceras* species of ammonite fossils. The *Kosmoceras* has occasionally been recorded from the Callovian of the Middle East, though it is much more common to the north in the Caucasus (Kiselev et al., 2013).

### 3.7 Radiolarian Bedded Chert Lithofacies (RBCL)

#### 3.7.1 Field description

The radiolarian bedded chert lithofacies (RBCL) is thin to medium-bedded, dark grey to black in colour. The thickness of chert beds ranges mainly from 5 to 10 cm (Figure 3.17, A–B). The bedded cherts normally extend laterally several hundred metres (Figure 3.17, C), but they can also appear as short lensoidal shapes 10–100 cm. Perhaps the most prominent feature in the bedded chert is a symmetrical triple-layered structure (Figure 3.17, D–E): a middle black siliceous layer sandwiched between upper and lower yellowish–brown layers. Some scattered rip–up clasts of bedded cherts were found within the *posidonia*-bearing limestone lithofacies (PBLL) (Figure 3.11, E). Imprinted ammonite moulds on the bedding surfaces are common (Figure 3.17, F), but their taxonomic identity cannot be determined with confidence due to poor preservation.

The bedded cherts are normally interbedded with both *posidonia*-bearing limestone lithofacies (PBLL) and back shale and argillaceous limestone lithofacies (BSALL) (Figure 3.17, B). The RBCL at the upper part of the Sargelu Formation, which has been recorded in all localities, extends laterally for hundreds of kilometres. Their black colour and

siliceous lithology makes them easily distinguishable in the studied area, so it can be used as a marker bed at the Middle and Upper–Jurassic boundary.

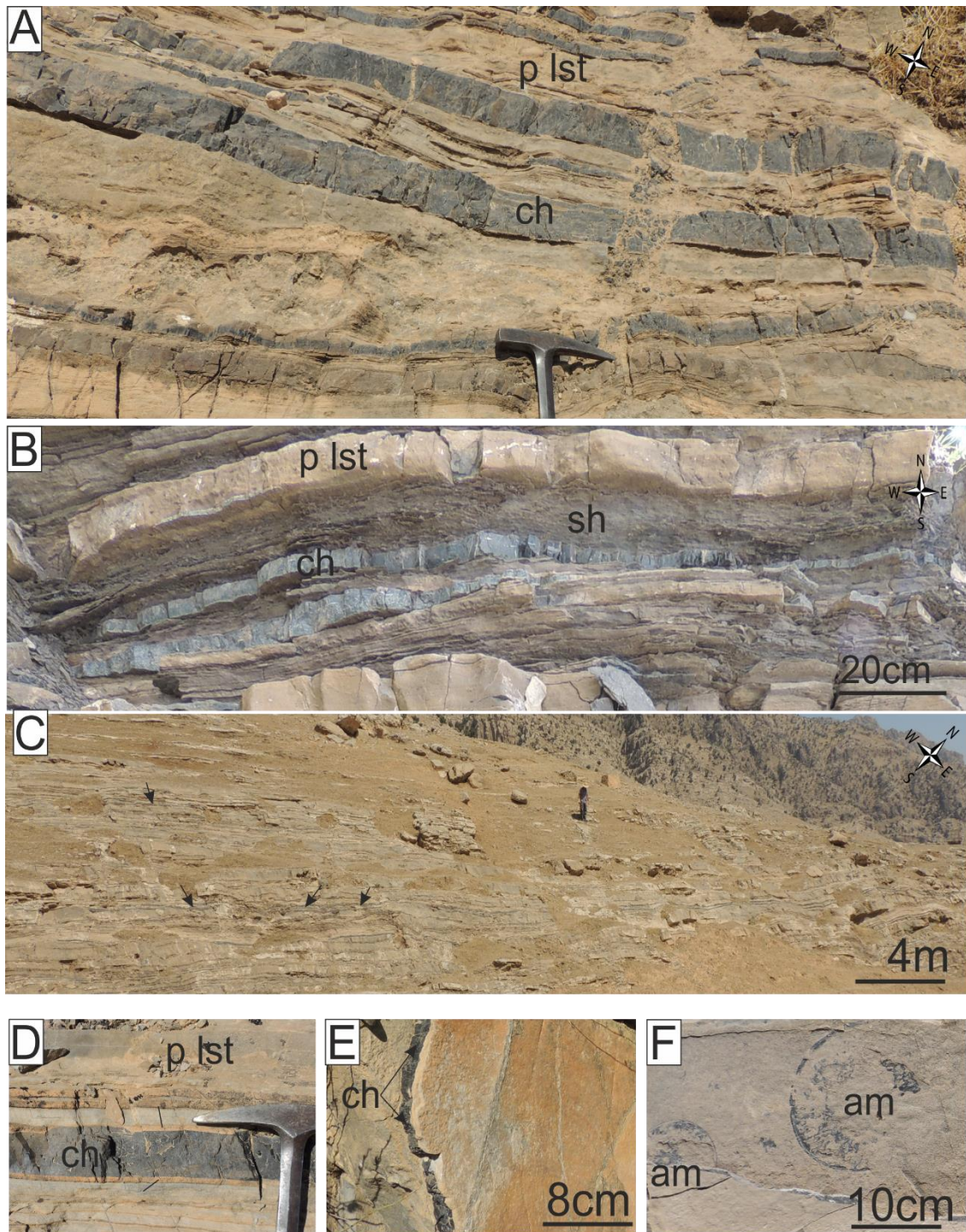


Figure 3.17: A; thin to medium–bedded cherts alternating with, *Posidonia*-bearing limestone, Hanjera location. B; interbedding between bedded chert, *Posidonia*-bearing limestone, and black shale, Banik location. C; general sight of the upper part of the Sargelu Formation showing dominance of bedded chert (black arrows), Hanjera location. D; Close–up photograph showing structures described as triple–layered of bedded chert (ch) E; bedding surface of bedded chert (ch) showing yellowish–brown colour of triple–layered structure F; bedded chert surface showing imprinted ammonite moulds (am), the photographs from D to F are from Barsarin locality.

### 3.7.2 Microscopic description

Microscope study shows that the bedded chert is principally composed of two different lithologies; i) radiolarian chert (Figure 3.18, A), and ii) silicified *Posidonia* layers (Figure 3.18, B). The former represents the major constituent of the bedded chert, whereas the latter is observed only in a few cases. The silicified *Posidonia* layers, distinguishable for possessing lamination (Figures 3.18, B; and 3.19, C), always co-exist with radiolarian chert, but the contacts between them are normally sharp (Figure 3.18, B). A detailed description of these two types of bedded silica is as follows:

**1- Radiolarian chert:** The matrices in the radiolarian chert are commonly light brown in colour, and gradually turn into darker brown around the radiolarian tests (Figure 3.18, C). The matrix background demonstrates a richness of scattered black spots, up to 0.5–0.2 mm across (Figures 3.20, A–C; and 3.21 A–C), each of which probably represents a different cross-sections of radiolarian tests.

Densely packed radiolarian fossils may make up over 85% of the bulk of the bedded chert. The radiolarian shells are homogeneously distributed in the bedded chert, and no terrigenous associations have been observed (Figures 3.18 A–C; and 3.20 A–C). Although the majority of radiolarian tests are severely damaged in terms of dissolution, their traces can be seen as small circular or irregular holes filled with silicate and organic materials (Figures 3.18, A; 3.19, A). Classification of radiolarians is difficult due to the poor preservation (3.20, A–C). Only a few relatively well-preserved tests have been recognized, which perhaps represent *Cinguloturris carpatica* Dumitrica fossil 100–300 µm in size (Figure 3.21, A–C). Besides, the bedded radiolarian cherts occasionally include a few partially or completely silicified, broken and folded thin-shelled bivalves that often lie parallel to the bedding surfaces. Additionally, some scattered silicified *Posidonia* coalescent debris were observed (Figure 3.19, A–B).

**2- Silicified *Posidonia*:** This type of bedded chert consists of partial or complete silica replacing the pre-existing carbonate rocks, and they are normally interlayering or overlaying the radiolarian chert within a singular bedded chert. It comprises densely-packed thin bivalve's packstone that lie parallel to the bedding surface, and usually alternate with the radiolarian cherts (Figures 3.18, B; and 3.19, C). It also includes some lensoidal bodies up to 0.9 mm in length and 0.4 mm across that are composed of silicified clusters or scattered single-crystals of dolomite. The amount of these crystals varies greatly from place to place, and they may show gradually increasing in amount upward with regards to the *Posidonia* contribution (Figure 3.19, C).

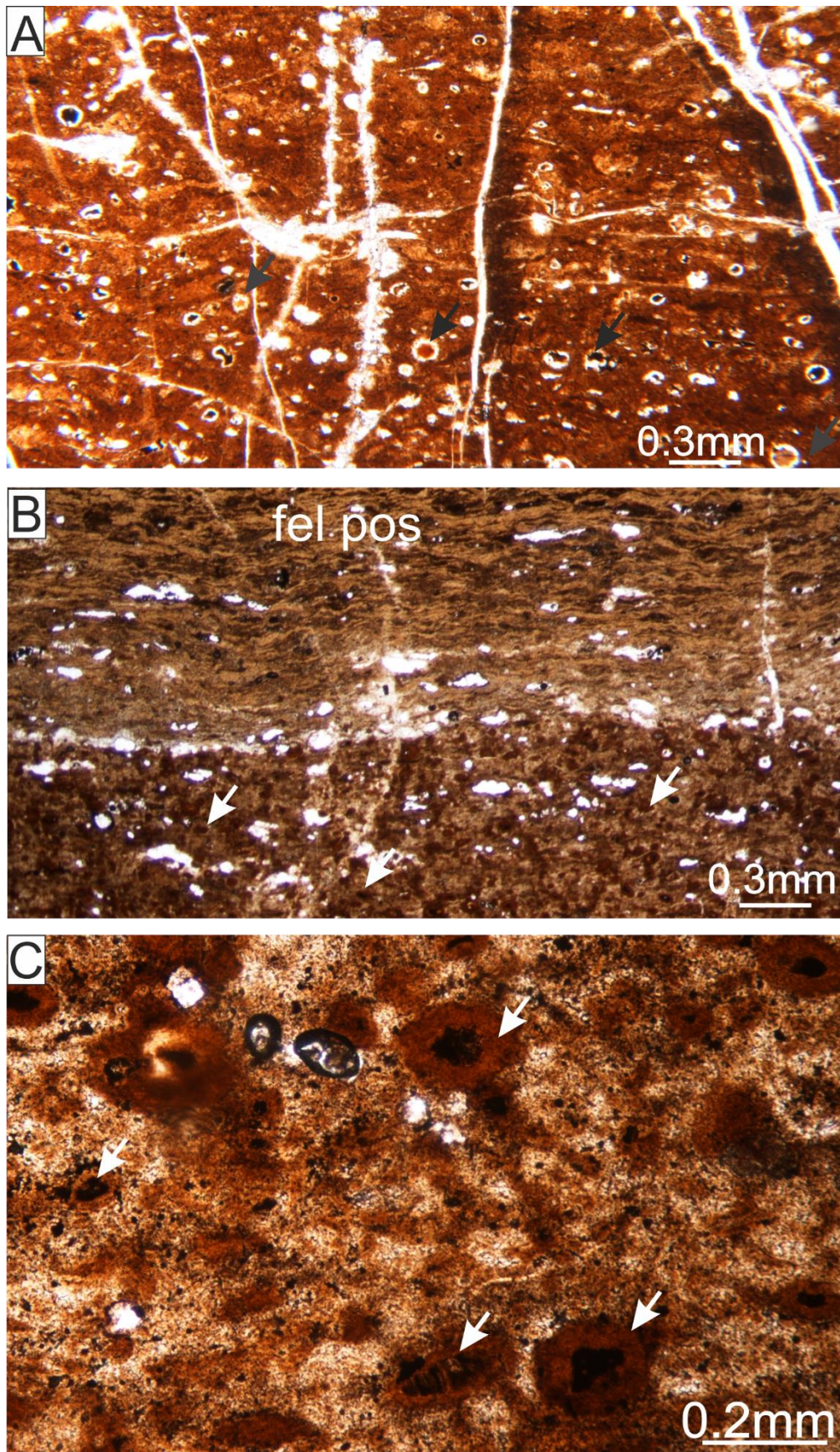


Figure 3.18: A; bedded chert showing numerous dissolved radiolarian tests (black arrows). B; photomicrograph showing both radiolarian chert at the bottom, and silicified filamentous *Posidonia* (fel pos) at the top of the photograph. Note the sharp boundary between them. C; close-up photomicrograph of bedded chert showing dark-brown coloured radiolarians (white arrows). All photos are PPL, Hanjera location

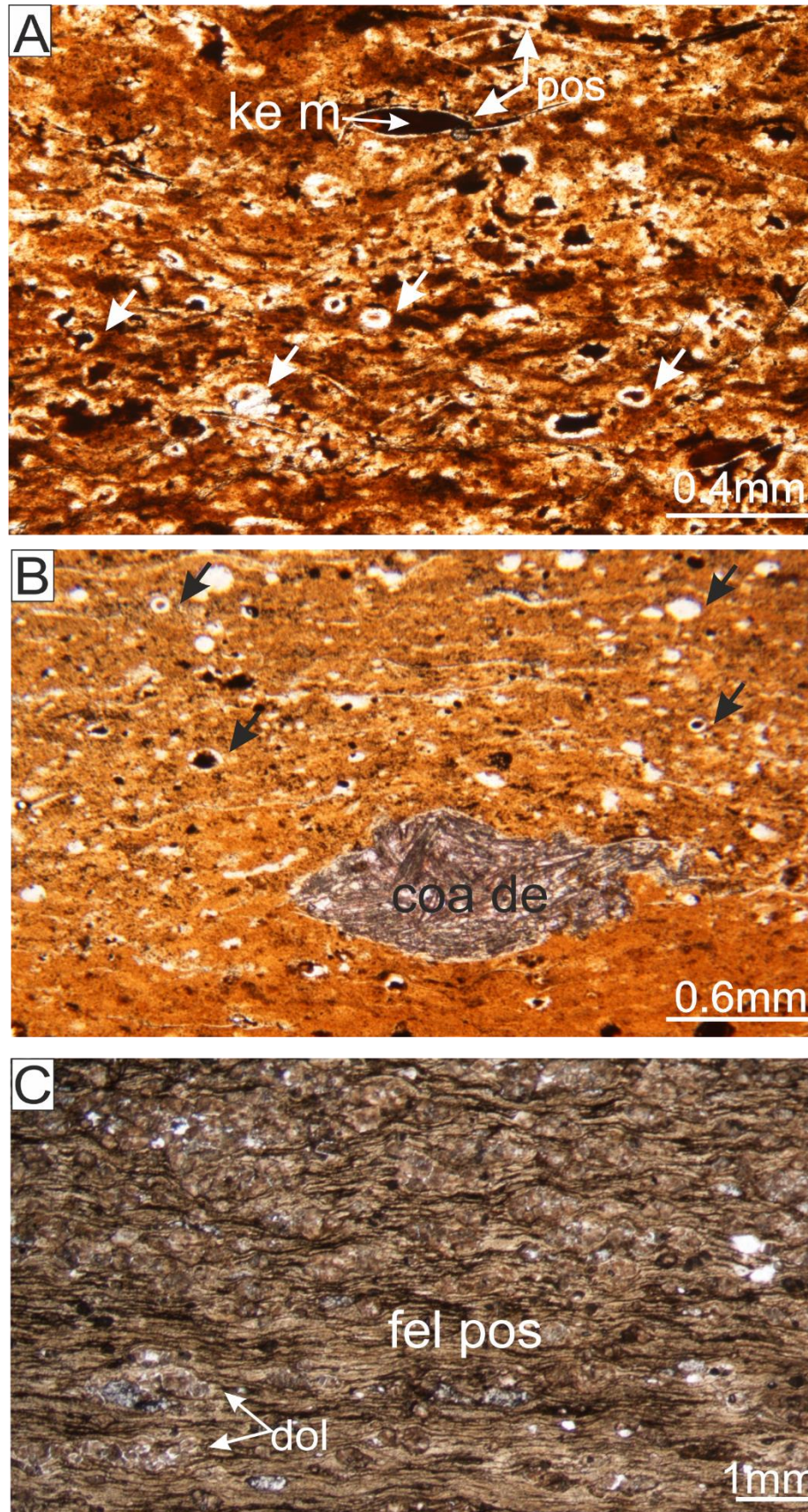


figure 3.19: A; bedded chert showing radiolarian pore–space and sheltered pores filled with kerogeneous matter (Ke m), note scattered *Posidonia* shells. B; bedded chert showing silicified coalescent debris, black arrows pointing to the radiolarian trace. C; completely silicified filamentous *Posidonia* comprises densely packed thin bivalves which lie parallel to the bedding surface; note proportion of dolomite crystals (dol) gradually increased upward. All photos are PPL, Gara location.

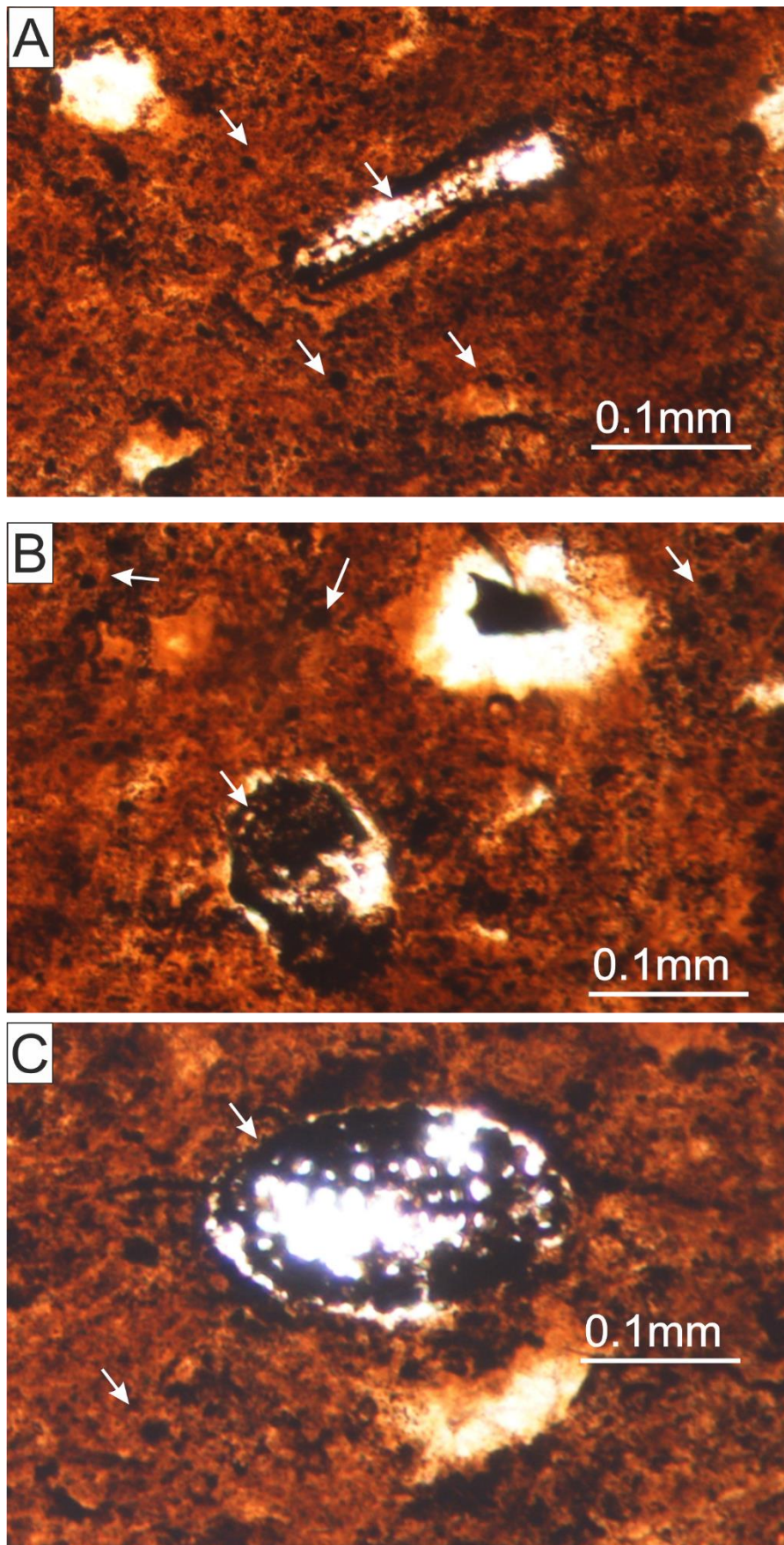


Figure 3.20; photomicrographs bedded chert with various kinds of radiolaria; their origin cannot be ascertained, due to the poor preservation of their outer wall. Note the groundmass contains a great number of perhaps radiolarian test ghosts (white arrows) Banik location.

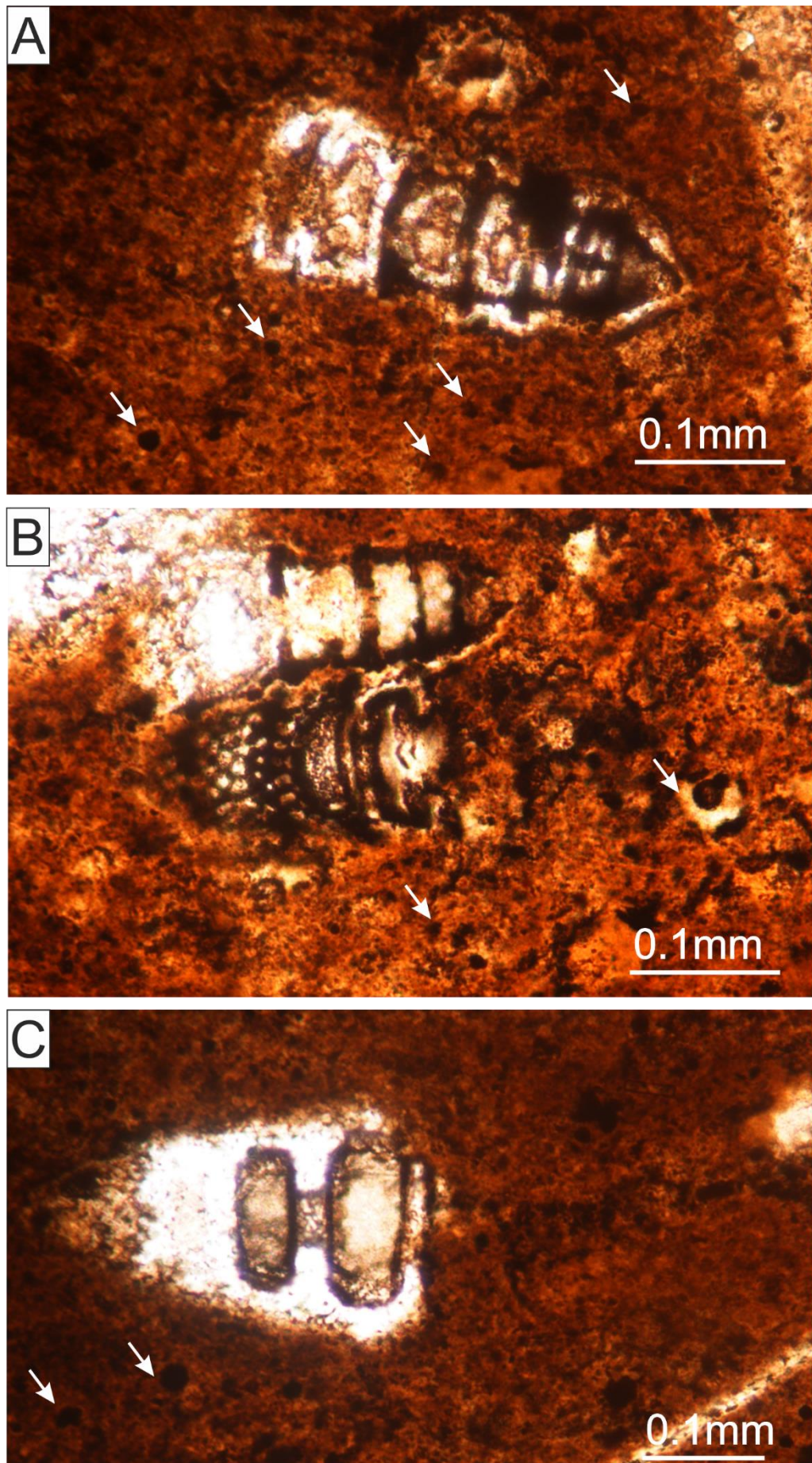


Figure 3.21: (A–C) photomicrographs showing *Cinguloturris carpatica* Dumitrica. Note the groundmass contains a great number of perhaps radiolarian test ghosts (white arrows). All photos are PPL, Chnaran Location.

### 3.7.3 Interpretation

Introduction:

Microcrystalline quartz can be precipitated directly from silica saturated water in some local basins, perhaps as a consequence of volcanic ash dissolution. In contrast, the modern and ancient ocean waters are grossly undersaturated with respect to silica precipitation, where the average dissolved silica concentration is about 1–4 ppm (Heath, 1974). Therefore, it is unlikely that chalcedony or microquartz of bedded chert was precipitated directly by inorganic processes from highly undersaturated ocean water. Such processes cannot account for many bedded successions of nearly pure chert that occur in the geologic record.

Bedded cherts are products of a wide variety of different depositional environments and diagenetic processes, which are reflected by differences in rock type (Figure 3.22). They can be subdivided into four main groups depending on type and abundance of siliceous organic constituents (Boggs, 2009):

- 1- Diatomaceous deposits.
- 2- Siliceous spicule deposits of invertebrate organisms, particularly sponges.
- 3- Bedded cherts containing few or no siliceous skeletal remains.
- 4- Radiolarian deposits.

For the Sargelu Formation, the most widely accepted possible origin of bedded chert sources is radiolarians because large amounts of radiolaria are found in them (Figures 3.18–3.21). The first three groups cannot be considered as a silica source for this formation simply because diatomaceous deposits have occurred in rocks since the Cretaceous, and no sponges were observed.

Radiolarians are single-celled silica-secreting planktonic organisms. The earliest known rare radiolaria date back to the Early Cambrian period, but the most prolific appearances of radiolarians were recorded from the Ordovician to the Early Cretaceous Periods, during which the radiolarians were considered important rock-formers (Jonse and Murchey 1986) (Figure 3.22). From the Late Cretaceous onwards, the radiolarian's role as rock-formers was reduced in the pelagic environments, perhaps as a consequence of the dominance of foraminifers, coccolithophorids, and diatoms (Jonse and Murchey, 1986).

The previous evidence suggests that the principal silica source for the bedded chert strata in the Sargelu Formation is biogenic silica from opal-secreting radiolarian organisms. The transformation of the silica polymorphs from opal-A to opal-CT (cristobalite / tridymite) to chert is a common diagenetic process in muddy sediments that contain significant quantities of opaline skeletal remains, such as radiolarian oozes. So, the possible source of silica in the Sargelu Formation is dissolution of the opaline skeletons of radiolarians. The rate of silica diagenesis is controlled by many factors, including time, interstitial-water, temperature, Ph, and lithology (Boggs, 2009; Jonse and Murchey, 1986).

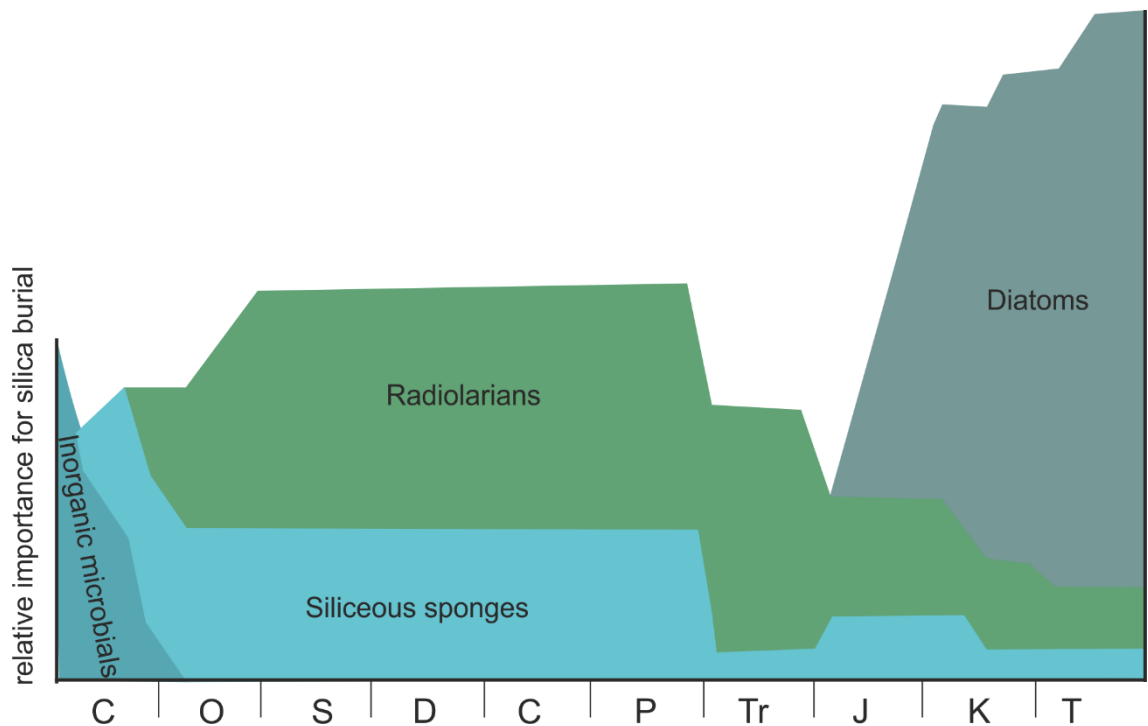


Figure 3.22: diagram showing the relative role of different organisms for extraction of silica from seawater since the beginning of the Cambrian Period (modified from Kidder and Erwin, 2001)

### 3.7.3.1 Age

Although bedded chert of the Sargelu Formation has several types of radiolarians, only *Cinguloturris carpatica* Dumitrica was identified (Figure 3.21, A–C) because most other radiolarians are poorly preserved (Figure 3.20, A–C). Radiolarians are of great importance as an age and bathymetric indicator (De Wever, 1989). The well-controlled taxa *Cinguloturris carpatica* is found to have appeared for the first time in Late Bathonian and lasted up to Early Callovian (Danelian, 1996; Beccaro and Lazar, 2007; Tekin, 2009; Tekin, 2012; Gorican *et al.*, 2012). Moreover, the determined radiolaria is quite similar to those suggested from the Callovian age of the Mediterranean by Baumgartner *et al.* (1995). Thus, the upper part of the Sargelu Formation with the presence of *Cinguloturris carpatica* Dumitrica could tentatively be dated as Late Bathonian–Early Callovian age.

### 3.7.3.2 Silica preservation and depth

Silica ooze is normally concentrated in modern deep oceans below the CCD forming siliceous oozes composed entirely of biogenic silica of radiolaria tests and diatom frustules. According to Tomescu (2004), bedded chert could also occur above the CCD or beneath shallower waters on the shelf, when these conditions fulfilment: fertile surface water, paucity of calcareous planktonic production, and very low terrigenous sediment input. Nelson (1995) suggested that the radiolarian formation is known to be strongly temperature dependent, and low surface temperatures enhance their preservation. Furthermore, widespread radiolarian chert accumulation could be related to cold-water upwelling current (pope, 2001, 2002, and 2003), which may not be preferred by calcareous fauna.

On the other hand, Jenkyns and Winterer (1982) concluded that the preservation and accumulation of radiolarians can be enhanced by an intense upwelling current for the following reasons: (1) phytoplankton productivity is promoted by high nutrient levels in upwelling systems. This produces a higher rate of radiolarian productivity and deposition of radiolarian-rich deposits, where increased rates of radiolarian deposition act inversely with the rate of dissolution of siliceous skeletons on burial; (2) CCD levels will elevate due to high rates of organic matter production beneath upwelling zones, and this can enhance radiolarian–preservation; (3) high organic content prevents the dissolution of silica by providing a film around the tests. So, the bedded chert of Sargelu Formation may provide a good clue to the high phytoplankton productivities and upwelling current (See section 3.8 for details).

Bedded cherts are regarded as primary accumulations of biogenic silica that can form in both deep and shallow water (Tomescu, 2004). From the total biogenic silica production, 97.5% are recycled to sea water before settling on the floor and only 2.5% will be preserved in the sediment as a biogenic silica ooze (Tomescu, 2004). Although siliceous tests of radiolarian are not resistant to dissolution in the undersaturated oceanic water with respect to silica, they are normally found at the bottom of the oceans. Modern analogues studies on the resistance of radiolarian and diatom shells to dissolution in the sea water reveal that the siliceous tests could be protected from external influences if they are surrounded by organic aggregates or embedded in a fecal pellet. In this case, they can be transported to the bottom of the ocean safely (Schrader, 1971; Ferrante and Parker, 1977; Casey et al., 1979; De Wever, 2014).

Although, its environment is generally interpreted as being deposited under anoxic condition of basinal origin, the exact palaeobathymetry of bedded chert formation in the Sargelu formation is still uncertain (Buday, 1980; Jassim and Goff, 2006; Aqrabi et al., 2010). It cannot be stated with certainty the depth of the bedded cherts, because they lack indicative sedimentary structures or fauna. Leinnen (1979) examined the relationship between dissolution, accumulation rate of biogenic opal and palaeodepth at the different range of depths. The results suggested that radiolarian dissolution was almost independent of depth, where dissolution of radiolarian can occur at the different depth level. So, poorly preserved or partially dissolved radiolarian may not indicate depositional water depth.

Boggs (2009) demonstrated that the radiolarian cherts mainly occur in two different facies: a) associated with mafic volcanic rocks such as pillow basalts, turbidite sandstones, and pelagic limestones, which are an excellent indicator to a deep-water origin; and b) the association between radiolarian cherts and limestones may suggest deposition at shallower depths of perhaps 200–1000 m (Boggs, 2009). So, the latter alternative can be regarded as the most likely facies that can be applied to the Sargelu Formation, especially their facies association with posidonia-bearing limestone supports shallower depositional environment above the CCD.

### 3.7.3.3 The existence of bedded chert

Although radiolarians have been reported from the Middle Cambrian in the Georgina Basin, Queensland, Australia in the relatively shallow water (Won and Below 1999; Won and Aims, 2002), their existences are limited into a narrow range of location and time. It has been noted that the radiolarites are abundantly distributed at the top Callovian and

Late Jurassic Epoch across the Neotethyan regions (Jenkyns and Winterer, 1982), but acme radiolarian events occurred during the Bathonian–Callovian age in the Neotethys realm, Circum–Mediterranean, Alpine Belts, and Zagros mountains (Figure 3.23). It seems that distribution and abundance of radiolarites occurred concurrently with the Neotethys Sea development through the Triassic–Jurassic Periods (Jenkyns and Winterer, 1982).

Bedded chert does not exist in the subsurface sections just about 60 km western to the studied area, whereas no reports in the eastern extension of the Sargelu Formation due to thrusting over Jurassic successions. However, about 60 km south-eastern of the studied area in Kermanshah area, western Iran, massive radiolarian successions of Middle–Late Jurassic have been reported by Gharib and De Wever (2010), which perhaps have links with the Sargelu Formation chert.

The Kermanshah chert are usually underlain or accompanied by ophiolite pillow lavas sequences. However, no ophiolites were observed in the studied sections. These ophiolites are assumed to be derived from the Neotethyan Ocean. De Wever (1996) stated that the long–held assumption of a relationship between the volcanic processes and abundance of radiolarians is incorrect. It is well known today that there is a strong positive relationship between radiolarian abundance in sediments and high-productivity areas and more generally under all water–mass of active upwelling current. The depositional basin of the Kermanshah radiolarian bedded chert is characterised by narrow elongated basin, which extend for hundred kilometres from Turkey to Oman, but are a few tens kilometres in width. Likewise, De Wever, (1989) found that the radiolarian bedded chert is usually intercalated with other sedimentary rocks belonging to nappes in the faulted blocks of a rifting margin.

#### 3.7.3.4 Colour variations in bedded chert

Colours are of great importance in determining the absence or presence of carbonaceous organic material and the oxidation state of iron and other metals in the chert (Jonse and Murchey, 1986). According to De Wever (1995) radiolarian chert could occur in different colours. Black coloured chert called phtanite, it is a term that originally used by French geologists to describe black coloured radiolarian bedded chert; the blackish colour is probably resulted from the organic material (Kremer, 2005; Puelles et al., 2014). The colour variations in bedded chert may also provide information about depositional environments. Black bedded cherts usually indicate a relatively shallow continental margin environment (De Wever et al., 2005; 2001). The black colour of the

bedded cherts in the Sargelu Formation may infer the relatively shallow environment with presence of carbonaceous organic material.

#### 3.7.3.5 Triple-layered structure

The triple-layered structure is perhaps the most distinguishable structure that has been recorded in chert beds at all localities (Figure 3.17, D–E). A similar structure reported by Iijima *et al.* (1985) in the Late Palaeozoic and Early Mesozoic sediments of Neo, Inuyama, and Kuzuu Districts in the Inner Chichibu terrain in Japan. It has been suggested that such structures may be resulted from segregation of silica from a silica gel–clay–water mixture during early diagenetic processes (Iijima *et al.*, 1985).

#### 3.7.4 Radiolarian formation and upwelling current

Today, it is generally agreed that the bedded chert deposits in pelagic waters are regularly linked to periods of high productivity of silica-secreting organisms such as diatoms, and radiolaria. Many studies focus on the hypothesis about a relationship between upwelling current and high radiolarian productivity (Figures 3.24; 3.25, 3.26) (Jonse and Murchey, 1986; De Wever, 1989; Bartolini *et al.*, 1999; Kidder and Erwin, 2001; Flugel, 2010; Voros, 2012). Moreover, mass accumulation of *Posidonia*, which is quite common in the Sargelu Formation, could be explained by the upwelling current zones. There are many examples that illustrate that the upwelling current has a significant impact on the radiolarian chert deposition. These are:

- a. Absence of radiolarites in the Atlantic Ocean in the Early Cretaceous (Figure 3.27) can be linked to the absence of upwelling in this basin and the large distance of this basin from areas of upwelling. (De Wever, 1989; Wever *et al.*, 2014).
- b. Tomescu (2004) noticed the presence of a close relationship between upwelling current and radiolarian bedded chert formation. Accordingly, the chert acmes are estimated to be concurrent with the upwelling by the late Ordovician, whereas an absence of chert abundance in the Early Silurian may reflect sluggish ocean circulation.
- c. Top of the Late Jurassic is distinguished by a complete and sudden disappearance of radiolarites, which may be attributed to a change in circulation from gyres that were producing upwelling in the Tethyan basin (De Wever, 1989). This abrupt biophysical change in the Neotethys is related to the change in circulation due to a latitudinal flow through Central America, which drastically changed the current pattern from a gyre in the Neotethyan basin, and its associated upwelling current (De Wever, 1989).

- d. Long duration of radiolarite deposition on the eastern margin of Oman of the Arabian plate, in Neotethys Sea (Figure 3.24), continued until the Late Cretaceous. This area is inferred to have remained under the influence of the upwelling conditions (De Wever, 1989).

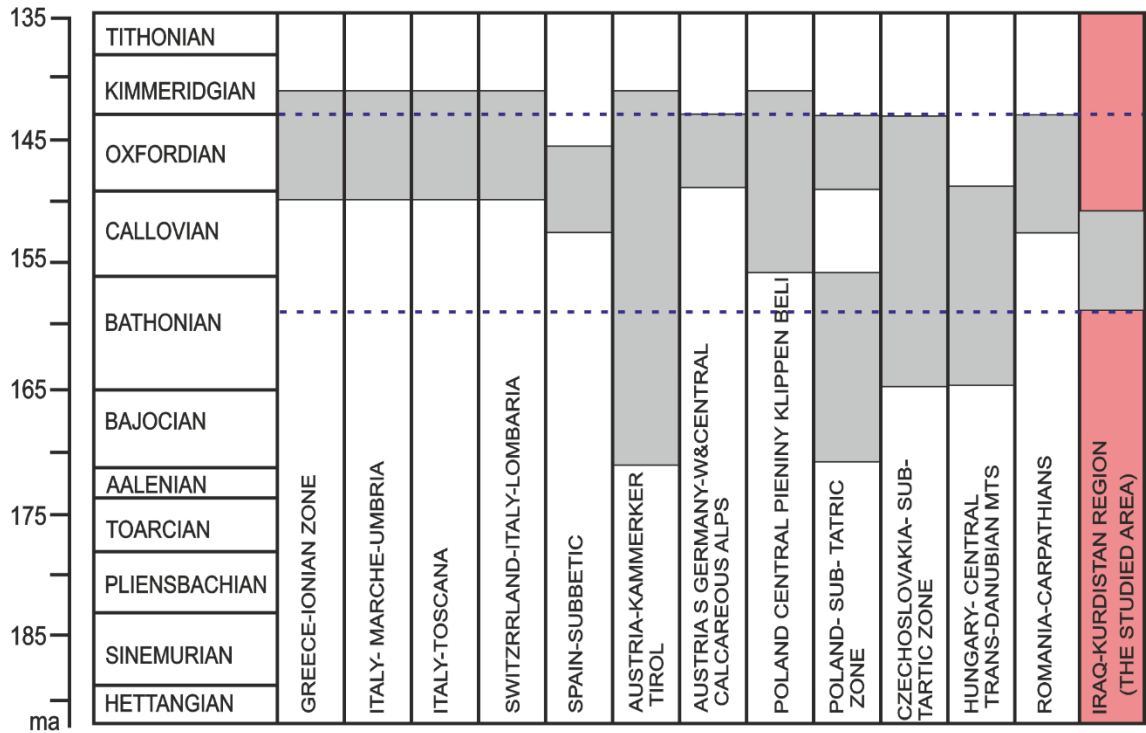


Figure 3.23: Distribution and age of Jurassic ribbon radiolarites in the continental-margin sequences of the Neo-Tethys. Note the radiolarites are usually followed by pelagic facies such as Ammonitico Rosso or pelagic oolites, and are highly diachronous. (Modified from Jenkyns and Winterer, 1982).

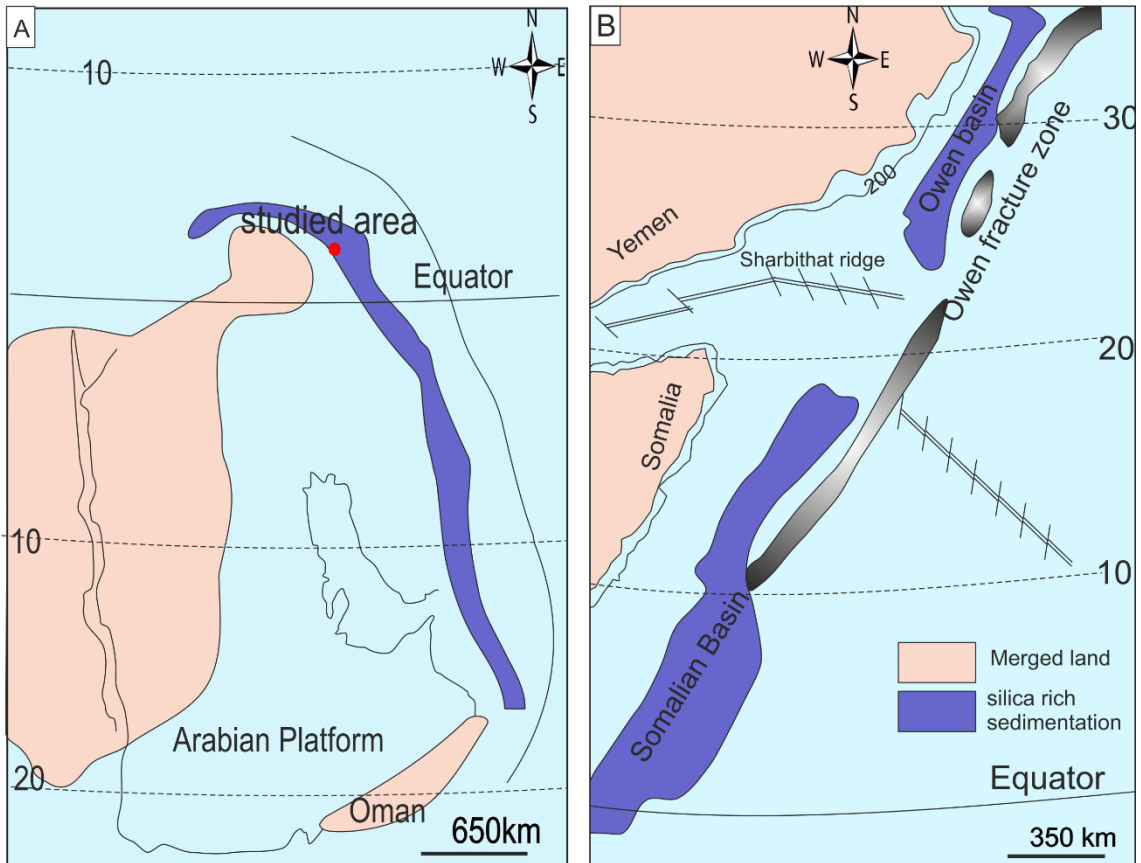


Figure 3.24: Comparison between the Hawasina Basin (A) which could be considered an extension to the studied Sargelu basin of Middle-Jurassic time with modern Somalia and Owen basins (B). Note, both recent and ancient, are at similar zones of intense upwelling. (Modified from De Wever and Baudin, 1996).

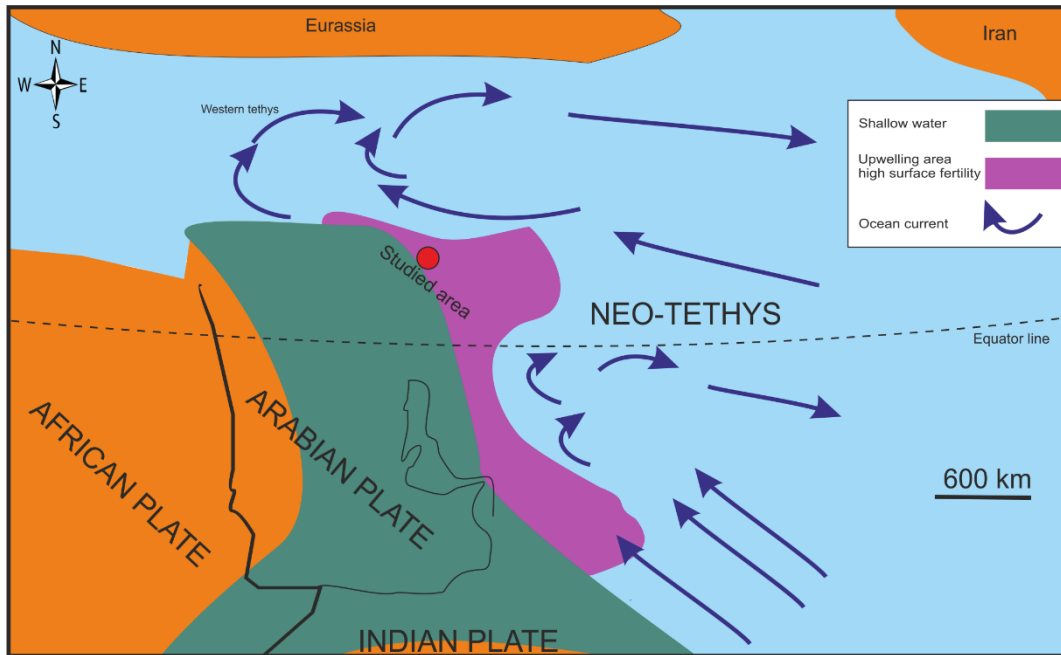


Fig 3.25: diagram showing a simplified upwelling area with high surface fertility and principal sedimentary palaeoenvironments. Note the effects the equatorial current system on the Western Neotethyan of the Arabian Margin and the studied area during Callovian age (modified from Baumgartner and Föllmi, 2013).

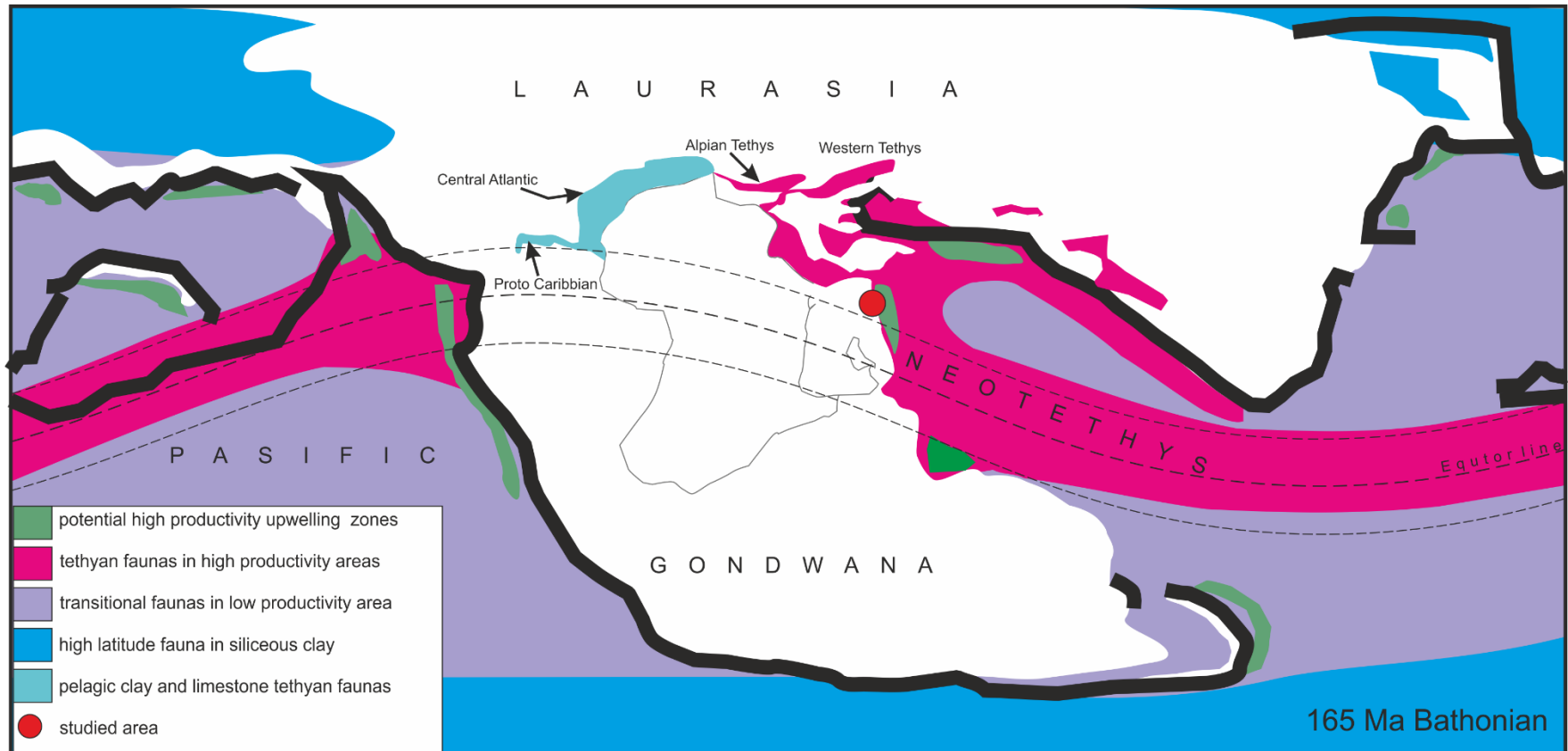


Figure 3.26: Palaeogeographic map showing major oceanic high productivities of radiolarian bio-provenance and potential high productivity upwelling zones during Bathonian age (modified from Baumgartner and Föllmi, 2013).

### 3.8 Potential mechanism for the high-productivity

Radiolarites are defined as chert–shale couplets; this feature was conspicuously common in the Mesozoic stratigraphy of the Neotethyan realm. There are controversial views on what stimulated the palaeo–productivity, and in particular, the exact mechanism for the origin of radiolarites deposits. Based on results obtained from the deep-sea drilling project, Berger and Winterer, (1974), and Hsu and Jenkyns (1974) assumed that the radiolarians may accumulate at depth exceeding 4 km in the calcite compensation depth (CCD) model. In contrast, Baumgartner *et al.* (1985), De Wever (1996), and Baumgartner and Föllmi (2013) found that the long–held assumption of a relationship between deep basinal environments and abundance of radiolarian bedded chert is erroneous. There are well-proven recent analogues in the Somali and Owen basins (Young and Kindle, 1994; Schulz *et al.*, 1996) confirming that radiolarian abundances in sediments are related to high-productivity of fauna and mostly under the ocean of active upwelling current in relatively shallow marginal basins (Figure 3.24). Baumgartner *et al.* (1985) pointed to the prevailing thick units of radiolarites deposition in the narrow troughs of relatively shallow marginal basins in Western Neotethys Ocean during Mesozoic period.

De Wever and Baudin (1996) stated that there are links between productivity of radiolaria and opening events of Neotethys during Middle–Upper Jurassic, Kimmeridgian and Cenomanian. These time intervals corresponding to three different steps in the evolution of the Neotethyan realm, and high productivity. Others are related radiolarian bloom and bedded chert formation to environmental control factors, including changes in nutrient fluxes (Price, 1977; Murray *et al.*, 1992; De Wever and Baudin, 1996; Onoue and Yoshida 2010; Gorican *et al.*, 2012; Baumgartner and Föllmi, 2013).

De Wever *et al.* (1994, 2001) and Baumgartner and Föllmi (2013) concluded that the formation of the bedded chert or radiolarites could be related to several causative factors, though the Caribbean river plume, and equatorial upwelling current models may represent the two most widely accepted recent analogous model.

#### 3.8.1 The Caribbean river plume model

Well documented recent analogue of a river plume model of the Amazon River can help to interpret some Mesozoic radiolarian successions in the western neo–Tethys. Based on Cherubin and Richardson (2007), the river plumes of the Amazon had a great effect on productivity and can produce seasonal eutrophication of the southern Caribbean Sea. This model is applicable for areas that are characterized by high productivity with no

existence of upwelling current. This is presented as a probable alternative model for nutrient dispersal in the Western Tethys and as a possible alternative to monsoonal-driving upwelling current.

Baumgartner and Föllmi (2013) has applied this model successfully in interpreting radiolarites deposition in areas such as Western Tethys, Central Atlantic and the Proto-Caribbean Sea as was termed “the Mediterranean ocean basins” (Figure 3.26), and this model may have taken place in the oceanic bodies characterized with limited water circulation. It is more acceptable for the areas in which palaeo-latitudes at the Middle Jurassic Neotethyan basins were located between 20° and 40°. According to Baumgartner and Föllmi (2013) Caribbean river plume cannot be compared with the likely mesotrophic situation of the Middle Jurassic Tethys, because it is characterized by abundant reef growth in its euphotic areas, and the limited mechanism of nutrient supply to the surface waters by influx of low water salinity lids.

### 3.8.2 Equatorial upwelling current

The second model, which has been well documented in the recent analogues, is equatorial upwelling current. The monsoonal-driving upwelling currents of modern analogues are well-documented in the Somali and Owen basins (Figure 3.24), Western Indian Ocean, the eastern margin of the Arabian Plate (Young and Kindle, 1994; Schulz *et al.*, 1996), and in the Gulf of California (De Wever, 1989; Baumgartner and Föllmi, 2013). The upwelling currents are estimated as the main mechanism that produces high fertility and accumulation rates of radiolarians. De Wever and Baudin (1995) conducted a comprehensive study on monsoonal-driving upwelling current for both recent analogues and Jurassic ages, and produced a set of palaeoenvironmental maps of the Neotethyan realm (Figure 3.24).

De Wever *et al.* (1994, 2001) and Baumgartner and Föllmi (2013) revealed that the Jurassic seasonal upwelling current had contributed to high accretion rates of radiolarites off the Arabian margin in the Neotethys. Based on De Wever *et al.* (2014), the seasonal upwelling current and high productivities are well-accepted as the main factors that result in radiolarian-rich deposits in some Jurassic palaeobasins. De Wever and Baudin (1995) suggested that fertility was one of the most imperative requirements that governed the radiolarites formation in the Mesozoic Tethys. Based on these palaeogeographic maps produced by De Wever and Baudin (1996) and Baumgartner and Föllmi (2013), the Sargelu Formation must be located within an ancient monsoonal-driving upwelling current (Figures 3.24 and 3.25). These maps provide a good basis to integrate

information on organic–carbon-rich facies and radiolarites for obtaining a more coherent picture of their distribution with respect to climate, circulation changes and tectonic. De Wever *et al.* (2014) found that the decreasing of radiolarian deposits during Early Cenozoic in Neotethys are linked to the absence of monsoonal current, when the Indian continent was crossing the Tethyan region (Figure 3.27).

The prevailing black–coloured radiolarian bedded chert with black shale at the base of the Neotethyan depositions, are an indicator of anoxic or dysoxic circumstances and the original presence of organic matter. Such bedded chert is assumed to be occurred in the monsoonal upwelling system (Baumgartner and Föllmi, 2013, Suzuki, 1998) and it is the most appropriate model to apply to the eastern Arabian Plate margin and the upper part of the Sargelu Formation cherts. Accordingly, by taking into account recent analogues, it can be proposed that seasonal monsoonal upwelling model can explain radiolarite deposition in the central Neotethyan basins during Jurassic, and it is probably the main source for chert formation at the upper part of Sargelu Formation.

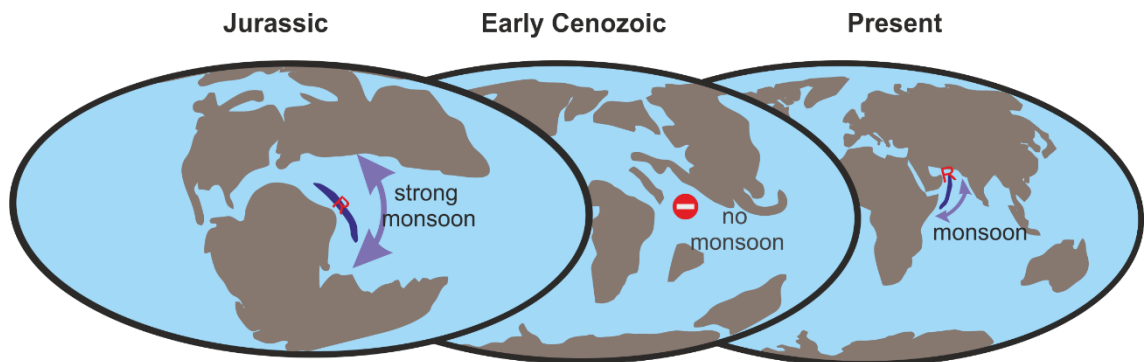


Figure 3. 27: diagram showing relationship between radiolarites(R) and monsoonal activates at different periods (Modified from DE Wever et al., 2014).

### 3.9 *Posidonia* and radiolaria relation

The co-occurrence of radiolarian chert and *Posidonia* are frequently reported from Middle Permian to Late Jurassic pelagic sedimentation in the Northern Alps, Oman, South China, Sicily, Timor, British Columbia, Central Apennines, Monte Cetona, southern Tuscany in Italy, and the Tatra Mountains in Poland (Conti, 1986; Jach, 2007; Onoue and Yoshida, 2010; Onoue et al., 2011; Baumgartner and Föllmi, 2013). Jach (2007) studied the relationship among *Posidonia*, radiolaria facies, high productivity, and deepening-upward in the Tatra Mountains in Poland. It has been revealed that the *Posidonia*-bearing limestone facies usually preceded by drowned basin, which is, in turn developed to radiolarian cherts facies. The existence of *Posidonia*-bearing limestones in the drowned basin represents an intermediate stage during the basin evolution towards radiolarite formation and deepening upward (Figure 3.28). This is quite comparable to *Posidonia* limestone and radiolarian bedded chert of Sargelu Formation, which underlain by drowned Sehkaniyan Formation (Numan, 1997), where at all studied sections, the radiolarian bedded cherts are always preceded by *Posidonia* facies (Figure 3.3).

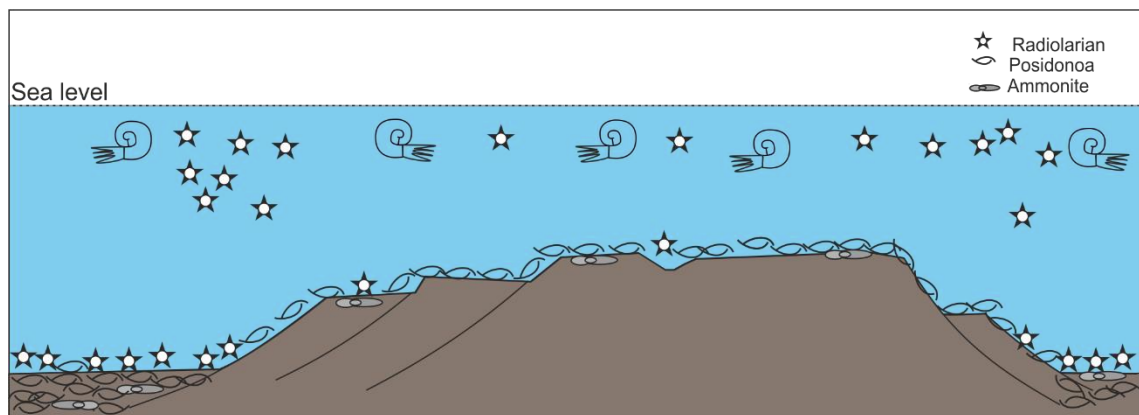


Figure 3.28: depositional model showing relation between *Posidonia*-bearing limestone and radiolaria (modified from Jach, 2007).

### 3.10 Palaeobasin geometry

The fulfilment condition for radiolarites is high-fertility, which is intimately connected to the upwelling current. Some ancient high fertility basins in Neotethys are comparable with the recent active monsoonal upwellings of Owen and Somalia basins (De Wever 2014), and generally accepted suppositions that the palaeobasin geometry of bedded chert is elongated basins (gutters). (Figure 3.24). Moreover, the majority of Mesozoic bedded cherts seem to have been deposited in the elongated basins or gutters with restricted oceanic circulation in small ocean settings with their own specific oceanographic characteristics (Jenkyns and Winterer, 1982; De Wever, 1989; De Wever and Baudin, 1996; De Wever et al., 2014).

The depositional basins of the bedded chert are estimated not to exceed 250 km wide in most places in the world and are most likely to have been deposited in the gutters basins (Figures 3.24, and 3.25). This suggestion is based on the limited occurrence of bedded cherts in the western Neotethys which has never been much longer than the dimensions of the present-day Red Sea, or Gulf of Aden. The Gulf of California, is the best-known modern example of an elongated basin model, characterized by upwelling current and high-productivity condition (De Wever, 1989).

The exact geometry of the depositional basin of the Sargelu Formation is not known. Both of eastern and western margins of the Gotnia Basin, in which the Sargelu Formation was deposited, were obscured by overthrusting during the Late Cretaceous and erosion during the Neocomian uplift respectively (Numan, 1997). Ancient and recent analogues have been compared in order to approach or predict the nature of palaeobasinal geometry of the studied bedded chert formation.

Numan (1997) has pointed to the opening of the Neotethys and split off the Iranian and Anatolian Plates further north from the Arabian Plate during Triassic–Jurassic Periods. The rifting led to extensive changes from a unified state basin of pre-Permian period in the Middle East region into segmented new sedimentation realms in Iraq and neighbouring countries as well. This visualization is based on drastic variation of lateral facies observed in Gotnia Basin with respect to thickness (see Chapter 2). The Neotethys opening at the eastern part of the Arabian Plate initiated graben and uplifts. Developing of Anah graben and Chemchemal uplift dissected the Gotnia Basin into sub-basins (Buday, 1980; Ziegler, 2001; Sharland *et al.*, 2001; Jassim and Goff, 2006; more detail

in Chapter 2). The following points demonstrate that the Sargelu Formation may have been deposited in a relatively narrow and elongated basin.

- a. The palaeobasin of the bedded chert-bearing the Sargelu Formation occurred as a narrow elongated basin, mostly for 450 km long and about 70 km wide. Most beds are found along the NW–SE striking, and these perhaps display compatible with palaeobasin margin of the Neotethys margin (Figure 3.1).
- b. Log sections of recently discovered oil-fields, which are at about 30–40 km southwestern of the studied sections a (Figure 3.1), reveal the existence of considerable evaporite intervals with no chert bands within the Sargelu Formation (Fatah and Mohialdeen, 2016). This dramatic change in depositional environments within a short distance from being a basinal open marine to partially evaporitic environments may indicate isolation of studied section from the rest of the basin or western side. This may also support the disintegration of Gotnia Jurassic palaeobasin into several separated sub-basins.
- c. The bedded cherts of the Sargelu Formation do not exist in the subsurface sections of Kirkuk area which located about 90 km to the west of the studied area (Figure 3.1). This emphasises that the bedded chert of the Sargelu Formation was deposited in a limited narrow elongated basin that does not exceed 200 km in width. It may also support the hypothesis of segmentation of Kurdistan sequences from the rest of the Iraqi shelf through Chemchemal palaeo–bathymetric high (Figure 3.29). Inorganic geochemical analyses have been conducted on black shale samples of Sargelu Formation by Elyas (2014). The type locality of Sargelu Formation and Sheikhan–4 well that located about 50 km westward to the studied exposures have been chosen for this purpose. The results show a drastic difference between the Sargelu type location and Sheikhan–4 with respect to the shale origin. It has been revealed that the clay minerals of Sargelu type locality are derived from marine most probably from volcanic activities, whereas the clays of Sheikhan–4 are from terrigenous material. This may support the conclusion that the depositional basin of the Sargelu Formation must be isolated from the main basin (Gotnia Basin) (Figure 3.29).
- d. Gayara and Al-Gibouri (2015) concluded that the great variation in thickness and depositional environment of Jurassic synchronous successions of Western Iraq may be linked to the tectonic control as a result of segmentation of the main basin into different sub-basins.
- e. Gharib and De Wever (2010) have studied the distribution of the Middle–Jurassic radiolarian in Kermanshah area, western Iran, which is located about 60 km to the southwest of the study area (Figure 3.1). They found that radiolarians were deposited

in the narrow and elongated basin. Regionally depositional basin extended along the eastern passive margin of Arabian plate from the Hawasina series, Oman in the south, continuing northward to Kermanshah in western Iran and ending with the Kocali series in Turkey (Figure 3.24, A). Kurdistan exposures of Middle Jurassic sediments can be correlated to the Kermanshah Formation. Moreover, the Sargelu Formation of Kurdistan could be considered as an extension of the same depositional platform of the Kermanshah deposition.

Furlo basin succession in Italy, probably represents a good model for complex pattern of intra-basinal fragmentation, which developed from drowning and rifting during Early Jurassic (Donatelli and Tramontana, 2013). The co-existence of extreme variation of depositional environments such as peritidal, condensed Ammonitico rosso, posidonia-bearing limestones, and basinal cherty pelagic within a short lateral and vertical distance could indicate the break-up of the carbonate platform. Furthermore, Soussi and Ben Ismail (2000), and Robertson & Searle (1990) have found the control of tectonic faults on the sedimentation of central Tunisia and Oman during Jurassic period (Figures 3.30, and 31). The Jurassic successions in the study area show abrupt vertical facies changes from restricted shallow platform and lagoonal Sarki and Sehkaniyan Formation of Early Jurassic to open marine and basinal Sargelu and Naokelekan Formations of Middle-Late Jurassic; they are capped by sabkha Barsarin Formation of Late Jurassic. Moreover, dramatic lateral facies changes between Kurdistan exposures and the western subsurface Jurassic sections are also very prominent (for more detail see Chapter 2). The abrupt vertical and lateral changes with respect to the facies and thickness may suggest tectono-stratigraphic controlling model for Jurassic succession in the study area. Consequently, this suggest that the rifting may create a complex pattern of several small intrabasinal morpho-structural highs, which developed from the drowned the Early Jurassic carbonate platform (Figure 3.29).

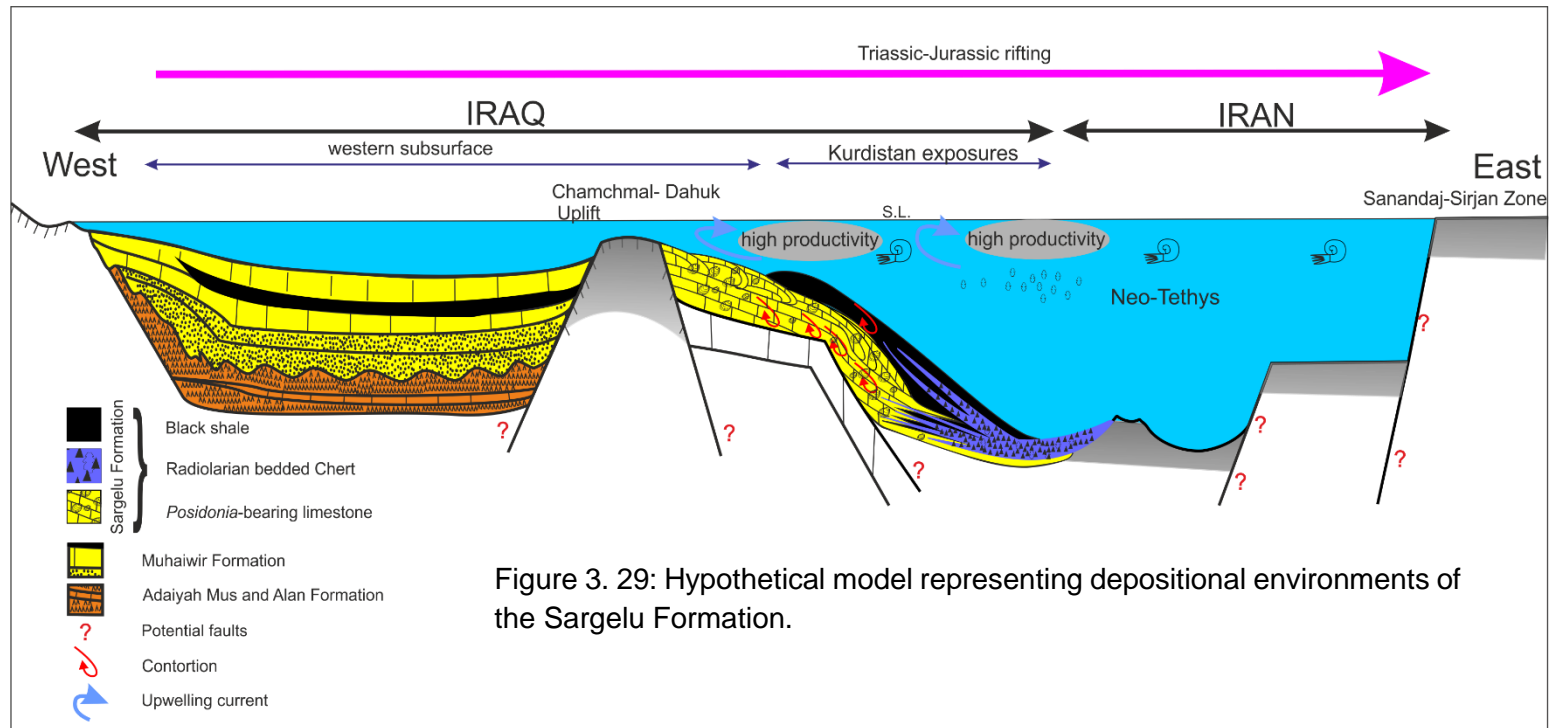


Figure 3.29: Hypothetical model representing depositional environments of the Sargelu Formation.

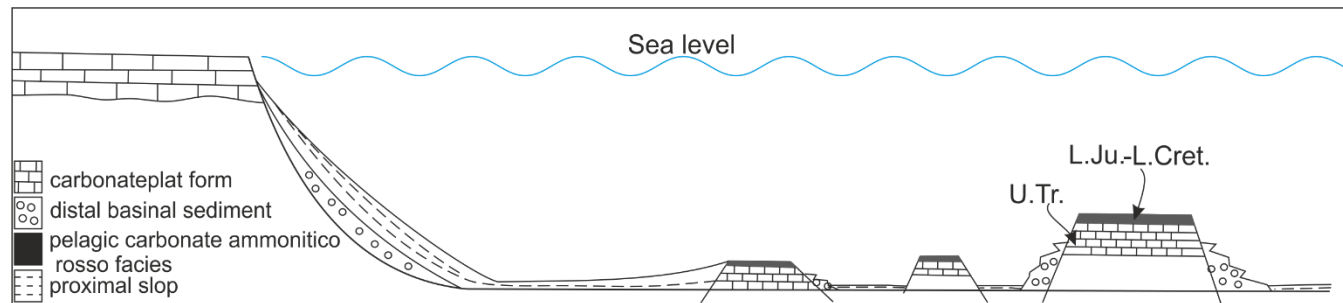


Figure 3.30: Restored relations of the passive margin sediments and the tectonic fault control of the Oman rifted margin (Modified from Robertson & Searle, 1990).

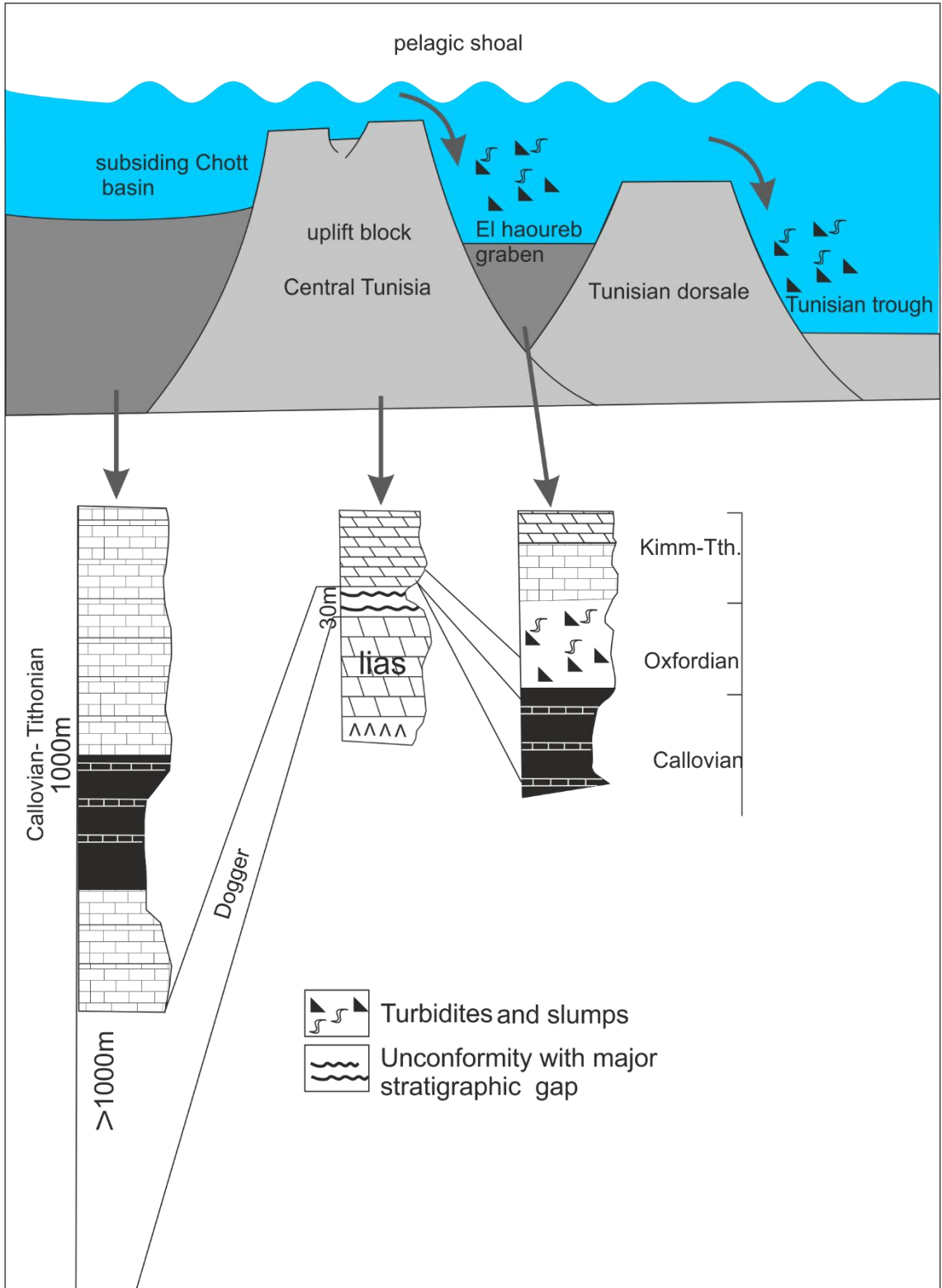


Figure 3.31: Simplified tectonic diagram showing the main palaeogeographic domains in central Tunisia and the main Jurassic faults which controlling the sedimentation. Note the great variation in facies and thickness between the Jurassic rocks (from Soussi and Ben Ismail, 2000).

### 3.11 Resedimentation

This study attempts to provide some evidence for the presence of resedimentation, which has never been reported before in the Sargelu Formation. Therefore, this research will provide some initial observations and interpretations that may form the basis for more detailed studies in the future. The upper part of Sargelu Formation comprises mixed strata composed of alternating lithofacies of posidonia-bearing limestones, black shale, and bedded cherts (Figure 3.17, A). Up until now, the causes of the co-occurrence these three lithofacies are still unknown. The main enigmatic question is simply: by what depositional process do they form, do their periodical repetitions follow specific depositional patterns, or do they occur randomly?

Submarine mass transportation and redeposition can be produced by rock falls, slides, slumps, turbidity currents, debris flows, or grain flows (Figure 3.32). Resedimented clastics may be additionally reworked by deep-marine bottom currents, termed "contourites". Gravity flows, which are also called sediment downslope flow, consist of turbidity, grain flows, and debris flows (Flügel, 2010). The following sections focus on two different processes of resedimentation; namely turbidity currents and slumps.

### 3.12 Turbidity currents

Sediment that was deposited from a turbidity current can be defined as a turbidite. Turbidites are characterized by graded bedding, and may equally demonstrate moderate sorting and a vertical sequence of distinct sedimentary structures (Flügel, 2010). Bouma (1962) was the first who identified, described and interpreted, the turbidite sequences through a siliciclastic succession (Figure 3.33). The Bouma Sequence model is an ideal turbidite sequence that consists of a well-defined vertical succession of five units, and they will be discussed in the next sections.

Although turbidity currents cannot be easily detected in deep-marine settings, they have been deduced through observations by its impact on infrastructures, such as cable failures. Much knowledge of turbidity current deposition has been inferred from extensive research on their deposits from laboratory flume experiments, which have a well-established theoretical basis (Reading, 2009).

Reading (2009) found out that turbidity currents are the most important process for transportation of coarse-grained sediment into a deep-sea setting, where suspensions of sediment are usually sustained by fluid turbulence. Final products of turbidity currents

are various types of turbidite beds or turbidites. Accordingly, the thickness and internal sedimentary structures of the turbidite successions can vary significantly (Figure 3.33). The main controlling factors that lead to variations are the sediment composition, distance between the source and proximal to distal place of deposition, density of the turbidity current, and topography of the depositional environment (Allen, 1985; Einsele, 2000).

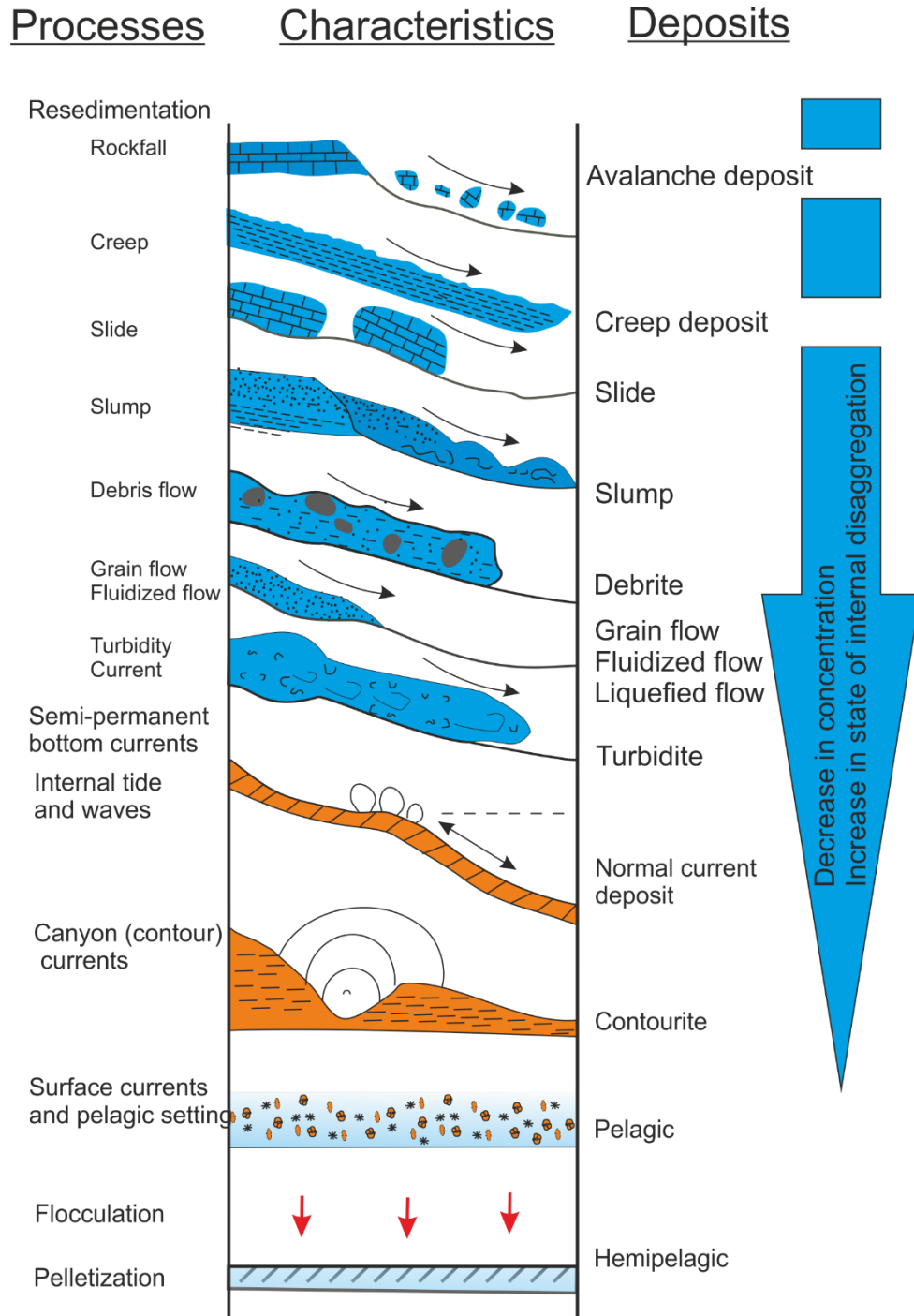


Figure 3.32: the range of different processes that occur in deep sea and their products (adapted from Stow, 1992; Reading, 2009).

Furthermore, a gradual deceleration of turbidity currents downslope may lead to deposition of their sediment load in a predictable order. This can be observed from laboratory flume experiment, which reproduced specific internal structures (Allen, 1985). Trends which have been identified by (Bouma, 1962) were supported by experimental results (Bridge and Demicco, 2008), and various sub-models were introduced by different authors since then, Einsele (2000) identified four categories of turbidites which are as the following:

#### 3.12.1 Coarse-grained turbidites

Coarse-grained turbidites, which are deposited by high-density turbidity currents, can carry pebble to boulder-sized clasts as bedload of the current flow. Commonly coarse-grained turbidites are deposited within a short-distance downslope in proximal areas in relation to the sediment sources and seem to occur preferentially in the wide feeder channels of deep-sea fans. The clasts are usually transported by traction, and the deposits demonstrate initial traction sedimentation and clast to clast contacts. Consequently, a finer part of the sediment will turn into suspension and creates a turbulent flow through dispersive water pressures which may result in formation of laminated or graded intervals (Lowe, 1982; Einsele, 2000; Kettle, 2012). Coarse-grained turbidites have very rarely been observed in studied sections.

#### 3.12.2 Medium-grained sandy turbidites (siliciclastics and carbonates)

The classic model for medium-grained sands and sand–mud turbidites was first presented by Bouma (1962). Five intervals of parallel sandstone beds Ta–e with an ordered sequence of internal lamination have been recognized in the complete sequence (Figure 3.33).

- A. Graded interval (Ta); it is the lowest interval that often shows normal grading, which indicate a high-flow regime, and lacks depositional lamination (Figure 3.33). It is usually associated with water escape structure, and this structure is usually interpreted to indicate rapid deposition in overlying strata, causing forceful expulsion of water during rapid gravity loading. The lowermost Bouma division may be underlain by a coarse-grained, inverse graded traction carpet. (Hsu, 1989; Einsele, 2000; Shanmugam, 2006; Bridge and Demicco, 2008; Hüneke and Mulder, 2011). This division has been recorded frequently during field study, and will be discussed in detail in the section 3.13.

- B. Plane laminated sand interval (Tb); it is distinguished by parallel lamination, and it is ascribed to deposition under upper-flow-regime and reflects traction structures (Figure 3.33). The boundary between the Tb and the overlying Tc intervals marks the transition from the upper- to lower-low system (Einsele, 2000; Shanmugam, 2006). The laminated posidonia-bearing limestone may represent this interval, and it will be discussed in detail in the section 3.13.
- C. Ripple cross-bedded interval (Tc); it represents the lower flow regime and is characterized by ripple cross-lamination (Figure 3.33). This interval of the Bouma sequence forms as a result of fallout of sand from suspension and current traction, and has less energy than the underlying Tb interval (Hsu, 1989; Einsele, 2000; Shanmugam, 2006; Bridge and Demicco, 2008; Hüneke and Mulder, 2011). No ideal structure for Tc interval were observed.
- D. Laminated mud interval (Td); it is ascribed to deposition under lower-flow regime forming planar laminations (Figure 3.33). The Td interval can be identified by lamination and very delicate grain sorting on the bed, and has been explained as mixed traction suspension sedimentation (Hsu, 1989; Einsele, 2000; Shanmugam, 2006; Bridge and Demicco, 2008; Hüneke and Mulder, 2011).
- E. Structureless mud interval (Te); it is slowly originated from suspension load sedimentation, and often demonstrates bioturbation structures (Einsele, 2000; Hüneke and Mulder, 2011).

The Bouma sequence usually displays a transition from the dominance of sedimentation by traction middle parts to sedimentation-dominated distal parts by suspension fallout at upper part. Normal fining upward are not restricted to the Ta division only, but the grain size tends to decrease up through the (Ta–e) divisions (Walker, 1965; Komar, 1985). Similarly, the thickness of individual laminae or cross-bedding sets can show a decrease from bottom to top (Hüneke and Mulder, 2011). Partial turbidite sequences are relatively common, whereas complete sequences are seldom encountered in nature. The suspension fallout-dominated interval Td may be rarer than other units, which represent the fine-grained parts of the Bouma turbidite sequence, have been rarely recorded from turbidite sequences (Stow, 1992; Shanmugam, 2006; Hüneke and Mulder, 2011).

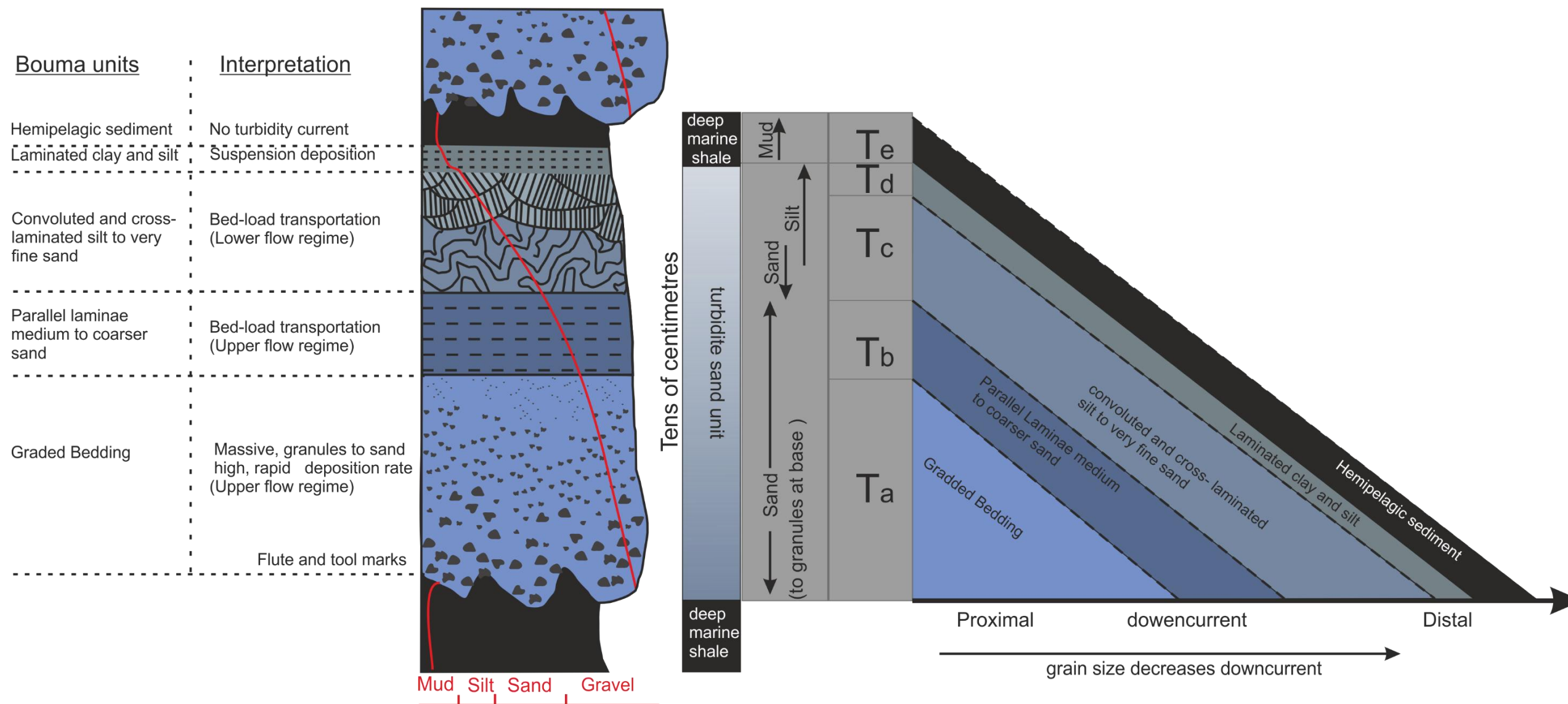


Figure 3.33: Diagram showing different intervals of the Bouma Sequence model with depositional interpretation (adapted from Bouma, 1962).

### 3.12.3 Carbonate turbidites

Soon after the first recognition of turbidite structures by Bouma (1962) researchers realized that the turbidite sequences could be present in many other lithological and structural configurations. The Bouma sequence, which often represents medium-grained turbidites, cannot accommodate all different kinds of turbidites, especially if they were carbonate, coarse- or fine-grained sediments. Carbonate turbidites are similar to siliciclastic turbidites in terms of theoretical mechanisms of turbidity current. However, they show considerable differences in terms of the nature of their occurrence (Reading, 2009; Flügel, 2010). Biogenic carbonate particles usually behave hydraulically different from siliciclastic sand particles, and are usually distinguished by early lithification and prominent large clasts. Moreover, in contrast to the siliciclastic turbidites, in which the grain size depends largely on the distance of transportation, the ecological limitations in the source area and taphonomic criteria control the size of the bioclastic particles in carbonate turbidites.

Meischner (1964) developed a new model for carbonate turbidites called allodapic limestones (Figure 3.34), which is more compatible with the carbonate turbidites or calciturbidites. The terms allodapic limestones or calciturbidites refer to carbonate sediments that originated elsewhere and were re-deposited by turbidity currents and display graded carbonate beds. It usually comprises skeletal and/or carbonate mud material that formed on carbonate shelves, platforms rims, and slopes (Einsele, 2000; Flügel, 2010). Allodapic limestone is pretty much identical to the Bouma model, but the main distinguishing characteristics of the allodapic limestones or carbonate turbidites are described below (Einsele, 2000).

- I. Medium-grained siliciclastic particles of the Bouma Ta and Tb intervals may be replaced by skeletal of fossils > 2mm with miner radiolaria or diatoms particles (zone one, Figure 3.34).
- II. Instead of the silt divisions Td–Te of the Bouma model, a chert layer is deposited at the top of carbonate turbidity, which was formed diagenetically from diatoms, radiolarians or sponge needles (zone two–three, Figure 3.34). Capping the top of a carbonate turbidite with bedded marine cherts of radiolarian siliceous ooze is an important process which indicates non-turbidity periods.

Accordingly, a graded carbonate turbidite can show distinctive pass sharply in its vertical succession in terms of grain size, resulting in a rapid change from relatively coarse grains of zone one interval to fine grains of bedded cherts of zone two.

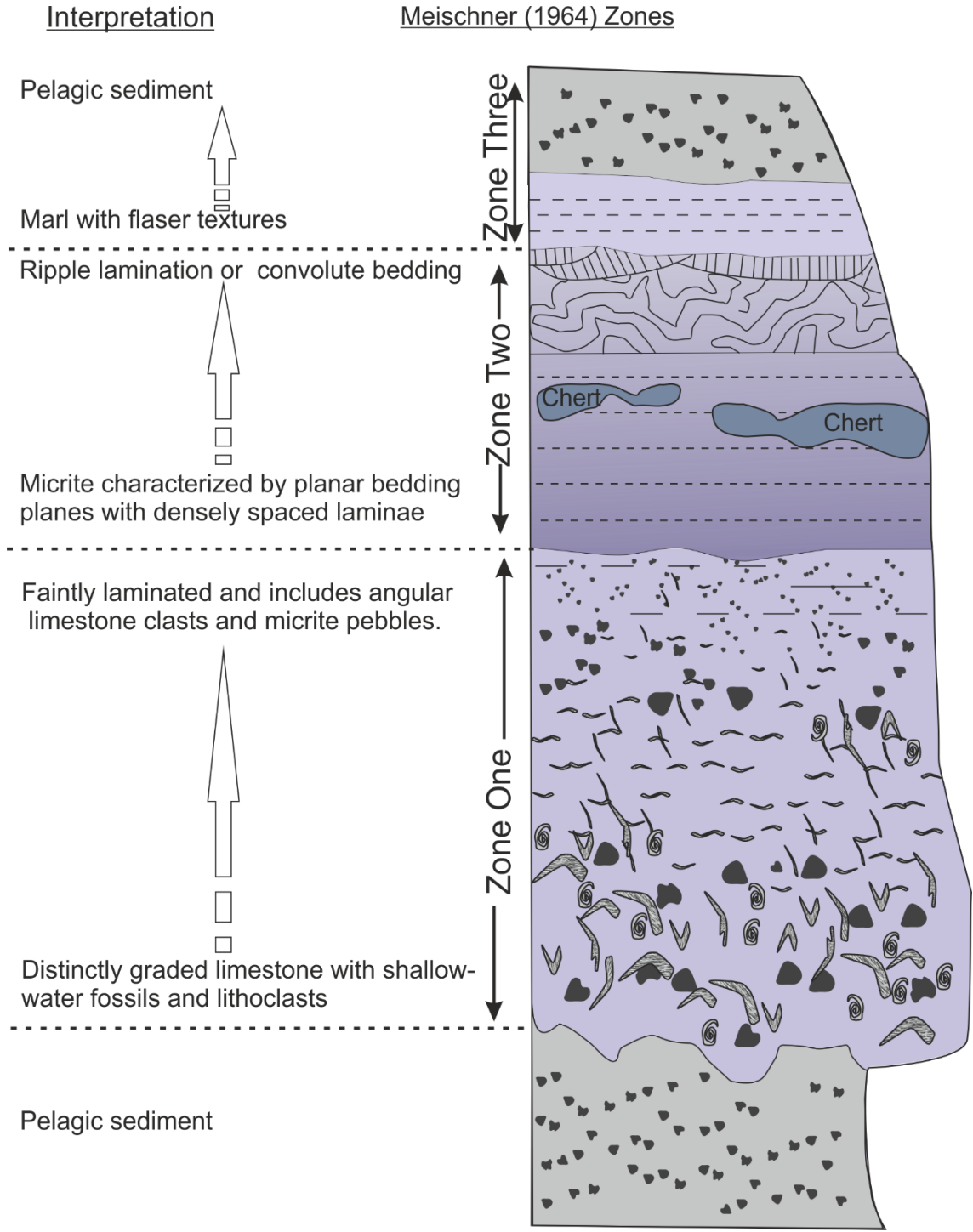


Figure 3.34: Meischner Sequence showing ideal allodapic limestone turbidity current model and its subdivisions (adapted from Meischner, 1964).

### 3.13 Turbidites of the Sargelu Formation

The black shale, radiolarian bedded chert and *Posidonia*-bearing limestone member BRPLM at the upper part of the Sargelu Formation comprises a mixture of three main different lithofacies alternating with each other at intervals of several decimetres thick showing a wide variations in terms of lithologies and sedimentary structures. The lithofacies are as follows:

- 1) *Posidonia*-bearing limestone lithofacies (P BLL)
- 2) Radiolarian bedded chert lithofacies (RBCL)
- 3) Black shale and argillaceous limestone lithofacies (BSALL)

Previous descriptions of outcrops by (Balaky, 2004; Sherwani and Balaky, 2006) give an impression that these lithofacies are chaotically distributed, and this could be because of relatively irregular repetitions of admixture of different lithofacies within a short span of thickness. However, current study may confirm exactly the opposite, where the BRPLM consists of specific repeated packs of admixture of different lithofacies (Figure 3.11). Each pack often shows the following vertical succession from bottom to top: a) graded bedding, b) laminated structures, and c) bedded chert or black shale. This kind of arrangement of sedimentary structures is comparable to the Meischner model, and may predict the existence of turbidite structures (Figure 3.35). The following points will provide some evidence for the existence of turbidites in the Sargelu Formation.

- **Graded bedding;** Graded bedding is the most distinguishable feature of the calciturbidite, which is exposed by a fining-upward sequence (Figure 3.35). They are relatively common throughout the upper part of the Sargelu Formation, and are present as 8–40 cm thick beds which comprise medium-grained wackestone to packstone (Figure 3.36). The bioclasts are usually characterized by a low diversity of fossils and a high abundance of well-sorted *Posidonia*. The graded bedding structure can stand out more clearly if there were enough amount of ammonite shells in the sediment. The larger size of ammonite shells will rest at the bottom of the bedding, whereas the size decreases gradually upward with *Posidonia* dominance at the top (Figure 3.35). In many cases graded beds display erosional surfaces, and they can be inferred in deposits by the existence of “probable rip-up” clasts of chert in the sequence (Figure 3. 11, E).

- **Parallel lamination**; the graded bedded limestone is usually followed by thinly bedded, clearly laminated *Posidonia*-bearing limestone (Figure 3.11). Parallel laminated limestones are distinguished by included horizontally laid, dense packing of thin-shelled bivalve with scattered coalescent particles. Microscopic examination revealed that the coalescent debris clasts comprise flocculated *Posidonia* valves, and their internal texture display rolling textures (Figure 3.14, C–D). This suggest that these clasts were probably generated from re-sedimentation.
- **Rare occurrence of ripple lamination**; no ripple lamination was observed in the field studies. Scarcity of occurrence of ripple lamination in carbonate turbidites was also emphasized by many other researchers (Hsu, 1989; Einsele, 2000; Shanmugam, 2006; Bridge and Demicco, 2008; Flügel, 2010; Hüneke and Mulder, 2011). Perhaps the taphonomic criterion is the main controlling factor that is behind the absence of ripple structure in the calciturbidite of the Sargelu Formation, where well-sorted, equally sized *Posidonia* shells of about 2 mm in diametre represent the majority of the calciturbidite components. The sediments are narrow size–range distribution, and lack grading in grain size, especially fine grains or mud often are unavailable for later stage of the lower flow regime of turbidity current to form ripple lamination. As a result the calciturbidite succession of the Sargelu Formation lacks ripple lamination, and pass sharply from sand-sized grains into bedded chert or shale are very ubiquitous in carbonate turbidites.
- **Chert beds as an alternative to Td–Te intervals**; bedded cherts in the BRPLM can be considered as an identifier in the Sargelu Formation exposures, which represent a distinguishing feature of the upper part of the Sargelu Formation and can be seen ubiquitously in studied outcrops (Figure 3.17, A–E). The chert exposed at the top of a calciturbidite is a crucial tool to distinguish it from siliciclastic turbidite. Interbedding between calciturbidites and bedded cherts have been recorded in many slope and base of slope apron environments (Al-Riyami et al., 2002; Yılmaz, 2006; Rubert et al., 2012; Baumgartner and Föllmi, 2013). According to Meischner (1964), instead of the Td–Te divisions of the Bouma model, the cherts can be considered as a supplementary division that caps the top of the carbonate turbidite sequence. Siliceous ooze accumulations in the Sargelu Formation are an important indicator for a non-turbidity period or a low-density tail to the turbidity currents (Figure 3.35).

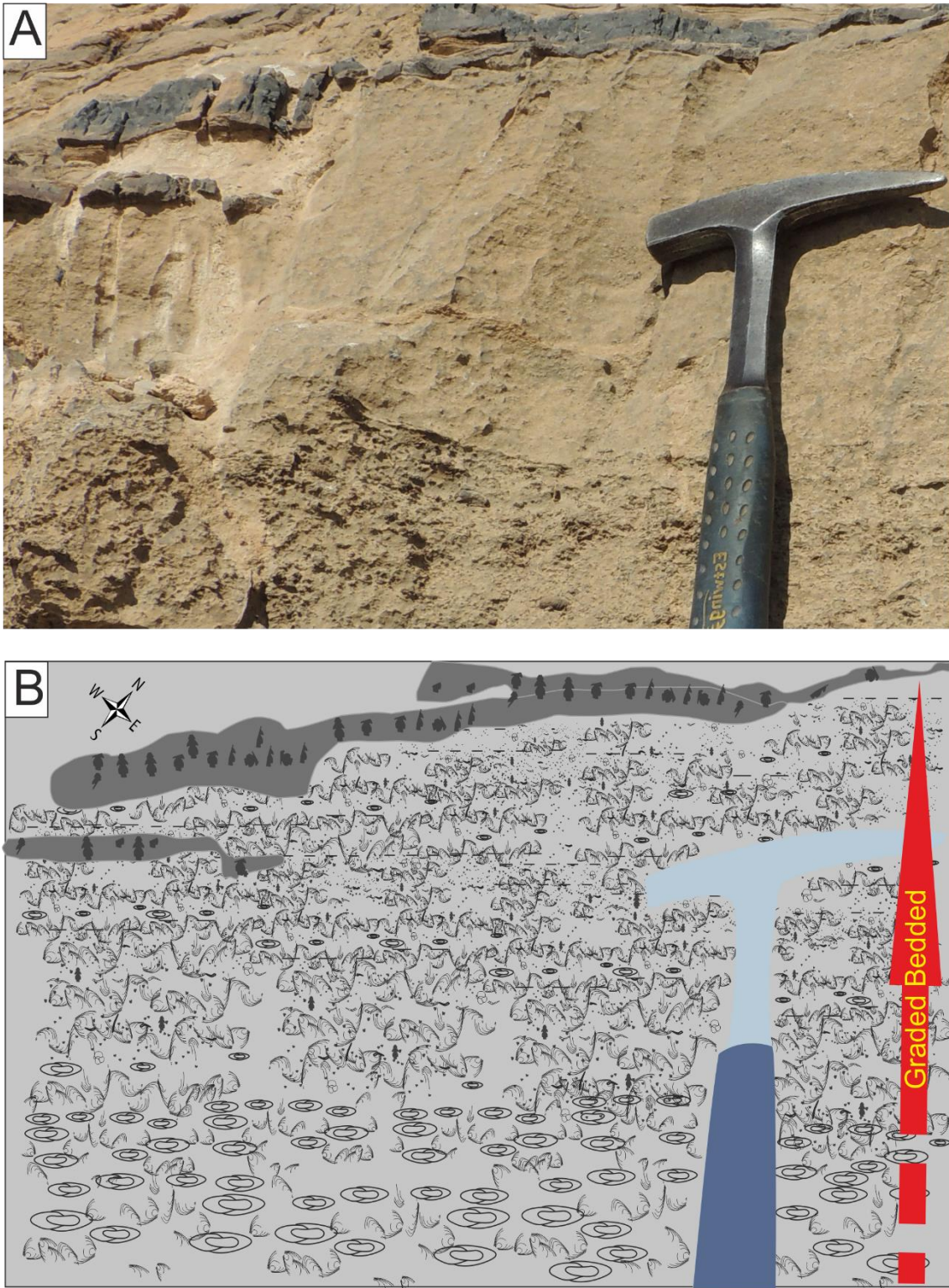


Figure 3.35: Cross-sectional view of *Posidonia*-bearing limestone and thin-bedded chert showing gradual fining upward. Note, the dominance of large ammonite at the base, while the lighter shells of *Posidonia* are concentrated at the top of the bed. The radiolarian bedded chert represents the non-turbidite period on the top of this section, Hanjera location.

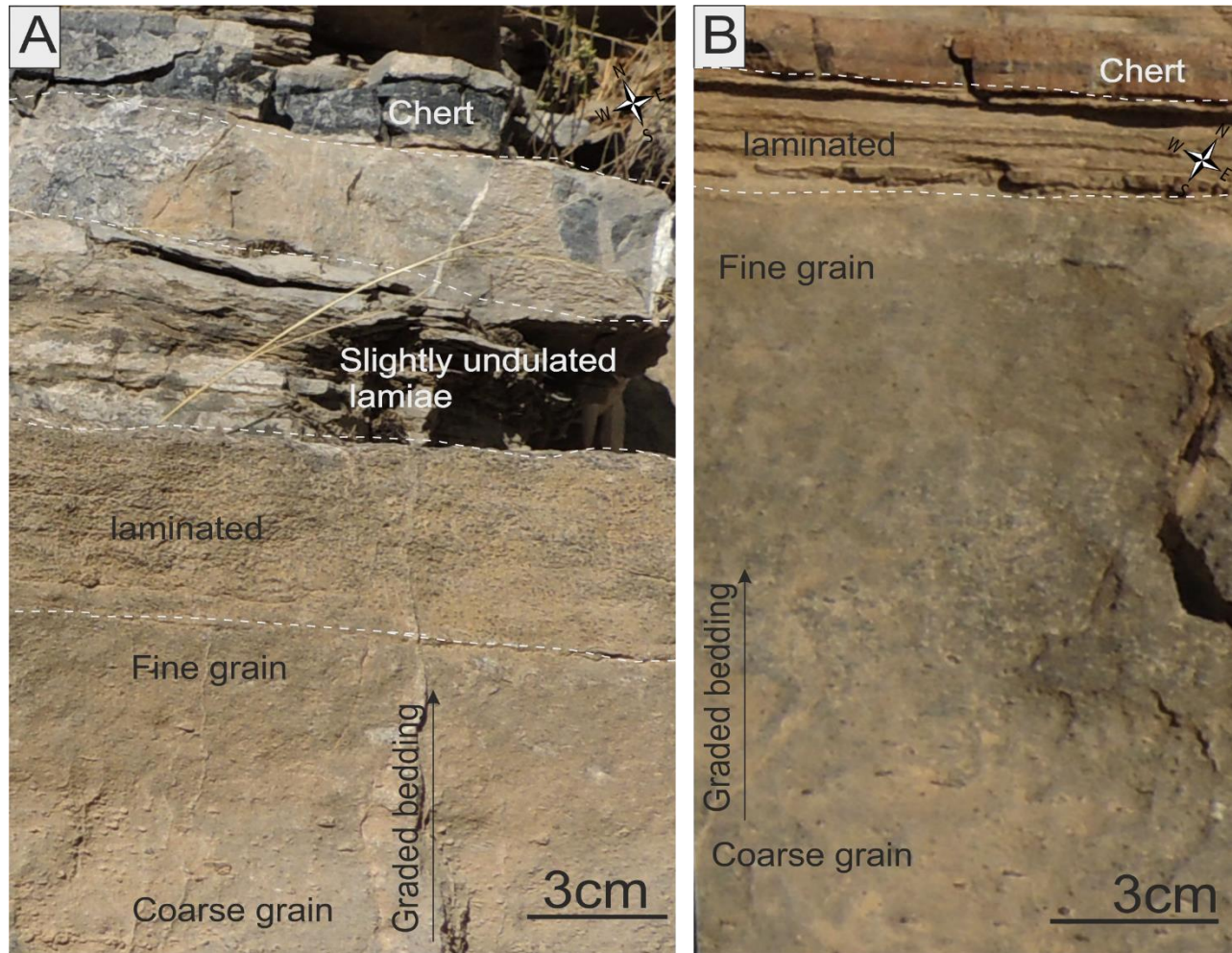


Figure 3.36: photographs showing normal graded bedding and laminated structures in *Posidonia*-bearing limestone, which may suggest turbidity processes. Note the bedded cherts cap the turbidite limestone. A and B are Chnaran and Hanjera locations respectively.

### 3.14 Mutual relationship between different lithofacies

Couplets of, bedded chert and black shale, posidonia-bearing limestone and bedded chert, or posidonia-bearing limestone and black shale in pelagic deposit sequences are quite common and they have been described by many researchers (Conti, 1986; Suzuki et al., 1998; Renata, 2007; Baumgartner and Föllmi, 2013). In contrast, the upper part of the Sargelu Formation, which is called BRPLM, is characterized by interbedding of posidonia-bearing limestone PBLL, radiolarian bedded chert RBCL, and shale BSALL, which is not a prevalent case in comparison with other analogues. The keys to solving the problem of the co-occurrence of bedded chert, different textures of posidonia-bearing limestone, and shale lie in the understanding and interpretation of the mutual relationship between different lithofacies. This chapter attempts to decipher this relationship, but future research will be required to develop an explanatory model to help understand the mutual relationship between different lithofacies.

Three recurring types of lithofacies beds are encountered in the BRPLM: PBLL, RBCL and BSALL. Although these different lithofacies seemed to be chaotically arranged, they may show a kind of turbidite sedimentary sequence (Figures. 3.35, 3.36, and 3.37). The BRPLM, to some extent, display different textures which are similar to allodapic limestone turbidites of the model or to their equivalents in Bouma's Sequence. Some of the Meischner's model zones "one, two, and three" (Figure 3.34) can be identified in the BRPLM beds. The suggested model is described in ascending order as the following points.

- i. **Turbidite PBLL**; It mainly consists of posidonia bearing limestone, and often includes the following structures: i) a basal graded division displays a fining-upward structure, and could also contain some rip-up clasts of the eroded underlying bedded cherts (Figures 3.11, 3.35, 3.36, and 3.37). This division may represent the zone one of the Meischner model or the Ta of Bouma sequence, ii) parallel-laminated limestone represents lower part of the second zone of the Meischner model that is characterized by planar bedding planes, and is the equivalent to the Tb of the Bouma model. Furthermore, in very few cases a convoluted and disturbed posidonia-rich laminae were observed (Figure 3.11 D), and overly the laminated part of zone two of the Meischner model and are rich in coalescent debris, may represent upper part of the Meischner model.
- ii. **Non-Turbidite RBCL**; the black bedded chert mainly consists of radiolarians, and sometimes displays an eroded surface. The RBCL is interpreted to represent

hemipelagic sediments, and are inferred as the non-turbidity periods that usually cap the turbidite sequence of the PBLL (Figures 3.36, and 3.37).

iii.

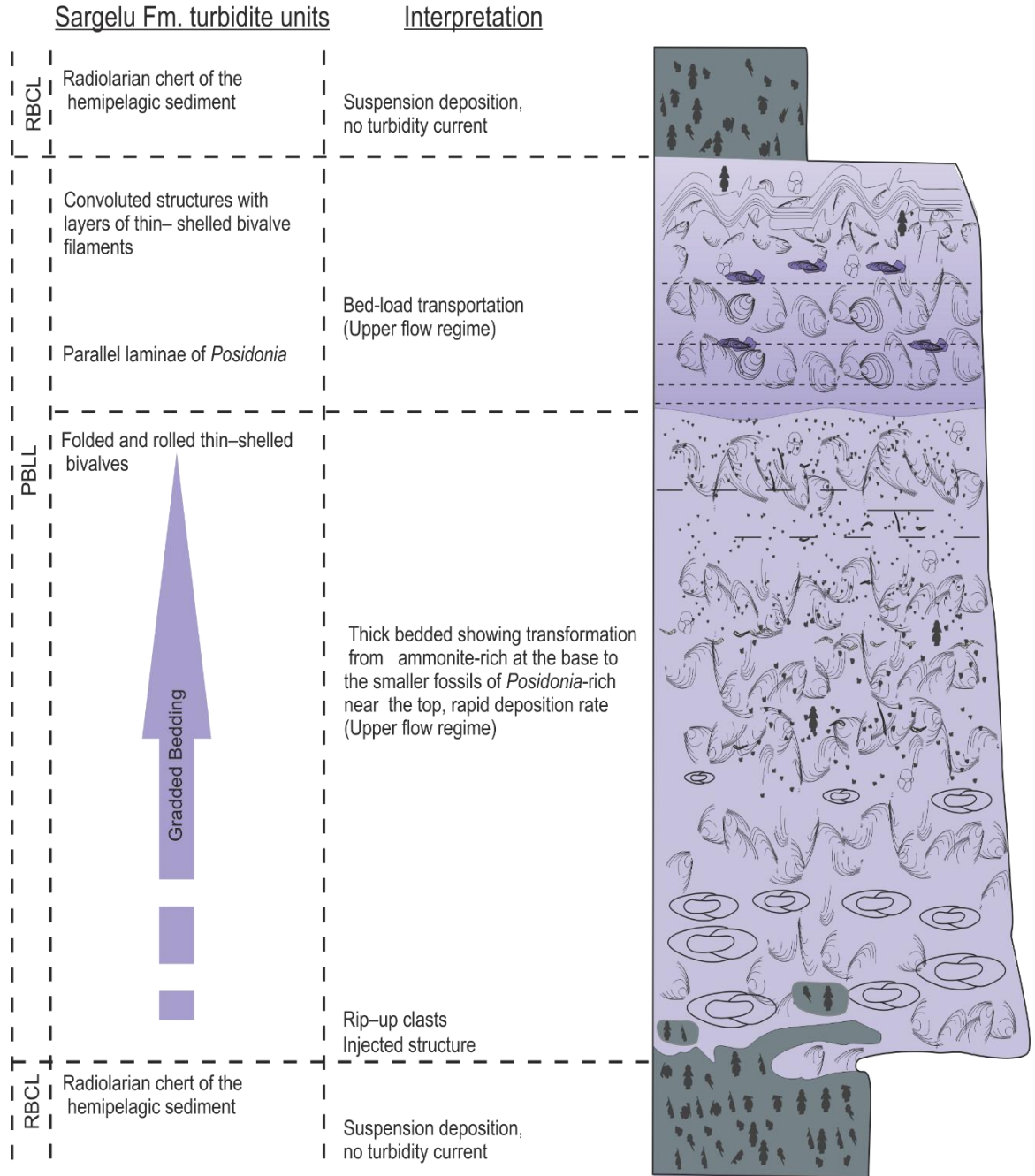


Figure 3.37: Generalized turbidity model of the upper part of the Sargelu Formation showing turbidity units and their interpretation.

### 3.15 Initiation of turbidity current

There are several causes that trigger a sediment gravity flow, including overloading in areas with high sedimentation rates, earthquakes, over steepening in rapidly prograding areas, and the topography of submarine slopes (e.g. angle and length of a slope). The differences in the density of the suspension (interstitial water) and the overlying water body also represent driving forces of turbidity currents (Kenter, 1990; Posamentier and Walker, 2006; Hüneke and Mulder, 2011). Additionally, recent studies have reported that the fluid escape e.g. biogenic methane gas within organic-rich sediments (Imbert, 2011) is perhaps a common phenomenon on an ocean floor which can cause liquefaction structures. All of these mentioned factors may result in sediment gravity flows (Hüneke and Mulder, 2011).

As discussed in the section 3.10, the fault-induced steepening of the platform margin of the depositional basin or “Gotnia Basin” has produced a submarine topography, which may have triggered the generation of turbidity currents resulting in the formation of turbidite successions in the Sargelu Formation. Moreover, fluid escaping from organic-rich sediments may represent an additional acceptable concept for triggering a sediment gravity flow to form the upper part of Sargelu Formation, which is rich in the organic matter.

### 3.16 Distance from source

Turbidites display a wide variety of sedimentary successions in nature, and these variations may reflect their proximity or distality to the sediment source area. A proximal turbidity current contains relatively coarse material, which subject more grain to grain interactions. However, distal turbidite sediments comprise finer grains that have been transported over longer distances, and the sediment is derived via suspended-load fallout. According to the (Flügel, 2010) turbidites can be differentiated into three main categories: proximal, intermediate or Bouma, and distal turbidites:

- (a) Proximal Turbidites; deposited relatively close to the source area, and have limited interbedding with pelagic sediment. They often show excellent traction carpet units.
- (b) Intermediate turbidites; which are represented by the Bouma or Allodapic sequences; they consist of interbedding pelagic sediments with a characteristic succession of sedimentary structures that demonstrate clear graded bedding. They may have oriented erosion and sole markings at the base of bedding.

- (c) Distal Turbidites; deposited far away from the source area, and are distinguished by thin structures of fine-grained bedded layers with well-developed cross-laminations, and lack massive intervals.

The field observations and microscopic studies indicate that the Sargelu Formation consists of turbidity deposits, which show interbedded pelagic sediments and clear graded bedding with few sole marks. These characters tend to be more comparable to the second category.

### 3.17 Folded Unit

The most prominent feature of the top of the Sargelu Formation is the existence of intense folded structures. The folded structure was observed at all localities (Figures 3.2 A, 3.38), and their intensity often increases westwards. The folded unit is 2 to 5 metres thick (Figure 3.8). It mainly comprises black shale and rare interbeds of *Posidonia*-bearing limestone and bedded chert. The lithofacies association in the folded unit of the upper part of the Sargelu Formation is quite similar to what have been described in the underlying lithofacies by taking into account the following considerations:

- (a) The folded unit is characterized by a dominance of organic-rich black shale in comparison to the underlying member (Figure 3.8).
- (b) The bedded cherts and *Posidonia*-bearing limestone disappear gradually upward in the folded unit.
- (c) The *Posidonia* shells show dramatic reduction in size up to 2 mm (Figure 3.12, F).

Although thin-section examination revealed widespread micro-folded laminae with imbricated and broken thin-shelled bivalves occurring through the middle to upper succession (Figure 3.14, E–F and 3.15 B–C), two macrostructure phases of folded carbonate have been documented during the field studies (Figure 3.8, A–C). The macro-folded structures were observed as slightly folded in the PBL and intensely folded at the top of the BSALL. The current study focuses on the latter folded structure.

#### 3.17.1 Slumping

Many different processes can result in folded structures of sedimentary rocks, such as hydration of anhydrite, tectonic folding, and downslope slumping of sediment. The first possibility can be neglected, because no evaporites were observed. As mentioned previously, the studied folded units are always overlain and underlain by non-folded beds. Bridge and Demicco (2008) have stated that the existence of the folded strata

within undeformed strata can be used to distinguish syn-depositional folding from tectonic folding. Accordingly, the folded structures at the top of the Sargelu Formation can be attributed to syn-depositional folding, which may be produced by gravitational processes. Perry and Taylor (2007) categorized sediment transportation from gravitational processes into three main mechanisms: (i) slides and slumps, (ii) rock falls, and (iii) mass flows, and all three mechanisms could occur along a continuum spectrum (Figure 3.32). The folded structure of the Sargelu Formation is comparable to the slide and slump category for the following reasons:

- A slump can be defined as a structure that originated from mass sliding and creeping of semi-consolidated sediment, in which the sedimentary strata display plastic deformation and remain coherent during slumping. In slumps, the original sedimentary structures are normally disrupted or destroyed (Tucker and Wright, 1990; Bridge and Demicco, 2008). In contrary, according to Flügel (2010) slides can be defined as the movement of rigid masses that are internally undeformed. Based on the previous definitions; the folded structure of the Sargelu Formation is most likely located within the slide–slump category which might have occurred on a slope.
- Early lithification is easily detectable in the studied folded beds, where despite intense folded structures, the bedding kept their parameters very well and their structural borders were not deformed (Figure 3.38). Sometimes, the bedding rupture occurred without any turbulence or liquid behaviour. Interbedding between semi-lithified chert and posidonia-bearing limestone with soft black shale may promote deformation, such as; crinkled and isolated irregular folded structures. Based on field observations, the folded structures of the beds may be attributed to the downslope slumping of sediment under the influence of gravity rather than sliding. The slumped masses can be preserved in either the downslope or adjacent basins.
- The existence of a tongue-like or lobe structure on some bedding surfaces of the Sargelu Formation may suggest slumping process (Figure 3.5, C). Such structure has also observed by Balaky (2004) at Gara location (Figure 3.1). Similarly, Kenter (1990), Kenter and Campbell (1991), and Harris (1994) have found lobe structure in their study on gravitational-deposited sediment, and considered it as evidence for slumped masses. They have assumed that the lobes may have been formed by the effects of creeping with initial dissection and compressional folding of strata, and they may indicate a slope angle of up to 25–40 degrees.

### 3.18 The morphology of slopes

Based on the previous interpretation, the Sargelu Formation may have been deposited during syn-rift passive margin systems, and, as a consequence many normal faults were perhaps developed, which resulted in basin segmentations. Most evidence suggests prevailing turbidity and slumped structures transported on a sloped surface. The morphologies of slopes are controlled by many factors, such as depositional fabric subsidence, sea-level, plate motion, oceanographic setting, climate, and wind direction (Kenter and Schlager, 1989; Kenter, 1990). In order to understand their influence on the slopes; the following points will be discussed briefly.

- **Palaeowind direction:** Schlager and Ginsburg (1981), Reading (1996), and Reading (2009) have found out that the palaeowind direction has a great impact on sedimentation. It is also important to determine whether the slopes are in a leeward or windward location. Along windward platform margins, many coarse carbonates are moved into the platform. On the contrary, along leeward platform margins, sediment is commonly moved off-platform, onto the adjoining slope and into the neighbouring basin.
- **Sediment composition Fabrics;** Kenter (1990) has stated that the geometry of submarine slopes can be controlled by the composition of slope sediments. Calcareous sediments for the same grain size build always steeper slopes than siliciclastic sediments. In general modern siliciclastic slopes may range between 5°–15°, whereas calcareous sediment can occur at slope angles up to 40° and may even be significantly steeper. Furthermore, slope angle of carbonate platforms can be influenced greatly by types of depositional fabrics. Grain-supported fabrics show great differences in terms of slope angle in comparison to mud-supported ones. The latter often can result in slope angles up to 15°, whereas grain-supported fabrics with minor or no proportion of a mud-supported matrix construct relatively high-angle slopes that may range between 12° and 40° (Kenter, 1990).

Because none of the earlier researches on the Sargelu Formation have considered the existence of a slope environment in the studied area, it is hard to assess slope angles, prevailing palaeowind direction, and morphology. However, the dominance of a wackestone to packstone carbonate fabric may suggest that the Sargelu Formation was deposited at: (a) leeward of the platform, which is also indicated by the absence of grainstone, (b) the expected slope angles is probably much shallower than 15°.

### 3.19 Transformations between different kinds of gravity deposits

Many different types of turbidites can be produced from a single gravity depositional process. It can be occurred either on the scale of two beds within an individual turbidite, or on the scale of the whole succession. For example, late stages of high-density turbidity currents can transform into low-density turbidity currents; each stage has its own distinct sequence of internal structures within individual beds (Figures 3.39, and 3.40). The transformation between different kinds of gravity deposits can be used as an effective tool to interpret an energy level and distance from the source (Flügel, 2010). Hüneke and Mulder (2011) stated that the transfer facies from graded bedding into laminated sedimentary structures indicates an upward decrease in the energy level, which shows a transfer from concentrated flow to turbulent flow deposit. The transformation from the turbidity regime to slumping structures of the upper part of the Sargelu Formation can be clearly indicated in the field successions.



Figure 3.38: Slumped structure showing folded beds, note the bedding kept their parameters (red arrows) which indicate early lithification, Gara location.

### 3.20 Summary

Basically, the Sargelu Formation is divided into three members as follows: BSDM, MPLM and BRPLM. The current study focuses on the BRPLM which is in turn divided into three lithofacies: PBLL, RBCL and BSALL. Commonly, these lithofacies alternate with each other at intervals of several decimetres, and the results in this study show clear interaction between them, which is embodied in the allodapic limestone turbidity model.

PBLL is dominated by thin-shelled bivalves of *Posidonia*, with some poorly preserved ammonites and aptychi. In some cases, the vertical section of the PBLL shows normal graded bedding, which is followed by parallel and then undulating laminae of the posidonia-rich limestone. Beds of the PBLL are mostly overlain or underlain by bedded cherts or black shales. Commonly, the preservation of *Posidonia* shells in the BRPLM changes from base to top into the following different styles: broken, butterfly, horizontal disarticulated valves, articulated with closed valves and cone-in-cone which imply environmental changes from shallow to deep water environments. The prominent PBLL is principally composed of radiolarian chert with few silicified *Posidonia* layers, and is interbedded with both RBCL and BSALL. The PBLL decreases westward of the study area until it vanishes completely just about 60 km in the subsurface sections. It has been suggested here that the bedded chert is located at the periphery of the main radiolarian depositional basin of Kermanshah of Iran. The monsoonal-driven upwelling current model could be contributed to high productivities and high accumulation rates for radiolarites.

Careful examination of the sedimentary structures of the different lithofacies reveals the common presence of resedimentation or turbidity structures in the upper part of the Sargelu Formation. The stacked packages of different lithofacies follow a particular order, and each package often shows the following vertical succession from bottom to top: graded bedding, laminated structures and bedded chert or black shale, which is comparable to the allodapic carbonate deposition or turbidite structures.

Based on the coexistence of the *Kosmoceras* species of ammonite, *Posidonia ornati* Quenstedt and *Cinguloturris carpatica* Dumitrica, the possible age range may change from the Bathonian–Bajocian to the Bathonian–Middle Callovian.

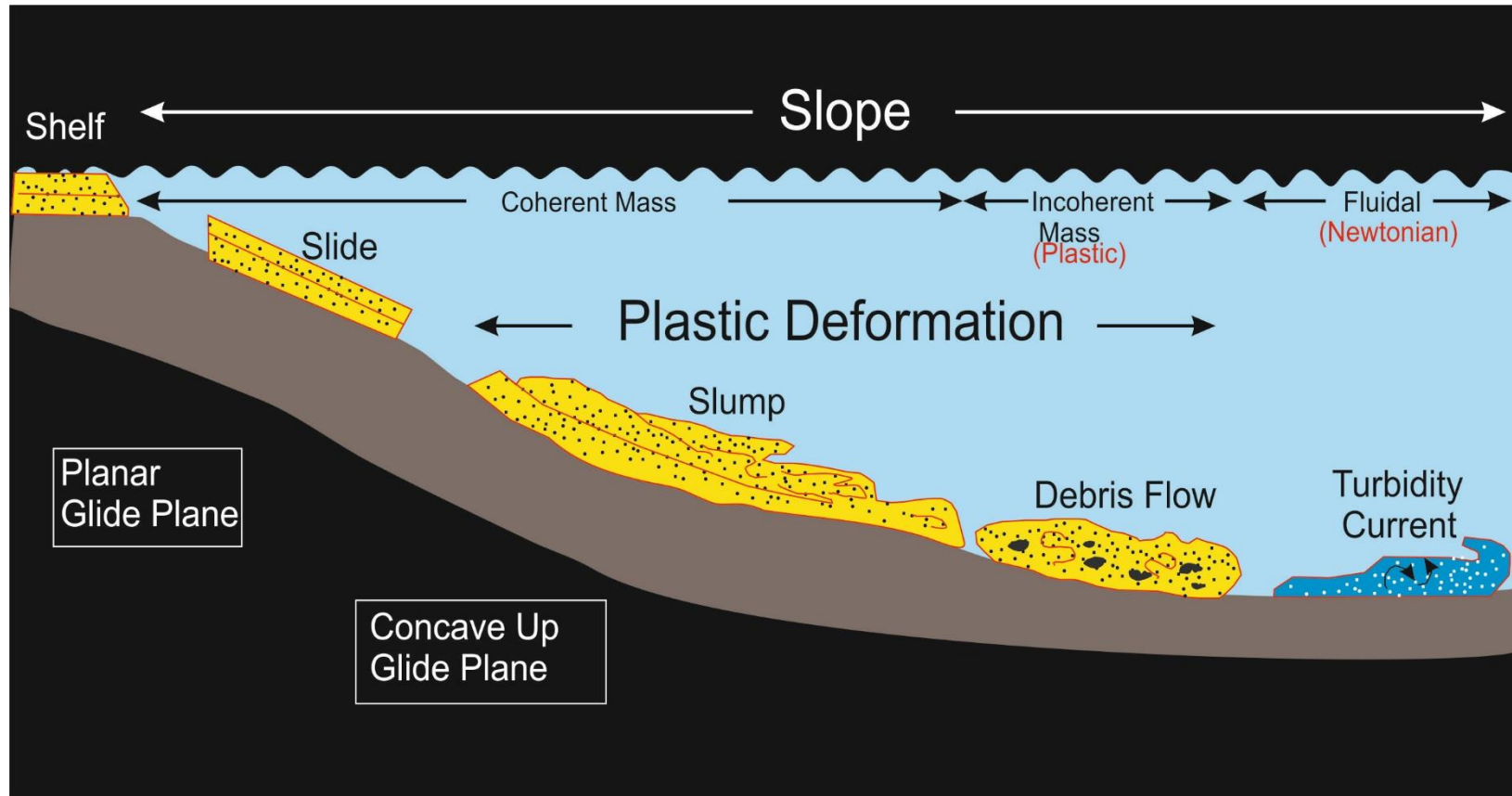


Figure 3.39: Schematic diagram showing different types of gravity-driven processes which transport sediments into deep water environments (modified from Shanmugam 2006).

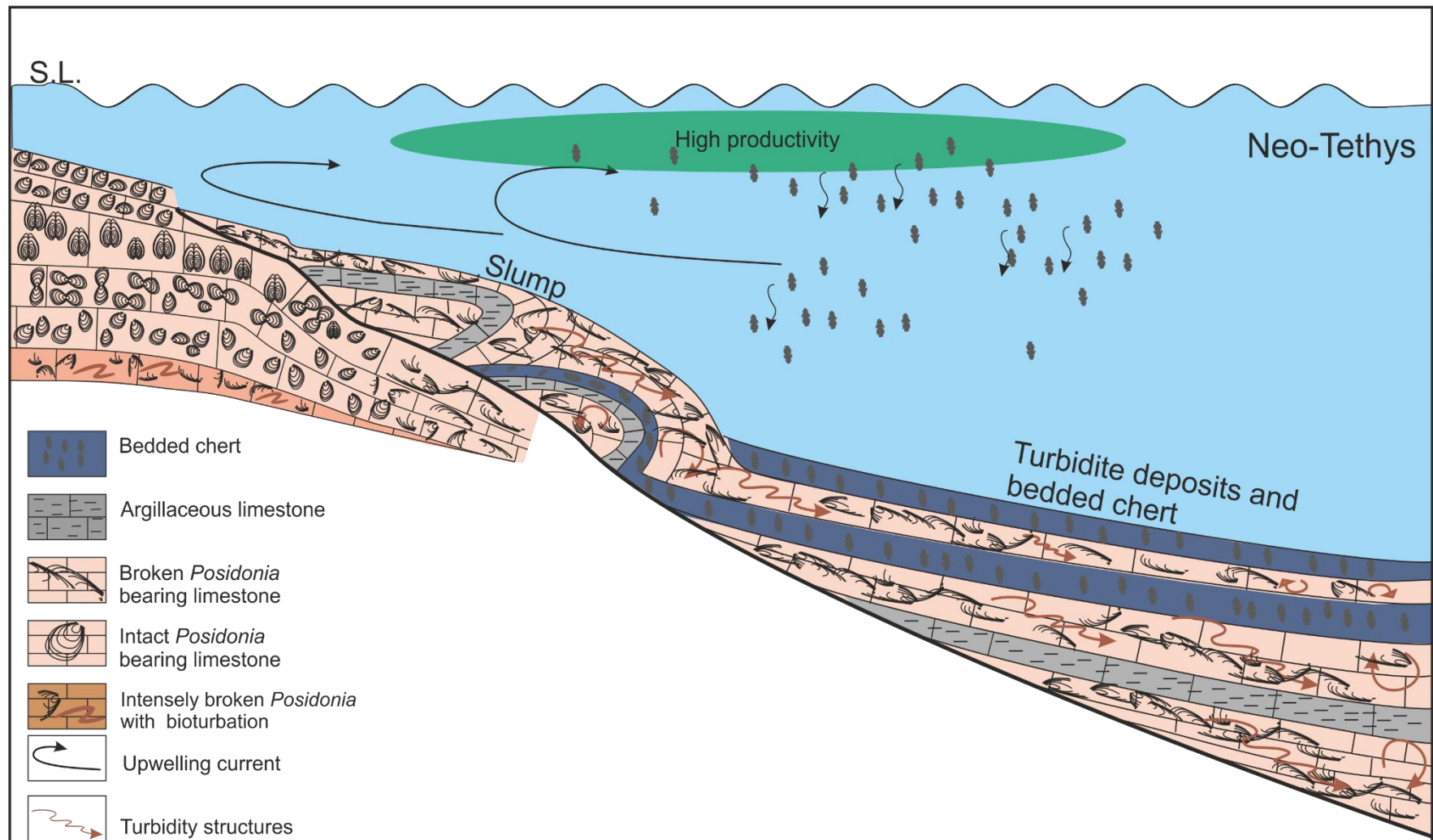


Figure 3.40: Hypothetical diagram showing upwelling current, high productivity and slumping structures of the upper part of the Sargelu Formation during Bathonian age. Note transformation gravity deposition from a relatively shallow slump to deeper turbidite deposits.

## **CHAPTER FOUR**

### **4 DESCRIPTION AND INTERPRETATION OF THE NAOKELEKAN FORMATION OXFORDIAN-EARLY KIMMERIDGIAN**

## 4.1 Aims

- To describe lithofacies in detail and establish a better understanding of depositional environments through field description, petrography, and microfacies analyses for seven selected sections of the Oxfordian–Early Kimmeridgian age in the Kurdistan region exposures.
- To interpret distributions, and transitions, between different lithofacies. To determine the causative factors in the sharp environmental changes from open-marine pelagic sedimentation to sabkha environments. What does this mean in terms of depositional processes and environments? Consequently, what can be inferred from these sharp lithofacies transitions?
- To understand the nature of the boundary lines between different lithostratigraphic members, as this has previously been poorly defined.

## 4.2 Facies analysis

Naokelekan Formation was first described near Naokelekan village (Figure 4.1), in the imbricated zone, in northern Iraq (Bellen et al., 1959). The formation is one of the most well-known organic-rich Jurassic successions of Iraq (Buday, 1980; Jassim and Goff 2006; Aqrabi et al., 2010). The Naokelekan Formation was subdivided by Bellen et al. (1959) into three members: i) the lower member, which is 7 metres thick, consists of thin-bedded, extremely bituminous limestones, dolomites, and bituminous calcareous shales (coal horizon of informal field nomenclature). ii) the middle member, about 4 metres, comprises dark grey, hard, mottled limestones with ammonite traces (Mottled bed of informal field nomenclature), iii) the uppermost 3 metres are laminated shaly limestone. Spath (1950) studied ammonites from the mottled member of the upper Jurassic of the Kurdistan area, and he determined the age of the formation to be Late Oxfordian to Early Kimmeridgian. Based on new observations and descriptions of the outcrops and petrographical study, the Naokelekan Formation can now be subdivided into five different lithologic members (Figures 4.2, and 4.3). The Naokelekan Formation members comprise:

1. Black shale member (BSM)
2. Carbonaceous limestone member (CLM)
3. Medium-bedded microbial-bearing limestone member (MBMLM)
4. Thick-bedded mottled limestone member (TBMLM)
5. Argillaceous limestone member (ALM)

### 4.3 Black shale member (BSM)

#### Field description

Black shale occurrence in Jurassic successions of the Kurdistan region has been recorded in the upper part of the Sargelu Formation, Bajocian–Bathonian, and the base of the Naokelekan Formation, Oxfordian–Early Kimmeridgian. They are considered a major source rock for Iraqi oil (Jassim and Goff, 2006; Ahmad, 2007; Hussein et al., 2013; Al-Ameri et al., 2013; Hussein et al., 2013; Abdula, 2014; Al-Ameri and Al-Nagshbandi, 2014).

Black shale member (BSM) represents the base of the Naokelekan Formation. It is black to dark grey in colour, highly fissile kerogeneous shale, with the bed thickness ranging from 10 to 30 cm. The black shales are normally interbedded with a few thin beds 5–10 cm of dark grey dolomites (Figure 4.4, A–B). In addition, there is a unit of dark-coloured lensoidal limestone, about 0.35 m thick and up to 1 m in length.

#### Microscopic description

Thin-section studies show crudely laminated mudstone, including a few poorly preserved planktonic *Protoglobigerina* foraminifera, and some small unidentified fossils 0.1–0.5 millimetres in size (Figure 4.6 A–B). This member is rich in probable calcareous nanofossils “coccoliths” relative to other faunas. The nanofossils, which are 8–15 microns in diameter, are round–ovate spheres. Their central openings, which are filled by organic matter, range from 0.04 to 0.08 millimetres in diameter (Figure 4.6, C). The nanofossils make up more than 85 % of the rock mass. The black shale beds are mainly composed of a mixture of clay minerals, silicates, and organic matter together with calcareous nanofossils.

The top of the BSM is distinguished by coarse-crystalline, saccharoidal dolomite. The dolomite crystals, which are unstained with Alizarin Red S, display cloudy, and euhedral to subhedral shapes, ranging from 0.150–0.250 mm in diameter (Figure 4.6, D). Intercrystalline porosity forms about 5–8 % of the bulk rock, which is infilled by black structureless organic material (Figure 4.6, D). A geochemical analysis of organic matter revealed the presence of black structureless materials of kerogen, which are insoluble in organic solvents (Salae, 2001). The microscopic study of the organic matter displays dark brown, segmented and branched forms of unidentifiable nature (Figure 4.6, E).

Anastomosing stylolites are common, black matter often concentrating on their surfaces (Figure 4.6, A).

#### 4.3.1 Bajocian–Bathonian and Oxfordian–Early Kimmeridgian boundary

The boundary between the base of the Naokelekan Formation and the top of the Sargelu Formation is represented by a black shale-dominant interval, so it is hard to determine the contact line between Bajocian–Bathonian and Oxfordian–Early Kimmeridgian age accurately. It is preferable to depend on the characteristic features of the top of the Bajocian–Bathonian rather than the base of the Oxfordian–Early Kimmeridgian for two reasons. Firstly, the top of the Sargelu Formation is laterally extensive for hundreds of kilometres and can be observed at all locations. It is very distinctive, and its diagnostic features are similar at all locations, where the top of the Sargelu Formation shows convoluted bedding and contains *Posidonia*-bearing chert and limestone as well as black shale (Figure 4.5, A–E). Secondly, the black shale member of the Naokelekan Formation do not appear at all locations clearly, and do not show prominent characteristics. Therefore, its base cannot be used for establishing lithostratigraphic correlation. The Naokelekan black shale member normally rest sharply on the convoluted bedding unit.

The black shale member in the Banik location that has been traditionally called “coal horizon,” was interpreted to represent the base of the Naokelekan Formation (Figure 3.8, B). However detailed study of the member reveals that this organic-rich black shale interval most likely belongs to the upper part of the Sargelu Formation. This interpretation is based on two facts: (i) this member demonstrates convoluting structure, which specifically belongs to the Sargelu Formation Environment, (ii) this interval is rich in *Posidonia* fossils.

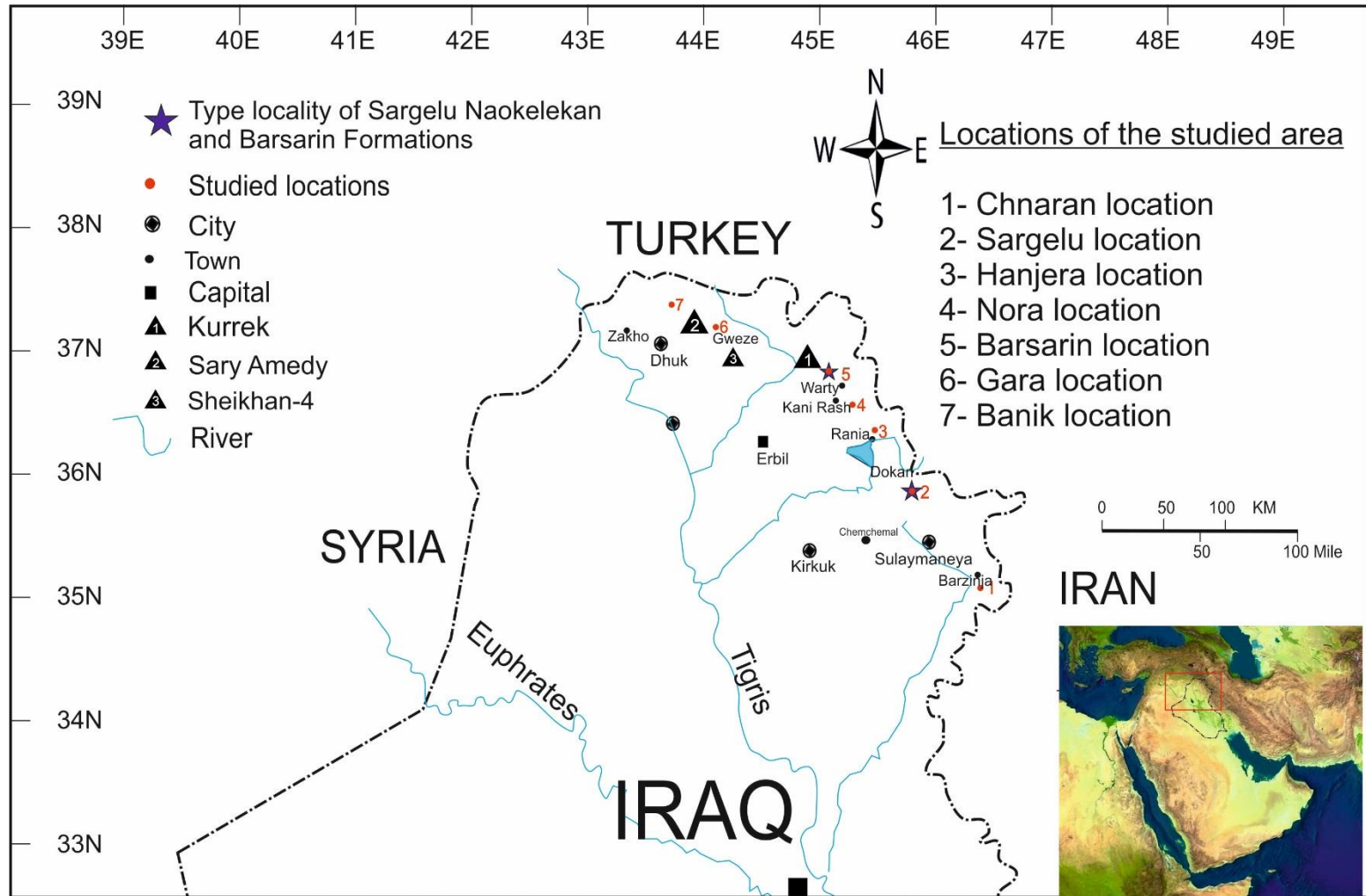


Figure 4.1: Different locations of the studied areas in northern Iraq, Kurdistan region.

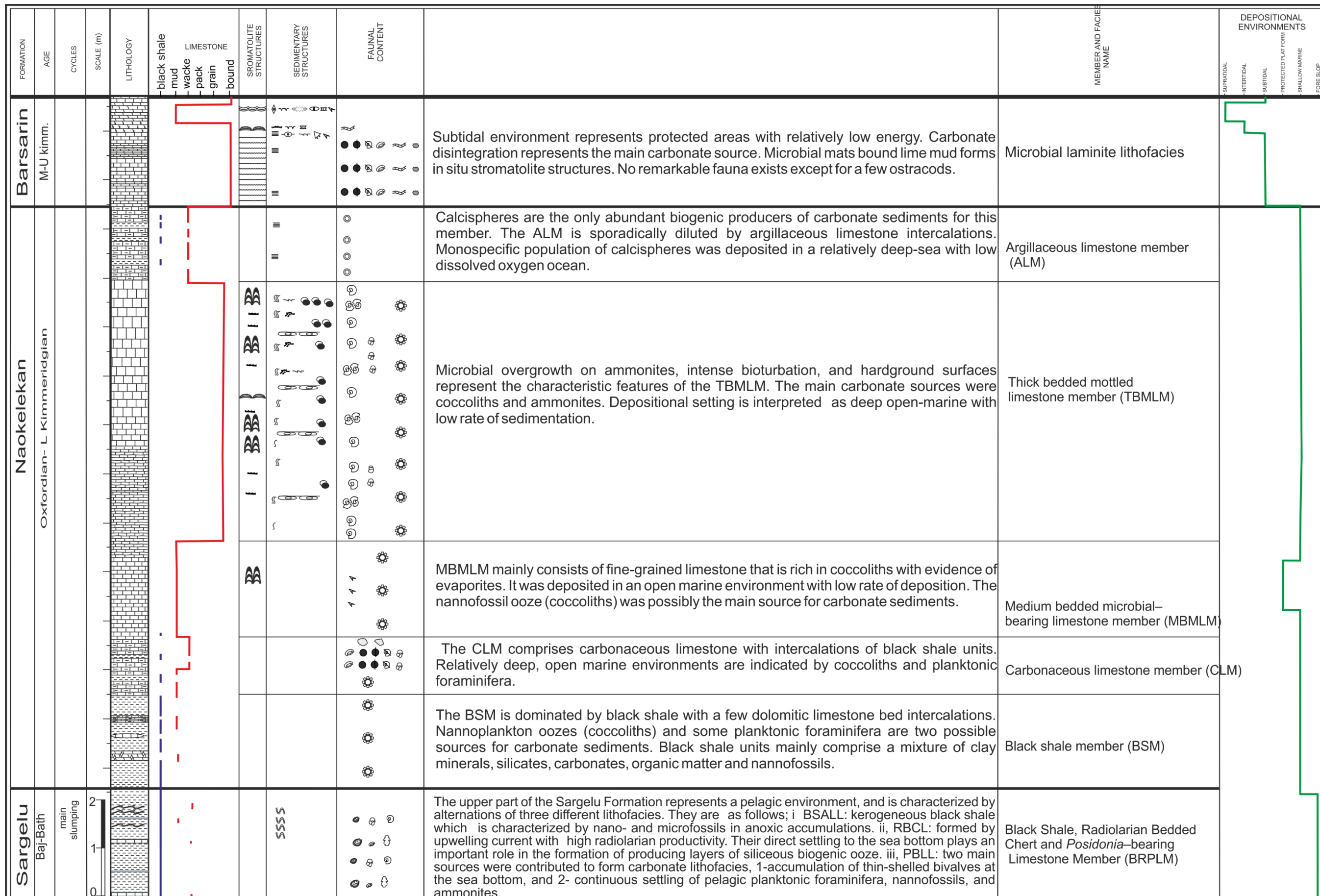


Figure 4.2: Generalized stratigraphic column of the Naokelekan Formation showing different members and the nature of underlying and overlaying contacts with Sargelu and Barsarin

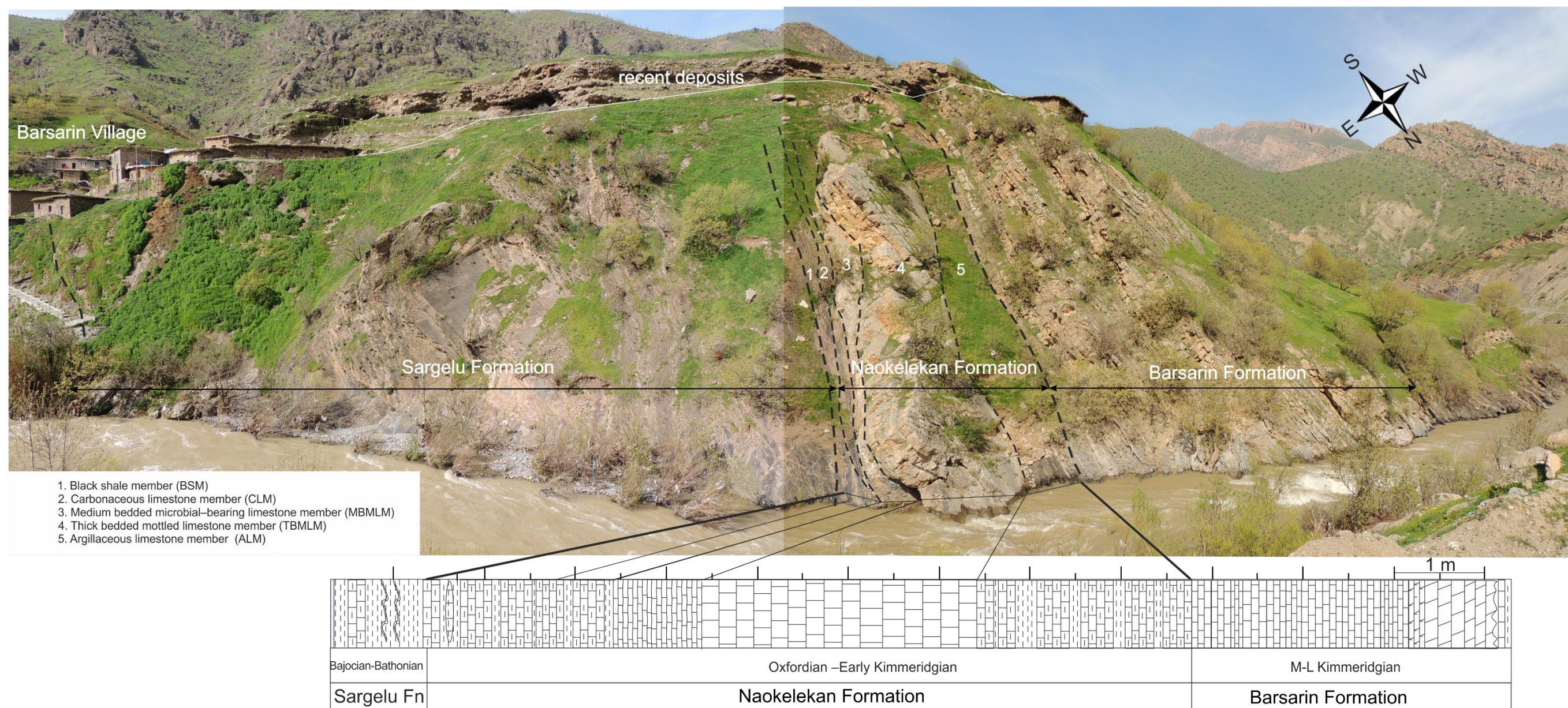


Figure 4.3: Panoramic photography showing the M-U Jurassic succession at Barsarin village locality. The Naokelekan Formation is represented by five different members BSM, CLM, MBMLM, TBMLM and ALM.



Figure 4.4: A; Black shale intercalated with a few dolomite beds. Note the sharp contact with the overlying medium-bedded microbial-bearing limestone member, Sargelu location. B; detail of black square in figure (A) showing black shale and few dolomite beds.

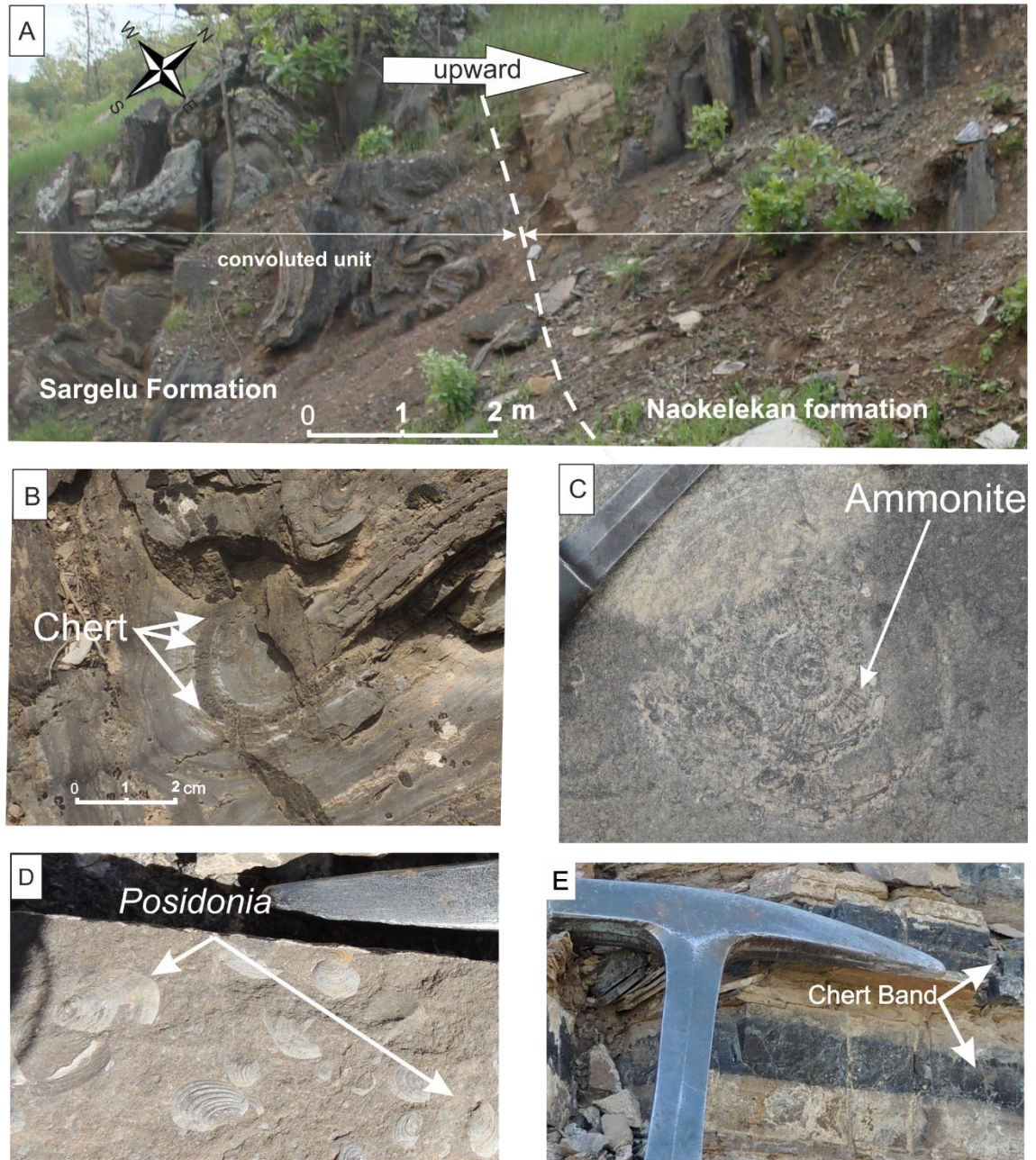


Figure 4.5: A; contact between the Naokelekan and Sargelu formations (dashed line). Note the changes from convoluted structures at the top of the Sargelu Formation to normal bedding at the base of black shale member of the Naokelekan Formation, Gara location. B, C, D, and E; detailed photographs representing the characteristics of the convoluted chert bands, ammonite, *Posidonia*, and bedded cherts respectively; they show unique diagnostic features of the top of the Sargelu Formation at all locations. B and C are from Gara location, whereas C and D are from Nora location.

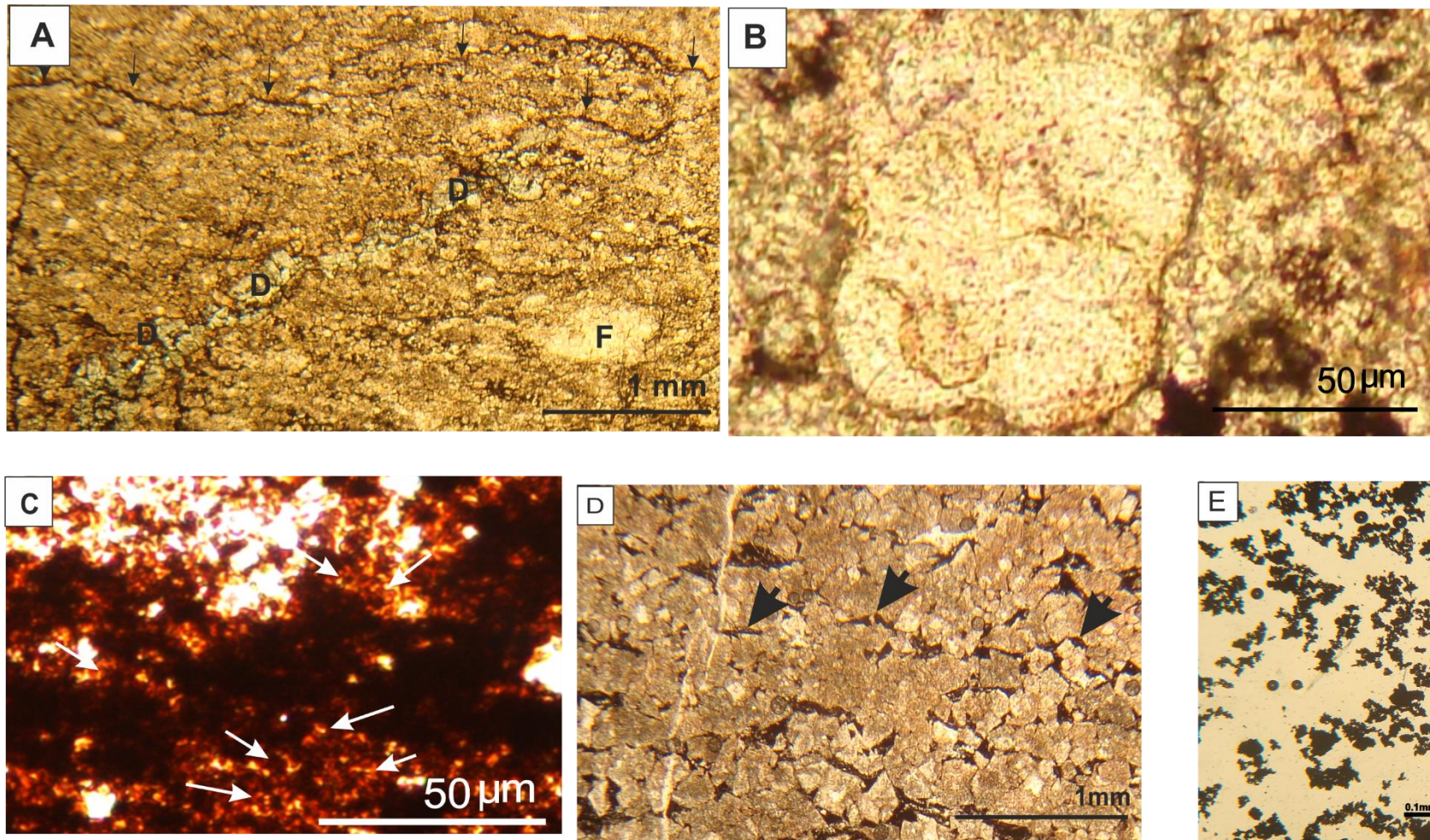


Figure 4.6: Black shale member: A; crudely laminated carbonaceous wackestone, including poorly preserved fossils (F), few dolomitized crystals (D), and organic materials are often concentrated on stylolites surfaces (black arrows), stained with Alizarin Red S, Hanjera location. B; poorly preserved planktonic *Protoglobigerina* foraminifera Barsarin location. C; Round to ovate-shaped nannofossils; each include central opening and are filled with organic material (white arrows), Hanjera location. D; subhedral to euhedral dolomites, note intercrystalline pores infilled by organic material (black arrows), Banik location, E; amorphous organic matter, showing dark segmented and branched forms. (All of the images are in the plane polarised light), Barsarin location.

### 4.3.2 Interpretation

According to Wignall (1994), any black coloured organic rich, fine grained sediment can be defined as black shale. The black colour is in part due to the presence of organic carbon, and abundance of pyrites. Emeis and Weissert (2009), and Trabucho-Alexander et al. (2012) are of the opinion that black shale is quite challenging to define as well as to classify, because they assume that black shale is a collective noun for a group of rocks with varying origins. More attention should be given to the sedimentary processes that lead to their formation, which is important for the Naokelekan black shale because multiple possible processes of its formation need to be considered.

The coexistence of *Protoglobigerina* and coccoliths can prove hemipelagic environments (Armstrong and Brasier, 2005). This kind of faunal association is comparable to the BSM of the Naokelekan Formation, where coexistence of *Protoglobigerina* and coccolith is quite common. Moreover, black shale is assumed to be of hemipelagic deposition by many authors, and the shales tend to form in relatively deep, restricted basins where reducing conditions prevail and abundant organic matter is preserved (Wignall, 1994; Selley, 2000; Boggs 2009). So, a hemipelagic depositional environment can be inferred for black shale member.

At the present time, organic-rich carbonates do not accumulate in the deep basins of oceans. For this reason, there are no recent analogues for the ancient pelagic or hemipelagic black shale depositions. Reading (1996) stated that the black shale accumulation theoretically can be determined by two end members:

(i) enhanced supply; this represents the areas of high surface water productivity for which the best modern example is the Gulf of California. Accumulation of black shale may occur if the surface-water productivity is high and/or there are plant rich terrestrial sources. The main factors controlling black shale preservation are oxygen concentration in the bottom water, sedimentation rate, particle size, and seafloor profile (Demaison and Moor, 1980). The high concentration of calcareous nannofossils relative to other faunas in the Naokelekan black shale member (Figure 4.6, C), especially in Banik location (Figure 4.1), may support enhanced supply as an acceptable model for this member, which is indicative of the high surface water productivity.

(ii) enhanced preservation; in this kind, the productivity is low but highly anoxic sea water preserves the black shale. The Black Sea is a good sample for this model. However, Trabucho-Alexander et al. (2012) found that the enhanced preservation model of the

Black Sea cannot be applied to ancient black shale, due to such extreme requirements being imposed on the deposition of black shale in the Black Sea. The Black Sea model cannot be applied to the black shale of the Naokelekan Formation and this because of the fundamental oceanographic differences between them. The Jurassic successions of the Kurdistan region were deposited in the passive margin of the Neotethys Ocean in contrast to the closed Black Sea.

#### 4.3.3 Oceanic Anoxic Events (OAE)

The deposition of organic-rich black shale in the Palaeozoic and Mesozoic Eras occurred in similar facies and over a wide area at specific times, and it seems to be a global event. This led Schlanger and Jenkyns (1976), and Jenkyns (1988) to the assumption that black shales were deposited synchronously and globally within narrow time envelopes, which were termed Oceanic Anoxic Events. Shale dominant intervals in the Middle–Upper Jurassic are not confined to northern Iraq's territory only, but they also occurred in many other areas of the AP. However, the shale intervals were not deposited concurrently (Alsharhan and Narin, 2003), and this may suggest that the deposition of the black shale of the Naokelekan Formation is a local event rather than to be OAE.

### 4.4 Carbonaceous limestone member (CLM)

#### Field Description

The thickness of the carbonaceous limestone member (CLM) ranges from 1.15 to 1.9 metres, and it is represented by thin to medium-bedded 7–15 cm thick, kerogeneous and dark grey limestone, with thin intercalations of black shales. The most conspicuous feature of this member is a gradual upward decrease in the amount of shale, and increase in limestone (Figure 4.7). This member is present at Chnaran, Hanjera, Nora, Barsarin, and Gara locations (Figure 4.1). Based on field observations, this member can be subdivided into two parts in ascending order:

1–The lower 0.6 metres consists of dark grey, medium to thin-bedded carbonaceous limestone, with thin-bedded black shale intercalations, (Figure 4.7).

2–The upper 0.65 metres comprises dark grey, thin-bedded highly fissile and fossiliferous limestone (Figure 4.7).

Its upper contact with the overlying medium-bedded microbial-bearing limestone member is sharp, and the boundary can be determined by the disappearance of the black shale intercalation in the MBMLM.

#### Microscopic description

1–The lower part: It may be subdivided depending on crystal fabric into two categories: (i) it exhibits different grain sizes of recrystallized calcite grains that are subhedral to anhedral in shape (Figure 4.8, A), and the crystal sizes range between 0.05 and 0.1 mm. Few selectively dolomitized fossils 1 mm in size have been observed (Figure 4.8, A). (ii) Inequigranular fabric (Figure 4.8, B) displays mixtures of calcite crystals, up to 0.2 mm across. Anastomosing stylolites are common, with black material concentrated on their surfaces. Study of the amorphous organic matter showed flaky tissues (Batten, 1982), and granular elements (Figure 4.8, C).

2–The upper part: The lithology varies from being mudstone at the base, to wackestone at the top of this member. It is rich in microfossils, which are represented by different kinds of foraminifers (Figure 4.9, A–D). The planktonic *Protoglobigerina* makes up the majority of fossil contents. Also few elongate uniserial and biserial benthic forams were observed (Figure 4.9, C). All fossil moulds and pores are filled with calcite cement (Figure 4.9, A–D). High magnification of thin-sections shows high abundance of small ring-shaped nannofossils, which perhaps represent coccoliths, 10–30  $\mu\text{m}$  in size. It seems that most of the detrital matrix grains were derived from the breakdown of coccoliths (Figure 4.9, E), and their intra-interstitial pores are infilled by kerogeneous matter.

The topmost 30 cm is substantially different from the lower 35 cm of this member. It comprises mixtures between angular and rounded grains 0.05–0.1 mm in size. The grains are moderately sorted and loosely packed, and they are partially or completely micritized with an indistinct nucleus and micritic envelopes. Although the overall texture can be classified as wackestone (Figure 4.9, H), in a few places engulfed micritized grains in calcite sparite appear as grainstone (Figure 4.9, G). Very few planktonic forms, fossils fragments and some angular chert grains are also observed (Figure 4.9, F).



Figure 4.7: carbonaceous member subdivisions: (a); medium to thin-bedded carbonaceous limestone, and (b); thin-bedded highly fissile and recrystallized carbonaceous limestone. Note, carbonaceous limestone member is underlain and overlain by black shale member, and medium microbial-bearing limestone member respectively, the shale amount decreasing upward can be clearly observed, Nora location.

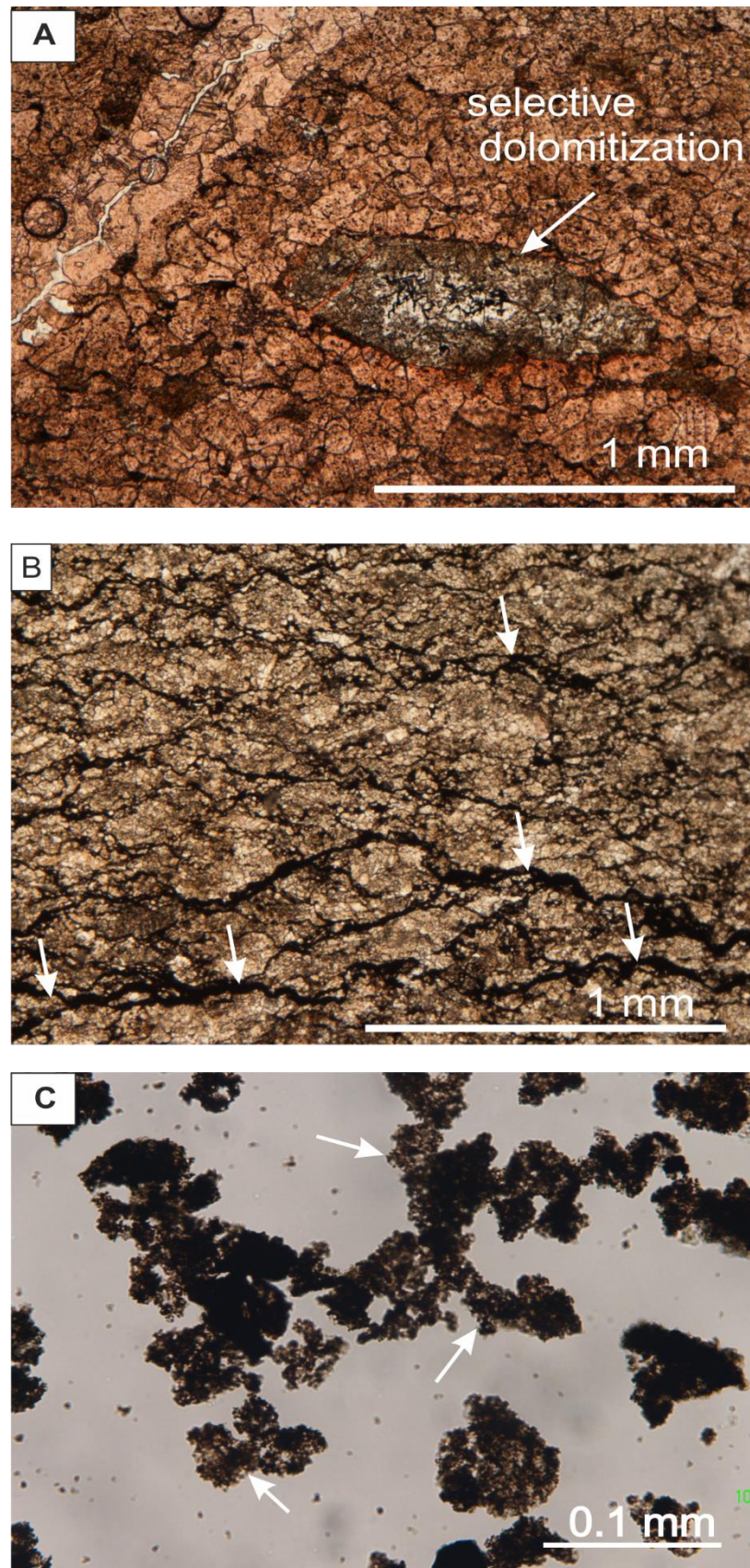


Figure 4.8: A; stained recrystallized limestone with Alizarin Red S showing selective dolomitization. B; Inequigranular fabric showing different grain-size of calcite, subhedral to anhedral, bituminous material superimposing anastomosing stylolites (white arrows). C; amorphous organic matters of carbonaceous limestone member showing flimsy tissues. All of the images are in plane polarised light, Barsarin location.

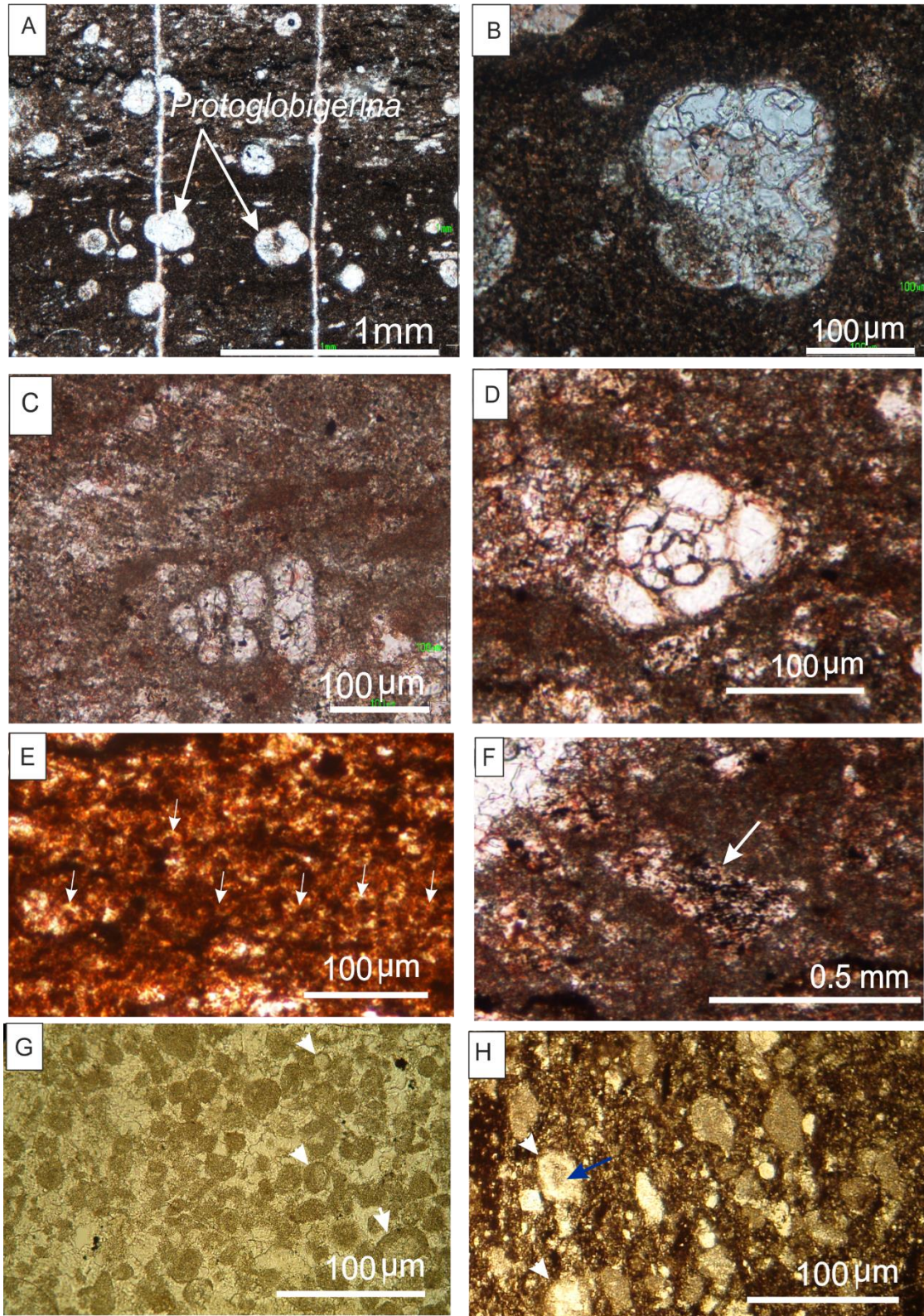


Figure 4.9: A; photomicrograph showing *Protoglobigerina* foraminifers (white arrows) that make up the majority of fossil contents of the upper unit of carbonaceous limestone member, Hanjera location. B; calcite cement infilling *Protoglobigerina* fossil moulds, Hanjera location. C; Biserial forams, Gara location. D; unidentified foraminifera, Gara location. E; small ring-shaped nanofossils, perhaps coccoliths (white arrows), Barsarin location. F; chert grains (white arrows), Gara location. G; engulfed micritized grains in calcite sparite, note some enveloped grains (white arrows), Hanjera location. H; partially or completely micritized angular grains (white arrows), Gara location. All of the images are in plane polarised light.

#### 4.4.1 Interpretation

##### 4.4.1.1 Micro- and nannofossils

*Protoglobigerina* are dominant microfossils in this member that make up more than 20 % of some horizons in the bulk rock. These small planktonic foraminifera have been previously observed and described in the Sargelu Formation, Bajocian–Bathonian age in the current study (see Chapter Three). The second important component in carbonaceous limestone member is coccoliths association (Figure 4.9, E), which form the majority of the groundmass, and they usually make up 90% of the micrite constituents. The coccolith occurrences in the Naokelekan Formation started during the black shale member and lasted until the top of the mottled limestone member (Figure 4.2).

Louis (2007), in his investigation in France and Switzerland about Early–Middle Oxfordian sediments, observed an association between coccoliths and *Protoglobigerina* in hemipelagic sediments. Furthermore, Armstrong and Brasier (2005) stated that the *Globigerina* planktonic foraminifera associations with coccoliths are significant contributors to deep-sea sedimentation. A microscope with a high magnification shows a great contribution of coccoliths on rock building in the CLM (fig 4.9, E). A lack of sedimentary structures, the dominance of *Protoglobigerina* planktonic foraminifera and coccoliths, and the scarcity of benthic foraminifera in the CLM suggests a relatively deep-water depositional environment, and may be below wave base. The existence of elongated shells of benthic foraminifera (Figure 4.9, C) points to the soft muddy substrate (Brasier, 1980).

##### 4.4.1.2 OAE and development of *Protoglobigerina*

There is a consensus between the scientists on the hemipelagic origin of *Protoglobigerina* fossils (Jansa et al., 1984; Fels, 1993; Jansa, Fleet et al., 2002; Armstrong and Brasier, 2005; Vedrine, 2007; Bellier, 2010; Andreea, 2012; Haas, 2012). The first occurrence of *Protoglobigerina* was recorded directly after the Toarcian age. They most likely developed from benthic forams as a result of the Toarcian oceanic anoxic event (OAE). The Early Toarcian possibly followed by a massive release of gas hydrates resulted in development of *Protoglobigerina* (Hart, 2003; Fribourg & Kiel, 2005; Fadel, 2012). This theory is consistent with the Middle–Upper Jurassic succession of Kurdistan where planktonic *Protoglobigerina* first occurred with local OAE appearance in the upper part of Sargelu Formation.

#### 4.4.1.3 Micritized grains

Concerning the micritized grains in the topmost 30 cm, it seems probable that a major proportion of the grains are angular (Fig 4.9, H), which suggests non-fecal peloids. The micritization process normally takes place through the alteration of clasts or bioclasts by endolithic algae, fungi and bacterial activities (termed microbial micritization) just on the sea floor, whereas envelopes are produced by the incomplete microbial micritization process (Tucker and Wright, 1990; Bathurst, 1975). There are two hypotheses, which may explain the origin of micritized grains of the topmost of carbonaceous limestone member:

1–Micritized grains in the CLM are comparable, to some extent, with Flügel's (2004) definition of the pseudopeloids of the Bahamian sediments. He stated that the pseudopeloid grains are peloids that originated from micritized ooids (Figure 4.9, G). Thus, based on Flügel's description, the origin of micritic grains can be attributed to the ooids on pelagic swells. A similar occurrence of pseudopeloids in submarine pelagic swells is emphasized by Lakschewitz et al. (1991) in the Chiemgau Alps in Germany, in the Late Jurassic period.

Due to the uncertainty and weak remnant textural characteristics of micritized grains at the top of carbonaceous limestone member, these grains cannot be identified certainly as ooids. Also, some grains display irregular contacts between the micritic envelope and the core textures which point to micrite coat rather than oolites. For the reasons mentioned above, micritized clasts cannot be undoubtedly determined as oolitic.

2–Bathurst (1975) found that the micritized skeletal debris forms a considerable part of the recent lime sand in the Bimini Lagoon. He stated that the microbial boring on skeletal grains is the main cause for yielding micritization. The boring normally weakens the limestone grains as they are mechanically suited to becoming rounded shape. This model cannot be applied to the carbonaceous limestone member because of the prevailing hemipelagic fauna such as *Protoglobigerina* and lack of any shallow or lagoonal indications.

Based on the evidence above, the formation of the micritized grains seems to be related to the first hypothesis. This inference is supported by the pelagic faunal elements such as coccoliths and *Protoglobigerina* association.

## 4.5 Medium-bedded microbial-bearing limestone member (MBMLM)

### Field description

The medium-bedded microbial-bearing limestone member (MBMLM) is dark grey, thin- to medium-bedded limestone, laminated in places. The bedding is highly fractured with no visible fossils, and is characterized by uniform and steady lateral extension (Figure 4.10, A). At the Chnaran section (Figure 4.1), at about 30 cm above the base of this member, a dark grey, medium-bedded 15–30 cm mudstone displays thick laminae. The bedding is characterized by elongated lensoidal structures 4–5 m in length (Figure 4.10, D), and small, scaled fractures occurred on upper and lower bedding planes (Figure 4.10, F). These fractures were completely filled by the overlying sediments.

The previous studies, which were carried out by local geological researchers, considered both TBMLM and MBMLM as one member that was traditionally called a “mottled member” (Bellen et al., 1959; Buday, 1980; Al-Sayab et al. 1982; Jassim and Goff, 2006; Aqrabi et al., 2010). However, the current study has revealed the existence of two different members in the traditional “mottled member”. Each of them has its own significant characteristics that will be discussed in detail in the next sections.

The upper boundary with the overlying thick-bedded mottled limestone member is sharp, and is marked by the first appearance of mottled textures. Both MBMLM and TBMLM are always overlain and underlain by a softer limestone and dominant black shale lithologies at all locations. The soft black shale is easily weathered, producing prominent cliffs of MBMLM and TBMLM in the outcrops (Figure 4.11, C). It is laterally extensive for hundreds of kilometres with constant thickness, where it can be readily recognized at all locations (Figure 4.34).

### Microscopic description

The MBMLM is composed of crudely laminated mudstone that contain a few scattered crystals of calcite spars, 30–50  $\mu\text{m}$  in size, which are floating in the micritic calcite matrix (Figure 4.10, C). At the top of this member, a considerable proportion of small lath and stellate shaped calcite pseudomorphs of evaporite have been observed, and the pseudomorph sizes range from 0.1 to 0.4 mm (Figure 4.10, B). High magnification light microscope study shows signs of microbial filaments as well (Figure 4.10, E).

Scanning electron microscope (SEM) analysis indicates that the MBMLM contains numerous probable calcareous nanofossils. These objects are elliptical to circular and between 6–11  $\mu\text{m}$  in diameter (Figure 4.10, G). They have a narrow rim and open central area, and the central area has a hole ranging from 2 to 5  $\mu\text{m}$  in diameter. The rings are relatively intact, but broken and fragmented rings are also common. SEM observations indicate that probable nanofossils are randomly arranged, and are surrounded by inconspicuous features of small calcite spar and by fragments ranging between 1–3  $\mu\text{m}$  across.

#### 4.5.1 Interpretation

Facies transition between MBMLM and TBMLM is marked by the first appearance of mottling texture (Figure 4.11, B). Both members are totally different. The former member comprises nanofossils, microbialites with probable calcite pseudomorphs after evaporite crystals and devoid of any ammonites, whereas the latter is characterized by existence of mottling texture, dense microbial growth and horizons of mass ammonite accumulation (Figure 4.13, B). For this reason, in the present study, the traditional mottled unit have been subdivided into two different members, MBMLM and TBMLM (Figure 4.11, A). The most important distinguishing characteristics for each member are summarized in the table 4.1:

The most probable hypothesis for the nanofossils origin is coccoliths. Other microfossils (e.g. calcispheres, radiolaria, and tintinnids) can be excluded due to their larger size normally  $>40 \mu\text{m}$ , whereas all nanofossils in the MBMLM are from 5–10  $\mu\text{m}$ . Moreover, morphologically coccoliths are different from other fossils; where the tintinnids appear as spherical to elongate, U-or V-shaped grains, the radiolaria display sieve-like fabric and are mostly siliceous, and the calcisphere lack internal structures (Scholle, 2003; Armstrong and Brasier, 2005).

Thin-section studies show scattered lathe, rosette shaped calcite pseudomorphs of evaporite, with no signs of any desiccation features such as tepee, mud-cracks, and solution collapses associations. In contrast, a lot of lensoidal shapes of micrite, coccoliths and microbial bacteria are associated. The member is completely barren of micro–macro fauna.

The occurrence of pseudomorphs of evaporite in association with coccoliths and microbial structures, which is seen very commonly in the Chnaran and Rania locations, have never been previously described in the Naokelekan Formation, and is extremely

puzzling. The depositional environment of the evaporite pseudomorphs is difficult to interpret because the associated fauna such as coccoliths are usually considered to be formed in open-sea. Furthermore, the sediments immediately underlying and overlaying this member have definitive faunal evidence of a distinct open-marine sequence.

Characteristics	Thick-bedded mottled limestone member	Medium-bedded microbial-bearing limestone member
Micro–macro fauna	Rich in ammonite and planktonic foraminifera	None
Nannofossils	Rich in coccoliths	Rich in coccoliths
Textures	Mottled	No mottling observed
Stromatolites	Laterally linked and columnar are common	Rich in microbial filaments
Bioturbation	Very common	None
Bedding thickness	Thick to massive	Medium
Evaporite pseudomorphs	None	Observed in places

Table 4.1: Comparison between thick-bedded mottled limestone member and medium-bedded microbial-bearing limestone member.

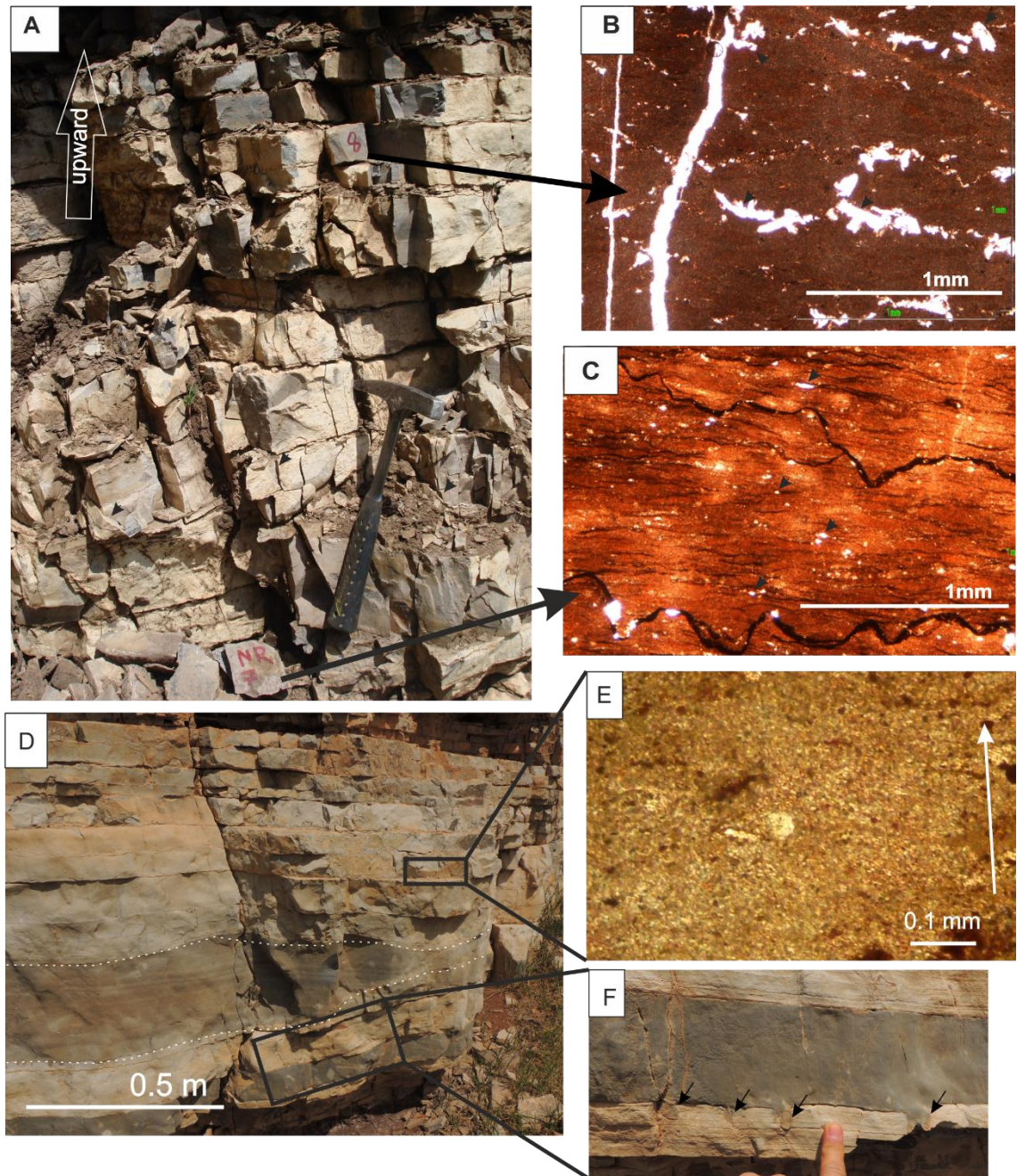


Figure 4.10: A; highly fractured, and well bedded MBMLM, Chnaran location. B; photomicrograph of the upper part of the MBMLM showing small lath shapes of limestone pseudomorphs of evaporite, Banik location. C, crudely laminated mudstone, including small scattered calcite spars, Banik location. D; Lower part of the MBMLM showing elongated lensoidal structures (white dashed line), Chnaran location. E; microbial bacteria, note the direction of microbial growth are parallel to the white arrow, Chnaran location. F; small scaled segmented bedding at lower part of the medium-bedded microbial-bearing limestone member, Chnaran location. G; Elliptical to circular calcareous nanofossils constitute the majority of the components of the rock sample, Chnaran location. (B, C, and E images are in the plane polarised light).

1. Black shale member (BSM)
2. Carbonaceous limestone member (CLM)
3. Medium bedded microbial-bearing limestone member (MBMLM)
4. Thick bedded mottled limestone member (TBMM)
5. Argillaceous limestone member (ALM)

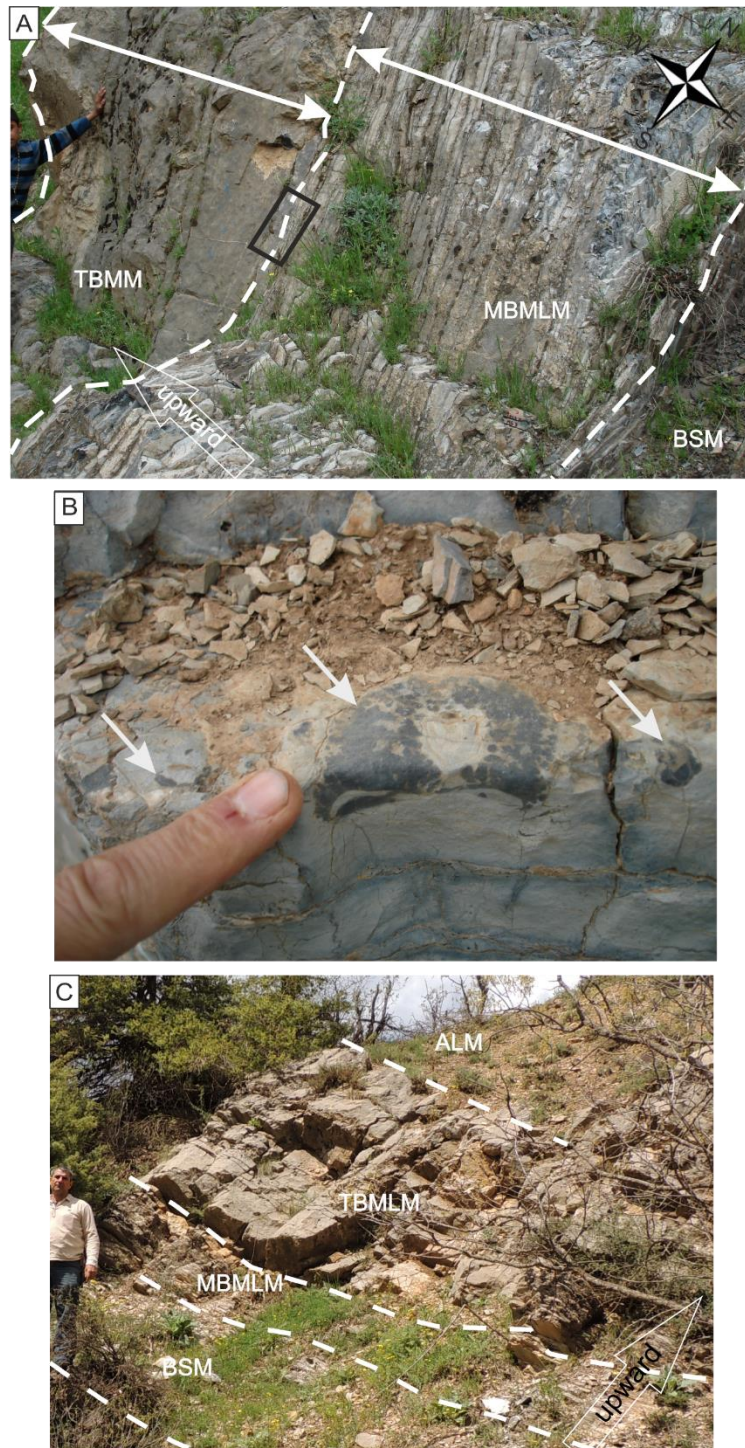


Figure 4.11: A; upper and lower sharp boundaries of medium-bedded microbial-bearing limestone member. Note, both MBMLM and TBMLM are completely devoid of black shale, sargelu location. B; Detail of the black rectangle of figure (A) shows first appearance of mottling (white arrows). C, both MBMLM and TBMLM appear as prominent cliffs in the outcrops; this is due to the existence of low resistance, soft limestone with predominant black shale lithologies that underlain and overlain them, Gara location. The soft black shale rock can be easily weathered, producing cliffs of MBMLM to TBMLM at all locations.

#### 4.5.1.1 Depositional models for evaporite

Modern evaporites are accumulating in a variety of non-marine and marginal-marine settings, whereas many thick sequences of ancient evaporites have been formed in laterally extensive, shallow to deep-water basins. Based on origin and facies association, the evaporite formation is interpreted in three different hypotheses (Boggs, 2009):

- 1) Subaerial evaporites; well documented modern evaporites accumulate in sabkha or salt flats, especially at Abu Dhabi on the Arabian side of the Persian Gulf (Trucial Coast).
- 2) Shallow subaqueous evaporites; shallow subaqueous evaporites accumulate in the marginal-marine environment in coastal salinas, are particularly common in southern and Western Australia (Warren, 2006).
- 3) Deep-water evaporites; there are no recent equivalents for deep water ancient marine evaporites environments. The Dead Sea in the west of Jordan may represent the only recent example of ancient deep-sea evaporite. The interpretation of ancient deep-water evaporites is generally based on theoretical considerations (Schreiber and Friedman, 1976).

All the evidence and facies associations support the postulation that the MBMLM are fairly deep during the deposition of the Oxfordian sediments. The evaporite deposition in is MBMLM is very comparable to the evaporation from a brine surface model of Kendall (1978, 1992), which stated: "in deep water, evaporite facies the brine is at near saturation with respect to the gypsum. The crystal growth probably occurs at the air-water interface and crystals settle through the water column pelagic rain."

## 4.6 Thick-bedded mottled limestone member (TBMLM)

### Field Description

Thick-bedded mottled limestone member (TBMLM) is dark grey to grey mottled limestone. About one-third of the lower part is characterized by medium bedding 10–15 cm, whereas the rest is represented by thick beds 30–45 cm, but can sometimes be massive >100 cm (Figure 4.12, A–B), both medium and thick beds show irregular or undulating bedding planes (Figure 4.12, C). The TBMLM appears persistent throughout the studied area. This member tends to form a prominent cliff, and can be readily traced in the field at all locations (Figures 4.11, C, 4.12, A, and 4.34).

The mottling is composed of dark and light patches (Figure 4.12, B–C). The terminologies of dark and light coloured patches are based on the reflection of light on the weathering surfaces. The patches that are saturated with kerogen appear lighter on the weathered surface, may be due to oxidized kerogen. Patches mainly display elongate to irregular shapes; and they often have sharp boundaries (Figure 13, A). The lighter patches often contain dark organic matter in pores, and according to Salae (2001), these dark matters consist of kerogeneous material (Fig 4.12, D), whereas lighter patches often include a very little amount or devoid of black organic matter. In addition to colour contrast, the mottling shows hardness, texture, and carbonate content differences.

Bedding surfaces in the uppermost part of this member often show horizons rich in accumulations of ammonite fossils (Figure 4.13, B). The ammonite fossils cannot be easily classified due to laminated overgrowths on their shells, which appear as darker patches on the exposed bedding surfaces (Figure 4.13, B), and are particularly difficult to sample. Locally, the overgrowths on ammonite fossils appear as small spherical, and hemi-spherical nodules. Moreover, some ammonite fossils show partially eroded shells (Figure 4.13, B). Sutured seam stylolites are common (Figure 4.13, C). The upper boundary with the overlying argillaceous limestone member is dramatically sharp, and is readily recognizable in the field due to rapid changes from the buff-coloured massive rigid mottled limestone to the overlying dark, soft, black shale and argillaceous limestone (Figure 4.14).

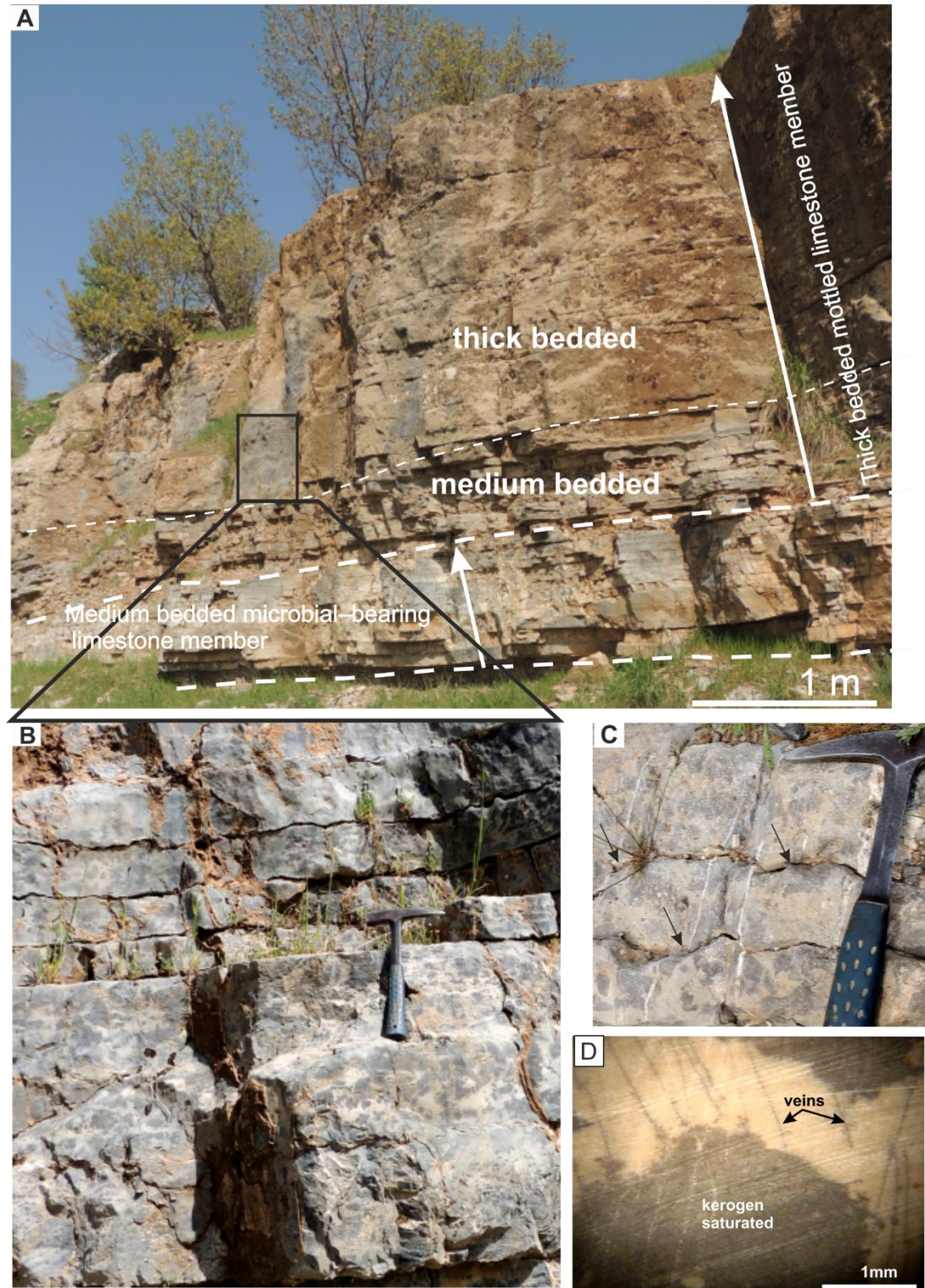


Figure 4.12: A; thick-bedded mottled limestone member appears persistent and forms a prominent cliff. B; bedding thickness variation and detail of dark and light patches. C; thick beds show irregular or undulating bedding planes (black arrows). D; polished surface showing differential colouring formed by highly porous bitumen saturated filling matrix and dense lithified dark patches. Note the veins are also saturated with kerogen (black arrows). The image is taken under reflected light. All photos are from Chnaran location.



Figure 4.13: A; vertical section view; sharp boundary between light (L) and dark (D) patches, (white arrows). Red arrows show scattered dark non-laminated patches surrounded by light patches. B; bedding plane showing numerous ammonite fossils, some with small dark nodular overgrowths, while others show signs of dissolution on their shells. C; stylolites parallel to bedding. All photos are from Nora location.

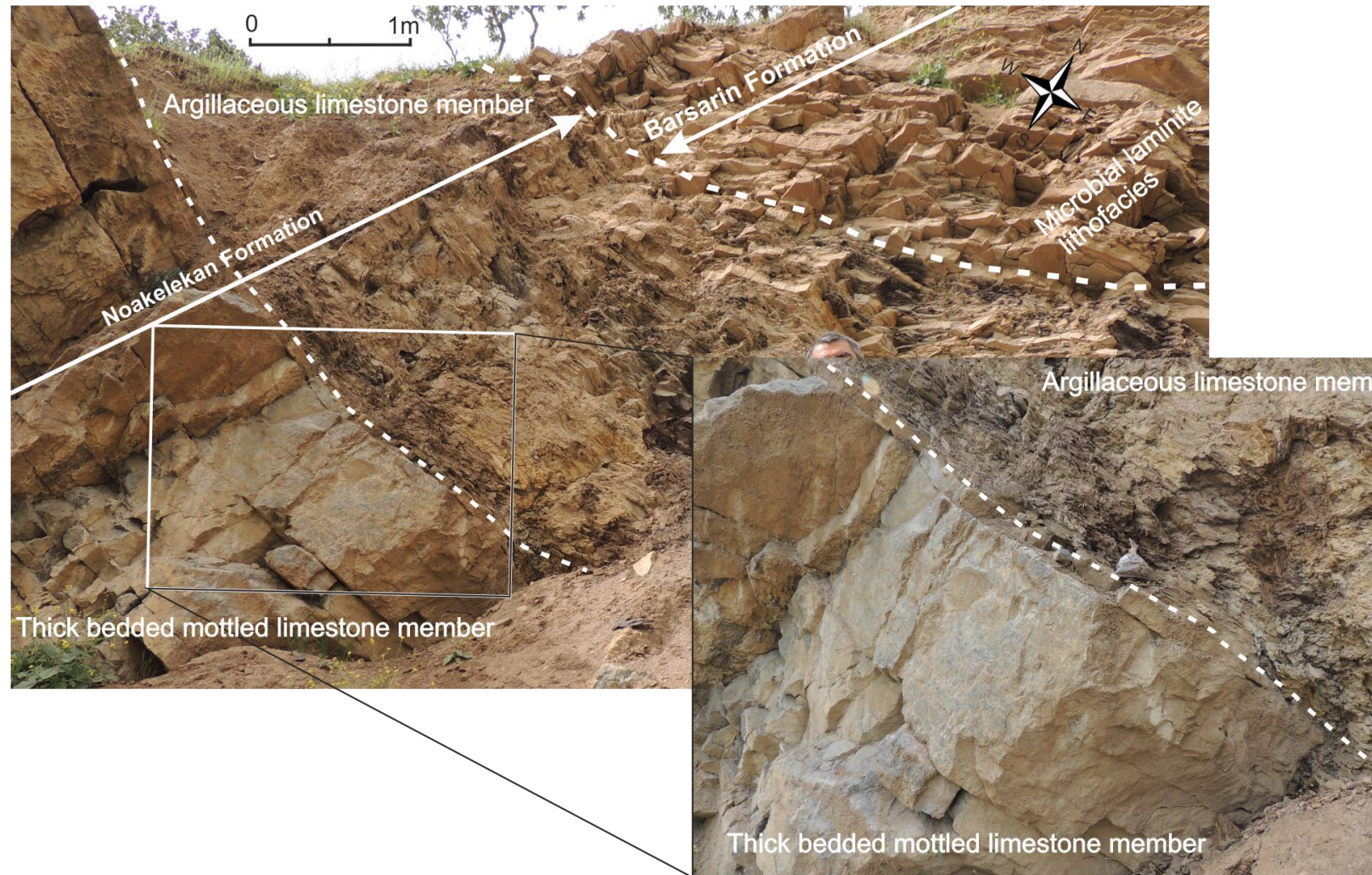


Figure 4.14: Sharp contact between TBMLM and the overlying ALM (dashed line). Note the dramatic change from microbial bacteria-rich thick-bedded mottled limestone to the shale dominated lithofacies. The upper boundary between argillaceous limestone member with microbial laminitite lithofacies is sharp also, Barsarin location.

Based on colour difference, the mottled limestone patches can be subdivided into two main categories, dark and light patches:

#### 4.6.1 Dark patches

Field observations reveal that the dark patches are composed of fine grained limestone; they appear either as laminated (Figures 4.15 and 4.16, A–B) or non-laminated patches (Figures 4.15 and 4.16, F), with eroded surfaces where the laminae are truncated (Figures 4.15 and 4.13, A). Dark patches, which often have close association with ammonites and nodular limestones, range from millimetres to several centimetres in diameter and are partially surrounded by, or embedded in, light patches (Figures 4.15, 4.16, A–D, and 4.17). They seem harder and more resistant to weathering, and are standing out whereas surrounded lighter patches seem recessive (Figures 4.13, A–C, and 4.16, E). The dark patch structures are roughly elongated to irregular in shape, but the overall view of the dark patches on the vertical section view display zones of horizontally aligned of detached structures (Figure 4.17). The dark patches and nodular limestones often lie parallel with the bedding surface, and do not generally cross the bedding boundaries (Figures 4.15, 4.18 A–B). The dark patches can be subdivided on the basis of the existence of lamination into laminated dark patches and non-laminated dark patches:

##### 4.6.1.1 Laminated dark patches

Chnaran, Sargelu, and Nora areas (Figure 4.1) can be considered the best locations for study of laminated dark patches due to their good preservation. Usually, dark laminae appear as overgrowths or coating on the ammonite shells and nodular limestones (Figures 4.15, 4.16, A–D, and 4.17). The laminated dark patches may be subdivided in terms of arrangements into three main kinds, and the lamination will be described according to the Hoffman's (1976) terms: (i) high relief laterally linked hemispheres (Figure 4.18 A), (ii) small vertically stacked columnar laminae up to 8 cm high (Figure 4.18, B), and (iii) concentric coating (Figure 4.18, C). The laminae often appear as thin crudely wavy layers, often with no distinctive colour or mineralogy between from light and dark grey laminae on a fresh surface, whereas on differentially weathered surfaces low contrast couplets of grey, and dark grey can be clearly observed.

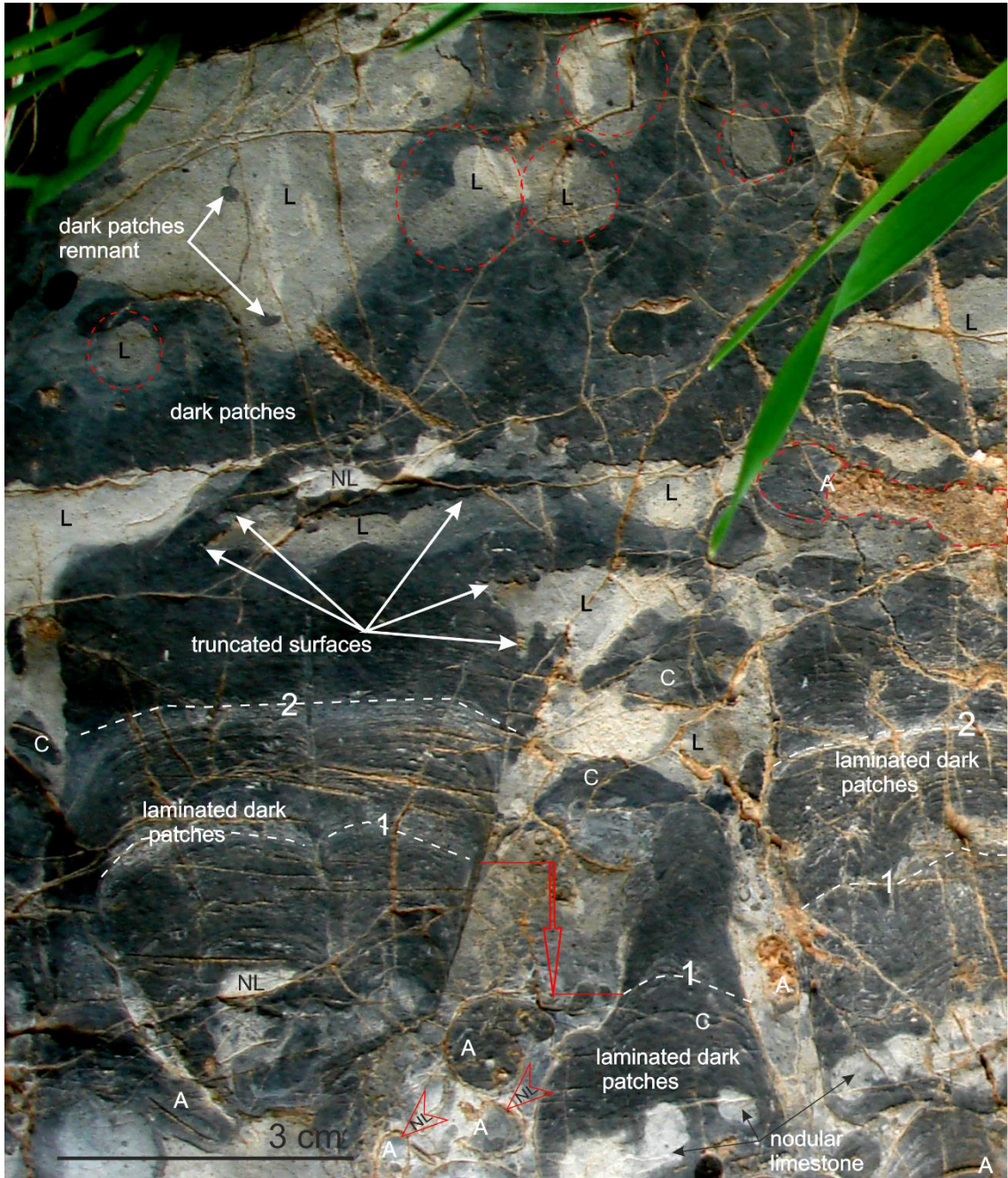


Figure 4.15: A cross section showing distribution and arrangements of the dark and light patches. The laminated dark patches normally develop on the nodular limestones (NL) and ammonite shells (A). The NLs are usually aligned in a row. Well-preserved laminated dark patches can be observed at the bottom of the photograph, which display columnar shape overgrowth on the NLs. Note lamination contrast decreases gradually upward and passes into massive dark patches, and they appear in several stacked packages (white dashed lines). Truncated surfaces can be clearly seen at the top of laminated dark patched columns. Many dark patch collapses (C) can be observed (middle bottom) with about 1.5 cm displacement of section (red arrow). Many of the dark patches appear as remnants, and they are engulfed by light patches (top left). Note most of the light patches display rounded outline (red dashed circles), Nora location.

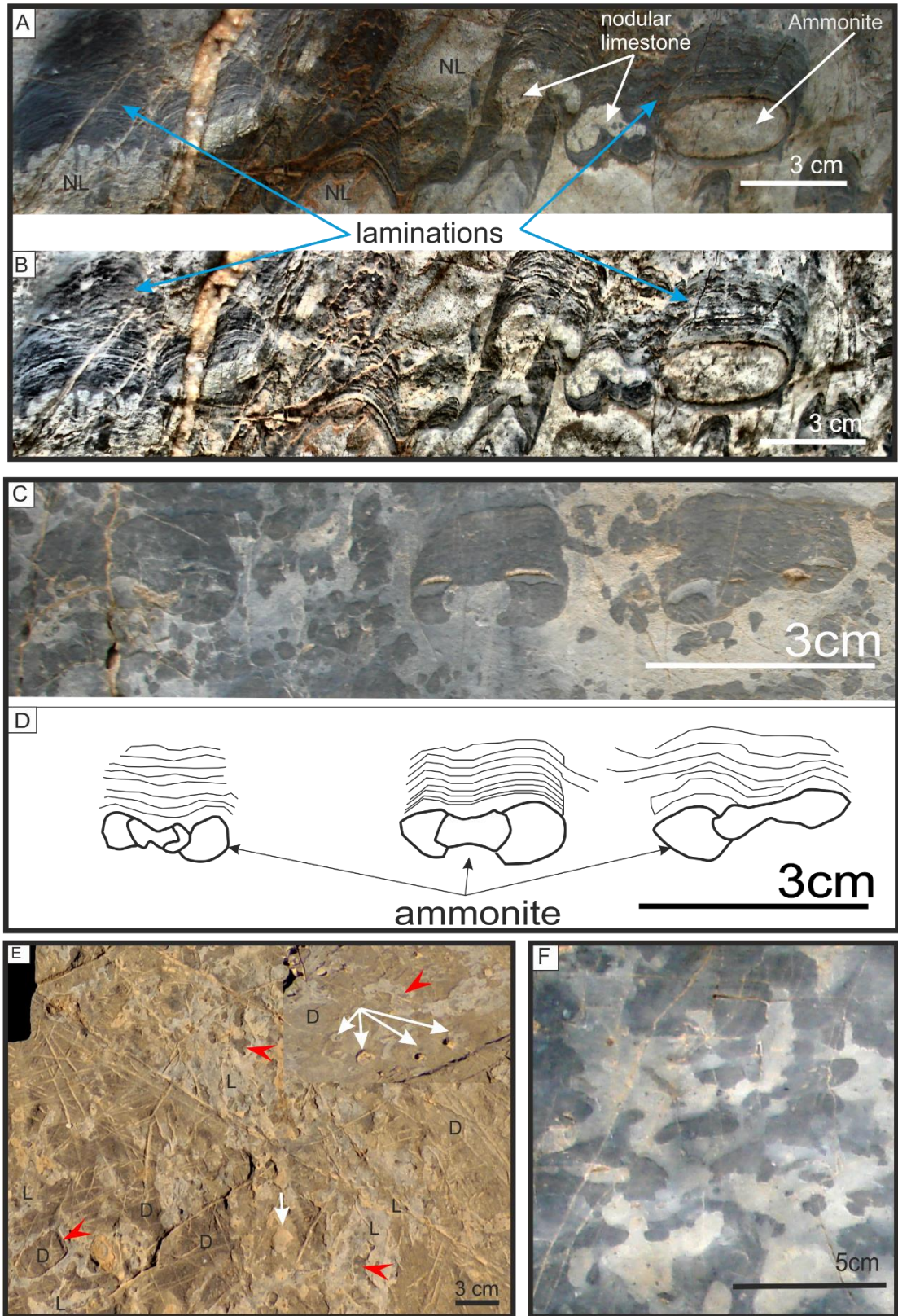


Figure 4.16: A; and B; laminated dark patches growing on ammonite shell and nodular limestones (NL). Note, (B) is the artistic effected photo. C and D; photograph and sketch showing laminated dark patches stacking on ammonite shells. E; bedding plane surface showing dark patches (D) appear resistant and are standing out, and light patches (L) appear as recessive producing pits (Light arrows). Note remnants of dark patches are engulfed by light patches. F; typical non-laminated mottled limestone comprises dark and light patches, Photos from Chnaran location.

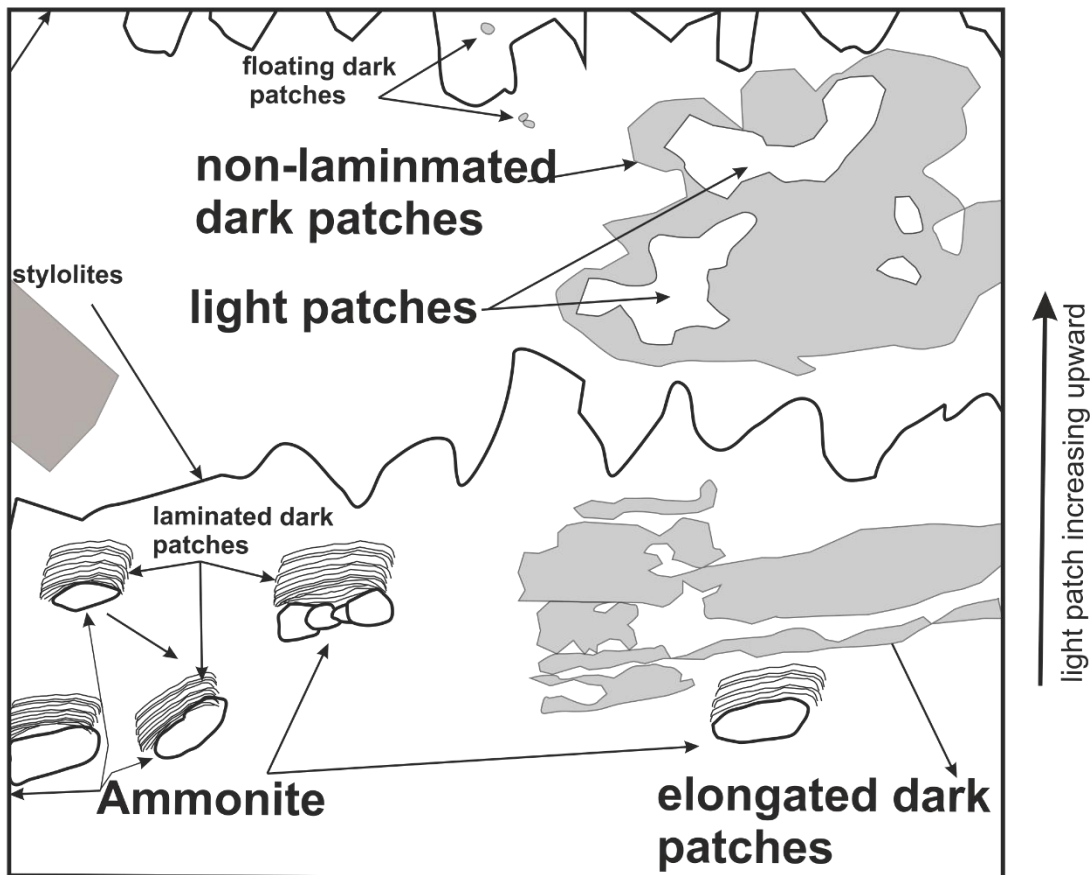


Figure 4.17: vertical section view showing differential resistance to weathering (top of the photo), the light patches appear as recessive producing pits, while the dark patches appear more resistance and standing out. Bottom of the photograph shows intimate association between laminated dark patches and ammonite fossils. The white dashed ellipsoidal shapes show lamination stacking on ammonites. Note that, light proportion increasing upward, their occurrence changes upward from elongated parallel laminated patches at the base to the massive non-laminated patches (left of the photo), Nora location.

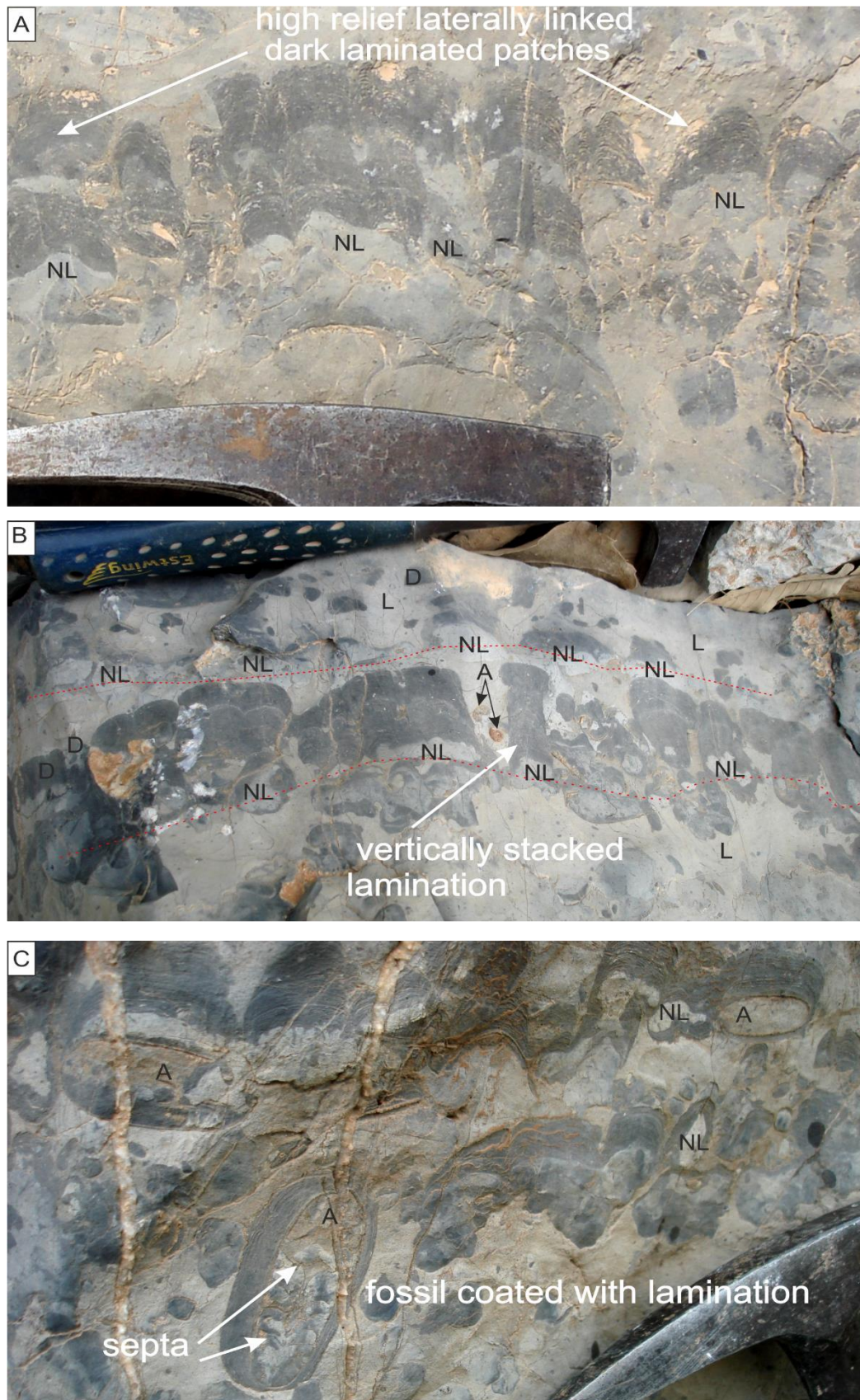


Figure 4.18: Thick-bedded mottled limestone member showing three different kinds of laminated dark patch textures. A; high relief laterally linked hemisphere. Note the laterally linked laminated structures stacking on nodular limestones (NL). B; small vertically stacked columnar and scattered dark patches (D) in light patches (L). Note that nodular limestone often appears in rows (red dash lines) C; concentric lamination coating ammonite (bottom left), the septa of the ammonite fossil can be seen clearly. Note dark laminated patches are normally stacks on the ammonites (A), and nodular limestones (NL), photos from Chnaran location.

## Thin-sections

Thin-sections of the laminated dark patches show crudely, uneven laminated mudstone. The laminae, which are 0.1–0.5 mm thick, appear as weak couplets of dark fine and coarse calcite grains with hemispherical growths of fine wavy laminated material (Figure 4.19, A–B). The dark patches contain numerous peloidal bodies that are rounded to irregular in shape and surrounded by microsparite (Figure 4.20, A and C), 0.01–1 mm in diameter.

Horizons of irregular chambers of encrusting foraminifera are observed, ovate or short vermiculate in shape 0.1–0.4 mm and up to 0.03 mm across, and their pores were infilled by calcite spar (Figure 4.19, C–D). Their axial sections often display two or three coiling, and they are lying tangentially and superimposed on the surface of laminae. Laminated dark patches are also rich in spherical objects with micritized walls, and their pores are completely infilled by calcite cement 0.1 mm in size. They may represent calcispheres (Figure 4.20, A).

The dark patches are rich in elongated and tube-shaped microbial filaments that show parallel rows of small calcite spar, several hundred microns in length and up to 40 microns thick. The rows generally oriented perpendicularly on laminae surfaces (Fig 4.19, C and 4.20, B). The (SEM) study shows few signs of microbial filaments as well (Figure 4.20, D).

### 4.6.1.2 Non-laminated dark patches

This kind is very common, and it can be recognized readily at all locations. They are fine grained limestone with irregular dark patches (Figure 4.21, A–C). The lithology of dark grey structureless patches is similar to the laminated dark patches. The only dissimilarity between them is the lack of lamination in the former one.

Microscopically, the non-laminated dark patches, which are rich in small elongated tubes of microbial filaments, 10–30  $\mu\text{m}$  across, display compact mudstone to wackestone (Figures 4.22, A–B and 4.23). Ammonites, and fossil debris have not been frequently encountered; they are normally engulfed in the fine micritic matrix (figure 4.22, A–B). Irregular dark spot grains 0.1–0.2 mm in size, peloids, and few calcispheres also have been recorded (figure 4.22, C).

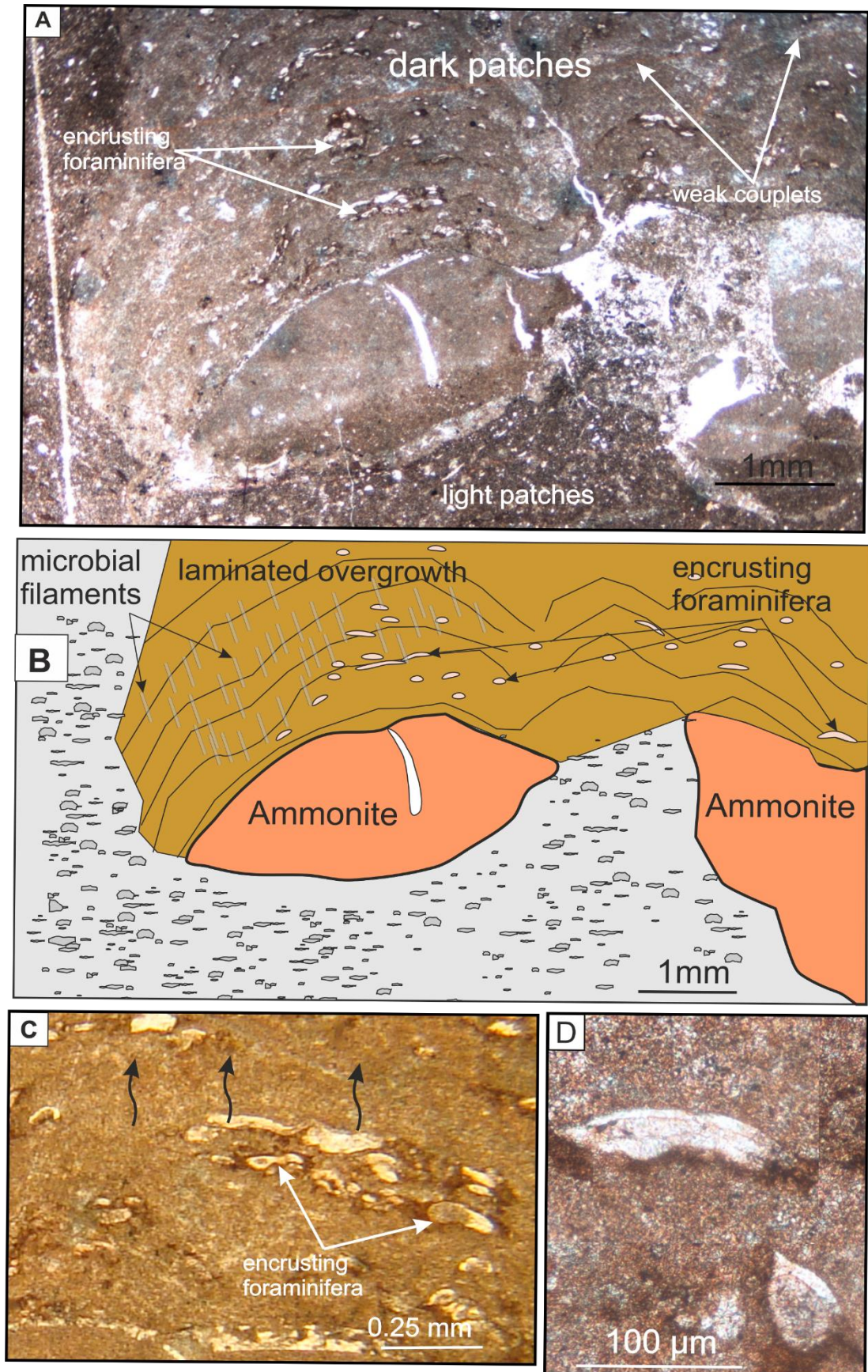


Figure 4.19: A; dark laminated patches over growth on ammonite shells, the lamina couplets consisting of fine dark and coarse-grained calcite spars. The dark patches are surrounded by light patches (bottom and left). Note that encrusting foraminifera, are lying tangentially along lamination surfaces. B; a sketch representing the details of the photo (A). C; photomicrograph showing filaments grow perpendicularly on the laminations (black arrows), with encrusting foraminifera (white arrows). D; detailed encrusting foraminifera, note horizons of irregular chambers. All photos are from Barsarin locality.

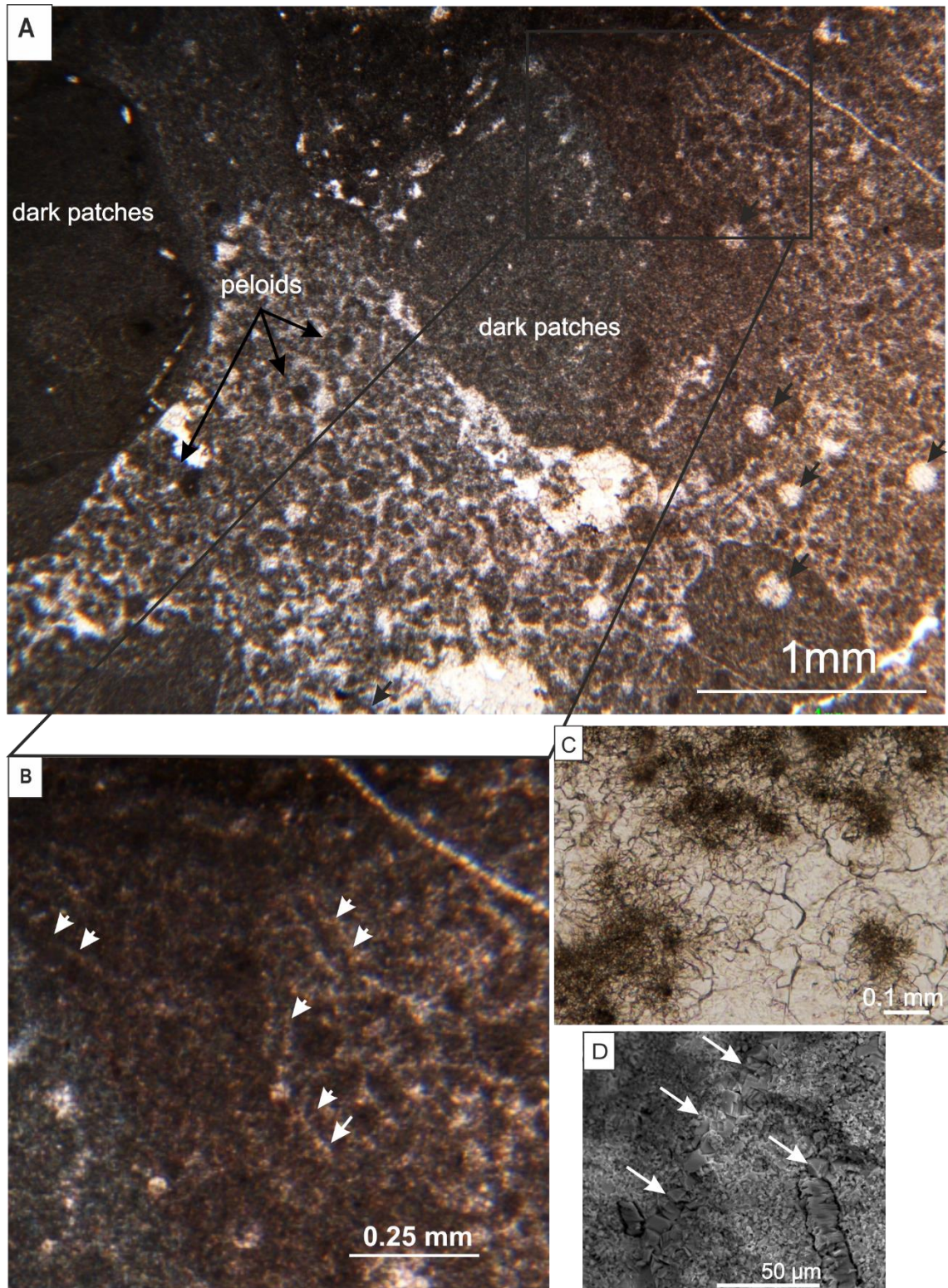


Figure 4.20: Micro-fabric of laminated dark patches, rich in different size of peloids, calcispheres (black arrows), and large clasts. B; detail of the black rectangle in (A), showing microbial filaments (white arrows). C; rounded to irregular shape peloidal structures surrounded by microsparite. D; SEM photograph filament traces (white arrows) in darker patches. The images A, B, and C are taken under polarised light. All photos are from Hanjera locality

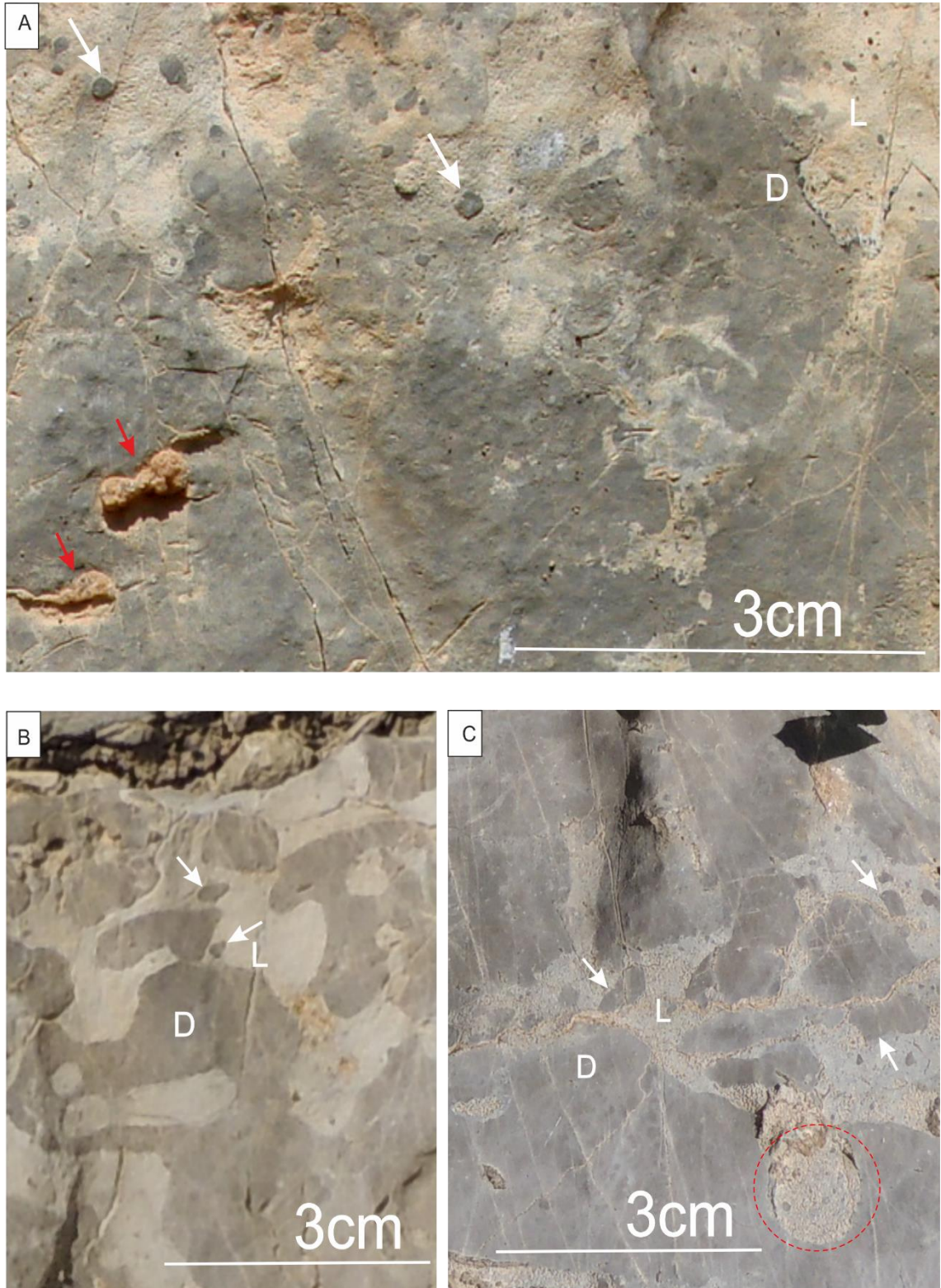


Figure 4.21: cross-section views show dark grey structureless patches (D) and light patches (L) at different locations A; Nora location, B; Barsarin location, and C; Gara location. Red arrows point to the ammonite fossils, while the white arrows show dark patches engulfed by light patches (L). Note rounded light patch penetrating dark patch (dashed red circles).

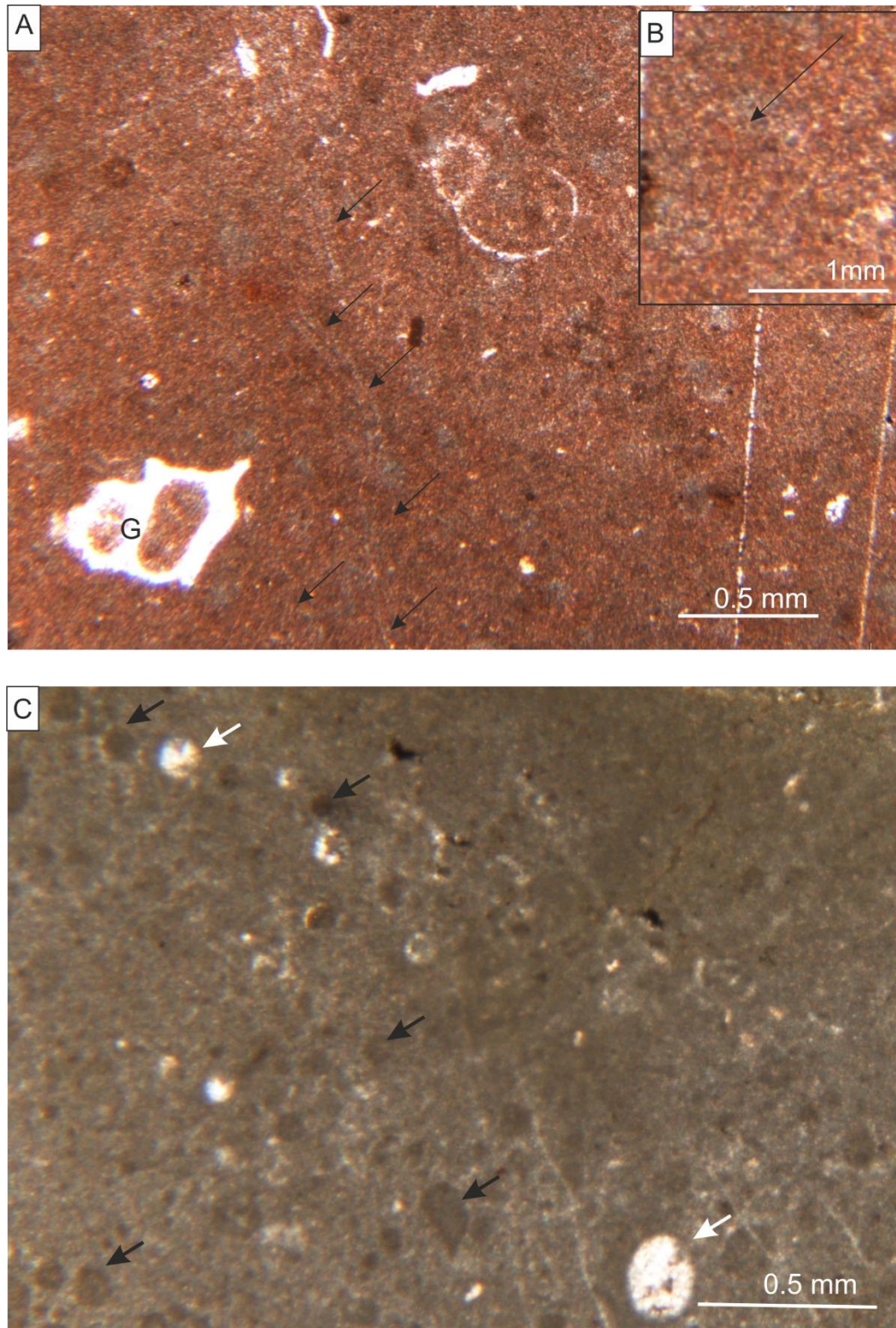


Figure 4.22: A; dark structureless patch contains a lot of microbial filament traces (black arrows), and few bioclasts and gastropods are also included (G), Hanjera location. B; photomicrograph shows detailed microbial filament. C; structureless dark patches containing peloidal shapes (black arrows) and calcispheres (white arrows). Both images are in the plane polarised light, Barsarin location.

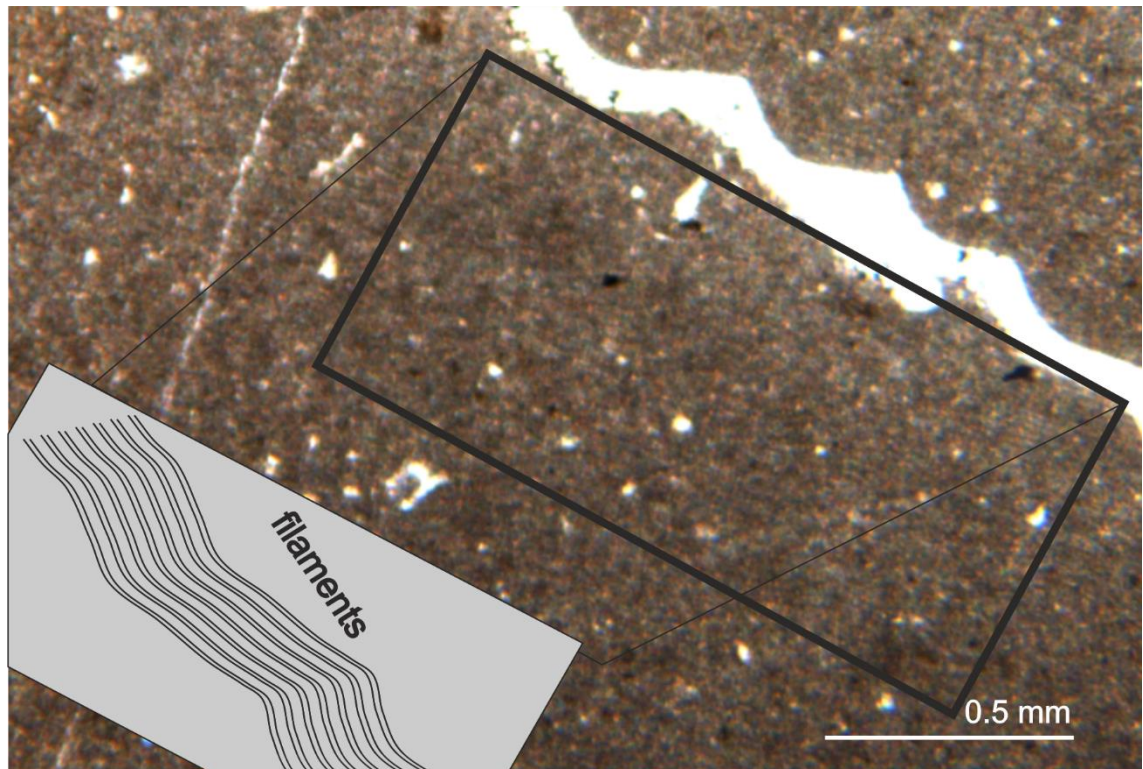


Figure 4.23: photomicrograph showing microbial filaments over growth on an ammonite shell. Note, the sketch of the microbial filaments has similar direction with the microbial of microphotograph. It can help to recognize the texture easily if they are compared, plane polarised light.

#### 4.6.2 Light patches

These patches are grey in colour, and light grey on the weathered surface. The light patches, which are rich in a kerogenous matter (Salae, 2001), are characterized by including a lot of small scattered darker patches up to centimetres in size (Figure 4.21, A–C). Light patches seem relatively softer than dark ones, as they show less resistance to weathering by comparison with dark patches. As a result, the light patches display recessive profile, whereas surrounding dark patches are more resistant and stand out.

In vertical sections, the light patches generally appear in three main patterns in the field (figure 4.24); they are in ascending order: (i) elongate irregular and horizontal light patches alternating with dark patches. Light patch diameters are up to 2 cm, and patches can be traced laterally for several decimetres. (ii) irregularly surrounding or penetrating the dark patches, sub-vertically and penetrating down for several centimetres. (iii) Some horizons in the middle part of the mottled member are completely dominated by light patches, with scattered small dark patch remnants (Figure 4.24). In many cases, more than one stage of light patches can be observed.

On some bedding planes, the light patches occur as small rounded pits 1–2 cm in diameter, forming sieve textures or rounded net-shaped pits, which are completely surrounded by large darker patches with or without cracks textures (Figures 4.25, A–B). Light patches normally include different-sizes of dark patches up to centimetre-scale.

In thin-section, the light patches are wackestone which is rich in different sizes of peloids, angular remnants of dark patches, unidentified micritized fossils, and shell debris (Figure 4.26, A). The dark patch remnants, which are a few millimetres up to few centimetres in size (Figure 4.26, B), are normally devoid of kerogenous materials, and sometimes are surrounded by dark spots (Figure 4.26, C). The boundaries between dark and light patches are smooth and sharp (Figure 4.21, B–C). The porosity in light patches is about 5–7 %, and the pores are mostly filled by kerogenous materials (Figure 4.26, B). Light and scanning electron microscope studies reveal similarities between dark and light patches in terms of the nannofossils they contain, whereas the basic differences between dark and light patches are that the light patches are devoid of microbial filaments and contain a higher proportion of the kerogenous material.



Figure 4.24: Photograph showing increasing in the light patches proportion upward by comparison with dark patches. Note, the variation of the light patches arrangement upward, from elongate parallel at the base to irregular patches in the middle, and to the dominance of light patches at the top.

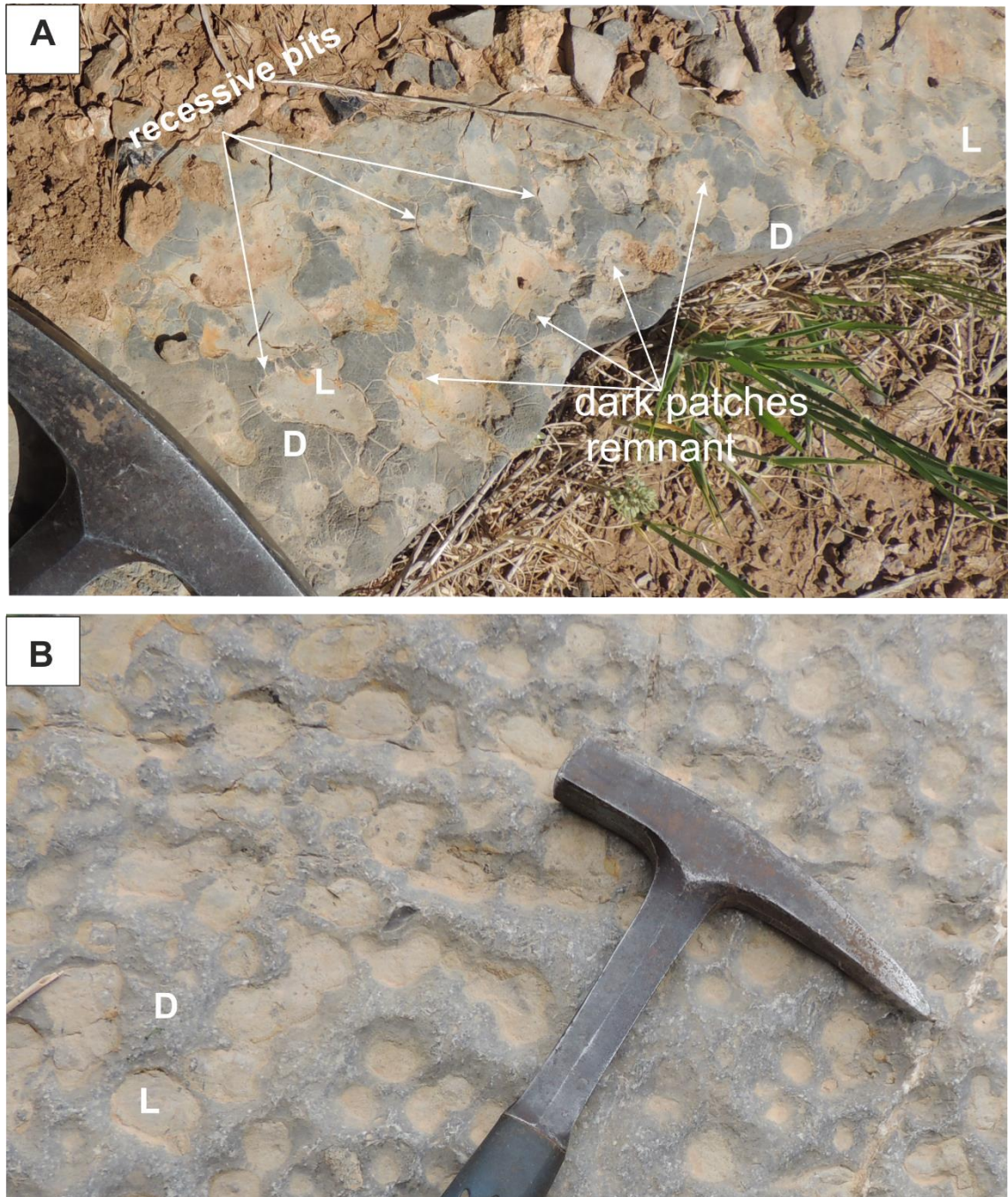


Figure 4.25: A; bedding plane surface view shows differential weathering effects and rounded net-shaped pits on the mottled member. The light patches (L) always appear recessive and less resistance than the darker patches (D). Note cracks in dark patches and dark patch remnants in the light patch matrixes, Chnaran location. B; bedding plane exhibiting differential weathering at Hanjera location, but no cracks were observed in the dark patches at this location.

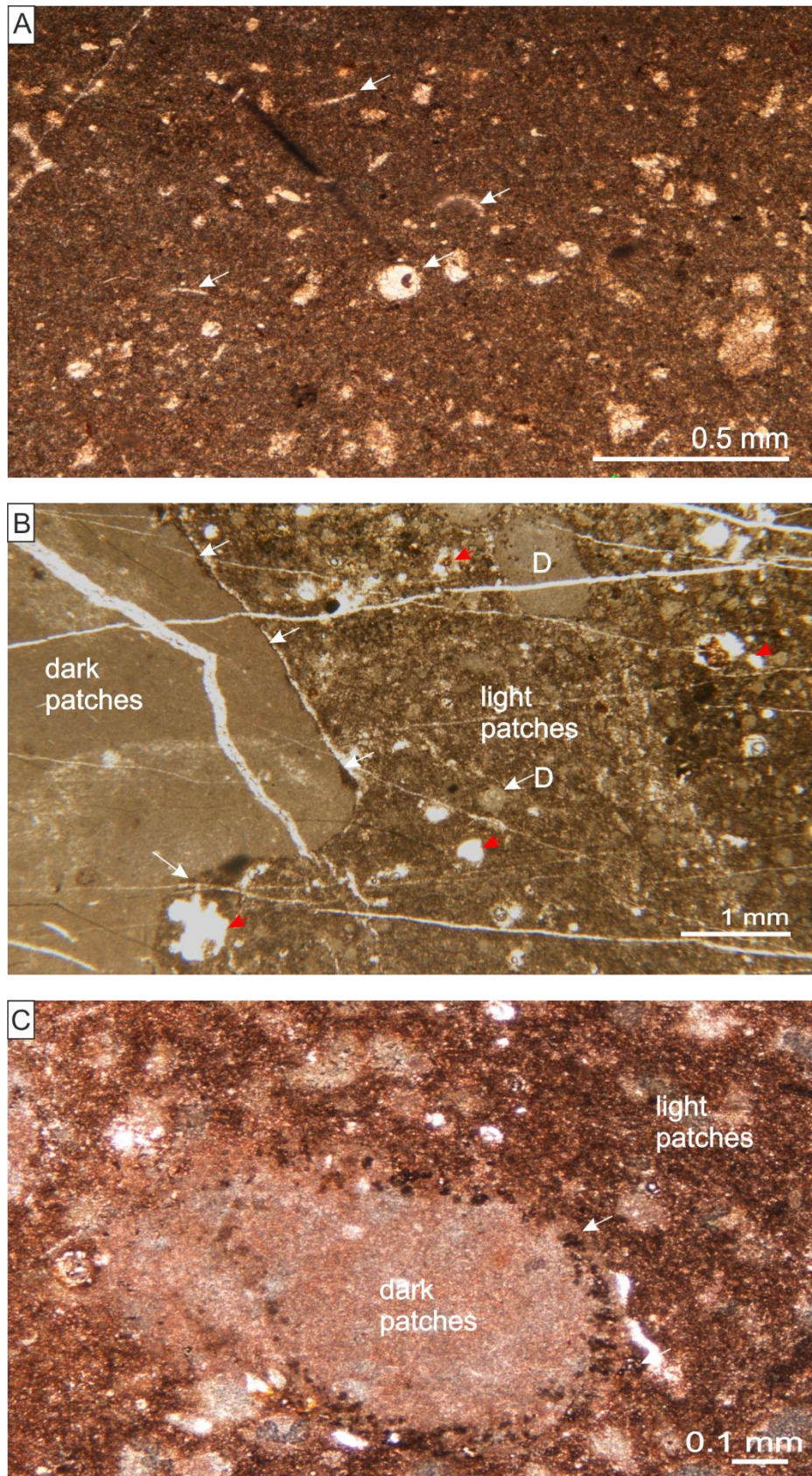
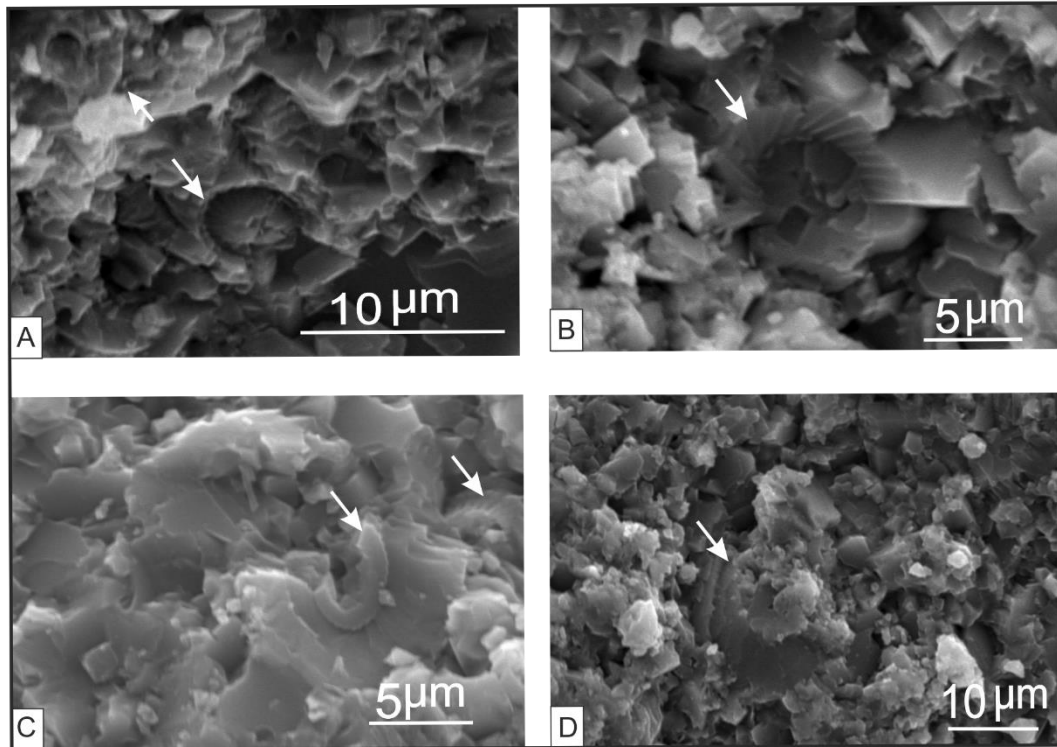


Figure 4.26: A; Fossil debris and calcispheres in the light patches (white arrows). B; shows a sharp boundary between dark and light patches (white arrows), scattered dark patch remnants (D), and fossil fragments are quite common in the light patches. Note the porous texture in the light patches (red arrows) C; dark spots growing on a floated dark patch surface that floated in the light patch matrix. All the images are in the plane polarised light, Barsarin location.

## I- dark patches



## II- light patches

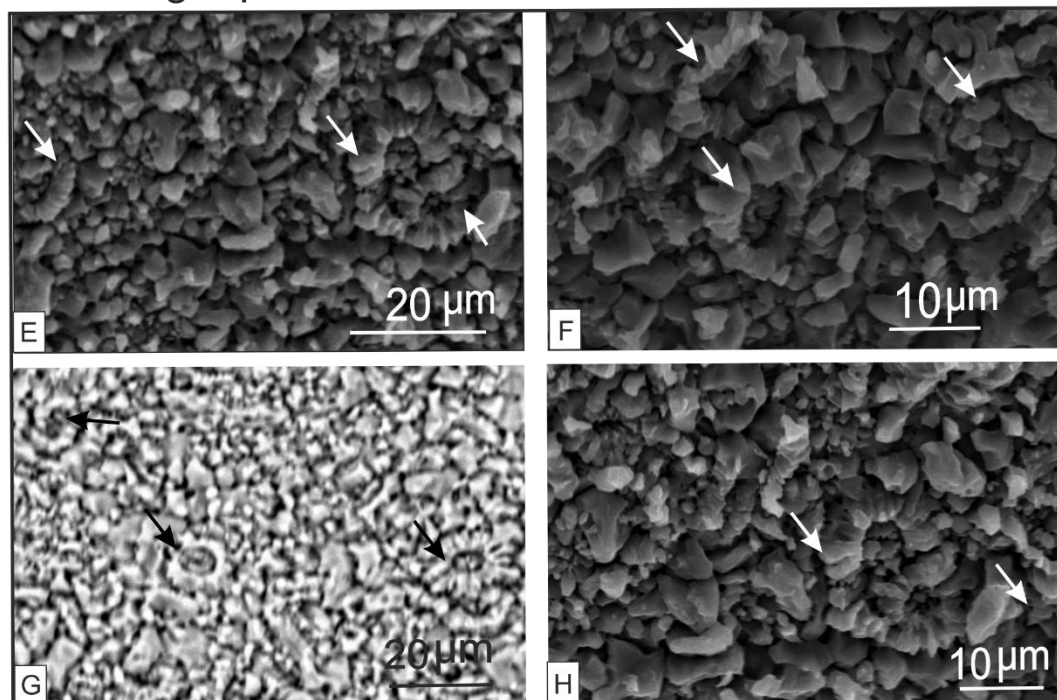


Figure 4.27: Scanning electron microscope photographs showing both dark (I) and light (II) patches. The SEM analysis reveals dominance of nanofossils in both dark and light patches (arrows). A, B, C, and D represent SEM images of dark patches, which clearly show nanofossils with their rim platelets, and crystals usually display sharp edges, low porosity and rather tightly interlocked, Chnaran location. E, F, G, and H show images of nanofossils in the light patches, the crystals appear in rounded, sub-unhedral. They seem more porous by comparison with darker patches. Note, the main difference between dark and light patches is related to the crystal roundness, Chnaran location.

### 4.6.3 Scanning electron microscope (SEM)

Scanning electron microscope (SEM) analysis indicates that, both the dark (Fig 4.27, A–D) and light (Figure 4.27, E–H) patches of mottled limestone member contain numerous probable calcareous nanofossils. These objects are elliptical to circular and between 5–10  $\mu\text{m}$  in diameter. They have a narrow rim and open central area. The central area has a hole ranging from 2 to 5  $\mu\text{m}$  in diameter, which is often occupied by a cluster of small calcite spars, and they show rosette-shape 2–4  $\mu\text{m}$  thick (Figure 4.27, A–H). In a few cases, the rims can clearly show defined platelets with sharp edges (Figure 4.27, B–C), whereas the majority of rosettes rims have coalesced. The rings are relatively intact, but broken and fragmented rings are also common. SEM observations indicate that probable nanofossils are randomly arranged, and are surrounded by inconspicuous features of small calcite spar and by fragments ranging between 1–3  $\mu\text{m}$  across (Figure 4.27). Some overgrowths on the rosette rim make the rings appear larger. The main differences between dark and light patches are the degree of crystallinity, where light patches relatively appear sub-anhedral (Figure 4.27, E–H) in comparison with sub-euhedral darker patches (Figure 4.27, A–D).

### 4.6.4 Interpretation

The first description of the thick-bedded mottled limestone member of the Naokelekan Formation was made in 1950 (Bellen et al., 1959). To determine the depositional palaeoenvironment and the origin of mottled textures were a big challenge, mainly for the following reasons:

- When the Naokelekan Formation was first described by Wetzel and Morton (1950, in Bellen et al., 1959), microbial structure was not well-known.
- Most of the recent researches have excluded the probabilities of existence of stromatolites, and this is perhaps due to the presence of ammonites and some planktonic foraminifera.
- The original textures of the microbialites were partially or completely obscured by bioturbation at all localities, therefore, determining their original texture was not easy.

The TBMLM is characterized by thick-bedded limestone and mottled textures. This member includes a large amount of coccoliths and ammonites. In addition, there is considerable evidence of microbial filament existence, supporting their role in the dark patch formation. The combination of field description with microfacies analysis indicates

that the TBMLM formed in a relatively deep water environment. This interpretation is supported by the following:

#### 4.6.4.1 Hypotheses on mottling formation

Mottled texture can be formed in a number of different ways, and there are various causes that control their formation. These can be broadly classified into several types, which are as follows:

A. Dolomitization control; the best example is mottled carbonate rocks in the Middle Devonian of eastern Nevada (Osmond, 1956). The development of the mottled pattern was interpreted as a result of partial or differential dolomitization, which may follow a pattern established at the time of deposition. Mottling seems to be connected to the rate of burial and associated expulsion of connate interstitial liquids. The diagenetically formed mottled rocks can be distinguished by possessing diffuse contact with the unaltered rocks. Also, it is possible to observe the continuation of a primary structure between mottled patches; lamination remnants of unaltered rocks can be observed on diagenetically altered parts.

The mottled texture in the TBMLM displays sharp boundaries between patches, with no primary structure continuation between them. Also, no dolomitization has been recorded in dark or light patches, whereas the patches are different in the texture, and spar proportion (Figure 4.27, A–H). For this reason; the diagenetic origin for the TBMLM is excluded.

B. Pigmentation control; Manley et al. (1975) found that the mottled texture in the Sequatchie Formation Upper Ordovician near Ringgold, Georgia, USA formed due to the presence of diagenetic hematite, which was formed by iron oxides or iron expelled from detrital chlorite. No Fe-rich minerals or evidence for mineral expulsion are observed in the mottled textures of the TBMLM; therefore, this model is excluded.

C. Fracture control; mottled texture can be related to brecciation in carbonate rocks (Flügel, 2004). It can appear as two main types. Firstly, breccia related to seismic events, which appears as laterally continuous limestone beds composed of intraclasts, and associated with deformation structures. Secondly, Impact breccia; this kind is generally characterized by strongly fractured clasts, and the ground mass contains a large number of fragmented particles.

The main characteristic of breccia mottles is the prevalence of vugs that filled with cement, bent rock, sheared textures, and heavily veined rocks (Torok, 2000; Flügel,

2004). No cement filling vugs or bent structures were observed in the Naokelekan Formation mottling. The geometry of light patches generally seems to be rounded in outline, smoothly curved, and tube-like in shape (Figure 4.21). This in turn excludes the fractured controlling origin. Therefore, a fracture control origin is excluded.

- D. Calcrete control; mottled nodular beds may form as a result of pedogenic processes. Irregular water diffusion through soil in the vadose zone may cause an irregular distribution of iron oxides/hydroxides. Calcrete mottling is often associated with the effect of root rhizoturbation. Root moulds show downward branching and reduction in width that can be used to distinguish them from burrows (Flügel, 2004). This type of colour mottling is common in lacustrine and floodplain muds (Tucker and Wright, 2009; Tandon et al., 1998). No indications of calcrete or rhizoturbation are present in TBMLM where the mottling member does not show any branching or downward size reduction. Therefore, calcrete control is excluded.
- E. Bioturbation control; with the exception of some cases which lead to mottling in carbonate rocks, most of which have been mentioned above, bioturbation can be considered as the major factor forming mottled textures (Laporte, 1971; Rubin and Friedman, 1977; Scholle, 2003; Flügel 2004; Horbury and Qing, 2004; Boggs 2009; Tucker and Wright, 1990). Differentiations in colour and texture are common features in mottled fabrics, which have resulted from bioturbation (Flügel, 2004). The mottled patches within TBMLM display different textures, which may be caused by the homogenization and transformation of micrite and microbial rich dark patches into the higher porosity and microsparitic light patches, where both macro and micro-structures of microbial textures display interruptions and disturbance by bioturbation (Figures 4.15 and 4.19 A–B). Therefore, bioturbation control is a plausible model for formation of the TBMLM.

Characteristics	Light patches	Dark patches
Colour on fresh surface	dark grey	grey to buff
Macrofabric	structureless	laminated and non-laminated
Weathering	recessive, producing pits	resistant to weathering, and are standing out
Association	no preferred association	surrounding and stacking ammonites and nodular limestones
Appearance	circular or ovate shapes are common feature	irregular and angular
Fauna	rich in coccolith	rich in coccolith
Microbial	none	filaments were observed
Cross cutting relation	often filling the accommodation space was created by bioturbation or scouring	laminations were interrupted by bioturbation. Most likely the dark patches were penetrated by small rounded light pits
Kerogen content	relatively higher	relatively low
Porosity	relatively higher	lower porosity

Table 4.2: Comparison between dark and light patches.

#### 4.6.4.2 Mottling characteristics

From the previous mentioned models and available evidence, it can be concluded that the mottled texture in the Naokelekan Formation is formed through bioturbation. A summary of the evidence is outlined in the (table 4.2) and the following points:

- a- It seems that the precursor textures were disrupted and truncated by bioturbation (Figures 4.13, A and 4.15), and subsequently, the tunnels, which lack any specific structure, are backfilled with matrix, whereas the microbial filaments can only be observed in darker patches (Figures 4.19, C; 4.20, B; and 4.22, B). Based on cross cutting relationships, the dark patches demonstrate excavation by small rounded light pits (Fig 4.16, E, and 4.21, C). From the previous relationship, it can be inferred that the dark patches were initially formed by microbial structures, which had subsequently penetrated and the light patches were formed.
- b- Mottled colour and texture differentiation (Figures 4.15, 4.21, C) are a characteristic of bioturbation.
- c- Despite the textural difference between dark and light patches, the light and scanning electron microscopic studies indicate that both light and dark patches share the same kinds of nannofossils (Figure 4.27), which suggested that they were derived from the same sources. The darker patches mainly consist of microbialites that have grown on nodular limestone and ammonite shells (Figures 4.16, A–D, 4.17, 4.18, A–C, and 4.19, A–B). The light patches, which seem to be devoid of any microbial activity, are richer in kerogen, and include a lot of scattered remnants of darker patches (Figure 4.26, A–B).
- d- The light and dark patches in the TBMLM often display sharp boundaries (Figure 4.26, B), which is one of the diagnostic features of mottling resulting from bioturbation.
- e- Lack of pigmentation diffusion between mottled patches may imply bioturbation rather than diagenesis.
- f- According to Scholle (2003), collapsed structures are distinctive features of bioturbation; perhaps the scattered dark patches remnant in the light patches formed by the collapse structures (Figures 4.15, and 4.26, B).
- g- The burrowing origin was suggested because of the existence of the recessive rounded pits on bedding surfaces at many localities (Figures 4.16, E, and 4.25, A–B).
- h- The microbial overgrowth on ammonite in the TBMLM is very comparable to the nodular limestone of “Ammonitico rosso” in the Alpine–Mediterranean Jurassic.

Jenkyns (1974) studied these nodules, and he assumed that these nodules were formed by syn-depositional diagenetic processes near sediment-water interface in the pelagic facies (It will be discussed in Chapter Seven in detail).

#### 4.6.4.3 Potential origin of the dark laminated patches

Both macro-and microfabrics, and structures in the TBMLM indicate that the dark patches are formed by microbial activity, where the light and scanning electron microscopic studies show filament traces in the dark patches (Figures 4.19, C; 4.20, B & D; 4.22, A–B; and 23). Stromatolite structures are usually constructed in specific geometric arrangements. Logan et al. (1964) classified stromatolites (microbial mat) on the basis of their geometric shapes (hemispheroidal and spheroids) from, which stromatolites and oncolites are built. According to Logan et al. (1964), stromatolites can be divided into three main types of arrangement: laterally linked hemispheroids (LLH), vertical stacked hemispheroids (VH), and spherical structures (SS). The dark laminated patches in the TBMLM are strikingly comparable to those which have been described by Logan et al. (1964) (Fig 4.28).

The Chnaran, Nora, Hanjera and Barsarin sections (Fig 4.1) are different from the other sections in the field exposures, where both microbial overgrowths on ammonites and oncolite structures are usually clear and easily observable as a macrostructure (Figures 4.15, 4.16, A–D, 4.17, A–C, and 4.18), whereas in the other locations, the microbial structures were revealed by delicate thin-section detection (Figures 4.20, A, and 4.22, A–B). In comparison with Logan's classification (1964), the TBMLM mainly contains two kinds of stromatolites: high relief laterally linked hemisphere stromatolites and small vertically stacked hemisphere or columnar stromatolites (Figure 4.28).

Oncolite contents gradually increase upward. The appearance of oncolites near the top of the TBMLM may suggest an increase in energy. The palaeocurrent action on the sea floor of the TBMLM can be explained by existence of oncolites (see Chapter 7). The Interrelationships between occurrences of oncolites, high structural relief, and ammonitico rosso, and facies breaks or hiatuses in sedimentation are reported repeatedly (Jenkyns, 1971; Playford et al., 1976; Peryt, 1983; Martire, 1992; Dromart et al., 1994; Flügel, 2010; Reolid and Nieto, 2010).

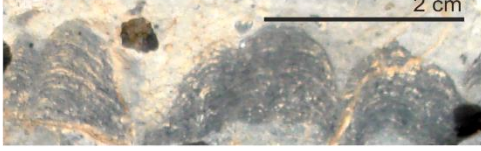
Stromatolites in the Noakelekan Formation	modified from Logan 1964	
	descriptions	vertical section of stromatolite structures
		Laterally linked hemisphere
		Vertically stacked hemisphere

Figure 4.28: diagram showing comparison between Naokelekan Formation microbial structures and modified Logan et al. (1964) model, Chnaran location.

#### 4.6.4.4 Nannofossils

The most probable hypothesis for the nannofossils origin is coccoliths. Other mineralized microfossils (e.g. calcispheres, radiolaria, and tintinnids) can be excluded due to their larger size normally >40 microns, whereas all nannofossils in the mottled limestone member are from 5–10 microns. As well as coccoliths have internal structures and are different morphologically. Tintinnids appear as spherical to elongate with U- or V-shaped grains, whereas radiolarians display sieve-like fabric and mostly siliceous. However, calcisphere have not any internal structures, (Scholle, 2003; Armstrong and Brasier, 2005).

#### 4.6.5 Discussion

##### 4.6.5.1 Bioturbation

The formation of the mottled texture is interpreted here to result from bioturbation. The original sedimentary fabrics of microbial stromatolites “dark patches” were deformed extensively by bioturbation “light patches.” The bioturbation activities are common features that truncate, erode, and disturb the microbial lamination (Figure. 4.15). The textural differentiation between the bioturbated patches, and the parent rocks can be easily observed in the field (Figures 4.16, E–F, and 4.21, A–C). Mottled texture was formed by a complex pattern of bioturbation with irregular and horizontal to sub-vertical burrowing. The burrow diameters are up to 1 cm across on average, thicker in some places. Burrows can be traced laterally for several decimetres, whereas sub-vertical burrows penetrate down up to several centimetres (Figure 4.24). By comparing with the description of Hattin (1971), the burrows may attribute to *Thalassinoides*, but due to the intense bioturbation, it is difficult to be classified.

The deformation in the original fabric of micritic limestone in the mottled structure ranges from 60 to 80 % compared with Droser and Bottjer’s (1986) classification of bioturbation categories and standard chart of bioturbation comparison. Many dark patch collapses were brought about by burrowing activities (Figure 4.15). The remnant dark patches still retain their fabric details and are typically engulfed by light patches. (Figures 4.13, A, 4.21, A–C), which is mostly reworked. In many cases, more than one stage of burrowing was observed (Figure 4.29, B). In some layers, in which the original fabric was completely removed due to the intense bioturbation, homogenized were occurred on parent rock (Figure 4.29, A). It is very hard to recognize the type of ichnofauna, which was responsible for forming the mottling texture, or identify the burrow type.

The existence of sub-angular dark patches remnant in the light patches, with preservation of their primary textures and distinctively sharp boundary outlines imply lithification of dark patches prior to their dispersion in the light patches (Figures 4.13, A; 4.21, B; 4.26, B). Furthermore, firmground to hardground substrate can be indicated by accumulation of cephalopod shells in large numbers at the top of some bedding surfaces (Fig 4.13, B) which may also indicate a shellground (Junkeys, 1974; Taylor et al., 2003).

### **A–Bioturbation and rate of sedimentation**

There is much research pointing to the reverse relationship between the rate of sedimentation and bioturbation. The abundance of bioturbation fabric and dark patch distribution in light patches can be used as evidence of a low sedimentation rate (Shourd and Levien, 1976; Goldring, 1995; Taylor et al., 2003). It is noticeable that the sedimentation rate impacts on the degree of burrowing activities. A lower rate of sedimentation is often accompanied by intense frequency of bioturbation. According to McIlroy (2004) trace fossil preservation can be located between two end members: a) distinctly burrowed and b) indistinctly burrowed (burrow mottled). McIlroy (2004) argued that rates of deposition can control the type of trace fossils: a very low depositional rate may result in a texture with a mottled and homogenized appearance, where the original sedimentary structure cannot be recognized.

### **B–Bioturbation and kerogen impregnation**

The dark patches or “parent rocks” normally consist of very compact mudstone–wackestone to bindstone. Their lack of kerogen may be related to the early lithification. The early lithification may be indicated by the existence of the scattered dark patches lags in the light patches, which may indicate burrowing in a firmground or hardground substrate. In contrast, the light patches, interpreted here as resulting from bioturbation, are richer in kerogen than the host rock, i.e. dark patches (Figure 26, A–C). The richness in kerogen may be due to less compaction and/or cementation. Pemberton and Gingras (2005), and Tonkin et al. (2010) demonstrated that burrows which excavate into a firm ground substrate have a great influence on altering petrophysical characteristics, with the potential to improve reservoir properties.

### **C–Bioturbation and oxygenated condition**

Intense bioturbation in the TBMLM may indicate well oxygenated condition, as suggested by: (i) absence of reduction indicator minerals of iron rich minerals such as glauconite and pyrite occurred (Berner, 1981), (ii) relative absence of organic matter, and (iii) there is a well evidenced relationship between increasing bioturbation and oxygenation, as introduced by many researchers (Hattin, 1971; Ekdale and Mason, 1988; Goldring, 1995; Savrda, 1995; Taylor et al., 2003; Wetzel, 2010; Monaco et al., 2012).

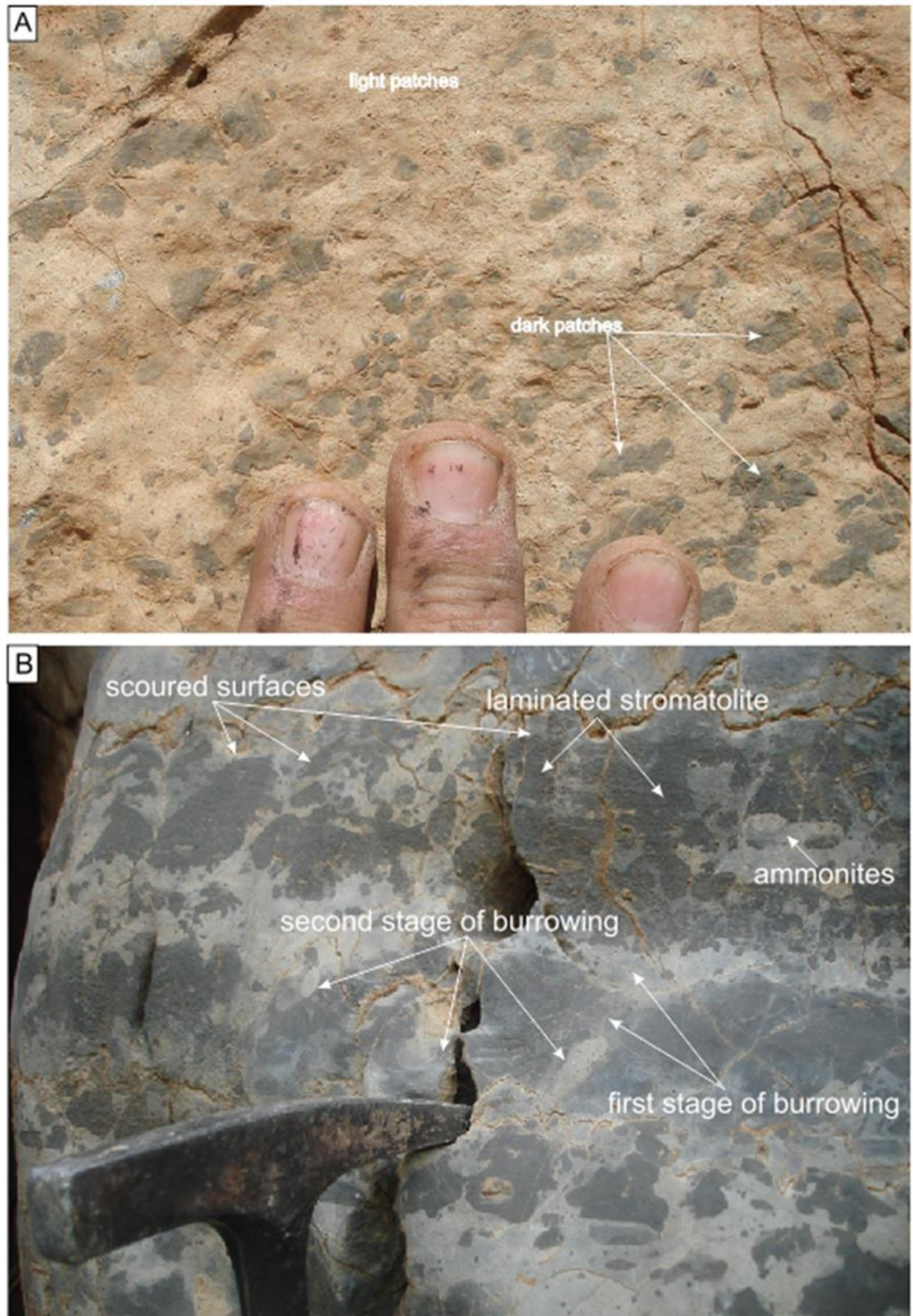


Figure 4.29 A; homogenized texture of mottled limestone member contains scattered remnants of dark patches, Gara location. B; photograph showing different stages of bioturbation and scoured surface of laminated stromatolites, Chnaran location.

#### 4.6.5.2 Microbial filaments and stromatolite forming environments

The Proterozoic Eon reflects an acme of abundance of diversity of microbial stromatolites (Riding, 1994). During this time, stromatolites were widely distributed in shallow-water environments. Since the Phanerozoic Eon the distribution of microbial stromatolites has declined. This decline was attributed to two main factors: firstly, biological evolution, and secondly, environmental factors (Riding, 1994).

The appearance of eukaryote metazoan is the main biological factor which led to the microbial decline (Riding, 1994). Many studies of ancient carbonate environments have demonstrated antipathetic relations between burrowing invertebrates, predators and microbial texture preservation (Garrett, 1970; Cussey and Friedman, 1976). The second factor may be related to the decrease of CO<sub>2</sub> pressure and increase of oxygen, and this change in environmental conditions from anaerobic to aerobic was probably caused by photosynthesis of cyanobacteria, which originated in the early stages of microbial evolution.

Since Phanerozoic the stromatolite structures can only survive in harsh environments where competition is reduced and the metazoan grazers are sufficiently rare. Saline restricted subtidal, hypersaline or/and highly fluctuating intertidal environments are optimal for the growth of stromatolites (Kendall and Skipwith, 1968; Gebelien, 1969; Friedman et al., 1973; Cussey and Friedman, 1976).

In fact, most Phanerozoic microbial stromatolites are recorded in peritidal environments (Riding, 1994), whereas the deep microbial stromatolite is quite infrequent. The fundamental characteristic for both deep and shallow stromatolites is the lamination (Hoffman, 1976), but for each type, there are distinctive characteristics (Table 4.3).

Characteristics	Peritidal stromatolites  (Shinn, 1968; Monty, 1976; Gill, 1977; Osborne et al., 1982).	Deep stromatolites  (Playford, 1976; Misik, 1993; George ,1999)
morphology	fenestrae pores are quite frequent in the internal and intrastromatolite mud laminae.	Fenestral porosity fabrics absent, usually finely laminated
occurrence	peritidal environments	Characteristically in condensed sequences grew on depositional slopes, and drowned reefs.
evidence of exposure	Desiccations, scoured surfaces, tepee structures gypsum crystals or their pseudomorphs.	None
associated fossils	Fauna often show high tolerance to harsh environments; peloids	pelagic faunas are common
response to sea-level fluctuation	Common; the effect of cyclicity and sea-level fluctuation can be seen clearly.	No clear effect
modern samples	Trucial Coast	Red Sea

Table 4.3: Comparison between deep and peritidal stromatolites.

The diagnostic features of the microbial structures in the TBMLM showing thin laminae, absence of fenestral porosity, growth on ammonite shells, and coccoliths association, are comparable in many ways to that of the description Playford et al. (1976), Misik (1993), and George (1999) in the table 4.3, so, it can be inferred that the microbial stromatolites in the mottled limestone of Naokelekan Formation formed in deep water environments (Figures 4.15, A–D, 4.17 and 4.27). Playford et al. (1976) have estimated the bathymetry of deep water stromatolites above 100 m below sea-level, and they assumed that the microbial structures can grow very slowly at localities where little or no platform–derived sediment could be provided, this may explain the absence of land or platform derived sediments.

Recent analogous examples in the Red Sea have been reported by Brachert and Dullo (1991) who pointed to the deep water microbial formation below the occurrence of living calcareous red algae from 120 m down to 215 m. In this bathymetric range, the microbial stromatolites are slowly accreted on the narrow shelf which sticks out from vertical reefal surfaces in the Red Sea; the stromatolites were also characterized by the absence of fenestral porosity.

#### 4.6.6 Summary of TBMLM formation

Based on the previous discussion, the mottled formation can be summarized briefly into the following points:

- The formation of the mottled texture is interpreted here to result from bioturbation.
- The original sedimentary fabrics are formed by microbial stromatolites “dark patches”
- Microbial stromatolites were deformed extensively by bioturbation producing “light patches”.
- The bioturbation activities are common features that truncate, erode, and disturb the microbial laminations.
- Facies association; ammonites, coccoliths, and deep-sea microbial stromatolites can indicate relatively deep water environment.

## 4.7 Argillaceous limestone member (ALM)

### Field Description

The ALM is black, thin to medium-bedded carbonaceous limestone, with thin-bedded intercalations of black argillaceous limestone and black shales (Figures 4.14, and 4.30, A & B).

### Microscopic description

The ALM is mainly composed of a calcispheric packstone, and no other fossils have been recorded. The calcispheres, which often show segmented walls with relatively large pores at the centre 0.010–0.030 mm across, are often intact, round-shaped grains, and 0.02–0.05 mm across. Many broken calcispheres are observed as well. The interstitial and intra-calcispheric pores are filled with organic matter (Figure 4.31 A).

#### 4.7.1 Microscopic evidence for the transition from ALM to MLL (Oxfordian–Early Kimmeridgian and Middle–Late Kimmeridgian boundary)

The boundary between the ALM and microbial laminite lithofacies (MLL) represents a contact between Oxfordian–Early Kimmeridgian Naokelekan Formation and Middle–Late Kimmeridgian Barsarin formation respectively (Figure 4.30, A–C). The contact between the ALM of Naokelekan Formation and the MLL of the Barsarin Formation seems to be sharp in term of facies change. The contact is marked by disappearance of calcispheric packstone of the ALM, which is rapidly overlain by microbial dominate bindstone of the MLL.

The base of the MLL is marked by first appearance of crudely laminated mudstone (Figures 4.31, B and 4.32, B). The laminae displays a wavy and anastomosing pattern, with no clear couplets of dark micrite and microsparite. Lensoidal and elongated shapes of micrite layers ranging from 0.3–0.5 mm, often containing microbial filaments (Figure 4.32, C) and scattered minute lath-shapes 20–30 microns long are common (Figure 4.32, D), which are filled by clear microspar (3–5 $\mu$ m). The laminae are locally disrupted horizontally by laminoidal fenestral layers up to 1–3 mm long and 0.5mm thick. This dramatic facies change from the ALM to the MLL can be seen much clearer in thin-section analysis than from the outcrop sections. In thin-section the contact can be determined by sharp changes in lithofacies from the calcispheric argillaceous limestone

member to the crudely laminated limestone with signs of evaporites at the base of the Late Kimmeridgian (Figure 4.31, A, B).

The laminoidal fenestral layers at the base in the MLL are occupied completely or partially by different kinds of calcite spar, micrite, and kerogenous matter. The fenestral filling materials can be categorized as follows: (i) anhedral to subhedral light drusy calcite spars: two distinct generations of spars can be distinguished; the cement is clear, ranging from 0.001–0.25 mm across, and crystal sizes increase from the pore wall to the centre of cavities (Figure 4.32, E); (ii) Fine, light brown mosaic equicrystalline spar (Figure 4.33, A) 0.05–0.1 mm in diameter, and the spars normally display rosette-shapes (Figure 4.33, B). The sharing of one fenestra cavity between equicrystalline and drusy calcite spars can be observed quite frequently (Figure 4.33, C). (iii) Lensoidal and rhomb-shaped micrite pseudomorphs of evaporite. The rhomb-shaped micrite normally associate with dolomite, partially dedolomitized, and completely dedolomitized minerals (Figure 4.33, D, and E). The rhomb-shaped micrite can be distinguished from the microbial-rich micrite through their specific and limited shapes and colour contrast, which appears darker than the main micrite textures. (iv) Kerogen-rich fenestrae: relatively narrow fenestrae 0.1 mm thick and ranging from 1–2 mm across; infilled by kerogen and some floated dolomite rhombs (Figure 4.33, F). This kind is dominantly observed in the lower part of the sequence. The study of the amorphous organic matter showed dark, solid granular structures (Figure 4.32, F).



Figure 4.30: A; boundary between argillaceous limestone member of the Naokelekan Formation (B) and microbial laminated lithofacies of the Barsarin Formation (C). The white dashed line shows sharp change in lithofacies from black shale dominance to the stromatolitic strata. This boundary is traditionally considered as a Naokelekan and Barsarin Formations contact. B; detail of argillaceous limestone member of the Naokelekan Formation, note the black shale dominance with few limestone beds intercalations. C; thin to medium-bedded MLL in the Barsarin Formation.

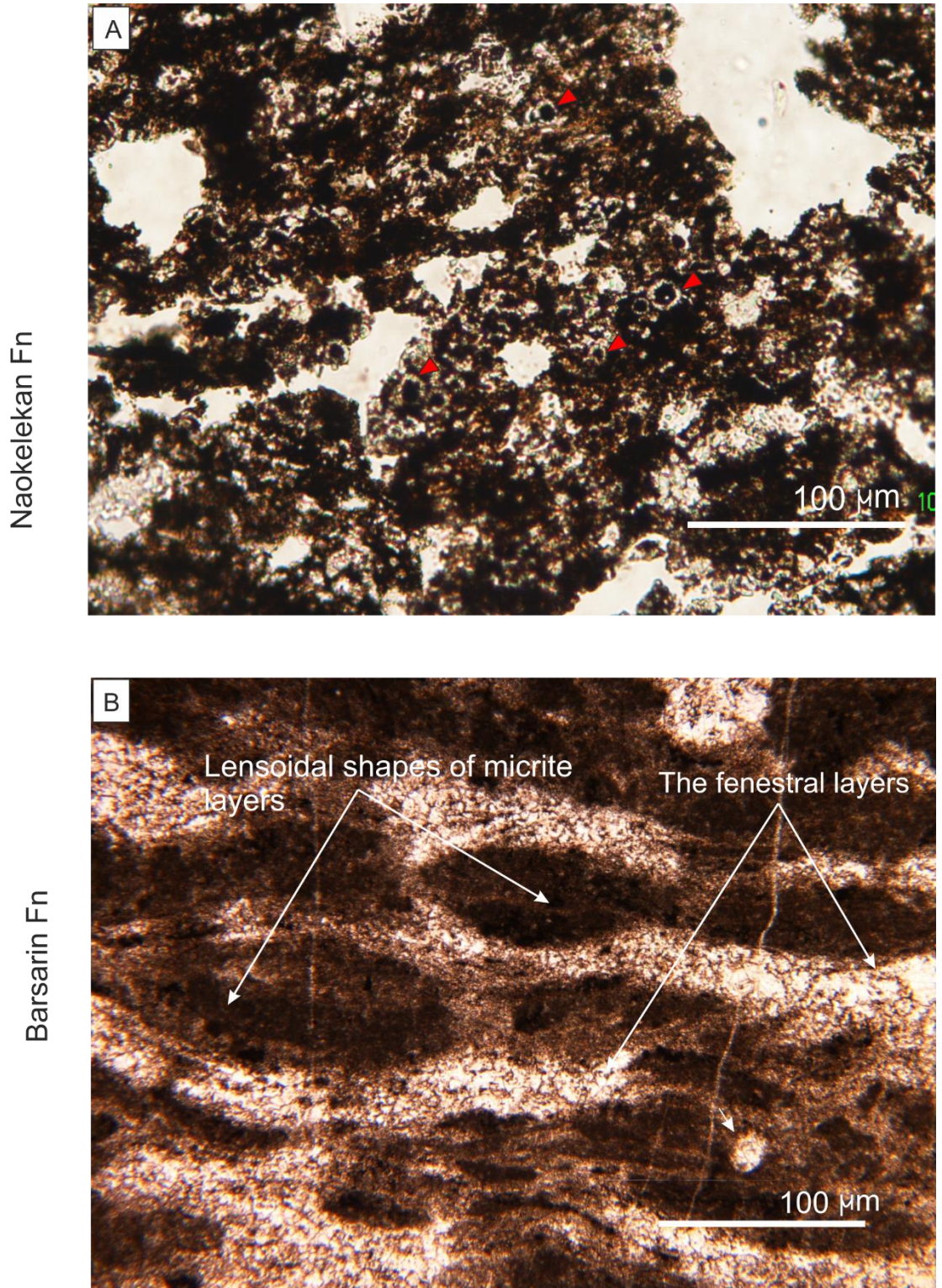


Figure 4.31: Sharp lithofacies change between argillaceous limestone member ALM (A) and microbial laminate lithofacies MLL (B) shows a dramatic change from pelagic calcisphere deposition to the peritidal sabkha environments (see Chapter 3). A; Calcispheric monospecific in argillaceous limestone member (red arrows), the inter- and intra-calcispheres pores are infilled by kerogen materials, PPL. B; photomicrograph shows alternating dark laminoid of evaporitic and microbial-rich mudstone and layers of fenestral light sparry calcite. PPL. Both photomicrographs are from Barsarin location.

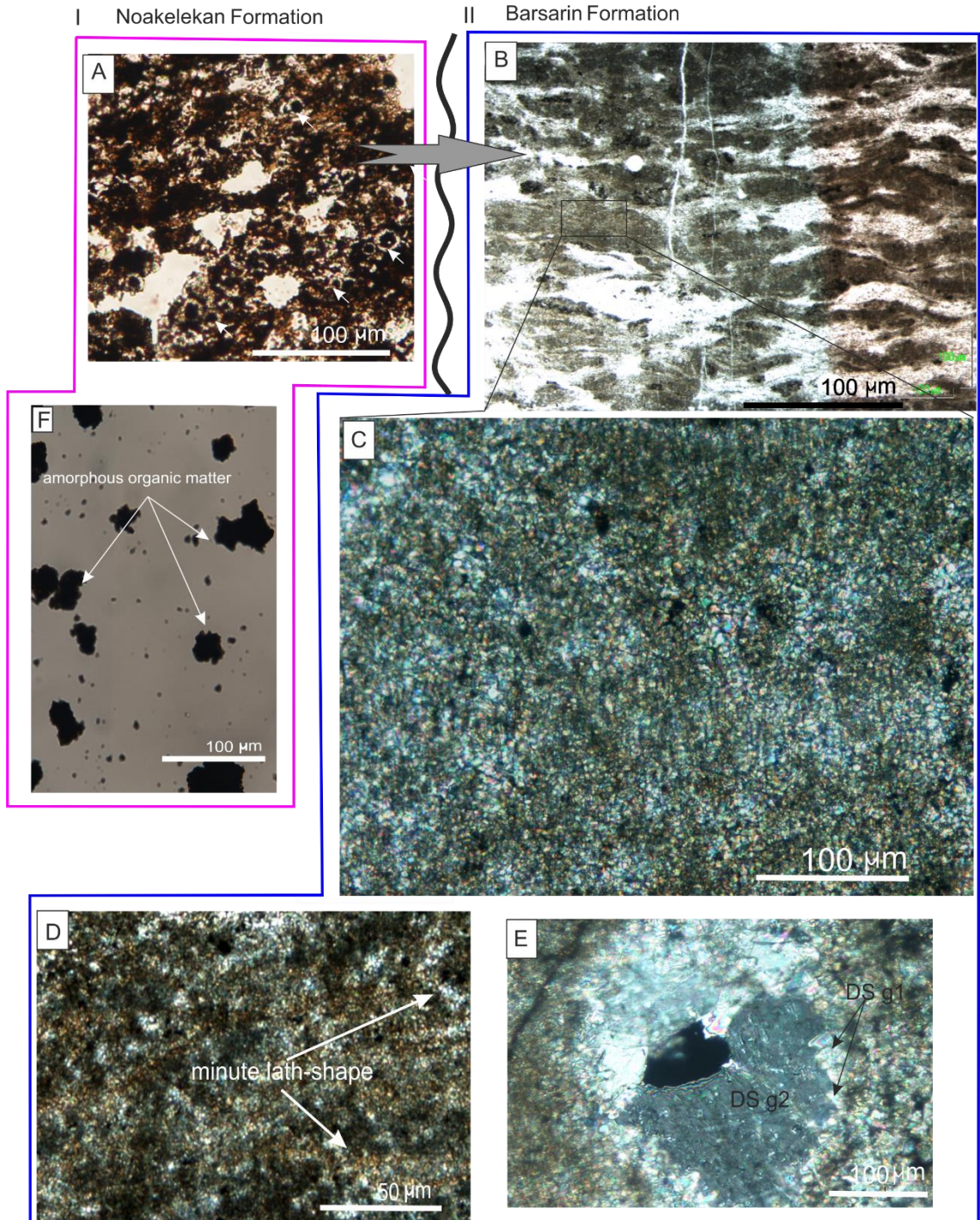


Figure 4.32: details of lithological change from the Naokelekan (I) to the Barsarin Formation (II). The wide grey arrow pointing to the dramatic lithofacies change. A; calcispheric packstone in argillaceous limestone member (white arrows), PPL. B; laminoid layers of light sparry calcite in between dark microbial-rich mudstone, PPL. C; detail of the black square showing microbial filaments, XP. D; mudstone contains scattered minute lath-shape PPL. E; two distinct generations of drusy cement can be distinguished DSg1 and DS g2 respectively, XP. F; amorphous organic matter shows dark solid granular structures, PPL. All photomicrographs are from Barsarin location.

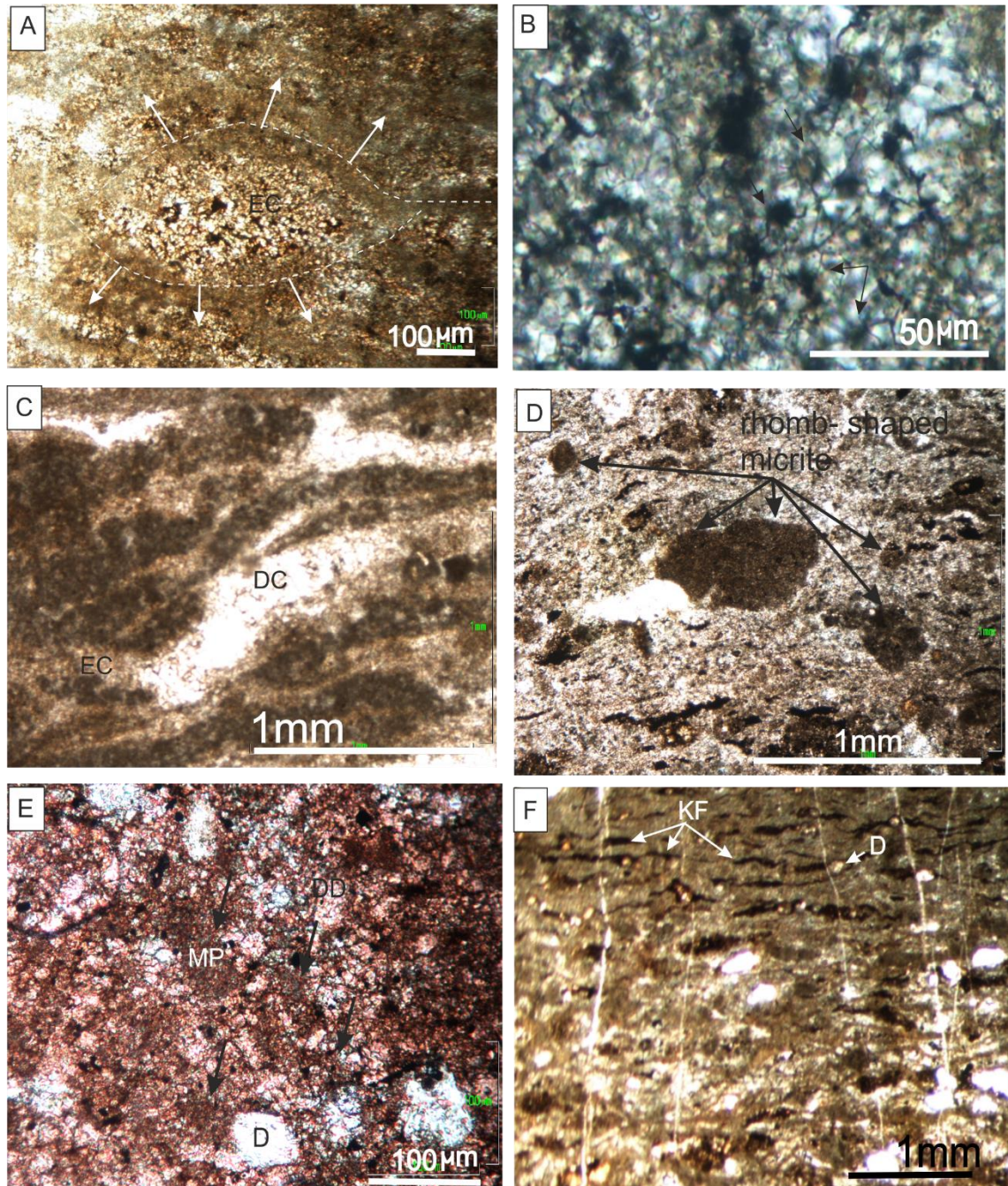


Figure 4.33: A; Lamination bent around fenestral calcite (EC), the white arrows pointing to the lamination displacement. B; rosette-shape spars in light brown fine mosaic equicrystalline calcite (black arrows). C; fenestra cavity occupied by equicrystalline (EC) and drusy (DC) calcite spars. D; rhomb-shaped micrite in mudstone (black arrows). E; thin-section showing rhomb-shaped micrite (MP) associated with dolomite, Alizarin Red S (D), partially dedolomitized, and completely dedolomitized (DD) minerals. F; narrow, Kerogen-rich fenestrae (KF) at the top of photomicrograph, including some floated dolomite rhombs (D), all the images are in plane polarised light. All photomicrographs are from Gara location.

#### 4.7.2 Facies interpretation of the ALM

A monospecific population of calcispheres is a feature of the argillaceous limestone member. The dominant assemblage makes more than 90% of the bulk rock (Figure 4.31, A). The prevalence of calcispheres was observed in this member in all locations. The widespread occurrences of calcispheres at the top of the Naokelekan Formation for more than 450 kilometres can be an effective tool for correlation.

The abundance of calcispheres is concomitant with the absence of all other faunas and floras such as ammonite benthic and planktonic forms. The production and settling of calcispheres represent the major sediment sources of the ALM, and micrite mainly provided by the disintegration of calcisphere (Figure 4.31, A). Calcispheres could be the main producer of carbonate sediments (Marszalek, 1975).

##### 4.7.2.1 Calcispheres

Calcisphere is a term referring to spherical or oval-shaped microfossils, regardless of their origin. This term was first used by (Williamson in 1880, in Bathurst, 1974); the spheres are constructed of a calcite wall enclosing a spherical central opening. The biological affinity of calcispheres is unknown and represents a matter of controversy (Wendler, 2002; Flügel, 2004; Versteegh et al. 2009).

The term (calcisphere) is inconsistently used by researchers. The morphological and taxonomical concepts lack formal definition, and for these reasons Versteegh et al. (2009) have suggested a new term “calcitarcha” to include calcareous microfossils with a central cavity enclosed by a wall of single or multiple layers, their biological affinities unknown.

##### 4.7.2.2 Potential origins of calcispheres “calcitarcha”

In general, the authors attributed the origin of calcispheres or “calcitarcha” to two types of algal cysts, and these are classified based on their occurrence in Palaeozoic and Mezo–Cenozoic (Wendler, 2002; Bathurst, 1975; Flügel, 2004).

1–Dasyclad green algae cysts (Chlorophyta): Many authors have suggested that calcispheres could be related to reproductive bodies (gametangia) of unknown dasycladacean algae (Rupp, 1967; Wray, 1977; Brasier, 1988). These kinds of cysts were common in the Palaeozoic Era successions, and their affinity to calcareous spheres is unknown. Rupp (1967) has compared non-spinose calcitarcha of the Devonian and

Carboniferous periods with modern dasycladacean reproductive cysts, and he discovered similarities in size and shape between them. Commonly, their sizes range between 0.1 and 0.5 mm and their central pores are characteristically 0.14 to 0.185 mm across.

This kind of calcisphere is well-known in the Devonian and Carboniferous periods of the Palaeozoic Era, often occurring in restricted and semi-restricted, lagoonal, and back-reef environments. Recent analogues of reproductive cysts of green algae have been studied by (Marszalek, 1975). He revealed that periodic blooms occurred of dasycladacean in shallow-water and sheltered environments in the Florida Keys. In contrast, Masters and Scott (1978) noted that calcispheres "calcitarcha" could exist in both deep and shallow warm-water, but they appear more abundant and distinctive in deeper water facies. Their abundance in the deep sea is explained by the relatively slower accumulation of other calcareous producers. However, calcispheres appear locally less abundant in shallow-water facies due to the dilution by a contribution of other organisms of carbonate production.

2-calcified dinoflagellate algae (Pyrrhophyta): The sizes of this kind of calcispheres are relatively small when compared with the green algae gametangia cysts, and range from 10 to 100  $\mu\text{m}$ , with an average of about 40  $\mu\text{m}$  (Keupp, 1991).

This kind of cysts has been observed predominantly in sediments of the deep shelf, slope and basinal settings. Additionally, their presence has been recorded in inner shelf environments as well. The calcispheres may occur with remarkable abundance in low energy facies in the innermost platform area (Masters and Scott, 1978; Riding, 1996). The Mesozoic calcitarcha affinities to the calcareous dinoflagellates have been emphasized by many authors (Masters and Scott, 1978; Versteegh et al., 2009).

Calcispheres are much more abundant within the Tethyan Sea than elsewhere on record, so it can be deduced that they are generated by organisms probably favouring niches located in sub-tropical latitudes climatic zones (Riding, 1996). Recent analogues of calcareous dinoflagellate cysts are known from a wide climatic range of neritic and pelagic environments, and it seems that they prefer tropical conditions rather than temperate regions.

Based on morphology characteristics and facies association, the calcitarcha of ALM are comparable to calcareous dinoflagellate cysts:

- i- Morphologically: calcitarcha are relatively small. Their sizes in the studied member range from 0.02 to 0.05 mm and this comparable to the dinoflagellate rather than dasyclad green algae.
- ii- Facies association: lack of shallow-water structures, green algae, and other kinds of shallow-water fauna can exclude shallow-water environments from argillaceous limestone member.

Hart (1991) described how there were a great abundance and widespread occurrence of calcitarcha “calcisphere” in Southern England and many other parts of Europe in the Lower Turonian strata. The extreme abundance of calcispheric facies was considered as a near-global bioevent. This event directly succeeded the well-known Late Cenomanian extinction event and carbon isotope excursion.

Hart (1991) stated that the abundance and monospecific population of the calcispheres next to the carbon isotope excursion may point to the unusual environmental conditions. The high abundance of calcispheres, which appears to be the result of an expansion of the oceanic oxygen minimum zone, is due to abundant flood from various localities of South Western Europe. Furthermore, Banner (1972) noted the abundance of calcitarcha in Tethyan environments, and he emphasized that the late Cenomanian calcispheres were deposited in open marine setting with normal salinity and a temperature of 20–25°C, and he assumed that the high abundance of calcispheres could occur in nutrient-rich surface water. Also, Jarvis (1988), and Souza (2011) have postulated a relationship between calcitarcha bioevent, and low rate of dissolved oxygen in the seas, which resulted in high abundance of calcitarcha. The abundance of the organic-rich monospecific calcitarcha in the ALM sight across the studied area (Figure 4.34), and the dramatically sharp change in facies, indicate a major change in palaeoceanography.

## 4.8 Summary

The organic-rich Naokelekan Formation is subdivided into five members, from base to top: BSM, CLM, MBMLM, TBMLM and ALM. In general, this formation was deposited in open-marine conditions, and is well-known for condensed intervals. Both BSM and CLM are dominated by organic matter. The amount of shale commonly decreases gradually upward within BSM whereas limestone beds increases upward. Abundant planktonic *Protoglobigerina* foraminifera and coccoliths discovered within both BSM and CLM suggest hemipelagic environments.

Both MBMLM and TBMLM represent condensed, prominent carbonate rock members in the Naokelekan Formation, which are overlain and underlain by softer strata. The bedding in MBMLM is characterized by uniform and steady lateral extension and it is devoid of any ammonites or visible fossils, but totally dominated by the large number of coccoliths and coccolith remains with microbial filaments. Some probable calcite pseudomorphs after evaporite crystals were observed as well. The facies associations suggest fairly deep-water with a brine surface model of Kendall (1978, 1992).

The TBMLM is considered to be of great importance for determining the palaeoenvironments, as discussed in the next chapters. This member is marked by the first appearance of mottled textures, and the mottling appears as dark and light patches in outcrops. The different textures of the mottled patches within the TBMLM were formed by bioturbation. The TBMLM consists of microbial stromatolite overgrowths on ammonite shells, encrusting foraminifera, coccoliths, and oncolites. The microbial overgrowth on ammonite is very similar to the ammonitico rosso facies. Many hardground substrates are indicated by accumulation of cephalopod shells in large numbers at the top of bedding surfaces. The combination of hardground, microbial stromatolite overgrowths and bioturbation suggests a condensed interval in well-oxygenated normal marine water. At all localities, the TBMLM is capped by the argillaceous limestone member, and its upper boundary is dramatically sharp.

The ALM is mainly composed of the monospecific population of calcispheres, and no other fossils have been recorded. The calcispheres are comparable to calcareous dinoflagellate cysts, and suggest that the ALM was deposited in a relatively restricted deep-sea with low dissolved oxygen ocean.

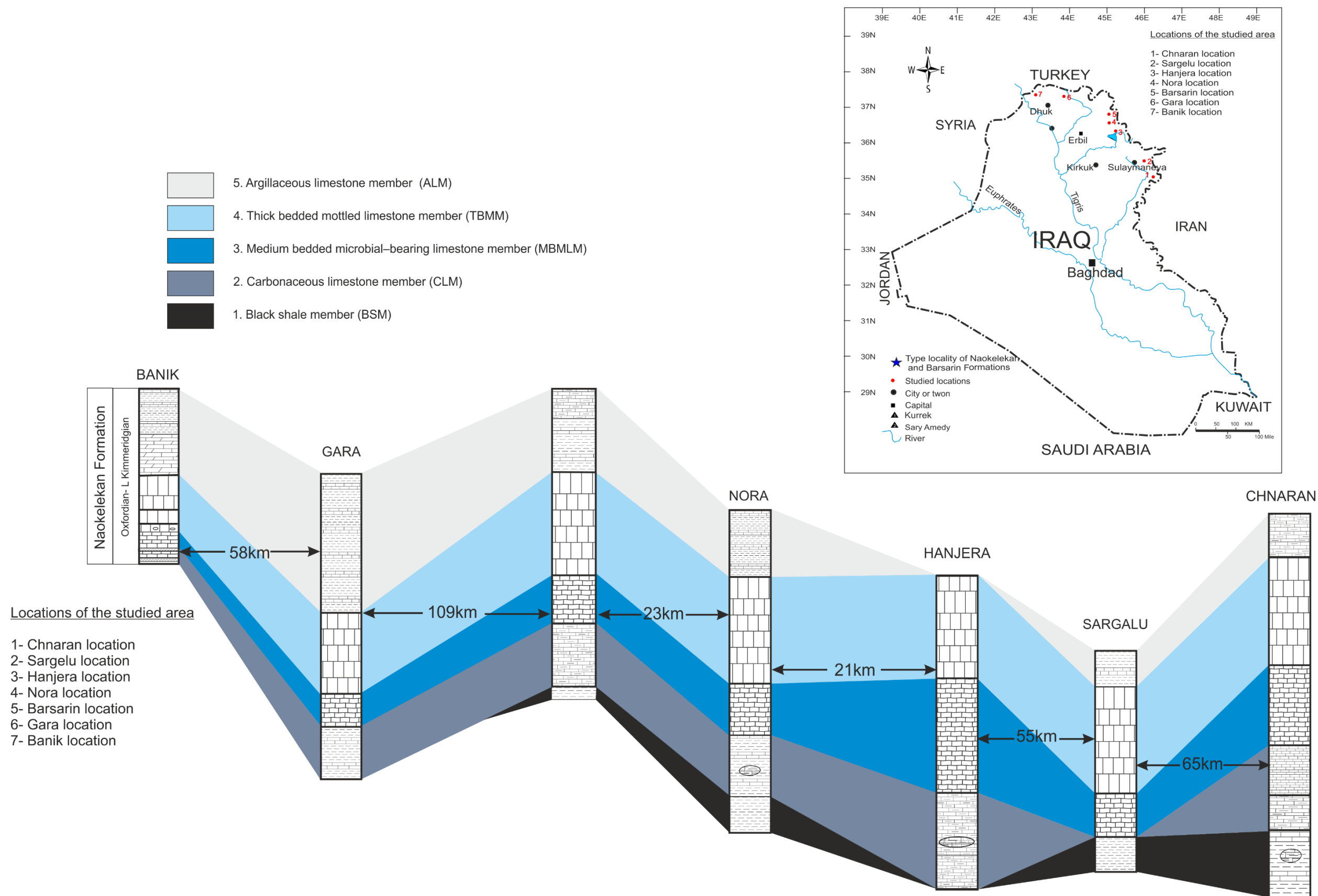


Figure 4.34 diagram showing distribution of member types of the Naokelekan Formation in Kurdistan exposures and lithostratigraphy correlation between different members. Note TBMLM, MBMLM as well as ALM are all laterally extensive for hundred kilometres.

## **CHAPTER FIVE**

# **5 DESCRIPTION AND INTERPRETATION OF THE BARSARIN FORMATION MID-LATE KIMMERIDGIAN**

## 5.1 Introduction

The Barsarin Formation was first described at Barsarin village (Figure 5.1) in northern Iraq, Kurdistan Region, as “laminated limestones and dolomitic limestones, some fluffy-textured, locally cherty, alternately in normal beds and in brecciated, crumbled and contorted beds” (Bellen et al., 1959). This formation is devoid of fossils. The age has been estimated from stratigraphic position, i.e. based upon well-constrained ages of the Naokelekan and Chia Gara Formations that respectively underlie and overlie the Barsarin Formation. Spath (1950) studied ammonite fossils of the Naokelekan Formation in Kurdistan Region, and assigning the top of the mottled limestone member of the Naokelekan Formation to Early Kimmeridgian. Howarth (1992) studied ammonites of the Chia Gara Formation, the base of which was determined to be Tithonian in age. Thus, the Barsarin Formation strata must be Middle–Late Kimmeridgian.

Seven different locations have been described in detail (Figure 5.1, attached appendix). The Barsarin Formation thickness ranges between 23 m in the Chnaran and 40 m in the Banik area, the formation clearly shows a westward thickness increase. Three lithofacies can be distinguished (Figures 5.2, and 5.3). From oldest to youngest, these are:

- 1- Microbial laminite lithofacies (MLL)
- 2- Blister–flat laminated lithofacies (BFLL)
- 3- Thick-bedded dolomite–limestone lithofacies (TBDLL)

A prominent characteristic of the Barsarin Formation is the repetition of lithofacies assemblages, in which each assemblage usually begins with a microbial laminite lithofacies, followed by blister–flat laminated lithofacies, and ends with thick-bedded dolomite–limestone lithofacies. The numbers of repeated lithofacies differ from one place to another. For instance, at Barsarin village, the highest number to be recorded in the outcrop where nine repetitions have been recorded. By contrast at Gara location, only five lithofacies repetitions were observed. The different lithofacies often show a specific arrangement, where it normally commences with the MLL and passes upwards into the BFLL to be capped by the TBDLL.

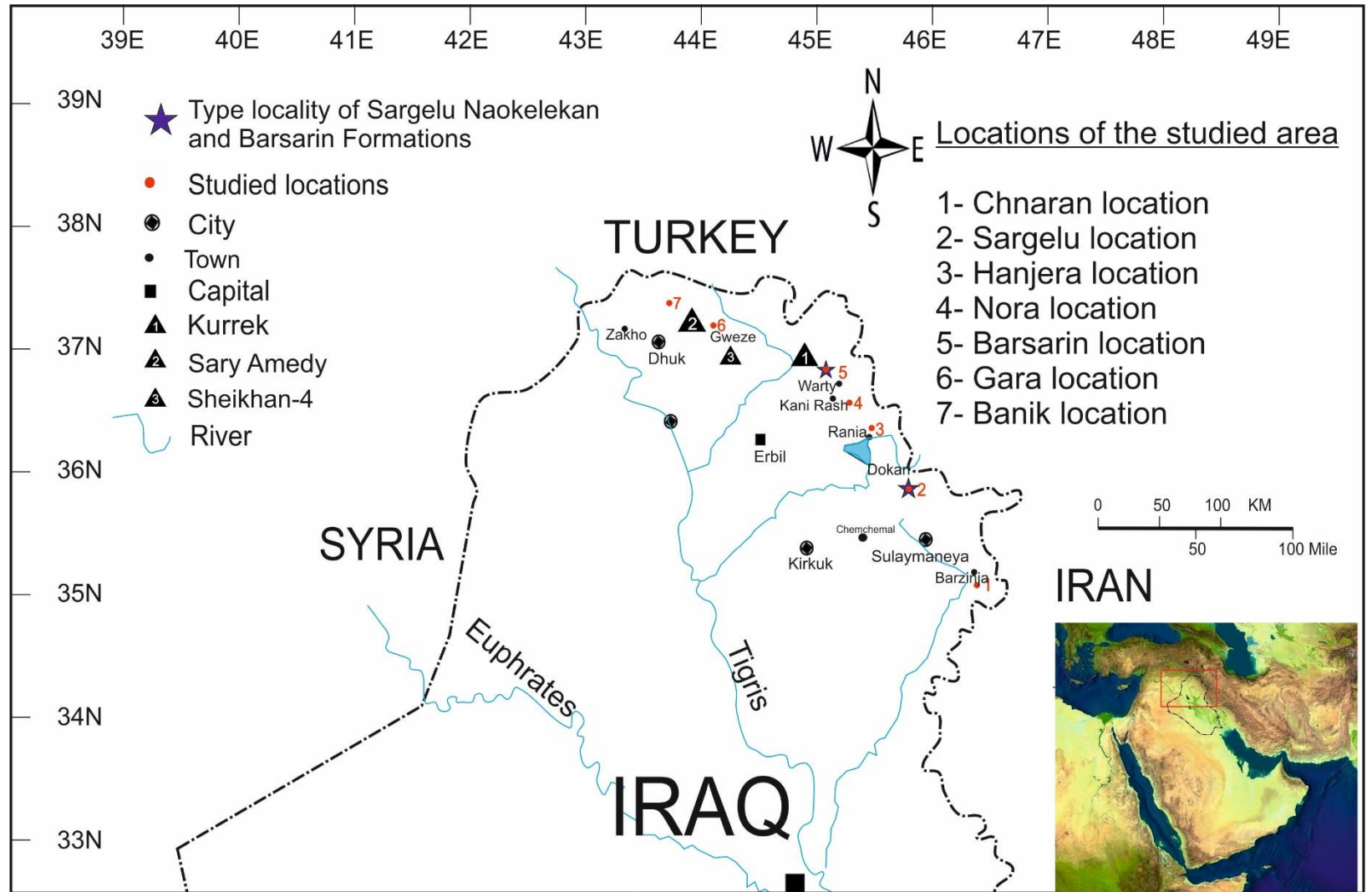


Figure 5.1: Different locations of the studied area in northern Iraq, Kurdistan region.

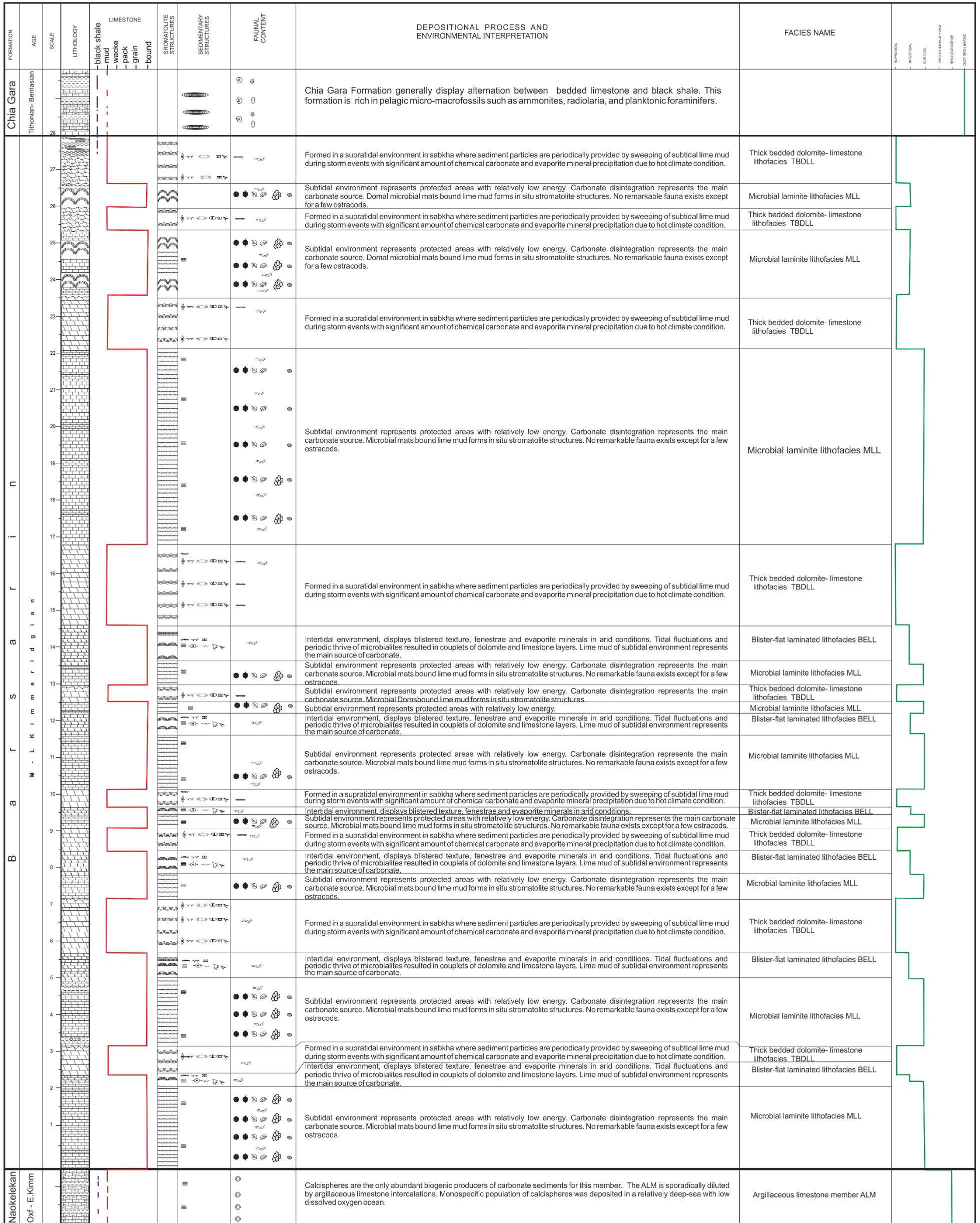


Figure 5.2: Generalized stratigraphic column of the Barsarin Formation showing different lithofacies and the nature of the underlying and overlying contacts with the Naokelekan and Chia Gara Formations respectively.

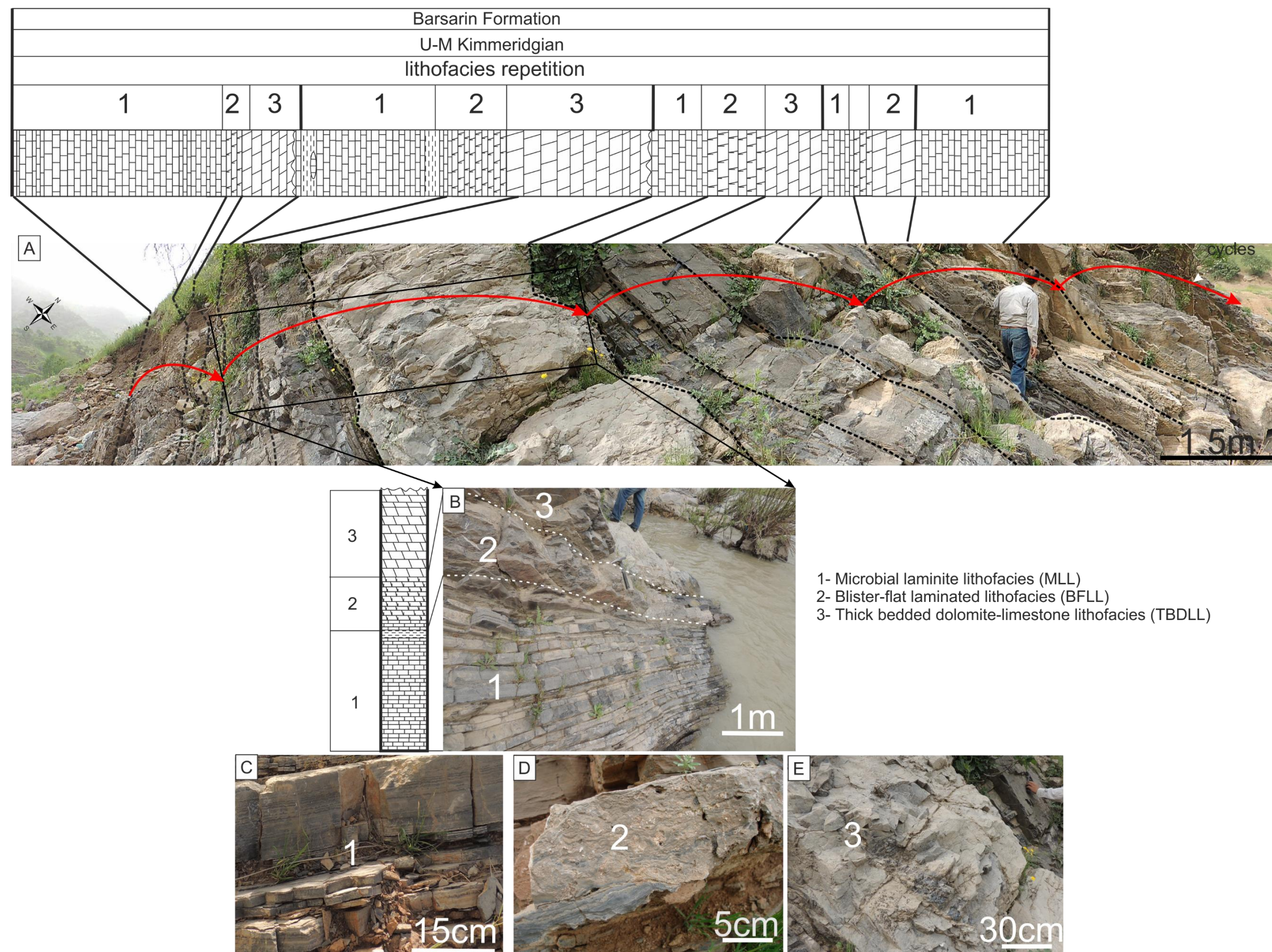


Figure 5.3: A; diagram showing panoramic photograph and lithostratigraphic log of the lower part of the Barsarin Formation, note a repetition of lithofacies (curved red arrows). B; photograph and stratigraphic log displaying typical arrangement of different lithofacies as the following order, from the bottom to top: 1- Microbial laminite lithofacies, 2- Blister-flat laminated lithofacies, 3- Thick-bedded dolomite-limestone lithofacies. C; microbial laminite lithofacies, which characterized by medium-bedded limestone and straight intralamination. D; blister-flat laminated lithofacies showing fenestra, desiccation feature and chert grains. E; thick-bedded lithofacies, including intraclasts, evaporites, and large chert nodules. All photographs are from Barsarin location.

## 5.2 Microbial laminite lithofacies (MLL).

### Field description

The microbial laminite lithofacies are often underlain and overlain by TBDLL and BFLL respectively. The MLL can be easily distinguished in the field by its possessing thin-to medium-bedded limestone and domal structures. Furthermore, in terms of colour, sedimentary structures, and mineralogical composition, the MLL exhibits a remarkable contrast with underlying and overlying lithofacies, where the MLL shows dark grey, medium-bedded, and straight laminated limestone (Figure 5.3, A and C). In contrast to the MLL, the BFLL is grey in colour with blistered textures of dolomitic limestone (Figure 5.3, D), whereas the TBDLL is often massive and buff in colour, and it contains chert nodules and brecciated dolomite (Figure 5.3, E). Relatively regular arrangements of the different kinds of lithofacies in the Barsarin Formation were revealed by field observations, which begin with MLL and pass upwards into blistered-flat to be capped by massive dolomite limestone lithofacies (Figures 5.3, B; and 5.4, C).

The MLL can be divided into two main categories on the basis of bedding morphology: (i) planar morphology and (ii) domal morphology. Generally, the MLL is mainly constituted from planar morphology. However, in the upper part of studied sections, the planar beds alternate with domal morphology for 2–4 intervals.

MLL is dark grey limestone (Figure 5.4, A), and light grey on weathering surface (Figure 5.4, B). Bed thickness ranges from medium 10–15 cm to thin 5–9 cm (Figure 5.4, C), which are thinly laminated with couplets of dark fine and light coarse calcitic laminae. The laminae often display crude to distinct fabrics, and they are slightly undulated, up to 1–3 mm thick (Figure 5.4, A–B). The vertical sections normally show differentially weathered surfaces with low relief contrast between dark and light laminae (Figure 5.4, B). The bedding planes often show tufts and pinnacle textures that rise some millimetres above the bedding surface (Figure 5.4, D). Few contorted laminae are observed in places, which appear as a series of small concentric undulated structure 10–15 cm across within individual beds, whereas the strata above and below are relatively unaffected (Figure 5.4, E). The MLL in the lowermost and uppermost parts of the studied sections sometimes alternate with medium-bedded black shale that includes some lensoid structures of limestone. The lenses are about 30 cm across and up to 15 cm thick (Figure 5.4, C).

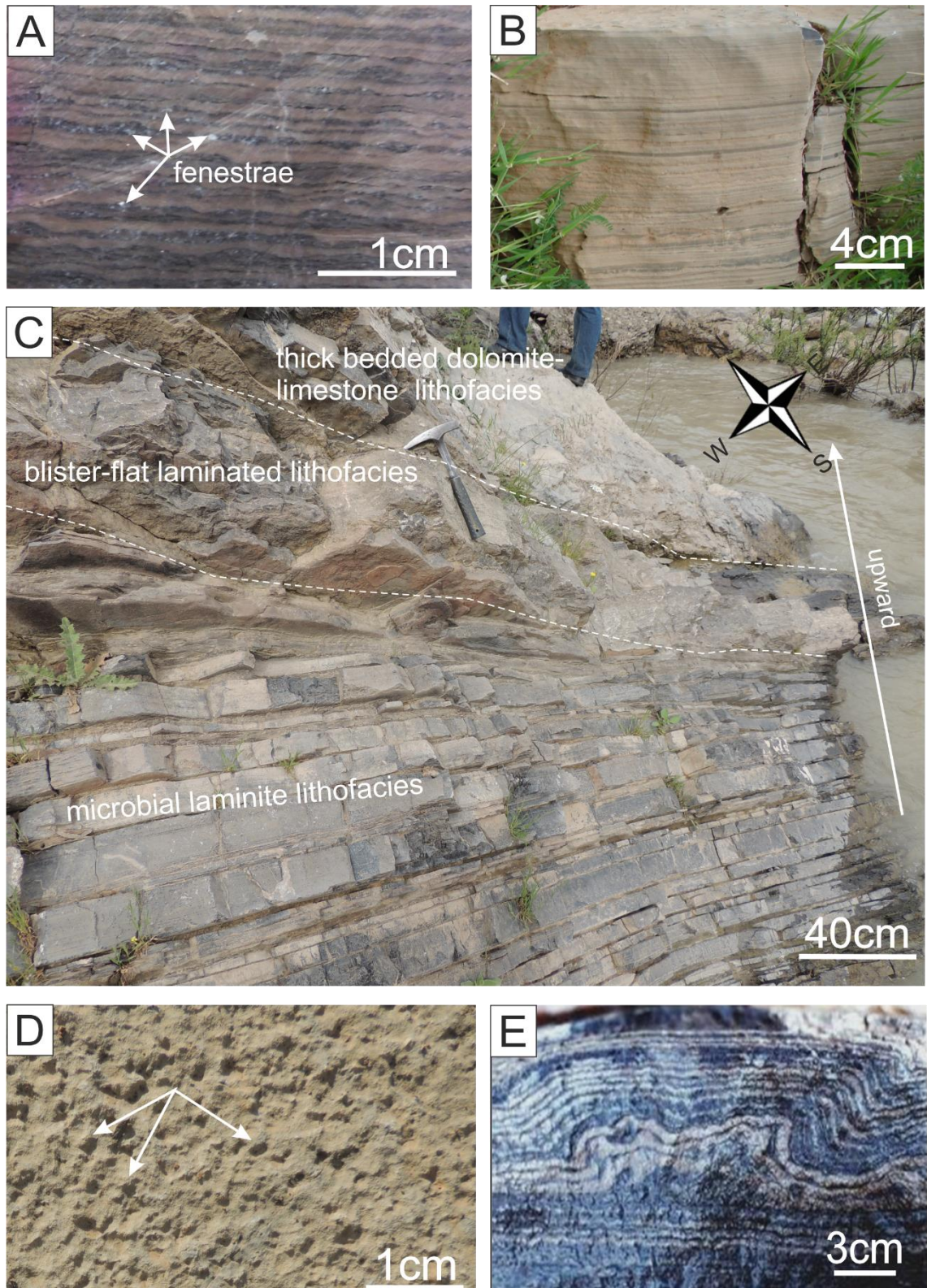
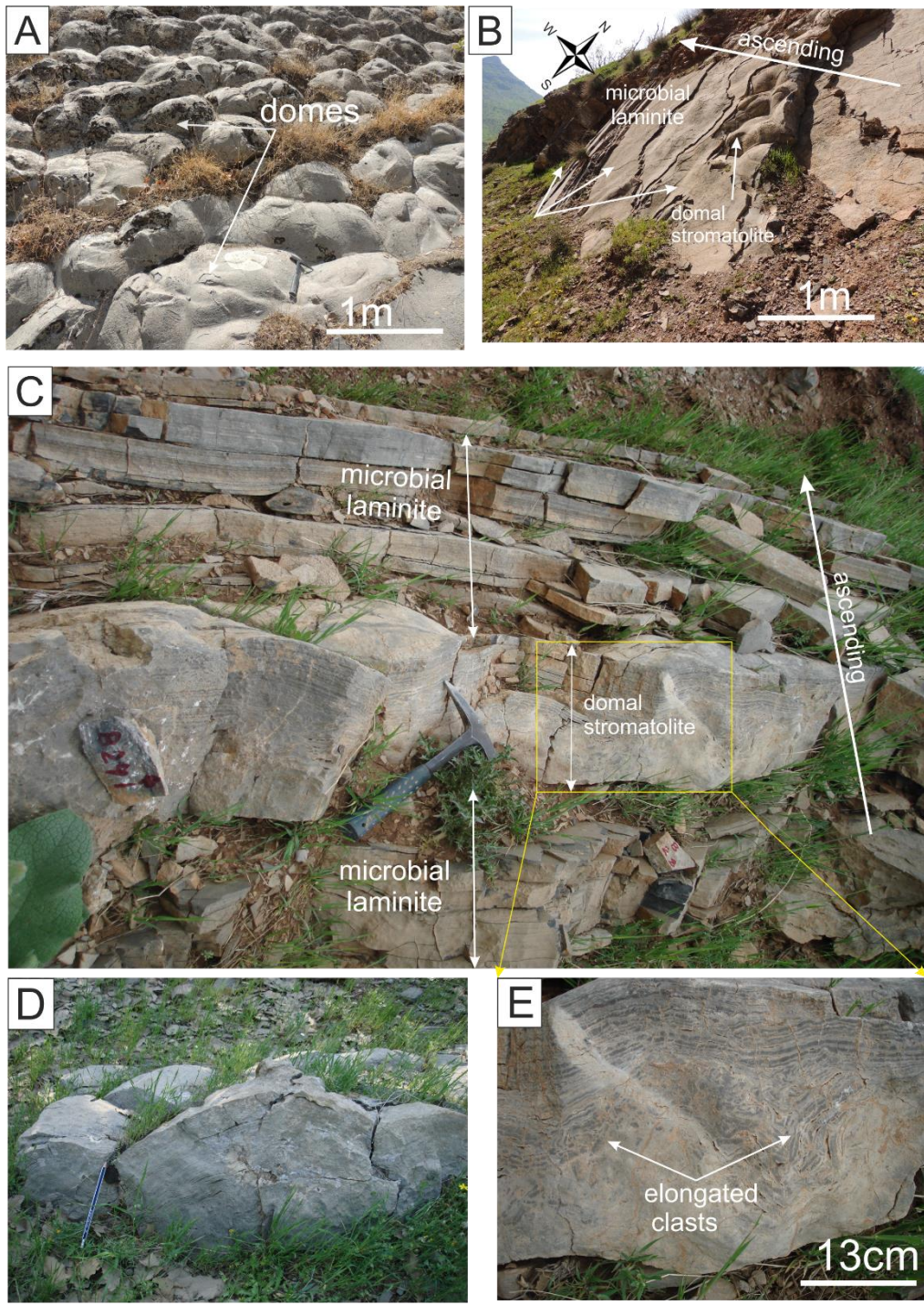


Figure 5.4: Microbial laminite lithofacies MLL. A; polished slab showing couplets of light coarse and dark fine calcitic laminae. The laminae show undulating macrofabric, note small fenestrae fabrics. B; vertical section showing low relief contrast on the differentially weathered surface showing straight lamination and couplet of dark light laminae with C; microbial laminite lithofacies displaying thin- to medium-bedded limestone, with few black argillaceous limestone interbedding. D; bedding planes of MLL showing tufts texture (white arrows). E; cross-sectional view showing contorted laminae structure, note the lower laminae are not affected by contortion. All photographs are from Barsarin location.



modified from Logan et al. (1964)	
descriptions	Vertical section of the stromatolite structures
 <p>close lateral</p>	laterally linked hemisphere mode-C
 <p>space lateral</p>	laterally linked hemisphere mode-S

Figure 5.5: Domal stromatolites from different locations. A; top view showing domal stromatolite at Barsarin Village. B; partially exposed domal stromatolites, showing alternation between domal and planar beddings. Note the latter bedding attempt to compensate underlying depression surfaces. C; cross sectional view showing alternation between domal stromatolite and planar bedding, Barsarin Village. D; domal stromatolites at Nora location, the pencil is about 15 cm. E; dome cores include large elongated clasts, Chnaran location. F; a sketch representing two types of laterally linked hemisphere mode C and S, modified form Logan et al. (1964).

The domal stromatolite morphologies in the MLL can be only observed in the upper part of the sections. It is dark grey, medium-bedded limestone, always alternating with planar bedding of the MLL (Figure 5.5, A–C), and the domes show low relief and thin to thick lamination. Based on the classification of the Logan (1964), domes can be considered as close laterally linked hemispheroidal stromatolite (C–LLH) (Figure 5.5, F). The domes are about 30–40 cm in diameter, and the synoptic relief of the dome is about 15–25 cm (Fig 5.5, D). Some dome cores include large voids, which are partially filled with large elongated clasts, up to few 5 cm across (Figure 5.5, E).

#### Microscopic description

Microbial laminite lithofacies mainly shows continuous laminae with couplets of micrite and microsparite. The laminations vary from crude to distinct microfabrics, and often show couplets of relatively thick light microsparite and thin dark micritic laminae (Figure 5.6, A). The MLL mainly comprise clotted microtexture, or as it is also termed “texture grumeleuse (Cayeux, 1935)” (Figure 5.6, B). The clotted microtexture, which surrounded by sub-millimetre size of calcite cement infilled fenestrae, appears as many little irregular clots up to 0.15 millimetres across, of an extremely fine crystalline calcite, standing out as dark grey colour in a matrix of granular calcite. The fenestral vugs exhibit lath to irregular shapes, and are arranged more or less concordant to lamination. Fenestrae may be completely or partially filled calcite cement and or kerogen (Figures 5.4, A; 5.6, A–C; and 5.8, B–C). Some ovoid-shaped dark brown to black, favreimid-like fecal pellets 0.3–0.8 mm in diameter have been observed (Figure 5.6, C), which are characterized by small micritic bodies with sieve-like structure.

Significant amounts of polygonal-shaped and inclusion-rich calcite spars 0.4–0.6 mm across have been observed, some spars have a lumen in the centre (Figures 5.6, D; and 5.8, B). The calcite spars often form clusters of rounded to elongate aggregate bodies up to 1.5 mm across. These clusters perhaps were derived from reproductive organs of green algae, but due to the ambiguity of their outer wall, their origin cannot be ascertained, and they will not be further discussed in this work. A few intact ostracod carapaces 0.17–0.2 mm in size are infilled by calcite cement, and few poorly preserved fossils 0.250–0.3 mm in size are also present (Figure 5.7, A). The dark laminae are rich in elongate tube-shaped microbial filaments, several hundred microns in length and up

to 60  $\mu\text{m}$  thick (Figure 5.7, C), whereas the lighter laminae normally display some radial structures of calcite spars up to 0.1 mm in size, which have lumen at the centre (Figure 5.7, B). Scattered clusters of dolomite and partially dedolomitized rhombs 0.05–0.07 mm across have been observed (Figure 5.7, D, and E). The dolomite rhombs are embedded in lensoidal organic-rich vugs. Some light brown micritic bodies which have rhombic-shape frameworks are also observed (Figure 5.7, D).

The domal stromatolites are microscopically similar to the planar bedding textures, which consist of couplets of dark fine and light microsparitic laminae (Figure 5.8, A). The darker laminae in domal stromatolite are thinner and strongly affected by stylolitization, whereas the lighter laminae are thicker and display much resistant to pressure solution. Both types of laminations are rich with clotted microtexture, inclusion-rich calcite spars (Figure 5.8, A–C), and rod-shaped peloids (Figure 5.8, D). Laminoid fenestrae structures are also common, and some of them show lath or rhombic shapes (Figure 5.8, A–C).

Two types of pressure dissolution are present in the MLL; non-sutured seam stylolite (Figure 5.7, E), and sutured seam stylolite (Figure 5.8, A). Non-sutured seam solution, anastomosing swarms run parallel to the lamination, where some fine-grained 0.03–0.05 mm cloudy dolomite rhombs are present, few of which are partially stained with Alizarin Red S, indicating effective dedolomitization (Figure 5.7, E).

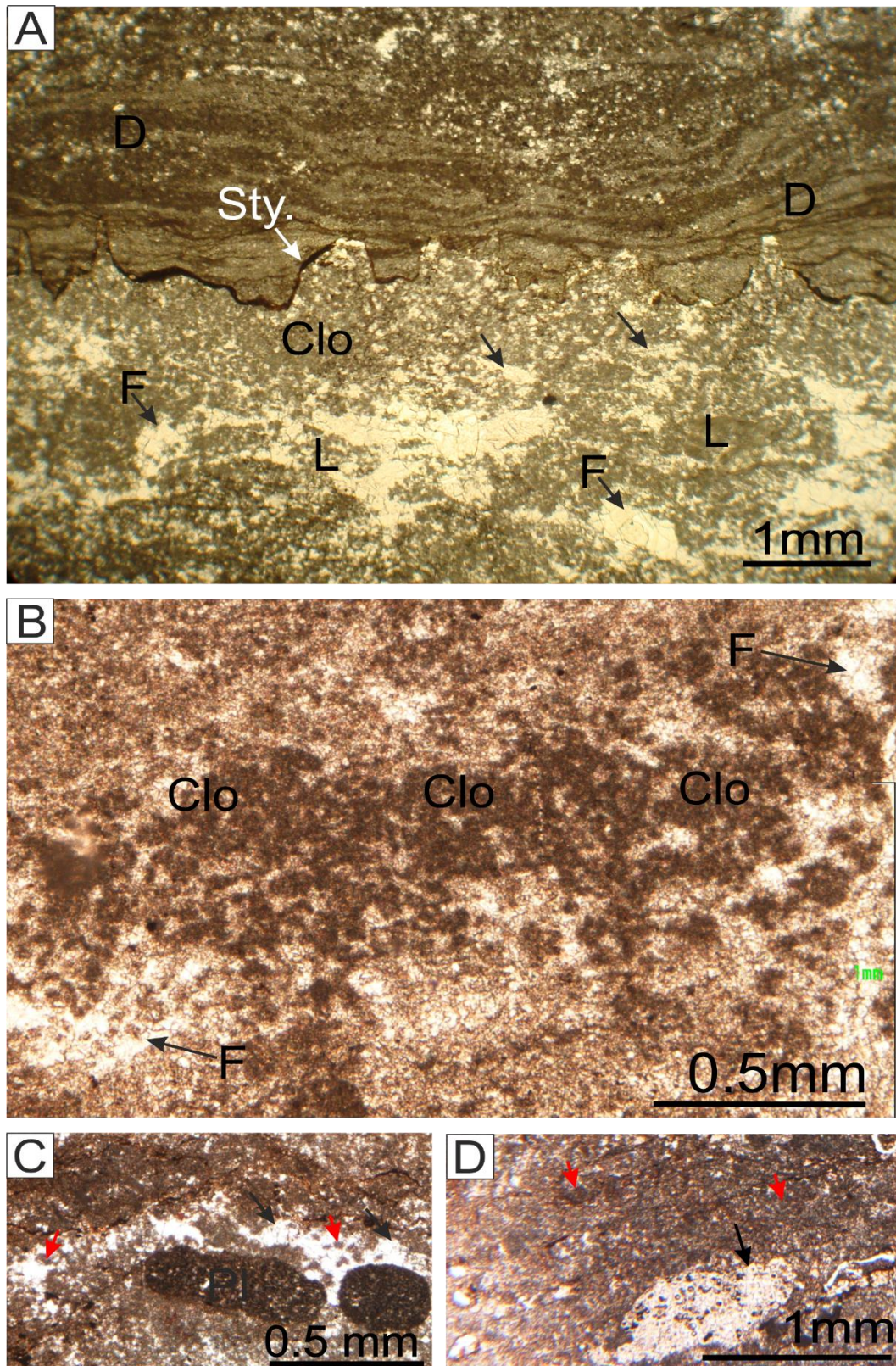


Figure 5.6: Microbial laminite lithofacies. A; laminated couplet, showing thin dark laminae (D), and thick light laminae (L), they both are rich in clotted microtextures (Clo). Note that the thin dark laminae are much susceptible to pressure solution. The black arrows point to the fenestrae (F), and some of which show lath-shaped outlines. B; microbial laminite lithofacies shows dominance of clotted microtextures and fenestrae, Alizarin Red S. C; dark spotted fecal pellets in the light laminae, are characterized by sieve-like structure. Note clotted dominance (red arrows). D; inclusion-rich calcite spars (black arrow), showing calcite spar clusters, and some spars have a lumen in the centre. Note the dominance of clotted microstructures (red arrows), Alizarin Red S. All of the images are in plane polarised light All photographs are from Chnaran location.

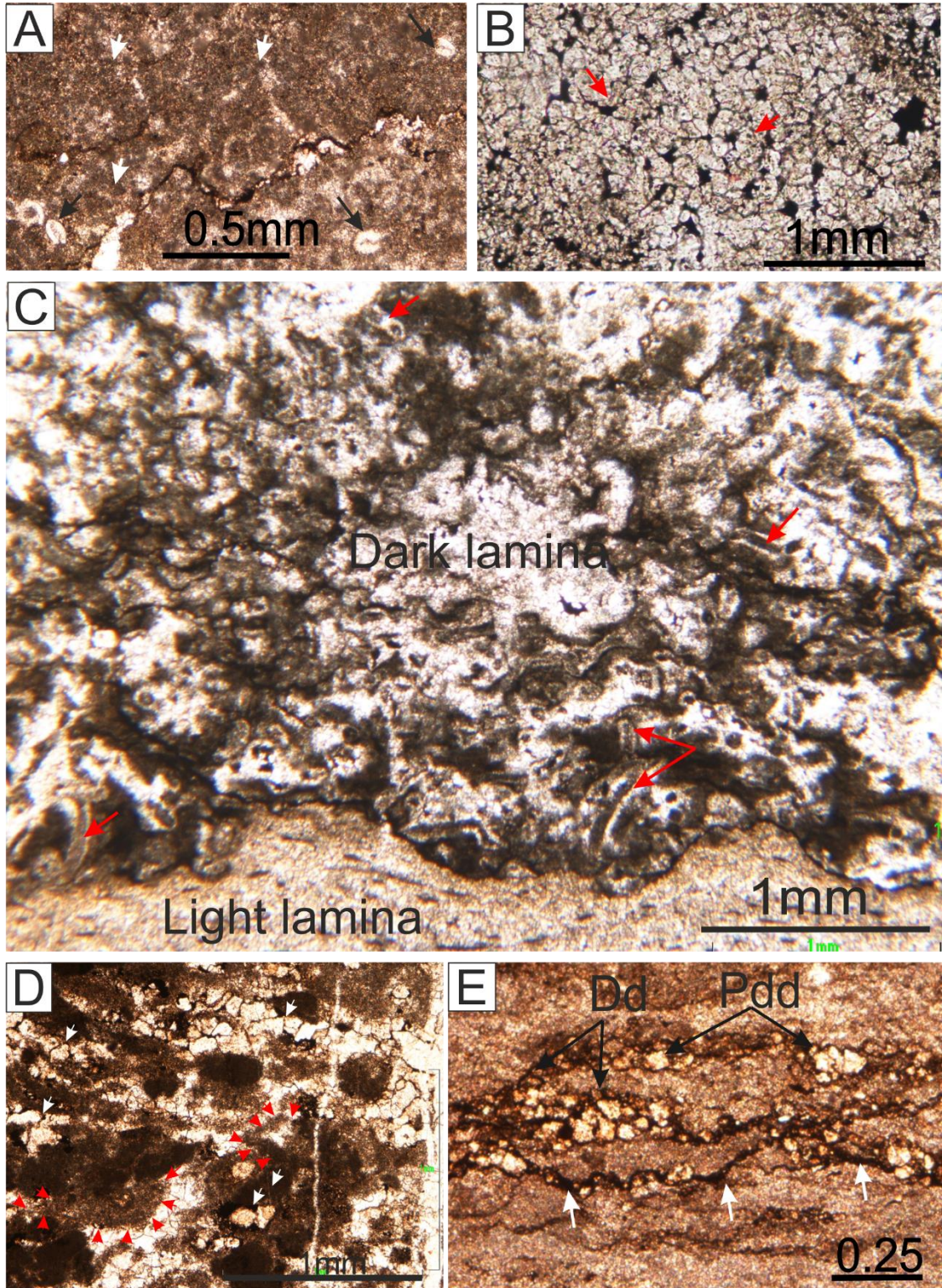


Figure 5.7: A; intact oyster carapaces are infilled by calcite cement (black arrows), and clotted structures (white arrows), Alizarin Red S. B; radial structures of calcite spars showing dark pores at their centre (red arrows). C; a microfabric of dark lamina showing microbial filaments (red arrows). D; partially dedolomitized rhombs floating in a micritic matrix (white arrows), note organic matter infilling the intercrystalline pores. The red arrows surround a rhomb-shaped micrite, Alizarin Red S. E; anastomosing swarms run parallel to lamination, where some partially or completely dedolomitized are present, Alizarin Red S. All of the images are in the plane polarised light, Hanjera location.

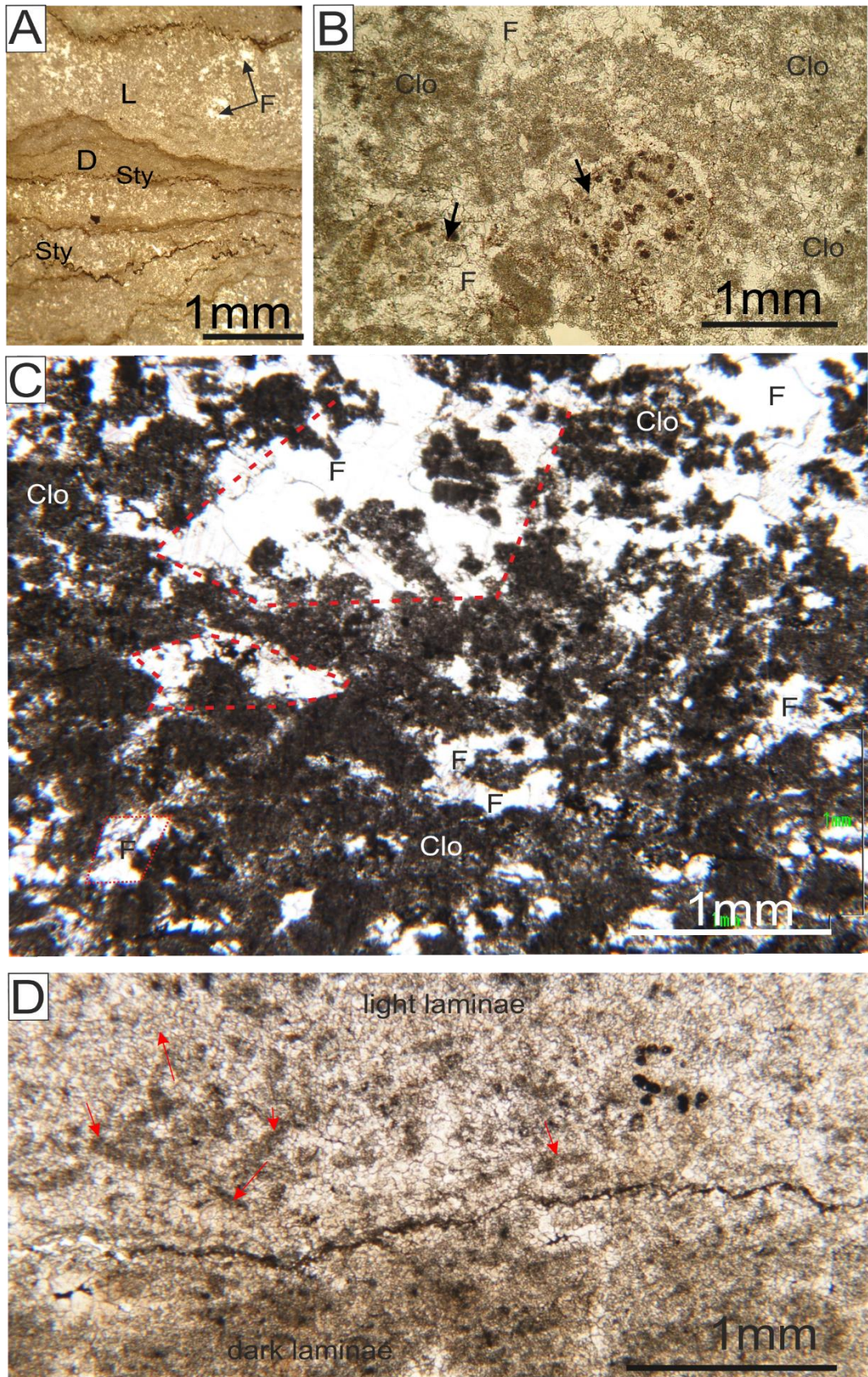


Figure 5.8 A; couplets of dark fine (D) and light microsparite (L) laminae. The light laminae are rich in fenestral fabrics (F). Note the dark laminae are so susceptible to pressure solution. B; photomicrograph showing inclusion-rich calcite spars (black arrows), with fenestral fabrics (F), and clotted microstructures (Clo). C; fenestral fabrics (F) display rhomb-shaped outlines (dashed red lines), note the dominance of the clotted microstructures (Clo); D; Rod shaped peloids (red arrows). All of the images are in plane polarised light, Gara location.

### 5.2.1 Interpretation

The microbial laminite lithofacies MLL is interpreted to record microbially dominated sedimentation in a protected subtidal environment. This interpretation is supported by the following:

#### 5.2.1.1 Clotted microtexture and microbial filaments

Clotted microtexture is a peloidal texture that exists abundantly in both dark and light laminae of the MLL. Their ultrastructure is quite different from the fecal pellet grains, where the clotted microtextures have irregular shapes and blurred outlines, and they lack specific internal structure, up to 0.150 mm in size (Figures 5.6, A–B and 5.8, C). It has been concluded that clotted microtexture can form by microbially produced peloids (Guo and Riding, 1992; Riding, 2000). They are a characteristic feature of microfabric stromatolitic lithofacies, and are found in both recent analogues and ancient deposits.

Many researchers have emphasized that the clotted fabrics are widespread in microbial communities, which create a microenvironment conducive to carbonate precipitation (Chafetz, 1986; Kennard & James, 1986; Riding and Sharma, 1998; Turner, 2000). Sun and Wright (1989), working on Upper Jurassic clotted microtexture, found evidence of their origin, from their occurrence in stromatolite crusts, and interpreted them to be a probable microbial product. This is quite applicable to MLL where paucity of fauna may have led to microbial structure preservation and development.

A microbialites role is also supported by some well-preserved filaments (Figure 5.7, C). Tufts and pinnacles on bedding surfaces (Figure 5.4, D) may also indicate the presence of a microbial mat, as similar sedimentary structures occurred in modern peritidal environments in the south coast of Tunisia (Gerdes, 2000). Radial structures of calcite spars in MLL (Figure 5.7, B) resemble the bacteria loci that are described by Chafetz (1986).

#### 5.2.1.2 Pellets

Favreimid-like fecal pellets are frequently observed in thin-sections of MLL (Figure 5.6, C). These microcoprolites can be easily recognized by their sieve-like structure that may be caused by calcite-filled canals (Flügel, 2010). Accumulations of favreimid fecal peloids in the latest Jurassic shallow-marine and restricted lagoon limestones were very common (Flügel, 2010).

#### 5.2.1.3 Fenestral fabric

Fenestra or window; was first defined by Tebbutt et al. (1965) as “a primary or penecontemporaneous gap in rock framework, larger than grain-supported interstices”. The term fenestra now can be used for any kind of a hole of any shape in a rock or consolidated sediment (Demicco and Hardie 1994).

The formation of fenestral vugs in MLL is suggested to be related to bio-activities of microbial mats or breaking down organic matter. Since all fenestrae are surrounded by clotted microtexture of microbialites, their origin can be linked to the microbial existent. Fenestrae are a common texture in modern peritidal carbonate environments, (Shinn, 1983; Flügel, 2004; Boggs, 2009; Tucker and Wright, 2009).

#### 5.2.1.4 Hypersaline environments and laminae preservation

MLL is mainly composed of limestone with a clotted microtexture, a few ostracod carapaces, and favreimid-like fecal pellets. The absence of fossils, except for a few ostracod carapaces, and rare fecal pellets (Figures 5.6, C and 5.7, A), together with rare evaporite pseudomorphs (Figures 5.6, A and 5.8, C) suggest hypersaline conditions. Moreover, the adjacent evaporite-rich lithofacies, such as blister-flat laminated lithofacies and thick-bedded dolomite-limestone lithofacies, which overlie and underlie MLL respectively, also show indications of hypersalinity and sabkha environment (see next sections 5.3 and 5.4).

The deposition of MLL in hypersaline environments may imply that the hypersalinity was beyond the threshold of predator tolerance, so that grazing behaviour was subdued or absent (Park, 1977). Consequently, organosedimentary or microbial mat structures can thrive, and prevail. This can be inferred by the paucity of skeletal micro or macro fauna, and perfectly preserved original lamination in MLL.

A low-energy tidal flat can be inferred by perfectly preserved lamination, with the existence of intact ostracods and pellets. Tucker and Wright (1990) stated that the pellets and intact ostracod carapaces are common constituents in protected environments such as lagoons and tidal flats due to the absence of wave action.

#### 5.2.1.5 Plastic deformation structures

Few contorted laminae are observed in the MLL (Figure 5.4, E), but their plastic behaviour may point to the presence of prelithified cohesive microbial surface binding

laminae (Schmidt, 1965; Schieber, 2007). Laminated contorted beds are more commonly found in shallow-water settings (Pruss et al, 2010). Assereto and Kendall (1977) and Kendall and Warren (1987) have observed similar textures of MLL plastic deformation texture in both ancient and recent subtidal environments.

#### 5.2.1.6 Domal stromatolites morphology

The domal stromatolites are conspicuous microbial sedimentary structures in the Barsarin Formation (Figures 5.2 and 5.5, A–E). Domal stromatolites have been well documented in modern environments. They often occur in hypersaline water in subtidal environments with moderate current movement (Gebelein, 1969; Playford and Cockbain, 1976; Kinsman and Park, 1976; Noffke, 2004). In general, domes are well developed in the upper part of the Barsarin Formation at all localities (Figure 5.5, D). The domes, which are often interbedded with planar beds of MLL (Figure 5.5, C), are of the close linkage laterally linked hemispheroid (C–LLH) (Figure 5.5, F). The domes show gently undulating lamination and are up to 30–40 cm wide and 15–25 cm high. They are found in two or three intervals as shown between 23.5 and 26.6 m on the logged succession (Figure 5.2).

Some modern domal structures show development of the void pockets under the domal crest. The voids are related to gas entrapment (Bathurst 1975; Warren 1982). At Chnaran location (Figure 5.1), partial breakages of lithified laminated rocks owing to a collapse into an opening were observed (Figure 5.5, C and E). Similar collapses in domal carbonate stromatolites were reported by Walter et al. (1973) in the modern Coorong Lakes on the south-eastern coast of Australia.

Domes may be considered as the modification of microbial mats in areas of high sediment supply. This may occur in areas of somewhat reduced surface abrasion (Gebelein, 1969; Braga et al., 1995; Draganits and Noffke, 2004). It seems that the periodic wetting and drying by tidal fluctuations are more effective on the crest where rapid lithification occurs (Logan et al., 1964). Dome crests may be partially exposed and dried during low tide, subsequently leading to early lithification, whilst the depressions are submerged for longer and consequently less lithified (Logan et al., 1964). Rapid alternation between domed stromatolites and planar beddings may reflect tidal fluctuation from lower intertidal to subtidal respectively, preventing the formation of stacked hemispheroid stromatolites. As well as the formation of domal stromatolites in subtidal–lower intertidal environments have been confirmed by many studies (Gebelein, 1969; Playford and Cockbain, 1976; Kinsman and Park, 1976; Warren, 1982; Ricketi,

1983; Sami and James, 1994; Noffke, 2004). Overall, the Barsarin Formation domes cannot be considered as mid–upper, intertidal or supratidal due to the absence of signs of desiccation. Therefore, lower–intertidal to shallow subtidal environments are the plausible for formation of domal stromatolites.

#### 5.2.1.7 Conclusions

Based on the previous discussion, it can be concluded that the MLL represents a relatively hypersaline subtidal environment and an isolated water body, relatively less liable for precipitation of evaporites. The current action and sediment supply may increase upward when the domal stromatolites begin to appear.

These results suggest that the clotted fabrics represent the most widespread microbial community in the MLL, which can create a microenvironment conducive to carbonate precipitation (Chafetz, 1986; Kennard & James, 1986; Riding and Sharma, 1998; Turner, 2000). Hoffman (1974), Warren and Kendal (1985), and Warren (1991) have assumed that most MLL and domal stromatolites are confined to, or otherwise formed under, subtidal environments. They usually form in relatively saline and protected environments where the current action is weak. Fauna are absent so grazing activity is minimal. Emergent desiccation features, which provide evidence of subaerial exposure such as mud cracks, tepee structures, are completely absent in the MLL. Therefore, subtidal rather than inter–supra tidal environments are indicated.

### 5.3 Blister–flat laminated lithofacies (BFL)

#### Field description

Blistered–flat laminite limestone lithofacies (BFL) is underlain and overlain by MLL and thick-bedded dolomite–limestone lithofacies (TBLL) respectively. This lithofacies can be easily distinguished in the field due to its blistered structures. Furthermore, in terms of bedding thickness and colour, BFL exhibits a remarkable contrast with the underlying and overlying lithofacies, where the BFL appears grey medium-bedded as compared with thin-to medium-bedded MLL and buff thick-bedded TBLL respectively (Figures 5.3, B–E and 5.9, A).

The BFL usually displays thinly laminated with couplets of calcite and dolomite. The calcite laminae are grey and recessive up to 3 mm thick, whereas dolomite laminae are buff and standing out up to 1 mm thick (Figures 5.9 B–C and 5.10, A–B). This lithofacies is rich with fractured flat–clasts derived from underlying or adjacent rocks (Figure 5.10,

C–D), they often show identical lithology to the BFLL, and are about 1–3 cm in size. Scattered small chert grains 1–3 mm in diameter are frequently observed (Figure 5.9, D).

The BFLL can be subdivided on the basis of lamination structures into blistered and flat laminae (Figure 5.9, B). The former displays wrinkle to irregular structures of small-scale dome-shaped laminations and (Figure 5.10, A). The blistered laminae are laterally linked hemisphere (LLH), which are closely spaced; therefore, based on the classification of Logan et al. (1964) can be symbolized as (C–LLH). Furthermore, the blistered laminae are distinguished by the existence of disrupted and scoured surfaces (Figure 5.10, A), laminoid-fenestral fabrics (Figure 5.9, C), and chert nodules (Figure 5.9, D). By contrast, the flat laminae display straight laminations, and they lack laminoid-fenestral fabric pockets and small chert nodules (Figure 5.9, B).

The laminoid interlayered fenestrae in the blistered laminae are relatively large 1–4 cm across and up to 2 cm thick, and they make up 6–9 % of the bulk of the lithofacies (Figures 5.9, C and 5.10, B). The fenestrae are lenticular to hemispheroidal in shape, normally with flat floor and convex roof. They lie parallel or subparallel to lamination, and are partially or completely infilled by calcite cement and kerogen (Figures 5.9, C and 5.10 B and E). The bedding–plane surfaces that directly overlie fenestrae, exhibit rounded to ovate pustule textures (Figure 5.10, E).

The coexistence of blistered and flat lamination in the same rock unit is very prevalent, and they often alternate with each other, and mostly the sequence begins with blistered laminae, then followed by flat one (Figures 5.9, B and 5.10, A–B). At some sections, the repetition between blistered and flat laminae occurs two or three times, and the sequence is often capped with flat–laminated textures (Figure 5.9, B).

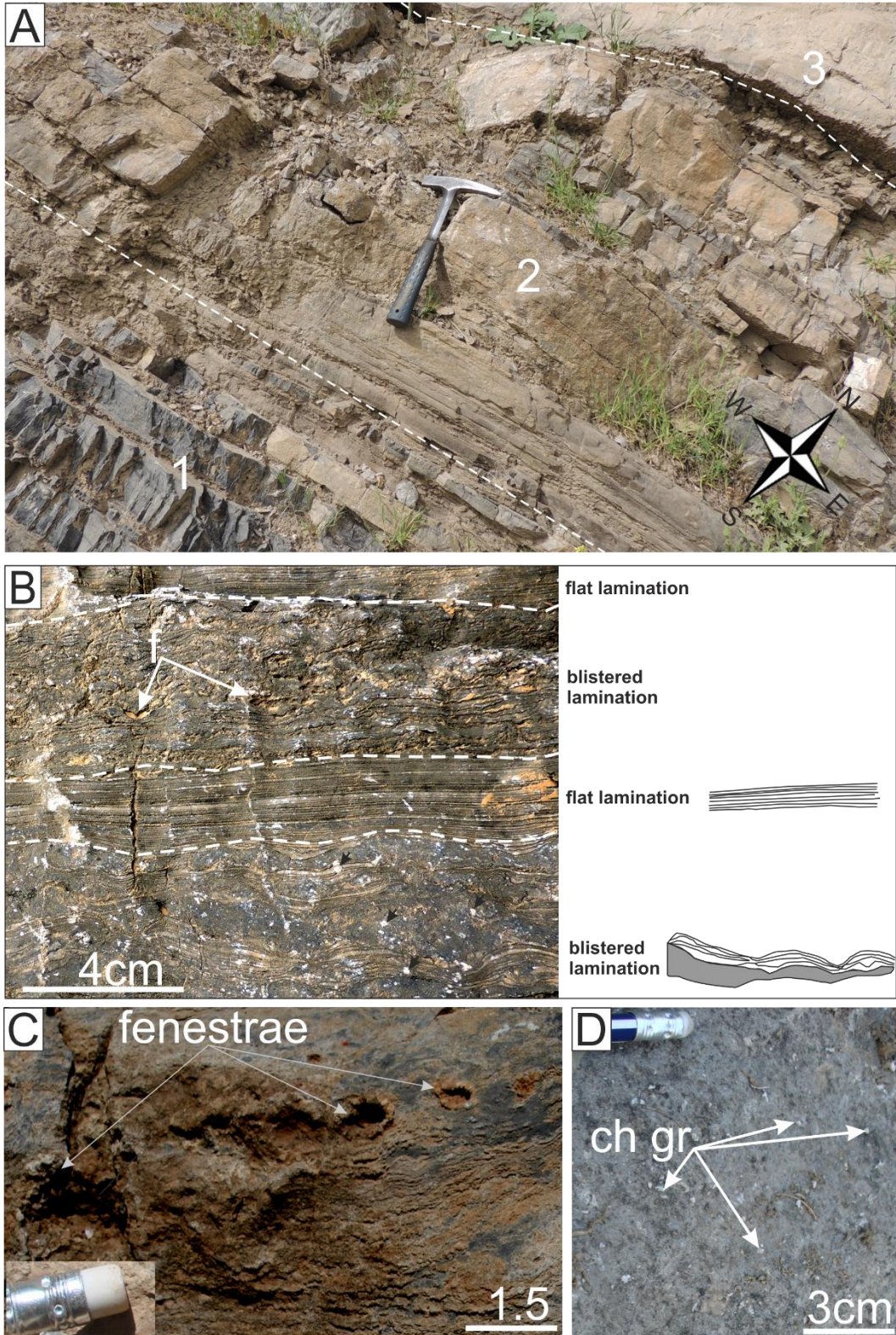


Figure 5.9: A; the Barsarin Formation exposure showing blistered-flat lamination lithofacies (2) is underlain by microbial laminite lithofacies (1), and overlain by thick-bedded dolomite lithofacies (3) respectively. Note the colour contrast between different lithofacies, and the white dashed lines showing sharp boundary between them, Gara location. B; alternating between blistered and flat laminae, lamination always begins with blistered then followed by flat laminae. Note the dominance of fenestrae (f) in the blistered laminae, white spots representing chert grains (black arrows), Barsarin location. C; fenestrae showing partially infilling by calcite cement in blistered fabrics. D; chert grain (ch gr) standing out due to differential weathering. Both C and D are from Nora location.

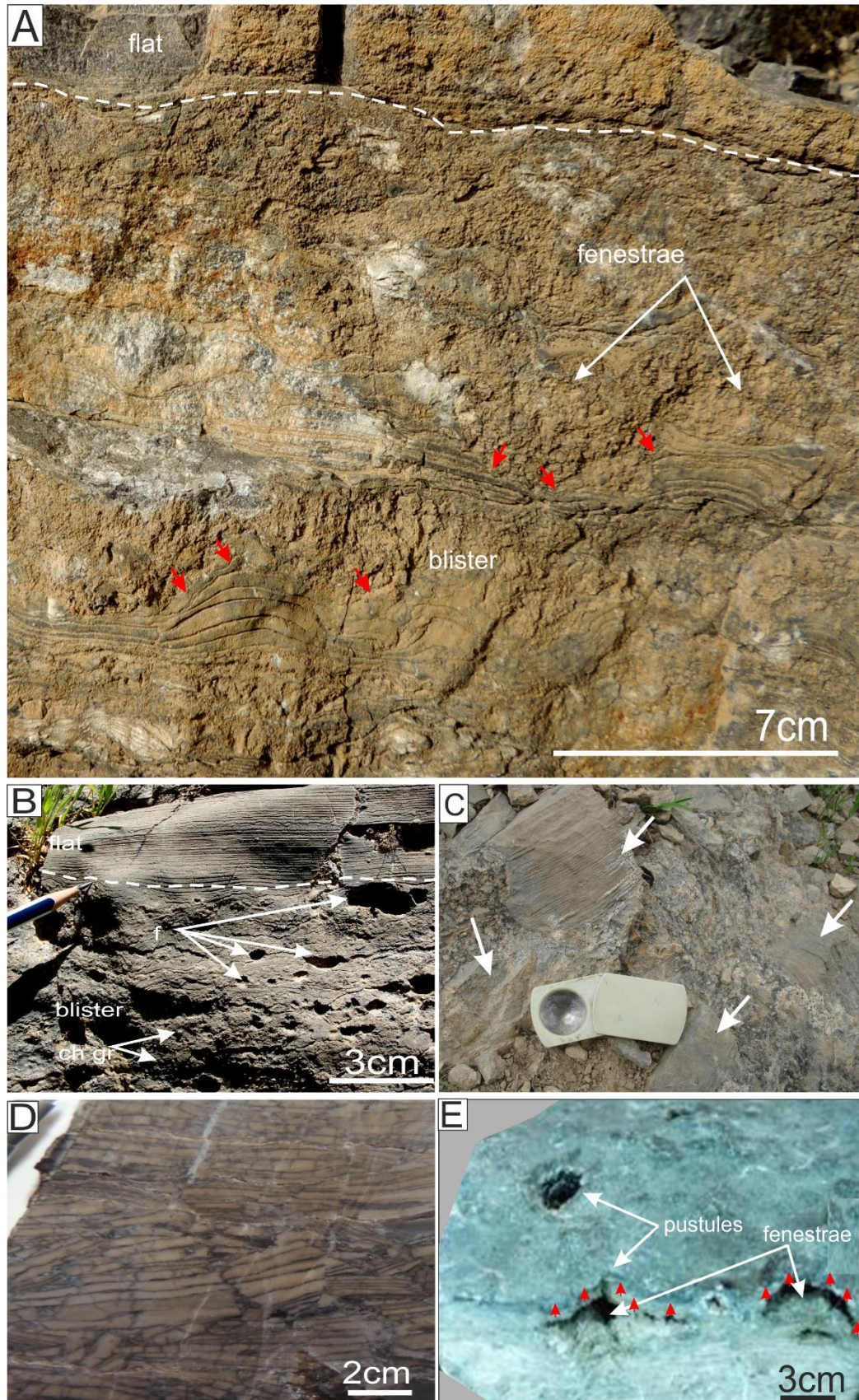


Figure 5.10: A; blistered- flat lamination lithofacies, the sequence normally commences with blistered then followed by flat laminae. The boundary between blistered and flat laminae is determined by white dashed line. The red arrows pointing to the scoured surfaces, note completely filled fenestra, Banik location. B; blistered-flat laminae with common fenestrae, Nora location. C; intraformational clasts showing identical lithology to flat laminated structures, Gara location. D; Polished blistered-flat laminated lithofacies slab showing fractures and intraformational clasts, Barsarin location. E; large fenestrae, note the pustules on the surface of sample, and pushed up laminae (red arrows), Barsarin location.

### Microscopic description

The BFLl usually displays sinuous and distinct lamination with couplets of dolomite and calcite spars (Figures 5.11, A and 5.12, A). In some cases, instead of the dolomite laminae, a fine-grained, dark laminated calcite occurs, which is rich in microbial filaments (Figures 5.11, C and 5.13, A–C), so at the absence of the dolomite laminae the couplets will comprise of coarse-light and dark–fine calcite spar laminae.

**The calcite spar laminae**, which are often rich in gypsum pseudomorphs (Figure 5.12 C–F), range from 0.2–3 mm in thickness. Calcite crystal sizes are coarser in the light laminae in comparison with the darker one, with individual crystals ranging from 0.02 to 0.05 mm diameter, (Figure 5.11, C). Moreover, the considerable amount of radial stellate masses have been observed in the calcite spar laminae, 0.03–0.05 mm in size (Figure 5.12, G).

The majority of spar crystals are cloudy and inclusion-rich which may correspond to relics of micrite, and the spars have curved boundaries as well (Figure 5.11, B). Based on Bathurst (1975) and Flügel (2010) criteria for neomorphism, the calcite spars in BFLl could be interpreted as a neomorphosed micrite, the major features that emphasising neomorphism origin are abbreviated in the following points:

- i. Often unclear and unclean appearance, with curved and engulfed crystal boundaries.
- ii. Contacts between calcite spars are not sharp.
- iii. Absence of different generations of spars.
- iv. A joining point of three intercrystalline boundaries “triple junctions” with all angles are  $< 180^\circ$ .
- v. Do not show increasing crystal size away from a grain surface.

**The dolomite-rich laminae** are thinner and darker in colour, and are up to 0.5 mm thick (Figure 5.12, A). Dolomite crystals are subhedral in shape, 0.1–0.5 mm across, and they have cloudy centers and clear rims. (Figure 5.12, B). The dolomite rhombs may show fitted pressure dissolution, where the pressure solution surfaces are superimposed on dolomite laminae, dark laminae are affected by sutured seam stylolite dissolution, to the degree of complete dissolution in places (Figure 5.11, A).

Elongate and tube-shaped microbial filaments are observed in some non-dolomitized dark laminae that show parallel rows of small calcite spar, up to 1 mm in length and about 70  $\mu\text{m}$  thick, often associated with evaporite pseudomorphs (Figure 5.13, A–C).

Authigenic silica comprising length–slow chalcedony, megaquartz, and microcrystalline quartz up to 3 mm has been encountered (Figures 5.12, C–D, 5.14, A–C). Some dolomite rhombs are engulfed by length–slow chalcedony or single megaquartz crystals, resulting in the poikilotopic textures (Figure 5.14, A).

The evaporite pseudomorphs in the BFL are filled either by dolomite (Figure 5.14, E), calcite (Figure 5.14, B, and D) or silica minerals (Figures 5.14, A–D). Furthermore, some micritic lensoidal shapes have been observed, implying probable existence of evaporite pseudomorphs (Figures 5.14, C). Mostly, the pseudomorphs are 1–2 mm in length, and normally associated with chert grains and flat clasts. Fractured flat clasts are observed up to 2 cm in length and 5 mm thick, and they often lie parallel to beddings.

The cavities of fenestrae are partially or completely infilled by coarse equant calcite cement of two or three generations. The cements often show clear and straight crystal boundaries with increasing crystal size away from the cavity wall surface. Various generations of cements can be distinguished either by a stage of kerogenous films that separate different generations or by the presence of distinctive micro–unconformity on corroded crystal surfaces (Figure 5.14, F). The first generations of calcite cement are cloudy subhedral few hundred microns in size, they often followed by kerogenous layers. The second generation of calcite cement crystals is clear, subhedral to anhedral, up to 1 mm in size, also followed by second kerogenous layers, and then the third–generation starts.

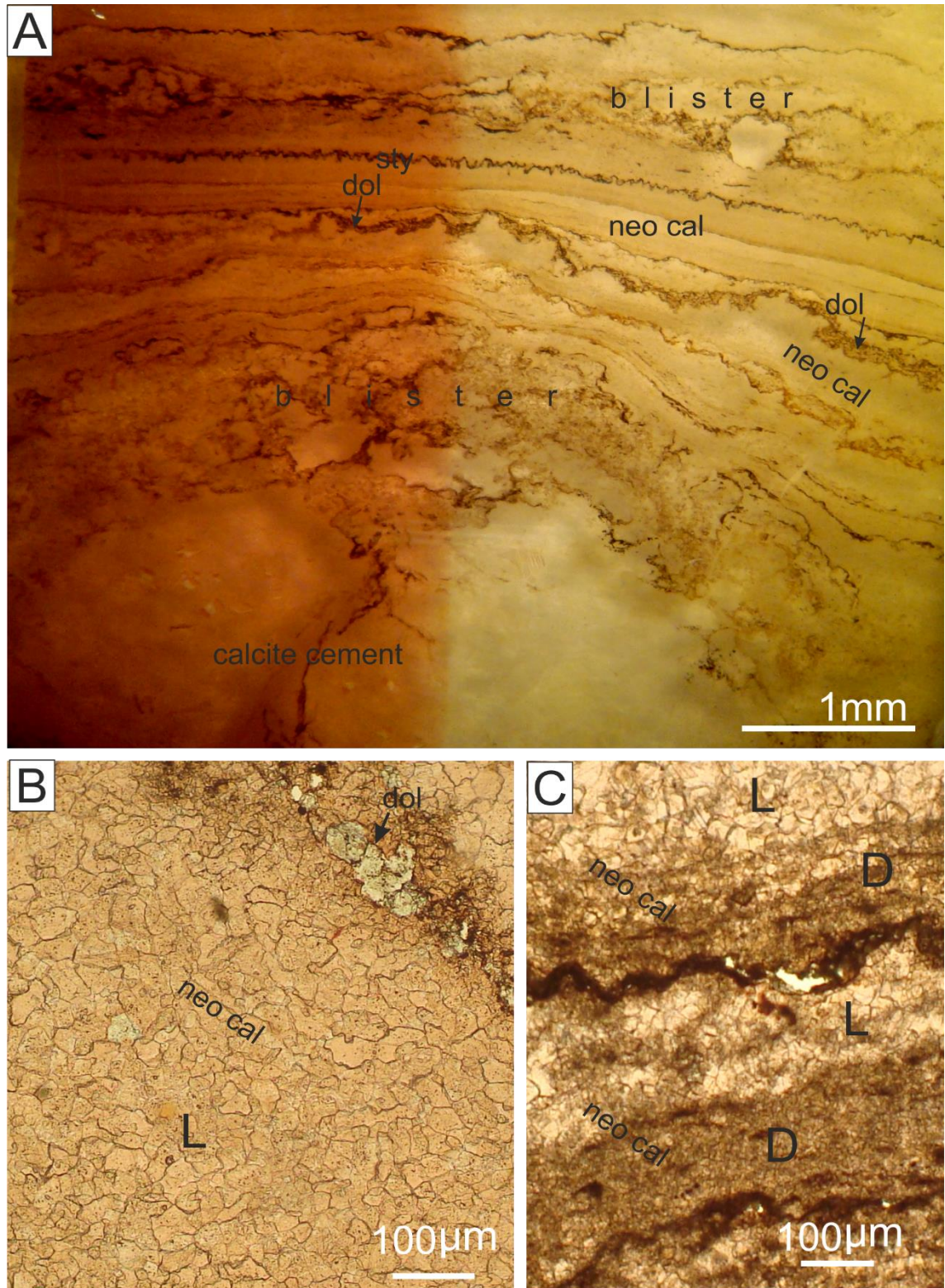


Figure 5.11: A; blister-flat laminated lithofacies, as illustrated in reflected-light, showing large fenestrae at the base that infilled by calcite cement. The blistered laminae showing couplets of dolomite (dol) and calcite spar laminae (neo cal). Note the darker laminae are thinner and susceptible to stylolitization. B; neomorphosed calcite in the light laminae (L), note irregular boundaries of calcite crystals. C; alternation between dark (D) and light (L) laminae. The calcite crystal sizes are coarser in the light laminae in comparison with the darker one. all photomicrographs are from Barsarin location.

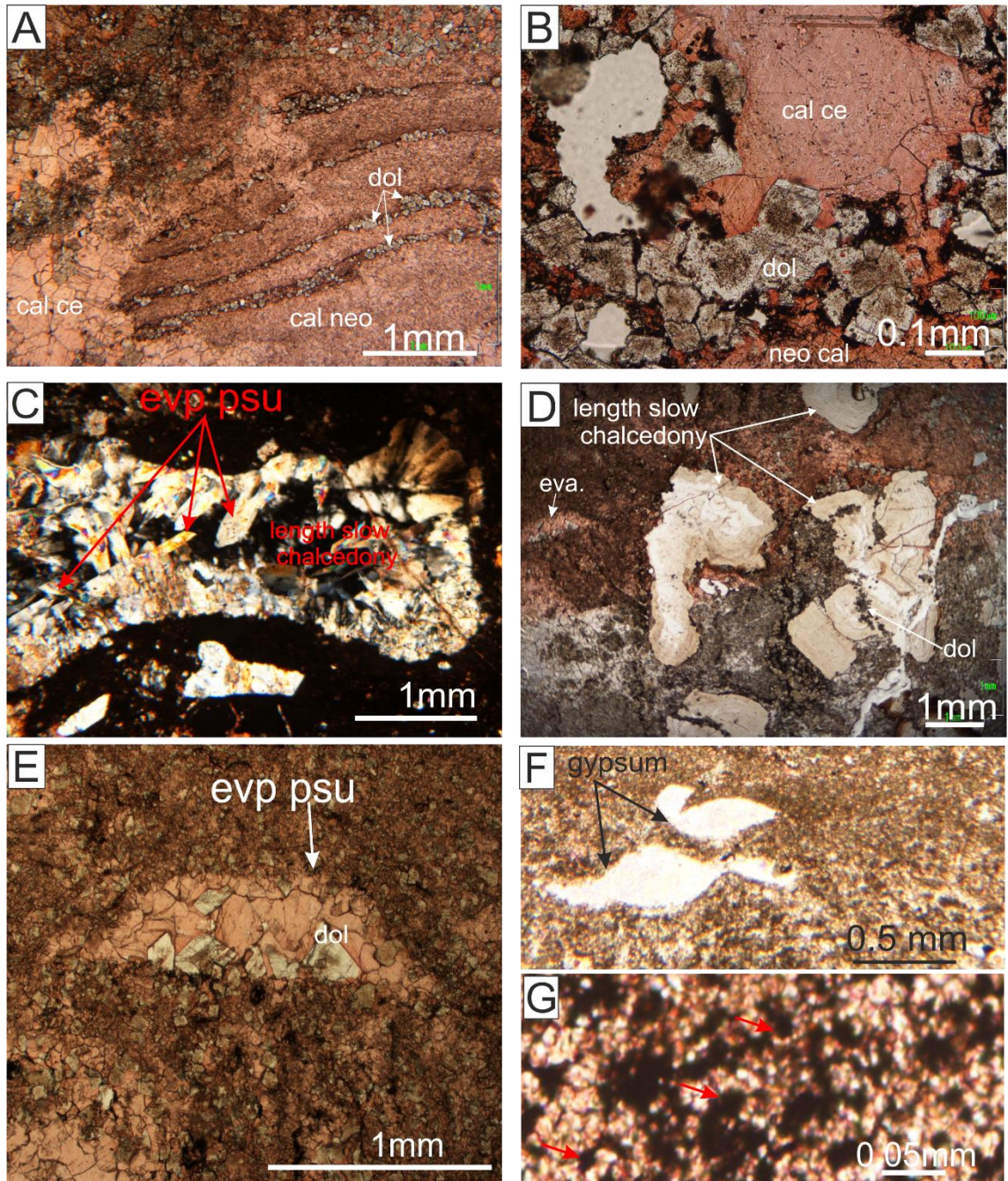


Figure 5.12: A; distinct lamination of dolomite (dol) and neomorphosed calcite (neo cal) couplets, note large fenestrae at left of photo B; dolomite crystals (dol) showing cloudy centre and clear rim. C; length-slow chalcedony including relicts of evaporite pseudomorphs (eva psu). D; photomicrograph showing poikilotopic length-slow chalcedony with dolomite crystals associated with evaporite (eva.) .E; evaporite pseudomorph is infilled by dolomite and calcite cements , note the dolomite crystals usually lining the wall of pore. F; calcite pseudomorphs of gypsum. G; radial stellate masses in the neomorphosed laminae (red arrows). All photomicrographs are from Barsarin location.

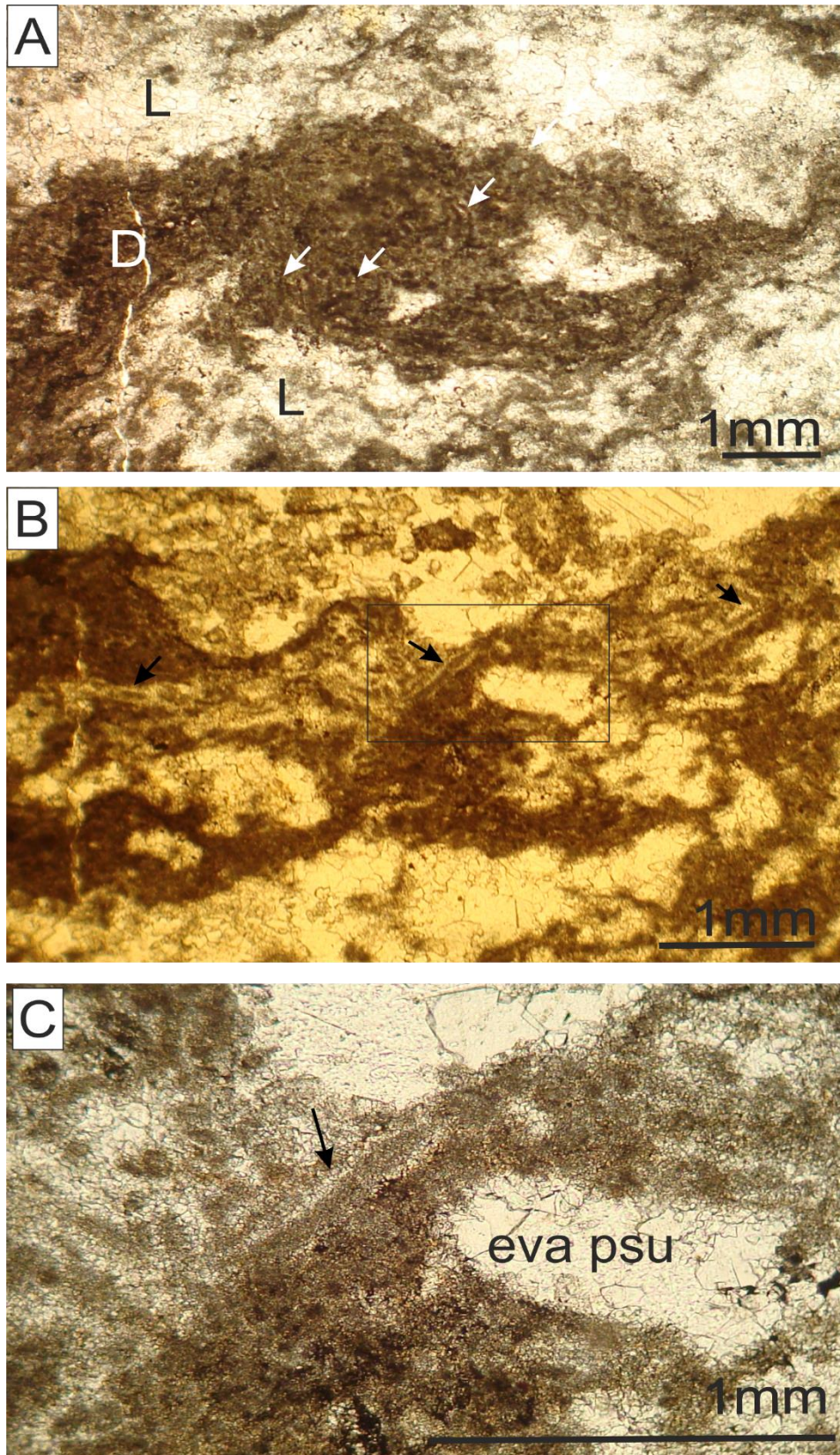


Figure 5.13: A; Clusters and arrays of cyanobacterial filaments (white arrows) in the darker laminae (D) surrounded by lighter laminae (L) with many signs of evaporite pseudomorphs (red arrows) B; Photomicrograph showing filaments in the dark micritic laminae (black arrows). C; detailed of black square showing evaporite pseudomorph (eva psu), and microbial filaments, note the filament wall consists of small calcite spar (black arrow). All photomicrographs are from Chnaran location.

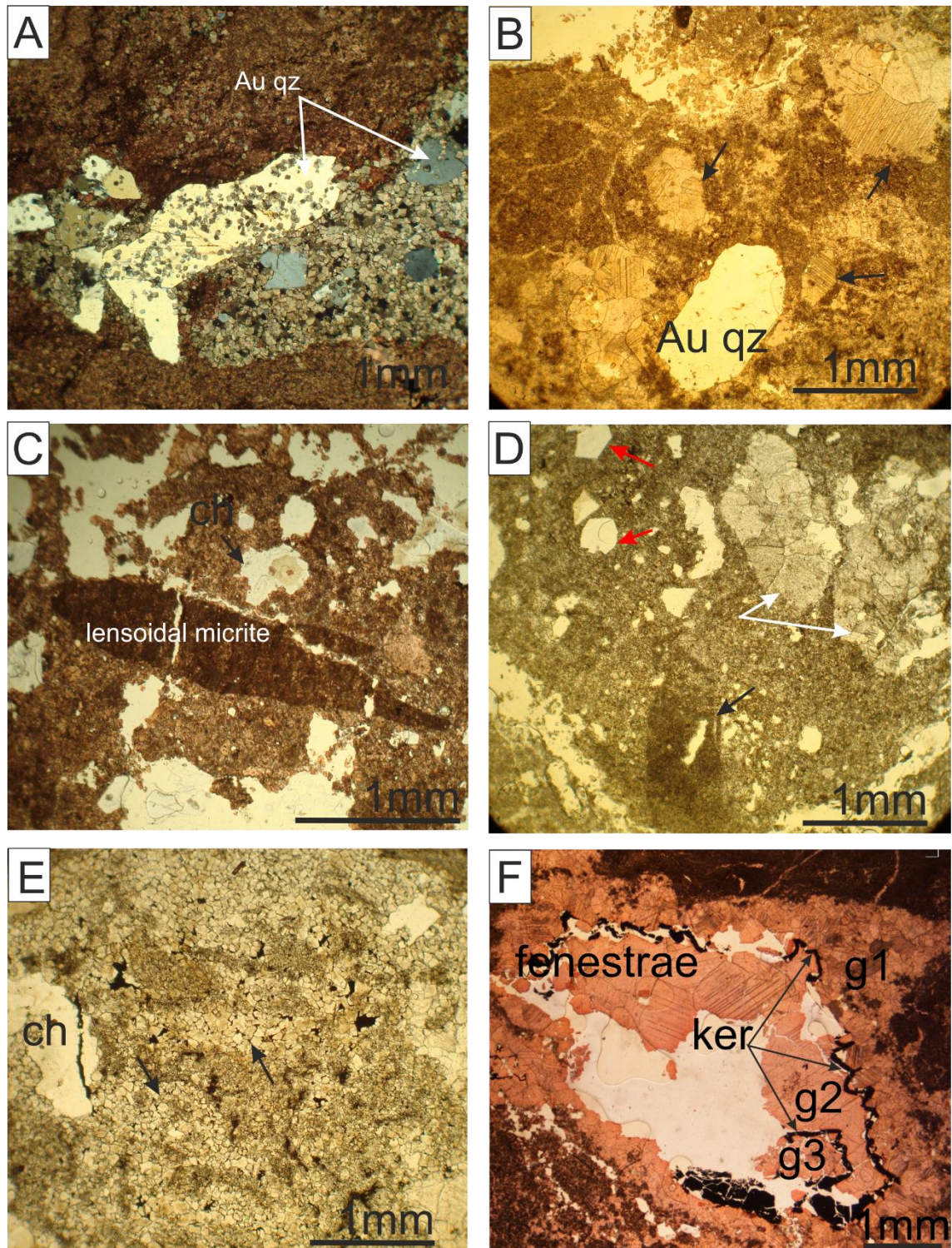


Figure 5.14: A; dolomite rhombs within (Au qz) crystals forming poikilotopic texture. B; calcite cement pseudomorphs of gypsum (black arrows) and authigenic quartz (Au qz) C; Lensoidal and rhomb-shaped micrite pseudomorphs of evaporite associated with length-slow chalcedony (ch). D; photomicrograph showing two kinds of evaporite pseudomorphs; white arrows pointing to the calcite cement pseudomorphs of gypsum, while the black arrow is pointing to the lath-like micrite pseudomorphs of evaporite, they associated with authigenic quartz (red arrows). E; dolomite rhombs infilling in the lath shape pseudomorphs of gypsum also associated with chert grains (ch). F; partially infilled fenestrae calcite cement by three generations g1, g2, and g3 respectively. Various generations of cement can be distinguished by kerogenous films (ker). All photomicrographs are from Barsarin location.

### 5.3.1 Interpretation

The BFL is characterized by structures of blistered–flat lamination and thinly laminated couplets of calcite and dolomite. This lithofacies includes large elongations to hemispheroidal interlayered fenestrae, scattered small chert grains, gypsum moulds or their pseudomorphs, and flat clasts. In addition, there is considerable evidence of microbial mat existence, supporting their role in the blistered structure formation. The combination of field description with microfacies analysis indicates that the BFL formed in intertidal environments; this interpretation will be discussed in more detail in the next sections.

#### 5.3.1.1 Blistered–flat fabrics related to microbial mats

1–Blistered laminae: extensive evidence for microbial presence or their activities in the blistered laminae have been recorded, such as well-preserved microbial filaments (Fig 5.13, A–C), blistered textures, dolomite laminae related to microbial mats (Fig 5.12, A), and gas trapped pockets under microbial mats (Figures 5.9, C and 5.10, B and E); as will be discussed in detail in the next sections.

The blistered fabrics in BFL (Figures 5.9, B and 5.10, A) are very comparable to modern convoluted microbial mats that are described by various authors (Illing et al., 1965; Kendall and Skipwith, 1968; Kinsman and Park, 1976; Kendall et al, 2002; Bouougri and Porada, 2010) on the Trucial coast of the Arabian Gulf, and by Gunatilaka, (1975), on Northern Ceylon Island. The ancient blistered stromatolites and their relationship to the microbialites are described by Leeder, (1975) and Dill et al. (2005) from the Northumberland basin and the Miocene Dam Formation in Qatar respectively.

Recent analogues emphasized that blister structures may form by gas generation below the microbial mat in the intertidal zone. Released gases are often trapped in pockets under microbial films made “leathery” due to considerable exposure and desiccation (Gunatilaka, 1975, Kendall and Skipwith, 1968; Noffke et al., 2001; Salae, 2002; Dill et al 2005; Haas 2004; Bosak 2009; Cuadrado et al 2013; Cuadrado et al, 2014).

2–flat laminae; although petrographic components of the flat laminae are quite similar to the blistered laminae, the flat laminae differ from blistered laminae in a number of important ways: (i) lack of small chert nodules (ii) absence of wrinkled laminae structures, (iii) lack of interlayered laminoid-fenestral fabric pockets, and (iv) lack of scoured surfaces (Figures 5.9, B and 5.10, A). The absence of laminoid-fenestral fabrics in the

flat laminae may be related to the relatively high rigidity of flat lamination, and suggesting early lithification. Depositional sequences in the BFL always commence with blistered and are capped by flat fabrics.

The coexistence of blistered shapes of microbial structures (Figures 5.9, B, and 5.10, A), evaporite minerals or their pseudomorphs (Figure 5.12 C–F), with laminoid fenestrae (5.10, E) may suggest that the rocks were deposited in intertidal environments of a hypersaline sea in arid climates (Illing et al., 1965; Kendall and Skipwith, 1968; Kinsman and Park, 1976). Most interpretations suggest a mid–upper intertidal environment for blister type stromatolites (Kendall and Skipwith, 1968; Noffke et al., 2001; Kendall, 2002; Haas 2004; Dill et al 2005; Allwood, 2006; Bosak 2009; Cuadrado et al 2013). Kendall and Skipwith, (1968) and Kendall et al. (2002) studied a similar type of blister–flat microbial stromatolite from a Holocene tidal flat complex of the Arabian Gulf coast, Abu Dhabi, and they suggested that blistered–flat fabrics developed in upper–intertidal to lower–supratidal environments and are subjected to relatively long periods of exposure, since signs of desiccation have frequently been encountered at the BFL. Desiccation is inferred from the presence evaporites (Figure 5.12 A–F). Rapid alternation between blister and flat textures may reflect the fluctuation of sea-level from lower to upper intertidal zones respectively or could be flooding from storms as in Abu Dhabi. In summary, these results show that the blistered–flat fabrics in BFL of the Barsarin Formation originated from microbial mats. They most probably deposited in mid–upper intertidal environments.

#### 5.3.1.2 Fenestrate (Open Space Structure)

The term *fenestra* or window was introduced for the first time by Tebbut et al. (1965), and they defined the term as “a primary or penecontemporaneous gap in rock framework, larger than grain-supported interstices.” Blistered laminae in the BFL are distinguished by the dominance of laminoid interlayered fenestrae 1–4 cm across, which are partially or completely infilled by calcite cement and kerogen (Figures 5.9, C; 5.10 B and E).

Grover and Read (1978) have classified fenestral fabrics into three main types: (i) laminoid fenestrae: generally appear parallel or subparallel to the lamination, occurring particularly in microbial carbonate by gas trapping; (ii) irregular fenestrae: irregular to equidimensional in shape, several millimetres across, shows little preferred orientation to bedding, formed simply by desiccation; (iii) tubular fenestrae: this kind is created mainly by burrowing organisms or plant roots. Based on the facies associations both second and third types of fenestrae can be excluded as no burrows, no plant roots, and

no irregular fenestrae were observed in the BFLL. The most likely type is laminoid fenestral for the following reasons:

Fenestrae pores are quite common in modern peritidal environments (Bathurst, 1975; Shinn, 1968; 1983, Trucker et al., 2009). They occur in the internal and intrastromatolite mud laminae, and are produced by gas being released through decaying organisms or cyanobacterial activity (Monty, 1976; Gill, 1977; Osborne et al., 1982; Flügel, 2004). This may result in the detachment of superficial microbial mats whereas the trapped air may rise and accumulate under the surface film producing pustule textures when the laminae are soft, so flat floor and convex roofs can strongly imply gas trapped pressure (Figures 5.10, E and 5.11, A). It is easy to observe intimate relationship between pustular and fenestrae in the FBLL, where the laminoid fenestrae are always overlaid by pustules textures in all places. Also, Monty (1976); Bosak et al. (2010) stated that the gas released through microbial activities can lead to perceivable morphological biosignatures.

Gas trapping, laminoid-fenestral and pustule formation with blistered structures, and microbial filaments all together can be considered as crucial evidence for microbial activities (Bosak et al., 2010). Shinn (1968) stressed that the fenestral fabric in modern carbonate settings is most abundant in inter-lower supratidal dolomitic sediments and never present in subtidal ones.

#### 5.3.1.3 Evaporite

Small gypsum crystals or their pseudomorph association can often be seen in the blister-flats in the Barsarin Formation at all locations (Figures 5.12, C–F and Fig 5.14, B–E). Displacement of the host sediments by interstitial growth of evaporite minerals were recorded frequently in the intertidal zone (Choi and Jones, 1988, James 1984; Kendall 1984). Evaporite minerals and their association with desiccation features indicate hypersaline conditions and subaerial exposure. Kinsman and Park (1976) in a study of the microbial belt and coastal sabkha evolution in Trucial Coast of the Arabian Gulf, pointed out that the evaporite mineral formation by capillary water beneath the microbial flat at low tide can lead to the blistered textures formation, where the microbial mat acts as an impermeable membrane which prevents tidal water from flushing the ground water. It is reasonable to assume that interstitial growth of evaporite minerals were not the only factor that may produce blisters because in some areas of study sections the blisters are present where there is no sign of evaporite.

#### 5.3.1.4 Dolomite related to microbial mats (Interlayered Dolomite)

The couplets of dolomite and calcite represent the second most prominent feature after blister fabric. Dolomite minerals in the blistered–flat structures appear as undulated and irregular laminae, which alternate with neomorphosed calcite laminae (Fig 5.12, A).

The interlayering of dolomite and calcite can be considered as an important criterion in distinguishing blistered and flat lithofacies from other lithofacies. It can be easily recognized on the weathered surfaces as well as in thin-sections (Figures 5.9, B, and 5.12, A). Comparable examples from ancient and recent analogs have been reported by various authors (Laporte, 1967; West et al., 1968; Gebelein and Hoffman, 1973; Hoffman, 1974). They interpreted ancient interlaminated dolomite and limestone on the millimetre scales by comparison with recent examples of microbial mats in tidal flats, which were composed of an alternation of microbial mat and particulate carbonate laminae. The microbial laminae would correspond to the dolomite, whereas the layer particulate carbonate laminae correspond to neomorphosed calcite layers. Friedman et al. (1973) in their study on Holocene of the Aqaba Gulf introduced an excellent example of alternating laminae of high Mg–calcite and aragonite. They claimed that a microenvironment can be created by microbial mat in which magnesium becomes rich in the organic matter. Furthermore, Gebelein and Hoffman (1973) emphasized that filament sheaths are very rich in magnesium ions. The organic material in the microbial sheaths will remain stable and does not decompose or release until long after deposition. The released  $Mg^{2+}$  goes on to form dolomite more or less in situ in the microenvironment of microbial mat layer. This type of dolomite was referred to by Chilingar et al., (1979 a&b) as “model stressing solid source of magnesium”. Laboratory experiments carried out by Gebelein and Hoffman (1973) support this hypothesis; they found that the magnesium concentrations in the microbial sheaths are 3 to 4 times higher, relative to sea water media. It was found that enough magnesium can concentrate in the 2 mm thick microbial layer to produce a dolomite lamination 1mm thick.

Recent studies found that the decomposition of microbial sheaths and the release of  $Mg^{2+}$  into the interstitial water are not the main causes behind dolomitized layers, but it seems that the dolomitization occurred in early diagenetic stages mediated by microbial activity (Rao et al., 2003; Van Lith et al., 2003; Vasconcelos et al., 2006 and Sanchez et al., 2009). Modern carbonate deposition analog studies regarding interlayering of dolomite and calcite at Lagoa Vermelha, Brazil, and experimental research concerning bacterial populations with mineral forming processes have been carried out by Van Lith et al. (2003), Vasconcelos et al. (2006), and Sanchez et al. (2009). They determined unique

microenvironmental conditions causing high Mg–calcite and dolomite formation and their interlayering with calcite laminae. They found that the calcite precipitation occurred in the uppermost layers of the microbial mat, where oxygenic photosynthesis and aerobic respiration prevailed, whereas dolomite minerals precipitated in the underlying anoxic layers of the microbial mat, where sulphide oxidation and sulphate reduction prevailed, and producing Mg concentrations.

Moreover, Van Lith et al. (2003) emphasized the vital action of microbes in dolomite formation. They discovered that inorganic changes in the conditions alone cannot prompt dolomite precipitation, but that the cyanobacterial cell wall can act as a nucleus for precipitation and, together with the metabolic activity, can trigger the precipitation of dolomites. Rao et al. (2003) have studied microbial dolomite crust formations from the Late Pleistocene in western India. They suggested that decaying organic sheaths associated with sulphate–reducing cyanobacteria promoted dolomite formation. The microbialites may have provided the nuclei for the origin of dolomites in many ancient carbonate successions (Rao et al., 2003; Van Lith et al. 2003; McKenzie and Vasconcelos, 2009). The microbial–related dolomites are interpreted to have formed under anoxic sulphate–reducing and hypersaline conditions, and dolomitization is considered a biomineral formed in the early stages of diagenesis.

### 5.3.2 Conclusion

Blister and fenestrae structures in the Barsarin Formation have practical applications, environmental significance, and are easily recognizable in the field. They can be considered as additional evidence of intertidal environments (Shinn et al., 1968; Monty, 1976; Grover and Read, 1978; Wright et al., 1990; Bain and Kindler, 1994; Tucker and Wright, 2009). From the previous discussion, and with regard to the methods which lead to dolomitization, it can be concluded that the dolomite laminae in the blistered–flat lamination lithofacies have a close relationship with microbial mat. All the evidence such as blister–flat structures, microbial mats, laminoidal fenestrae, laminated dolomite, evaporite mineral or their pseudomorphs emphasizes that the blister–flat textures originated from microbial mat in the intertidal environments.

## 5.4 Thick-bedded dolomite–limestone lithofacies (TBDLL)

Field description:

Thick-bedded dolomite–limestone lithofacies (TBDLL) is characterized indurated dolomite and/or limestone, light grey in colour, buff on weathering, displaying finely crystalline with intensively fractured textures. The TBDLL generally comprises two major lithologies (1) dolomite and (2) limestone. The TBDLL often begin with dolomitized units followed by limestone or thick laminated dolomite units (Figure 5.15).

Chert nodules and intraclasts make the main constituent of the TBDLL, which can be recognized easily in the outcrop sections. Based on their morphology and size, several different kinds of chert nodule have been observed, and they can be subdivided into three main categories: (i), elongated black chert nodules with lamination, 2–10 cm in length (Figure 5.16, A); (ii) large lensoidal chert nodules, range from 20–40 cm across (Figure 5.16, B); and (iii) small scattered chert nodules, few millimetres across in size (Figure 5.16, C). The study of the outcrop sections shows a higher distribution of chert nodules in the lower part than the upper part in the Barsarin Formation succession, and their amount within the TBDLL decreases gradually upward as well. The chert nodules, which are normally overlain by intraclast breccias, mainly occupy lower part of the TBDLL.

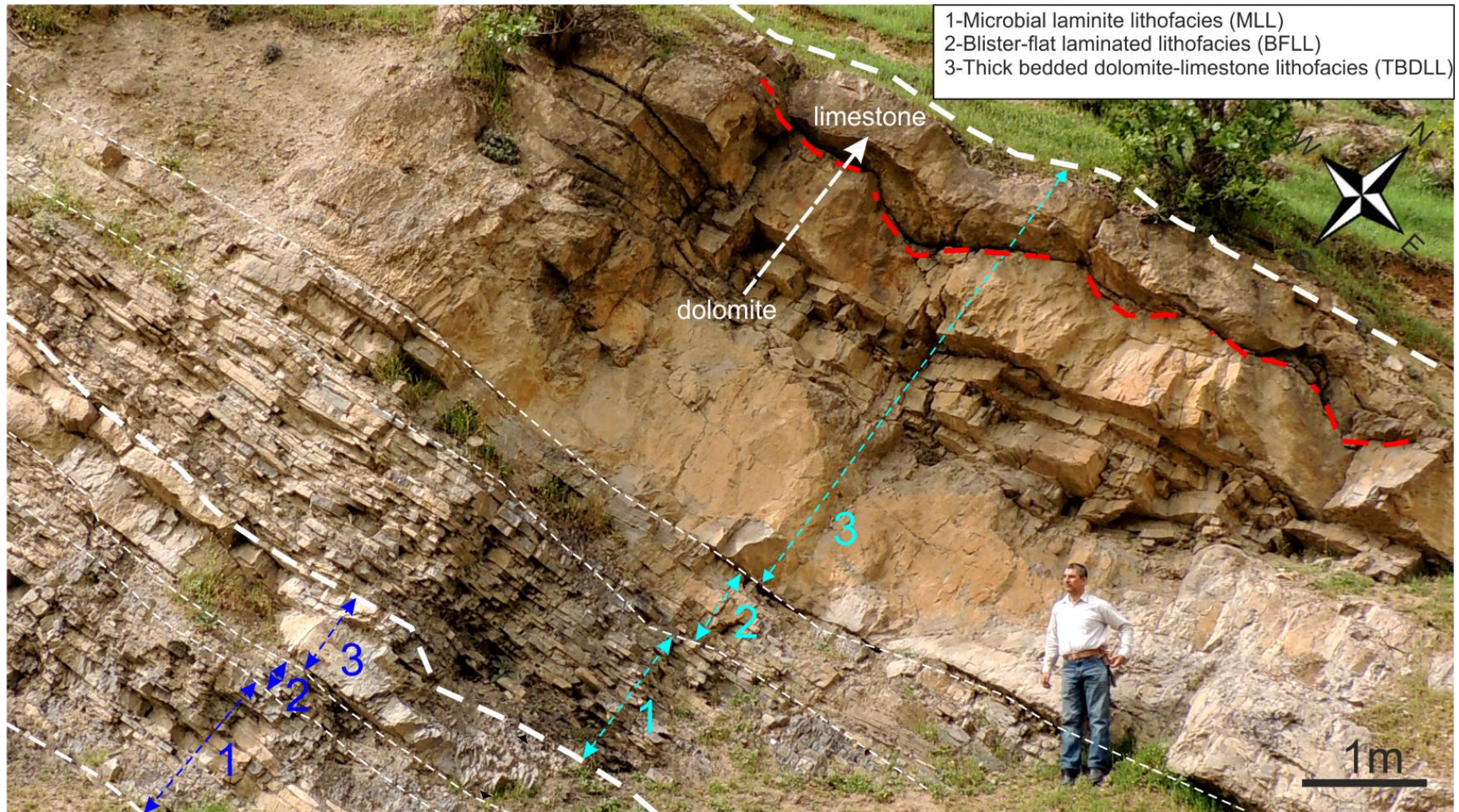
The Intraclasts, which represent a common feature in the TBDLL, consist of polygenetic carbonates: (i) large intraclasts, up to 10 cm in size, show clear preserved internal precursor structures of blistered–flat lamination, from which they have been derived, (Figure 5.16, D), (ii) intraclasts show distinct lamination with couplets of fine-crystalline dolomite and limestone laminae up to 6 cm in size (Figure 5.16, E), and (iii) fine-crystalline dolomite clasts that have similar characteristics of the thick-bedded dolomite–limestone lithofacies up to 5 cm in size. (Figure 5.16, F) The colour contrast between the intraclasts and the matrix is very clear on weathered surfaces as displaying buff and brown colour respectively (Figure 5.16, F). Except intraclasts, the deformed and intensively cracked beds are common, where the bedding can still be followed for tens of centimetres (Figure 5.16, G).

Scoured surfaces, polygonal cracks, and tepee structures are well observed at the top of this lithofacies (Figure 5.17, A–D). Horizons of red to yellow colour, highly porous, and brecciated carbonate-rich soil-like crusts exist on the top of the TBDLL, which often separate thick-bedded dolomite–limestone lithofacies and the MLL (Figure 5.18, A–B).

Kurrek and Sary Amedy areas, specifically the Erbil and Dhuk (Figure 5.1) represent the only two locations in the studied area that have thick units of chicken-wire evaporite deposition up to 2 m thickness (Figure 5.17, E–F).

In all locations, the top of the Barsarin Formation succession is normally occupied by the TBDLL. The bedding nature of the TBDLL shows dramatic changes when approaching to the top of the Barsarin Formation, which displays: (i) noticeable undulation and tilting structures, (ii) disturbed bedding, (iii) lobe-shaped structures (Figure 5.19, A), and (iv) gradual upward increase of black shale intercalation. The top of this lithofacies represents the boundary between the Barsarin and the Chia Gara Formations.

The upper boundary of the Barsarin Formation can be easily identified in the field signified by a gradational lithological change from thick dolomite–limestone lithofacies on the top of the Barsarin Formation to the black shale dominant Chia Gara Formation (Figure 5.19, B). In contrast to the underlying Barsarin Formation, the Chia Gara Formation is uniformly bedded and rich with fossils, especially radiolaria and ammonites (Mohyaldin, 2008). In addition, the lower part of the Chia Gara Formation is marked by large discoidal structures termed “phacoidal” Van Bellen et al. (1959) (Figure 5.19, C). The phacoidal structure can be defined as a large lensoid structure up to a metre across and half metre thick, floating within thick-bedded black shales 10–50 cm thickness.



5.15: Photograph showing stratigraphic section of the lower part of the Barsarin Formation which consists of three different lithofacies (1, 2, and 3). The section normally begins with MLL, and it is followed by the BFLL, while the TBDLL always rests on the top of the succession which displays massive, light buff colour. The boundary between dolomite and limestone lithology in the TBDLL is marked by the existence of tepee structures (red dashed line). Note there are repetitions of different lithofacies in spite of difference of thickness between repeated lithofacies, Barsarin location.

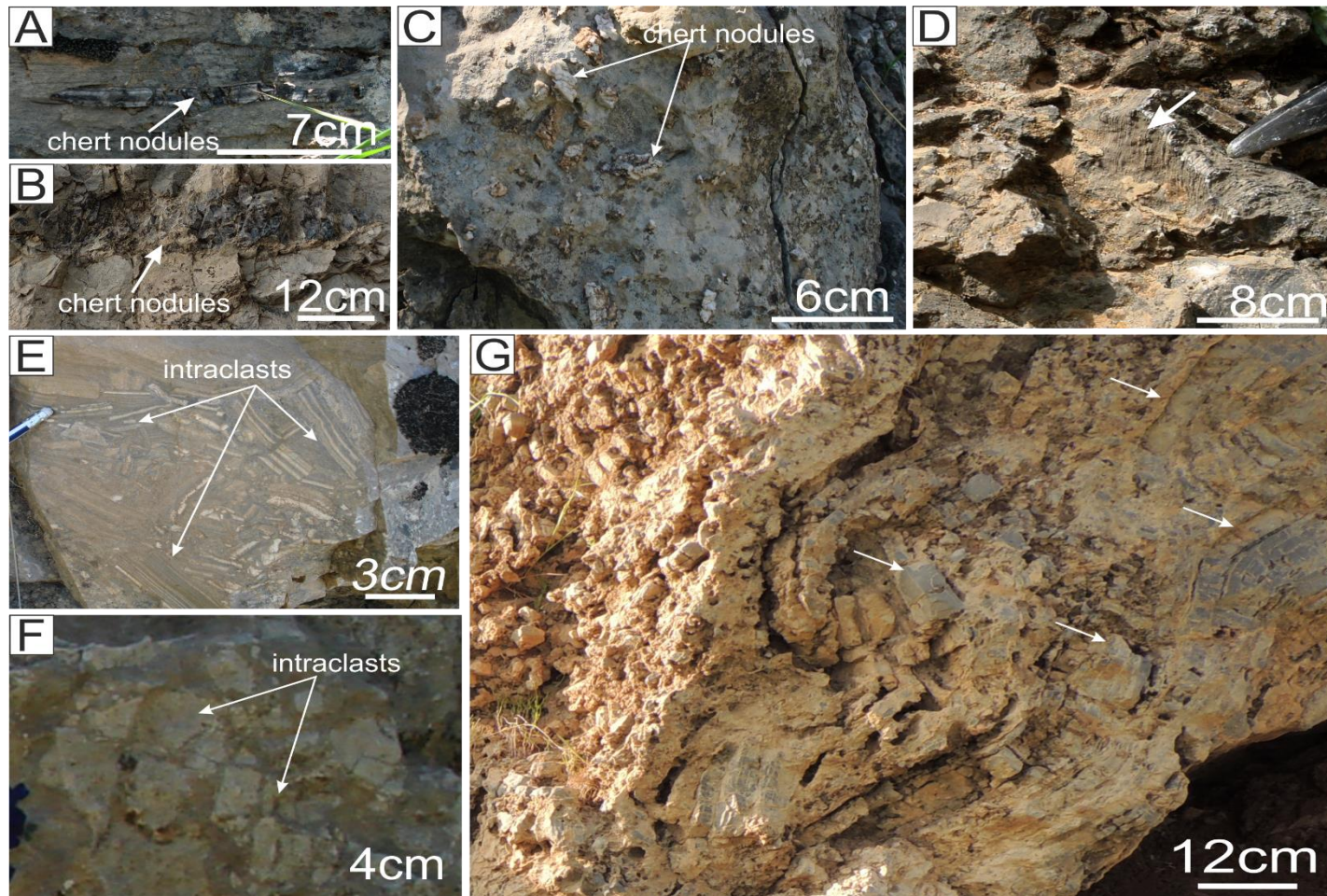


Figure 5.16: A; Black, laminated, and elongated chert nodules, note the preservation of original lamination B; large lensoidal chert nodules C; scattered chert nodules in the massive dolomite lithofacies. D; intraclasts derived from blister-flat lithofacies in the thick-bedded dolomite-limestone lithofacies. E; Intraclasts show distinct intralamination macrofabric with couplets of dark and light colour. F; Structureless dolomitic clasts have similar characteristics of the thick-bedded dolomite limestone lithofacies. G; Deformed and intensely fractured bedding, note precursor bedding still can be followed.

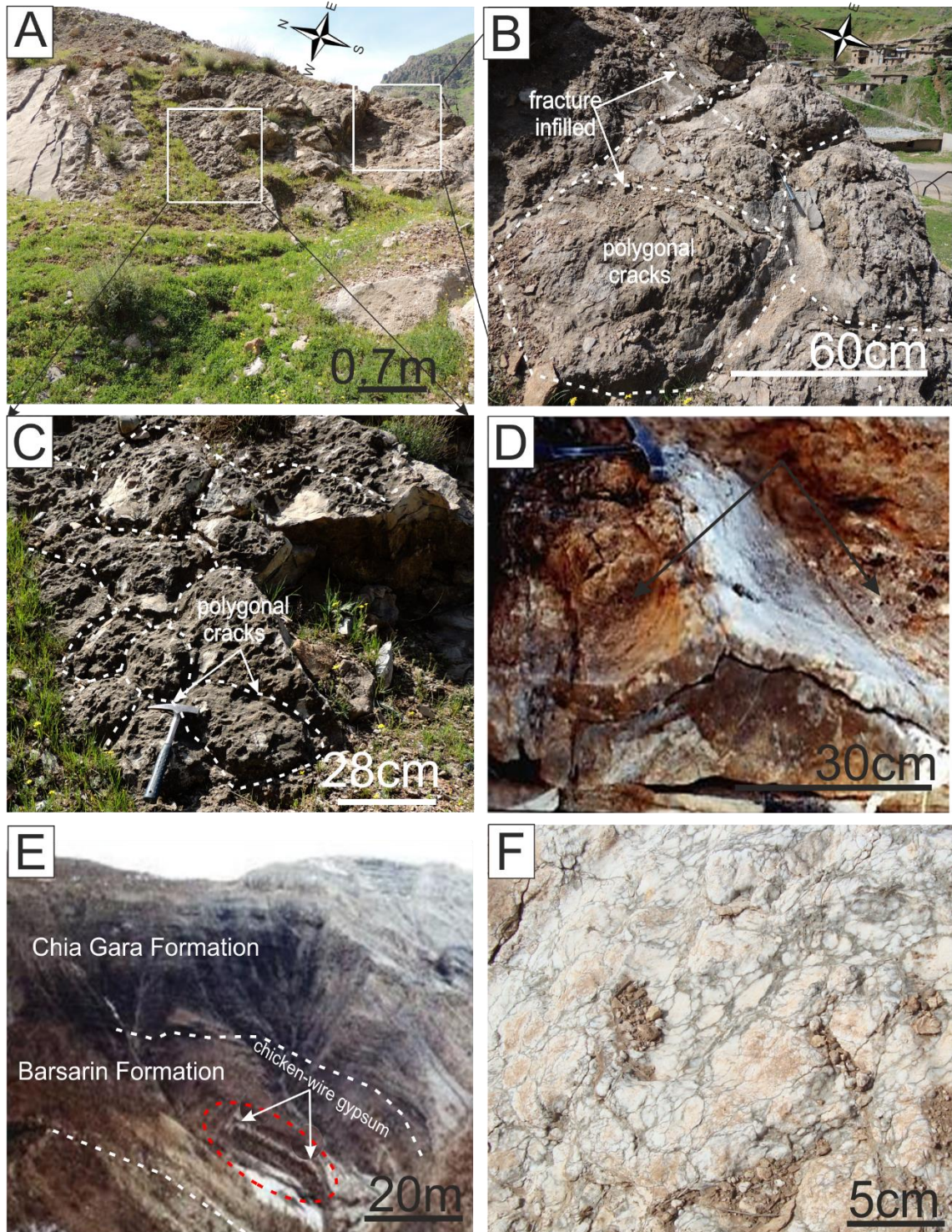


Figure 5.17: A; showing two intervals of polygonal mudcrack at the top of thick-bedded dolomite-limestone lithofacies. B; detail of the white square in the (A) photo showing polygonal fracture networks which are filled with limestone sediments. C; detail of the white square in the (A) photo showing polygonal crack network. D; desiccation feature on the top of the TBDLL displaying tepee and saucer-shaped structures. E; gypsum beds in the TBDLL. F; detail of the red dashed oval in (F) photo showing chicken-wire texture of gypsum. The A-D photographs are from Barsarin location, whereas the E and F photographs are from Karrk location.

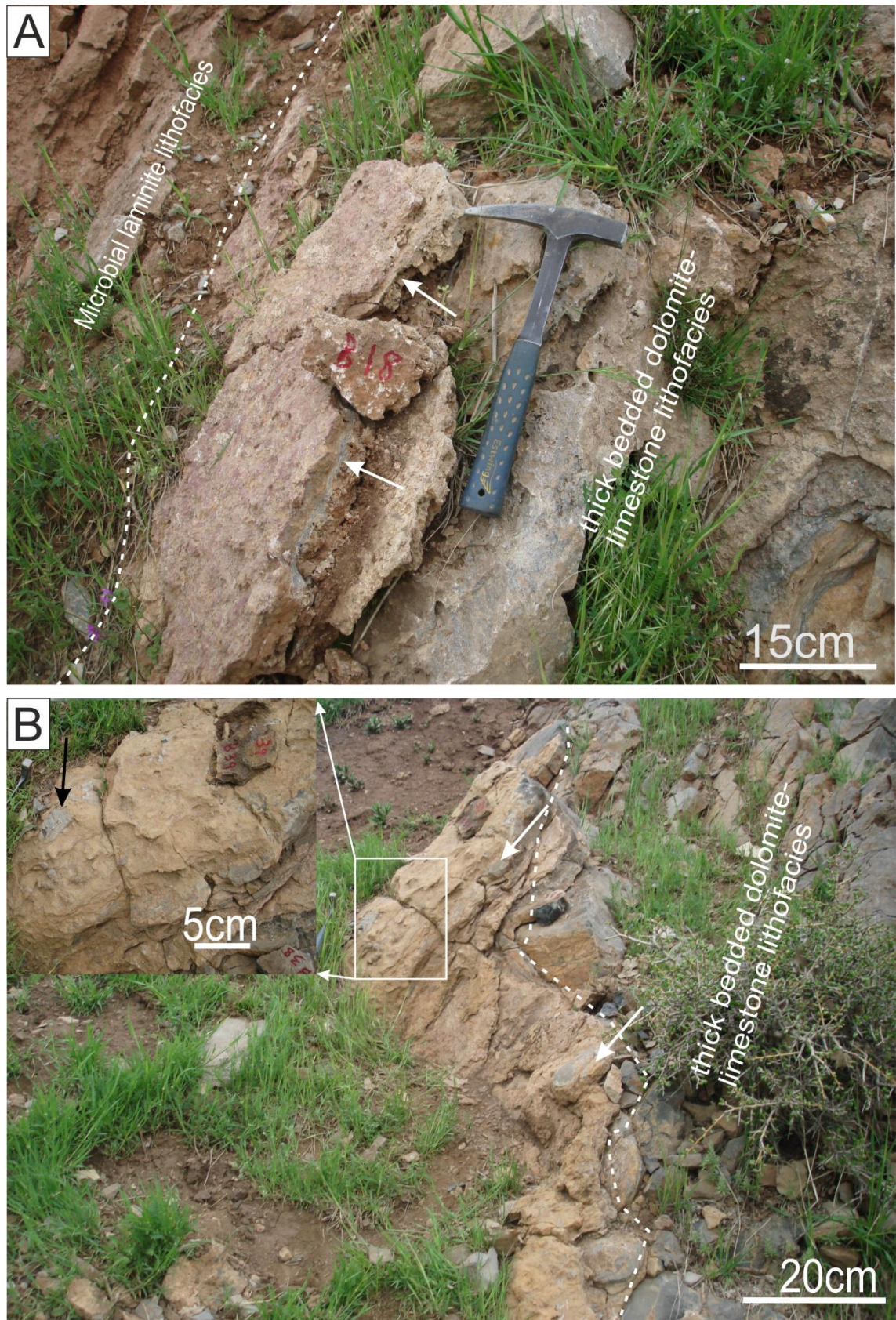


Figure 5.18: A; red coloured highly porous and brecciated carbonate-rich soil-like horizon (white arrows) separating thick-bedded dolomite-limestone lithofacies and microbial laminite lithofacies. B; irregular surface at the top of the TBDLL showing brecciated yellowish. C; detail of the white rectangle in the (B) photo the white arrows a pointing to the breccias. Photographs are from Chnaran location

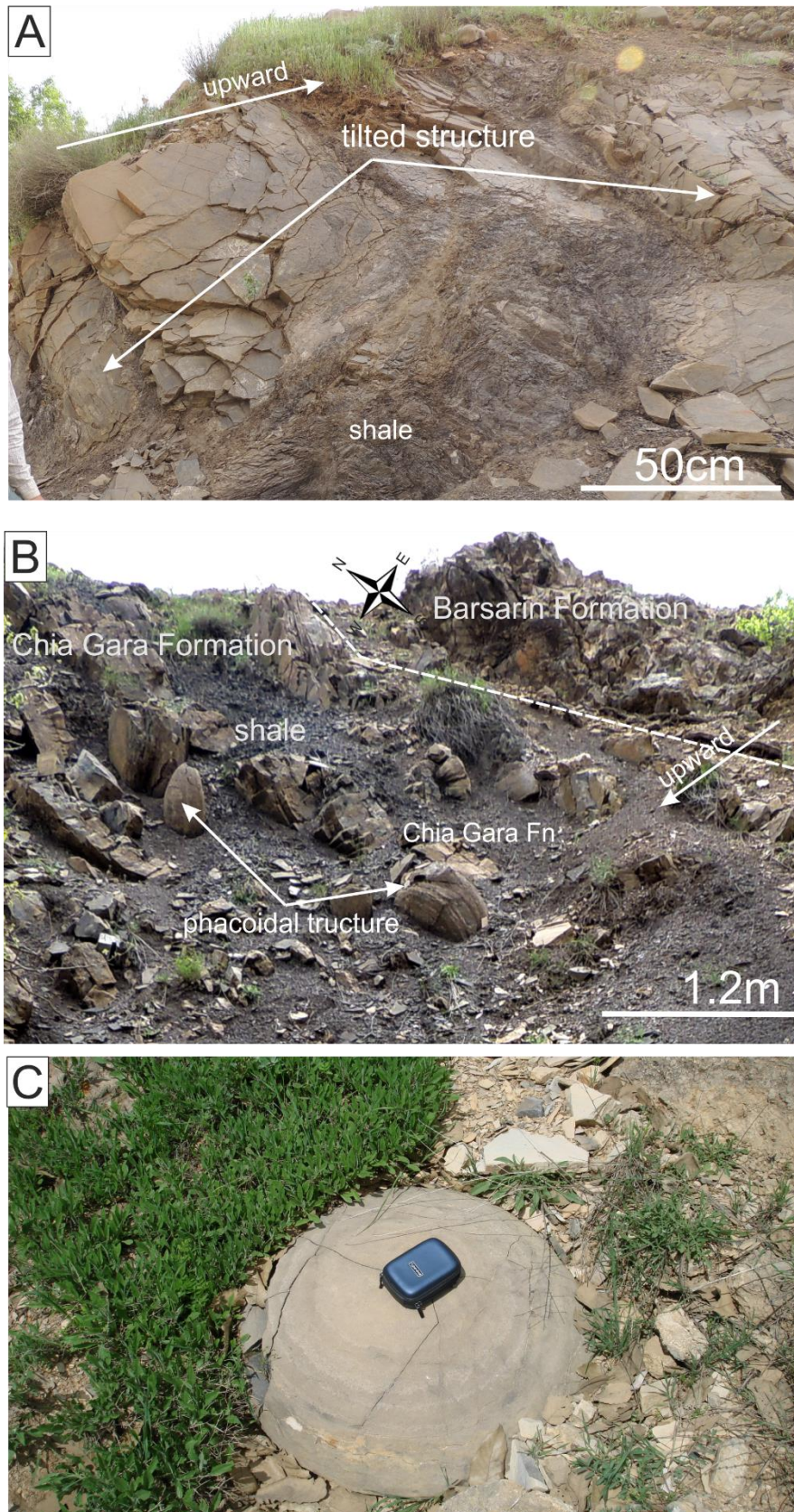


Figure 5.19: A; thick bedding dolomite unit in the top of the Barsarin Formation displays noticeable undulation and tilted structures, Barsarin location. B; the boundary between Barsarin and Chia Gara Formations (white dashed line), showing lithological change from massive dolomite of the Barsarin Formation to the black shale dominance of Chia Gara Formation, which distinguished by possessing large discoidal structures “phacoidal structure”, Gara location. C eroded large discoidal structures of Chia Gara Formation, Gara location.

#### Microscopic description:

Generally, two main textures can be distinguished in the TBDLL: 1–dolomitized mudstone and mudstone with intraclasts, and 2–laminated dolomite with couplets.

1–Dolomitized mudstone and mudstone with intraclasts is predominantly composed of dolomitic intraclasts that possess weak internal lamination of dark–coloured dolomitized mudstone. The intraclasts generally appear as flat-shaped clasts with truncated surfaces (Figure 5.20, A–D), which are often embedded in a mosaic dolospar and/or dolomite (Figure 5.20, A–B).

Millimetre-sized evaporite minerals and their pseudomorphs are widely spread in the TBDLL, and they can be seen within or around the intraclasts. In many cases, the existence of evaporite mineral or their pseudomorphs in the intraclasts may result in fenestrae formation (Figures 5.20, C, E and 5.21, A–B, and I).

Some of the fractured porous and the fenestral structures that related to the evaporite pseudomorphs are filled with compact coarse-crystalline dolomite which exhibit sweeping extinction, up to 0.2 mm in size (Figure 5.21, C–D). On the other hand, the fenestral vugs with short wedge-shaped fractures, 1–2 mm in size, are infilled by calcite cement that includes poikilotopically fine-crystalline dolomite rhombs 0.020–0.025 mm in size (Figure 5.21, F). Authigenic silica (Figure 5.21, D), spherulite, length slow chalcedony and megaquartz have been frequently recorded in thin-section studies (Figure 5.21, E and G). Elongated ghosts of anhydrite laths and silicified dolomite rhombs are observed in some of the large chert nodules (Figure 5.21, H). Some irregular dark peloids with the diameters from 0.15 to 0.200 mm are also observed (Figure 5.21, D).

2–Laminated dolomite with microbialites can be subdivided into two main kinds:

A–Laminated dolomitized mudstone shows distinct lamination with couplets of laminoid fenestral fabric and dolomitized mudstone, which contain microbial clotted microtexture (Figure 5.22, C–F), elongated peloids (Figure 5.22, A–B), and few peloids (Figure 5.22, F). The elongated peloids, up to 1 mm long and 0.1 mm thick, are devoid of internal structure (Figure 5.22, B), and are mainly embedded in the dolomitic calcite microsparite.

The fenestral structures are up to 1.2 mm in length and 0.13 mm thick, and commonly distinguished by a sharp outline reminiscent of evaporite moulds. They are normally filled by clear mosaic dolomite spars and may constitute up to 30% of the rock (Figure 5.22, C–F). The fenestrae cavities in the lower part of the studied sections are filled or lined by dolomite crystals and followed by calcite cement or kerogen (Figure 5.22 C–D); whereas at the upper part, the fenestrae cavities are often occupied by poikilotopic blocky calcite–dolomite spars of 3–4 mm in size (Figure 5.22 D–E).

B–Couplets of fine crystalline dolomite and coarse poikilotopic blocky calcite laminae display distinct lamination and include dolomitized mudstone intraclasts up to few millimetres thick. The poikilotopic block calcite laminae are up to 1 mm in thickness with rhombs of dolomite up to 0.08 mm in size (Figure 5.23, A–B). Dolomite rhombs in the poikilotopic blocky calcite laminae tend to concentrate on the external part of the laminae. Some poikilotopic blocky calcite pseudomorphs of gypsum, which often consist of single-crystal calcite, have been observed in the dolomitized mudstone as well. In places, entire blocky calcite laminae are replaced by the saccharoidal dolomites, and the interstitial pores are infilled by calcite cements or kerogen (Figure 5.23, C).

Sutured seam stylolites are common in this lithofacies: they often run parallel to lamination, and commonly occur between the laminae boundaries. Some fine-grained 0.02–0.07 mm cloudy dolomite rhombs are present, and a few of which are calcite, indicating effective dedolomitization. Some of the stylolites have been distorted by dissolution collapse breccia, and non-sutured seam stylolites are also observed.

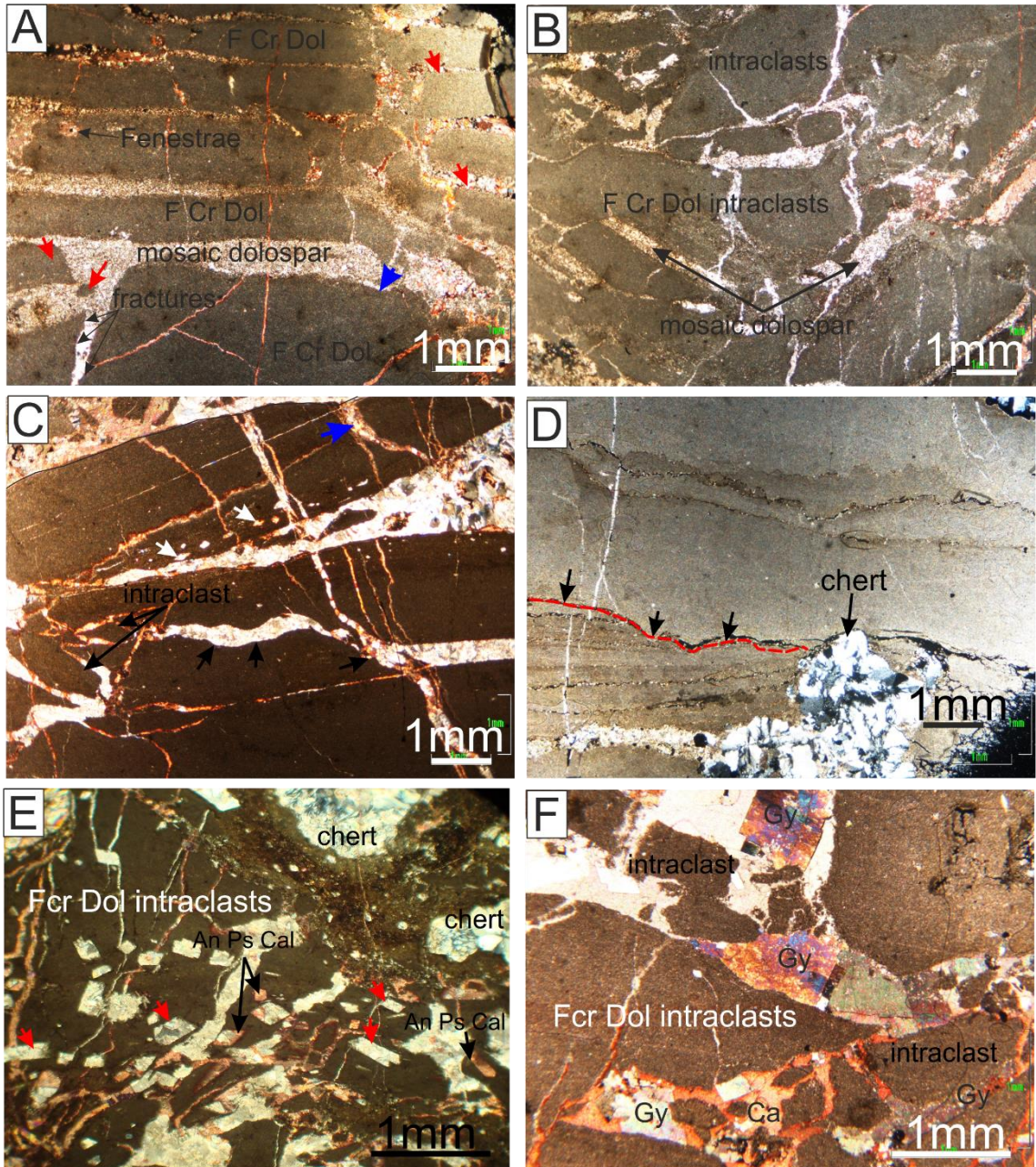


Figure 5.20: A; fine crystalline dolomite (F Cr Dol) showing intraclasts (red arrows), fenestrae structures, truncated, and fractured laminae (blue arrow); note most intraclasts are surrounded by mosaic dolospar. B; fine crystalline dolomite intraclasts and mosaic dolospar (F Cr Dol). C; intraclasts of fine crystalline dolomite showing fenestrae structures related to the calcite pseudomorphs of evaporite (white arrow), fractures (blue arrows), and truncated surface. D; Fine crystalline laminated dolomite displaying truncated surface (dash red line), and chert grains. E; fine crystalline dolomite intraclasts showing association between anhydrite crystal (red arrows), calcite pseudomorphs of evaporite (An Ps Cal) and chert grains; note most of the anhydrite have occurred within dolomite laminae. F; fine crystalline dolomite intraclasts are infilled with coarse crystalline gypsum (Gy) and few calcite cements (Ca). Note the intraclasts float in the calcite and gypsum cements. All Photomicrographs are from Gara location.

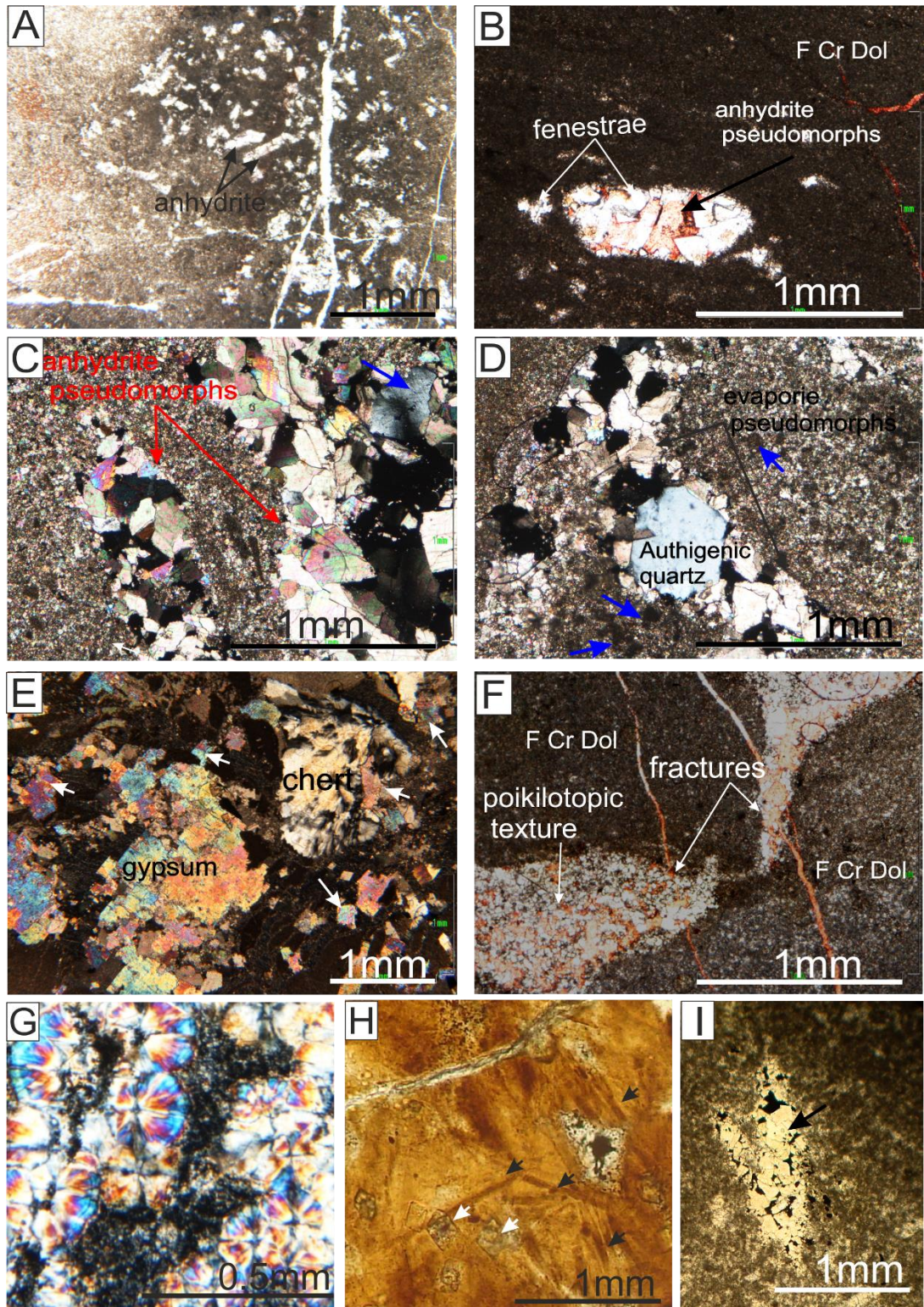


Figure 5.21: A; anhydrite lath shapes in fine crystalline dolomite show fenestral structures. B; fenestral structures are formed by calcite pseudomorphs of evaporite in microcrystalline dolomite, note the vug-filling cement sequences consist of the clear dolomite crystals followed by calcite cement. C; large lathe-shaped anhydrite moulds filled by coarse crystalline dolomite; note sweeping extinction. D; large evaporite pseudomorph moulds are infilled by authigenic quartz and coarse crystalline dolomite, blue arrows pointing to the clotted microtexture. E; gypsum and length slow chalcedony association in the fine crystalline dolomite. F; calcite cement showing poikilotopic textures infilling fractures of fine crystalline dolomite. G; Spherulites showing radially arranged fibres in the thick-bedded dolomite-limestone lithofacies. H; chert nodules, show ghosts of anhydrite laths (black arrows) and silicified dolomite rhombs inclusions (white arrows) I; swallowtail gypsum in the clotted microtexture. All Photomicrographs are from Barsarin location.

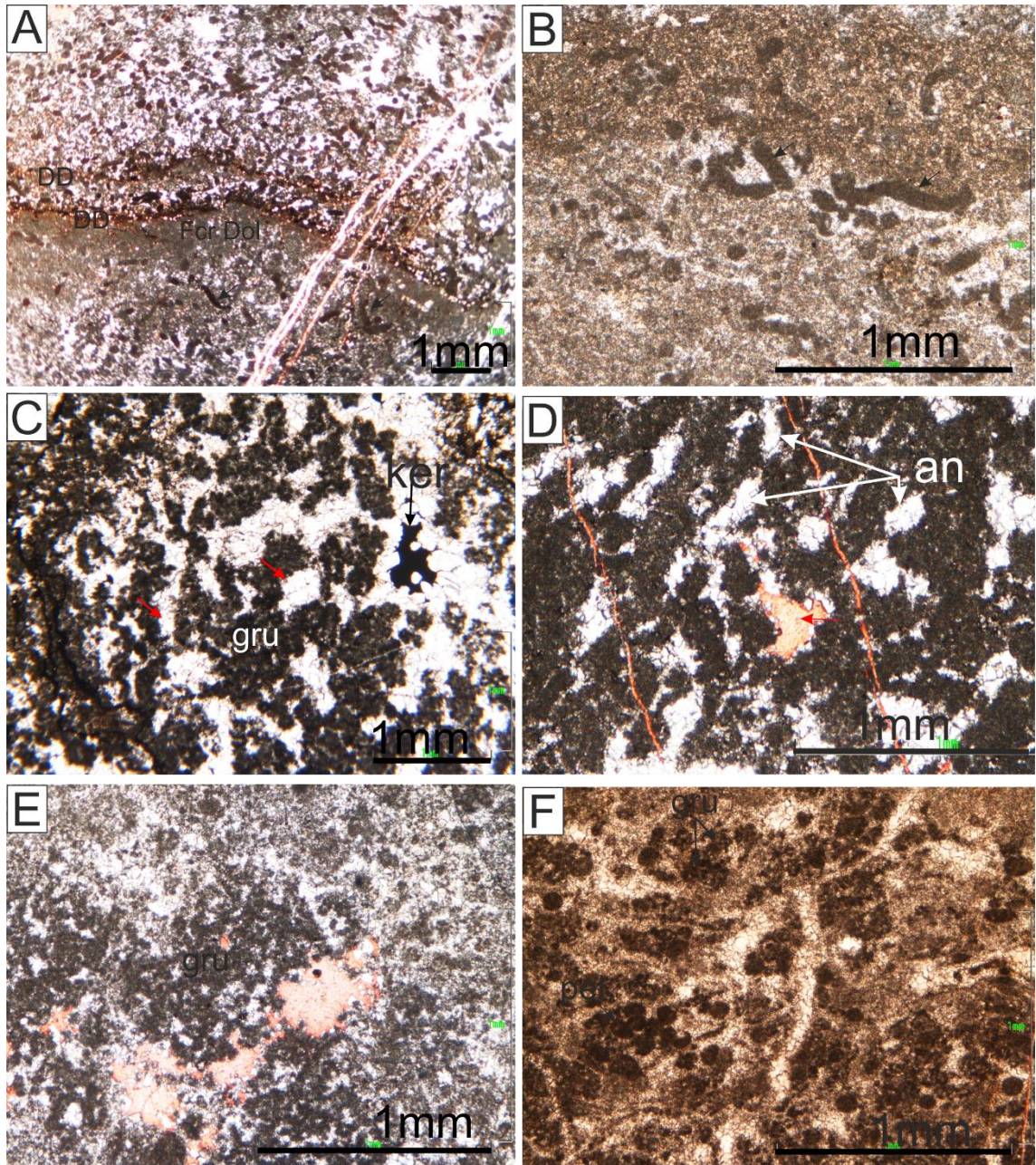


Figure 5.22: couplets of fine crystalline dolomitized mudstone and fenestral dolomite, note that the fenestral dolomite laminae are much richer with elongated peloids than darker one. B; detailed of elongated peloids, black arrows pointing to the elongated peloids. C; dolomitized mudstone showing grumeleuse (gru) or clotted "microtexture (clo) dolomite pseudomorphs of anhydrite (red arrows) with some cavities that are infilled by kerogen (ker). D; dolomitized mudstone and dolomite pseudomorphs of anhydrite (an) displaying fenestral texture; note the evaporite pore-filling sequence consists of a clear dolomite followed by calcite cement (red arrows). E; photomicrograph showing association between clotted microtexture, dolomite and calcite pseudomorphs of evaporites. F; microcrystalline dolomite forming from peloids (pel) and clotted microtexture (clo). All Photomicrographs are from Nora location.

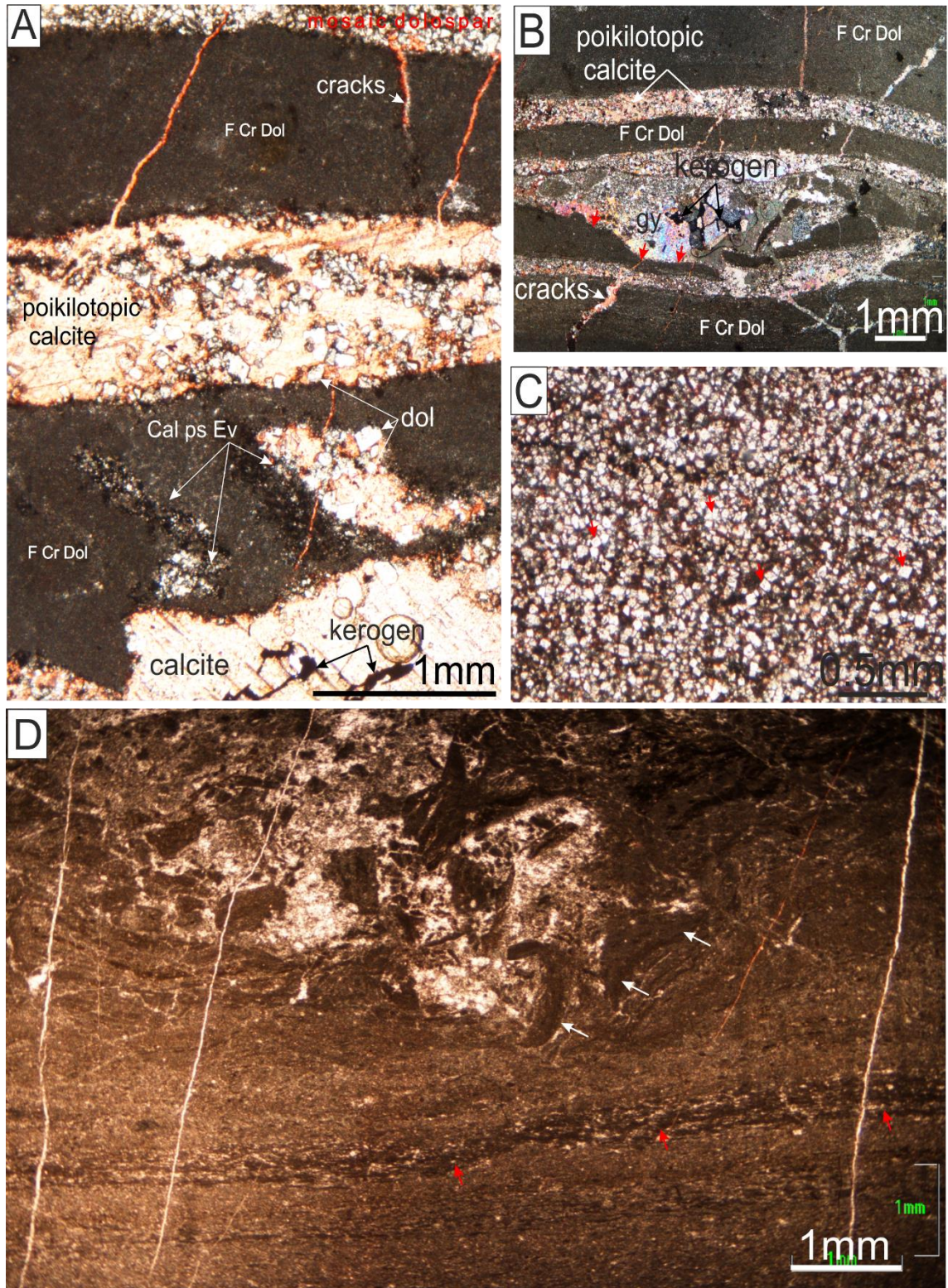


Figure 5.23: Couplets of fine crystalline dolomite (F Cr Dol) and coarse poikilotopic blocky calcite laminae, Note dolomicrite including calcite pseudomorphs of evaporite, while poikilotopic blocky calcite laminae containing rhombs of dolomite and kerogen. B; Couplets of fine crystalline dolomite (F Cr Dol) and coarse poikilotopic blocky calcite laminae including intraclasts, and gypsum, note truncated surface (red arrows) (gy) C; saccharoidal dolomite crystals (red arrows) are engulfed by blocky calcite cement. D; fragments of penecontemporaneous dolomitized carbonates showing deformation structures (white arrows). Note clot-rich laminae (red arrows), they may represent microbial laminae. All Photomicrographs are from Barsarin location.

### 5.4.1 Interpretation

Thick-bedded dolomite–limestone lithofacies (TBDLL) is interpreted to record desiccation and evaporation of minerals dominated sedimentation in a sabkha environment. This interpretation is supported by the sections which present a detailed interpretation of this facies association in terms of (1) fine crystalline dolomite, (2) desiccation and brecciations, (3) evaporate minerals and (4) silicification.

#### 5.4.1.1 Desiccation structures

The top of the TBDLL is disrupted by horizons of polygonal mudcrack and saucer-shaped or tepee structures, which are interpreted to be desiccation structures (Fig 5.15). The desiccation cracks are indicators of periods of non-deposition and subaerial exposures. They normally occur in fine-grained carbonate sediments developed under an arid or semi-arid climate (Flügel, 2004).

Tepee is a desiccated sedimentary structure that commonly exhibit saucer-shaped and polygonal cracks. They are found mostly in ancient and modern supratidal environments (Assereto and Kendal, 1977; Kendall and Warren, 1987). Thick units of tepee structures can be accounted for prolonged episodes of exposure between storm tides (Tucker and Wright, 1990). Based on Assereto and Kendall's (1977) classification, the tepee structures of the TBDLL seem to be in a mature phase (Figure 5.17, D).

In comparison to the recent analogous of the Arabian Gulf, Bahamas, and coastal saline in South Australia (Shinn et al., 1965; Kendall and Skipwith, 1968; Warren, 1982; Alsharhan and Kendall, 2003; Bontognali et al., 2010; Sadooni, 2010), upper intertidal to supratidal environments are inferred for TBDLL.

#### 5.4.1.2 Evaporites and intraclasts

Evaporite minerals and the evidence of their former presence can be seen in both macro- and micro-scales quite frequently. The evaporite minerals often occur as gypsum and anhydrite in four different shapes. The anhydrite may be represented by lath shapes (Figures 5.20, E and 5.21 A–C) or nodular (chicken wire) textures (Figure 5.17, F), whereas the gypsums may appear as lensoidal or swallowtail gypsum (Figure 5.21, I).

The evaporite minerals have great environmental importance, and have been frequently cited as a key tool for recognizing the supratidal environment, in which gypsum and anhydrite appear in the uppermost intertidal and supratidal zones in the sabkha

environments on the Trucial Coast in the Arabian Gulf (Park, 1977). All petrographic characteristics of evaporite minerals and their association with penecontemporaneous dolomite and intraclasts in the TBDLL (Figures 5.20, C, E–F and 5.21, A–E) have a nearly perfect match with modern sabkha analogue. Nodular anhydrites (Figure 5.17, E–F) “chicken wire” are formed by penecontemporaneous diagenetic products within the capillary zone of unconsolidated sediments in exposed supratidal flats of arid regions in sabkha, and they were quite common in ancient evaporitic supratidal flats (Curtis et al., 1963; Illing et al., 1965; Butler, 1969; Evans et al., 1969; Handford, 1981; Warren, 1991).

The intraclast breccias are the abundant constituents in the TBDLL, and they strongly appear to be of polygenic origin. Selley (2000) divided breccias into two main types: they either form as dissolution–evaporite collapse or deposits in very proximal environments, in which the clasts have not yet undergone rounding, and abrasion. The formation of intraclasts in the TBDLL are inferred to be related to the dissolution–evaporite collapse (Figure 5.16, G), for their association to the evaporitic mineral or pseudomorph (Figure 5.20, E–F). Some intraclast breccias may form through evaporite mineral growth or reworked fragments of penecontemporaneous dolomitized carbonate through the wave action on the tidal flat, particularly during storm tide on the supratidal environments. However, this kind of breccia occurs on smaller scale, usually weakly consolidated carbonate sediments. Intraformational breccia is filled by dolomite cement (Figure 5.23, D).

#### 5.4.1.3 Dolomite related to sabkha environments

The TBDLL mainly comprises fine crystalline dolomite associated with evaporite minerals or their pseudomorphs (Figure 5.20, C, E, and F), intraclasts, and collapsed breccias related to evaporites. The association of fine grain or penecontemporaneous dolomite and gypsum in recent supratidal settings is well established, particularly on the Trucial Coast of the Arabian Gulf (Wells, 1962; Curtis et al., 1963; Illing et al., 1965; Shinn et al., 1965; Kinsman and Patterson, 1973; Yechieli and Wood, 2002; Alsharhan and Kendall, 2003; Bontognali et al., 2010; Sadooni, 2010). The evaporite–dolomite phase has also been described from ancient deposits (Laporte, 1967; Matter, 1967; Roehl, 1967; Rabet, 1981; Alsharhan 1993; Tourir, 2009; Meister et al., 2013). By analogy with the recent sediments, it may be concluded that TBDLL was formed on an evaporitic carbonate tidal flat of the sabkha environment; since a great bulk of recent similar dolomite occurs in the supratidal portion of tidal flats. This model, i.e. penecontemporaneous dolomitized carbonate appears to be well-documented in modern systems with strong support from experimental work in that it is only from a high

Mg/Ca ratio, high salinity brine that a dolomite can be precipitated in the laboratory at low temperatures (Hardie, 1987).

However, recent studies on the Trucial Coast argued that the high Mg/Ca ratio is not the only controlling factor of penecontemporaneous dolomitization, instead dolomitization can form within exopolymeric substances (EPS). In this model, dolomite precipitation is linked to microbialites that can tolerate high pH and alkalinity and lowers sulphate concentrations of interstitial waters (Bontognali et al., 2010; Sadooni, 2010). The microbialites in TBDLL mostly occur as thin mats that are rich in fenestral structures and clotted microtexture (Figure 5.22, C–F). The clotted microtexture is related to a variety of microbialites which usually lacks clear lamination (see section 5.2.1.A for more detail) (Aitken, 1967; Wray, 1977; Flügel, 2004). The microbial mats may form in the TBDLL immediately after each inundation and storm tides, but laminations are scarcely preserved because of their later destruction by desiccation and/or evaporative mineral growth.

Based on mentioned evidence above, there is a close similarity between the TBDLL of the Barsarin Formation and the supratidal of the sabkha model of Trucial Coast, Arabian Gulf. This presumption is based on, firstly, evidence of highly arid conditions; carbonate sediments of sabkha setting contain evaporites or their relict features within the dolomite fabrics; and secondly, a shallowing-upward succession cross-sectional profile. There may be shallowing-upward trends in these strata, but in order to establish that correctly it needs to statistical analysis. The evidence for shallowing-upward in the Barsarin Formation is indicated by marine sedimentation succession, which normally commenced with a sudden subtidal environment over an earlier supratidal sabkha. Since marine regressions result in progradation producing a profile comprising (i) microbial laminite lithofacies, subtidal, (ii) blister flat stromatolite, intertidal, and (iii) thick-bedded dolomite–limestone lithofacies, supratidal. The shallowing-upward succession and facies association in the Barsarin Formation resemble, in many ways, the Trucial Coast sabkha model.

Based on studies about the Trucial Coat of Arabian Gulf, Kinsman and Park (1976) and Patterson and Kinsman (1981, 1982) revealed that the dolomitized units always followed by limestone. According to their study, the early dolomitization took place through evaporite pumping or ascending brine solute at a narrow strandline at the boundary between inner sabkha and upper intertidal zones; whereas the limestone unit represents an outer sabkha zone (Fig 5.24).

The dolomite–limestone successions in the TBDLL are very comparable to the Trucial Coast model that described by Patterson and Kinsman (1981, 1982), where the thick-bedded dolomites in the TBDLL are normally followed by thick-bedded limestone (Figures 5.15 and 5.24). It is suggested that the dolomite may occur in inner sabkha and upper part of the intertidal zone. The limestone is believed to represent an outer sabkha zone, which seems to be away from the effect of evaporite pumping or ascending brine solute, where no dolomitization occurs. In particular, the TBDLL sediments are completely devoid of terrigenous components, indicating that the major sediment sources supplying the sabkha perhaps derived from: (i) chemical precipitation and (ii) storm periods, which sweep sediments from the subtidal zone.

#### 5.4.1.4 Silicification

The TBDLL in lower part of the Barsarin Formation sequence is characterized by widespread existence of siliceous minerals. The common associations of silica, evaporite minerals or their pseudomorphs, breccias, and desiccation structures can be considered as a most prominent diagnostic feature of the TBDLL. Large chert nodules up to 40 cm comprising a length slow chalcedony and spherulites can be frequently observed throughout the lithofacies (Figure 5.21D–E, and G–H), specifically in the lower part of the TBDLL, which are often overlain by intraformational breccia or collapsed breccia.

In the thick-bedded dolomite–limestone lithofacies, relics of evaporite minerals are noticeable within and adjacent to the silicate minerals (Figure 5.21, E, and G–H), since silica minerals have been indisputably determined as a common evaporite replacing mineral (Siedlecka, 1976). It has been concluded that the silicate minerals most probably occurred by replacing sulphate minerals (Folk and Pittman, 1971; Siedlecka, 1972; Chowns and Elkins, 1974; Tucker, 1976; Siedlecka, 1976; Milliken, 1979; Friedman, 1980; Heaney, 1995; El Khoriby, 2005). Intimate association between silica and evaporite minerals and their pseudomorphs distribution in silica suggests that the chert nodules are most likely formed by replacing sulphate minerals.

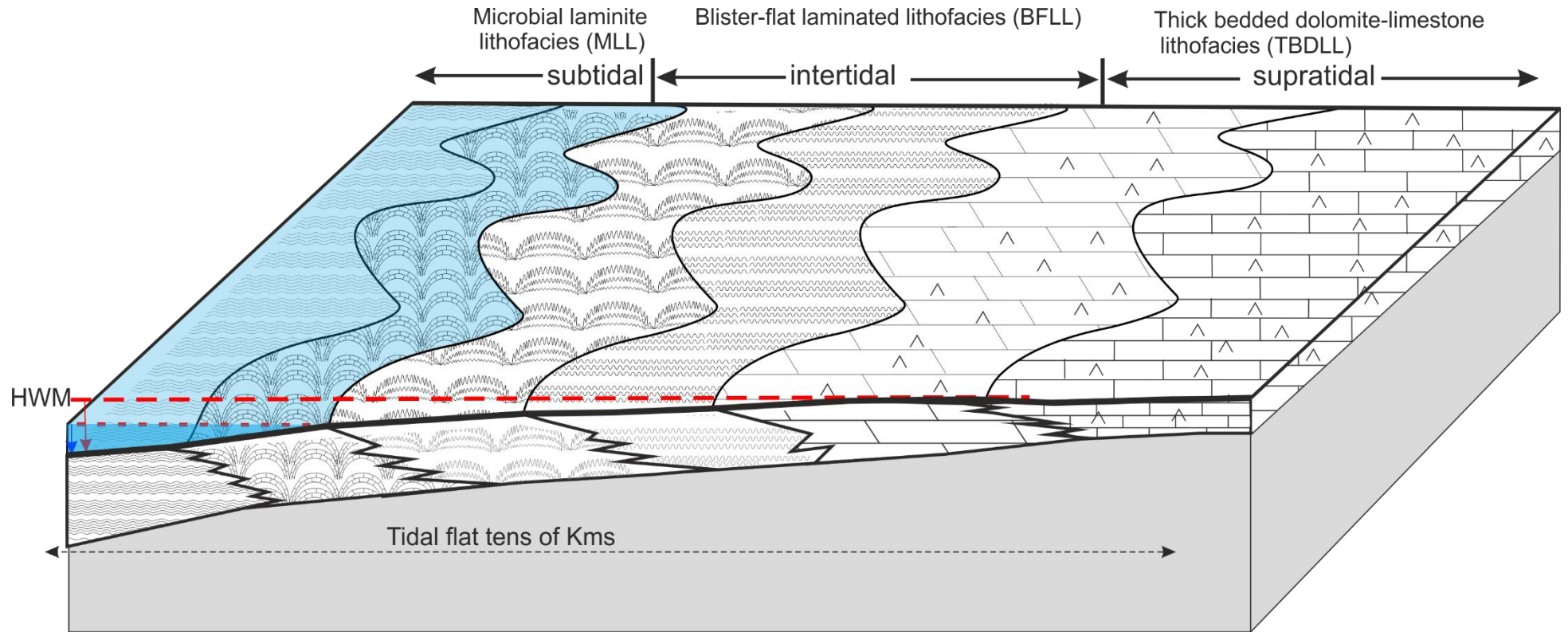


Figure 5.24: Depositional model showing different lithofacies locations of the Barsarin Formation on a tidal flat.

#### 5.4.2 Conclusions

TBDLL always overlies the BFLL, and underlies the MLL. Generally, this lithofacies is buff in colour, fine-crystalline dolomite, which includes large lensoidal cherts, gypsum, anhydrite, and often displays an irregular upper boundary (Figure 5.15). Signs of desiccation have been frequently encountered, which could be inferred from the presence of polygonal cracks, and tepee structures. The intraclasts origins have been interpreted from their similarity to the BFLL and TBDLL, and lack of the terrigenous clasts in the TBDLL may suggest that the clasts are considered to be of intraformational origin.

Gypsum, anhydrite, and their pseudomorphs seem to be closely associated with the silica minerals. Evaporite occurrence in all localities is of microscopic scale, but in the Kurrek and Sary Amedy areas, in Erbil and Dhuk (Figure 5.1) respectively, they are represented by two units of chicken-wire gypsum up to a few metres thick. Field and microscopic studies indicate that evaporites are a major constituent in the TBDLL, but only a minor one in the BFLL and rarely observed in the MLL, so the increasing evaporative conditions upwards can be seen clearly in the sequence.

Fossils are very few, and are represented by fecal pellets and some horizons of elongated peloids that perhaps represent *Aggregatella pseudohieroglyphicus* Elliot, which may represent microcoprolites (Elliott, 1962). According to (Gayara and Minas, 1996) existence of elongated peloids indicates high salinity and a supratidal environment. The clotted microtexture is common microbialites and usually lack clear lamination. By the analogy with the recent sediments, it can be concluded that the TBDLL formed in an evaporative carbonate tidal flat of the sabkha environment, since a great bulk of fine crystalline dolomite associated with gypsum or their pseudomorphs, desiccation structure, clotted microtexture, and fenestrae occur in the supratidal portion of tidal flats.

## 5.5 Summary

Chapter five gives the description and interpretation of the Middle–Late Kimmeridgian Barsarin Formation from seven localities in northern Iraq. The results confirm the dominant nature of the microbial stromatolites. Also, the occurrence of the Barsarin Formation in repeated microbial laminite lithofacies, blister–flat laminated lithofacies and thickly bedded dolomite–limestone lithofacies cycles with the presence of evaporite and desiccation structures such as polygonal mud cracks, tepees and flat–pebbles are all consistent with peritidal sabkha conditions. Up to nine shallowing-upward cycles were recorded in the type locality.

The subtidal facies is suggested for microbial laminite lithofacies, since no subaerial exposure surfaces are confirmed. The presence of the MLL in association with domal stromatolite structures suggests the continuous submergence conditions with relatively high saline water. Paucity of fauna and well preserved laminae suggest that the depositional condition was above the tolerance for the majority of the fauna, which may have led to microbial structure preservation and development.

Blistered–flat laminite fabrics are very comparable to modern convoluted microbial mats, and are interpreted to be intertidal facies. On the basis of the lamination structures, the BFLL is subdivided into blistered and flat laminae. The former, which displays wrinkle structures, was occurred in the lower part of the intertidal zone, as indicated by the existence of disrupted and scoured surfaces, evaporite mineral or their pseudomorphs, and laminoid-fenestral fabrics. However, the flat laminae that represent the upper intertidal zone, display straight laminations, and lack laminoid-fenestral fabric pockets. The couplets of dolomite and calcite represent periodic microbial mats flourish with siliciclastic sediments fluctuations. It is concluded that the dolomite laminae in the BFLL have a close relationship with microbial mat.

Thick-bedded dolomite–limestone lithofacies is indurated, finely crystalline dolomite and/or limestone with intensively fractured textures. The TBDLL is often massive and begins with dolomitized beds followed by limestone beds. Many scoured surfaces, polygonal cracks, and tepee structures are well-developed at the top of this lithofacies. Intraclasts, evaporite crystals and chert nodules are the major constituents of the TBDLL. Also, thick units of chicken-wire evaporite deposition of up to 2 m thickness are observed. The TBDLL is interpreted to have occurred in the supratidal sabkha environment. This interpretation is supported by the existence of penecontemporaneous dolomitization, desiccation, dissolution brecciation, evaporite minerals and silicification.

*CHAPTER SIX*

*6 SEQUENCE STRATIGRAPHY OF THE SARGELU,  
NAOKELEKAN AND BARSARIN FORMATIONS  
MID-LATE JURASSIC*

## 6.1 Aims

- Subdivide the strata in the study area successions into sequence stratigraphic units, including systems tracts and sequences, including high-frequency sequences if possible.
- Assess the relationships between eustatic sea-level changes, tectonic subsidence and uplift, and pelagic sedimentation.
- Attempt to correlate the sequence development on the Arabian plate with sequences defined with the study area.

## 6.2 Introduction

Sequence stratigraphy is a method that deals with the subdivision of strata into genetic packages of isochronous units. Each package is inferred to represent a cyclic change in sea-level and/or sediment supply, which is bounded by unconformities and their correlative conformities. In sequence stratigraphy, the boundaries and different facies that correspond to same time–lines can be traced across entire basins. Sequence stratigraphy can be a useful tool for understanding and predicting the distribution of petroleum system elements (Moore, 2001; Coe, 2003; Catuneanu, 2006; Catuneanu et al., 2011).

Sequences are composed of packages of genetically linked depositional systems termed “systems tracts” (Moore, 2001). The term “depositional system” was introduced by Fisher and McGowen (1969) describing assemblages of lithofacies genetically linked by a common set of depositional processes, such as rivers, deltas and slope depositional systems (Schlager, 2000). Depositional sequences can be defined as a relatively conformable succession of genetically related strata bounded top and base by unconformities and their correlative conformities (Vail et al., 1977). Sequences ought to be as succession of strata, deposited during a complete accommodation cycle.

The last four decades, sequence stratigraphy has provided an important tool in sedimentary basin analysis of continental margins that are fed by siliciclastic sediments (Vail et al., 1977; Wilgus et al., 1988). However, the mechanism behind the sequence development of carbonate rocks differs significantly from that of siliciclastic sediments that are derived from processes of weathering, erosion, transport and deposition. In contrast, carbonate rocks are produced in specific areas called carbonate factories, either as direct precipitation from seawater or by the skeletons of marine organisms (Bosence and Wilson, 2003). Most carbonates were formed close to where they are now

rather than being transported into the depositional basin from the nearby land area. Sequence stratigraphic can be applied to carbonates as well (Sarg, 1988; Schlager, 2005), but it is necessary to modify sequence stratigraphy to be applicable on carbonate settings. For example, in a carbonate setting turbidites appear in highstand systems tracts when platforms are at a maximum of productivity (Schlager, 1989).

This chapter describes the sequence stratigraphy of the Jurassic succession of northern Iraq and more particularly, the Sargelu, Naokelekan and Barsarin Formations. These Jurassic formations are the most prolific oil-bearing interval in Iraq, and their succession comprises interbedded carbonates, organic-rich shale and evaporites. The carbonate units often form reservoirs capped by a thick evaporite unit. The topmost Jurassic system in almost all regions of the Arabian Plate (AP) is overlain by thick evaporite units of the Gotnia, Hith, or Barsarin Formations. In chapter 3, 4, and 5 the detail interpretation of deposition environments was made in order to ascertain the possible environment and the factors that control sedimentation in the study sections.

### **6.3 Potential difficulties in sequence stratigraphy application in the study area**

#### **6.3.1 Post collision deformation**

The eastern and western margins of Gotnia Basin are not known precisely due to overthrust structures that occurred in the Late Cretaceous period and erosion during the Neocomian uplift (Numan, 1997). The study area is also located within the collision area between the Arabian and Persian blocks, and many reverse faults developed along initially extensional normal faults.

#### **6.3.2 Geometry of the basin**

The geometry of the basin is an important issue that needs to be considered when studying the basin. Platforms could be attached or unattached to adjacent continental landmass. The former type may represent rimmed carbonate platforms, epeiric platforms or ramps, which are often characterised by mixing carbonates with land-derived siliciclastic sediments. However, isolated platforms are unattached and are often devoid of the terrigenous influx (Bosence and Wilson, 2003). Evidence presented in previous chapters suggests complete absence of terrigenous components within the studied facies of Middle–Late Jurassic Period, even the upper Jurassic sabkha facies of the Barsarin Formation has no terrigenous sediment content. Basin analysis studies in Chapter 7 assumed a tilted fault block model for the Middle–Late Jurassic.

Based on what have been discussed in the previous chapters, the depositional basin of the Middle to Upper Jurassic condensed successions of Kurdistan region most likely developed on the bathymetric high. More important challenges from the primary model arise when we deal with the peculiar stratigraphic sequences resulting from the sedimentation of a submarine isolated fault block. Besides, the lack of detailed seismic investigations has made the understanding of the basin development and stratigraphy difficult. Reconstruction of the basin to its original form is crucial to understanding the sequence stratigraphy.

#### **6.4 Sequence boundaries on submarine plateaus**

Sequence boundaries can be easily observed in carbonate platform top areas because of clear subaerial erosion, basinward shift of coastal onlap facies, produced by a relative falls in sea-level (Wilgus et al., 1988). However, on a distal submarine bathymetric high or distal basin floor, sequence boundaries can be found along with stratigraphic gaps occurring on non-depositional or slightly erosional submarine surfaces, often marked by hardgrounds (Vera and Martín–Algarra, 1994; George, 1999; Nieto et al., 2011). Although in the study area, Bajocian–Lower Kimmeridgian sequence strata could be formed either as a condensed interval on a distal basin floor or on an isolated bathymetric high, the discussion in the Chapter 7 suggests that the condensed intervals are most likely formed on the bathymetric high. So, it is envisaged that the geometric and sedimentological criteria of the normal shallow-water platform top strata are probably absent in the study basin. For that reason, the sequence boundaries that have been recorded on the carbonate platform top in the shallower part of the western part of the Gotnia Basin will not be easily recognised in the study area, see chapter 2 for detail.

The coastal sediments and angular relationships between different sequences packages are usually not clear in the distal deep-marine basin, so the sedimentological and bathymetric criteria of the isolated pelagic plateau may not be applicable for deducing relative deepening or shallowing of the sea–bottom. However, Martire (1992) pointed out that a stratigraphic sequence as a record of the interaction between sea-level fluctuations and sedimentation may be assumed as sequence boundaries, and that the sedimentary events match sea-level falls.

## 6.5 Sequence boundaries

According to Schlager (2005) and Saller et al. (1993) sequence boundaries are often accompanied by widespread marine erosion and a hiatus. Sequence boundaries are subdivided into three main types:

### 6.5.1 Type 1 sequence boundaries

It is an unconformity, distinguished by fluvial incision and stream rejuvenation and sedimentary bypass of the shelf. It demonstrates an abrupt seaward shift of facies and coastal onlap and developed during relative sea-level falls below the shelf break of the preceding sequence. This is inferred to be due to the rate of eustatic fall, which was higher than the rate of basin subsidence at the depositional shoreline break, resulting in a relative fall in sea-level at that position (Schlager, 2005).

### 6.5.2 Type 2 sequence boundaries

Carbonate sequence boundary unconformity developed when relative sea-level falls to a position between the shelf break and old shoreline, and only the inner part of shelf subjected to subaerial erosion (Myers and Milton, 1996; Schlager, 2005). SB2 occurs when the rate of eustatic sea-level fall is less than the subsidence rate at the shelf edge (relative sea-level rise at the shelf edge), but exceeds the rate of subsidence at the shoreline (Schlager, 2005; Catuneanu, 2006).

### 6.5.3 Type 3 sequence boundaries or drowning unconformity

This kind of sequence boundary suggests no fall of relative sea-level, but it develops when sea-level rises faster than the system can aggrade. The Sb3 is often accompanied by a significant marine hiatus and marine erosion is normally prominent over the sequence boundary, particularly on drowned carbonate platforms (Saller et al., 1993; Schlager, 2005). Schlager (1999) identified Sb3 sequence boundaries as the boundary of a drowning unconformity within the carbonate sequence stratigraphy.

Based on Buday (1980), Jassim and Goff (2006), Sissakian (2013), Gayara and Al-Gibouri (2015) the western side of Gotnia Basin is characterised by carbonate–siliciclastic sequences with many subaerial unconformities. In contrast, the entire Middle–Upper Jurassic successions in the east are carbonate strata and lacks subaerial unconformities (for detail see Chapter 2). The western side of the basin may include type

1 sequence boundaries, but within the study area, Type 3 drowning unconformities are more dominant though Type 1 boundaries do occur (discussed in section 6.8.2).

## 6.6 Depositional sequences

According to Catuneanu et al. (2009) a depositional sequence can be defined as a succession of strata that was deposited during a full cycle of change in accommodation or sediment supply. In the studied basin strata are mostly deep-water facies, so depositional sequences from Bathonian to Early Kimmeridgian are mostly not bounded by subaerial unconformities. However, the Middle–Late Kimmeridgian Barsarin Formation shows high-frequency sequences, and each one of those is presumably capped by a subaerial exposure surface. The top of the Naokelekan Formation Early Kimmeridgian does show the significant possible sequence boundary where the transition from basinal facies to Sabkha facies occurs, representing a basinward shift (Figure 6.1). Within each sequence, deepening trends define the transgressive system tract (TST), and shallowing trends define the highstand system tract (HST). The point of transition from deepening to shallowing is interpreted to represent a maximum flooding surface (mfs).

The long-term eustatic curve of Miller et al. (2005) and the relative sea-level interpretation of the Jurassic strata of western Gotnia Basin show opposite trends with respect to the deepening (Figure 6.1). According to Miller et al. (2005), Jurassic eustasy shows deepening upward whereas the Jurassic in the study area shows long term shallowing-upward. Thus, even if the Miller et al. (2005) curve is an accurate record of Jurassic eustasy this eustatic history is not expressed in the relative sea-level history implied by the study area, possible because: the area is dominated by tectonic movements within a passive margin, and the eustatic signal is overprinted by a more dominant tectonic signal or because depositional water depths were too deep to record the influence of eustasy, or because autocyclicity or other forms of more complex stratal responses overprinted any eustatic signal.

The following section will discuss sequence stratigraphy of the latest Triassic to Jurassic successions in general and Middle–Late Jurassic in detail. Based on the evidence in Chapters 3, 4 and 5, this duration is divided into three depositional sequences, and they are of the third-order sequence (Figure 6.1).

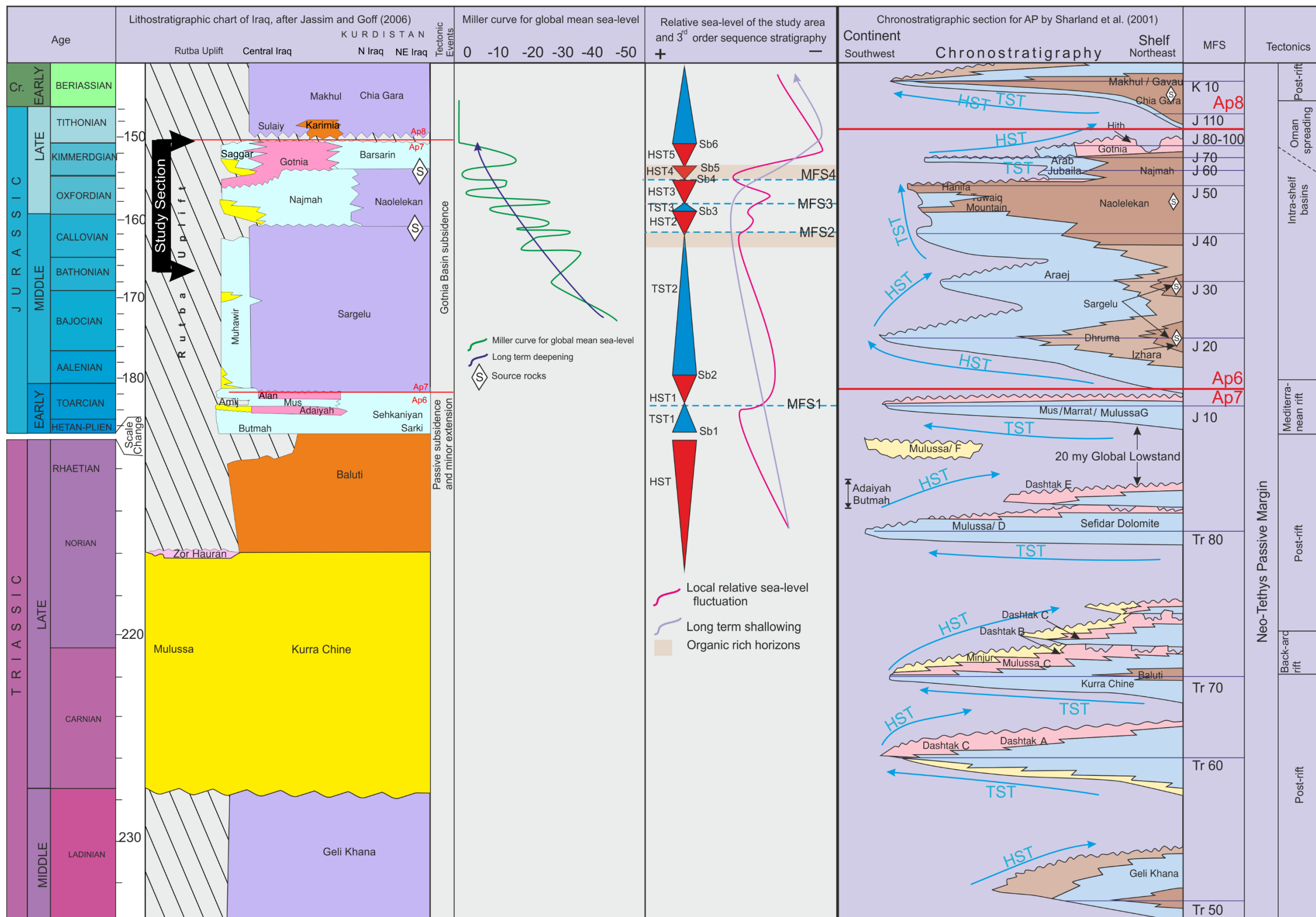


Figure 6.1: Generalized stratigraphic correlation between Iraq and Arabian Plate (AP) showing comparison between tectonic, eustatic, relative sea-level development. Note 3<sup>rd</sup> order sequence stratigraphy with relative sea-level exhibit a reverse pattern with Miller's curve, where the latter curve shows deepening upward, whereas the relative sea-level of study area shows shallowing upwards.

## 6.7 Depositional sequence 1 (Upper Triassic–Lower Jurassic)

Second order sequences have been identified through application of detailed description and interpretations of evidence. There will be an attempt to apply third–order sequence stratigraphy as well.

The lower sequence boundary (Sb1) of the depositional sequence DS1 in the study area corresponds to the Triassic–Jurassic boundary, which also coincides with the contact between Baluti and Sarki Formations. Based on Al-Juboury and McCann (2015) the DS1 was distinguished by a thick palaeosol developed during the Rhaetian–Sinemurian. Regionally, relative sea-level was low during the Early Jurassic for 20 million years (Al-Husseini, 1997; Alsharhan and Nairn, 2003; Sharland et al., 2001; Sadooni and Alsharhan, 2004). After a prolonged period of non-deposition over wide areas of the Central Arabian Plate, a thick hiatus produced the pre-Marrat Formation unconformity. In contrast, Lower Jurassic successions in the northern part of AP, i.e. the correlative conformity in Iraq and the study area are relatively complete, and characterised by TST strata contain undifferentiated shallow carbonate–evaporites representing low rates of subsidence. The TST in the study area may include Sarki and parts of the Sehkaniyan Formations (Figure 6.1) (Sharland et al., 2001; Al-Juboury and McCann, 2015).

The MFS1 in the DS1 correlate to the globally recognised Toarcian transgression. Although the sequence stratigraphic framework of the AP is characterised by prominent fluctuations in sea-level change, these variations are difficult to recognise in the study area. The MFS1 of Toarcian age in Iraq could be located at the Lithiotis limestone of the Sehkaniyan Formation within the study area and/or its equivalent to the base of the Mus Formation. The Marrat Formation of Saudi Arabia is also rich in *Spiriferina* brachiopod and Lithiotis limestone which is reported to be similar to strata observed in the basal Mus and Sehkaniyan Formations (Sharland et al., 2001; Jassim and Goff, 2006).

After MFS1 Toarcian, the undifferentiated evaporite–carbonate system of HST1 was formed, where a progressive fall in the relative sea-level resulted in the formation of the Upper Marrat, Alan and upper part of Sehkaniyan Formations, that is distinguished by evaporite deposition (Figure 6.1). Large areas in the AP were subjected to exposure during late Toarcian–Aalenian, whereas the Toarcian transgression persisted for longer in many regions globally (Röhl, 2005) characterised by widespread occurrence of organic-rich mudstones, called Posidonia black shales.

## 6.8 Depositional sequence 2 (Middle Jurassic)

### 6.8.1 Sequence boundary (Sb2)

Despite destructive dolomitization, the contact between the Sehkaniyan and Sargelu Formations is marked by clear transitions from massive to medium-bedded limestone, which probably correlate with Sb2 (Buday, 1980). The Sb2 characterized the rapid transformation from eroded surfaces with rip-up breccia of evaporitic dolomite Sehkaniyan Formation to a basinal facies of the Sargelu Formation (Figure 6.2). However, with the lack of biostratigraphic and geochemical evidence, caution must be applied, as the destructive dolomitization eliminated and destroyed almost all the original textures at the Sb2.

Generally, the Late Toarcian to Early Aalenian hiatus of the AP and surrounded area coincided with an eustatic fall in global sea-level (Ziegler, 2001). During Late Toarcian–Aalenian a second depositional hiatus took place in the Jurassic period in the central AP, where the sea-level dropped about 75 metres (Al-Husseini, 1997). The study area was perhaps affected by this hiatus, but due to the destructive dolomitization at the boundary between Sargelu and Sehkaniyan Formations it is difficult to ascertain to which extent they were affected. Based on Tucker (1993), the destructive dolomitization may infer relative sea-level fall sequences. This means that the basal saccharoidal dolomite member (BSDM) could be part of the relative sea-level fall period, and the sb2 located at the base of the middle posidonia limestone member (MPLM) (Figure 6.2).

The transition from the Sehkaniyan to the Sargelu suggests abrupt drowning from evaporitic shallow-intertidal environment to basinal facies. Traditionally, the top of Sehkaniyan Formation has been considered to be Pliensbachian–Early Toarcian whereas lower part of the Sargelu Formation was assumed to be Bajocian (Buday, 1980). Accordingly, Late Toarcian–Aalenian could be absent in the studied area, but there is a need for further research in order to establish strong evidence regarding this hiatus (Figure 6.2). This boundary could be defined as a type 3 of sequence boundary, corresponding to platform drowning, and it often forms by fast sea-level rises or subsides. Consequently, a transgressive systems tract of the Sargelu Formation directly overlies the preceding highstand systems tract of Sehkaniyan formation. According to Jassim and Goff (2006), a significant marine hiatus was also identified on the Sb2 surface.

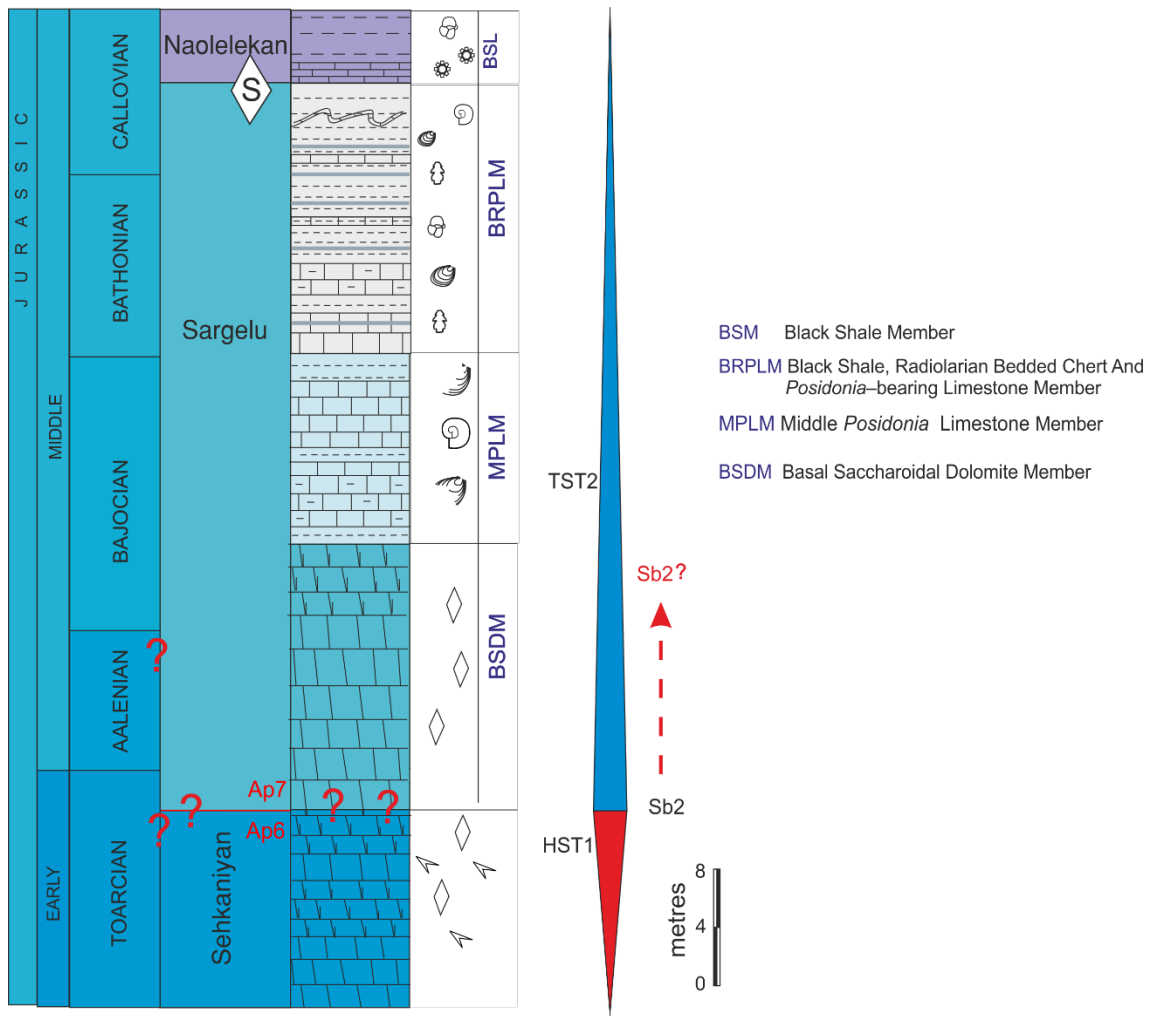


Figure 6.2: diagram showing sequence stratigraphy and facies change between Sehkaniyan and Sargelu formations of Early - Middle Jurassic. Note, the *Posidonia* and radiolarian-rich Sargelu Formation rest on an evaporitic Sehkaniyan Formation strata, and this shows clear transitions from shallow evaporitic facies to pelagic condition. The question marks point to the uncertainty of the lower boundary of the Sargelu Formation owing to destructive dolomitization, while the dashed red arrow suggests the probable Sb2.

### 6.8.2 Drowning

If relative sea-level increase outpaces production rate, then the platform will produce a drowning unconformity surface, characterized by a very rapid facies change from shallow-water carbonates to deep shelf, slope or basinal deposits (Bosence and Wilson, 2003; Emery and Myers, 2009).

From Toarcian age onwards, a large epipelagic Arabian Platform was created in the Gotnia Basin. The thinning and extension of the Gotnia Basin during lithospheric stretching resulted in the collapse and drowning of the pre-Toarcian platform (Aqrabi et al., 2010). The rifting may extend from the eastern margin of the Arabian Platform along Oman up to northern Iraq (Robertson and Searle, 1990; Stampfli et al., 2001; Robertson, 2007). Based on Jassim and Goff (2006) the eastern margin of the Gotnia Basin may be

subjected to normal faulting, generating horst and graben structures across the study area. As a consequence of these phases of extensional faulting, the pre-existing Sehkaniyan shallow basin fragmented into sub-basin environments that accompanied a rapid platform deepening (Aqrabi et al., 2010). Clari and Martire (1996) considered the abrupt facies change from shallow to deep facies to be a sign of deepening related to the sudden drowning of the shallow pre-existing platform. Facies change between Sehkaniyan and Sargelu formations of Early–Middle Jurassic may indicate the drowning events in the studied area, where the Sargelu Formation which is rich with *Posidonia* and radiolarian fauna, rests suddenly on an evaporitic Sehkaniyan Formation strata that shows clear transitions from intertidal evaporitic settings to pelagic environment over relatively small vertical thickness.

### 6.8.3 TST2 *Posidonia* and radiolarians-rich facies

During Early Bajocian, i.e. about 170 million years ago relative sea-level rose again and continued until the Middle–Callovia (Sharland et al., 2001). During this interval the Neotethys Ocean expanded and transgressed westward onto the Arabian Craton. The appearance of ammonite *Shirbuirnia fastigata* in the Arabian Basin of the lower part of the Dhurma Formation may imply the impact of the sea-level rise, whereas appearance of posidonia-bearing limestone in the Sargelu Formation represents the starting TST2 within the study area (Figure 6.1). This stage most probably resulted from rifting in the Mediterranean region. As a consequence of the increase rate of subsidence, many intra-shelf basins developed and were separated by platform areas during the rifting and reactivated passive margin.

The suggested Sb2 in the current study matches the major sequence boundary between Ap6 and AP7 (Figure 6.1). The TST2, which developed on the Sb2, is characterised by dominance of carbonate deposition with subordinate evaporites. Commonly, the depositional condition, seems to be changed into a more open-marine condition during Bathonian Bajocian. The deepening is indicated by the following evidence:

- The appearance of *Posidonia*, ammonites and *Protoglobigerina* foraminifera represents a clear decrease in energy, and it can be assumed that lower energy conditions probably means deeper water.
- The relationship between *Posidonia* and radiolarian in the Sargelu Formation strata clearly suggests facies change from shallow to deep-water environment (see Chapter 3). The facies change from the underlying intertidal Sehkaniyan Formation into posidonia-rich strata upward and then into radiolaria dominance

at upper part of the Sargelu Formation is interpreted as facies change from shallow to deep-water environment.

- Different phases of preservation of thin-shelled bivalves *Posidonia* from base to top provides the clue about deepening of the basin. The transition from broken to articulate thin-shelled bivalves was accompanied by gradually increasing radiolaria occurrence, and black shale association upward, which may support deepening and transgression of the basin (See Chapter 3).
  - At the beginning, the thin-shelled bivalves of the MPLM appear as intensely broken fragmented shells, showing no preferred orientation, and this may imply current and bioturbation dominance.
  - The thin-shelled bivalve in the subsequent strata exhibit different styles of preservation along their upward development over time, they change from intact disarticulated to articulate and then to close valves.

Sharland et al. (2001) revised the Arabian Plate sequence stratigraphy but proposed many more sequence stratigraphic subdivisions in the western side of Gotnia and Arabia Basin than are observed within the study area. Many locations within the Gotnia and Arabian Basins were influenced by sea-level fall and subaerial exposures, whereas the study area was continuously submerged. For example:

- i. There are reports (Alsharhan and Nairn, 2003) of relative sea-level fall resulting in extensive subaerial exposure and development of Bajocian–Bathonian age sequence bounding unconformities.
- ii. In the Arabian Basin, the lower unit of the Bajocian Lower Dhurma Shale is underlain and overlain by clear unconformities.
- iii. Most west to northwest parts of Iraq were characterized by subaerial exposure during the Bathonian age (Buday, 1980).

Subsequent to this dropping of relative sea-level, a MFS2 of the Early Bathonian was recorded in many places, which was indicated by the existence of the ammonite *Micromphalites* and foraminifera zone *Riyadhella arabica* in Middle Dhurma (Figure 6.1) (Sharland et al., 2001). The marly limestone unit near the base of the Muhaiwir Formation at western of Iraq could represent subsurface equivalent to mfs of Early Bathonian. These fluctuations in depositional sequences and subaerial exposures cannot be observed in the study area. The TST2 of the Sargelu Formation in the study area does not show any depositional interruption or unconformities (Balaky, 2004), and the deepening continued until lower part of Naokelekan, which implies continuous submergence of Middle–Late Jurassic subsystem in the study area.

#### 6.8.4 MFS2

Through Middle Callovian time the AP was covered with a broad transgressive sea. The flooding probably resulted from a combination of an eustatic rise in sea-level and increases in rate of subsidence that started with formation of intra-shelf basins (Murriss, 1984). The differential subsidence resulted in the development of many trough and bathymetric high structures throughout the area. The trough areas are distinguished by their richness of organic-rich rock deposition, where shales and deeper-marine carbonates were accumulated (Al-Husseini, 1997). Commonly, the Bajocian–Bathonian strata pass upward from destructive dolomitization to posidonia-bearing limestone and bedded chert sediments, including organic-rich shale intervals, but organic-rich shale reached its apex during Middle Callovian. The MFS2 is located between the black shale, radiolarian bedded chert and posidonia-bearing limestone member (BRPLM) of Sargelu and black shale member (BSM) of Naokelekan (Figure 6.3 and Figure 6.4). The top of the (BRPLM) displays the highest abundance of pelagic fauna such as Radiolarians, *Protoglobigerina* Foraminifera, ammonite, and coccoliths, whereas the BSM shows gradually decreasing upward of pelagic fauna Figure 6.3).

Biostratigraphic evidence from subsurface strata of Middle–Callovian age in northern Iraq indicates that the shale unit at base of the Najmah Formation, which is underlain and overlain by shallower environments, represents a transgressive pulse. The MFS2 of the Basinal Naokelekan Formation of Kurdistan outcrops could correlate to the lower Najmah shale (Sadooni, 1997). Sharland et al. (2001) found that the Najmah Formation may be developed following the J40 flood or MFS2, and it could be a relative ‘forced regressive wedge’ detached downdip by large distance from earlier HST oolite shoals of the Muhaiwir Formation. Accordingly, in central Iraq, the Najmah may be developed following a minor flooding–back, overlain by an unconformity surface that developed on the Sargelu Formation basin margin. The transgressive period in the Najmah Formation in Iraq is quite comparable with that observed in the Upper Sargelu Formation of Kuwait (Yousif and Nouman, 1997) and with the Tuwaiq Mountain Formation of Saudi Arabia (Murriss, 1980; Droste, 1990). Furthermore, Matos (1997) observed a transgression of Middle–Callovian strata over Bathonian–Early Callovian unconformably strata in the United Arab Emirates.



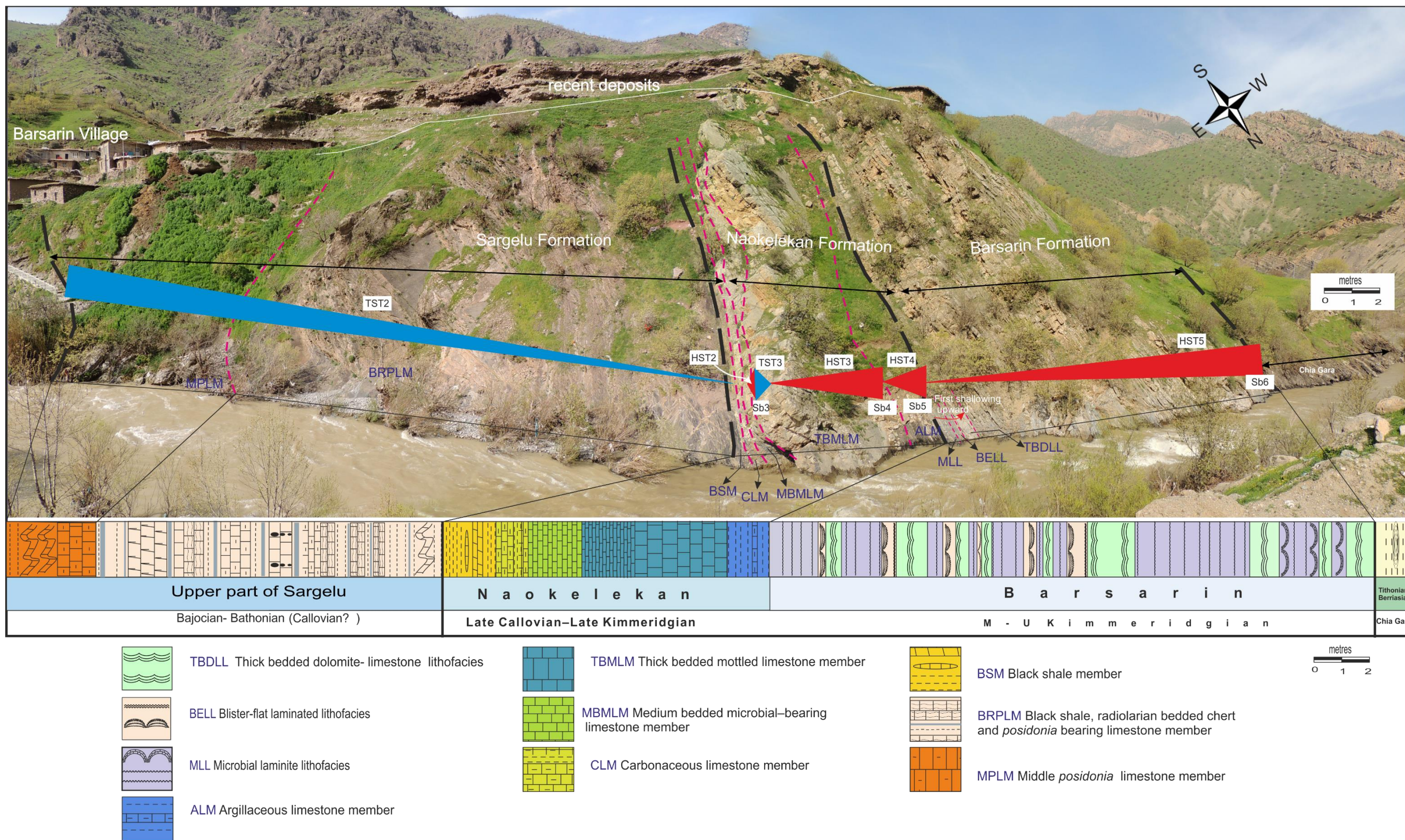


Figure 6.4: diagram showing panorama of field section in Barsarin locality with stratigraphic column and sequence stratigraphy of the upper part of the Sargelu- Naokelekan-Barsarin and Chia -Gara Formations. The presented sequence stratigraphy is 3<sup>rd</sup> order, Barsarin location.

### 6.8.5 HST2

Short-duration highstand carbonates HST2 of the carbonaceous limestone member (CLM) and medium-bedded microbial-bearing limestone member (MBMLM) of the Naokelekan Formation were deposited over deeper-water facies of the black shale member (BSM) of the Naokelekan and Sargelu Formations. The MBMLM shows a gradual upward decrease of ammonites, radiolaria and planktonic foraminifera. Strata at the top of this systems tract were not subjected to exposure as the western section of Gotnia Basin, but a clear shallowing with many signs of evaporation and probable oolites have been recorded near to the top (Figure 6.3, and 6.4).

## 6.9 Depositional sequence 3 (Late Callovian–Oxfordian)

### 6.9.1 Sb3

The Sb3 is clearly marked by a sharp facies transition from a medium-bedded microbial-bearing limestone member (MBMLM), which differs from the overlying thick-bedded mottled limestone member (TBMLM) in that the (MBMLM) represents deposition in restricted conditions, and contains indications of evaporitic deposits with no visible fossils. In all sections, the TBMLM is characterised by a significant number of microbial stromatolites over the ammonite bearing layers (Figures 6.3, and 6.4). The transition from the MBMLM to the lower part of the TBMLM implies HST2 to TST3 transition. The bedding surface at the top of the MBMLM could be a combined sequence boundary Sb3 with maximum flooding surface, which is determined based on facies change from the restricted condition with signs of evaporitic deposits to open-marine conditions of TBMLM.

### 6.9.2 TST3 microbial rich Medium-bedded facies

In the Middle Oxfordian of Iraq, the shallow-water Najmah Formation was deposited along the west bank of the Tigris River (Figure 5.1), whereas the condensed basinal Naokelekan Formation was deposited at the east of the river and in the basin centre (Bellen et al., 1959; Buday, 1980; Jassim and Goff, 2006). After Sb3, further marine transgressions occurred in the study area. The TST3 is represented by a medium-bedded part of the TBMLM which is rich with deep-sea microbial filaments and coccoliths (Figures 6.4, and 6.5)

According to Droste (1990), J50 was a mfs of the Middle Oxfordian age (Figure 6.1), determined by *Perisphinctes plicatilis* ammonite zone, in the AP during this span of time. It is well represented within the lower Hanifa Formation in the subsurface of offshore Qatar and the upper Tuwaiq Mountain Formation of onshore Abu Dhabi (De Matos and Hulstrand, 1995; Sharland et al., 2001). However, the J50 mfs Middle Oxfordian was not recorded in the studied area. It is likely that the mfs of the AP does not directly relate to the eustatic sea-level curve, being somewhat localised in the AP, based on ammonite ages within the thick-bedded mottled member which continued deposition in the study area without any interruption. Although at most localities across the AP shale source rocks were deposited during Middle Oxfordian, ammonite fossils suggest that the condensed carbonate facies was deposited during this period instead of shale facies. The impact of mfs J50 on the Naokelekan Formation appears minimal. It is interpreted that the condensed facies extended from Lower to Upper Oxfordian strata, and the MFS3 perhaps occurred earlier than the mfs of J50 of the AP. The mfs of J50 is interpreted as a sequence that was driven by a combination of subsidence and eustasy.

### 6.9.3 HST3 Mottled facies

The HST3 developed during the formation of the upper part of the thick-bedded mottled limestone member (TBMLM), which is characterised by massive bedding. The TBMLM may represent the most controversial member of the Oxfordian deposition in the study area. It generally comprises microbial stromatolite overgrowths on ammonite shells, bioturbation, encrusting foraminifera, coccoliths, and oncolites (Figure 6.3). Bioturbation and oncolites seem to increase upward. The basin analysis study suggested a condensed facies within a mottled facies (see Chapter 7). Impact of relative sea-level falls that affected the carbonate platform top elsewhere on the AP is not clear in this member in the study area, most likely because they accumulated in deep-water where depth and energy changes related to relative sea-level cycles had little or no impact.

Martire (1992) proposed that the condensed pelagic successions usually deposit during periods of HST when a slowed down current activity allows the preservation of the pelagic input, and the lowstand may generate hardgrounds as a result of acceleration winnowing prevented deposition. The depositional history of the Naokelekan Formation is characterised by slow wholly pelagic sedimentation, probably subjected to sweeping by current action. Much evidence suggests the pelagic environment of TBMLM, and the likely palaeobathymetry is few hundred metres for the condensed strata in the Naokelekan Formation.

## 6.10 Depositional sequence 4 (Late Oxfordian–Late Kimmeridgian)

### 6.10.1 Sb4

On top of the mottled member, some horizons of the microbial stromatolite overgrowth on ammonites are characteristic of hardground surfaces, associated with a hiatus and a low rate of sedimentation. The top of mottled facies, which shows hardgrounds and many bioturbation intervals represent the Sb4. Low rate of sedimentation and hardground is indicated by dense microbial growth on ammonites and horizons of mass ammonite accumulation. Reolid et al. (2010) suggested a close relationship between hardgrounds and condensed facies. The hardground surfaces of the TBMLM include encrusted ferruginous layers, deep-marine, stromatolites, and oncoids with a core that mainly comprises ammonites and/or pelagic calcareous clastics. Based on Martín–Algarra (2000) stromatolite overgrowths on ammonites usually occur on in starved basins and on bathymetric highs, and they represent discontinuity and break in sedimentation periods. The Sb4 may be the equivalent to the Early Kimmeridgian sequence boundary. The last facies of Naokelekan argillaceous limestone may represent the onset of a new sequence. The bedding surface at the top of the TBMLM could be a combined sequence boundary and maximum flooding surface, based on the following considerations: (1) The lowstand systems–tract facies of the TBMLM may generate horizons of the microbial stromatolite overgrowth on ammonites as a result of accelerated winnowing prevented deposition, the action of currents can be clearly seen on oncolites. (2) Presence of calcispheres in the last facies of the Naokelekan Formation, the argillaceous limestone, may suggest the beginning of a new transgressive period.

### 6.10.2 HST4 calcispheres-rich facies

The break–up of the depositional basin of the AP peaked during the Early Kimmeridgian when several isolated intra-shelf basins and sub-basins developed (Sharland et al., 2001) (see Chapter 2). The field observations show that the uppermost part of the Naokelekan Formation is locally represented by calcispheric argillaceous limestone, and is characterised by euxinic environments. The abrupt change from well-aerated to anoxic conditions may suggest a tectonic control. Lyons et al. (2003) observed that the abrupt transition from well oxic to anoxic condition occurred in response to increasing productivity resulting from the rise in sea-level and corresponding increase in surface water nutrient availability. The blooms of calcispheres appear to correlate with the sea-

level rise when a widespread oceanographic change took place, which coincided with a global change observed in the oceans (Dias–Brito, 2000; Wilkinson, 2011).

mfs 60 is well recognised in the upper part of Hanifa Formation in Saudi Arabia and Abu Dhabi, where the shales of the Hanifa Formation overlie anhydrite formations (Droste, 1990; De Matos and Hulstrand, 1995). The HST4 and MFS4 in the study area are comparable to the mfs 60 of the Early Kimmeridgian of the AP. According to Aigner (1989) the topography of the passive margin basin was responsible for the deposition of prolific source rocks in the Late Jurassic of Eastern Arabia. A major rise in eustatic sea-level during the late Oxfordian could be the main cause of the development of this Hanifa intrashelf basin (Aigner, 1989). High organic content in the Early Kimmeridgian tended to be deposited in the deepest part of the basin under anoxic conditions that supported preservation of organic matter.

### **6.11 Problematic boundary between Early and Middle Kimmeridgian**

As it was described in the Chapter 4, the argillaceous limestone member (ALM) of the topmost of the Naokelekan formation assumed to be Early Kimmeridgian, is overlain by a sabkha facies of the Barsarin Formation of Middle–Late Kimmeridgian age. Palaeogeographic changes from Lower to Middle Kimmeridgian successions, which represent an abrupt shift from basinal to sabkha environment, are considered problematic in sequence stratigraphy. The current study supports previous investigations that showed a change from pelagic environment of Early Kimmeridgian to the shallow sabkha of Middle Kimmeridgian that occurred through a few metres with no unconformities or stratigraphic interruption.

The top bedding surface of the Lower Kimmeridgian strata of the ALM, which was deposited in a basinal environment, does not show any indication of subaerial exposure, and the subsequent Middle Kimmeridgian Barsarin Formation sabkha facies overlies the ALM across a sharp contact. The boundary between ALM and the base of Barsarin Formation Sb5 can be considered as a second major sequence boundary. This study of the TBMLM boundary surface Sb4 provides evidence for hardground development and deep-sea microbial stromatolite overgrowth and accumulation of a typical ammonitico rosso facies with a possible associated hiatus (see Chapter 7). The appearance of oncolites near the top of mottled facies may represent an increase in energy, and it can be assumed that higher–energy conditions could mean shallower water. However, the fall in relative sea-level during Sb5 is more unequivocal because the Barsarin Formation

includes many desiccation features such as, mud-cracks, tepee structures, nodules gypsum (chicken-wire), and dissolution collapses.

Considering the comparison diagram between the eustatic curves of Miller et al. (2005) and the relative sea-level constructed here, no correspondences between the eustatic curve and Naokelekan can be seen. According to Miller et al. (2005), the eustatic sea-level shows a rising tendency over the Middle–Late Jurassic, whereas the general trend of the study area shows clear 2nd order shallowing-upward sequences during this time (Figure 6.1). Abrupt facies change, deepening and shallowing trends are therefore more likely due to tectonic control, rather than the response to eustatic sea-level changes. One possible interpretation is uplift during the Early Kimmeridgian period.

#### 6.11.1 HST5 Sabkha facies

The Middle–Late Kimmeridgian represents the almost final stages of infill of basins generated after the Toarcian rifting. Both the Arabian and Gotnia Basins are characterized in this interpretation by repetition of several shallowing-upward cycles (Figure 6.5). Generally, the Barsarin Formation (see Chapter 2), includes nine shallowing-upward cycles in the type locality. However, in this interval, the Gotnia Formation in both Iraq and Kuwait with the Arab Formation D in most parts of Arabian Gulf is well known for four main shallowing-upward cycles. The cycles often comprise interbedded evaporite and carbonate strata, and halite often caps these cycles in southern Iraq, Kuwait and Saudi Arabia (Al-Silwadi et al., 1996; Yousif and Nouman, 1997). Both the halite and the carbonates, essentially represent HST sediments, capped by late HST to LST regressive evaporites.



### 6.11.2 The Barsarin sequence

A prominent characteristic of this sequence is the repetition of lithofacies representing shallowing-upward cycles. The numbers of repeated lithofacies in study area differ from one place to another. The contrast in cycle numbers among the various localities is significant, because if these cycles were forced by eustasy, or even by relative sea-level, we would expect to observe the same number on cycles. Thus, it can be concluded that this variation in cycle numbers is perhaps controlled by local fault block tectonics, or they are autocycles.

Generally, 6 to 9 cycles have been recorded that often display an arrangement starting with microbial laminate lithofacies (MLL) and passing upward into the blister flat stromatolite (BFLL) and then into thick-bedded dolomite–limestone lithofacies (TBDLL) (Figure 6.6). The shallowing-upward in the Barsarin Formation can be indicated by a marine sedimentation succession, which normally begins with a subtidal environment over an earlier supratidal sabkha facies. Marine regression results in a progradation, producing a profile comprising (i) MLL of subtidal environment, (ii) BFLL, of intertidal environment, and (iii) TBDLL, of supratidal environment. The shallowing-upward succession and facies association in the Barsarin Formation can be compared in many ways with the Trucial Coast sabkha model (for details see Chapter 5). The entire Barsarin Formation can be considered to be a 3<sup>rd</sup> order regressive supersequence, and it can be divided into two groups, where the lower group shows the blister–flat microbial dominance in an intertidal facies whereas the upper one is characterised by the appearance of domal stromatolite structures. These shallowing-upward facies have been called cycles by numerous researchers e.g. (Wilson, 1975; Goodwin and Anderson, 1985; Gani and Bhattacharya, 2007). However, shallowing-upward strata have also been called "parasequences" (Wilgus et al., 1988; Van Wagoner et al., 1990). The parasequence in its original definition is a regional metre-scale cycle with an upward–shallowing succession of facies bounded marine flooding surface. A marine flooding surface can be defined here as a lithological discontinuity with a sudden shift of facies that generally indicates an abrupt increase in water depth (Catuneanu et al., 2011).

Nine subdivisions of shallowing-upward high-frequency cycles with distinctive repetition of different facies, which may help lithological correlation, have been recorded in the Barsarin Formation. A complete cycle contains three different facies that show a shallowing-upward sequence (Figure 6.6). An ideal shallowing-upward high-frequency cycle is composed of three components:

1) Microbial laminite lithofacies at the basal surface overlain by subtidal facies that represents early TST.

2) Blistered–flat microbialite lithofacies of intertidal environment, representing the lower part of HST. The flat lamination microbialites are distinguished from blistered lamination by: (i) the flat textures are much richer than blister texture in evaporites as a sign of approaching to the upper part of intertidal environment (ii) the lack of pustular and fenestrae structures indicate that the flat textures are relatively located far from tidal influence comparison with blistered one. The sequence starts with blister then followed by flat one. Both textures formed by direct carbonate precipitation and trapped micritic particles, which were generated by fragmentation of algae in a subtidal environment.

3) Thick dolo–mudstones (TBDLL) with dominance of anhydrite of supratidal environment. The latest stages of HST are usually capped by thick unit of massive dolomite lithofacies, which is generally composed of low-permeability, evaporitic dolomite/limestone, and evaporite solution breccias mudstones, which characterised by including, length–slow chalcedony, chert nodules, evaporite pseudomorphs, and tepee with polygonal structures.

High-frequency sea-level fluctuations with climatically induced productivity cycles (Van Wagoner et al., 1990; Elder et al., 1994; Leyrer et al., 1999). The potential causative factors for high-frequency cycles have been a subject of controversy for several years (Moore, 2001; Emery and Myers, 2009). Based on Moore (2001) and Schlager (2005) two main mechanisms could be responsible for parasequences: 1) Milankovitch cyclicity, orbital perturbations force climate changes, where the growth and retreat of ice sheets can cause high-frequency eustatic cycles. 2) Subsidence in combination with normal sedimentation processes which could lead to high-frequency cycles termed autocycles (Schlanger and Jenkyns, 1976). Bosence et al. (2009) found that the variability of cycles from one location to another may suggest a tectonic control. So, active extensional faults may explain the difference in stacked peritidal cycle numbers in the Barsarin Formation from location to location.

Ginsburg (1971), James (1984), and Moore (2001) argued that the sediment source for tidal flat sedimentation might be covered by progradation of a tidal flat shoreline. Here, sedimentation will cease, but subsidence causes transgression and the cycle will be repeated. The repetition of different facies of several parasequences can be interpreted as transgressive–regressive periods. Disordered vertical successions could take place

when amplitudes of eustatic fluctuations are high, or when autocyclic processes dominate and accordingly drown the periodic external signal (Burgess, 2006).

Deposition of the first sequence at all localities in the study area, commenced by the formation of a relatively thick early TST of the parasequence and followed by the deposition of a late HST, are associated with progressive shallowing-upwards. The top of each cycle or the late HST is characterised by including evidence of subaerial exposure surfaces on top of the sequence. The polygonal cracks, tepee structures and evaporite minerals are considered here to represent deposition as part of late-stage HST, indicating a regressive fall in the relative sea-level capping the parasequence sets (Figure 6.6). The high-frequency cycles in the Barsarin Formation range in thickness from 0.5 to 4 metres. Some of the Barsarin Formation parasequences do not represent typical cycles due to the lack of one of the facies, so the quantitative analysis might be useful in future research (Burgess, 2016).

### 6.11.3 **Sb6**

The upper contact between the Barsarin and Chia Gara Formations could represent a combined sequence boundary Sb6 with maximum flooding surface between Kimmeridgian and Middle Tithonian strata. Strata at the top of the Barsarin Formation displays clear evidence for desiccation, such as tepee and polygonal mudcrack structures with many signs of evaporite pseudomorphs. At all localities, the Barsarin Formation is sharply overlain by basinal marine strata of the Chia Gara Formation. The Chia Gara Formation, Middle Tithonian–Berriasian comprises thin-bedded limestone and black shales, including ammonite and radiolarian fossils. This boundary could be a second drowning event which occurred between Kimmeridgian and Middle Tithonian age. The Chia Gara transgression covered a large area in Iraq, because the shallow-water and sabkha; the Gotnia Formation is also abruptly overlain by the basinal Chia Gara Formation.

## 6.12 **Summary**

Chapter five discusses the sequence stratigraphy of the latest Triassic to Jurassic successions in general and of the Middle–Late Jurassic in detail. Based on the evidence provided in chapters 2, 3, 4 and 5, this duration is divided into four depositional sequences of the third-order sequence which are as follows: the depositional sequence one consists of the latest Triassic to Early Jurassic Period, the depositional sequences two of the Middle Jurassic Period, the depositional sequence three of the Late Callovian–

Oxfordian and the depositional sequences four of the Late Oxfordian–Late Kimmeridgian.

The depositional sequence one corresponds to the Triassic–Jurassic boundary which coincides with the contact between Baluti and Sarki Formations. Studies point to a development as a thick palaeosol during the Rhaetian–Sinemurian. The depositional sequence two presents a drowning unconformity surface between the pelagic Sargelu Formation, which is rich in *Posidonia* and radiolarian fauna, and the evaporitic Sehkaniyan Formation strata of the pre-Toarcian platform. The depositional sequences two and three commonly contain pelagic facies such as *Posidonia* limestone, radiolarian bedded chert, and ammonitico rosso facies.

The sequence stratigraphic study confirms that there are no subaerial exposures within the depositional sequences two and three. The stratigraphic subdivision development in the study area that was continuously submerged, does not have clear sequence boundaries or other direct evidence for sea-level variations. Thus, the sequence boundaries are presumably a correlative conformity to successions of a sequence boundary unconformity on the platform top at western and shallower part of Gotnia Basin. The depositional sequences four focuses on sabkha Barsarin Formation. A prominent characteristic of this sequence is the repetition of lithofacies with shallowing-upward facies successions. The repetition of different facies of several parasequences is interpreted as transgressive–regressive periods.

Sequence stratigraphic analysis discovered incompatibility between the long-term eustatic curve of Miller et al. (2005), the regional sea-level changes of the study area and synchronized successions in different areas in the AP. It seems that the global sea-level change pattern shows long term deepening during Middle–Late Jurassic, whereas the general trend of the study area shows long term shallowing. This contrast is interpreted to be a result of the tectonic movement controls within a passive margin over sea-level fluctuation. Consequently, the eustatic signal is overprinted by a more dominant tectonic signal. Accordingly, the abrupt facies changes, and deepening or shallowing trends are likely due to tectonic control, rather than the response to eustatic sea-level fluctuations.

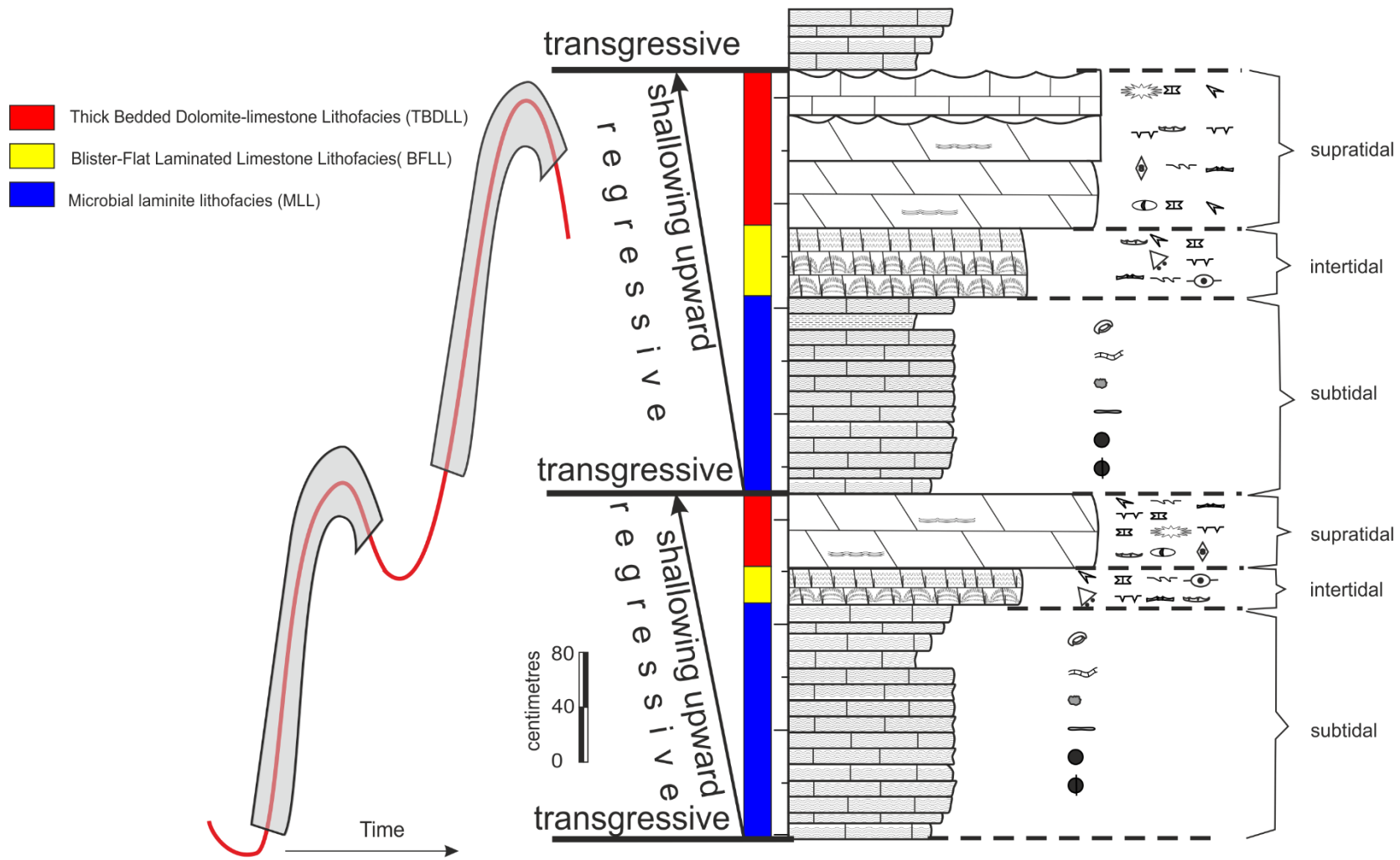


Figure 6.6: Diagram showing typical shallowing upward succession of two selected cycles of the Barsarin Formation with their relationship to fluctuating of sea-level.

## *CHAPTER SEVEN*

### *7 ANALYSIS OF A CONDENSED INTERVAL ON A NEOTETHYAN MARGIN: IMPLICATIONS FOR BASIN EVOLUTION*

## 7.1 Aims

In Chapter 4, the thick-bedded mottled limestone member (TBMLM) of the Naokelekan Formation was interpreted to be deep-sea microbial stromatolites with low sedimentation rate leading into condensation. This chapter aims to:

- Study and understand in detail, which processes control condensed facies formation in the Naokelekan Formation.
- Demonstrate that this condensed facies could be explained by tectonic controls, eustatic sea-level change, sediment supply and production and/or current activities.
- Suggest potential relations between these variables by outlining a comprehensive conceptual model that may be useful for the interpretation of condensed facies of the study area.
- Decipher the causes of the ammonitico rosso formation in condensed successions in the study area, and find an appropriate analogue in this respect.

Chapter 7 is divided into four main sections. The first section is an introduction, which briefly describe the relationship between different facies and defines the condensations. The second section discusses palaeobasin setting, tectonic development and provides examples of bathymetric highs as a potential model. The third section conducts an overview of the nature of microbial stromatolite overgrowth on ammonites to produce "ammonitico rosso," and discusses the factors that control condensed facies such as low sedimentation rates, palaeocurrent, and paucity of planktonic organisms. The final sections discuss issues related to depth and climate control and the Naokelekan and Barsarin Formation boundary.

## 7.2 Introduction

The Late Jurassic Naokelekan Formation of Kurdistan characterized by condensed intervals, is equivalent to the subsurface Najmah Formation (Figures 7.1 and 7.2). The depositional environment of the condensed facies of the Naokelekan Formation has been described and interpreted in detail in Chapter 4. In summary, the Naokelekan Formation is regarded as a key organic-rich Jurassic succession in Iraq and surrounding countries (Buday, 1980; Jassim and Goff, 2006; Aqrabi et al., 2010), and it has been considered an important source rock for the petroleum system in Iraq. Although the depositional environment of the Naokelekan Formation is characterized by pelagic sedimentation, the topmost part of the thick-bedded mottled limestone member (TBMLM), and the base of medium-bedded microbial-bearing limestone member

(MBMLM) include evidence for relatively shallow environments such as oolites and oncolites. Deep-sea microbial stromatolite overgrowths on ammonite shells, oncolites, bioturbation, encrusting foraminifera, coccoliths, and calcispheres represent the most distinctive features of the Naokelekan Formation, which can be prominently observed at all localities throughout the study area ( Figures 4.3). In the studied Naokelekan Formation outcrops, five members have been recognised (Figure 4.3). From bottom to top of the formation, these are as follows:

1. Black shale member (BSM)
2. Carbonaceous limestone member (CLM)
3. Medium-bedded microbial-bearing limestone member (MBMLM)
4. Thick-bedded mottled limestone member (TBMLM)
5. Argillaceous limestone member (ALM)

The Najmah Formation was first described from the Najmah well in the Foothill Zone (Bellen et al., 1959) (Figure 7.2), and the formation exists in Mesopotamia and Stable Shelf Zones as well (Figure 7.1). In contrast to the Naokelekan Formation, the Najma Formation is relatively thick, and the total thickness of the formation could reach up to 485 metres in the southern depocentres (Figure 7. 2, B). The Najmah Formation represents a calcareous neritic facies with episodic intercalations of lagoonal facies (Buday, 1980). Based on Jassim and Goff (2006) the formation can be divided into four parts; these are in ascending order: i) fine-grained, featureless, recrystallized limestones with relict fauna or oolitic grains, ii) oolitic and pseudo-oolitic limestones with an abundance of macrofossil debris; iii) coarsely crystalline dolomites; and iv) fluffy-textured limestones with thin anhydrite layers intercalation, and in some subsurface sections thin units of black shale are present.

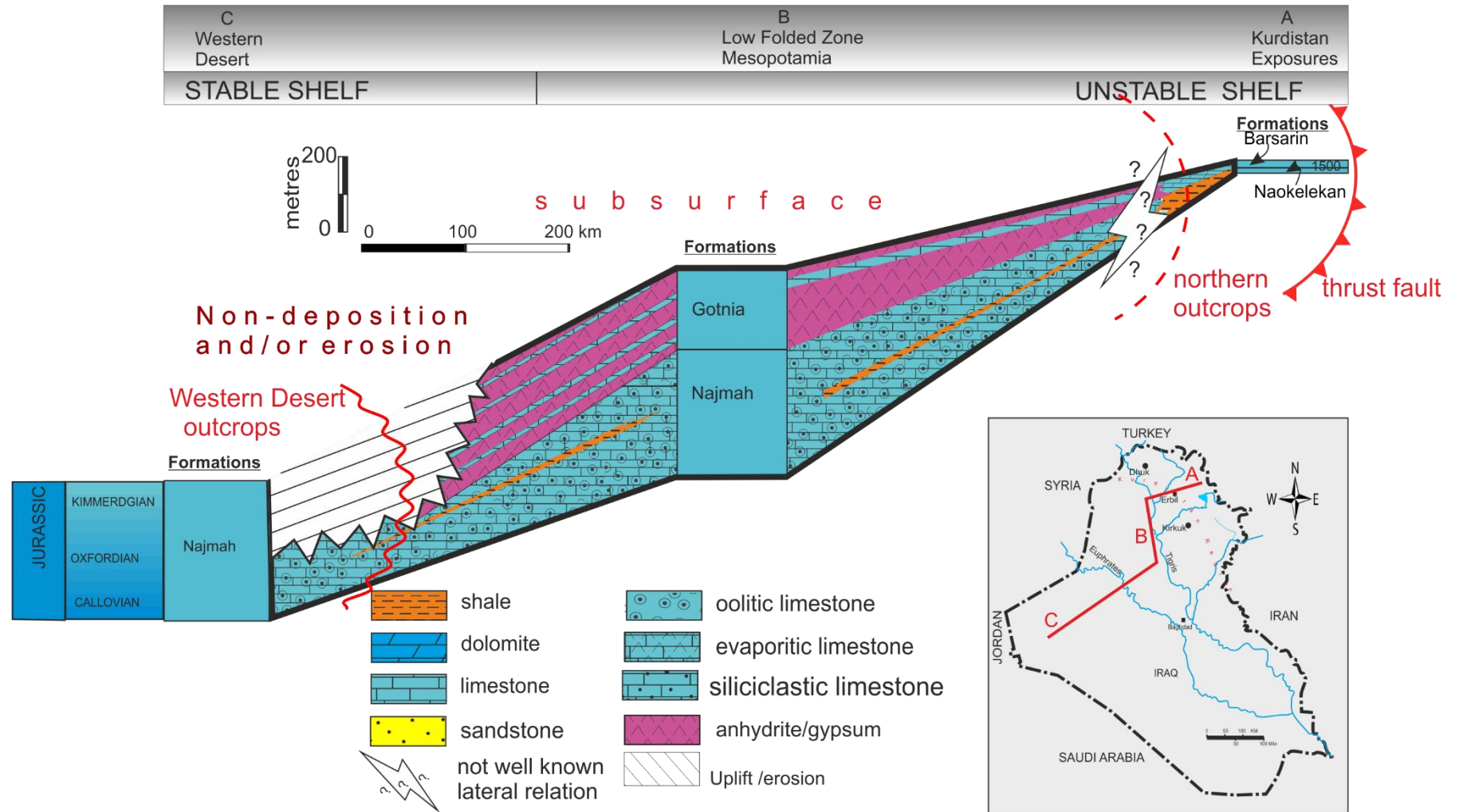


Figure 7.1: Diagram showing poorly understood lateral facies changes from Naokelekan to the subsurface section of Najmah Formation. Note thrust fault at northeast and erosion at southwest resulted in ambiguity in the basin-margin.

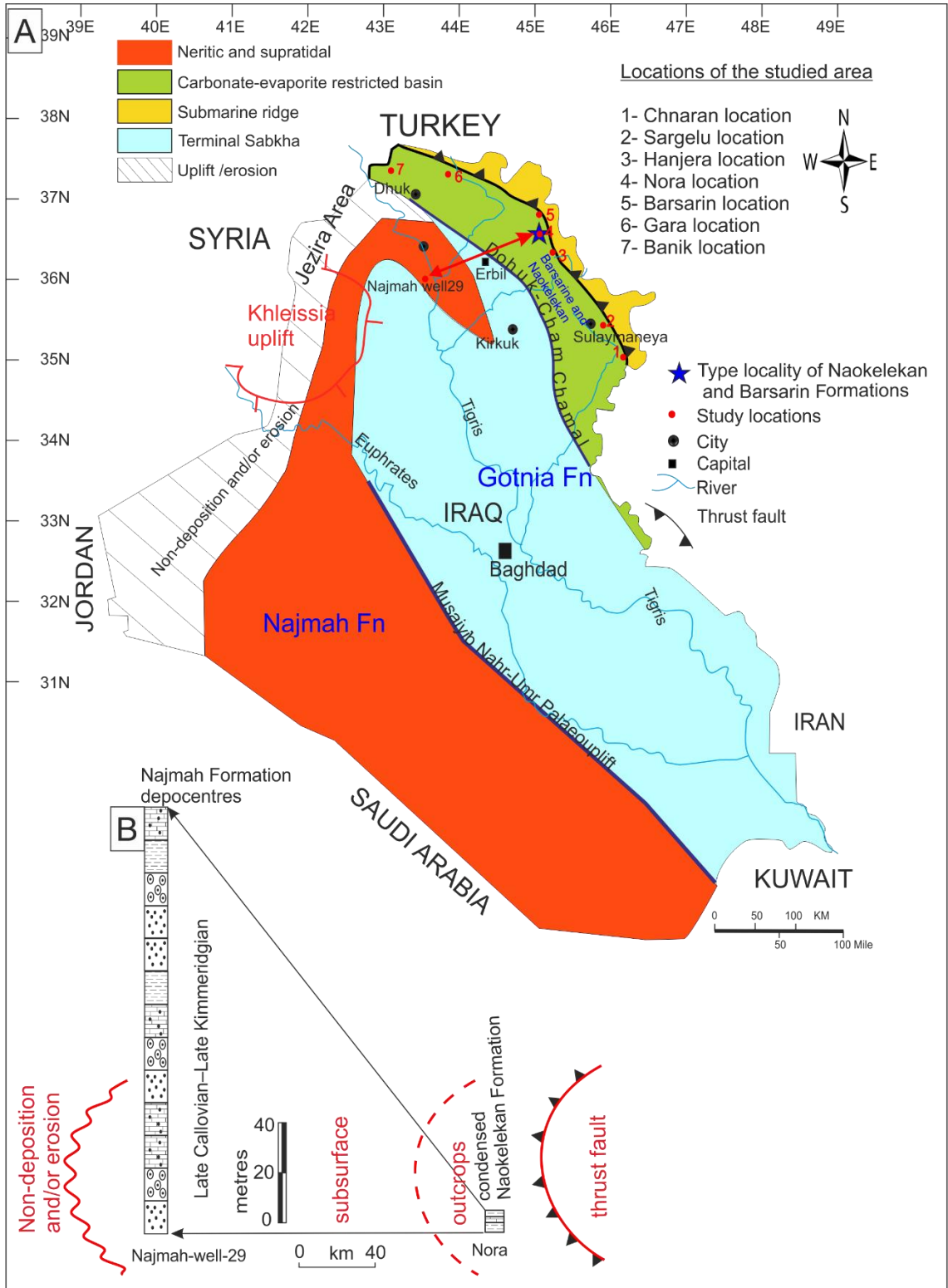


Figure 7.2: A; The palaeogeographic of Late Jurassic of Iraq, after Jassim and Goff (2006). (B) Correlation between condensed Naokelekan and Naimah Formations.

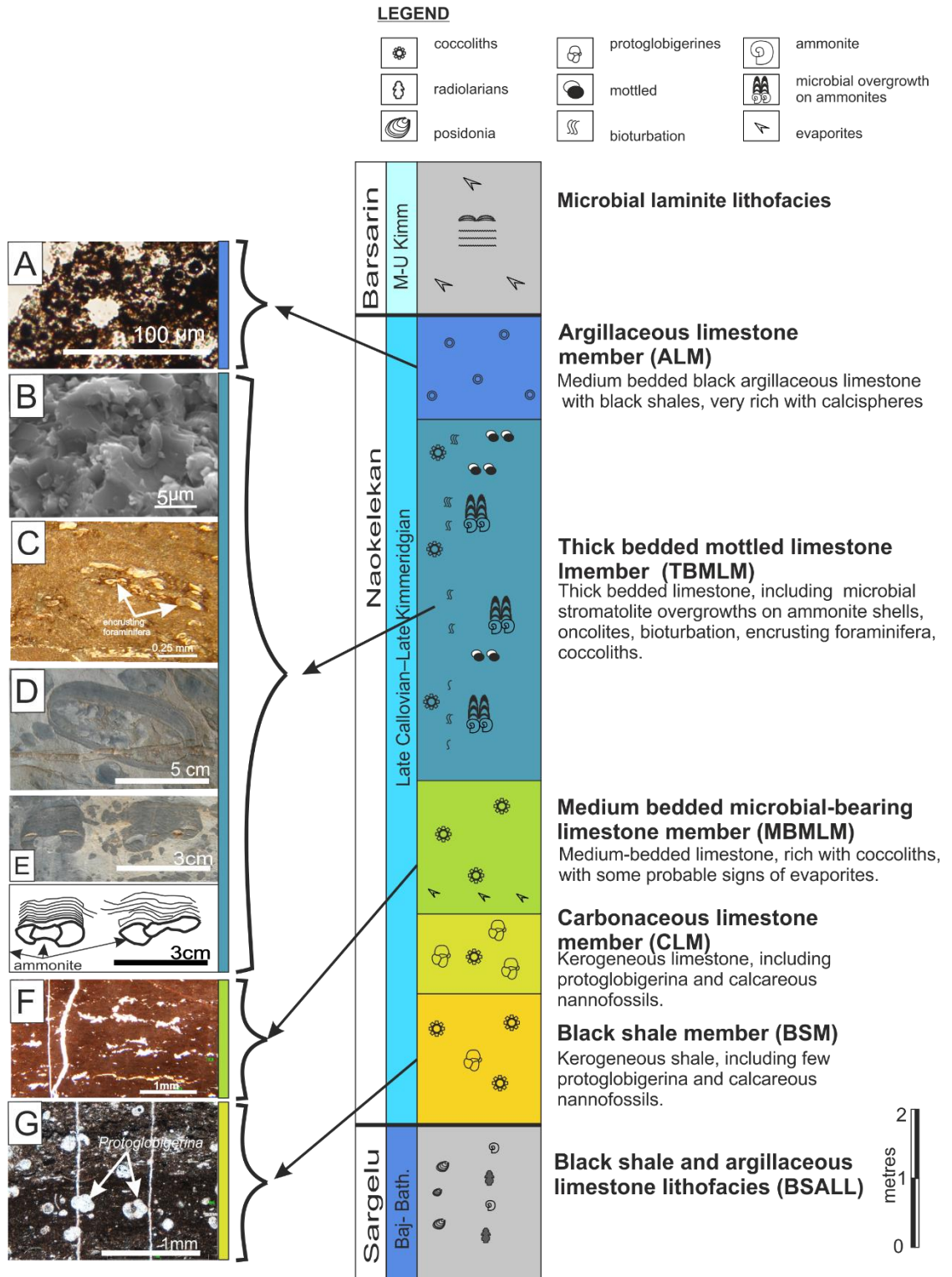


Figure 7.3: Simplified stratigraphic column of the Naokelekan Formation showing different lithofacies and the nature of underlying and overlying contacts with Sargelu and Barsarin. Left column represents the different characteristic feature for each lithofacies, and they are: (A) calcispheres, (B) coccoliths, (C) encrusting foraminifera, (D) oncolites, (E) microbial stromatolite overgrowth on ammonite shells, (F) signs of evaporites, and (G) *Protoglobigerina*.

Two main problems arise when studying Middle–Upper Jurassic palaeobasin of Iraq where neither Gotnia Basin margin, nor lateral relationships between different formations are observed. So far, lateral facies changes from Najmah to Naokelekan Formations are very poorly understood (Figures 7.1 and 7.2 ). Ditmar and the Iraqi–Soviet Team (1971) suggested that a significant lateral facies change is most likely located 50 km east of Kirkuk city, which may coincide with the Chemchemal–Dhuk palaeo uplift (Figure 7.2 A). The geometry of the palaeobasin is unclear due to uncertainties of location of both western and eastern margins of the Gotnia Basin (Figure 7.2 A and B). The western margin of the basin was exposed to erosion during the Neocomian Uplift (Numan, 1997; Aqrawi et al., 2010), when large areas around the Khleisia High were uplifted (Figure 7.2 A). Accordingly, the Najma Formation was partially or completely eroded at the western margin of the basin and unconformably overlain by the Aptian successions. Furthermore, the location of the northern margin is completely unknown because of overthrusting of an ophiolite complex onto the Jurassic succession during the Cretaceous–Neogene period (Figure 7.2 A).

The Naokelekan Formation is one of the thinnest formations in the Jurassic of northern Iraq (Bellen et al., 1959). The formation rarely exceeds 14 metres in thickness and covers an age span from the Late Callovian to the Early Kimmeridgian, i.e. more than 10 m.y. Even corrected mechanical compaction and chemical or pressure solution, the average sedimentation rate for the whole formation is only a few millimetres per ky. Spath (1950) studied the Late Jurassic ammonites of northern Iraq and first suggested the possibility of a significant time gap between the base of the Chia Gara and top of the Sargelu Formations, i.e. the time span between Callovian and Lower Tithonian. Spath (1950) also first suggested the presence of a depositional hiatus or maybe breaks within the Naokelekan Formation, most likely on the top of the TBMLM. Therefore, the mottled member may comprise numerous coalesced condensed sections, which form a composite condensed section.

Bellen et al. (1959) in their original work in the Kurdistan region recommended reviewing previous studies and pointed out that further detailed studies are necessary to identify the causes of condensation. However, very few studies were carried out to reveal the nature and causes of condensed intervals, and to determine their depositional setting. Recently, Jassim et al. (1984), and Aqrawi et al. (2010) have assumed that the sedimentary successions of the Naokelekan and Barsarin Formations were deposited in a starved basin.

### 7.3 Condensation facies

Condensed facies are generally defined by a strongly reduced stratigraphic record and are often associated with marine hiatuses. Condensed facies might be expressed as a period of high pelagic fossil concentration, or as a hardground caused by lithification (Jenkyns, 1971; Fels and Seyfried, 1993; Flügel, 2010). Condensed strata can occur for many reasons, including: low sedimentation rates during transgression, or sediment starvation during platform drowning. Low sedimentation rates could also occur on a faulted or elevated bathymetric high as a result of the lack of terrigenous influx, current sweeping and reworking sediments.

- **Condensed section related to transgression;** it is characterised by sediment starvation and by essential marker horizons in the sequence stratigraphic architecture of a basin. The condensed sections usually appear as thin marine horizons and commonly show pelagic to hemipelagic sedimentation, burrowed horizons, presence of apparent hiatuses, and hardgrounds. Furthermore, they may include authigenic minerals, such as glauconite, siderite, phosphate, or high faunal abundances. Deposition of organic-rich shales with high gamma readings is typical of many condensed sections (Loutit, 1988; Catuneanu, 2006; Messina et al., 2007; Bjorlykke, 2015). This description is generally applicable to siliciclastic depositional basins with standard physiography of the shelf–slope–basin.
- **The condensed facies on the bathymetric highs;** Because of the high topography, usually, this kind of condensed carbonate facies lacks siliciclastic input. Condensed facies developed on bathymetric highs, was common during Jurassic rifting and breakup of a continental mass in the Neotethys. Episodes of hiatus and low deposition rate usually interrupt this facies, which are expected to have a strong relationship with ammonitico rosso facies phenomenon. The ammonitico rosso facies is well-defined in the Jurassic of the European epicontinental areas and in the southern margin of the Neotethys, and it is characterized by combination between ferruginous oncoids, ammonites, coccoliths, intense bioturbations, hardgrounds, and microbial stromatolites facies (Figure 7.4) (Jenkyns, 1974; Pallini and Schiavinotto, 1981; Winterer and Bosellini, 1981; Massari, 1983; Stampfli et al., 1991; Cecca et al., 1992; Martire, 1992; Monaco, 1992; Bohm and Brachert, 1993; Santantonio, 1993; Zempolich, 1993; Winterer and Sarti, 1994; Norris and Hallam, 1995; Rojay and Altiner, 1998; luczynski, 2002; Dromart et al., 2003; Gill et al., 2004; Cecca et al., 2005; Reolid et al., 2005; Martire et al., 2006; Rais et al., 2007; Reolid and Molina,

2010; Reolid et al., 2010; Reolid and Nieto, 2010; Massari and Westphal, 2011; Vörös, 2012).

The condensed intervals in the study area are characterised by deep-sea microbial stromatolite overgrowths on ammonite shells with oncolites, which makes up a major constituent of ammonitico rosso facies (Figure 7.3 D and E). Although the condensed ammonitico rosso facies have been widely studied in Europe, the local geologists of Iraq and surrounding areas are unfamiliar with this kind of facies. This facies seems to be comparable in many respects to the thick-bedded mottled limestone member of the Naokelekan Formation such as deep-sea microbial stromatolites, oncolites, hardgrounds, and facies association with *Posidonia* (Figure 7.5). There are many possible scenarios which can explain the development of condensed facies. In the next sections, different cases of condensation are discussed from a theoretical point of view as well as by a comparison with the actual well-documented Jurassic succession of the northwestern Neotethys Ocean.

In southern Iraq and Kuwait, a condensed argillaceous organic-rich limestone unit within middle part of Najmah Formation was reported as well, but its relationship with ammonitico rosso of TBMLM is unclear (Yousif and Nouman, 1997; Sadooni, 1997; Strohmenger et al., 1998). This unit suggests that parts Najmah Formation were probably deeper than the traditional shallow-water facies as described at its type locality (Bellen et al., 1959), and it is more likely related to similar environmental condition of the Naokelekan Formation (i.e. basinal facies). This suggests that the condensed facies could extend far southward, and further investigations may be needed to determine the nature of Najmah Formation.

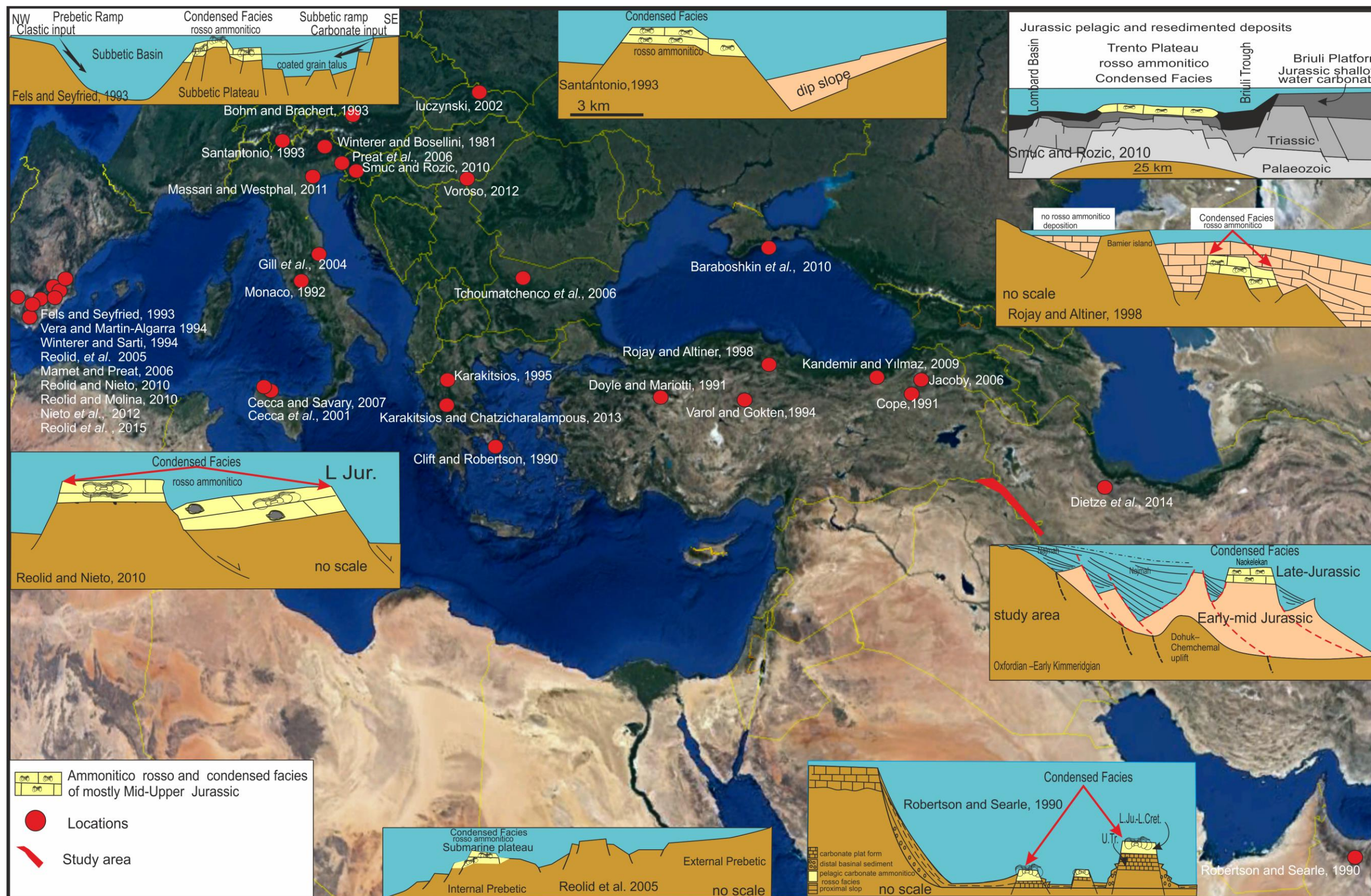


Figure 7.4: Distribution of the rosso ammonitico and condensed facies across Northern Neotethys Ocean. Note growing of condensed facies over the bathymetric highs in passive margins.

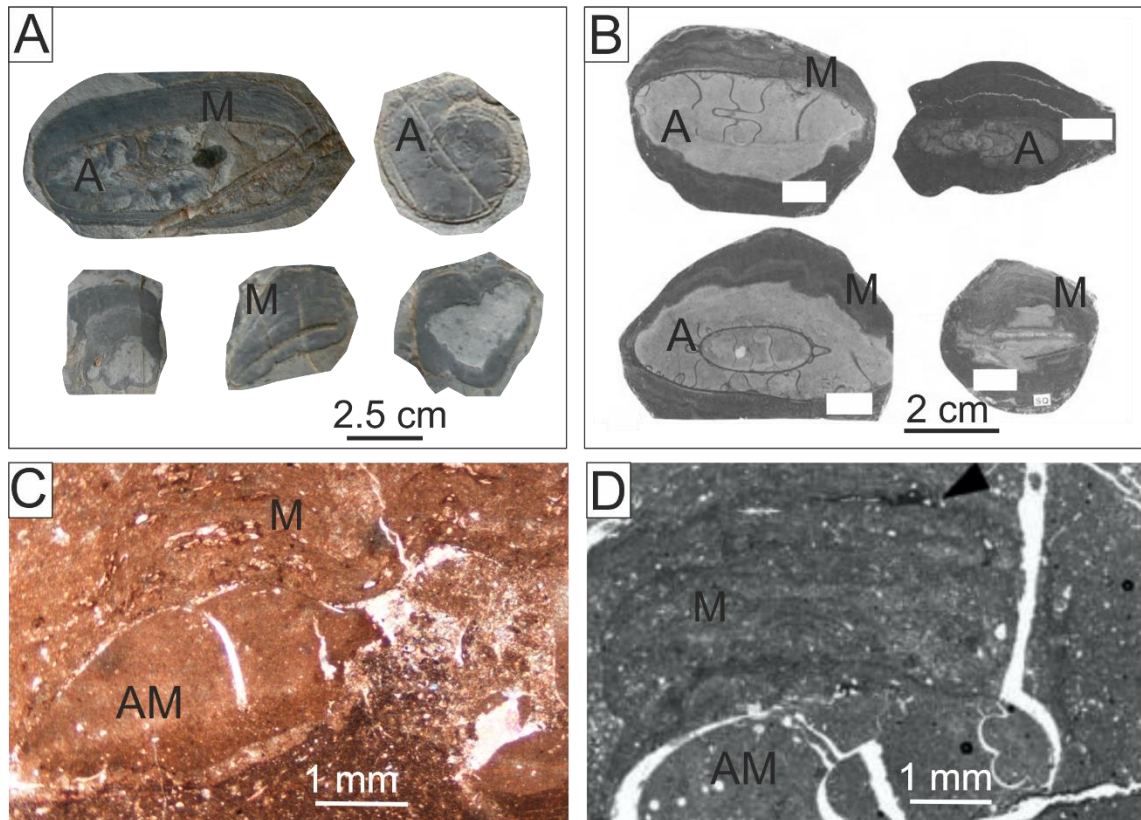


Figure 7.5: (A) Oncoids in the thick-bedded mottled limestone unit TBMLM, Naokelekan Formation. (B) Oncoids of the Betic Cordillera, Southern Spain, modified from Vera and Martín-Algarra (1994). Both (A and B) photos show oncoidal structure of the pelagic microbial stromatolites (M) with cores formed by ammonite shells (AM). Note the striking similarity between the two studies.

(C) Photomicrograph showing microbial overgrowth on ammonites in the TBMLM, Naokelekan Formation. (D) Microbial overgrowth on ammonites, Middle Oxfordian lithofacies in the Prebetic Zone, Betic Cordillera, southern Spain (Reolid et al. 2010). Note the similarity between Photomicrograph of C and D as well. Both photos are PPL.

## 7.4 Condensed facies and tectonic setting

The condensed facies could occur either on (1) starved basin floor or (2) bathymetric high.

### 7.4.1 Starved basin floor

Condensed facies can occur in a sediment starved deep-sea basin floor. Deep-sea carbonate starvation, which led to the condensed facies development, could occur through trapping of sediments by sub-marine barriers, sweeping by currents, and/or low carbonate production as a result of sea-level fall. However, there are some basic differences between the bathymetric high and starved basin floors, which need to be taken into account; they are: (1) the ammonitico rosso facies has been always reported

on bathymetric high, whereas condensed sediments in starved deep basin floor lack ammonitico rosso facies, and no reports have recorded yet (2) Robertson et al. (2016) argued that the starved basins are characterised by hemipelagic and eupelagic sedimentation, discontinuously, and are affected by resedimentation or gravity–flow deposits events bringing material from nearby elevations, whereas no gravity–flow deposits can occur bathymetric high (3) The starving basin floor does not show large lateral variation in thickness with adjacent sections such that occur between graben and horst, whereas the lateral differentiation in thickness with adjacent sections is quite prominent in the bathymetric high. Hence, as condensed Naokelekan Formation lacks gravity–flow deposits, and exhibits lateral variation in facies and thickness, the possibility of being a condensed of starved deep-sea basin floor is low.

#### 7.4.2 Bathymetric high

The palaeotopography is perhaps the predominant controlling factor in formation of condensed intervals. Previous researchers agreed that the condensed and/or ammonitico rosso ammonite-rich carbonates occur on structural highs bounded by submarine troughs (Cecca et al., 2005; Reolid and Nieto, 2010; Reolid et al., 2015). The bathymetric high have been reported with a different nomenclature, such as pelagic swells, seamounts, pelagic ridges, deep submarine horsts, submarine plateau, and/or tilted blocks (Figures 7.4 and 7.6). For example, Misik (1993) and Cecca et al. (2005) pointed to condensed deposition on the swells, whereas Martire (1992) stated that the condensed facies deposited on the isolated plateau, but based on Jenkyns (1971) the condensed pelagic limestone of Sicily may be occurred seamounts. In spite of different terms, the condensed facies on the various high palaeotopography structures seems to share lithological characteristics, where they are characterised by hardgrounds encrusted by ferromanganese nodules with stromatolitic overgrowths on ammonite shell (Figure 7.6). Devleeschouwer et al. (2002) confirmed high-elevation submarine topography that originated either as a volcanic seamount, pelagic swells, or as tectonic fault–bounded rises, which can lead to condensed pelagic cephalopods limestone formation as well. The great challenge here is determining the kind of bathymetric high, and also to reveal the reasons that led to the condensation.

### 7.5 Tectonics

The Neotethys started to open and broaden up in the Late Permian, and the ocean continued to expand progressively into the Jurassic period along the southern part of Europe and eastern side of Arabian Plate (AP) (Sharland et al., 2001; Ziegler, 2001).

Extensional rifting resulted in the formation of a passive margin at the eastern part of the AP, and many grabens, troughs and submarine plateaus were developed during Late Triassic–Late Jurassic Neotethyan Ocean. Accordingly, the Neotethys basin of Jurassic period was mostly segmented into many sub-basins controlled by tectonic faults (see chapter 2 for details). The compartmented basin of western Neotethys Ocean during the Jurassic maybe had many fault-bounded sub-parallel ridges and troughs. Winterer and Bosellini (1981), Martire (1992) Fels and Seyfried (1993), Misik (1993), Winterer and Sarti (1994), Martire et al. (2006) Rais et al. (2007), and Nieto et al. (2012) observed close relationships between tectonic activity and condensed facies, where the condensed facies have always developed on the swelled pelagic plateau, tilted faulted blocks, or submarine plateaus.

In the study area, no clear evidence of structural control on the Gotnia Basin was discovered, and no studies have provided convincing evidence that syn-rift extension and magmatism occurred during the Late Jurassic in Kurdistan Region. However, global plate tectonic reconstructions of the peri–Tethyan confirm rifting during Jurassic period (Ziegler, 2001; Stampfli et al., 2001; Stampfli and Borel, 2002). Furthermore, Studies in Oman and Iran introduced evidence supporting continental rifting with development of many fault-controlled bathymetric highs in the Arabian Plate margin (Fontaine, 1989; Robertson, 2007). So, in the current study, evidence is primarily from researchers elsewhere in Arabian Plate who had better structural data showing fault control persistent into Jurassic time. Evidence is as follows:

1. Normal faulting is documented in numerous field–based structural studies in Oman and Iran area (Robertson et al., 1990; Stampfli et al., 1991; Stampfli et al., 2001; Ghasemi and Talbot, 2006; Robertson, 2007). The faults represent Permian and Triassic–Jurassic rifting of the continental margin of AP, which created an extensive set of deep grabens separated by elevated horst blocks.
2. The association of magmatism during Triassic–Jurassic successions may suggest evidence of crustal thinning and rifting of Neo-Tethyan ocean crust. The extensional magmatism is well documented in Oman at the basement of the Hawasina Basin and the Sahtan Group, and it is also well characterized in Iran as well (Bechennec et al., 1990; Rabu et al., 1990; Glennie, 1992; Ziegler, 2001; Ghasemi and Talbot, 2006).

3. Ali et al. (2013) studied seismic stratigraphy and subsidence history of the United Arab Emirates rifted margin and overlying foreland basins. Based on the seismic results the Toarcian–Oxfordian represents syn-rift deposition.

Based on the previous arguments, it can be assumed that Gotnia Basin is probably controlled by syn-rift structure, which is formed by extensional processes similar to those occurred in Oman and Iran. So, Each Sargelu Naokelekan and Barsarin Formations could be syn-rift depositional sediment.

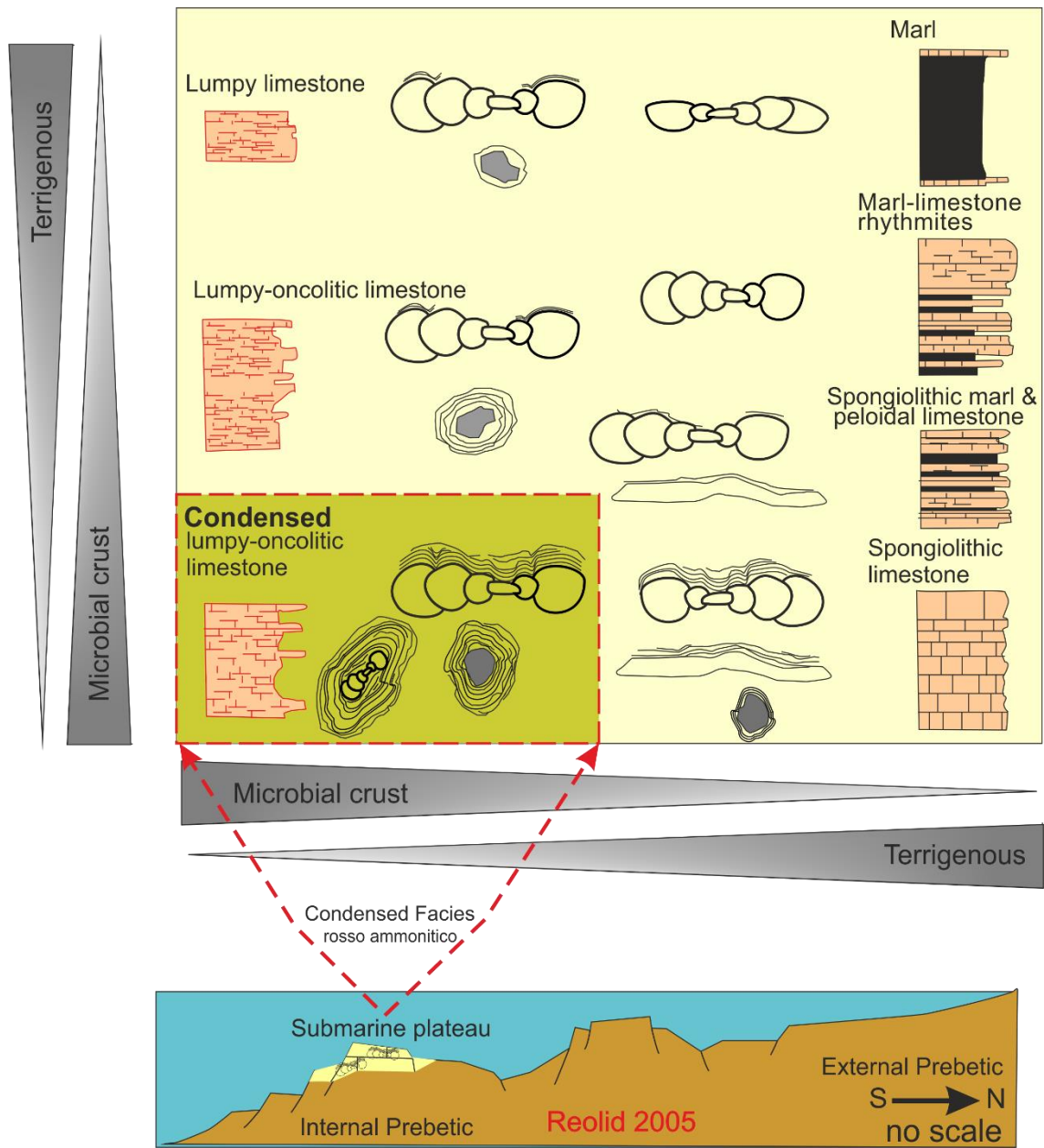


Figure 7.6: distributions and abundance of microbial rosso ammonitico on the intra Prebetic Zone, southern Spain during Middle Oxfordian - Lower Kimmeridgian. Note, the influence of the terrigenous influx in condensed facies formation, and the lack of terrigenous sedimentations were because of low rate sedimentation and isolated platform modified from Reolid et al (2005).

## 7.6 Evidence for fault controlled bathymetry

Burgess et al. (2013) found that there are different types of submarine palaeobathymetric high features such as isolated carbonate buildups (ICBs), erosional remnants, volcanoes, and tilted fault blocks. It has been argued that if studies have poor-quality two-dimensional data, it will be difficult to determine the identity of the bathymetry high structure because of the similarity between ICBs and non-ICB structures. For this reason, they analysed more than 230 two-dimensional seismic images in order to determine the possibility of using the seismic methodology to identify ICBs accurately. In the next sections, some identification criteria of Burgess et al. (2013) will be applied on the Naokelekan condensed facies to determine the type of bathymetric high, which are characterised by the following:

No erosional remnants and volcano palaeo-highs were observed or reported in the study area, so the bathymetric high could be either an ICBs or tilted fault blocks. Although Burgess et al. (2013) identification criteria were basically derived for seismic applications in order to distinguish ICBs from non-ICB features, the available data in the current study will focus only on regional and stratigraphic constrains. TBMLM of the Naokelekan Formation is characterised by:

1. The palaeolatitude during Late Jurassic was tropical.
2. Late Jurassic succession was appropriate for carbonate products (Figure 7.7).
3. Based on sequence stratigraphy the late Jurassic succession is occurred during a long term (1–10 m.y.) regressive trend.
4. No evidence available to confirm that the Naokelekan Formation was developed on the bathymetric high structural trend.
5. Siliciclastic input was consistently absent during all Jurassic period in the study area, which may suggest potential bathymetric high.
6. Condensed Naokelekan Formation is laterally adjacent to a thick succession of siliciclastic-carbonate interbedded facies.

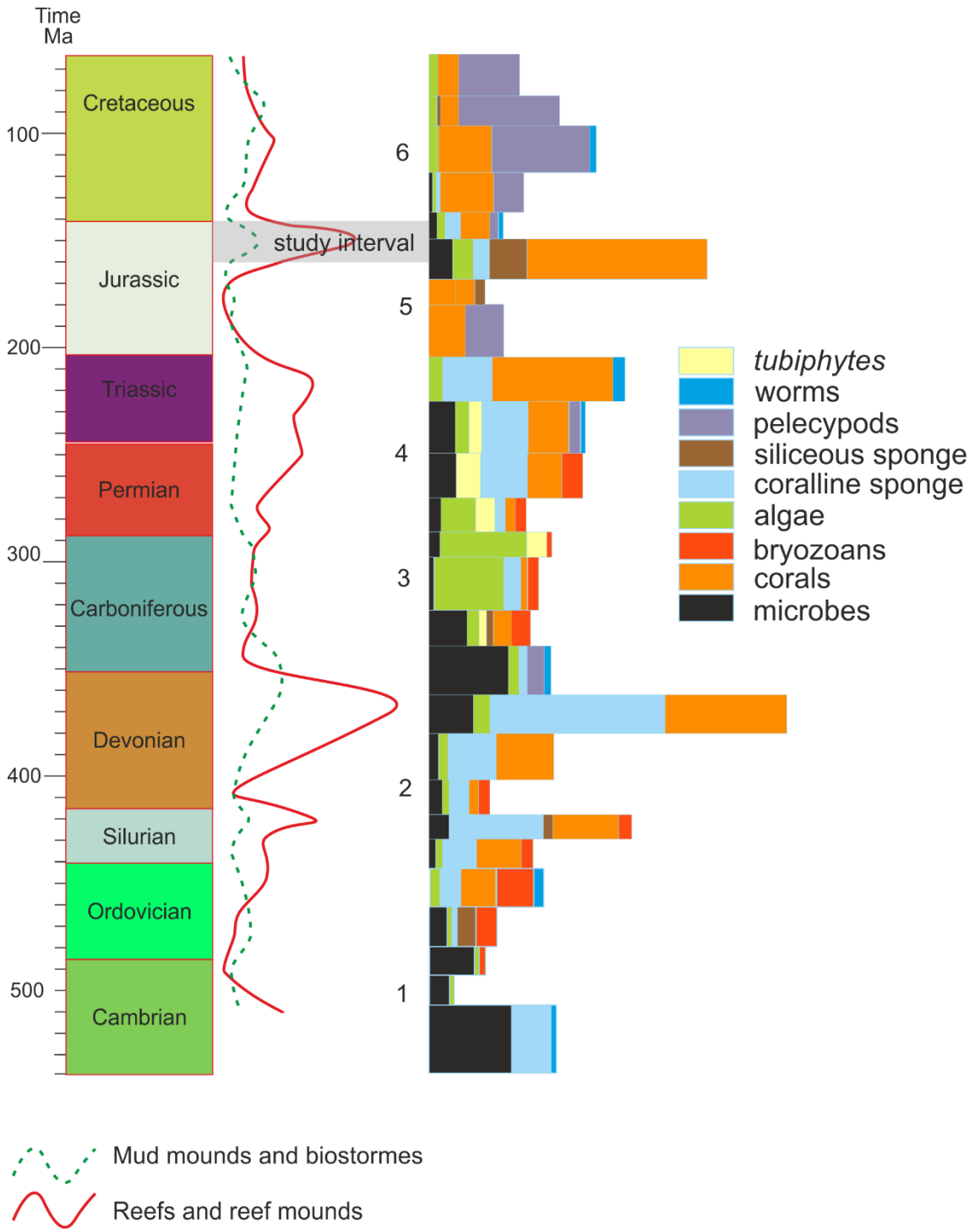


Figure 7.7: Diagram showing prevailing Phanerozoic reef types and reef builders. The left column represents cumulative curves of reefs and reef mounds and the number of mud mounds and biostormes from Cambrian to Cretaceous. Right column is the cumulative number of reefs in which a particular reef builder is prevailing, Modified from Kiessling et al. (1999).

Significant difference in thickness may suggest local difference in subsidence. Extensive thick sequence of sediment and its equivalent condensed sequence show a correlation between tectonic position and thickness; where the condensed units occur at tectonic high along the crests, whereas the thickest sections are downthrown of the fault (Chapman et al., 1978). The occurrence condensed facies juxtaposed to thick sequence, which is controlled by tectonic faults, is well presented in the seismic analysis of passive margin and extensional basins of Australia (Holford et al., 2013). The tectonic control could be assumed in the study area through the existence of condensed formation next to the depocentres, which may suggest subsidence creating high accommodation for Najmah in a graben, whereas condensed Naokelekan may deposit on a horst. Furthermore, Depositional succession in the Gotnia Basin was thicker at the eastern side than the western side during Early–Middle Jurassic. This pattern of the thickness distribution is distinctively reversed during Callovian to Kimmeridgian ages, which may be related into tectonic development change in the tectonic (Figure 7.1). For instance; both Naokelekan and Barsarin Formations of the eastern side of the basin, which their ages ranged from Late Callovian–Late Kimmeridgian, are about 35 metres in thickness. However, in the same span of time, Najmah and the Gotnia Formations were about 530 metres (Figures 7.1 and 7.2).

Additionally, Murriss (1984) pointed to the segmentation of the AP margin by rifting, and it has been argued that the Gotnia Basin partially separated from the main Neotethys Ocean by bathymetric highs. Accordingly, a series of the parallel basins adjacent to shallow platforms were developed. The basins comprise the southwestern shelf, the southern trough or the Gotnia Basin, and the eastern trough or Fares Basin, whereas the middle ridge or Kurdistan Block separates each of the Gotnia and Fares Basins. The difference in subsidence rates could occur by reactivation of basement fault, and this is compatible with geophysical study (Ali et al., 2013), who also stated that reactivated Permian Faults during Middle–Late Jurassic resulted in subsidence with syn-rift deposition in the AP. So the Middle–Late Jurassic reactivated fault control assumption could be accepted for interpreting the bathymetric high. Thus, as a principle, it can be assumed that the Permian faults were reactivated during Middle–Late Jurassic time as tilted fault blocks, and bathymetric highs were developed. In comparison to the ICBs the condensed facies shows depositional thinning relative to the adjacent area, whereas the ICBs demonstrates depositional thickening relative to adjacent carbonate strata. So, it can exclude ICBs as a palaeo bathymetric high for study area.

Bosence (2005) identified eight main types of tectonosedimentary environments within which Cenozoic carbonate platforms occur. Available evidence suggests that the study basin is best classified as fault-block platforms. This kind of platform mainly develops in marine rift basins, point to clear differentiation in thickness, where thicken in carbonate ramp stratigraphies down hanging wall dip slopes and thin onto footwall highs. Although the term bathymetric high seems to be most suitable, the previous argues suggests that the TBMLM can be considered as a kind of developed ammonitico rosso facies on fault-block platform or tilted fault block high. (Figure 7.8).

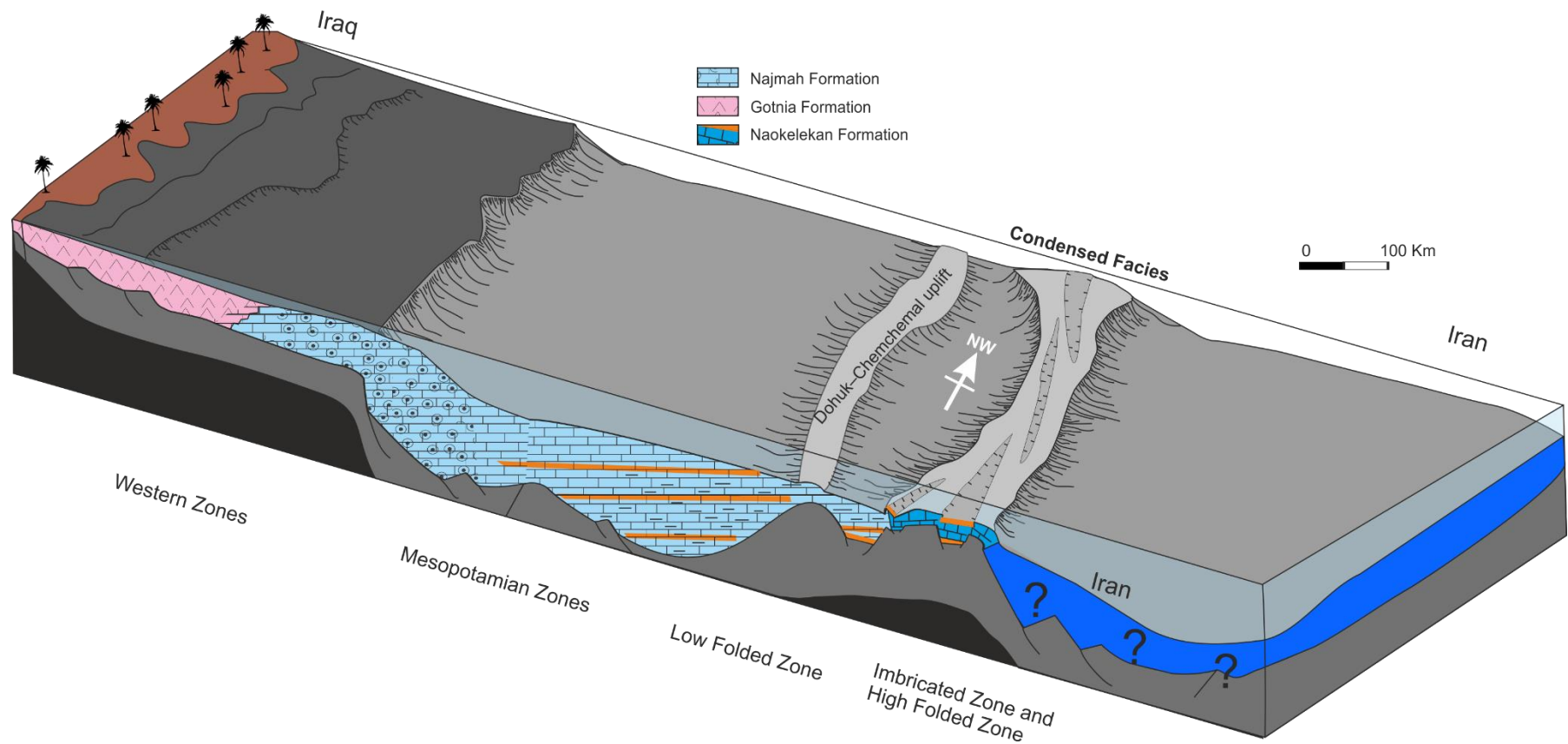


Figure 7.8: hypothetical model for fault-block platform of condensed facies in the Naokelekan Formation during Oxfordian. The condensed facies of the Naokelekan Formation, which is about 14 meters in thickness, was assumed to be developed on the bathymetric high. Synchronous deposition of carbonate and siliciclastic sediments of Najmah Formation, which is about 500 meters in thickness, also deposited in a short lateral distance from the condensed facies.

## 7.7 Eustatic and relative sea-level control

Besides the lack of compatibility between the eustatic curve of Miller et al. (2005) and the regional sea-level changes of the study area ( see section 6.6), a clear contrast can also be found by the effect of eustasy between synchronized successions in different areas in the AP with respect to the global scale.

**Incompatibility with the global eustatic curves:** Based on Miller et al. (2005) the global sea-level change pattern shows long term deepening during Middle–Late Jurassic. However, stacking patterns in the study area shows long term shallowing with a clear sudden transition from deep to shallow water in this time span (Figure 7.9). The following examples help to clarify the contrast in response to global sea-level change between Western Europe and Arabian Plate areas:

Norris and Hallam (1995) studied facies variations across the Middle–Late Jurassic boundary in Western Europe and the relationship to sea-level changes. Comparison of bathymetric curves from different regions led to identification of a regional sea-level rise across Western Europe during the Callovian–Early Oxfordian age, and this change has been considered to be eustatic in origin. In contrast to the Western Europe strata, in Saudi Arabia, Abu Dhabi, Qatar, Bahrain, and large areas of Iraq, strata record exposures during the Callovian (see Chapter 2). This hiatus due to RSL fall is also supported by widespread marine erosion in eastern Lebanon and Sinai, and the hiatus is well represented in Tuwaiq Mountain Limestone as well. Likewise, in north-western parts of the AP, Hirsch and Picard (1988) and Hirsch et al. (1995) introduced evidence that suggest subaerial exposure during the end of the Middle–Late Callovian age. Discrepancies between the eustatic curve of (Miller et al., 2005) and the record of local relative sea-level change can be explained by local fault control that led to abrupt vertical and lateral facies change among Naokelekan, Barsarin and Najmah successions.

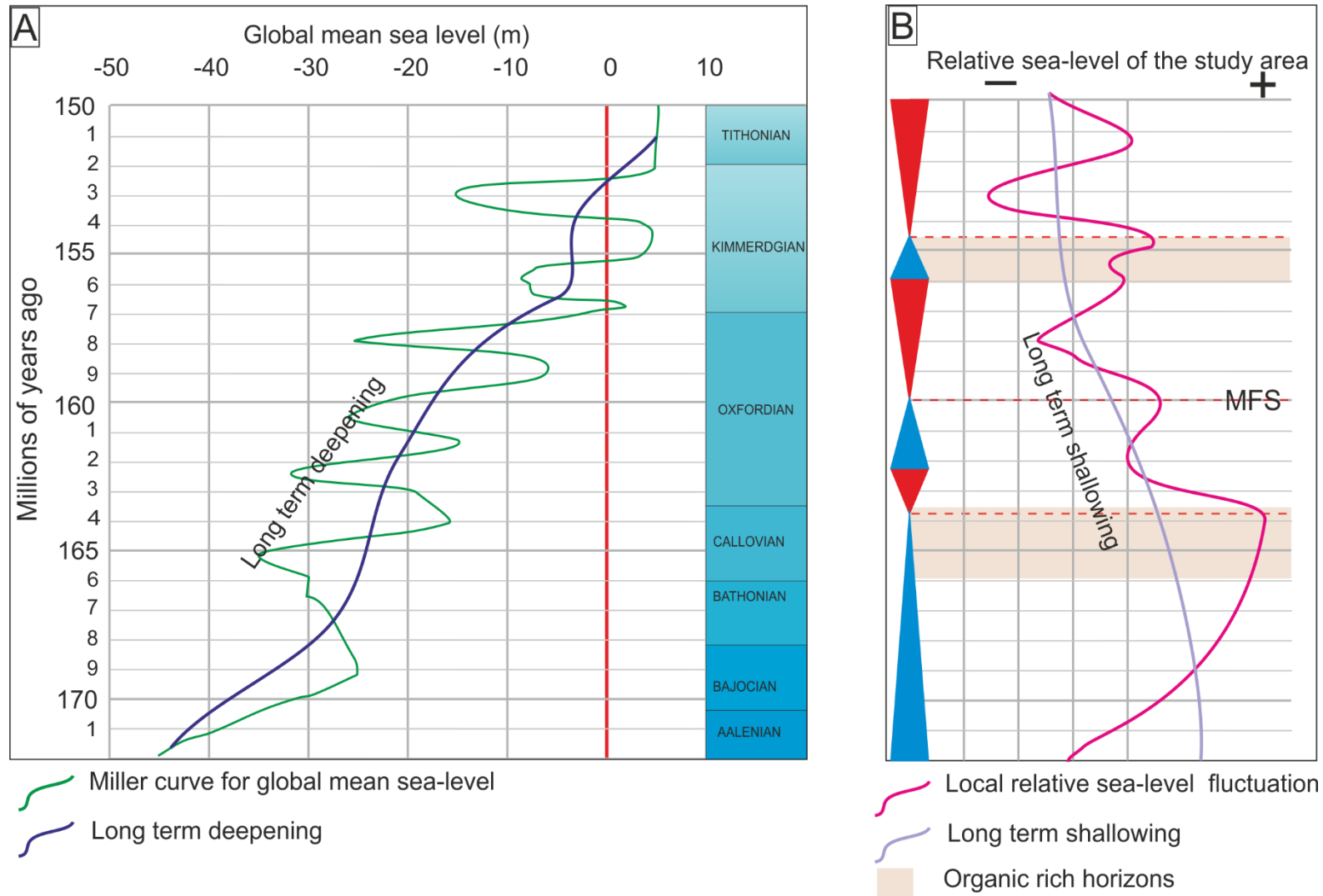


Figure 7.9: Correlation between global mean sea-level of Miller (2005) and relative sea-level Fluctuation in the study area. Note, the curves are found to exhibit a reverse behaviour, where Miller's curve shows deepening upward, whereas the relative sea-level shows shallowing upwards.

## 7.8 Gotnia Basin accommodation

According to seismic data by Ali et al. (2013) the Neotethys Ocean was progressively rifted during the Middle–Late Jurassic in the AP (Figure 7.10). Rifting processes resulted in horst–graben basins trending north/northwest to the southeast (Sharland et al., 2001; Jassim and Goff, 2006). The passive margin development with differential subsidence is well-documented in Oman sequences (Figure 7.11 A) (Pratt and Smewing, 1990; Rabu et al., 1990; Robertson and Searle, 1990; Robertson, 2007). Jassim and Goff (2006) considered that this phase of Oman rifting may extend further north along the margin of the AP, separating an outer carbonate ridge from the restricted Gotnia Basin.

The previous evidence suggests that the Middle–Late Jurassic perhaps was deposited on tilted fault blocks. Murriss (1984); Strohmenger et al. (1998); Yousif and Nouman (1997) recorded condensation facies on the middle Najmah formation in Kuwait, and on the western of Surmeh or Fars Basins at the main Neotethys Ocean, but only Robertson and Searle (1990) clearly reported condensed ammonitico rosso facies on a bathymetric high in Oman (Figure 7.11 A). It seems that the studied Late Jurassic condensed facies probably extended regionally further toward the southeastern part of AP. An extensional model with subsidence of passive continental margins, can be applied on the AP tectonic setting. This is due to the particular geodynamic setting in which the deposition of condensed Naokelekan Formation took place, tens of kilometres wide and a hundred–kilometres–long isolated tilted fault block (Figure 7.8). This palaeogeographic block unit, which is completely free of both terrigenous and carbonate allochthonous inputs, is bordered by two deeper basins; the main Gotnia Basin to the west and the “Fars Basin” to the east. The former basin plays a crucial role in trapping all sediments coming from the western highlands of the Arabian shield and adjacent carbonate platform. The geodynamic setting of the study basin is quite comparable to the isolated submarine Trento Plateau which was described as a rifted continental margin of the Ligurian arm of the Tethyan Ocean (Winterer and Bosellini, 1981; Martire, 1992; Masetti et al., 2012).

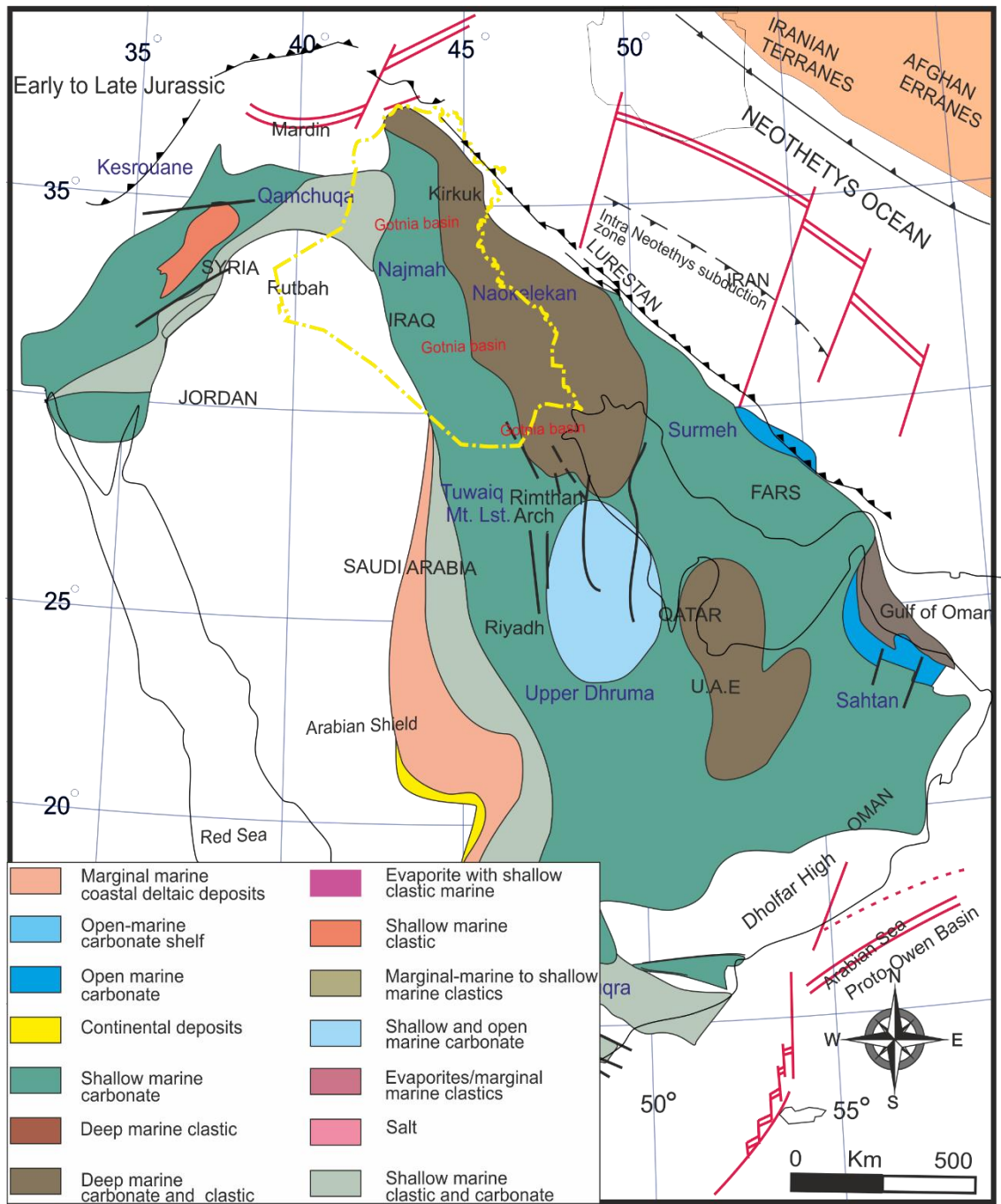


Figure: 7.10: Palaeofacies of the Late Jurassic in the Arabian Plate, which is characterized by including differential intra-plate subsidence that resulted in the development of intrashelf basins on the plate, modified from Ziegler (2001).

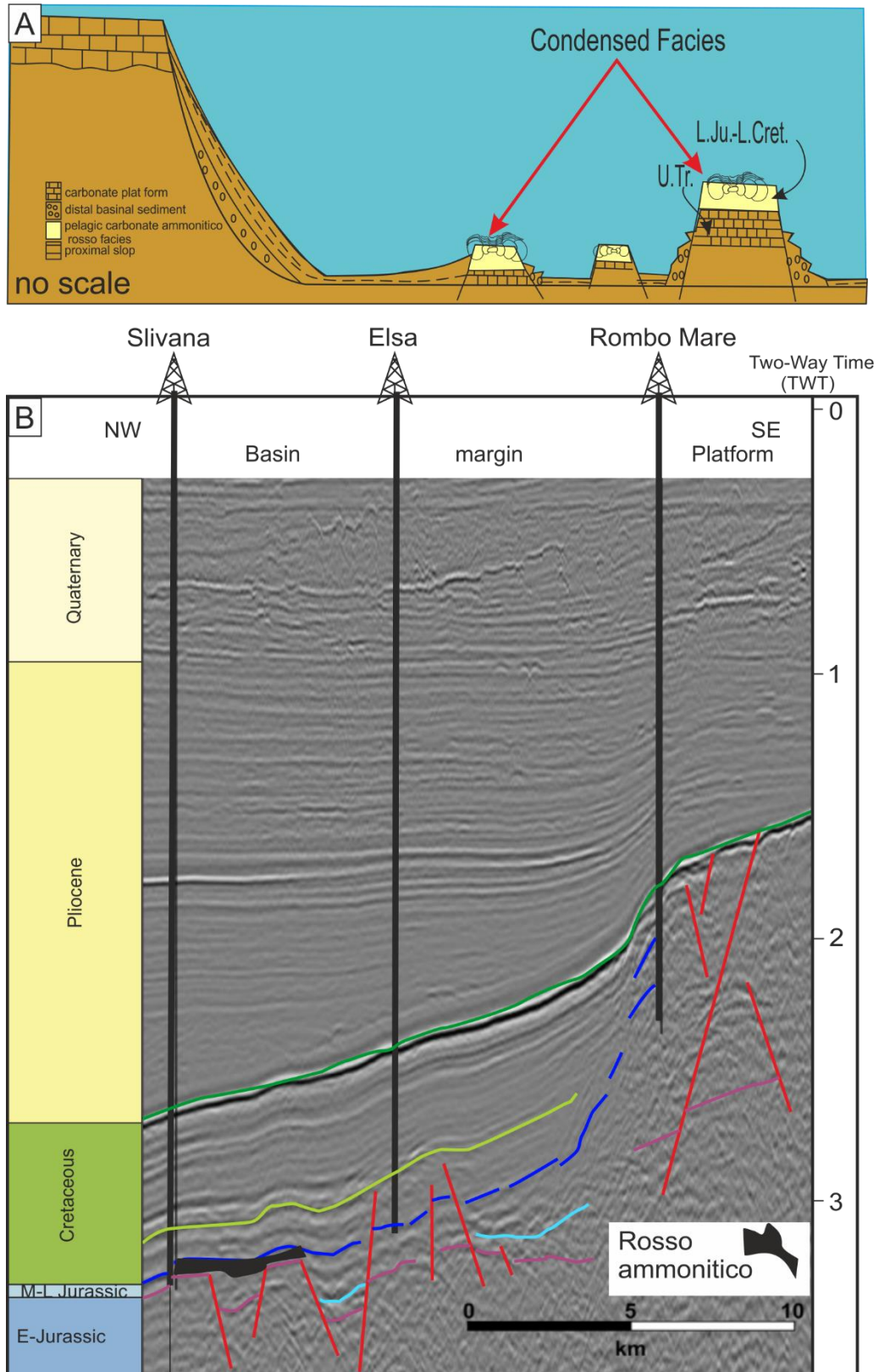


Figure: 7.11: (A); The passive margin development with differential subsidence in Oman showing condensed rosso ammonitico facies development on a bathymetric high in Oman. Modified from Robertson and Searle, 1990 (B); Seism-stratigraphic interpretation of showing the Jurassic extensional fault from the north-western margin of the Apulian Platform, Italy. Note Rosso ammonitico development on the faulted blocks. Modified from Santantonio et al. (2013).

## 7.9 Microbial stromatolite overgrowth on ammonites “ammonitico rosso”

Since the recognition of microbial stromatolites, the general impression was that they are unequivocal indicators of shallow-water conditions. However, this interpretation has changed in the last three decades and investigations on stratigraphic succession of different regions of the Neotethys Ocean in the Jurassic or Cretaceous periods are not compatible with shallow-water settings. It has been revealed that deep-marine stromatolites range from photic to an aphotic origin. A comparison between deep and shallow microbial characteristics is presented in Chapter 5. Numerous examples of pelagic microbial stromatolite overgrowths have been recorded in the Jurassic (Jenkyns, 1971; Jenkyns, 1974; Bernoulli and Jenkyns, 1974; Pallini and Schiavinotto, 1981; Winterer and Bosellini, 1981; Massari, 1983; Massari and Dieni, 1983; Clift and Robertson, 1990; Stampfli et al., 1991; Doyle and Mariotti, 1991; Cope, 1991; Cecca et al., 1992; Monaco, 1992; Martire, 1992; Bohm and Brachert, 1993; Santantonio, 1993; Zempolich, 1993; Winterer and Sarti, 1994; Varol and Gökten, 1994; Martín-Algarra and Vera, 1994; Vera and Martín-Algarra, 1994; Norris and Hallam, 1995; Karakitsios, 1995; Pratt, 1995; Rojay and Altiner, 1998; Martín-Algarra, 2000; Iuczynski, 2002; Dromart et al., 2003; Gill et al., 2004; Cecca et al., 2005; Reolid et al., 2005; Tchoumatchenco et al., 2006; Jacoby, 2006; Martire et al., 2006; Preat et al., 2006; Mamet and Pr eat, 2006; Rais et al., 2007; Cecca and Savary, 2007; Bernoulli and Jenkyns, 2009; Kandemir and Yılmaz, 2009; Reolid et al., 2010; Reolid and Molina, 2010; Baraboshkin et al., 2010; Smuc and Rozic, 2010; Reolid and Nieto, 2010; Massari and Westphal, 2011; V or os, 2012; Karakitsios and Chatzicharalampous, 2013; Reolid et al., 2015). Phanerozoic pelagic stromatolites are considered as a precise indicator of low sedimentation rates, and condensed and/or reduced facies bearing many sedimentary gaps. Although pelagic microbial stromatolites are widespread and abundant during the Jurassic, they have been recorded in different stages of geological history as well. Some Palaeozoic examples of deep-water microbialite have been reported (Playford and Cockbain, 1969; Playford et al., 1976; George, 1999). Similarly, few recent examples from the present pelagic stromatolites have been documented as well (Playford and Cockbain, 1976; Brachert and Dullo, 1991; Brachert, 1999).

Based on the previous discussion, microbial overgrowth on ammonites or clasts represents a characteristic feature of condensed facies (Figures 7.3, 7.5, and 7.12). Middle to Late Jurassic ammonitico rosso condensed facies frequently include microbial overgrowth on ammonites. The ammonitico rosso is one of the best well-documented

facies in the whole history of the Neotethys Ocean because of its peculiar palaeontologic and lithologic characteristics. Due to abundant ammonite fossils, the biostratigraphy of ammonitico rosso is precisely controlled as well. Ammonitico rosso occurrences range between Late Permian and Berriasian, and they have never been reported post-Berriasian age (Stampfli et al., 1991; Cecca et al., 1992). It seems that the ammonitico rosso occurred concurrently with the timing of passive margin evolution of the Neotethys Ocean (Figure 7.1). Bohm and Brachert (1993) investigated some deep-water stromatolite units from the Middle–Jurassic of southern Germany (Posidonien–Schiefer, Amaltheen–Ton) and of the Northern Calcareous Alps (Adneter Kalk, Klauskalk). Their interpretation suggests that the deep-sea microbial stromatolite as a rule forms during intervals of very low rate of sedimentation in extremely starved basins, and they normally occur in association with, intense bioturbation, hardgrounds or ferromanganese crusts (Vera and Martín–Algarra, 1994; George, 1999). Furthermore, intense bioturbation may indicate a low rate of sedimentation (Shourd and Levin, 1976; Goldring, 1995; Taylor et al., 2003). Because of their occurrence on bathymetric high or distal basin floor, typical platform components or shelf derived sediment such as coated grains, phototrophic benthos, shells of plankton and nekton are usually absent in this facies as well. In the Naokelekan Formation, clear evidence for condensed facies, pelagic microbial stromatolites overgrowth on ammonite shells, and oncolites have been recorded, which is quite similar to the ammonitico rosso deposition of Jurassic succession (Figures 7.5 and 7.12).

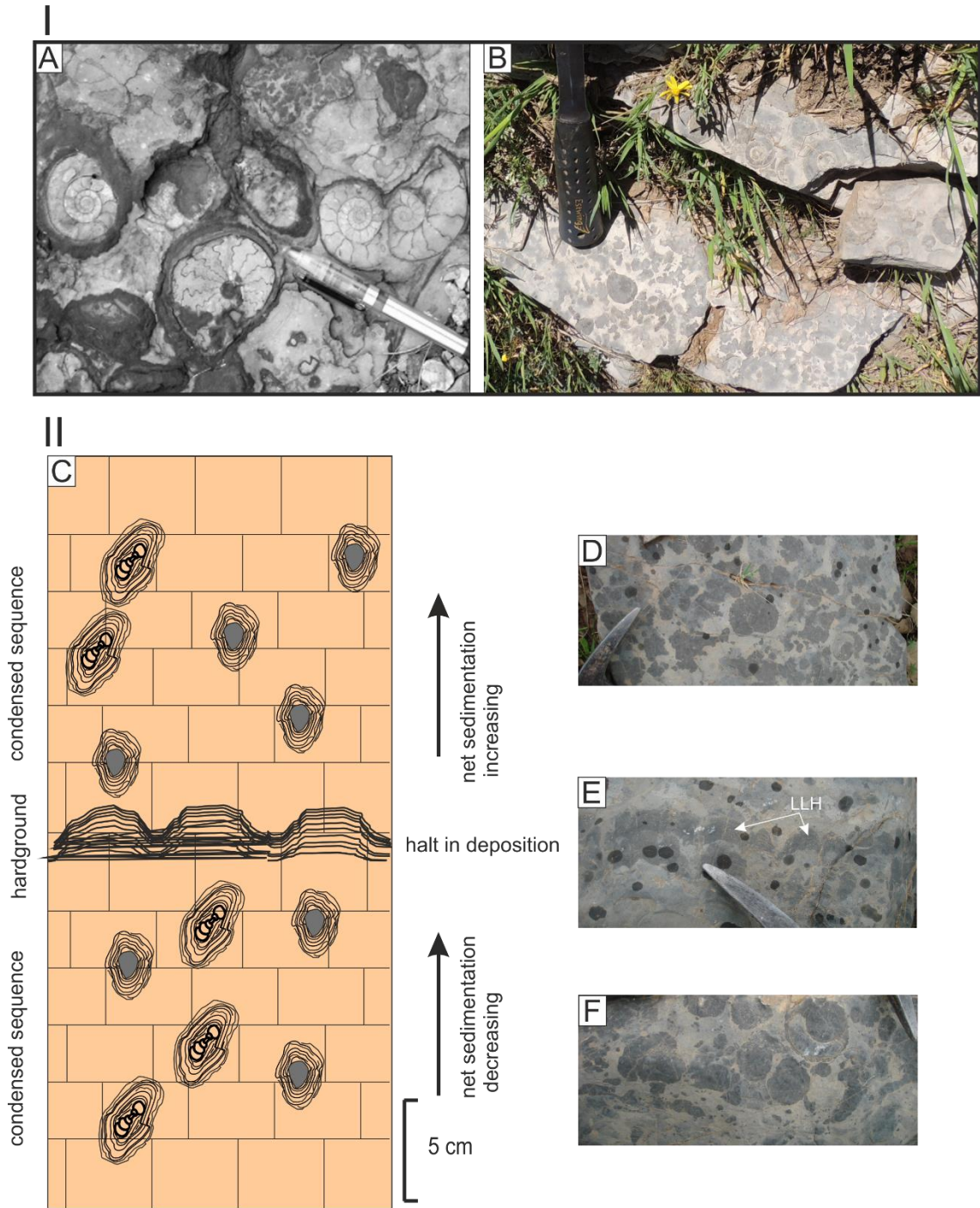


Figure 7.12: I- Comparison between; (A) a slab showing taphonomy of cephalopod assemblages with hardground of macro-encrustations of ammonites of the Jurassic microbial from pelagic swells of the External Subbetic, Spain (Reolid et al 2010) and (B) bedding plane surface showing numerous ammonite fossils, some with small dark microbials overgrowth.

II- (C) idealised diagram of a condensed sequence showing hardground with the laterally linked hemisphere microbial stromatolites interrupting two condensed sequenced modified from Jenkyns (1971). Likewise, photos D, E and F showing transformation from microbial oncolites -laterally linked stromatolites white arrows (LLH).

### 7.9.1 Condense ammonitico rosso facies and bathymetry high

The basin extensional phases produce normal faults, which led into development many horst and graben. The differentiation in the ocean floor topography gave rise to considerable accommodation variation between horst and graben. Consequently, relatively condensed carbonate successions deposited on the horsts whereas thick successions deposited in the troughs (Ziegler, 2001). Usually, synrift basins display juxtaposition of condensed and thick successions within the depositional basin. This relation is well documented in the worldwide passive margins (Hocking, 1988; Fabbi and Santantonio, 2012; Holford et al., 2013; Grain et al., 2013).

No modern analogues are known for the ammonitico rosso facies, so the current argument relies on analogue research suggesting deep-sea microbial overgrowth on ammonites of the Jurassic ammonitico rosso facies. There is no direct evidence that the TBMLM of the Naokelekan Formation was deposited on a bathymetric high, but numerous researches introduced evidence suggests that development of condensed facies and ammonitico rosso stromatolites on bathymetric highs are contemporaneous with the development of syn-rift structures in the Jurassic Neotethys (Martire, 1992; Fels and Seyfried, 1993). For example, Santantonio et al. (2013) combined seismic data with wells and studied the Jurassic–Cretaceous in Apulia Platform, Southern Italy. The 2D and 3D seismic analysis emphasized the development of condensed ammonitico rosso on the horst plateau (Figure 7.11 B). Also, Robertson et al. (1990) reconstructed the tectonic development in Oman, and it has been found that the ammonitico rosso pelagic limestones are locally accumulated on the bathymetric high.

### 7.9.2 Disappearance of ammonitico rosso

Cecca et al. (1992) traced the appearance, development, and disappearance of the peculiar stromatolitic condensed facies. They found that the appearance of microbial condensed facies ranges between Late Permian to Berriasian, and bloomed during the Jurassic. The causes of their disappearance after the Berriasian are still controversial, but it probably related to the demise of rifting in the western Tethys area during Late Jurassic–Early Cretaceous, and incipient sinking of continental margins due to thermal subsidence, as well as the blooming of rock-forming plankton during the Tethyan Realm (Cecca et al., 1992).

However, it has been argued that the oceanic chemistry changes by the end of the Jurassic period may have led to the disappearance of ammonitico rosso facies. This

assumption can explain the lack of ammonitico rosso on the present-day rifted margins (Cecca et al., 1992). Ocean chemistry of during Middle Jurassic to Early Cretaceous was different from that of the recent ocean. The changes commenced in the Early Aptian. Jenkyns (1974); Cecca et al. (1992) argued that precipitation of Mg calcite from seawater is as an important source for ammonitico rosso formation. The proportion of magnesium in pelagic carbonates significantly decreased around the Kimmeridgian–Tithonian boundary and precisely since the late Barremian. So, based on the Mg/Ca ratio, it can distinguish between pre-Aptian periods when precipitation of inorganic aragonite was promoted and post-Aptian to present time with enhanced calcite precipitation.

## **7.10 Factors controlling condensed intervals related to Jurassic ammonitico rosso**

Detail study on low sedimentation rates, prevailing winds and currents controlling factor, paucity of planktonic organisms, and hardgrounds have been carried out on the occurrence of condensed intervals in Neotethys Ocean of the Jurassic period.

### **7.10.1 Current sweeping and reworking**

Condensed ammonitico rosso facies that is thought to have developed in a particular environment of topographic high, usually shows significant influence by currents. Based on Jenkyns (1971) and Misik (1993) sweeping and reworking process on the bathymetric high actively contributed to reduce the sediment thickness. The influence of current on the carbonate platform is well understood in Little Bahama Bank (Schlager and Ginsburg, 1981; Reading, 1996; Reading, 2009). It has been found out that the current has a great impact on sedimentation. At windward platform margins, many coarse carbonates are swept into the platform, whereas along leeward platform margins, sediment is commonly moved off-platform, onto the adjoining slope and into the neighbouring basin. The palaeocurrent action on the sea floor of the TBMLM can be deduced by existence of oncolites (Figures 7.3 D and 7.5 A) (see Chapter 4). The Interrelationships between occurrences of oncolites, high structural relief, and ammonitico rosso facies are reported repeatedly (Jenkyns, 1971; Martire, 1992; Reolid and Nieto, 2010).

Martire (1992) studied Late Jurassic sequence stratigraphy of condensed ammonitico rosso limestones of pelagic sediments of the south Alps in Italy. The study concluded that the formation of condensed successions may be controlled by faults and current activities. The rifting and passive continental margins cause the formation of many fault-bounded plateaus and troughs. The shelf-derived sediments are mostly trapped in the

intervening troughs, whereas limited particle rain of planktonic or nektonic organisms deposited on these isolated plateaus. Later, these pelagic sediments were swept by currents into adjacent deep-water troughs (Martire, 1992; Massari and Westphal, 2011). The precipitated particles and early cementation on the submarine plateau seem to be greatly controlled by the degree of winnowing. The continuous current activity may sweep up sediments from the plateau into troughs, and as a result of that, condensed structures may form on palaeobathymetric high (Martire, 1992; Massari and Westphal, 2011).

Although prevalence of well-oxygenated conditions during deposition of the TBMLM are indicated by intense bioturbation of sediments and abundance of ammonites, microfossil associations have rarely been observed in condensed facies of the TBMLM. However, Microfossils such as radiolarians and foraminifers were abundant in nearby sections in Iraq and Iran during Late Jurassic. The TBMLM comprises two main size-classes of skeletal grains, and they are represented by coccoliths 8–15 microns, and ammonites which are up to 15 centimetres across. It seems clear that the skeletal grains were distributed at two extreme ends, which represented by a bimodal histogram (Figure 7.13). This model could reflect the impact of currents on the condensed facies in the Naakelekan Formation. The nannofossils, i.e. coccoliths were preserved because of microbial trapping and binding, whereas the other microfossils were not small enough to be captured by trapping, and they were most probably swept up. The ammonites were heavy enough to be over the carrying capacity of currents, so they are most likely overturned and rolled by current and as results many oncolites were developed.

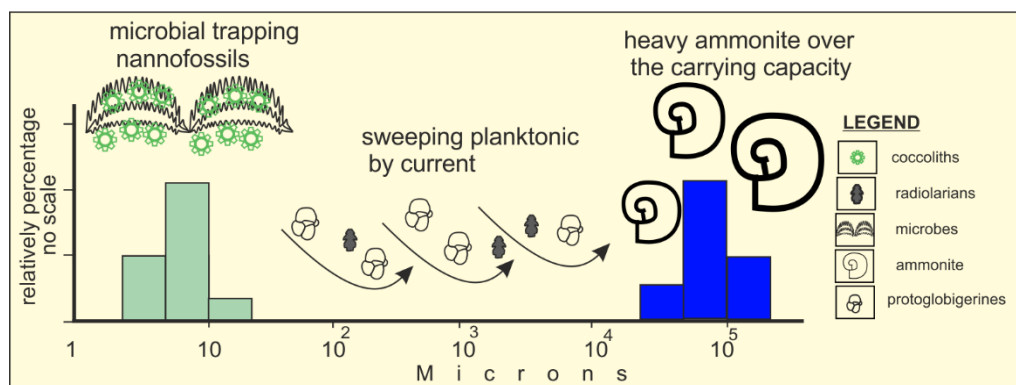


Figure 7.13: diagram showing current impact on the condensed intervals. A bimodal histogram explaining that only trapped coccoliths and ammonite could preserve on the tilted fault block, while the rest size were swept away by current.

### 7.10.2 Rate of sedimentation

Low sedimentation rate can be indicated by abundant stromatolites, because the microbial mat cannot flourish and survive in relatively high sedimentation rates. Generally, formation mechanisms of microbial stromatolite follow the same principle either in deep or in shallow-water. In both environments, an obstruction factor is required to block influx of transported sediments.

- Sediment input in shallow water could be limited through different kinds of barrier such as reefs or shoals. Gerdes and Krumbein (1994) presented numerous recent analogue localities of microbial mat growth in shallow water that have been protected from sediment infestation by barriers, such as Spencer Gulf, South Australia, Laguna Mormona, Baja Cal., Mexico, Andros Island, Bahamas, Plum Island, Massachusetts, and Mellum Isl southern North Sea.
- Sediment input in deep water could be limited through bathymetric high, graben or troughs. For the study area, the graben could be more probable, which resulted in the sediment trap. Consequently, the condition on the bathymetric high will be most suitable for microbial growth.

Low rate of sedimentation is favourable for growth of microbial stromatolites, whereas high sediment inputs inhibit and suppress microbial growth (Eriksson et al., 2010; Gerdes, 2010). Seong–Joo et al. (2000) suggested that the maximum microbial development occurred synchronously with the low sedimentation rates or during brief sedimentary pauses. It seems likely that there is a characteristic association of Phanerozoic deep-water stromatolites with condensed intervals (Playford and Cockbain, 1976). Playford and Cockbain (1976); Browne (2011) studied modern oceanic stromatolites and sedimentation rate, and the study revealed that the deep-water microbial stromatolites could survive only through low sedimentation rate settings. Additionally, Shourd and Levin (1976), Goldring Goldring (1995) and Taylor et al. (2003) pointed to the reverse relationship between the rate of sedimentation and bioturbation for more detail (see section 4.6.5 B). Furthermore, the existence of oncolites on open-sea platform sequences can also imply breaks or hiatuses in sedimentation (Playford et al., 1976; Peryt, 1983; Dromart et al., 1994; Flügel, 2010).

Martire (1992); Massari and Westphal (2011) studied condensed pelagic succession of ammonitico rosso facies on a palaeobathymetric high of Late Bajocian–Tithonian age in the Trento Plateau, Southern Alps. They discovered that the condensed facies occurred on a horst block of the southern continental margin of the Neotethys Ocean. Based on

Massari and Westphal (2011) the rates of sedimentation on palaeobathymetric high were exceedingly low, which was about few millimetres per thousand years with many stratigraphic gaps.

As it has been argued that two main processes were involved in the condensed facies deposit of Naokelekan Formation: minimal sediment input and reworking. The paucity of planktonic foraminifera during most of the Jurassic could be an additional reason for stratigraphic condensation as well. Development of the TBMLM on a bathymetric high or tilted fault block appears to be fundamental reason controlling condensed facies formation, where the faulted block receives a minimal supply of terrigenous clastics, platform-derived sediment, and nutrients from the mainland. As a consequence, the opportunity arises for growth of microbial stromatolites in condensed facies.

### 7.10.3 Paucity of planktonic organisms

Paucity of planktonic organisms simply reflects the fact that the bloom of these organisms occurred in later times, i.e. during the Cretaceous. Massari and Westphal (2011); Bernoulli and Jenkyns (1974) considered Middle–Late Jurassic Neotethys as a time of condensed pelagic sedimentation, because continental margins, which situated far from continental areas, isolated platforms or bathymetric high blocks were generally subjected to significant deficiency in sediment supply.

### 7.10.4 Hardground and low rate of sedimentation

Flügel (2010) and Reolid et al. (2010) highlighted the close relationship between marine carbonate hard grounds and condensed facies. Hardgrounds may result from a discontinuity or break in sedimentation, which can be indicated by dense microbial growth and horizons of mass ammonite accumulation. These surfaces may include encrusted ferruginous layers, deep-sea stromatolites, and oncoids with a core that mainly comprises ammonites and/or pelagic calcareous clastics. Vera and Martín-Algarra (1994), Misik (1993), Martín-Algarra (2000) stated that the stromatolite growth always accounts on swell structures and in extremely starved basin with a very low rate of sedimentation, their bedding surface could represent discontinuity periods. Under these starved conditions, microbial communities and, in a lesser extent, encrusting foraminifera can survive.

Most of the previously mentioned features in condensed facies and hardground are quite comparable with those reported in the TBMLM (Figure 7. 12, A–E) (see chapter 4 for

more details). Microbial growth on ammonites, for example, which is quite comparable to the ammonitico rosso facies, is the most noticeable feature that distinguishes this member from the underlying and overlying members. The second remarkable feature may be the mottling, which was interpreted to be the result of highly bioturbated sediments in well-oxygenated conditions and low average sedimentation rate.

Although more evidence is required to prove presence of hardgrounds in the study area, firmground to hardground substrate might be assumed to be present by the accumulation of cephalopod skeletons in large numbers at the top of the bedding surfaces in the ammonite-rich horizons. The ammonites may construct more than 60 percentage of macro-invertebrate, which usually concentrated at the top of bedding surfaces (Figure 7.12, B). There are also other indications of hardgrounds, for example: colonized microbial crusts grown on ammonite shells and lithoclasts signifying to a hardground strata (Nieto et al., 2012), or a very slow growth of deep-sea stromatolites as evidenced by the occurrence of micro-borings between stromatolite layers (Figure 7.5, A and C). Early lithification can be indicated by angular, dense, compact, and well-cemented lithoclasts, and often appears as scattered clasts in the burrow filling matrix.

Moreover, Spath (1950) studied ammonites in this study area, and his results confirmed a discontinuity or break in sedimentation within the mottled facies as well. Based on ammonite studies by Spath (1950), the age of Both Naokelekan and Barsarin Formations, which are about 35 metres in thickness, ranges from Late Callovian–Oxfordian–Late Kimmeridgian.

#### 7.10.5 Depth

As no modern analogue has been recorded yet for ammonitico rosso stromatolites facies, the palaeobathymetry and depositional environments are still controversial (Martire et al., 2006). The depth at which deep-water stromatolite and rosso ammonites were deposited has been much debated in the past because no recent analogue has been found yet. In classical papers on pelagic basins and the evolution of tectono-sedimentary systems, deep-water stromatolite and rosso ammonites are assumed to be deposited at 1000 metres depth (Jenkyns, 1974; Winterer and Bosellini, 1981). A few years later, this figure was completely revised based on the Deep-Sea Drilling Project data, and they found that the depth must be a few hundreds of metres (Winterer, 1998; Martire et al., 2006). Furthermore, recently, the sedimentologic and palaeontologic evidence of the Jurassic succession of the Southern Alps demonstrated that the ammonitico rosso stromatolites were deposited in even shallower water than previously

thought. Monaco (1992); Massari and Westphal (2011) have reported hummocky cross stratified beds interlayered with ammonitico rosso facies, which suggests deposition above the storm wave base. Furthermore, the existence of hermatypic corals, and zooxanthellae, which represent lower photic zone habitats, were reported in places in rosso ammonites stromatolites facies (Gill et al., 2004).

Although low sedimentation rates with condensed facies can occur in a range of different water depths from shallow to deep water, basically, based on available evidence, TBMLM could have formed in a range of depths from near sea-level to deep water just above the CCD. However, by comparing with the description of Hattin (1971), the burrows in the TBMLM of the Naokelekan Formation may attribute to *Thalassinoides* bioturbation, but due to the intense bioturbation, it is difficult to be classified. *Thalassinoides* can be habituated at lower rates of sedimentation (Taylor et al., 2003), and according to Massari and Westphal (2011) coexistence of ammonites with intense burrowing may suggest normal salinity, well-oxygenated conditions, low average sedimentation rate, oligotrophic environments, and photic zone. It is important to notice that there is a lack of direct conclusive evidence concerning the depth of condensed facies in the study area. Based on the above discussion, it can be deduced that the condensed facies of ammonitico rosso were mostly occurred within very few hundred metres depths.

#### 7.10.6 Climate controlled

The Jurassic represents one of the warm periods during the Phanerozoic Earth history and is generally characterised by a paucity of direct evidence for ice ages. However, the existence of some certain deposits, such as dropstones and glendonites in this period is still highly debated (Price, 1999). A series of studies on this question have been conducted by several researchers (Price, 1999; Veizer et al., 2000; Cecca et al., 2001; Dromart et al., 2003; Cecca et al., 2005; Brigaud et al., 2009). Geochemical and biogeographical studies in the northern and Central Europe Mediterranean area, North and East Africa, Middle East, and Central Asia carried out over the last two decades have presented evidence for climatic fluctuations in the Northern Hemisphere during Late Callovian and Early Oxfordian (Padden et al., 2001; Dromart et al., 2003; Tremolada et al., 2006; Rais et al., 2007; Louis-Schmid et al., 2007). It has been found that the condensed facies, which were mainly widespread in the latest Middle Jurassic period, were largely ended by a cold climatic period, and the cooling episodes were usually followed by a significantly warmer period.

Dromart et al. (2003) studied ammonite migrations, and presented stable  $\delta^{18}\text{O}$  isotope data from shark teeth to determine palaeotemperatures for the Late Jurassic. They suggested that climate can control ammonite migration; cold-water ammonite (boreal) can replace the warmer water ammonite (Tethyan) during cool times (Figure 7.14). The results revealed evidence of cooling during Late Callovian–Early Oxfordian that post-dated Toarcian–Callovian widespread organic-rich deposition, and the cooling event coincided with a sudden fall in sea-level. The temperature fall was basically determined by the migration of cold-water ammonite (boreal) towards subtropical latitudes during the Late Callovian–Early Oxfordian age. Cecca et al. (2005) studied palaeoclimatic controls of biogeographic and sedimentary events in the Tethyan during the Oxfordian. They used larger data sources to verify the results of (Price, 1999; Dromart et al., 2003). The palaeotemperature trends have been inferred from oxygen isotopes of belemnites. Based on the carbon isotope excursion results, a cooling event may be lasted about 1 my, which is consistently coupled with the dearth of carbonate production and condensed facies occurrence on swell structures. According to Vörös (2012), temperature deterioration is attributed to  $\text{CO}_2$  depletion in the atmosphere via enhanced organic carbon burial in pre-Upper Callovian age and acted as an inverse greenhouse effect because of the widespread absence of Lower Oxfordian reefal formation and Late Callovian–Early Oxfordian crisis in carbonate production.

Nieto et al. (2012), Rais et al. (2007) have studied stratigraphic breaks in the ammonitico rosso facies with the evolution of pelagic swells from hardground analysis of Middle–Late Jurassic in Eastern External Subbetic, Southern Spain, and in the Helvetic of the Swiss submarine high. They reported deep-sea microbial overgrowth on ammonites and hardground features, which are indicative of low rates of sedimentation, and their occurrence coincides with cold global temperatures. The cold events were usually followed by relative sea-level falls, and are characterised by the low rate of sedimentation, sediment erosion, and early diagenesis with many horizons of hardgrounds. Martire et al. (2006) studied a proposal of lithostratigraphic ordering and formalization of ammonitico rosso, *Posidonia* and *Saccocoma* facies of Middle–Late Jurassic in northern Italy, and obtained similar results with regard to the relationship between climate and condensed facies. The results suggested that the climatic and oceanographic changes reducing carbonate production were perhaps one of the factors that led to the formation of condensed facies. This interpretation is supported by the existence of ammonitico rosso Veronese condensed succession, which usually occurs in very low rate of sedimentation of the Upper Bajocian–Tithonian.

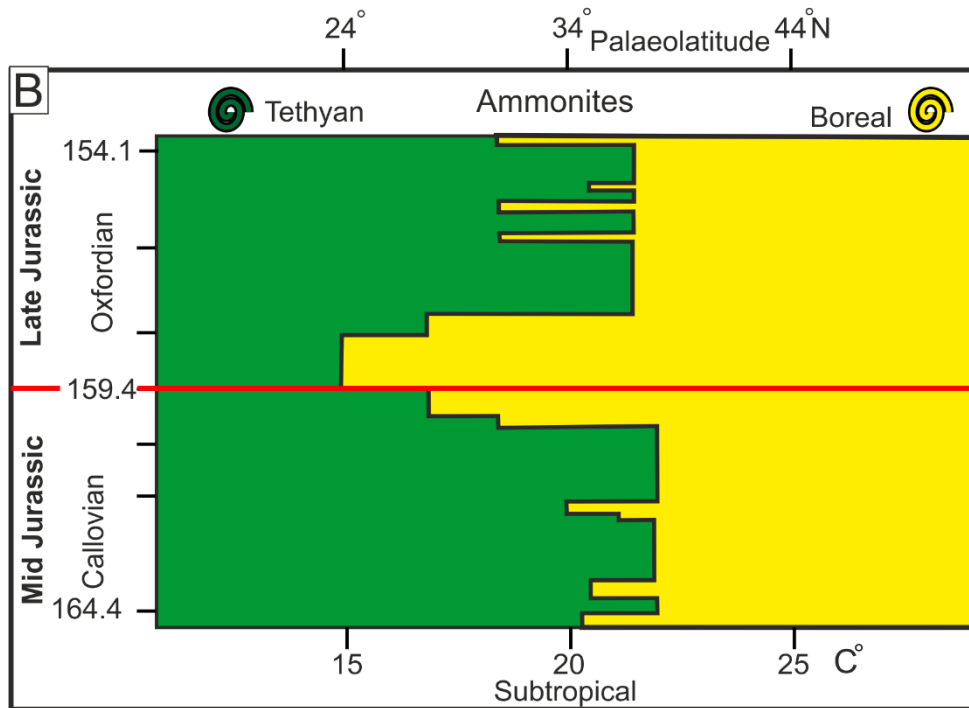
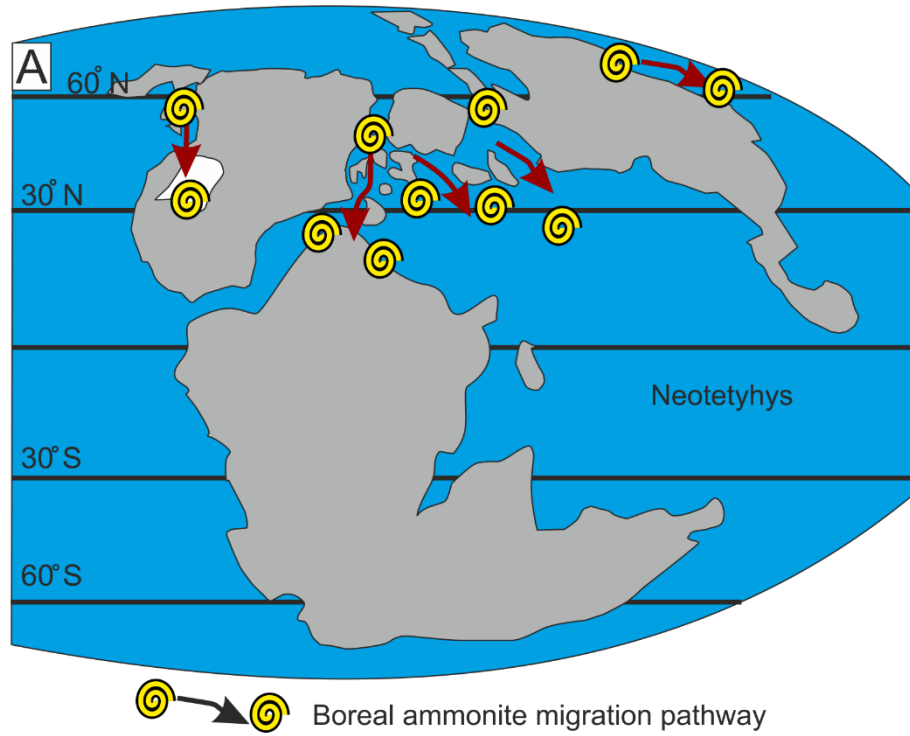


Figure 7.14: (A) Palaeogeographic diagram showing migrations and distributions of boreal ammonite. Note migration towards subtropical latitudes of boreal ammonite fauna during the Late Callovian-Early Oxfordian age. (B) Distribution of different of Boreal and Tethyan ammonites during Bathonian- Oxfordian age and their relationship to the palaeotemperature, modified from Dromart et al., 2003.

### 7.11 Naokelekan Barsarin boundary

The Naokelekan/ Barsarin Formations boundary at all localities, which is represented by the boundary between the Early and Middle Kimmeridgian age, shows basinal facies transition to sabkha facies in short time span. The abrupt facies changes imply large water–depth variation, and this change is important in understanding basin development. The palaeodepth of the Naokelekan Formation is estimated as having been about 200 metres at the time of the Early Kimmeridgian, whereas the Barsarin Formation is peritidal.

The dropping of sea-level from 200 to 0 metres depth has not been registered globally during the Early/ Late Kimmeridgian age. According to Miller et al. (2005) the eustatic sea-level fall from Early to Middle Kimmeridgian was about 20 metres suggesting that the relative sea-level fall observed in the field area was not eustatic. From the previous discussion, this dropping of sea-level is not considered to be Eustatically controlled, especially the long-term eustatic trend was toward deepening as shown by Miller et al. (2005).

Numan (1997) interpreted that this abrupt facies change is controlled by tectonic processes, and it is considered here to represent time of incipient subduction between Arabian and Persian plates. However, global plate tectonic reconstructions of peri-Tethys confirm continuation of Neotethys in extension during Jurassic period, and their studies confirm that subduction commenced later in Cretaceous (Stampfli et al., 2001; Ziegler, 2001; Sharland et al., 2001). Gulf of Suez could be the best model for uplifted block that occurred during extension, where significant uplift occurred contemporaneous directly to adjacent subsidence (Omar et al., 1989; Cross et al., 1998). Bosence (2005) has also pointed to the rifted Gulf of Suez as an uplifted fault block platform model, where shallow marine setting overlies deeper sediments. It can be assumed that a synchronous uplift and subsidence within an extensional basin regime would be the probable processes for abrupt lateral and vertical variation, where a fault block uplifted at depositional basin of Naokelekan and Barsarin Formations with adjacent subsidence at Gotnia and Najma Formations basin. So, a model for study area could be uplifted fault block platform. Late stages of Gotnia Basin development indicate that there was a great influence of the uplifted block on the basin, which led to isolation from the main ocean for several times, and as a result thick cycles of evaporite strata were developed during Late Jurassic.

## 7.12 Discussion

Although the existence of condensed Naokelekan Formation of Late Callovian–Early Kimmeridgian has been recognised for a long time by (Bellen et al., 1959), the causes and controlling factors have not yet been clearly identified. An important challenge arises from the suggested model, because study area suffers a lack of seismic and tectonic studies. The main features of the studied condensed facies are: microbial stromatolite overgrowth on bathymetric and high basin floor deposits, where no siliciclastic sediment supply exists from the continental shelf or land-derived sediment. The Jurassic succession of the Naokelekan Formation shows sufficient evidence and sedimentological features to suggest that this formation is comparable to the ammonitico rosso facies that in turn gives clues to the understanding of the relevant processes. No modern analogue of ammonitico rosso has yet been found. So, the condensed facies of the Naokelekan Formation correlated with the ancient ammonitico rosso analogue. The most important commonalities between the TBMLM and ancient condensed ammonitico rosso analogies are:

- 1) Existence of deep-sea microbial stromatolite overgrowth on ammonites with coccoliths groundmass.
- 2) Characterised by low sedimentation rate, hiatus, bioturbation, and hardground surfaces.
- 3) An obvious impact of currents on the condensed intervals is its contribution in sweeping sediments.
- 4) Always appear as a condense successions.
- 5) Ammonitico rosso facies usually occurs vertically adjacent to the *Posidonia*, radiolarian bedded chert facies.
- 6) Their occurrence specified a particular time period which is usually Middle–Late Jurassic.
- 7) They occur on the pelagic bathymetric highs. The TBMLM facies is entirely carbonate sediments and usually lack terrestrial inputs.

Clearly, the ammonitico rosso facies has been sufficiently studied in Europe. These studies emphasize that the development of the ammonitico rosso facies occurred on bathymetric high within condensed facies during Middle–Late Jurassic rifting. The importance of this section lies in the tectonic development and sequence pattern which are quite comparable to those that have been described from the Middle–Late Jurassic sequence of Europe. Similarly, the seismic studies in combination with synthesis of the tectonic and sedimentological evolution of the eastern margin of the AP during Jurassic

period suggest rifted basin development with prevalence of graben and fault blocks. Numerous studies pointed to the occurrence of the ammonitico rosso on the bathymetric highs, and the provided evidence from seismic data suggests that the bathymetric highs refer to fault blocks. Jassim and Goff (2006) assumed that this phase of rifting may extend further north along the margin of the AP into the study area, but, again no conclusive evidence for this extension exists. The ammonitico rosso in condensed facies is relatively unfamiliar in the AP or the study area and only very few studies exist. Middle–Late Jurassic successions of Callovian to Oxfordian age in the central Pontides Basin in Turkey, may represent the nearest reported location to the study area that contains ammonitico rosso facies (Rojay and Altiner, 1998).

Based on the previous arguments, there are two possible interpretations: (1) the ammonitico rosso facies of the TBMLM could be developed on a titled fault block bathymetric high. (2) The ammonitico facies developed under similar conditions on the distal basin floor, with no high present. Based on the available evidence, the first possibility is likely the correct explanation. However, the study area lacks any direct evidence for a bathymetric high, so the distal basin floor interpretation is also still possible. Further tectonic and seismic studies are needed to resolve this issue.

## *CHAPTER EIGHT*

### *8 DISCUSSION*

## **8.1 Tectonic development of the study area**

A significant geological problem in the study area is a deficiency of current scientific research on the tectonic development the study area. Almost all studies in the study area were focused on the post-basin fill deformation history of the area rather than on the tectonic evolution of the Mesozoic sedimentary basins. However, exposures showing complete successions from the Ordovician to recent make Kurdistan Region a suitable area to study and understand the tectonic history of the Neotethys Ocean. The study of the stratal stacking pattern in the study area is vital to understand the basin development which consists of rift basins that are strongly influenced by fault evolution. The reconstruction of basin development is challenging because of Late Cretaceous thrust fault deformation.

Early–Middle Permian rifting is interpreted to have taken place at the northeastern margin of the AP (Sharland et al., 2001). Multiple episodes of rifting occurred in the Triassic and Jurassic which are recorded in the sedimentary records in Oman and Iran (Robertson, 2007). The Neotethys opening and development of passive margin at the eastern side of the AP are documented in numerous studies which provide evidence for rifting and passive margin development that included fault–controlled basin developed in the Arabian palaeo–basin that persisted into the Jurassic period. However, the models that have been suggested in the current studies for the basin development require support from more detailed tectonic models. Until sufficient research on the tectonic development is completed, most of the basin-scale results presented are best regarded as testable hypotheses.

## **8.2 Correlation between subsurface sections and Kurdistan outcrops**

Review of the literature (see Chapter 2) indicates that the outcrops are poorly correlated to the nearby subsurface sections. For example, in Kirkuk oil–field, it is still unclear whether the Late Jurassic is represented by the Najmah/ Gotnia or the Naokelekan/ Barsarin Formations. This uncertainty is common even in modern wells that are drilled by newly involved companies.

Based on the results of this study the missing link between subsurface and outcrop sections is possibly located a few tens of kilometres west to southwest of the study area, where the facies seems to dramatically change with regards to thickness and lithological characteristics. This abrupt lateral facies change is most likely tectonically controlled.

About 30 km westward from a studied outcrop at subsurface, the condensed Naokelekan Formation appears as a relatively thick succession, and it is not a condensed section anymore. As it has been discussed in Chapter 7, the thin condensed section indicates very a specific environmental and basinal history. Similarly, the Barsarin Formation shows significant lateral facies changes from shallowing-upward cycles of sabkha environment into intervals of interfingering of thick anhydrite units and of carbonate rocks.

During comparison between studied outcrops with subsurface sections, the following conspicuous differences were observed in the subsurface sections:

- In subsurface sections, no condensed sections are recorded, whereas the thickness of Middle–Late Jurassic formations increases significantly.
- The boundary between the Naokelekan and Sargelu Formations in subsurface sections distinguished from outcrops by including clear evaporite intervals (Aqrawi et al., 2010).
- Based on internal reports of local oil companies, subsurface sections show shale–dominant facies in the Naokelekan Formation as well as the Sargelu Formation.
- Upper Jurassic strata in subsurface sections characterised by a dominance of evaporite intervals.

The difficulties in correlation between surface and subsurface section can be related to the following reasons:

- Both surface and subsurface sections generally lack detailed seismic surveys.
- It is obvious that the available bio–and chronostratigraphy data could be inaccurate or out of date because most of the studies were conducted half–century ago. The area needs to be better for both outcrop and subsurface sections, and additional Bio–chronostratigraphy, or magnetostratigraphic techniques must be used, especially for the Jurassic period which modestly depends on ammonite zones.
- The depositional environments of both subsurface and surface strata are also poorly studied and/or understood, and therefore, interpretations vary significantly.

### **8.3 Sargelu Formation**

The traditionally interpretation of the Sargelu Formation divides it into three members as the follows:

1. Basal Saccharoidal Dolomite member (BSDM)

2. Middle Posidonia Limestone member (MPLM)

3. Black Shale, Radiolarian Bedded Chert and *Posidonia*-bearing Limestone member (BRPLM)

The current study focuses on BRPLM, which has been subdivided for the first time into three distinct lithofacies. Basically these lithofacies alternate with each other at intervals of several decimetres thick, and the results show clear interaction between them, which embodied in the allodapic limestone turbidity model that will be discussed in the next sections. The lithofacies are as the follows:

1. *Posidonia*-bearing limestone lithofacies (PBLL)
2. Radiolarian bedded chert lithofacies (RBCL)
3. Black shale and argillaceous limestone lithofacies (BSALL)

### 8.3.1 Radiolarian bedded chert

Although the bedded chert of the Sargelu Formation represents the only clear radiolarian phenomenon in the entire stratigraphic section from Ordovician to Recent, there are almost no studies on the distribution and depositional processes for the radiolaria. The few researches that studied bedded chert of Sargelu never documented radiolarian fossils (Balaky, 2004; Sherwani and Balaky, 2006). The Bedded chert interval of the Middle Jurassic was used as a marker bed in Kurdistan outcrops where it is exposed widely and consistently within carbonate successions at all localities of Jurassic exposures.

500 metres thick radiolarian strata formed in a relatively deep offshore passive margin basin, in a 250 km wide belt that extends about 3000 km from Oman through the Kermanshah basins in Western Iran and into the Antalya Basin in Turkey (Bernoulli and Jenkyns, 2009; Agard, 2005; Baumgartner, 2013). The existence of radiolarians seems to be limited to a narrow range of space and time, and they are abundantly distributed at the Callovian and Late Jurassic Epoch across the eastern side of the Neotethyan (Gharib and De Wever, 2010). It seems that the distribution and abundance of the radiolarites coincide with carbonate platforms on the pelagic highs, and took place concurrently with the Neotethys Ocean development through the Triassic–Jurassic Periods controlled by faulted blocks along the rifted margins (Jenkyns and Winterer, 1982; Baumgartner, 2013). Despite reports on the existence of thick successions of Jurassic radiolarians in the nearby sections in Kermanshah, Iran (Gharib and De Wever 2010) no attempt was

made to find out how the Kermanshah radiolarian intervals are linked to the bedded chert of the study area.

The bedded chert intervals of the upper part of the Sargelu Formation are not as massive as the Kermanshah radiolarians, and they decrease westward until they vanish completely in the subsurface sections just about 60 km west of the studied area. The lateral variation in thickness from massive radiolarian in Kermanshah to relatively thin-sections of chert in the Sargelu Formation could suggest that the bedded chert of the studied area is located at the periphery of the main radiolarian depositional basin. The lateral extension of bedded chert between Sargelu Formation and Kermanshah cherts has not been traced yet, so the nature of the link between them can only be assumed until future studies approve/confirm this relationship.

### 8.3.2 Potential mechanism for the high-productivity

The long-held assumption that the depositional basin bedded cherts of Sargelu approaches the calcite compensation depth (CCD) has been questioned in the current study. It is well proven today that there is a strong positive relationship between an abundance of radiolarian and high-productivity areas. De Wever and Baudin (1995) suggested that fertility that governed the radiolarites formation in the Mesozoic Tethys is the imperative requirement rather than ocean depth. There are controversial views on what stimulated the palaeo-productivity, and in particular, the exact mechanism for the origin of radiolarites deposits.

The most accepted recent analogue model for high-productivity and causative factors of formation of the bedded chert or radiolarites could be the Caribbean river plume model or equatorial upwelling current model (De Wever et al., 1994, 2001; Baumgartner, 2013). The former model has been excluded because it is characterized by abundant reef growth in its euphotic areas, and the limited mechanism of nutrient supply to the surface waters by the influx of low water salinity lids, which is inapplicable to the study area. The equatorial upwelling current model, which is well documented in recent analogues, has been chosen to explain the radiolarites in study area. Upwelling currents of modern analogues are well-documented in the Somali and Owen basins, Western Indian Ocean and the eastern margin of the Arabian Plate (Young and Kindle, 1994), as well as in the Gulf of California (De Wever, 1989; Baumgartner 2013).

A comprehensive study on monsoonal-driven upwelling current for both recent analogues and Jurassic period by De Wever and Baudin (1995), De Wever et al. (2014),

and Baumgartner (2013) produced a set of palaeoenvironmental maps of the Neotethyan realm. Based on these palaeogeographic maps Jurassic seasonal upwelling current contributed to high productivities and high accumulation rates for radiolarites off the Arabian plate margin in the Neotethys. The Sargelu Formation may have been under the influence of an ancient monsoonal-driven upwelling current.

Much research was carried out on the Neotethyan radiolarian bedded chert (De Wever, 1989; Gharib and De Wever, 2010), it has been interpreted that the radiolarian usually intercalated with other sedimentary rocks belonging to nappes in the faulted blocks of a rifting. They found that radiolarians were deposited in the narrow and elongated basins, and regionally the depositional basin extended as a narrow strip along the eastern passive margin of Arabian plate. Likewise, the depositional basin of the Sargelu Formation bedded chert is assumed to have developed on the relatively narrow and elongated basin, which extends for hundred kilometres from Sirwan valley to Zakho but are a few tens of kilometres in width. The distribution of the Middle–Jurassic radiolarian chert on narrow and elongated basin in Kermanshah area, western Iran, which is about 60 km to the southwest of the current studying area, is the best example to understand how bedded chert developed in the study area.

### 8.3.3 *Posidonia*-bearing limestone

Despite an abundance of *Posidonia* fossils in both the MPLM and BRPLM, they did not get much attention from local geologists. Almost all studies on the upper part of the Sargelu Formation focused on petroleum investigations. This study attempts to present a new point of view and introduces *Posidonia* as a key to interpret the depositional environment, in particular, for re-drawing the depositional basin, which could be an introduction for a future, more detailed analysis on thin-shelled bivalves of Jurassic age. Although there are no modern analogues for the massive accumulation of *Posidonia* in the Recent Oceans, Toarcian *Posidonia* Shale of Central European Basin System is one of the most well-known events when the mass accumulation of thin-shelled bivalve occurred. The interpretations that presented herein depend on well-studied ancient analogue of Toarcian *Posidonia* Shale.

Based on the type of shell preservation, the PBLM and MPLM were classified into several categories. For example, the thin-shelled bivalves of *Posidonia* in the MPLM are broken into small fragments with no preferred orientation of the broken shells, whereas the PBLM shows a wide range of thin-shelled bivalve preservation, which appear to be distributed following specific arrangement upwards through the unit (i) intact disarticulated, (ii)

articulated with closed valves, (iii) folded with fragmented shells, and (iv) stripe-like or filamented *Posidonia*.

The development and variation in the shell preservation style are of great importance in determining the palaeoenvironment of MPLM Sargelu Formation. The transition from the intensely broken fragmented shells of the MPLM to the intact or fragmented bivalve shells of PBLM could imply a transition from a shallow depth where the storm event conditions are able to disturb the sea bottom to a low-energy depositional environment probably below fair-weather wave base. Furthermore, butterfly and articulated and cone-in-cone preservation of *Posidonia* may suggest low velocity turbidites and slow decay of articulating ligament in oxygen deficient waters. Preservation of articulated shells means in-situ accumulation *Posidonia*. The vertical variety may imply deepening upward.

The distribution of folded and rolled thin-shelled bivalves, which are rich with dispersed coalescent debris, increases gradually upward across the sections, and they may represent the dominant kind of preservation in comparison with the other kinds. Similar structures of folded thin-shelled bivalves have been observed by Navarro et al. (2008) and Negra et al. (2011) and have been interpreted as having formed through compaction. However, micro- and macrostructures in the current study provide evidence that may suggest other reasons, such as mass transportation and redeposition which result in folding and rolling structures in Sargelu Formation.

Breakage of the thin shells by compaction effects can probably be excluded because some layers of *Posidonia*-bearing limestone are not folded or broken even though they are directly above or below beds that contain broken, folded and rolled *Posidonia*. The existence of large slumping structure at the top of the Sargelu Formation suggests redeposition as well. Furthermore, the existence of a significant amount of *Posidonia* coalescent debris within folded and rolled shells indicates micro-slumping. Coalescent debris comprise flocculated *Posidonia* valves with internal folding and rolling textures. Furthermore, in some cases, thin-shelled bivalves demonstrate tangential alignment around ammonite shells or rigid materials, which may suggest folding or rolling rather than blockage by compaction.

#### 8.3.4 Age

Although the Sargelu Formation is very rich in different kinds of fossils, such as ammonites, thin shelled bivalves, and radiolarians, the age of the formation is still not

well-defined. No palaeontological and biostratigraphic studies have been carried out on the Sargelu Formation in the region for about six decades, and text books or recently published articles have simply repeated what has been reported in the first descriptions made for the formation by Bellen et al. (1959). There is an urgent need for more/detailed research to determine the accurate age of the formation. Recently, many studies on the radiolarians and ammonites were carried out in Iran, and there is a strong need to follow in their footsteps with prospective studies. Based on previous studies, the Sargelu Formation has been determined as Bathonian in age at the top (Bellen et al., 1959; Buday, 1980), but according to current results obtained in this study the formation age perhaps extends at least into the Middle–Callovian. The results are based on the following evidence:

- The thin-shelled bivalves are represented by *Posidonia ornati* Quenstedt, which has been observed first by Wetzel in 1948 (Bellen et al., 1959) in the Sargelu Formation type section. Based on Imlay (1945; 1963; and 1964); Waller and Stanley Jr (2005); and Cant (2001), the *Posidonia ornati* can be considered as an indicator for Bajocian to Callovian age.
- In spite of existence of different genera of radiolaria, only *Cinguloturris carpatica* Dumitrica was identified because the majority of them were poorly preserved. The well-controlled taxa *Cinguloturris carpatica* is found to have appeared for the first time in Late Bathonian and lasted up to Early Callovian.
- The Middle Callovian age is also ascertained through recording *Kosmoceras* species of ammonite fossils, where the *Kosmoceras* has occasionally been recorded from the Callovian of the Middle East, though it is much more common to the north in the Caucasus.

### 8.3.5 Resedimentation

The only thing that has been interpreted over the past decades conclusively is that the Sargelu formation was formed in a pelagic environment, but the sedimentology and palaeo–environments remained poorly understood. The upper part of the Sargelu Formation mainly comprises the combination of *Posidonia*-bearing limestones PBL, black shale BSALL, and bedded chert RBCL, which appear in alternating successions. Controls on changes from one facies to another were poorly understood. The main questions are: what does this co-existence mean, does their repetition follow specific depositional patterns, and how does this relationship between facies help to understand and interpret the depositional environments? The present study attempts to decipher this

relationship. Some evidence regarding the presence of re-sedimentation has been provided (Chapter 3), which has never been reported before in the Sargelu Formation. These initial observations and interpretations on re-sedimentation may stimulate further studies and debate about the issue with more detailed studies in the future.

### 8.3.6 Allodapic limestones or carbonate turbidites

Bouma (1962) was the first who described and interpreted the turbidite sequences through a siliciclastic succession. However, this model seems to be more applicable to siliciclastic sedimentary structures. Since the Sargelu Formation mainly comprises carbonate, Bouma's model of turbidites appears to be not well representative for the carbonate depositions. Theoretically, carbonate turbidites are similar to siliciclastic turbidites in terms of mechanisms of turbidity current, but they can be different in two basic aspects:

- Biogenic carbonate particles are usually distinguished from siliciclastic sediments by early lithification and prominent large clasts or boulders.
- In contrast to the siliciclastic turbidites, in which the grain size depends largely on the distance of transportation, the ecological limitations in the source area and taphonomic criteria control the size of the bioclastic particles in carbonate turbidites.

For this reason, the interpretation of turbidity in the Sargelu Formation has relied on the Meischner (1964) model which includes allodapic limestones as well and is more compatible with the carbonate turbidites or calciturbidites.

Careful examination of the internal sedimentary structures and the morphology of different lithofacies reveals the common presence of re-sedimentation or turbidity structures. It has been also discovered that the stacked packages of different lithofacies are not random but may follow a particular order, and further, future research with a quantitative analysis would need to fully understand mechanisms responsible for these relationship. Each package often shows the following vertical succession from bottom to top: a) graded bedding, b) laminated structures, and c) bedded chert or black shale. This kind of arrangement of sedimentary structures is comparable to the Meischner model, and may indicate turbidite structures. The main distinguishing characteristics of the allodapic limestones or carbonate turbidites in the Sargelu Formation are:

Graded bedding structures that fine upwards are relatively common throughout the lower part of the PBLL and is the best evidence for calciturbidite deposition, which is best

expressed by. Vertical differential grain size distribution in the graded bedding structures is best expressed by ammonite bioclasts concentrated at the bottom of graded beds, whereas the size decreases gradually upward with *Posidonia* bioclasts dominant at the top. The graded bedded structures are usually followed by thinly bedded clearly laminated posidonia-bearing limestone in the upper part of PBLL, but no ripple cross laminations were observed in the field studies, except for some folded structures. The scarcity of ripple lamination in the allodapic limestone seems to be common which was also emphasized by many other researchers (Hsu, 1989; Einsele, 2000; Shanmugam, 2006; Bridge and Demicco, 2008; Flügel, 2010; Hüneke and Mulder, 2011). In the current study, it has been assumed that the taphonomic criterion could be the main controlling factor that is behind the absence of ripple structures in the top unit of the PBLL. This is because the majority of calciturbidites comprise well-sorted *Posidonia* shells with narrow size-range distribution, and sediments lack fine grains or mud particles. Since fine grain particles are the main factor responsible for the later stage of the lower flow regime of turbidity current to form ripple lamination, the lack of them in the calciturbidite could result in the absence of ripple lamination. Accordingly, the allodapic successions usually pass sharply from sand-sized grains to bedded chert or shale. The bedded cherts in the BRPLM and the black shale of the BSALL are considered as a supplementary division that caps the top of the carbonate turbidite sequence, and their accumulations are an important indicator for a non-turbidity period or a low-density tail to the turbidity currents.

### 8.3.7 *Posidonia* and radiolaria relation

The co-occurrence between radiolarians and *Posidonia* facies that has been reported frequently by many researchers (Jach, 2007; Onoue and Yoshida, 2010; Onoue et al., 2011; Baumgartner, 2013), is important in terms of palaeobathymetry. The *Posidonia*-bearing limestones often appear as a transitional phase during the basin evolution between drowned basin and radiolarite facies, which commonly implies deepening upward. The radiolarians and *Posidonia* facies co-existence was also observed in the BRPLM, and is quite comparable to the studies mentioned above, but their importance was not evaluated by local geologists until now. It has been found in the study area that the *Posidonia*-bearing limestone facies is always underlain by shallow-water and tidal-flat carbonate sediments of Sehkaniyan Formation, which in turn gradually transitions into radiolarian cherts. This relation clearly suggests facies change from shallow to deep-water environment. The facies change from the underlying shallow-tidal Sehkaniyan Formation into *Posidonia*-rich strata upward and then into Radiolaria dominance at upper

part of the Sargelu formation could help to understand the drowning event in the studied area between Sehkaniyan and Sargelu Formations.

### 8.3.8 Fold structures

The upper part of the Sargelu Formation stands out for its folding structures, which were observed in all outcrops studied. The folded unit has an average thickness of 3 metres, is restricted to one stratigraphic interval, and consists mostly of black shale with rare interbeds of *Posidonia*-bearing limestone and bedded chert. This structure was originally reported by Bellen et al. (1959), but, like many other features of the Jurassic strata, the origin of this structure is still poorly understood. In addition to what has been described by previous studies about the folded unit, the detailed field studies and microscopic examinations in the current study revealed that macro-and microfolded structures are much wider range than that previously reported.

- The current observations suggest that folding in the Sargelu Formation occurred at least at two different intervals: 1) first folding structure has been recorded near the top of the MPLM. 2) The second folding structure is located at the top of the Sargelu Formation within the BRPLM, which represent the major folding event as reported by Bellen et al. (1959).
- Thin-section examination revealed widespread micro-folded laminations with imbricated and broken thin-shelled bivalves occurring through the middle to upper succession.
- Some bedding planes of the MPLM show lobate structures that may suggest sediment downslope flow.

This study concludes that the folding structures are most probably attributed to the downslope slumping of semi-consolidated sediment under the influence of gravity. The strata probably underwent plastic deformation and remained coherent during slumping. The slumping has been assumed based on the observations obtained in the field, where early lithification is easily detectable in the studied folded beds. In spite of extreme folded structures, the bedding remained coherent, and some bedding rupture occurred without any turbulence or liquid behaviour.

### 8.3.9 Oceanic Anoxic Events (OAE)

In contrast to the global Toarcian OAE, the AP in general was not impacted by the Toarcian global OAE. The AP was interrupted by a hiatus during the Early–Middle

Toarcian, and this time interval is equivalent to the megasequence boundary between AP6 and AP7. Sea-level dropped about 75 metres in the Middle Aalenian relative to the Toarcian stage (Al-Husseini, 1997), so marine deposition on the AP was interrupted by a hiatus in the Toarcian, except perhaps for the northernmost areas of the AP mostly was a shallow carbonate evaporite dominance environment with no signs for OAE during that span of time.

The Callovian–Early Oxfordian carbonate strata has been interrupted by the occasional deposition of organic-rich sediments forming the upper part of the Sargelu and lower part of Naokelekan Formations in the study area. The Hanifa formation in Saudi Arabia is organic rich strata, deposited in the Late Oxfordian age, time may be equivalent to the mottled member in the Naokelekan Formation. From previous discussion it can be concluded that neither organic-rich sediment formations of the study area nor other parts of AP were deposited concurrently. Furthermore, the interpreted pattern of eustasy for this interval from Miller et al. (2005) is not observed. Correlation between the Late Bathonian–Callovian hiatus in AP and global sea-level change curve of Miller et al. (2005) shows clear disagreement, when during Late Bathonian–Callovian the Miller curve mainly shows deepening whereas the AP generally subjected to the exposure during that time.

#### **8.4 Naokelekan Formation**

Special consideration has been given to the Naokelekan Formation in the current study, because some unresolved issues remain regarding: mottling, condensation intervals, deep-sea microbial overgrowths on ammonite shells, and a basinward shift of facies from deep marine to sabkha. The Naokelekan Formation was traditionally subdivided into three members, but based on new observations; it can now be subdivided into five different lithologic members, which are:

1. Black shale member (BSM)
2. Carbonaceous limestone member (CLM)
3. medium-bedded microbial-bearing limestone member (MBMLM)
4. Thick-bedded mottled limestone member (TBMLM)
5. Argillaceous limestone member (ALM)

#### 8.4.1 Black shale in the Naokelekan Formation

Lower part of the Naokelekan Formation mainly consists of black shale BSM with rare prominent carbonate beds, including a few poorly preserved planktonic *Protoglobigerina* foraminifera, and some small unidentified fossils and nannofossils. Black shale occurrence has been recorded in the upper part of the Sargelu Formation as well, so it is difficult to determine the contact between Naokelekan and Sargelu Formations. In fact, neither the lower boundary nor the age of the base of the Naokelekan Formation were determined accurately yet. Thus, the current study proposes to rely on the characteristic features at the top of the Sargelu Formation rather than the base of the Naokelekan Formation to determine their contact, for the following reasons:

- The top of the Sargelu Formation is laterally extensive and can be correlated over large areas, whereas the black shale member of the Naokelekan Formation do not appear at all localities which often replaced by carbonate strata.
- Diagnostic features at the top of the Sargelu Formation are quite distinctive and similar at all localities, where it shows slumping and contains *Posidonia* with radiolarian cherts. The Naokelekan black shale member rest sharply on the convoluted bedding unit.

The lower part of the Naokelekan Formation is characterised by a dominance of black shale, significant proportions of *Protoglobigerina* nannofossils were observed. Presently, no attempt was made to determine the age of the lower boundary of the formation, but it is recommended to utilize the *Protoglobigerina* fossils in order to determine the age of the base of the Naokelekan Formation. A lack of sedimentary structures, the dominance of coccoliths with *Protoglobigerina* planktonic foraminifera, and the scarcity of benthic foraminifera in the BSM and CLM may suggest a relatively deep-water depositional environment, and probably was below wave base.

#### 8.4.2 Carbonate units in the Naokelekan Formation

The carbonate unit of the Naokelekan Formation "MBMLM and TBMLM" usually stands out as a resistant ridge between soft more easily eroded shale-rich members. Previous studies considered this carbonate unit as one member that was traditionally known as "mottled limestone member" (Bellen et al., 1959; Buday, 1980; Al-Sayab et al.1982; Jassim and Goff, 2006; Aqrabi et al., 2010). However, more detailed examination in the

current study has revealed the existence of two different members in the mottled limestone unit. Each has its own significant characteristics that will be discussed in detail in the next sections.

The current study revealed that the MBMLM contains no ammonite or mottling texture. Moreover, at the top of this member, a considerable proportion of small lath-shaped limestone calcite pseudomorphs of evaporite with signs of microbial filaments have been observed, and SEM analysis shows that the MBMLM contains numerous probably calcareous nannofossils. The occurrence of pseudomorphs of evaporite in association with coccoliths, and microbial structures have never been previously reported in the Naokelekan Formation. The depositional environment of the evaporite pseudomorphs is difficult to interpret but commonly their association may imply a short period of restricted condition in open-sea, since the sediments that directly underlie and overlie this member have clear faunal evidence of a distinct open marine settings.

All evidence and facies associations within the MBMLM indicate deep water during deposition of the Oxfordian sediments. The evaporite deposition in the MBMLM is comparable to the evaporation from the brine surface model of Kendall (1978, 1992) which stated: "in deep water, evaporite facies the brine is at near saturation with respect to the gypsum. The crystal growth probably occurs along the air-water interface, and crystals settle through the water column as pelagic rain."

#### 8.4.3 Mottled limestone

The mottling texture, which appears as dark and light patches, is probably the most prominent texture in the Naokelekan Formation. Origin of the mottling has been discussed in detail in chapter 4. The mottled patches within TBMLM show different textures, and it has been found that bioturbation can be considered as the major factor forming mottled textures in the Naokelekan Formation. The mottled textures show various evidence of bioturbation including: a) abundance of disrupted and truncated textures, b) Lithologic difference between dark and light patches, c) sharp boundaries between light and dark patches d) lack of pigmentation diffusion between different patches, e) existence of collapsed clasts, f) existence of the recessive rounded pits on bedding surfaces.

Both macro-and microfabrics of the TBMLM reveal for the first time that the dark patches are formed by microbial activity. The dark patches mainly consist of very compact bindstone and can be considered as parent rocks. The diagnostic features of the

microbial structures in the TBMLM displaying thin laminae, absence of fenestral porosity, growth on ammonite shells, and coccoliths association, are comparable in many ways to deep water microbialites. The TBMLM mainly contains two kinds of microbial stromatolites; small vertically stacked hemisphere or columnar stromatolites and high relief laterally linked hemisphere stromatolites. The facies association suggests that the TBMLM represents a relatively deep water environment, and the associated ammonites, coccoliths, *protoglobigerina*, and deep-sea microbial stromatolites support this interpretation.

Through scanning electron microscope observation, additional important components of the Naokelekan and Sargelu Formations were discovered. SEM analysis demonstrates that the MBMLM contains numerous calcareous coccoliths. These objects form the majority of the groundmass, and they usually make up 90% of the micrite constituents. The appearance of coccoliths ranges from the upper part of the Sargelu Formation to the top of the mottled limestone member.

#### **8.4.4 Argillaceous limestone member and calcispheres**

The upper part of the Naokelekan Formation, which is represented by the argillaceous limestone member (ALM) in the current study, was traditionally well known for its organic-rich black shale, but its origin remained unknown since their initial descriptions almost 65 years ago. Microscopic study shows that the ALM is mainly composed of a calcispheric packstone containing kerogeneous material. No other fossils have been observed. A monospecific population of calcispheres makes up more than 90% of the bulk rock, which can be observed throughout the study area. The widespread occurrence of calcispheres at the top of the Naokelekan Formation for more than 450 kilometres can be a useful tool for correlation. Based on morphology characteristics, the calcispheres are more comparable to calcareous dinoflagellate cysts. The results of this study suggests that the ALM was deposited in a relatively deep-sea with low dissolved oxygen ocean.

## 8.5 Barsarin formation

The average thickness of the Barsarin Formation is estimated to be about 30 metres, and the formation clearly shows a westward thickness increase. The Barsarin Formation has been subdivided into three lithofacies, from oldest to youngest:

- Microbial laminite lithofacies (MLL)
- Blister–flat laminated lithofacies (BFLL)
- Thick-bedded dolomite–limestone lithofacies (TBDLL)

A distinctive characteristic of the Barsarin Formation is the repetition of lithofacies assemblages. Each assemblage usually begins with a microbial laminite lithofacies, followed by blister–flat laminated lithofacies, and ends with thick-bedded dolomite–limestone lithofacies. Field studies found that the numbers of repeated lithofacies vary from one place to another, e.g. at Barsarin village, nine repetitions have been recorded, whereas at Gara location, only five lithofacies repetitions were observed.

### 8.5.1 Microbial laminite lithofacies (MLL).

In the current study, it has been found out that the MLL is often overlain and underlain by BFLL and TBDLL respectively. Based on the bedding morphology, the MLL was subdivided into two main types, which are planar and domal morphologies. The former mainly constitutes the MLL, whereas the domal stromatolite morphology has been only observed in the upper part of the sections. MLL principally demonstrates continuous laminations with couplets of thin dark micrite and thick light microsparite laminae. The MLL mainly comprises clotted microtexture, or as it is also termed “texture grumeleuse”, and the results suggest that the clotted fabrics represent the most widespread microbial community in the MLL, which can create a microenvironment conducive to carbonate precipitation. The MLL includes numerous fenestrae, which may be related to gas entrapment, and the fenestrae cavities are completely or partially filled with calcite cement.

MLL is interpreted to record microbially dominated sedimentation in a protected subtidal environment. Based on the presented discussion, it can be concluded that the MLL represents a relatively hypersaline subtidal environment and an isolated water body, where the current action is weak, and relatively less liable for precipitation of evaporites. The current action and sediment supply may increase upward when the domal stromatolites begin to appear. Faunas are rare, so grazing activity is minimal. No

evidence of subaerial exposure such as mud cracks or tepee structures exist in the MLL. So, subtidal rather than inter- or supratidal environments are suggested.

#### 8.5.2 Blister-flat laminated lithofacies (BFLL)

The BFLL usually overlies the MLL, and can be easily distinguished in the field due to its blistered structures. The BFLL are usually laminated dolomite-calcite couplets. The blistered laminae display wrinkle to irregular structures of small-scale dome-shaped laminations which appear as a laterally linked hemisphere. Furthermore, it has found that the blistered laminae demonstrate disrupted and scoured surfaces with laminoid-fenestral fabrics. It has been found that these open-space structures occurred particularly in microbial carbonate by gas trapping under microbial mats made "leathery" due to considerable exposure and desiccation. Flat laminae have the same characteristics as blistered laminae, except that they lack laminoid-fenestral fabric pockets and small chert nodules. The absence of laminoid-fenestral fabrics in the flat laminae has been related to the relatively high rigidity of flat lamination, suggesting early lithification. The co-occurrence of blistered and flat laminations in the same bed is very common, and the succession usually begins with blistered laminae, and is followed by flat laminae. This order, i.e. repetition between blistered-flat laminae can occur for two or three times, and the succession is often capped with flat-laminated textures. Rapid alternation between blistered and flat textures may reflect sea-level fluctuations from lower to upper intertidal zones respectively, or could represent flooding events from storms as in analogue Abu Dhabi.

Evidence of cyanobacterial filaments suggests that the blistered-flat fabrics in BFLL originated from microbial mats. The coexistence of blistered and flat microbial structures with evaporite pseudomorphs, intraformational clasts and laminoid fenestrae could suggest that the BFLL was deposited in mid-upper intertidal environments of a hypersaline sea in arid climates, which is quite comparable to the blister-flat microbial stromatolite from a Holocene tidal flat complex of the Arabian Gulf coast, Abu Dhabi.

The couplets of dolomite and calcite represent the most characteristic feature of the BFLL, where the dolomite laminae appear as undulated and irregular layers and alternate with calcite laminae. It has been interpreted that the interlaminated dolomite and limestone in BFLL are comparable with modern analogues of microbial mats in tidal flats of Aqaba Gulf and Trucial Coast, which are composed of an alternation of microbial mats and particulate carbonate laminae, and were addressed as "dolomite related to microbial mats". In the current study, it has been found that the microbial laminae would

correspond to the dolomite because the Mg-rich organic material in the microbial sheaths will remain stable and does not decompose or release until long after deposition, and released Mg goes on to form dolomite more or less in situ in the microenvironment of microbial mat layer.

However, recent studies argued that the released Mg from decomposition of microbial sheaths is not the main cause behind interlaminated dolomite, but it seems that the dolomitization occurred during early diagenetic stages mediated by microbial activity. Modern carbonate deposition analog and experimental research concerning bacterial populations with mineral forming processes have revealed that unique microenvironmental conditions producing high Mg–calcite and dolomite formation and their interlayering with calcite laminae. It seems that calcite precipitation occurred in the uppermost layers of the microbial mat, where oxygenic photosynthesis and aerobic respiration prevailed, whereas dolomite minerals precipitated in the underlying anoxic layers of the microbial mat, where sulphide oxidation and sulphate reduction prevailed, and producing Mg concentrations. Furthermore, according to Rao et al. (2003) decaying organic sheaths associated with sulphate–reducing cyanobacteria promoted dolomite formation. The microbialites may have provided the nuclei for the origin of dolomites in many ancient carbonate successions. The microbial–related dolomites are interpreted to have formed under anoxic sulphate–reducing and hypersaline conditions, and dolomitization is considered as biominerally formed in the early stages of diagenesis.

### 8.5.3 Thick-bedded dolomite–limestone lithofacies (TBDLL)

The TBDLL is buff in colour, fine-crystalline dolomite and limestone, and it generally comprises two main lithologies; dolomite and limestone. The TBDLL sequences often begin with dolomitized units followed by limestone lithologies. The field observations show that the TBDLL always overlies the BFLL, and underlies the MLL. In summary, the TBDLL is characterised by including large lensoidal cherts, gypsum, and anhydrite, and often displays an irregular upper boundary. Signs of desiccation have been inferred from the presence of polygonal cracks, and tepee structures. Many horizons of intraclasts were recorded, and the TBDLL, similar to other lithofacies, show a lack of the terrigenous clasts. Therefore, these clasts have been considered to be of intraformational origin. In addition to providing further evidence for a dominance of desiccations features in this lithofacies, see Chapter 5, a model has been proposed to explain dolomitization as well. Also the relationship between evaporites and silicification has been interpreted.

#### 8.5.4 Dolomite related to sabkha environments

The TBDLL generally consists of fine crystalline dolomite which is associated with tepee structures, polygonal cracks, evaporite minerals or their pseudomorphs, intraclasts, and collapsed breccia related to evaporites, with rare fossils. By analogy with the recent sediments, it has been concluded that the TBDLL developed on an evaporitic carbonate tidal flat of the sabkha environment; since a great bulk of recent similar dolomite occurs in the supratidal portion of tidal flats. There is a remarkable similarity between the TBDLL and the supratidal of the sabkha model of Trucial Coast, Arabian Gulf. This presumption is based on evidence of highly arid conditions and shallowing-upward succession cross-sectional profile. The evaporite–dolomite phase has been described from ancient deposits as well (Roehl, 1967; Rabet, 1981; Alsharhan 1993; Tourir, 2009; Meister et al., 2013).

The penecontemporaneous dolomitization is well-documented in modern environments with strong support from experimental studies in that it can only form from a high Mg/Ca ratio (Hardie, 1987). The association of fine grain or penecontemporaneous dolomite and gypsum in recent supratidal settings is well documented, particularly on the Trucial Coast of the Arabian Gulf (Wells, 1962; Curtis et al., 1963; Illing et al., 1965; Shinn et al., 1965; Kinsman and Patterson, 1973; Yechieli and Wood, 2002; Alsharhan and Kendall, 2003; Bontognali et al., 2010; Sadooni, 2010). This study confirms that the early dolomitization took place through evaporite pumping or ascending brine solute at a narrow strandline at the boundary between inner sabkha and upper intertidal zones; whereas the limestone unit represents an outer sabkha zone. Consequently, in the shallowing-upward succession thick-bedded dolomites are followed by thick-bedded limestone, which indicate a basinward shift of facies from outer to inner supratidal zone. The shift of facies from dolomite to limestone is well interpreted in the Trucial Coast of the Arabian Gulf by Patterson and Kinsman (1981, 1982). However, new research on the Trucial Coast concluded that the high Mg/Ca ratio is not the only governing factor of penecontemporaneous dolomitization, but dolomite precipitation can form within exopolymeric substances (EPS) as well. In this new model, dolomitization is linked to microbialites that can tolerate high pH values and alkalinity and lowers sulphate concentrations of interstitial waters (Bontognali et al., 2010; Sadooni, 2010).

## 8.6 Sequence stratigraphy

Chapter 6 has studied in detail the sequence stratigraphy of the Jurassic successions which are the most prolific oil-bearing interval in Iraq. Investigations of sequence stratigraphy can be useful because it may lead to a better understanding of the basin development. The Jurassic succession in the study area comprises interbedded carbonates, organic-rich shale and evaporites, and the carbonate units often form the reservoirs which are capped and sealed by evaporite units.

Sequence stratigraphy is challenging in Kurdistan and needs more attention because: (1) the lack of high-resolution chronostratigraphy for either surface or subsurface sections has considerably reduced their utility for sequence stratigraphy application. (2) Late Cretaceous collision between the Arabian and Persian blocks resulted in the development of structural overprint, (3) Wide areas of the western margin of the Gotnia Basin are exposed to subaerial erosion, and (4) so far; no comprehensive seismic studies were conducted in this area, so the basin development and stratigraphy are poorly defined. Generally, the Late Triassic–Late Jurassic period has been subdivided into four depositional sequences of third order, which are Latest Triassic–Early Jurassic, Middle Jurassic, Late Callovian–Oxfordian, and Late Oxfordian–Early Kimmeridgian, but the current study has focused on the Middle–Late Jurassic period.

### 8.6.1 Sb2

Previous studies agreed that the boundary between AP6 and AP7 represents a major unconformity which occurred during Late Toarcian to Early Aalenian eustatic fall in global sea-level (Al-Husseini, 1997; Ziegler, 2001). Based on the local studies the contact between Sehkaniyan and Sargelu Formations matches this boundary, which is called Sb2 herein. However, the field observation revealed that the base of the Sargelu Formation or BSDM, was subjected to destructive dolomitization and all the original textures were eliminated and destroyed. So, there is yet no absolute certainty of the primary sedimentary or pre-dolomitization origin, and with the lack of biostratigraphic and geochemical evidence, caution must be applied. This doubt concerning the depositional origin of destructive dolomitization casts considerable uncertainty on attempts to determine the Sb2 position in the sections as well. According to this interpretation the basal saccharoidal dolomite member (BSDM) could be part of the relative sea-level fall period, and the Sb2 would be located at the base of the middle *Posidonia* limestone member (MPLM), i.e. the boundary of Sb2 probably occurred later than what was previously believed.

The relative sea-level rose during Early Bajocian and lasted until the end of the Callovian, and in the meantime; the Neotethys Ocean expanded and transgressed westward far onto the Arabian Craton (Sharland et al., 2001). This rise in the sea-level in the AP is consistent with the evidence that has been presented for the Sargelu Formation. Facies changes between Sehkaniyan and Sargelu Formations of Early–Middle Jurassic may indicate the deepening upward in the studied area, where the Sargelu Formation, which is rich in *Posidonia* and radiolarian fauna, rests abruptly on a shallow to intertidal Sehkaniyan Formation strata that shows clear transitions from shallow intertidal facies to pelagic environment over several metres. Most of the articles, either in AP or in Iraq considered relative sea-level rise in Bajocian–Callovian as an indication that the drowning events took place regionally, and most evidence support this as well.

However, the findings of the current study do not support the previous research which suggested that the base of Naokelekan Formation, i.e. the black shale member (BSM), was deposited in an intertidal environment. The results from this study indicate that the base of the Naokelekan Formation or the BSM represents a hemipelagic depositional environment. This contrast may explain the different interpretations of sequence stratigraphy between this and previous studies. Thus, Balaky (2014) has considered the top of the Sargelu Formation as a mfs during Bathonian age, whereas the present study suggests that this mfs may extend into Middle–Late Callovian age of the Naokelekan Formation that herein is called MFS2.

### 8.6.2 Sb3

As it has been mentioned previously, the traditional mottled limestone member has been subdivided into two members for the first time, which are MBMLM and TBMLM. Although no evidence for evaporites were reported from outcrops of the Sargelu and Naokelekan Formations, the recently drilled wells show horizons of evaporites about 40–60 km southwest of the study area (Fatah, 2014). However, for the first time some probable indications of evaporites were observed in the MBMLM, which has been interpreted that restricted conditions took place during deposition of the MBMLM. The existence of evaporites in the studied outcrops is inferred to represent sea-level fall. Based on the co-existence of probable signs of evaporitic, coccoliths and traces of microbes the Sb3, the base of MBMLM was suggested as a sequence boundary. There are no subaerial exposures. Thus Sb3 is presumably a correlative conformity to succession of a sequence boundary unconformity on the platform top at western and shallower part of Gotnia Basin. The biggest challenge here is the difficulty in correlation between correlative conformity

and unconformity boundary because: (1) the basin is poorly constrained, and palaeo–or chronostratigraphy is not supported by new technology and ammonite zonation data. (2) Stratigraphic subdivision development in the study area that was continuously submerged, do not show clear sequence boundary or other direct evidence for sea-level fluctuations.

### 8.6.3 HST3

Thick-bedded mottled limestone member (TBMLM) is the most controversial lithofacies of the Oxfordian deposition in the study area. A previous study considered mottled facies as a TST (Balaki 2014), but, herein, it has been suggested that the condensed pelagic successions were deposited during periods of HST when a slowed down current activity allows the preservation of the pelagic input, and the lowstand may generate hardgrounds as a result of acceleration winnowing prevented deposition. The disagreement of the current sequence stratigraphy might have been due to the difference in the interpretation with new subdivisions of facies. The basin analysis study confirmed that the condensed facies within the TBMLM is quite analogous to the condensed Ammonitico rosso Facies.

### 8.6.4 Sb4

The bedding surface at the top of the TBMLM could be a combined sequence boundary Sb4 with maximum flooding surface, which is determined based on the following considerations: (1) horizons of the microbial stromatolite overgrowth on ammonites, which are inferred to be characteristic of the hardground, associated with a hiatus and a low rate of sedimentation, recorded at the top of the mottled member. (2) Evidence of calcisphere in the last facies of Naokelekan argillaceous limestone may represent the onset of a new transgressive period.

### 8.6.5 Problematic boundary between Early–Middle Kimmeridgian

The boundary between the Early and Middle Kimmeridgian age, which represents the Naokelekan/ Barsarin Formations contact, shows an abrupt basinward shift of facies from Ammonitico Rosso to sabkha. The abrupt facies change indicates large water–depth variation, and this change is considered to be of great importance for the understanding of the basin development. According to Numan (1997), this abrupt facies change could be tectonically controlled, and represent timing of incipient subduction between Arabian and Persian plates. However tectonic studies confirm continuation of Neotethys in expansion through Jurassic time, and subduction commenced later in the

Cretaceous (Stampfli et al., 2001; Ziegler, 2001; Sharland et al., 2001). The current study assumed that the Gulf of Suez could be the best model for uplifted block that occurred during extensional periods, where significant uplift has been recorded contemporaneous directly to adjacent subsidence (Omar et al., 1989; Cross et al., 1998). Bosence (2005) has also pointed to the rifted Gulf of Suez as an uplifted fault block platform model, where a shallow marine setting overlies deeper sediments.

Previous literature considered Naokelekan and Barsarin formations as an unfilled accommodation space in the sediment-starved centre (Buday, 1980; Jassim and Goff, 2006; Aqrabi et al., 2010). If Naokelekan Formation strata were deposited in a deep basin, it would be difficult to explain what the mechanism responsible for this water depth change. Furthermore, it is considered impossible for the Barsarin Formation to be deposited in a deep starved basin as well, because there is significant observations consistent with supratidal environments. The abrupt facies changes from basinal marina to sabkha between Naokelekan and Barsarin Formations could be related to the sudden uplift that happened during extension processes rather than subduction, perhaps for these reasons (1) the subduction occurred later in the Cretaceous period (2) the sudden uplift of studied Upper Jurassic strata is comparable to uplifted fault block of Gulf of Suez.

#### 8.6.6 Sequence stratigraphy of Middle–Late Kimmeridgian

Despite the fact of the existence of an enormous number of publications concerning petroleum geology in the study area, research on the sequence stratigraphy on the Barsarin Formation was not performed. A prominent characteristic of this sequence, which is represented as HST4, is the repetition assemblages of lithofacies with shallowing-upward facies succession. Each assemblage usually begins with a microbial laminite lithofacies, followed by blister–flat laminated lithofacies, and ends with thick-bedded dolomite–limestone lithofacies. The numbers of repeated cycles in the study area differ from one place to another. Generally, six to nine cycles have been recorded that often display a sort of arrangement where it normally commences with microbial laminite lithofacies. Due to variations of cycle numbers in different localities within the study area, it has been inferred that these cycles could be controlled by relative sea-level rather than eustasy. Evidence from the global plate tectonic reconstruction suggests that extensional faults may generate the right amount of accommodation in the AP (Ziegler, 2001; Stampfli et al., 2001; Stampfli and Borel, 2002). The variability of cycles from one location to another cannot be dismissed from a tectonic control (Bosence et al., 2009).

So, the difference in stacked peritidal cycle numbers in the Barsarin Formation from location to location could be explained by evidence of active extensional faults.

The upper contact between the Barsarin and Chia Gara Formations could represent a combined sequence boundary Sb5 with maximum flooding surface of Chia Gara Formation. At the same time, it could be a second drowning event which occurred in the Middle Late Jurassic sequence, between Kimmeridgian and Tithonian. Last beading at in the Barsarin Formation displays clear evidence for desiccation, such as tepee and polygonal mudcrack structures with many signs of evaporite pseudomorphs. At all localities, the sabkha Barsarin Formation is sharply overlain by basinal marine strata of the Chia Gara Formation.

## 8.7 Condensed facies

Elliot and Bellen et al. (1959) were the first who pointed to the possible existence of condensed intervals in the Naokelekan Formation, and they principally assumed that the condensed intervals should be somewhere within the mottled member. Despite clear demands for further studies and extensive evaluation suggested by Bellen et al. (1959), the condensed facies did not receive sufficient consideration in the last six decades, and the causes behind these events have yet to be identified conclusively.

Based on the evidence presented in Chapter 7, the general conclusion is that the TBDLL may be considered as ammonitico rosso facies. The TBDLL is characterized by a combination of microbial stromatolite overgrowth on ammonites, oncoids, coccoliths, intense bioturbations, and hardgrounds. There are two theoretical models that can be offered to explain the ammonitico rosso development: (1) the ammonitico rosso facies of the TBDLL could have developed on a tilted fault block bathymetric high. (2) The ammonitico facies developed under similar conditions on the distal basin floor, with no high present. The present study has focused on the first model, i.e. ammonitico rosso on the bathymetric high. During literature review in Chapter 7, it has been observed that there are no articles available on a distal basin floor model so far. Although herein it has been focused mainly on bathymetric high, it is difficult to decide which one of these models is closer to the reality. Additional data should be collected in future that would allow to determine which hypothetical model is more correct.

Clearly, the ammonitico rosso facies has been sufficiently studied in Europe. These studies emphasize that the development of the ammonitico rosso facies occurred on bathymetric high within condensed facies during Middle–Late Jurassic rifting. The

importance of this section lies in the tectonic development and sequence pattern which are quite comparable to those that have been described from the Middle–Late Jurassic sequence in Europe. Similarly, the seismic studies in combination with synthesis of the tectonic and sedimentological evolution of the eastern margin of the AP during Jurassic period suggest rifted basin development with prevalence of graben and fault blocks. Numerous studies pointed to the occurrence of the ammonitico rosso on the bathymetric highs, and the provided evidence from seismic data suggests that the bathymetric highs developed on fault blocks. Jassim and Goff (2006) suggested that a phase of rifting interpreted to have occurred in Oman and may extend further north along the margin of the AP into the study area, but, again no conclusive evidence for this extension exists. The ammonitico rosso in condensed facies is relatively unfamiliar in the AP or the study area and only very few studies exist. Middle–Late Jurassic successions of Callovian to Oxfordian age in the central Pontides Basin in Turkey, may represent the nearest reported location to the study area that contains ammonitico rosso facies (Rojay and Altiner, 1998).

An important challenge arises from the suggested tilted fault block model when we deal with peculiar stratigraphic sequences resulting from sedimentation on a supposed palaeobathymetry, especially if the study area suffers a lack of seismic and tectonic studies. The main features of the study basin are: microbial stromatolite overgrowth on bathymetric and high basin floor deposits, where no siliciclastic sediment supply exists from the continental shelf or land–derived sediment. The Jurassic succession of the Naokelekan Formation shows sufficient evidence and sedimentological features to suggest that this formation is comparable to the ammonitico rosso facies that in turn gives clues to the understanding of the relevant processes. Although modern analogue of ammonitico rosso has not been found yet, the field and microscopic observations in the TBMLM of the Naokelekan Formation match those from the ancient ammonitico rosso analogue.

Based on the available evidence in Chapter 7, the ammonitico rosso most likely has developed on a tilted fault block bathymetric high, but the weak point is that the study area lacks direct evidence for bathymetric high, so the distal basin floor could be also potential environment until future tectonic and seismic studies will be performed to elucidate this issue. The most important similarities between the TBMLM and ancient condensed ammonitico rosso analogues are:

- Existence of deep-sea microbial stromatolite overgrowth on ammonites with coccoliths groundmass.
- Characterised by low sedimentation rate, hiatus, bioturbation, and hardground surfaces.
- An obvious impact of currents on the condensed intervals by its contribution in sweeping sediments.
- Always appear as condensed successions.
- Ammonitico rosso facies usually occurs vertically adjacent to the *Posidonia*, radiolarian bedded chert facies.
- Their occurrence specified a particular time period which is usually Middle–Late Jurassic.
- They occur on the pelagic bathymetric highs, and the sediments usually lack terrestrial inputs.

A few hundred metres is a reasonable depositional water depth to infer for condensed strata of the Naokelekan Formation. At the top of this depth range, the effects of wind-driven currents may be enough to sweep sediment. Martire (1992) stated that the condensed sequences ought to record climatic changes through reaction chains involving currents, climate, eustasy, and facies at this depth. The opportunity for sediment preservation on the condensed isolated plateau usually increases during relative high sea-level stands where the effect of a current is reduced. The onset of sedimentation of the mottled facies represents a highstand systems tract that seems to have occurred in the following middle and upper transgressive medium-bedded evaporite facies. According to Loutit (1988) and Martire (1992) the pelagic carbonate particles “planktonic rain” fall towards the bottom and they are mostly preserved on the plateau during low current activity.

## *CHAPTER NINE*

### *9 CONCLUSIONS AND RECOMMENDATIONS*

## 9.1 Conclusions

### 9.1.1 Sargelu Formation

1. This study strengthens the idea that the depositional basin of the AP in the Jurassic period occurred during progressive phase of the rifted margin on the epicontinental basin. During Middle–Late Jurassic time, the studied area was subjected to rifting and many horst and graben structures were formed in the depositional basin. The Middle–Late Jurassic Formation is interpreted to have been deposited on one of these horsts, and could be considered as fault–block platforms or tilted block highs.
2. Seasonal upwelling currents contributed to high productivity and accretion rates of radiolarites in the central Neotethyan basins during the Jurassic. This is likely to be the main cause of chert formation at the upper part of Sargelu Formation.
3. Previous evidence suggests that the principal silica source for the bedded chert in the Sargelu Formation is biogenic silica from opal–secreting radiolarian organisms. Densely packed radiolarian fossils may make up over 85% of the bulk of bedded cherts, and their radiolarian shells are homogeneously distributed in the bedded chert.
4. Bedded chert of the Sargelu formation could correlate to the Kermanshah radiolarian deposition, but the lateral extension of the bedded chert between Kurdistan Region and Kermanshah area has not been traced yet, so the link between these areas is assumed, pending future investigations.
5. This study suggests that development and variation in the shell preservation style are of great importance in determining the palaeoenvironment of MPLM Sargelu Formation. The transition from the intensely broken fragmented shells of the MPLM to the intact or fragmented bivalve shells of PBLL indicates a transition from shallow depth, where storm conditions disturb the sea bottom, to a low-energy depositional environment below fair–weather wave base.
6. Accurate examination of different lithofacies in the Sargelu Formation reveals the common presence of turbidity or allodapic succession. The following turbidite intervals were recognised: a) graded bedding, b) laminated structures, and c) bedded chert or black shale.
7. The posidonia-bearing limestones often appear as a transitional stage between the drowned basin of Sehkaniyan Formation and radiolarite sub-facies, this probably implies deepening upward.
8. Results indicate that the folding structures may be attributed to the downslope slumping of semi-consolidated sediment under the influence of gravity, in which the

sedimentary strata display plastic deformation and remain coherent during translation.

9. Facies changes between the Sehkaniyan and Sargelu formations of Early–Middle Jurassic suggest drowning events in the studied area, where the Sargelu Formation is rich with *Posidonia* and radiolarian fauna.
10. According to the current study the Sargelu Formation age may extend into the Middle–Calloviaian.
11. The depositional basin of the Sargelu Formation bedded chert is assumed to be developed on a relatively narrow and elongated basin, which extends for hundred kilometres from Sirwan valley to Zakho but are a few tens kilometres in width.

### 9.1.2 Naokelekan Formation

1. According to the outcrop observations and by comparing with those of subsurface sections along–strike length, the interpreted submarine tilted fault block structure in the study area is about 450 km, but the width is not well defined due to over–thrusting in the east. Regional correlations suggest that the condensed intervals could extend as an elongated structure into the Arabian Gulf.
2. The condensed facies of the Naokelekan Formation could be significantly influenced by unidirectional marine currents. Erosion and reworking by these currents led to a further reduction in sediment thickness.
3. It can be concluded that the mottled texture in the Naokelekan Formation is formed through bioturbation, and the intense bioturbation in the mottled facies imply an oxygenated environment.
4. It has been discovered for the first time that the dark patches are the pre-bioturbation sediment matrix deposited under the influence of microbial activity.
5. The condensed pelagic microbial stromatolite facies is interpreted to be developed on a bathymetric high, received a minimal supply of terrigenous and platform–derived sediment. However, the condensed stratigraphic could all represent a distal basin floor setting, with low sedimentation rates due to little micro–and nannoplankton pelagic production during most of the Jurassic, and slow microbial activity driving accumulation at sites away from sediment gravity–flow deposition.
6. The pelagic stromatolitic condensed facies of the Naokelekan Formation closely resembles ammonitico rosso facies developed on other Neotethyan margins.
7. Low sedimentation rates are indicated by intense bioturbation, intervals with firmground to hardground substrate, microbial crust overgrowths on ammonite shells and lithoclasts, and micro–borings between stromatolite lamination.

8. Coccoliths make up about 90 percent of the bulk of the particles usually being trapped by microbial stromatolites. The appearance of coccoliths occurred during deposition of the upper part of the Sargelu Formation and lasted until the top of the mottled limestone member.
9. Evaporite associations in the MBMLM of the Naokelekan Formation, may imply a short period of restricted conditions in open marine, since the sediments that are directly underlying and overlaying this u have definitive faunal evidence of a distinct open marine sequence.
10. Argillaceous limestone member in the Naokelekan Formation comprise a monospecific population of calcispheres. The widespread occurrences of calcispheres at the top of the Naokelekan Formation for more than 450 kilometres can be an effective tool for correlation.
11. Organic rich intervals in the study area and other parts of AP were not deposited concurrently, and the AP in general was not impacted by the Toarcian OAE.
12. Impact of relative sea-level oscillations that affected the carbonate platform top elsewhere on the AP was not clear in this formation in the study area, most likely because they accumulated in deep-water where depth and energy changes related to RSL cycles had little or no impact.

### 9.1.3 Barsarin Formation

1. The results suggested that the MLL represents a relatively saline subtidal environment and an isolated water body, relatively less liable for precipitation of evaporites than other facies of Barsarin Formation.
2. The blistered–flat fabrics in BFLL of the Barsarin Formation originated from microbial mats. Laminoidal fenestrae could suggest that blister structures were deposited in the mid–intertidal environments of a hypersaline sea in arid climates, whereas the flat laminae structures occurred at upper part of intertidal environment.
3. Great bulk of fine crystalline dolomite with gypsum or their pseudomorphs, and desiccation structures suggest that the TBDLL formed in an evaporative carbonate tidal flat of the sabkha environment.
4. Shallowing-upward cycles in the Barsarin Formation are concluded by a marine sedimentation succession, which normally begins with an abrupt subtidal environment over an earlier supratidal sabkha facies. The ideal shallowing cycles normally commences with microbial laminate lithofacies and passes upwards into blister flat stromatolite lithofacies to be capped by thick-bedded dolomite–limestone lithofacies.

5. All facies in the Barsarin Formation are completely devoid of terrigenous components, suggesting that the major sediment sources supplying the sabkha derived from; i) chemical precipitation, and ii) storm periods which sweep only carbonate sediments from the subtidal zone.
6. It has been concluded that the bedding surface at the top of TBMLM could be a combined sequence boundary and maximum flooding surface.

## 9.2 Recommendations

1. The Middle–Late Jurassic succession outcrops extend from southeast to northwest through eastern Iraq. The southeastern end of the outcrop approaches the Iranian border near Sirwan Valley, but because of political obstacles, it is not currently possible to correlate the studied succession with others located across the border. Based on this study the condensed section of the Naokelekan Formation most probably crossed the border to Iran, but no report has been published about them. Similarly, Jurassic successions at the northwest end of study area, which approach the Turkish border, have not been correlated with those in Turkey yet. So, there is an urgent need to find a correlation between Jurassic exposures in northern Iraq with each of those in Turkey and Iran, which are called Cudi and Surmeh group respectively.
2. Subsurface strata west of the study area in the Gotnia Basin are poorly linked and correlated to the Kurdistan outcrops. Improved biostratigraphy, well and seismic studies may help to find the subsurface lateral extension of the Jurassic strata.
3. Detailed further investigation of the tectonic development during Permian–Jurassic time in the study area is a required to understand how probable rifting episodes controlled accumulation of strata.
4. Trace the lateral extension of bedded chert between Sargelu Formation and Kermanshah radiolarians.
5. Further studies need to be carried out in order to understand turbidite structures or the characteristics of the allodapic limestones in Sargelu Formation.
6. We recommend applying biostratigraphic techniques using the *Protoglobigerina* and radiolarian fossils, in order to determine the age of the base of the Naokelekan and the top of Sargelu Formation.
7. There is serious doubt concerning the boundary between Sehkaniyan and Sargelu Formations in the study area which is deformed by destructive dolomitization. In order to relocate Sb2 positions precisely detail study on the depositional origin is needed.

There is also a need for further research in order to establish strong evidence regarding the existence or absence of Late Toarcian–Aalenian in the study area.

8. Construction of an ammonite zonation for these Jurassic strata is a pre-requisite for further sequence stratigraphy study.
9. More studies are needed to understand the association between pseudomorphs of evaporite in with coccoliths and microbial structures in the MBMLM.
10. Coccoliths are of great importance due to their applications in palaeoenvironment determination and age of the formations. There is an urgent need for research to identify the coccoliths as precisely as possible of the Middle–Late Jurassic of the study area.
11. The ammonitico rosso facies of the TBMLM could develop either on a bathymetric high or under similar conditions on the distal basin floor. Bathymetric high theory was discussed in Chapter 7 in detail. A future study investigating distal basin floor theory would be very interesting. It is recommended that extra field and seismic data should be collected to determine which hypothetical model is more likely.
12. Although two main hypotheses have been suggested to explain the possible origin of dolomitization in the Barsarin Formation, further detailed studies are needed to explain the possible mechanism of dolomitization and to determine which of the following hypotheses is closest to the truth.
  - Interlayered dolomite in the BFLL has been interpreted to be related to microbial mat, or dolomitization may have been occurred in early diagenetic stages mediated by microbial activity.
  - Evaporite pumping or exopolymeric substances (EPS) as a possible origin of dolomitization in the TBDLL.
13. Because numbers of possible high-frequency cycles differ from place to place in the Barsarin Formation, and locations do not represent typical cycles due to the lack of one of the facies, further quantitative analysis would be useful in order to interpret sequence stratigraphy.

## **References**

- Abdula, R.A., 2014. Hydrocarbon potential of Sargelu Formation and oil–source correlation, Iraqi Kurdistan. *Arabian Journal of Geosciences*, **8**, 5845–5868.
- Abdolizadeh, S., Maleki, Z. and Arian, M. 2016. Earthquake Hazard Zonation and Seismotectonics of the Bandar Abbas Area, Zagros, Iran. *Open Journal of Geology*, **6**, 210.
- Aigner, T. 1989. *Quantitative modeling of carbonate platforms: some examples*.
- Aitken, J.D. 1967. Classification and environmental significance of cryptalgal limestones and dolomites, with illustrations from the Cambrian and Ordovician of Southwestern Alberta. *Journal of Sedimentary Petrology*, **37**, 1163–1178.
- Al Ahmed, A. A. N. 2012. Determination and applications of chemical analysis to evaluate Jurassic hydrocarbon potentiality in Northern Iraq. *Arabian Journal of Geosciences*, **6**, 2941–2949.
- Al-Ahmed, A. 2006. *Organic geochemistry palynofacies and hydrocarbon potential of Sargelu Formation (Middle Jurassic) Northern Iraq*. PhD thesis, University of Baghdad.
- Al-Ameri, T. K., and Al-Nagshbandi, S. F. 2014. Age assessments and palynofacies of the Jurassic oil source rocks succession of North Iraq. *Arabian Journal of Geosciences*, **8**, 759–771.
- Al-Ameri, T. K., and Zumberge, J. 2012. Middle and upper Jurassic hydrocarbon potential of the Zagros fold Belt, North Iraq. *Marine and Petroleum Geology*, **36**, 13–34.
- Al-Ameri, T. K., Najaf, A. A., Al-Khafaji, A. S., Zumberge, J., and Pitman, J. 2013. Hydrocarbon potential of the Sargelu Formation, North Iraq. *Arabian Journal of Geosciences*, **7**, 987–1000.
- Al-Azzawi, A. M. N., and Dawood, R. M., 1996. Report on detailed geological survey in northwest of Kilo 160–Rutbah area. *GEOSURV*, int. rep. no. 2491.
- Al-Badry, A., 2012. *Stratigraphy and geochemistry of Jurassic formations in selected sections north Iraq*. Ph.D. thesis, University of Baghdad, Baghdad, Iraq, 162.
- Al-Husseini, M. I. 1997. Jurassic Sequence Stratigraphy of the Western and Southern Arabian Gulf. *GeoArabia*, **2**, 361–382.
- Ali, M. Y., Watts, A. B., and Searle, M. P. 2013. Seismic stratigraphy and subsidence history of the United Arab Emirates (UAE) rifted margin and overlying foreland basins. In: K. Al Hosani et al. (eds.) *Lithosphere Dynamics and Sedimentary Basins: The Arabian Plate and Analogues*. Frontiers in Earth Sciences, Springer–Verlag Berlin Heidelberg, 127–143.

- Al-Jaafary, A. S., and Hadi, A., 2015. Hydrocarbon potential, thermal maturation of the Jurassic sequences, and the genetic implication for the oil seeps in North Thrust Zone, North Iraq: *Arabian Journal of Geosciences*, **10**, 8089–8105.
- Al-Jiburi, B. S., and Karim, S. A. 2009. Contribution to the age determination of the Najmah Formation, from surface outcrops in the Iraqi Western Desert. *Iraqi Bulletin of Geology and Mining*, **5**, 1–8.
- Al-Juboury, A. I., and McCann, T. 2015. Petrological and geochemical interpretation of Triassic–Jurassic boundary sections from northern Iraq. *Geological Journal*, **50**, 157–172
- Allen, J. R. 1985. *Principles of physical sedimentology*. Chapman & Hall, London, 272 p.
- Allen, P. A., and Allen, J. R. 2013. *Basin analysis: Principles and application to petroleum play assessment*. John Wiley & Sons, 632 p.
- Allwood, A. C., Walter, M. R., Kamber, B. S., Marshall, C. P. & Burch, I. W. 2006. Stromatolite reef from the Early Archaean era of Australia. *Nature*, **441**, 714–718.
- Al-Mubarak, M., and Amin, R. M. 1983. Report on the regional geological mapping of the eastern part of the Western Desert and western part of the Southern Desert. *GEOSURV*, int. rep. no. 1380.
- Al-Naqib, S. Q., and Al-Juboury, A. I. 2014. A new look on the Jurassic formations of the western part of Iraq. *Arabian Journal of Geosciences*, **7**, 559–588.
- Al-Naqib, S. Q., Said, L. K., Taha, Y. M., Al-Sharbaty, F. A., Yakta, S. A., Hussain, M. S., Yacuob, I. I., and Al-Mukhtar, L. 1986. Detailed geological survey of Rutba area. *GEOSURV*, int. rep. no. 1560.
- Al-Riyami, K. K., Danelian, T., and Robertson, A. H. 2002. Radiolarian biochronology of Mesozoic deep-water successions in NW Syria and Cyprus. Implications for south-Tethyan evolution. *Terra Nova*, **14**, 271–280.
- Al-Sayab, A., Al-Ansari, N., Al-Rawi, D., Al-Jasim, J., Al-Omari, F. & Al-Shaikh, Z. 1982. *Geology of Iraq*. University of Mosul, (Arabic).
- Alsharhan, A. S. & Kendall, C. S. C. 2003. Holocene coastal carbonates and evaporites of the southern Arabian Gulf and their ancient analogues. *Earth–Science Reviews*, **61**, 191–243.
- Alsharhan, A. T. 1993. Facies and sedimentary environment of the Permian carbonates (Khuff Formation) in the United Arab Emirates. *Sedimentary Geology*, **84**, 89–99.
- Altinli, I. E. 1966. Geology of eastern and southeastern Anatolia: *Bulletin of the Mineral Research and Exploration Institute of Turkey*, **66**, 35–75.

- Andreea U.T. A. & Kristina G.J.E.C.I. 2012. Microfacies, sedimentary environments and evolution of carbonate deposits of mirdita, Albania—preliminary note. *Oltenia. Studii i comunicri. tiinele Naturii.* . **28**, 193–205.
- Aqrawi, A. A., Horbury, A. D., Horbury, A. D., and Sadoon, F. N. 2010. *The petroleum geology of Iraq*. Scientific Press, Beaconsfield, 560 p.
- Arian, M., and Noroozpour, H. 2015. Tectonic Geomorphology of Iran's Salt Structures: Open Journal of Geology, 5, 61.
- Armstrong, H. & Brasier, M. 2005. *Microfossils*, 2nd edn. , Blackwell publishing, 296 p.
- Assereto, R.L.A.M. & Kendall, C.G.St.C. 1977. Nature, origin and classification of peritidal tepee structures and related breccias. *Sedimentology*, **24**, 153–210.
- Baban, D. H., and Ahmed, S. M. 2013. Vitrinite reflectance as a tool for determining level of thermal maturity for the Upper Jurassic Naokelekan and Barsarin Formations in Sargelu location, Kurdistan Region, NE Iraq: *Arabian Journal of Geosciences*, **7**, 2269–2277.
- Bain, R. J. & Kindler, P. 1994. Irregular fenestrae in Bahamian eolianites; a rainstorm–induced origin. *Journal of Sedimentary Research*, **64**, 140–146.
- Balaky, S. M. H. 2004. *Stratigraphy and sedimentology of Sargelu Formation (Middle Jurassic) in selected sections in Erbil and Duhok Governorates–Iraqi Kurdistan*. MSc thesis, University of Salahaddin.
- Banner, F. 1972. Pithonella ovalis from the early Cenomanian of England. *Micropalaeontology*, **18**, 278–284.
- Baraboshkin, E. Y., Rogov, M., and Mileev, V. 2010. On the characteristics of the Ammonitico Rosso facies in Callovian (Middle Jurassic) sediments near planerskoe (East Crimea). *Moscow University Geology Bulletin*, **65**, 223–228.
- Bartolini, A., Baumgartner, P., and Guex, J. 1999. Middle and Late Jurassic radiolarian palaeoecology versus carbon–isotope stratigraphy. *Palaeogeography, Palaeoclimatology, Palaeoecology*, **145**, 43–60.
- Bathurst, R.G.C. 1975. *Carbonate sediments and their diagenesis*. Development in sedimentology 12, Elsevier Science, Inc., Amsterdam, 685 p.
- Baumgartner, P. O., and Föllmi, K. 2013. Mesozoic radiolarites–accumulation as a function of sea surface fertility on Tethyan margins and in ocean basins. *Sedimentology*, **60**, 292–318.
- Baumgartner, P.O., Bartolini, A., Carter, E.S., Conti, M., Cortese, G., Danelian, T., De Wever, P., Dumitrica, P., Dumitrica–Jud, R., Gorican, S. and Guex, J. 1995. Middle Jurassic to Early

- Cretaceous radiolarian biochronology of Tethys based on Unitary Associations. In: *Middle Jurassic to Lower Cretaceous Radiolaria of Tethys: Occurrences, Systematics, Biochronology*. Memoires de Geologie (Lausanne, Switzerland) Edited by: InterRad Jurassic–Cretaceous Working Group, **23**, 1013–1048.
- Beccaro, P., and Lazăr, I., 2007. Oxfordian and Callovian radiolarians from the Bucegi Massif and Piatra Craiului Mountains (Southern Carpathians, Romania). *Geol Carpat*, **58**, 305–320.
- Bechennec, F., Le Métour, J., Rabu, D., Bourdillon–de–Grissac, C., De Wever, P., Beurrier, M. t., and Villey, M. 1990. The Hawasina Nappes: stratigraphy, palaeogeography and structural evolution of a fragment of the south-Tethyan passive continental margin. *Geological Society, London, Special Publications*, **49**, 213–223.
- Bellen, R.C. van, Dunnington, H.V., Wetzels, R. & Morton, D. 1959. *Lexique Stratigraphique International*, Asie, Fascicule **10a**, Iraq. Paris, 333 p.
- Bellier, J. P., Mathieu R. & Granier B. 2010. *Short Treatise on Foraminiferology (Essential on modern and fossil Foraminifera)*. Court traité de foraminiférologie. L'essentiel sur les foraminifères actuels et fossils. Notebooks on Geology, Brest, Book 2010/02 (CG2010–B02), 104 p
- Berger, W.H., Winterer, E.L. 1974. Plate stratigraphy and the fluctuating carbonate line. In: Hsu, K.J., Jenkyns, H.C., Halm, A. (Eds.) *Pelagic Sediments: in Land and Under the Sea*. Special Publication of the International Association of Sedimentology, **1**, pp. 11–48.
- Bernoulli, D., Jenkyns, H. C., 1974. Alpine, Mediterranean and central Atlantic Mesozoic facies in relation to the early evolution of the Tethys. In: Dott Jr., R. H., Shaver, R. H. (Eds.), *Modern and Ancient Geosynclinal Sedimentation*. SEPM Special Publication 19, 129–160.
- Bernoulli, D. 2009. Ancient oceans and continental margins of the Alpine–Mediterranean Tethys: deciphering clues from Mesozoic pelagic sediments and ophiolites. *Sedimentology*, **56**, 149–190.
- Beydoun, Z. R., 1991. Arabian Plate Hydrocarbon Geology and Potential. A Plate Tectonic Approach. *AAPG Studies in geology*, Tulsa, Oklahoma, USA, **33**, 77 p.
- Bjorlykke, K., 2015. Petroleum geoscience: From sedimentary environments to rock physics. Springer Science & Business Media, 662 p.
- Boggs, S. 1995. *Principles of sedimentology and stratigraphy*. New Jersey: Prentice–Hall, 784 p.
- Boggs, S. 2009. *Petrology of sedimentary rocks*. Cambridge University Press, 600 p.
- Bohm, F., and Brachert, T. C. 1993. Deep-water stromatolites and Frutexites Maslov from the Early and Middle Jurassic of S–Germany and Austria. *Facies*, **28**, 145–168.

- Bontognali, T. R., Vasconcelos, C., Warthmann, R. J., Bernasconi, S. M., Dupraz, C., Strohmenger, C. J. & McKenzie, J. A. 2010. Dolomite formation within microbial mats in the coastal sabkha of Abu Dhabi (United Arab Emirates). *Sedimentology*, **57**, 824–844.
- Bosak, T., Bush, J. W. M., Flynn, M. R., Liang, B., Ono, S., Petroff, A. P. & Sim, M. S. 2010. Formation and stability of oxygen-rich bubbles that shape photosynthetic mats. *Geobiology*, **8**, 45–55.
- Bosak, T., Liang, B., Sim, M. S. & Petroff, A. P. 2009. Morphological record of oxygenic photosynthesis in conical stromatolites. *Proceedings of the National Academy of Sciences*, **106**, 10939–10943.
- Bosence, D. 2005. A genetic classification of carbonate platforms based on their basinal and tectonic settings in the Cenozoic. *Sedimentary Geology*, **175**, 49–72.
- Bosence, D., and Wilson, R. 2003. Carbonate depositional systems. In: Coe A, (ed.) *The sedimentary record of sea-level change*. Milton Keynes (UK) The Open University/Cambridge University Press, 209–233.
- Bosence, D., Procter, E., Aurell, M., Bel Kahla, A., Boudagher-Fadel, M., Casaglia, F., Cirilli, S., Mehdie, M., Nieto, L., Rey, J., Scherreiks, R., Soussi, M., Waltham, D., 2009. A dominant tectonic signal in high-frequency, peritidal carbonate cycles? A regional analysis of Liassic platforms from Western Tethys. *Journal of Sedimentary Research*. **79**, 389–415.
- Bouma, A. H., 1962. *Sedimentology of some flysch deposits*. Elsevier Amsterdam, 168 p.
- Brachert, T. C. 1999. Non-skeletal carbonate production and stromatolite growth within a Pleistocene deep ocean (Last Glacial Maximum, Red Sea). *Facies*, **40**, 211–228.
- Brachert, T. C., and Dullo, W., 1991. Laminar micrite crusts and associated foreslope processes, Red Sea. *Journal of Sedimentary Research*, **61**, 354–363.
- Braga, J.C., Martin, J.M. & Riding, R. 1995. Controls on microbial dome fabric development along a carbonate–siliciclastic shelf basin, Transect, Miocene, SE Spain. *Palaios*, **10**, pp.347–361.
- Brasier, M.D. 1980. *Microfossils*. George Allen and Unwin, London, 193 p.
- Bridge, J., and Demicco, R., 2008. *Earth surface processes, landforms and sediment deposits*. Cambridge University Press, 815 p.
- Brigaud, B., Durllet, C., Deconinck, J.–F., Vincent, B., Pucéat, E., Thierry, J., and Trouiller, A. 2009. Facies and climate/environmental changes recorded on a carbonate ramp: a sedimentological and geochemical approach on Middle Jurassic carbonates (Paris Basin, France). *Sedimentary Geology*, **222**, 181–206.

- Browne, K.M. 2011. Modern marine stromatolitic structures: The sediment dilemma. In: Tewari, V.C., Seckbach, J. (Eds.), *Stromatolites: Interaction of microbes with sediments*. Springer, New York, 291–312.
- Buday, T. 1980. *The regional geology of Iraq, stratigraphy and palaeogeography*, **1**, Dar Al-Kutib pub. University of Mosul, Iraq, 336 p.
- Burgess, P. M. 2016. Identifying ideal stratigraphic cycles using a quantitative optimization method. *Geology*, **44**, 443–446.
- Burgess, P. M., 2006. The signal and the noise: forward modelling of allocyclic and autocyclic processes influencing peritidal carbonate stacking patterns. *Journal of Sedimentary Research*, **76**, no. 962–977.
- Burgess, P. M., Winefield, P. Minzoni, M., and Elders, C. 2013. Methods for identification of isolated carbonate buildups from seismic reflection data. *AAPG bulletin*, **97**, 1071–1098.
- Butler, G.P. 1969. Modern evaporite deposition and geochemistry of coexisting brines, the sabkha, Trucial Coast, Arabian Gulf. *Journal of Sedimentary Petrology*, **39**, 70–89.
- Cant, A., 2001. Chapter 1: Mexico as the Western Margin of Pangea Based on Biogeographic Evidence from the Permian to the Lower Jurassic. *AAPG Memoir* **75**, 1–27
- Cantrell, D. L., and Hagerty, R. M., 1999. Microporosity in Arab Formation carbonates, Saudi Arabia. *GeoArabia*, **4**, 129–154.
- Carman, G. J., 1996. Structural elements of onshore Kuwait. *GeoArabia*, **1**, 239–266.
- Casey, R., Gust, L., Leavesley, A., Williams, D., Reynolds, R., Duis, T., and Spaw, J. M., 1979. Ecological niches of radiolarians, planktonic foraminiferans and pteropods inferred from studies on living forms in the Gulf of Mexico and adjacent waters. *Transac–Gulf Coast. Assoc Geol Soc*, **24**, 216–223
- Caswell, B. A., Coe, A. L., and Cohen, A. S., 2009. New range data for marine invertebrate species across the early Toarcian (Early Jurassic) mass extinction. *Journal of the Geological Society*, **166**, 859–872.
- Catuneanu, O., 2006. *Principles of sequence stratigraphy*. Elsevier, Amsterdam, 386 p.
- Cecca, F., and Savary, B., 2007. Palaeontological study of Middle Oxfordian–Early Kimmeridgian (Late Jurassic) ammonites from the Ammonitico rosso of Monte Inici (north-western Sicily, Italy). *Geodiversitas*, **29**, 507–548.
- Cecca, F., Fourcade, E., and Azéma, J., 1992. The disappearance of the “Ammonitico Rosso”: *Palaeogeography, Palaeoclimatology, Palaeoecology*. **99**, 55–70.

- Cecca, F., Martin Garin, B., Marchand, D., Lathuiliere, B., and Bartolini, A. 2005, Palaeoclimatic control of biogeographic and sedimentary events in Tethyan and peri-Tethyan areas during the Oxfordian (Late Jurassic): *Palaeogeography, Palaeoclimatology, Palaeoecology*, **222**, 10–32.
- Cecca, F., Savary, B., Bartolini, A., Remane, J., and Cordey, F. 2001. The Middle Jurassic–Lower Cretaceous Ammonitico rosso succession of Monte Inici (Trapanese Domain, western Sicily); sedimentology, biostratigraphy and isotope stratigraphy. *Bulletin de la Société géologique de France*, **172**, 647–659.
- Chafetz, H.S. 1986. Marine peloids: a product of bacterially induced precipitation of calcite. *Journal of Sedimentary Petrology*, **56**, 812–817.
- Chapman, G. R., Lippard, S. J., and Martyn, J. E., 1978. The stratigraphy and structure of the Kamasia Range, Kenya Rift Valley. *Journal of the Geological Society*, 135, 265–281.
- Chérubin, L. M., and Richardson, P. L., 2007, Caribbean current variability and the influence of the Amazon and Orinoco freshwater plumes: Deep Sea Research Part I. *Oceanographic Research Papers*, **54**, 1451–1473.
- Chilingar, G.V., Bissell, H.S. & Wolf, K.H. 1979. Diagenesis of carbonate sediments and epigenesis (or catagenesis) of limestones. In: Larsen, G. and Chilingar, G.V.(eds.) *Diagenesis in Sediments and Sedimentary Rocks*, **25A** 249–422, Elsevier, Amsterdam.
- Chilingar, G.V., Zenger, D.H., Bissell, H.J. and Wolf, K.H. 1979 (b). Dolomite and dolomitization. In: Larsen, G. and Chilingar, G.V. (eds.). *Diagenesis in Sediments and Sedimentary Rocks*, **25A**, 425–536, Elsevier, Amsterdam.
- Chowns, T.M. & Elkins, J.E. 1974. The origin of quartz geodes and cauliflower cherts through the silicification of anhydrite nodules. *Journal of Sedimentary Petrology*, **44**, pp. 885–903.
- Clift, P. D., and Robertson, A. H., 1990. Deep-water basins within the Mesozoic carbonate platform of Argolis, Greece: *Journal of the Geological Society*, **147**, 825–836.
- Conti, M., 1986. New data on the biostratigraphy of the Tuscan cherts at Monte Cetona (southern Tuscany, Italy). *Marine Micropalaeontology*, **11**, 107–112.
- Cope, J., 1991. Ammonite faunas of the Ammonitico Rosso of the Pontide Mountains, northern Anatolia. *Geologica Romana*, **27**, 303–325.
- Cross, N.E., Purser B.H., Bosence, D.W.J. 1998. The tectono–sedimentary evolution of a rift margin carbonate platform: Abu Shaar, Gulf of Suez, Egypt. In: Purser B.H., Bosence D.W.J. (eds.) *Sedimentary and tectonic evolution of rift basins—the Red Sea–Gulf of Aden*. Amsterdam, Netherlands, Chapman Hall Kluwers, 271–295.

- Cuadrado, D. G., Bournod, C. N., Pan, J. & Carmona, N. B. 2013. Microbially-induced sedimentary structures (MISS) as record of storm action in supratidal modern estuarine setting. *Sedimentary Geology*, **296**, 1–8.
- Cuadrado, D. G., Perillo, G. M. & Vitale, A. J. 2014. Modern microbial mats in siliciclastic tidal flats: Evolution, structure and the role of hydrodynamics. *Marine Geology*, **352**, 367–380
- Curtis, R., Evans, G., Kinsman, D.J.J. and Shearman, D.J. 1963. Association of dolomite and anhydrite in the recent sediments of the Persian Gulf. *Nature*, **197**, 679–680.
- Cussey, R. and Friedman, G.M. 1976. Antipathetic relations among algal structures and grazers in Dogger (Jurassic) carbonate rocks, Southeast of Paris, France. *American Association of Petroleum Geologists*, **60**, 612–615.
- Danelian, T., Robertson, A. H., and Dimitriadis, S. 1996. Age and significance of radiolarian sediments within basic extrusives of the marginal basin Guevgueli Ophiolite (northern Greece). *Geological Magazine*, **133**, 127–136.
- De Wever P. 1989. Radiolarians, radiolarites, and Mesozoic palaeogeography of the circum-Mediterranean Alpine belts. In: Hein J.R. & Obradovic J., Eds., *Siliceous deposits of the Tethys and Pacific regions*. Springer Verlag, New York, 31–49.
- De Wever, D., P, Caulet, J., Nigrini, C., and Caridroit, M. 2001. *Radiolarians in the Sedimentary Record*, Amsterdam, Netherlands. Gordon and Breach Science Publishers, 533 p.
- De Wever, P., and Baudin, F., 1996. Palaeogeography of radiolarite and organic-rich deposits in Mesozoic Tethys. *Geologische Rundschau*, **85**, 310–326.
- De Wever, P., O'Dogherty, L., and Gorican, S., 2014, Monsoon as a cause of radiolarite in the Tethyan realm: *Comptes Rendus Geoscience*, v. 346, no. 11–12, p. 287–297.
- Demaison, G.J. & Moore, G.T., 1980, Anoxic environments and oil source bed genesis. *American Association of Petroleum Geologists*, **64**, 1179–1209.
- Devleeschouwer, X., Herbosch, A., and Preat, A. 2002. Microfacies, sequence stratigraphy and clay mineralogy of a condensed deep-water section around the Frasnian/Famennian boundary (Steinbruch Schmidt, Germany). *Palaeogeography, palaeoclimatology, palaeoecology*, **181**, 171–193.
- Dias-Brito, D. 2000. Global stratigraphy, palaeobiogeography and palaeoecology of Albian–Maastrichtian pithonellid calcispheres: impact on Tethys configuration: *Cretaceous Research*, **21**, 315–349.

- Dill, H. G., Botz, R., Berner, Z., Stüben, D., Nasir, S. & Al-Saad, H. 2005. Sedimentary facies, mineralogy, and geochemistry of the sulphate-bearing Miocene Dam Formation in Qatar. *Sedimentary Geology*, **174**, 63–96.
- Ditmar, V., and Iraqi–Soviet Team, 1971. Geological conditions and hydrocarbon prospects of the Republic of Iraq (northern and central parts) (manuscript report): Iraq National Oil Company, Baghdad, Iraq.
- Doyle, P., and Mariotti, N., 1991. Jurassic and Lower Cretaceous belemnites from Northwestern Anatolia (Turkey): *Geologica Romana*, **27**, 347–379.
- Draganits, E. & Noffke, N. 2004. Siliciclastic stromatolites and other microbially induced sedimentary structures in an Early Devonian barrier–island environment (Muth Formation, NW Himalayas). *Journal of Sedimentary Research*, **74**, 191–202.
- Dromart, G., Gaillard, C., and Jansa, L., 1994. Deep-marine microbial structures in the Upper Jurassic of western Tethys, In: Bertrand–Sarfati, J., Monty, C. (Eds.), *Phanerozoic Stromatolites II*. Springer, 295–318.
- Dromart, G., Garcia, J. P., Picard, S., Atrops, F., Lécuyer, C., and Sheppard, S. M. F., 2003, Ice age at the Middle–Late Jurassic transition?. *Earth and Planetary Science Letters*, **213**, 205–220.
- Droste, H. 1990. Depositional cycles and source rock development in an epeiric intra-platform basin: the Hanifa Formation of the Arabian peninsula. *Sedimentary Geology*, **69**, 281–296.
- Einsele, G., 2000. The Interplay Between Sediment Supply, Subsidence, and Basin Fill. In Einsele, G., *Sedimentary Basins*. Springer, p. 480–540.
- Ekdale, A. & Mason, T. 1988. Characteristic trace–fossil associations in oxygen–poor sedimentary environments. *Geology*, **16**, 720–723.
- El Khoriby, E. M. 2005. Origin of the gypsum-rich silica nodules, Moghra Formation, northwest Qattara depression, western desert, Egypt. *Sedimentary Geology*, **177**, 41–55.
- Elliott, G. F. 1962. More microproblematica from the Middle East. *Micropalaeontology*, **8**, 29–44.
- Elyas, Y. K., 2014. *Inorganic Geochemistry of Black Shale in Sargelu Formation from Selected Sections in Iraqi Kurdistan Region*. PhD thesis, Salahaddin, 194 p.
- Emeis, K. C. & Weissert, H. 2009. Tethyan–Mediterranean organic carbon-rich sediments from Mesozoic black shales to sapropels. *Sedimentology*, **56**, 247–266.

- English, J. M., Lunn, G. A., Ferreira, L., and Yacu, G. 2015. Geologic evolution of the Iraqi Zagros, and its influence on the distribution of hydrocarbons in the Kurdistan region. *AAPG Bulletin*, **99**, 231–272.
- Eriksson, P. G., Sarkar, S., Samanta, P., Banerjee, S., Porada, H., and Catuneanu, O., 2010. Palaeoenvironmental context of microbial mat-related structures in siliciclastic rocks. In: Seckbach, J., Oren, A. (Eds.), *Microbial Mats: Modern and Ancient Microorganisms in Stratified Systems*. Springer, Amsterdam, 71–108.
- Etter, W., 1996. Pseudoplanktonic and benthic invertebrates in the Middle Jurassic Opalinum Clay, northern Switzerland: Palaeogeography, Palaeoclimatology, Palaeoecology, **126**, 325–341.
- Evans, G., Schmidt, V., Bush, P., and Nelson, H. 1969. Stratigraphy and geologic history of the sabkha, Abu Dhabi, Persian (Arabian) Gulf. *Sedimentology*, **12**, 145–159.
- Fabbi, S., and Santantonio, M., 2012. Footwall progradation in syn-rift carbonate platform–slope systems (Early Jurassic, Northern Apennines, Italy). *Sedimentary Geology*, **281**, 21–34.
- Fatah, S.S. 2014. *Source rock characterization and biomarker distribution of Sargelu Formation (Middle Jurassic), Miran Oil Field, Sulaimani area, Kurdistan Region, NE-Iraq*. MSc thesis University of Sulaimani, 103 p.
- Fatah, S.S. and Mohialdeen, I.M. 2016. Hydrocarbon generation potential and thermal maturity of Middle Jurassic Sargelu Formation in Miran Field, Sulaimani Area, Kurdistan Region, NE Iraq. *Journal of Zankoy Sulaimani*, Special Issue, GeoKurdistan II, 213–228.
- Fels, A. & Seyfried, H. 1993. “A la recherche du temps perdu”: on geological condensation, with examples from the Jurassic Subbetic Plateau in Southeastern Spain. *N.Jb. Geol. Pabiont. Abh*, **189**, 13–31.
- Fels, A., and Seyfried, H. 1993. A la recherche du temps perdu”: on geological condensation, with examples from the Jurassic Subbetic Plateau in Southeastern Spain, **189**, 13–31.
- Ferrante, J., and Parker, J., 1977, Transport of diatom frustules by copepod fecal pellets to the sediments of Lake Michigan. *Limnology and Oceanography*, **22**, 92–98.
- Flügel, E., 2004. *Microfacies of carbonate rocks. Analysis, Interpretation and Application*. Springer, Berlin Heidelberg, 976 p.
- Flügel, E., 2010. *Microfacies of carbonate rocks: analysis, interpretation and application*. Springer Science & Business Media, 984 p.
- Folk, R.L. & Pittman, J.S. 1971. Length–slow chalcedony: a new testament for vanished evaporites. *Journal of Sedimentary Petrology*, **41**, pp. 1045–1058.

- Fontaine, J., 1989. The Hezan Units: a fragment of the south neo-Tethyan passive continental margin in SE Turkey. *Journal of Petroleum Geology*, **12**, 29–50.
- Fouad, S. F. A., 2014. Western Zagros Fold-Thrust Belt, Part II: The High Folded Zone: *Iraqi Bull. Geol. Min.*, Special Issue, 53–71.
- Fouad, S. F. A., 2015. Tectonic map of Iraq, scale 1: 1000 000, 3rd edition. *Iraqi Bulletin of Geology and Mining*, **11**, no. 1.
- Fouad, S., 2010, Tectonic and structural evolution of the Mesopotamia Foredeep, Iraq. *Iraqi bull: Geol. and Min*, **6**, 41–53.
- Friedman, G.M. 1980. Dolomite is an evaporite mineral: evidence from the rock report and from sea marginal ponds of the Red Sea. In: Zenger, D.H., Dunham, J.B. & Ethington, R.L. (eds.) *Concepts and models of dolomitization*. SEPM, special publication, **28**, pp. 69–80.
- Friedman, G.M., Amiel, A.J., Braun, M. & Miller, D.S. 1973. Generation of carbonate particles and laminites in algal mats—Example from sea marginal hypersaline pool, Gulf of Aqaba, Red Sea. *American Association of Petroleum Geologists*, **43**, 541–557.
- Gardosh, M., Weimer, P., and Flexer, A. 2011. The sequence stratigraphy of Mesozoic successions in the Levant margin, southwestern Israel: A model for the evolution of southern Tethys margins: *AAPG Bulletin*, **95**, 1763–1793.
- Garrett, P. 1970. Deposit feeders limit development of stromatolites. *American Association of Petroleum Geologists*, **54**, 848 (Abs.).
- Gayara, A. D., and Al-Gibouri, A. S., 2015. Sequence stratigraphic analysis of the Lower Jurassic succession, Western Iraq: *Arabian Journal of Geosciences*, **8**, 5833–5843.
- Gayara, A.D. & Minas, H.A. 1996. On the quantification of biofacies: Biostratigraphic study of Najmah limestone Formation, Northern Iraq. *Iraqi Journal of science*, **37**, 115–133.
- Gebelein, C.D. 1969. Distribution, morphology, and accretion rate of recent subtidal algal stromatolites, Bermuda. *Journal of Sedimentary Petrology*, **39**, 49–69.
- Gebelein, C.D. and Hoffman, P. 1973. Algal origin of dolomite laminations in stromatolitic limestone. *Journal of Sedimentary Petrology*, **43**, 603–613.
- George, A. D. 1999. Deep-water stromatolites, Canning Basin, northwestern Australia. *Palaios*, **14**, 493–505.
- Gerdes, G. 2010. What are microbial mats?. In: *Microbial Mats: Modern and Ancient Microorganisms in Stratified Systems*, edited by J. Seckbach and A. Oren. Springer, Dordrecht, 3–25.

- Gerdes, G. Krumbein, W.E. & Noffke, N. 2000. Evaporite microbial sediments. In: R.E. Riding & S.M. Awramik (Eds.) *Microbial Sediments*. Springer, Berlin, 196–208.
- Gerdes, G., Krumbein, W. 1994. Peritidal potential stromatolites—a synopsis. In: *Phanerozoic Stromatolites II*, edited by Bertrand–Sarfati J, Monty. Springer, 101–129.
- Gharib, F., and De Wever, P., 2010. Radiolaires mésozoïques de la formation de Kermanshah (Iran): *Comptes Rendus Palevol*, **9**, 209–219.
- Ghasemi, A., and Talbot, C., 2006. A new tectonic scenario for the Sanandaj–Sirjan Zone (Iran). *Journal of Asian Earth Sciences*, **26**, 683–693.
- Gill, D. 1977. Salina A–1 Sabkha cycles and the Late Silurian palaeogeography of the Michigan Basin. *Journal of Sedimentary Petrology*, **47**, pp. 979–1017.
- Gill, G. A., Santantonio, M., and Lathuilière, B., 2004. The depth of pelagic deposits in the Tethyan Jurassic and the use of corals: an example from the Apennines: *Sedimentary Geology*, **166**, 311–334.
- Glennie K. W., 1992. Plate Tectonics and the Oman Mountains. *Tribulus*, **2**, 11–21.
- Goff, J. C., 2005. Origin and potential of unconventional Jurassic oil reservoirs on the Northern Arabian Plate. *14th SPE Middle East Oil and Gas Show and Conference*. United States, *Society of Petroleum Engineers*, 797–812.
- Goldring, R. 1995. Organisms and the substrate: response and effect. *Geological Society of London*, Special Publications, **83**, 151–180.
- Gorican, S., Pavsic, J., and Rosic, B. 2012. Bajocian to Tithonian age of radiolarian cherts in the Tolmin Basin (NW Slovenia). *Bulletin de la Societe geologique de France*, **183**, 369–382.
- Grain, S., Peace, W., Hooper, E., McCartain, E., Massara, P., Marshall, N., Lang, S., 2013. Beyond the Deltas: Late Triassic Isolated carbonate build-ups on the Exmouth plateau, Carnarvon Basin, Western Australia. In: *Proceedings the Sedimentary Basins of Western Australia IV. Petroleum Exploration Society of Australia*, Perth, WA.
- Grover, J. and Read, J.F. 1978. Fenestral and associated vadose diagenetic fabric of tidal flat carbonates, Middle Ordovician New Market Limestone, Southeastern Virginia. *Journal of Sedimentary Petrology*, **48**, 453–473.
- Gunatilaka, A. 1975. Some aspects of the biology and sedimentology of laminated algal mats from Manner Lagoon, Northwest Ceylon. *Sedimentary Geology*, **14**, 275–300.
- Guo, L. & Riding, R. 1992. Aragonite laminae in hot water travertine crusts, Rapolano Terme, Italy. *Sedimentology*, **39**, 1067–1079.

- Haas, J. 2004. Characteristics of peritidal facies and evidences for subaerial exposures in Dachstein-type cyclic platform carbonates in the Transdanubian Range, Hungary. *Facies*, **50**, 263–286.
- Hafid Bouougri, E. & Porada, H. 2010. Topographic control of mat–surface structures evolution: Examples from modern evaporitic carbonate (Abu Dhabi) and evaporitic siliciclastic (Tunisia) tidal flats. In *EGU General Assembly Conference Abstracts*, **12**, 10447.
- Handford, C.R. 1981. Coastal Sabkha and salt pan deposition of the Lower Clear Fork Formation (Permian). *Journal of Sedimentary Petrology*, **51**, 761–778.
- Haq, B. U., and Al-Qahtani, A. M., 2005, Phanerozoic cycles of sea-level change on the Arabian Platform: *GeoArabia*, **10**, 127–160.
- Hardie, L.A. 1987. Perspectives, dolomitization: A critical view of some current views. *Journal of Sedimentary Petrology*, **57**, 166–183.
- Harris, M. T., 1994. The foreslope and toe-of-slope facies of the Middle Triassic Latemar buildup (Dolomites, northern Italy): *Journal of Sedimentary Research*, **64**, 132–145.
- Hart, M. B. 1991. The Late Cenomanian calcisphere global bioevent. *Proceedings of the Ussher Society*, **7**, 413–417.
- Hart, M. B., Fitzpatrick, M. E. J. 1995. Kimmeridgian palaeoenvironments; a micropalaeontological perspective. *Proceedings–Ussher Society*, **8**, 433–433.
- Hattin, D. E. 1971. Widespread, synchronously deposited, burrow–mottled limestone beds in Greenhorn Limestone (Upper Cretaceous) of Kansas and southeastern Colorado. *American Association, of Petroleum Geologists*, **55**, 412–431.
- Hirsch, F., and Picard, L., 1988. The Jurassic facies in the Levant. *Journal of Petroleum Geology*, **11**, 277–308.
- Hirsch, F., Flexer, A., Rosenfeld, A., and Yellin-Dror, A. 1995. Palinspastic and crustal setting of the eastern Mediterranean. *Journal of Petroleum Geology*, **18**, 149–170.
- Hocking, R., 1988. Regional geology of the northern Carnarvon Basin, in Proceedings the North West Shelf, Australia: *Proc. Pet. Expl. Soc. Aust. Symp*, 97–114.
- Hoffman, P. 1974. Shallow and deep water stromatolites in Lower Proterozoic platform–to–basin facies change, Great Slave Lake. *American Association of Petroleum Geologists*, **58**, 856–867.
- Hoffman, P. 1976. Stromatolite morphogenesis in Shark Bay, Western Australia. In: Walter, M.R. (ed.) *Stromatolites*. Developments in Sedimentology, Elsevier, Amsterdam, **20**, 261–271.

- Hofmann, A., Dirks, P. H. & Jelsma, H. A. 2004. Shallowing-upward carbonate cycles in the Belingwe Greenstone Belt, Zimbabwe: a record of Archean sea-level oscillations. *Journal of Sedimentary Research*, **74**, 64–81.
- Holford, S., Schofield, N., Jackson, C., Magee, C., Green, P., and Duddy, I.R. 2013. Impacts of igneous intrusions on source and reservoir potential in prospective sedimentary basins along the western Australian continental margin, in: *Proceedings West Australian Basins Symposium*, 1–12.
- Horbury, A. D. & Qing, H. 2004. Pseudobreccias revealed as calcrete mottling and bioturbation in the Late Dinantian of the southern Lake District, UK. *Sedimentology*, **51**, 19–38.
- Howarth, M. K. 1992. Tithonian and Berriasian ammonites from the Chia Gara Formation in northern Iraq. *Palaeontology*, **35**, 597–655.
- Hsu, K. J., 1989. *Physical principles of sedimentology: a readable textbook for beginners and experts*. Springer–Verlag, New York, 233 p.
- Hüneke, H., and Mulder, T., 2011. *Deep-sea sediments*. Developments in Sedimentology,
- Hussein, F. S., El Kammar, M. M. & Sherwani, G. H. 2013. Organic Geochemical Assessment of Jurassic Source Rock from Duhok, North Iraq. *Journal of American Science*, **9**, 258–264
- Iijima, A., Matsumoto, R., and Tada, R., 1984. Mechanism of sedimentation of rhythmically bedded chert. *Sedimentary geology*, **41**, 221–233.
- Illing, L.V., Wells, A.S. & Taylor, J.C.M. 1965. Penecontemporary dolomite in the Persian (Arabian) Gulf. In: Pray, L.C. and Murray, R.C. (eds.) *Dolomitization and limestone diagenesis*. a symposium, SEPM, special publication, **13**, 89–111.
- Imbert, P., 2011, Industrial application of deep-sea sediments. In: Huneke, H., Mulder, T. (eds.), *Deep–Sea Sediments. Developments in Sedimentology*. Elsevier, Amsterdam, **63**, 715–764.
- Imlay, R. W. 1963. Jurassic fossils from southern California. *Journal of Palaeontology*, **37**, 97–107.
- Imlay, R. W. 1964. Middle Bajocian ammonites from the Cook Inlet region, Alaska. No. 418–B.
- Imlay, R. W., 1945. Jurassic fossils from the southern states. *Journal of Palaeontology*, **19**, 253–276.
- Jacoby, W. R., 2006. Three–directional extensional deformation and formation of the Liassic rift basins in the Eastern Pontides (NE Turkey): *Geologica Carpathica*, **57**, 337–346.
- Jansa, L. F. & Steiger, T. 1984. Mesozoic carbonate deposition on the outer continental margin off Morocco. Initial Rep DSDP, **79**, 857–891.

- Jarvis, I., Carson, G., Hart, M., Leary, P., & Tocher, B. 1988. The Cenomanian–Turonian (late Cretaceous) anoxic event in SW England: evidence from Hooken Cliffs near Beer, SE Devon. *Newsletters on Stratigraphy*, **18**, 147–164.
- Jassim, S. Z., Karim, S. A., Basi, M., Al Mubarak, M. A., and Munjir, J. 1984. *Final report on regional geological survey of Iraq, Geological Survey of Iraq*, v. **3**.
- Jassim, S.Z. and Goff, C. 2006. *Geology of Iraq*. Published by Dolin, 318 p.
- Jenkyns, H. C. 1974. Origin of red nodular limestones (Ammonitico Rosso, Knollenkalke) in the Mediterranean Jurassic: a diagenetic model. In: Hsu, K.J. and H.C. Jenkyns (eds), *Pelagic Sediments: On Land and Under the Sea*. Special Publication, **1**, 249–271.
- Jenkyns, H. C., 1971. The genesis of condensed sequences in the Tethyan Jurassic: Lethaia, **4**, 327–352.
- Jenkyns, H. C., 1988. The early Toarcian (Jurassic) anoxic event; stratigraphic, sedimentary and geochemical evidence. *American Journal of Science*, **288**, 101–151.
- Jenkyns, H. C., and Hsü, K. J., 1974. An Introduction. In: Hsu, K.J. and H.C. Jenkyns (eds), *Pelagic Sediments: On Land and Under the Sea*. Special Publication, **1**, 1–10.
- Jenkyns, H. C., and Winterer, E. L., 1982. Palaeoceanography of Mesozoic ribbon radiolarites. *Earth and Planetary Science Letters*, **60**, 351–375.
- Jones, D. L., and Murchey, B., 1986, Geologic significance of Palaeozoic and Mesozoic radiolarian chert: Annual Review of Earth and Planetary Sciences, v. 14, p. 455.
- Kadhim, S. A. R., and Nasr, F., 1971. Upper Jurassic prospect in Iraq 10th Iraqi Engineering congress. Baghdad, no. 4.
- Kandemir, R., and Yılmaz, C., 2009, Lithostratigraphy, facies, and deposition environment of the lower Jurassic Ammonitico Rosso type sediments (ARTS) in the Gümüşhane area, NE Turkey: Implications for the opening of the northern branch of the Neotethys Ocean. *Journal of Asian Earth Sciences*, **34**, 586–598.
- Karakitsios, V. 1995. The influence of preexisting structure and halokinesis on organic matter preservation and thrust system evolution in the Ionian Basin, Northwest Greece. *AAPG bulletin*, **79**, 960–980.
- Karakitsios, V., and Chatzicharalampous, E., 2013. Biostratigraphy and sedimentology of the Ionian zone ammonitico rosso in the Mavron Oros area (NW Epirus, Greece)–palaeogeographic implications: *Bulletin of the Geological Society of Greece*, **47**, 136–145.

- Karim, K. H., Koyi, H., Baziany, M. M., and Hessami, K., 2011. Significance of angular unconformities between Cretaceous and Tertiary strata in the northwestern segment of the Zagros fold–thrust belt, Kurdistan Region, NE Iraq. *Geological Magazine*, **148**, 925–939.
- Kauffman, E., 1978. Benthic environments and palaeoecology of the Posidonienschiefer (Toarcian). *Neues Jahrbuch, Geologie and Palaontologie, Abhandlungun*, 175, 18–36.
- Kauffman, G., 1981. Ecological reappraisal of the German Posidonienschiefer (Toarcian) and the stagnant basin model. In: Gray, J., Boucot, A.J. & Berry, B.N. (eds). *Communities of the Past*, Hutchison Ross, Stoudsberg, Pennsylvania, 311–381.
- Kendall A.C. 1992. Evaporites. In R.G. Walker and N.P. James (eds.). *Facies Models: Response to Sea-level Change*. Geological Association of Canada, 375–409.
- Kendall A.C. 1978. *Subaqueous evaporites*. Facies models Geoscience Canada, **8**, 124–138.
- Kendall, C.G.St.C. Alsharhan, A.S. & Cohen, A. 2002. The Holocene tidal flat complex of the Arabian Gulf coast of Abu Dhabi. *Sabkha Ecosystems*, **1**, 21–35.
- Kendall, C.G.St.C. and Skipwith, P.A.D'E. 1968. Recent algal mats of a Persian (Arabian) Gulf lagoon. *Journal of Sedimentary Petrology*, **38**, 1040–1058.
- Kendall, C.G.St.C. and Warren, J. 1987. A review of the origin and setting of tepee and their associated fabrics. *Sedimentology*, **34**, 1007–1027.
- Kennard, J. M. & James, N. P. 1986. Thrombolites and stromatolites: two distinct types of microbial structures. *Palaios*, **1**, 492–503.
- Kenter, J. A., 1990. Carbonate platform flanks: slope angle and sediment fabric. *Sedimentology*, **37**, 777–794.
- Kenter, J. A., and Campbell, A. E., 1991. Sedimentation on a Lower Jurassic carbonate platform flank: geometry, sediment fabric and related depositional structures (Djebel Bou Dahar, High Atlas, Morocco). *Sedimentary Geology*, **72**, 1–34.
- Kenter, J. A., and Schlager, W., 1989. A comparison of shear strength in calcareous and siliciclastic marine sediments. *Marine Geology*, **88**, 145–152.
- Kettle, S., 2012, *Resedimented carbonates from the Jurassic of Mallorca*. MPhil thesis, University of Birmingham, 303 p.
- Keupp, H. 1991. Fossil calcareous dinoflagellate cysts. In: Ridding, R. (Ed.), *Calcareous algae and stromatolites*. Springer Berlin Heidelberg, 267–286.

- Kidder, D. L., and Erwin, D. H. 2001. Secular Distribution of Biogenic Silica through the Phanerozoic: Comparison of Silica-Replaced Fossils and Bedded Cherts at the Series Level. *The Journal of Geology*, **109**, 509–522.
- Kinsman, D.J.J. and Park, R.K. 1976. Algal belt and coastal sabkha evolution, Trucial coast, Persian (Arabian) Gulf. In: Walter, M.R. (ed.) *Stromatolites*. Developments in Sedimentology, Elsevier, Amsterdam, 20, 421–433
- Kinsman, D.J.J. and Patterson, R.J. 1973. Dolomitization process in sabkha environment (abs.). *American Association of Petroleum Geologists*, **57**, 788–789.
- Kiselev, D., Rogov, M., Glinskikh, L., Guzhikov, A., Pimenov, M., Mikhailov, A., Dzyuba, O., Matveev, A., and Tesakova, E., 2013. Integrated stratigraphy of the reference sections for the Callovian–Oxfordian boundary in European Russia. *Volumina Jurassica*, **11**, 59–96.
- Komar, P. D. 1985. The hydraulic interpretation of turbidites from their grain sizes and sedimentary structures. *Sedimentology*, **32**, 395–407.
- Koyi, H., 1988. Experimental modeling of role of gravity and lateral shortening in Zagros mountain belt. *AAPG Bulletin*, **72**, 1381–1394.
- Kremer, B., and Kazmierczak, J., 2005, Cyanobacterial mats from Silurian black radiolarian cherts: phototrophic life at the edge of darkness. *Journal of Sedimentary Research*, **75**, 897–906.
- Lapointe, P., 1991. Sabkha vs. salt basin model for the Arab Formation understanding in the Umm Shaif Field, UAE. In: *Proceedings Middle East Oil Show, Society of Petroleum Engineers*, 523–533.
- Laporte, L.F. 1967. Carbonate deposition near mean sea-level and resultant facies mosaic: Manlius Formation (Lower Devonian) of New York State. *American Association of Petroleum Geologists*, **51**, 73–101.
- Lasemi, Y., and Jalilian, A. H., 2010. The Middle Jurassic basinal deposits of the Surmeh Formation in the Central Zagros Mountains, southwest Iran: facies, sequence stratigraphy, and controls. *Carbonates and Evaporites*, **25**, 283–295.
- Leeder, M. 1975. Lower Border Group (Tournaisian) stromatolites from the Northumberland Basin. *Scottish Journal of Geology*, **3**, 207–226.
- Leinen, M., 1979. Biogenic silica accumulation in the central equatorial Pacific and its implications for Cenozoic palaeoceanography. *Geological Society of America Bulletin*, **90**, 1310–1376.
- Littke, R., Leythaeuser, D., Rullkotter, J., and Baker, D. R., 1991, Keys to the depositional history of the *Posidonia* Shale (Toarcian) in the Hils Syncline, northern Germany. *Geological Society, London, Special Publications*, **58**, 311–333.

- Logan, B.W., Rezak, R. and Ginsburg, R.N. 1964. Classification and environmental significance of algal stromatolite. *The Journal of Geology*, **72**, 68–83.
- Louis-Schmid, B., Rais, P., Bernasconi, S. M., Pellenard, P., Collin, P. Y. & Weissert, H. 2007. Detailed record of the mid-Oxfordian (Late Jurassic) positive carbon-isotope excursion in two hemipelagic sections (France and Switzerland): A plate tectonic trigger. *Palaeogeography, Palaeoclimatology, Palaeoecology*, **248**, 459–472.
- Loutit, T.S., Hardenbol, J., Vail, P.R. and Baum, G.R., 1989. Condensed sections: the key to age determination and correlation of continental margin sequences. In: C.K. Wilgus, B.S. Hastings, C.G.St.C. Kendall, H.W. Posamentier, C.A. Ross and J.C. Van Wagoner et al. (Eds) *Sea-Level Changes: An Integrated Approach*. SEPM Special Publication, **42**, 183–214.
- Lowe, D. R., 1982. Sediment gravity flows: II Depositional models with special reference to the deposits of high-density turbidity currents. *Journal of Sedimentary Research*, **52**, 279–297
- Luczynski, P., 2002. Depositional evolution of the Middle Jurassic carbonate sediments in the high-tatric succession, Tatra Mountains, Western Carpathians, Poland. *Acta Geologica Polonica*, **52**, 365–378.
- Mackertich, D.S. and Samarrai A.I. 2015. History of hydrocarbon exploration in the Kurdistan Region of Iraq. *GeoArabia*, **20**, 181–220.
- Mamet, B., and Pr eat, A., 2006. Jurassic microfacies, Ammonitico rosso limestone, Subbetic Cordillera, Spain. *Revista Espa ola de Micropalaeontolog a*, **38**. 219–228.
- Manley, F. H., Ogren, D. E. & Webb, L. C. 1975. Mottled upper Ordovician carbonates in Northwest Georgia. *Journal of Sedimentary Research*, **45**, 615–617.
- Marszalek, D. S. 1975. Calcisphere ultrastructure and skeletal aragonite from the alga *Acetabularia antillana*. *Journal of Sedimentary Research*, **45**, 266–271.
- Martin-Algarra, A. 2000. Bacterially mediated authigenesis in Mesozoic stromatolites from condensed pelagic sediments (Betic Cordillera, Southern Spain).
- Mart n-Algarra, A., and Vera, J., 1994. Mesozoic pelagic phosphate stromatolites from the Penibetic (Betic Cordillera, southern Spain). In: Bertrand-Sarfati J, Monty C (eds) *Phanerozoic Stromatolites II*, Springer, 345–391.
- Martire, L., 1992. Sequence stratigraphy and condensed pelagic sediments. An example from the Ammonitico rosso Veronese, northeastern Italy: *Palaeogeography, Palaeoclimatology, Palaeoecology*, **94**, 169–191.

- Martire, L., Clari, P., Lozar, F., and Pavia, G. 2006. The Ammonitico rosso Veronese (Middle–Upper Jurassic of the Trento Plateau): a proposal of lithostratigraphic ordering and formalization. *Rivista Italiana di Palaeontologia e Stratigrafia*, **112**, 227–250.
- Masetti, D., Fantoni, R., Romano, R., Sartorio, D., and Trevisani, E., 2012. Tectonostratigraphic evolution of the Jurassic extensional basins of the eastern southern Alps and Adriatic foreland based on an integrated study of surface and subsurface data. *AAPG bulletin*, **96**, 2065–2089.
- Massari, F., 1983. Oncoids and stromatolites in the Ammonitico rosso sequences (Middle–Upper Jurassic) of the Venetian Alps. In: Peryt T. (ed) *Coated grains*. Springer, Berlin Heidelberg New York, 358–366.
- Massari, F., and Dieni, I. 1983. Pelagic oncoids and ooids in the Middle–Upper Jurassic of Eastern Sardinia. In: Peryt T. (ed) *Coated grains*. Springer, Berlin Heidelberg New York, 367–376.
- Massari, F., and Westphal, H., 2011. Microbialites in the Middle–Upper Jurassic Ammonitico Rosso of the Southern Alps (Italy). In: Tewari, C., and Seckbach, J. (eds) *Stromatolites: Interaction of Microbes with Sediments*. Springer, 223–250.
- Masters, B. A. & Scott, R. W. 1978. Microstructure, affinities and systematics of Cretaceous calcispheres. *Micropalaeontology*, **24**, 210–221.
- Matter, A. 1967. Tidal flat deposits in the Ordovician of Western Maryland. *Journal of Sedimentary Petrology*, **37**, 601–609.
- McIlroy, D. 2004. Some ichnological concepts, methodologies, applications and frontiers. *Geological Society, London, Special Publications*, **228**.
- McRoberts, C. A., 2011. Late Triassic Bivalvia (Chiefly Halobiidae and Monotidae) from the Pardonet Formation, Williston Lake Area, Northeastern British Columbia, Canada. *Journal of Palaeontology*, **85**, 613–664.
- Meesook, A., Sha, J., Yamee, C., and Saengsrichan, W., 2009. Faunal associations, palaeoecology and palaeoenvironment of marine Jurassic rocks in the Mae Sot, Phop Phra, and Umphang areas, western Thailand: Science in China Series D. Earth Sciences, **52**, 2001–2023.
- Meischner, K., 1964. Allodapische Kalke Turbidite in Riff-nahen Sedimentationsbecken. In: Bouma AH, Brouwer A (eds) *Turbidites*. Elsevier, Amsterdam, 156–191.
- Meister, P., Mckenzie, J. A., Bernasconi, S. M. and Brack, P. 2013. Dolomite formation in the shallow seas of the Alpine Triassic. *Sedimentology*, **60**, 270–291.
- Messina, C., Rosso, M. A., Sciuto, F., Di, I., Maniscalco, R., and Sanfilippo, R., 2007. Anatomy of a transgressive systems tract revealed by integrated sedimentological and palaeoecological

- study: the Barcellona Pozzo di Gotto Basin, northeastern Sicily, Italy. In: Nichols, G., Williams, E. and Paola, C., (eds) *Sedimentary Processes and Basins—A Tribute to Peter Friend*. Blackwell, **38**, 367–400.
- Miller, K. G., Kominz, M. A., Browning, J. V., Wright, J. D., Mountain, G. S., Katz, M. E., Sugarman, P. J., Cramer, B. S., Christie–Blick, N., and Pekar, S. F., 2005. The Phanerozoic record of global sea-level change: *Science*, **310**, 1293–1298.
- Milliken, K.L. 1979. The silicified evaporite syndrome—Two aspects of silicification history of former evaporite nodules from Southern Kentucky and Northern Tennessee. *Journal of Sedimentary Petrology*, **49**, 245–256.
- Misik, M. 1993. The Czorsztyn Submarine Ridge (Jurassic–Lower retaceous, Pieniny Klippen Belt): An Example of a Pelagic Swell, *Mitt. Osterr.Geol.Ges.*, **86**. 133–140.
- Mohyaldin, I. J., 2008. *Source rock appraisal and oil/source correlation for the Chia Gara Formation, PhD thesis*. University of Sulaimani, 235 p.
- Monaco, P. and Trecci, t. 2012. Taphonomy and ichnofabric of the trace fossil *Avetoichnus luisae* Uchman and Rattazzi, 2011 in Palaeogene deep-sea fine-grained turbidites: examples from Italy, Poland and Spain. *Bollettino della Società Palaeontologica Italiana*, **51**, 24.
- Monaco, P. 1992, Hummocky cross-stratified deposits and turbidites in some sequences of the Umbria–Marche area (central Italy) during the Toarcian. *Sedimentary Geology*, **77**, 123–142.
- Monty, C.L.V. 1976. The origin and development of cryptalgal fabrics. In: Walter, M.R. (ed.). *Stromatolites*. , **20**, 193–200.
- Murray, R. W., Jones, D. L., and ten Brink, M. R. B., 1992, Diagenetic formation of bedded chert: Evidence from chemistry of the chert–shale couplet: *Geology*, v. 20, no. 3, p. 271–274.
- Murris, R., 1984, Middle East: stratigraphic evolution and oil habitat.
- Alsharhan. A., and, Nairn, A. 2003. *Sedimentary basins and petroleum geology of the Middle East*. Elsevier, 843.
- Navabpour, P., Angelier, J., and Barrier, E. 2011. Brittle tectonic reconstruction of palaeo–extension inherited from Mesozoic rifting in West Zagros (Kermanshah, Iran). *Journal of the Geological Society*, **168**, 979–994.
- Navarro, V., Molina, J. M., and Ruiz–Ortiz, P. A. 2008. Filament lumachelle on top of Middle Jurassic oolite limestones: event deposits marking the drowning of a Tethysian carbonate platform (Subbetic, southern Spain). *Facies*, 55, no. 1, p. 89–102.

- Negra, M. H., Zagrarni, M. F., Hanini, A., and Strasser, A. 2011. The filament event near the Cenomanian–Turonian boundary in Tunisia. filament origin and environmental signification. *Bulletin de la Société Géologique de France*, **182**, 507–519.
- Nelson, D. M., Tréguer, P., Brzezinski, M. A., Leynaert, A., and Quéguiner, B. 1995. Production and dissolution of biogenic silica in the ocean: revised global estimates, comparison with regional data and relationship to biogenic sedimentation. *Global Biogeochemical Cycles*, **9**, 359–372.
- Neumann, A.C. and Land, L.S. 1975. Lime mud deposition and calcareous algae in the Bight of Abaco, Bahamas: A budget. *Journal of Sedimentary Petrology*, **45**, 763–786.
- Nieto, L. M., Reolid, M., Molina, J. M., Ruiz–Ortiz, P. A., Jiménez–Millán, J., and Rey, J. 2012. Evolution of pelagic swells from hardground analysis (Bathonian–Oxfordian, Eastern External Subbetic, southern Spain). *Facies*, **58**, 389–414.
- Noffke, N., Gerdes, G., Klenke, T. and Krumbein, W. E. 2001. Microbially induced sedimentary structures: a new category within the classification of primary sedimentary structures. *Journal of Sedimentary Research*, **71**, 649–656.
- Norris, M. S., and Hallam, A. 1995. Facies variations across the Middle–Upper Jurassic boundary in Western Europe and the relationship to sea-level changes. *Palaeogeography, Palaeoclimatology, Palaeoecology*, **116**, 189–245.
- Numan, N. M. 1997. A plate tectonic scenario for the Phanerozoic succession in Iraq. *Iraqi Geological Journal*, **30**, 85–110.
- Omar, G. I., Steckler, M. S., Buck, W. R., and Kohn, B. P., 1989, Fission–track analysis of basement apatites at the western margin of the Gulf of Suez rift, Egypt: evidence for synchronicity of uplift and subsidence. *Earth and Planetary Science Letters*, **94**, 316–328.
- Omer, M. F. 2012. *Sedimentology and Geochemistry of Khabour Formation in Northern Iraq*. PhD thesis, Baghdad University, Iraq.
- Onoue, T., and Yoshida, A. 2010. Depositional response to the Late Triassic ascent of calcareous plankton in pelagic mid–oceanic plate deposits of Japan. *Journal of Asian Earth Sciences*, **37**, 312–321.
- Onoue, T., Nikaido, T., Zamoras, L. R., and Matsuoka, A. 2011. Preservation of larval bivalve shells in a radiolarian chert in the Late Triassic (Early Norian) interval of the Malampaya Sound Group, Calamian Island, western Philippines. *Marine Micropalaeontology*, **79**, 58–65.

- Osborne, R. H., Licari, G. R., and Link, M. H. 1982. Modern lacustrine stromatolites, Walker Lake, Nevada. *Sedimentary Geology*, **32**, 39–61.
- Oschmann, W., 1993, Environmental oxygen fluctuations and the adaptive response of marine benthic organisms: *Journal of the Geological Society*, v. 150, no. 1, p. 187–191.
- Osmond, J. C. 1956. "Mottled carbonate rocks in the Middle Devonian of eastern Nevada." *Journal of Sedimentary petrology*, **26**, 32–41.
- Othman, R., 1990, *Generation, migration and maturation of the hydrocarbons, Northern Iraq (Upper Jurassic–Lower Cretaceous)*. M.Sc. Thesis, University of Salahaddin (arabic), 208 p.
- Padden, M., Weissert, H., and de Rafelis, M. 2001. Evidence for Late Jurassic release of methane from gas hydrate. *Geology*, **29**, 223–226.
- Pallini, G., Schiavinotto, F., 1981. Upper Carixian Lower Domerian Sphinctozoa and ammonites from some sequences in central Apennines. In: Farinacci, A., Elmi, S. (Eds.) *Ammonitico rosso Symposium Proceedings*. Edizioni Tecnoscienza, Roma, 521–535.
- Park, R.K. 1977. The preservation potential of some recent stromatolites. *Sedimentology*, **24**, 485–506.
- Parrish, J. T., Droser, M. L., and Bottjer, D. J. 2001. A Triassic upwelling zone: the Shublik Formation, arctic Alaska, USA. *Journal of Sedimentary Research*, **71**, 272–285.
- Patterson, R.J. and Kinsman, D.J.J. 1981. Hydrologic framework of a sabkha along Arabian Gulf. *Amer. American Association of Petroleum Geologists*, **65**, 1457–1475.
- Patterson, R.J. and Kinsman, D.J.J. 1982. Formation of diagenetic dolomite in coastal sabkha along Arabian (Persian) Gulf. *American Association of Petroleum Geologists*, **66**, 28–43.
- Pemberton, S. G. and Gingras, M. K. 2005. Classification and characterizations of biogenically enhanced permeability. *American Association of Petroleum Geologists*, **89**, 1493–1517.
- Perry, C., and Taylor, K. 2007. *Environmental sedimentology*. Blackwell publishing, 460 p.
- Peryt, T. M. 1983. Oncoids, Comments on recent developments. In: Peryt, T. M. (ed.) *Coated Grains*. Springer–Verlag, Berlin, Heidelberg, 273–275.
- Peryt, T. M., 1983. *Oncoids: comment to recent developments, Coated grains*. Springer, p. 273–275.
- Playford, P. E., and Cockbain, A. E. 1969. Algal stromatolites: deep water forms in the Devonian of Western Australia: *Science*, **165**, 1008–1010.

- Playford, P.E., Cockbain, A.E., 1976. Modern algal stromatolites at Hamelin Pool, a hypersaline barred basin in Shark Bay, Western Australia. In: Walter, M.R. (Ed.) *Stromatolites. Developments in Sedimentology*, Elsevier, Amsterdam, 20, 389–411.
- Pope, M. C., and Steffen, J. B. 2003. Widespread, prolonged late Middle to Late Ordovician upwelling in North America: A proxy record of glaciation. *Geology*, **31**, 63–66.
- Pope, M.C. 2002. Cherty facies of the Late Ordovician Montoya Group, southern New Mexico and western Texas: Implications for Laurentia oceanography and duration of Gondwana glaciation. In: Lueth, V., Giles, K.A., Lucas, S.G., Kues, B.S., Myers, R.G., Ulmer-Scholle, D. (eds.) *Geology of White Sands*. New Mexico Geological Society Fall Field Conference Guidebook, 53. New Mexico Geological Society, **53**, 159–165.
- Pope, M.C., and Steffen, J.B. 2001. Upwelling in the Montoya Group: evidence for prolonged Late Ordovician glaciation. *Geological Society of America Abstracts with Programs*, **33**, 214–215.
- Posamentier, H.W., Walker, R.G. 2006. *Facies models revisited*: SEPM (Society for Sedimentary Geology), **52**, 1–100.
- Pratt, B. R., 1995. The origin, biota and evolution of deep-water mud-mounds: Carbonate Mud-Mounds. Their Origin and Evolution. *Spec. Publ. Intern. Assoc. Sedimentol.*, **23**, 49–123.
- Pratt, B. R., and Smewing, J. D. 1990. Jurassic and Early Cretaceous platform margin configuration and evolution, central Oman Mountains: *Geological Society, London*, Special Publications, **49**, 69–88.
- Preat, A., Morano, S., Loreau, J.-P., Durlet, C., and Mamet, B. 2006. Petrography and biosedimentology of the Ammonitico rosso Veronese (Middle–Upper Jurassic, north-eastern Italy). *Facies*, **52**, 265–278.
- Price, G. D. 1999. The evidence and implications of polar ice during the Mesozoic. *Earth–Science Reviews*, **48**, 183–210.
- Price, I. 1977. Facies distinction and interpretation of primary cherts in a Mesozoic continental margin succession, Othris, Greece. *Sedimentary Geology*, **18**, 321–335.
- Pruss, S. B., Bosak, T., Macdonald, F. A., McLane, M. and Hoffman, P. F. 2010. Microbial facies in a Sturtian cap carbonate, the Rasthof Formation, Otavi Group, northern Namibia. *Precambrian Research*, **181**, 187–198.
- Puelles, P., Ábalos, B., and Fernández–Armas, S., 2014. Graphite and quartz petrofabrics: Examples from the Ediacaran black quartzites of the Ossa–Morena Zone (SW Iberia). *Tectonophysics*, **615**, 53–68.

- Rabet, A.M. 1981. Differentiation of environments of dolomite formation, Lower Cretaceous of Central Tunisia. *Sedimentology*, **28**, 331–352.
- Rabu, D., Le Métour, J., Bechennec, F., Beurrier, M., Villey, M., and De Grissac, C. B. J., 1990. Sedimentary aspects of the Eo–Alpine cycle on the northeast edge of the Arabian Platform (Oman Mountains). *Geological Society, London, Special Publications*, **49**, 49–68.
- Rais, P., Louis–Schmid, B., Bernasconi, S. M., and Weissert, H., 2007. Palaeoceanographic and palaeoclimatic reorganization around the Middle–Late Jurassic transition. *Palaeogeography, Palaeoclimatology, Palaeoecology*, **251**, 527–546.
- Rao, V. P., Kessarkar, P. M., Krumbein, W. E., Krajewski, K. P. and Schneider, R. J. 2003. Microbial dolomite crusts from the carbonate platform off western India. *Sedimentology*, **50**, 819–830.
- Reading, H. G., 2009. *Sedimentary environments: processes, facies and stratigraphy*. John Wiley and Sons, Chichester.
- Reading, H.G. 1996. *Sedimentary Environments: Processes, Facies and Stratigraphy* (3rd ed.): Oxford, Blackwell, 688 p.
- Renata, J., 2007, Bositra limestones—a step towards radiolarites: case study from the Tatra Mountains. *Annual Societatis Geologicae Poloniae*, **77**, 161–170.
- Reolid, M., and Molina, J. M., 2010. Serpulid–Frutexitis Assemblage from Shadow–Cryptic Environments in Jurassic Marine Caves, Betic Cordillera, Southern Spain. *Palaios*, **25**, 468–474.
- Reolid, M., Gaillard, C., Oloriz, F., and Rodríguez–Tovar, F. J. 2005. Microbial encrustations from the Middle Oxfordian–earliest Kimmeridgian lithofacies in the Prebetic Zone (Betic Cordillera, southern Spain): characterization, distribution and controlling factors *Facies*, **50**, 529–543.
- Reolid, M., Nieto, L. M., and Rey, J. 2010. Taphonomy of cephalopod assemblages from Middle Jurassic hardgrounds of pelagic swells (South–Iberian Palaeomargin, Western Tethys). *Palaeogeography, Palaeoclimatology, Palaeoecology*, **292**, 257–271.
- Reolid, M., Rivas, P., and Rodríguez–Tovar, F. J. 2015. Toarcian ammonitico rosso facies from the South Iberian Palaeomargin (Betic Cordillera, southern Spain): palaeoenvironmental reconstruction. *Facies*, **61**, 1–26.
- Reolid, P. M., and Nieto, L. M. 2010. Jurassic Fe–Mn macro-oncoids from pelagic swells of the External Subbetic (Spain): evidences of microbial origin. *Geologica Acta*, **8**, 151–168.

- Ricketts, B. D. 1983. The evolution of a middle Precambrian dolostone sequence; a spectrum of dolomitization regimes. *Journal of Sedimentary Petrology*, **53**, 565–586.
- Riding, R. 1994. Stromatolite survival and change: The significance of Shark Bay and Lee Stocking Island subtidal columns. In: Krumbein, E., Patterson, D.M. and Stal, L.J. (eds.) *Biostabilization of sediments*. Verlag, Berlin, 183–202.
- Riding, R. 2000. Microbial carbonates: the geological record of calcified bacterial–algal mats and biofilms. *Sedimentology*, **47**, 179–214.
- Riding, R. 2008. Abiogenic, microbial and hybrid authigenic carbonate crusts: components of Precambrian stromatolites. *Geologia Croatica*, **61**, 73–103.
- Rivas, P., Aguirre, J., and Braga, J., 1997. Entolium beds: Hiatal shell concentrations in starved pelagic settings (middle Liassic, SE Spain). *Eclogae Geologicae Helvetiae*, **90**, 293–302.
- Robertson, A. H. F. 2007. Overview of tectonic settings related to the rifting and opening of Mesozoic ocean basins in the Eastern Tethys: Oman, Himalayas and Eastern Mediterranean regions. *Geological Society, London, Special Publications*, **282**, 325–388.
- Robertson, A. H. F., Blome, C. D., Cooper, D. W. J., Kemp, A. E. S., and Searle, P. 1990. Evolution of the Arabian continental margin in the Dibba Zone, Northern Oman Mountains. *Geological Society, London, Special Publications*, **49**, 251–284.
- Robertson, A., and Searle, M. 1990. The northern Oman Tethyan continental margin: stratigraphy, structure, concepts and controversies. *Geological Society, London, Special Publications*, **49**, 3–25.
- Robertson, A., Parlak, O., Yıldırım, N., Dumitrica, P., and Taslı, K., 2016. Late Triassic rifting and Jurassic–Cretaceous passive margin development of the Southern Neotethys: evidence from the Adıyaman area, SE Turkey. *International Journal of Earth Sciences*, **105**, 167–201.
- Roehl, P.O. 1967. Stony Mountain (Ordovician) and Interlake (Silurian) facies analogs of recent low energy marine and subaerial carbonates, Bahamas. *American Association of Petroleum Geologists*, **51**, 1979–2032.
- Röhl, H. J., 2005. Lower Toarcian (Upper Liassic) black shales of the Central European epicontinental basin: a sequence stratigraphic case study from the SW German *Posidonia* Shale. In: Harris, N., (ed.) *the Deposition of Organic Carbon-rich Sediments: Models, Mechanisms, and Consequences*. SEPM, Special publication, **82**, 165–189.
- Röhl, H.-J., Schmid-Röhl, A., Oschmann, W., Frimmel, A., and Schwark, L. 2001. The *Posidonia* Shale (Lower Toarcian) of SW–Germany: an oxygen–depleted ecosystem controlled by

- sea-level and palaeoclimate. *Palaeogeography, Palaeoclimatology, Palaeoecology*, **165**, 27–52.
- Rojay, B., and Altiner, D., 1998. Middle Jurassic–Lower Cretaceous biostratigraphy in the Central Pontides (Turkey): remarks on palaeogeography and tectonic evolution. *Rivista Italiana di Palaeontologia e Stratigrafia*, **104**, 167–180.
- Rubert, Y., Jati, M., Loisy, C., Cerepi, A., Foto, G., and Muska, K., 2012. Sedimentology of re-sedimented carbonates: Facies and geometrical characterisation of an upper Cretaceous calciturbidite system in Albania. *Sedimentary Geology*, **257**, 63–77.
- Rubin, D. M., and Friedman, G. M. 1977. Intermittently emergent shelf carbonates: an example from the Cambro–Ordovician of eastern New York State. *Sedimentary Geology*, **19**, 81–106.
- Sadooni, F. N., 1997. Stratigraphy and petroleum prospects of Upper Jurassic carbonates in Iraq. *Petroleum Geoscience*, **3**, 233–243.
- Sadooni, F. N., Howari, F. and El-Saiy, A. 2010. Microbial dolomites from carbonate-evaporite sediments of the coastal sabkha of Abu Dhabi and their exploration implications. *Journal of Petroleum Geology*, **33**, 289–298.
- Salae, A. T. S., 2001. *Stratigraphy and sedimentology of the Upper Jurassic succession northern Iraq*. MSc thesis, University of Baghdad, 95 p.
- Sami, T. T. and James, N. P. 1994. Peritidal carbonate platform growth and cyclicity in an early Proterozoic foreland basin, upper Pethei Group, northwest Canada. *Journal of Sedimentary Research*, **64**, 111–131.
- Sanchez–Roman, M., Vasconcelos, C., Warthmann, R., Rivadeneyra, M. A. and McKenzie, J. A. 2009. Microbial Dolomite Precipitation under Aerobic Conditions: Results from Brejo do Espinho Lagoon (Brazil) and Culture Experiments. *Perspectives in Carbonate Geology: A Tribute to the Career of Robert Nathan Ginsburg*, IAS special publication **41**, 167–178
- Santantonio, M. 1993. Facies associations and evolution of pelagic carbonate platform/basin systems: examples from the Italian Jurassic. *Sedimentology*, **40**, 1039–1067.
- Santantonio, M., Scrocca, D., and Lipparini, L. 2013. The Ombrina–Rospo Plateau (Apulian Platform): Evolution of a carbonate platform and its margins during the Jurassic and Cretaceous. *Marine and Petroleum Geology*, **42**, 4–29.
- Savrda, C. E., 1995. Ichnologic applications in palaeoceanographic, palaeoclimatic, and sea-level studies. *Palaios*, **10**, 565–577.

- Schatz, W., 2005. Palaeoecology of the Triassic black shale bivalve *Daonella*—new insights into an old controversy. *Palaeogeography, Palaeoclimatology, Palaeoecology*, **216**, 189–201.
- Schettino, A., and Scotese, C., 2002. Global kinematic constraints to the tectonic history of the Mediterranean region and surrounding areas during the Jurassic and Cretaceous: *Journal of Virtual Explorer*, **8**, 145–160.
- Schieber, J., Bose, P. K., Eriksson, P.G Banerjee, S., Sarkar, S., Altermann W. and Catuneanu, O. 2007. *Atlas of microbial mat features preserved within the clastic record*. Elsevier.
- Schlager, W., and Ginsburg, R. N., 1981. Bahama carbonate platforms—the deep and the past. *Marine Geology*, **44**, 1–24.
- Schlanger, S. O. and Jenkyns, H. C. 1976. Cretaceous oceanic anoxic events: causes and consequences. *Geologie en mijnbouw*, **55**, 179–184.
- Schmid-Röhl, A., Röhl, H.J., Oschmann, W., Frimmel, A., and Schwark, L., 2002. Palaeoenvironmental reconstruction of Lower Toarcian epicontinental black shales (*Posidonia* Shale, SW Germany): global versus regional control. *Geobios*, **35**, 13–20.
- Schmidt, V. 1965. Facies, diagenesis, and related reservoir properties in the Gigas Beds (Upper Jurassic) Northwestern Germany. In: Pray, L.C. and Murray, R.C. (eds.) *Dolomitization and limestone diagenesis*. a symposium—SEPM, special publications, **13**, 124–168.
- Scholle, P.A. and Ulmer–Scholle, D.S., 2003. A Color Guide to the Petrography of Carbonate Rocks: Grains, Textures, Porosity, Diagenesis. *AAPG Memoir* **77**.
- Schrader, H. J., 1971. Fecal pellets: role in sedimentation of pelagic diatoms. *Science*. **174**, 55–57.
- Schreiber, B. C. and Friedman, G. M. 1976. Depositional environments of Upper Miocene (Messinian) evaporites of Sicily as determined from analysis of intercalated carbonates. *Sedimentology*, **23**, 255–270.
- Searle, M. P., 2007. Structural geometry, style and timing of deformation in the Hawasina Window, Al Jabal al Akhdar and Saih Hatat culminations, Oman Mountains: *GeoArabia*, **12**, 99–130.
- Seilacher, A., 1982. Ammonite shells as habitats in the *Posidonia* Shales of Holzmaden—floats or benthic islands. *Neues Jahrbuch für Geologie und Paläontologie, Monatshefte*, 99–115.
- Selley, R. C. 2000. *Applied sedimentology, 2nd edn*. Elsevier, 523 p.
- Seong–Joo, L., Browne, K. M., and Golubic, S. 2000. On stromatolite lamination. In: Riding, R.E., Awramik, S.M. (Eds.) *Microbial Sediments*. Springer–Verlag, Berlin, pp. 16–24
- Shanmugam, G. 1980. Rhythms in deep sea, fine-grained turbidite and debris-flow sequences, Middle Ordovician, eastern Tennessee. *Sedimentology*, **27**, 419–432.

- Shanmugam, G., 2006. *Deep-water Processes and Facies Models: Implications for Sandstone Petroleum Reservoirs*. Elsevier, Amsterdam, 476p.
- Sharland, P. R., Archer, R., Casey, D. M., Davies, R. B., S.H. Hall, A. P. H., Horbury, A. D., and Simmons, M. D., 2001, Arabian Plate Sequence Stratigraphy. *GeoArabia*, Special Publication **2**, 371 p.
- Sherwani, G. H., and Balaky, S. M. 2006. Black Chert, an interesting petrographic component within the upper part of Sargelu Formation (middle Jurassic)–North and Northeastern Iraqi Kurdistan. *Iraqi Bull. Geology and Mining*, **2**, 77–88.
- Shinn, E. A. 1983. Birdseyes, fenestrae, shrinkage pores, and loferites; a reevaluation. *Journal of Sedimentary Petrology*, **53**, 619–628.
- Shinn, E.A. 1968. Practical significance of Birdseye structure in carbonate rocks. *Journal of Sedimentary Petrology*, **38**, 215–223.
- Shinn, E.A., Ginsburg, R.N. and Lloyd, R.M. 1965. Recent supratidal dolomite from Andros Island, Bahamas. In: Pray, L.C. and Murray, R.C. (eds.) *Dolomitization and limestone diagenesis*. SEPM, special publication, **13**, 112–123.
- Shourd, M. L., and Levin, H. L. 1976. Chondrites in the upper Plattin Subgroup (middle Ordovician) of eastern Missouri. *Journal of Palaeontology*, **50**, 260–268.
- Siedlecka, A. 1972. Length–slow chalcedony and relicts of sulfate–evidences of evaporitic environments in the Upper Carboniferous and Permian beds of Bear Island, Svalbard. *Journal of Sedimentary Petrology*, **42**, 812–816.
- Siedlecka, A. 1976. Silicified Precambrian evaporite nodules from Northern Norway: a preliminary report. *Sedimentary Geology*, **16**, 161–175.
- Sissakian, V. K., 2000, The Geological map of Iraq, scale 1:000000, Geological Survey and Mining *GEOSURV*, Baghdad, Iraq.
- Sissakian, V. K., and Al-Jiburi, B. S. M. 2014, Stratigraphy of the high folded zone. *Iraqi Bull. Geol. Min., Special Issue*, **6**, 73–161
- Sissakian, V. K., and Mohammad, B. S. 2007. Geology of Iraqi Western Desert *Iraqi Bull. Geol. Min., Special Issue*, 51–124.
- Smuc, A., and Rozic, B., 2010. The Jurassic Prehodavci Formation of the Julian Alps: easternmost outcrops of Ammonitico rosso in the Southern Alps (NW Slovenia). *Swiss Journal of Geosciences*, **103**, 241–255.

- Soua, M., Zaghib-Turki, D., Ben Jemia, H., Smaoui, J. And Boukadi, A., 2011. Geochemical Record of the Cenomanian-Turonian Anoxic Event in Tunisia: Is it Correlative and Isochronous to the Biotic Signal. *Acta Geologica Sinica-English Edition*, **85**, 1310–1335.
- Soussi, M., and Ismaïl, M. B. 2000. Platform collapse and pelagic seamount facies. Jurassic development of central Tunisia. *Sedimentary Geology*, **133**, 93–113.
- Spath, L. F. 1950. A new Tithonian ammonoid fauna from Kurdistan Northern Iraq. *Bulletin of the British Museum (Natural History) Geology*, **1**, 95–137
- Spezzaferri, S., and Spiegler, D. 2005. Fossil planktic foraminifera (an overview). *Paläontologische Zeitschrift*, **79**, 149–166.
- Stampfli, G. M., and Borel, G. 2002. A plate tectonic model for the Palaeozoic and Mesozoic constrained by dynamic plate boundaries and restored synthetic oceanic isochrones. *Earth and Planetary Science Letters*, **196**, 17–33.
- Stampfli, G., Borel, G., Cavazza, W., Mosar, J., Ziegler, P.A. 2001. *The palaeotectonic atlas of the periTethyan domain*. European Geophysical Union, Karlsruhe 1 (CD).
- Stampfli, G., Marcoux, J., and Baud, A. 1991. Tethyan margins in space and time. *Palaeogeography, Palaeoclimatology, Palaeoecology*, **87**, 373–409.
- Steiger, T. and Jansa, L. F. 1984. *Jurassic limestones of the seaward edge of the Mazagan Carbonate Platform, Northwest African continental margin*. Morocco. Initial Rep DSDP, **79**, 449–491.
- Stow, D. A. V. 1992. *Deep-water Turbidite Systems*. Blackwell, 473 p.
- Strohmenger, C., Webb, S., Al-Kandari, J., Kaufman, J., and De Graff, J. 1998. *An Integrated Approach to Najmah–Sargelu Formation Fractured Carbonate Reservoir Prediction (Upper to Middle Jurassic) in the Gotnia Basin of Kuwait*. Proceedings Geo 98 Conference, Barhain.
- Sun, S. Q. and Wright, V. P. 1989. Peloidal fabrics in Upper Jurassic reefal limestones, Weald Basin, southern England. *Sedimentary Geology*, **65**, 165–181.
- Surdashy, A. M., 1999. *Sequence stratigraphic analysis of the Early–Jurassic central and northern Iraq*. PhD thesis (unpublished), Science College, University of Baghdad, Baghdad, Iraq, p. 145.
- Suzuki, N., Ishida, K., Shinomiya, Y., and Ishiga, H. 1998. High productivity in the earliest Triassic ocean: black shales, Southwest Japan. *Palaeogeography, Palaeoclimatology, Palaeoecology*, **141**, 53–65.

- Szabo, F., and Kheradpir, A., 1978. Permian and Triassic stratigraphy, Zagros basin, south-west Iran. *Journal of Petroleum Geology*, **1**, 57–82.
- Tandon, S. K., Andrews, J. E., Sood, A. and Mittal, S. 1998. Shrinkage and sediment supply control on multiple calcrete profile development: a case study from the Maastrichtian of central India. *Sedimentary Geology*, **119**, 25–45.
- Taylor, A., Goldring, R. and Gowland S. 2003. Analysis and application of ichnofabrics. *Earth–Science Reviews*, **60**, 227–259.
- Tchoumatchenco, P., Rabrenović, D., Radulović, B., and Radulović, V. 2006. Trans–border (east Serbia/west Bulgaria) correlation of the Jurassic sediments: main Jurassic palaeogeographic units. *Geoloski anali Balkanskoga poluostrva*, **67**, 13–17.
- Tekin, U. K., and Cemal Goncuoglu, M., 2009. Late Middle Jurassic (Late Bathonian–early Callovian) radiolarian cherts from the Neotethyan Bornova flysch zone, Spil Mountains, Western Turkey. *Stratigraphy and Geological Correlation*, **17**, 298–308.
- Tomescu, I., 2004. *The Ordovician: a window toward understanding abundance and migration patterns of biogenic chert and implications for palaeoclimate*. PhD thesis, Ohio University.
- Tonkin, N. S., McIlroy, D. Meyer, R. and Moore–Turpin, A. 2010. Bioturbation influence on reservoir quality: A case study from the Cretaceous Ben Nevis Formation, Jeanne d'Arc Basin, offshore Newfoundland, Canada. *AAPG Bulletin*, **94**, 1059–1078.
- Torok, A. 2000. Formation of dolomite mottling in Middle Triassic ramp carbonates (Southern Hungary). *Sedimentary Geology*, **131**, 131–145.
- Tour, J., Soussi, M. and Troudi, H. 2009. Polyphased dolomitization of a shoal–rimmed carbonate platform: example from the middle Turonian Bireno dolomites of central Tunisia. *Cretaceous Research*, **30**, 785–804.
- Trabucho–Alexandre, J., Dirkx, R., Veld, H., Klaver, G. and de Boer, P. L. 2012. Toarcian black shales in the Dutch Central Graben: Record of energetic, variable depositional conditions during an Oceanic Anoxic Event. *Journal of Sedimentary Research*, **82**, 104–120.
- Tremolada, F., Erba, E., van de Schootbrugge, B., and Mattioli, E. 2006, Calcareous nannofossil changes during the late Callovian–early Oxfordian cooling phase. *Marine Micropalaeontology*, **59**, 197–209.
- Tucker, M. E. and Wright, V. P. 2009. *Carbonate sedimentology*. John Wiley & Sons, p.
- Tucker, M. E., Wright, V. P. and Dickson J.A.D.1990. *Carbonate sedimentology*. Blackwell, London, 482 p.

- Tucker, M.E. 1976. Replaced evaporites from the Late Precambrian of Finnmark, Arctic, Norway. *Sedimentary Geology*, **10**, pp. 193–204.
- Tucker M.E. 1993. Carbonate diagenesis and sequence stratigraphy. In: Wright VP (ed) *Sedimentology review*, Blackwell, Oxford, 51–72.
- Turner, E. C., James, N. P. and Narbonne, G. M. 2000. Taphonomic control on microstructure in Early Neoproterozoic reefal stromatolites and thrombolites. *Palaios*, **15**, 87–111.
- Ulmer–Scholle, D. S. 2003. *A color guide to the petrography of carbonate rocks: grains, textures, porosity, diagenesis*. Published by American Association of Petroleum Geologists **77**.
- Van Lith, Y., Warthmann, R., Vasconcelos, C. and McKenzie, J. A. 2003. Microbial fossilization in carbonate sediments: a result of the bacterial surface involvement in dolomite precipitation. *Sedimentology*, **50**, 237–245.
- Van Wagoner, J. C., Mitchum, R., Campion, K., and Rahmanian, V. 1990. *Siliciclastic sequence stratigraphy in well logs, cores, and outcrops: concepts for high-resolution correlation of time and facies*.
- Varol, B., and Gökten, E. 1994. The facies properties and depositional environments of nodular limestones and red marly limestones (Ammonitico Rosso) in the Ankara Jurassic sequence, central Turkey. *Terra Nova*, **6**, 64–71.
- Vasconcelos, C., Warthmann, R., McKenzie, J. A., Visscher, P. T., Bittermann, A. G. and van Lith, Y. 2006. Lithifying microbial mats in Lagoa Vermelha, Brazil: modern Precambrian relics?. *Sedimentary Geology*, **185**, 175–183.
- Vedrine, S., and Strasser, A. 2007. *High-frequency palaeoenvironmental changes in mixed carbonate–siliciclastic sedimentary systems (Late Oxfordian, Switzerland, France, and southern Germany)*. PhD thesis, University of Fribourg.
- Veizer, J., Godderis, Y., and François, L. M. 2000. Evidence for decoupling of atmospheric CO<sub>2</sub> and global climate during the Phanerozoic eon. *Nature*, **408**, 698–701.
- Vera JA, Martín–Algarra A. 1994. Mesozoic stratigraphic breaks and pelagic stromatolites in the Betic Cordillera (Southern Spain). In: Bertrand–Sarfati J, Monty C (eds) *Phanerozoic stromatolites II*. Springer, 319–344.
- Versteegh, G. J., Servais, T., Streng, M., Munnecke, A. and Vachard, D. 2009. A discussion and proposal concerning the use of the term calcispheres. *Palaeontology*, **52**, 343–348.
- Vörös, A., 2012. Episodic sedimentation on a peri–Tethyan ridge through the Middle–Late Jurassic transition (Villány Mountains, southern Hungary). *Facies*, **58**, 415–443.

- Walker, R. 1965. The origin and significance of the internal sedimentary structures of turbidites, in Proceedings of the Yorkshire Geological and Polytechnic Society. *Geological Society of London*, **35**, 1–32.
- Waller, T. R., and Stanley Jr, G. D. 2005. Middle Triassic periomorphian Bivalvia (Mollusca) from the New Pass Range, west–central Nevada: systematics, biostratigraphy, palaeoecology, and palaeobiogeography. *Journal of Palaeontology*, **79**, 1–58.
- Walter, M. R., Golubic, S. and Preiss, W. V. 1973. Recent stromatolites from hydromagnesite and aragonite depositing lakes near the Coorong Lagoon, South Australia. *Journal of Sedimentary Petrology*, **43**, 1021–1030.
- Warren, J. K. 2006. *Evaporites: sediments, resources and hydrocarbons*, **1035**, Berlin: Springer.
- Warren, J.K. 1982. The hydrological significance of Holocene tepee, stromatolite and boxwork limestone in coastal salinas in South Australia. *Journal of Sedimentary Petrology*, **52**, 1171–1201.
- Warren, J.K., 1991. Sulfate dominated sea–marginal and platform evaporative settings. In: Melvin, J.L. (Ed.), *Evaporites, petroleum and mineral resources*. Developments in Sedimentology, **50**, 477–533 Elsevier, Amsterdam.
- Wells, A.J. 1962. Recent dolomite in the Persian (Arabian) Gulf. *Nature*, **194**, 274–275.
- Wendler, J., Grafe, K. U., and Willems, H. 2002. Palaeoecology of calcareous dinoflagellate cysts in the mid–Cenomanian Boreal Realm: implications for the reconstruction of palaeoceanography of the NW European shelf sea. *Cretaceous Research*, **23**, 213–229.
- West, I. M., Brandon, A., and Smith, M. 1968. A tidal flat evaporitic facies in the Visean of Ireland. *Journal of Sedimentary Research*, **38**, 1079–1093.
- Wetzel, A. 2010. Deep-sea ichnology: observations in modern sediments to interpret fossil counterparts. *Acta Geologica Polonica*, **60**, 125–138.
- Wignall, P. 1993. Distinguishing between oxygen and substrate control in fossil benthic assemblages. *Journal of the Geological Society*, **150**, 193–196.
- Wignall, P., and Simms, M. 1990. Pseudoplankton. *Palaeontology*, **33**, 359–378.
- Wignall, R B. 1994. *Black shales*. Oxford University Press, 127 p.
- Wilkinson, I. P., 2011, Pithonellid blooms in the Chalk of the Isle of Wight and their biostratigraphical potential. *Proceedings of the Geologists' Association*, **122**, 809–815.
- Winterer, E. L., and Bosellini, A. 1981. Subsidence and sedimentation on Jurassic passive continental margin, Southern Alps, Italy. *AAPG Bulletin*, **65**, 394–421.

- Winterer, E. 1998. Palaeobathymetry of mediterranean Tethyan Jurassic pelagic sediments: *Memorie della Societa Geologica Italiana*, **53**, 97–131.
- Winterer, E., and Sarti, M. 1994. Neptunian dykes and associated features in southern Spain: mechanics of formation and tectonic implications. *Sedimentology*, **41**, 1109–1132.
- Won, M.-Z., and Below, R. 1999. Cambrian Radiolaria from the Georgina Basin, Queensland, Australia. *Micropalaeontology*, **45**, 325–363.
- Won, M.-Z., and Iams, W. J. 2002. Late Cambrian radiolarian faunas and biostratigraphy of the Cow Head Group, western Newfoundland. *Journal of Palaeontology*, **76**, 1–33
- Wray, J.L. 1977. *Calcareous Algae*. Elsevier, Amsterdam, 185 p.
- Wright, V.P., Rise, A.C. and Munn, S.G. 1990. Intraplatform basin–fill deposits, from the Infracambrian Huqf Group, east Central Oman. In: Robertson, A.H.F., Searle, M.P. and Rise, A.C. (eds.) *The geology and tectonics of the Oman Region*. Geological Society of London, Special publication, **49**, 601–616.
- Yecheili, Y. and Wood, W. W. 2002. Hydrogeologic processes in saline systems: playas, sabkhas, and saline lakes. *Earth–Science Reviews*, **58**, 343–365.
- Yilmaz, C. 2006. Platform–slope transition during rifting: The mid–Cretaceous succession of the Amasya Region (Northern Anatolia), Turkey. *Journal of Asian Earth Sciences*, **27**, 194–206.
- Young, D. K., and Kindle, J. C., 1994. Physical processes affecting availability of dissolved silicate for diatom production in the Arabian Sea. *Journal of Geophysical Research*, **99**, 22619–22632.
- Yousif, S., and Nouman, G. 1997. Jurassic geology of Kuwait. *GeoArabia*, **2**, 91–110.
- Zempolich, W.G. 1993. The drowning succession in Jurassic carbonates of the Venetian Alps, Italy: a record of supercontinent breakup, gradual eustatic rise, and eutrophication of shallow-water environments, in Loucks, R.G., and Sarg, J.F. (eds.) *Carbonate Sequence Stratigraphy*. American Association of Petroleum Geologists, Memoir **57**, 63–105.
- Ziegler, M. A. 2001. Late Permian to Holocene palaeofacies evolution of the Arabian Plate and its hydrocarbon occurrences: *GeoArabia*, **6**, 445–504.

# APPENDIX

Full-field stratigraphic descriptions

Chnaran Location (567924, E3934178)

FORMATION	AGE	SCALE (m)	SAMPLE No.	LITHOLOGY	STROMATOLITE STRUCTURES	SEDIMENTARY STRUCTURES	FAUNAL CONTENT	FACIES NAME		
Barsarin	Mid-Late Kimmeridgian	0-11	BCh39					Thick bedded dolomite-limestone lithofacies TBDLL		
			BCh38					Thick bedded dolomite-limestone lithofacies TBDLL		
			BCh37					Thick bedded dolomite-limestone lithofacies TBDLL		
			2					BCh36	Microbial laminite lithofacies MLL	
			3					BCh35	Thick bedded dolomite-limestone lithofacies	
								BCh34	Microbial laminite lithofacies MLL	
								BCh33	Microbial laminite lithofacies MLL	
			4					BCh32	Microbial laminite lithofacies MLL	
								BCh31	Thick bedded dolomite-limestone lithofacies TBDLL	
			5					BCh30	Thick bedded dolomite-limestone lithofacies TBDLL	
								BCh29	Microbial laminite lithofacies MLL	
								BCh28	Microbial laminite lithofacies MLL	
								6	BCh27	Microbial laminite lithofacies MLL
								BCh26	Microbial laminite lithofacies MLL	
								7	BCh25	Microbial laminite lithofacies MLL
								BCh24	Microbial laminite lithofacies MLL	
								8	BCh23	Microbial laminite lithofacies MLL
								BCh22	Microbial laminite lithofacies MLL	
								9	BCh21	Microbial laminite lithofacies MLL
			10					BCh20	Microbial laminite lithofacies MLL	
								BCh19	Microbial laminite lithofacies MLL	
			11					BCh18	Thick bedded dolomite-limestone lithofacies TBDLL	
			12					BCh17	Blister-flat laminated lithofacies BFLL	
								BCh16	Blister-flat laminated lithofacies BFLL	
			13					BCh15	Microbial laminite lithofacies MLL	
								BCh14	Microbial laminite lithofacies MLL	
			15					BCh13	Thick bedded dolomite-limestone lithofacies TBDLL	
								BCh12	Thick bedded dolomite-limestone lithofacies TBDLL	
			16					BCh11	Microbial laminite lithofacies MLL	
								BCh10	Microbial laminite lithofacies MLL	
			18					BCh9	Thick bedded dolomite-limestone lithofacies TBDLL	
								BCh8	Blister-flat laminated lithofacies BFLL	
			20					BCh7	Microbial laminite lithofacies MLL	
								BCh6	Microbial laminite lithofacies MLL	
			22					BCh5	Thick bedded dolomite-limestone lithofacies TBDLL	
BCh4	Blister-flat laminated lithofacies BFLL									
23	BCh3	Microbial laminite lithofacies MLL								
	BCh2	Microbial laminite lithofacies MLL								
BCh1	Microbial laminite lithofacies MLL									
Naokelekan	Oxfordian-Early Kimmeridgian	12-35	NCh19					Argillaceous limestone member ALM		
			NCh18					Thick bedded mottled limestone member TBMLM		
			NCh17					Thick bedded mottled limestone member TBMLM		
			NCh16					Thick bedded mottled limestone member TBMLM		
			NCh15					Thick bedded mottled limestone member TBMLM		
			NCh14					Thick bedded mottled limestone member TBMLM		
			NCh13					Thick bedded mottled limestone member TBMLM		
			NCh12					Thick bedded mottled limestone member TBMLM		
			NCh11					Thick bedded mottled limestone member TBMLM		
			NCh10					Thick bedded mottled limestone member TBMLM		
			NCh9					Thick bedded mottled limestone member TBMLM		
			31					NCh8	Medium bedded microbial-bearing limestone member MBMLM	
								NCh7	Medium bedded microbial-bearing limestone member MBMLM	
			33					NCh6	Carbonaceous limestone member CLM	
								NCh5	Carbonaceous limestone member CLM	
			34					NCh4	Black shale member BSM	
NCh3	Black shale member BSM									
35	NCh2	Black shale member BSM								
	NCh1	Black shale member BSM								
Sargelu	Bajocian-Bathonian	0-3	SgCh25					Main Slump unit		
			SgCh24					Main Slump unit		
			SgCh23					Main Slump unit		
			SgCh22					Main Slump unit		
			SgCh21					Main Slump unit		
			SgCh20					Main Slump unit		
			SgCh19					Main Slump unit		
			SgCh18					Main Slump unit		
			SgCh17					Main Slump unit		
			SgCh16					Main Slump unit		
			SgCh15					Main Slump unit		
			SgCh14					Black shale, radiolarian bedded chert and <i>posidonia</i> -bearing limestone member BRPLM		
			SgCh13					Black shale, radiolarian bedded chert and <i>posidonia</i> -bearing limestone member BRPLM		
			SgCh12					Black shale, radiolarian bedded chert and <i>posidonia</i> -bearing limestone member BRPLM		
			SgCh11					Black shale, radiolarian bedded chert and <i>posidonia</i> -bearing limestone member BRPLM		
SgCh10	Black shale, radiolarian bedded chert and <i>posidonia</i> -bearing limestone member BRPLM									
SgCh9	Black shale, radiolarian bedded chert and <i>posidonia</i> -bearing limestone member BRPLM									
SgCh8	Black shale, radiolarian bedded chert and <i>posidonia</i> -bearing limestone member BRPLM									
SgCh7	Black shale, radiolarian bedded chert and <i>posidonia</i> -bearing limestone member BRPLM									
SgCh6	Black shale, radiolarian bedded chert and <i>posidonia</i> -bearing limestone member BRPLM									
SgCh5	Black shale, radiolarian bedded chert and <i>posidonia</i> -bearing limestone member BRPLM									
SgCh4	Black shale, radiolarian bedded chert and <i>posidonia</i> -bearing limestone member BRPLM									
SgCh3	Middle <i>posidonia</i> limestone member MPLM									
SgCh2	Middle <i>posidonia</i> limestone member MPLM									
SgCh1	Middle <i>posidonia</i> limestone member MPLM									

Sargelu Location (514783, E3969364)

FORMATION	AGE	SCALE (m)	SAMPLE No.	LITHOLOGY	STROMATOLITE STRUCTURES	SEDIMENTARY STRUCTURES	FAUNAL CONTENT	FACIES NAME					
Barsarin	Mid-Late Kimmeridgian	1 2 3 4 5 6 7 8 9	BS34					Microbial laminite lithofacies MLL					
			BS33										
			BS32										
			BS31										
			BS30										
			BS29										
			BS28										
			BS27										
			BS26										
			BS25										
			BS24										
			BS23					10 11 12 13 14 15 16 17					Thick bedded dolomite-limestone lithofacies TBDLL
			BS22										
			BS21										
			BS20										
			BS19										
			BS18										
			BS17										
			BS16										
			BS15										
			BS14										
			BS13										
			BS12										
BS11													
BS10	18 19 20 21 22 23					Blister-flat laminated lithofacies BFLL							
BS9													
BS8													
BS7													
BS6													
BS5													
BS4													
BS3													
BS2													
BS1													
Sargelu	Bajocian-Bathonian	3 2 1 0	SgCh25					Black shale, radiolarian bedded chert and <i>posidonia</i> -bearing limestone member BRPLM					
			SgCh24										
			SgCh23										
			SgCh22										
			SgCh21										
			SgCh20										
			SgCh19										
			SgCh18										
			SgCh17										
			SgCh16										
SgCh15													
SgCh14													
SgCh13													
SgCh12													
SgCh11													
SgCh10													
SgCh9	middle part of sargelu					Middle <i>posidonia</i> limestone member MPLM							
SgCh8													
SgCh7													
SgCh6													
SgCh5													
SgCh4													
SgCh3													
SgCh2													
SgCh1													
Naokelekan	Oxfordian-Early Kimmeridgian	24 25 26 27 28 29 30	NS9					Argillaceous limestone member ALM					
			NS8										
			NS7										
			NS6										
			NS5										
			NS4										
			NS3										
			NS2										
			NS1										
			Sargelu					Bajocian-Bathonian	3 2 1 0	SgCh25			
SgCh24													
SgCh23													
SgCh22													
SgCh21													
SgCh20													
SgCh19													
SgCh18													
SgCh17													
SgCh16													
SgCh15													
SgCh14													
SgCh13													
SgCh12													
SgCh11													
SgCh10													
SgCh9	middle part of sargelu					Middle <i>posidonia</i> limestone member MPLM							
SgCh8													
SgCh7													
SgCh6													
SgCh5													
SgCh4													
SgCh3													
SgCh2													
SgCh1													

Hanjera Lotion (486759. E 4015920)

FORMATION	AGE	SCALE (m)	SAMPLE No.	LITHOLOGY	STROMATOLITE STRUCTURES	SEDIMENTARY STRUCTURES	FAUNAL CONTENT	FACIES NAME
Barsarin	Mid-Late Kimmeridgian	0-30	BH55					Microbial laminite lithofacies MLL
			BH54					Microbial laminite lithofacies MLL
			BH53					Microbial laminite lithofacies MLL
			BH52					Microbial laminite lithofacies MLL
			BH51					Microbial laminite lithofacies MLL
			BH50					Microbial laminite lithofacies MLL
			BH49					Microbial laminite lithofacies MLL
			BH48					Microbial laminite lithofacies MLL
			BH47					Microbial laminite lithofacies MLL
			BH46					Microbial laminite lithofacies MLL
			BH45					Microbial laminite lithofacies MLL
			BH44					Microbial laminite lithofacies MLL
			BH43					Microbial laminite lithofacies MLL
			BH42					Microbial laminite lithofacies MLL
			BH41					Microbial laminite lithofacies MLL
			BH40					Microbial laminite lithofacies MLL
			BH39					Microbial laminite lithofacies MLL
			BH38					Microbial laminite lithofacies MLL
			BH37					Microbial laminite lithofacies MLL
			BH36					Microbial laminite lithofacies MLL
			BH35					Microbial laminite lithofacies MLL
			BH34					Microbial laminite lithofacies MLL
			BH33					Microbial laminite lithofacies MLL
			BH32					Microbial laminite lithofacies MLL
			BH31					Microbial laminite lithofacies MLL
			BH30					Microbial laminite lithofacies MLL
			BH29					Microbial laminite lithofacies MLL
			BH28					Microbial laminite lithofacies MLL
BH27	Microbial laminite lithofacies MLL							
BH26	Microbial laminite lithofacies MLL							
BH25	Microbial laminite lithofacies MLL							
BH24	Microbial laminite lithofacies MLL							
BH23	Microbial laminite lithofacies MLL							
BH22	Microbial laminite lithofacies MLL							
BH21	Microbial laminite lithofacies MLL							
BH20	Microbial laminite lithofacies MLL							
BH19	Microbial laminite lithofacies MLL							
BH18	Microbial laminite lithofacies MLL							
BH17	Microbial laminite lithofacies MLL							
BH16	Microbial laminite lithofacies MLL							
BH15	Microbial laminite lithofacies MLL							
BH14	Microbial laminite lithofacies MLL							
BH13	Microbial laminite lithofacies MLL							
BH12	Microbial laminite lithofacies MLL							
BH11	Microbial laminite lithofacies MLL							
BH10	Microbial laminite lithofacies MLL							
BH9	Microbial laminite lithofacies MLL							
BH8	Microbial laminite lithofacies MLL							
BH7	Microbial laminite lithofacies MLL							
BH6	Microbial laminite lithofacies MLL							
BH5	Microbial laminite lithofacies MLL							
BH4	Microbial laminite lithofacies MLL							
BH3	Microbial laminite lithofacies MLL							
BH2	Microbial laminite lithofacies MLL							
BH1	Microbial laminite lithofacies MLL							
BH53i	Microbial laminite lithofacies MLL							
BH52i	Microbial laminite lithofacies MLL							
BH51i	Microbial laminite lithofacies MLL							
BH50i	Microbial laminite lithofacies MLL							
BH49i	Microbial laminite lithofacies MLL							
BH48i	Microbial laminite lithofacies MLL							
BH47i	Microbial laminite lithofacies MLL							
BH46i	Microbial laminite lithofacies MLL							
BH45i	Microbial laminite lithofacies MLL							
BH44i	Microbial laminite lithofacies MLL							
Naokelekan	Oxfordian-Early Kimmeridgian	30-37	NH9					Thick bedded mottled limestone member TBMLM
			NH8					Thick bedded mottled limestone member TBMLM
			NH7					Thick bedded mottled limestone member TBMLM
			NH6					Thick bedded mottled limestone member TBMLM
			NH5					Thick bedded mottled limestone member TBMLM
			NH4					Thick bedded mottled limestone member TBMLM
			NH3					Thick bedded mottled limestone member TBMLM
			NH2					Thick bedded mottled limestone member TBMLM
			NH1					Thick bedded mottled limestone member TBMLM
			Sargelu					Bajocian-Bathonian
SgH17	Black shale, radiolarian bedded chert and <i>posidonia</i> -bearing limestone member BRPLM							
SgH16	Black shale, radiolarian bedded chert and <i>posidonia</i> -bearing limestone member BRPLM							
SgH15	Black shale, radiolarian bedded chert and <i>posidonia</i> -bearing limestone member BRPLM							
SgH14	Black shale, radiolarian bedded chert and <i>posidonia</i> -bearing limestone member BRPLM							
SgH13	Black shale, radiolarian bedded chert and <i>posidonia</i> -bearing limestone member BRPLM							
SgH12	Black shale, radiolarian bedded chert and <i>posidonia</i> -bearing limestone member BRPLM							
SgH11	Black shale, radiolarian bedded chert and <i>posidonia</i> -bearing limestone member BRPLM							
SgH10	Black shale, radiolarian bedded chert and <i>posidonia</i> -bearing limestone member BRPLM							
SgH9	Black shale, radiolarian bedded chert and <i>posidonia</i> -bearing limestone member BRPLM							
SgH8	Black shale, radiolarian bedded chert and <i>posidonia</i> -bearing limestone member BRPLM							
SgH7	Black shale, radiolarian bedded chert and <i>posidonia</i> -bearing limestone member BRPLM							
SgH6	Black shale, radiolarian bedded chert and <i>posidonia</i> -bearing limestone member BRPLM							
SgH5	Black shale, radiolarian bedded chert and <i>posidonia</i> -bearing limestone member BRPLM							
SgH4	Black shale, radiolarian bedded chert and <i>posidonia</i> -bearing limestone member BRPLM							
SgH3	Black shale, radiolarian bedded chert and <i>posidonia</i> -bearing limestone member BRPLM							
SgH2	Black shale, radiolarian bedded chert and <i>posidonia</i> -bearing limestone member BRPLM							
SgH1	Black shale, radiolarian bedded chert and <i>posidonia</i> -bearing limestone member BRPLM							

FORMATION	AGE	SCALE (m)	SAMPLE No.	LITHOLOGY	STROMATOLITE STRUCTURES	SEDIMENTARY STRUCTURES	FAUNAL CONTENT	FACIES NAME
Barsarin	Mid-Late Kimmeridgian	0-24	BN52					Microbial laminite lithofacies MLL
			BN51					Microbial laminite lithofacies MLL
			BN50					Microbial laminite lithofacies MLL
			BN49					Thick bedded dolomite-limestone lithofacies TBDLL
			BN48					Thick bedded dolomite-limestone lithofacies TBDLL
			BN47					Microbial laminite lithofacies MLL
			BN46					Microbial laminite lithofacies MLL
			BN45					Stratiform laminated limestone and domal stromatolite lithofacies SLLDSL
			BN44					Microbial laminite lithofacies MLL
			BN43					Thick bedded dolomite-limestone lithofacies TBDLL
			BN42					Blister-flat laminated lithofacies BFLL
			BN41					Microbial laminite lithofacies MLL
			BN40					Microbial laminite lithofacies MLL
			BN39					Microbial laminite lithofacies MLL
			BN38					Microbial laminite lithofacies MLL
			BN37					Microbial laminite lithofacies MLL
			BN36					Microbial laminite lithofacies MLL
			BN35					Microbial laminite lithofacies MLL
			BN34					Microbial laminite lithofacies MLL
			BN33					Microbial laminite lithofacies MLL
			BN32					Microbial laminite lithofacies MLL
			BN31					Microbial laminite lithofacies MLL
			BN30					Blister-flat laminated lithofacies BFLL
			BN29					Thick bedded dolomite-limestone lithofacies TBDLL
BN28	Blister-flat laminated lithofacies BFLL							
BN27	Microbial laminite lithofacies MLL							
BN26	Microbial laminite lithofacies MLL							
BN25	Thick bedded dolomite-limestone lithofacies TBDLL							
BN24	Thick bedded dolomite-limestone lithofacies TBDLL							
BN23	Thick bedded dolomite-limestone lithofacies TBDLL							
BN22	Thick bedded dolomite-limestone lithofacies TBDLL							
BN21	Blister-flat laminated lithofacies BFLL							
BN20	Blister-flat laminated lithofacies BFLL							
BN19	Blister-flat laminated lithofacies BFLL							
BN18	Microbial laminite lithofacies MLL							
BN17	Microbial laminite lithofacies MLL							
BN16	Thick bedded dolomite-limestone lithofacies TBDLL							
BN15	Microbial laminite lithofacies MLL							
BN14	Microbial laminite lithofacies MLL							
BN13	Blister-flat laminated lithofacies BFLL							
BN12	Blister-flat laminated lithofacies BFLL							
BN11	Blister-flat laminated lithofacies BFLL							
BN10	Blister-flat laminated lithofacies BFLL							
BN9	Microbial laminite lithofacies MLL							
BN8	Microbial laminite lithofacies MLL							
BN7	Microbial laminite lithofacies MLL							
BN6	Microbial laminite lithofacies MLL							
BN5	Microbial laminite lithofacies MLL							
BN4	Microbial laminite lithofacies MLL							
BN3	Microbial laminite lithofacies MLL							
BN2	Microbial laminite lithofacies MLL							
BN1	Microbial laminite lithofacies MLL							
Naokelekan	Oxfordian-Early Kimmeridgian	25-30	NN19					Argillaceous limestone member ALM
			NN18					Argillaceous limestone member ALM
			NN17					Argillaceous limestone member ALM
			NN16					Argillaceous limestone member ALM
			NN15					Thick bedded mottled limestone member TBMLM
			NN14					Thick bedded mottled limestone member TBMLM
			NN13					Thick bedded mottled limestone member TBMLM
			NN12					Thick bedded mottled limestone member TBMLM
			NN11					Thick bedded mottled limestone member TBMLM
			NN10					Thick bedded mottled limestone member TBMLM
			NN9					Medium bedded microbial-bearing limestone member MBMLM
			NN8b					Medium bedded microbial-bearing limestone member MBMLM
			NN8					Medium bedded microbial-bearing limestone member MBMLM
			NN7					Medium bedded microbial-bearing limestone member MBMLM
			NN6					Carbonaceous limestone member CLM
			NN5					Carbonaceous limestone member CLM
			NN4					Carbonaceous limestone member CLM
			NN3					Carbonaceous limestone member CLM
			NN2					Black shale member BSM
NN1	Black shale member BSM							
Sargelu	Bajocian-Bathonian	0-3	SgN23					Main Slump unit
			SgN22					Main Slump unit
			SgN21					Main Slump unit
			SgN20					upper part of sargelu
			SgN19					upper part of sargelu
			SgN18					upper part of sargelu
			SgN17					upper part of sargelu
			SgN16					upper part of sargelu
			SgN15					upper part of sargelu
			SgN14					upper part of sargelu
			SgN13					upper part of sargelu
			SgN12					upper part of sargelu
			SgN11					upper part of sargelu
SgN10	upper part of sargelu							
SgN9	upper part of sargelu							
SgN8	upper part of sargelu							
SgN7	upper part of sargelu							
SgN5	upper part of sargelu							
SgN5	middle part of sargelu							
SgN4	middle part of sargelu							
SgN3	middle part of sargelu							
SgN2	middle part of sargelu							
SgN1	First slump unit							
								Middle <i>posidonia</i> limestone member MPLM



Gara Location (368619, E4095981)

FORMATION	AGE	SCALE (m)	SAMPLE No.	LITHOLOGY	STROMATOLITE STRUCTURES	SEDIMENTARY STRUCTURES	FAUNAL CONTENT	FACIES NAME				
Barsarin	Mid-Late Kimmeridgian	1	BG50 BG49 BG48 BG47 BG46					Thick bedded dolomite-limestone lithofacies TBDLL				
		2	BG45 BG44 BG43					Microbial laminite lithofacies MLL				
		3	BG42					Thick bedded dolomite-limestone lithofacies TBDLL				
		4	BG41					Microbial laminite lithofacies MLL				
		5	BG40 BG39 BG38 BG37 BG36					Microbial laminite lithofacies MLL				
		6	BG35 BG34					Thick bedded dolomite-limestone lithofacies TBDLL				
		7	BG33					Thick bedded dolomite-limestone lithofacies TBDLL				
		8	BG32					Blister-flat laminated lithofacies BFLL				
		9	BG31					Thick bedded dolomite-limestone lithofacies TBDLL				
		10	BG30 BG29 BG28 BG27 BG26 BG25 BG24 BG23 BG22 BG21 BG20 BG19 BG18					Microbial laminite lithofacies MLL				
		11	BG17 BG16 BG15 BG14 BG13					Thick bedded mottled limestone member TBMLM				
		12	BG12					Blister-flat laminated lithofacies BFLL				
		13	BG11 BG10 BG9 BG8 BG7 BG6 BG5 BG4 BG3 BG2 BG1					Microbial laminite lithofacies MLL				
		Naokelekan	Oxfordian-Early Kimmeridgian	34	NG15 NG14 NG13 NG12 NG11 NG10 NG9					Argillaceous limestone member ALM		
				35	NG8 NG7 NG6 NG5					Thick bedded mottled limestone member TBMLM		
	36			NG4					Medium bedded microbial-bearing limestone member MBMLM			
	37			NG3 NG2 NG1					Carbonaceous limestone member CLM			
	Sargelu			Bajocian-Bathonian	38	SgG50 SgG48 SgG46 SgG45 SgG44 SgG43 SgG42 SgG41 SgG40 SgG39 SgG38 SgG37 SgG36 SgG35 SgG34 SgG33 SgG32 SgG31 SgG30 SgG29 SgG28 SgG27 SgG26 SgG25 SgG24 SgG23 SgG22 SgG21 SgG20 SgG19 SgG18 SgG17 SgG16 SgG15 SgG14 SgG13 SgG12 SgG11 SgG10 SgG9 SgG8 SgG7 SgG6 SgG5 SgG4 SgG3 SgG2 SgG1						Black shale, radiolarian bedded chert and <i>posidonia</i> -bearing limestone member BRPLM
					39						Middle <i>posidonia</i> limestone member MPLM	
					40							
					41							
					42							
					43							
		44										
		45										
		46										
		47										
	48											

Bank Location (319657, E4121871)

FORMATION	AGE	SCALE (m)	SAMPLE NO.	LITHOLOGY	STROMATOLITE STRUCTURES	SEDIMENTARY STRUCTURES	FAUNAL CONTENT	FACIES NAME	
Barsarin	Mid-Late Kimmeridgian	1	BZ53					Thick bedded dolomite-limestone lithofacies TBDLL	
		2	BZ52						
		3	BZ51						
		4	BZ50						Blister-flat laminated lithofacies BFLL
			BZ49						
			BZ48						
		5	BZ47						Thick bedded dolomite-limestone lithofacies TBDLL
			BZ46						
			BZ45						
		6	BZ44						Microbial laminite lithofacies MLL
			BZ43						
			BZ42						
		7	BZ41						Thick bedded dolomite-limestone lithofacies TBDLL
			BZ40						
			BZ39						
		8	BZ38						Blister-flat laminated lithofacies BFLL
			BZ37						
			BZ36						
		9	BZ35						Microbial laminite lithofacies MLL
			BZ34						
			BZ33						
		10	BZ32						Thick bedded dolomite-limestone lithofacies TBDLL
			BZ31						
			BZ30						
		11	BZ29						Blister-flat laminated lithofacies BFLL
			BZ28						
			BZ27						
		12	BZ26						Thick bedded dolomite-limestone lithofacies TBDLL
			BZ25						
			BZ24						
		13	BZ23						Microbial laminite lithofacies MLL
			BZ22						
			BZ21						
		14	BZ20						Thick bedded dolomite-limestone lithofacies TBDLL
			BZ19						
			BZ18						
		15	BZ17						Blister-flat laminated lithofacies BFLL
			BZ16						
			BZ15						
16	BZ14						Thick bedded dolomite-limestone lithofacies TBDLL		
	BZ13								
	BZ12								
17	BZ11						Microbial laminite lithofacies MLL		
	BZ10								
	BZ9								
18	BZ8						Thick bedded dolomite-limestone lithofacies TBDLL		
	BZ7								
	BZ6								
19	BZ5						Microbial laminite lithofacies MLL		
	BZ4								
	BZ3								
20	BZ2						Blister-flat laminated lithofacies BFLL		
	BZ1								
	BZ0								
Sargelu	Bajocian-Bathonian	0	NZ101					Black shale, radiolarian bedded chert and <i>posidonia</i> -bearing limestone member BRPLM	
		1	NZ99						
		2	NZ98						
		3	NZ97						
		4	NZ96						
		5	NZ95						
		6	NZ94						
		7	NZ93						
		8	NZ92						
		9	NZ91						
Naokelekan	Oxfordian-Early Kimmeridgian	40	NZ17					Argillaceous limestone member ALM	
		41	NZ16						
		42	NZ15						
		43	NZ14						
		44	NZ13						
Sargelu	Bajocian-Bathonian	0	NZ100					Middle <i>posidonia</i> limestone member MPLM	
		1	NZ99						
		2	NZ98						
		3	NZ97						
		4	NZ96						